Mission-Oriented Seismic Research Program

Annual Report

2007

M-OSRP

University of Houston

Sponsors and Advisory Board representatives

Corporate Sponsors

Amerada Hess ..... Scott Morton, Jacques Leveille
Anadarko ..... Roger Reagan
BP ..... Uwe Albertin
BHP ..... Michael Richardson
ChevronTexaco ..... Debbie Bones
ConocoPhillips ..... Douglas Foster, Robert Stolt
Devon Energy ..... Kenneth Beeney
Encana ..... William Goodway, David Mackidd
ENI-Agip ..... Michele Buia
ExxonMobil ..... Peter Traynin
Geotrace Technologies ..... Jaime Stein
GX Technology ..... Nick Bernitsas, Robert Bloor
IBM ..... Tom McClure
Landmark ..... Dave Diller
Petrochina Company Limited ..... Jixiang Xu
Petrobras ..... Neiva Zago
PGS ..... Martin Widmaier, Steve Kelly, Ruben Martinez
Repsol ..... Francisco Ortigosa Fernandez
Saudi Aramco ..... Yi Luo
Shell ..... Jonathan Sheiman
Statoil-Hydro ..... Lasse Amundsen
WesternGeco ..... Luis Canales, William Dragoset

Federal Support

DOE Basic Energy Sciences ..... Nick Woodward
NSF CMG ..... Henry A. Warchall

M-OSRP Personnel

Faculty

Lasse Amundsen (Statoil) ..... Adjunct Professor (Physics)
Douglas J. Foster[1] (ConocoPhillips) ..... Adjunct Professor (Physics)
Kristopher A. Innanen ..... Assistant Professor (Physics)
Robert G. Keys (ConocoPhillips) ..... Adjunct Professor (Physics)
Jacques Leveille (Amerada Hess) ..... Adjunct Professor (Physics)
Fang Liu ..... Research Assistant Professor (Physics)
Ken H. Matson (BP) ..... Adjunct Associate Professor (Physics)
Bogdan Nita (Assistant Professor, Montclair State U.) .... Adjunct Assistant Professor (Physics)
Jon Sheiman (Shell) ..... Adjunct Professor (Physics)
Robert H. Stolt (ConocoPhillips) ..... Adjunct Professor (Physics)
T. Hing Tan (Shell) ..... Adjunct Professor (Physics)
Arthur B. Weglein ..... Cullen Professor (Physics)
Daniel Whitmore (ConocoPhillips) ..... Adjunct Professor (Physics)

Ph.D. Students

Walter Kessinger ..... Geosciences
Shansong Jiang ..... Physics
Jose Eduardo Lira ..... Geosciences[2]
Xu Li ..... Physics
Zhiqiang Wang ..... Physics
Jim Mayhan ..... Physics
Shih-Ying Hsu ..... Physics
Min Wang ..... Physics
Dan Fisher ..... Physics
Zhicheng You ..... Physics
Jiming Zhang ..... Physics

Recent Alumni

Adriana Citlali Ramirez ..... Physics
Haiyan Zhang ..... Physics
Jingfeng Zhang ..... Physics
Fang Liu ..... Physics
Zhiqiang Guo ..... Geosciences
Francisco Miranda ..... Physics
Simon A. Shaw ..... Geosciences

Administrative Support

Jennifer Chin-Davis ..... Business Administrator
Nguyen Tran ..... Program Accountant
Angela Cowan ..... Program Coordinator
Joseph Ghobrial ..... Computer/IT Support
Jesse Weglein ..... Webmaster

[1]Chair, M-OSRP Advisory Board
[2]Petrobras, Brazil

Table of Contents

M-OSRP 2007 Introduction and Preface

This year has been another positive and productive year for M-OSRP. In this introduction to the 2007 Annual Report, we provide an executive summary of the program, from both the broad strategic goals and methods being pioneered, developed and tested, as well as progress and highlights and plans within specific projects. We begin by describing the origin of seismic E & P challenges. Then we note how these issues are addressed, in general, and what and how M-OSRP is pursuing, progressing, providing and contributing towards a comprehensive and effective response. We start with the origin of seismic challenges.

ALL SEISMIC METHODS MAKE ASSUMPTIONS AND ASSUMPTION SATISFACTION ALIGNS WITH ALGORITHMIC RELIABILITY, PREDICTABILITY AND EFFECTIVENESS

We recognize that: (1) seismic exploration methods have an established and strong track-record of effectiveness, and that effectiveness depends upon the satisfaction of assumptions and prerequisites behind seismic techniques and algorithms, and (2) when those same algorithmic prerequisites and assumptions are violated then seismic methods can and will fail and result in dry hole drilling.

TYPES OF ASSUMPTIONS

For our purposes, we find it useful to distinguish different types of algorithmic assumptions and requirements as follows: (1) assumptions on adequate types and extent of data collection, extrapolation and interpolation, (2) assumptions on adequate compute power for acceptable processing turn-around time, and (3) innate algorithmic assumptions or requirements. An innate algorithmic assumption is one that is not satisfied or resolvable by a more complete acquisition and adequate compute power.

Simple examples of innate imaging challenges are:(1) the inability under complex subsurface conditions, with current velocity analysis methods, to determine an adequate velocity model, given ideal acquisition and adequate compute capability, and (2) the inability to accurately image beneath a perfectly provided velocity model when a combination of lateral velocity and variable dip are involved in the overburden and/or if the geometry of the reflector is complex, corrugated and rapidly varying.

ASSUMPTION VIOLATION PRODUCES SEISMIC ALGORITHM FAILURE AND SEISMIC EXPLORATION CHALLENGES

Seismic processing algorithm assumption violations are behind all seismic processing breakdown and exploration challenges. M-OSRP, a research program designed to address pressing seismic challenges needs to begin with a clear, frank and forthright examination of the origin of these pitfalls and obstacles, and, in general, how that type of issue can be addressed. We are all aware of, and celebrate, and benefit from, the tremendously successful history of seismic processing and seismic exploration, and we owe a great debt to those that brought that capability to the petroleum industry. We also recognize that all processing methods make assumptions, and we need to recognize the flaws and pitfalls, as well, thereby enabling researchers to define and focus and improve upon our current seismic capability.

There is danger in defining the problem only in terms of the issues we wish to examine, or know how to address. The focus on acquisition and compute issues, often dominates the discussion, or the move to non-seismic techniques becomes more interesting, anything but examining and addressing the innate seismic processing assumptions and limitations.

HOW TO ADDRESS CHALLENGES: FIGURE OUT HOW TO EITHER SATISFY OR AVOID VIOLATED ASSUMPTIONS

We recognize that there are two reasonable ways and strategies to respond and address seismic challenges: (1) find a way to remove the prerequisite violation by directly satisfying the algorithm's need, or developing a new way to satisfy the previously violated assumption or requirement, or (2) develop a fundamentally new processing concept and method that produces the original sought after processing goal while entirely avoiding the current processing algorithm's need for a difficult or impossible to satisfy requirement or assumption. The goal is to provide a new contribution to the tool box of techniques to allow seismic capability to navigate a geologic configuration and to access a type of exploration play that is either currently precluded and inaccessible or is accessible but inadequately defined.

HOW M-OSRP ADDRESSES SPECIFIC CHALLENGES

In the Mission-Oriented Seismic Research Program, we adopt one or the other of these challenge response strategies depending on the specific issue we are addressing. For data acquisition, interpolation, and extrapolation our general inclination and response is to remove the prerequisite violation, and satisfy the demand of wave theoretic processing through: (1) demonstrating the E & P cost benefit and added-value that a more complete acquisition would provide, and (2) developing more effective methods for data extrapolation and interpolation (please see report by A.C. Ramirez et al). However, we also recognize the near term practical reality that doesnt expect as standard practice a fully 3D data collection, e.g., we anticipate limited coverage and sampling in the cross-line direction, and we therefore develop distinct imaging algorithms that are designed to provide the benefit of our new depth imaging concepts with either: (1) a full 3D acquisition, or (2)

the currently standard, more common and less complete 3D acquisition. To exemplify the latter type of algorithmic accommodation a new water speed migration required as the first step in the inverse series imaging algorithms (Fang Liu), that is a wave theoretic FK Stolt migration in the in-line direction, but is an aperture compensated Kirchhoff migration in the cross-line direction, and can be found in a paper in this Annual Report (Zhiqiang Wang et al) .

INNATE SEISMIC ALGORITHMIC ASSUMPTIONS: SATISFYING OR AVOIDING

For innate seismic processing algorithm assumptions, we suggest and encourage first trying to satisfy the needs of current imaging methods. If that fails, or if the assumptions themselves are too restrictive for situations of interest (e.g., assuming a 1D earth) , we suggest developing new algorithms with less restrictions and less daunting assumptions. We recognize that complex media and interfaces, (and sometimes with not so complicated subsurface conditions), can cause havoc with many mainstream seismic processing algorithm prerequisites, demands and requirements. The innate set of algorithmic limitations needs to be recognized and addressed simultaneously with acquisition and compute demands, to have a realistic and effective strategy for addressing the actual issues behind seismic exploration challenges that we face in the petroleum industry.

THE INVERSE SCATTERING SERIES AND AVOIDING THE NEED FOR ANY SUBSURFACE INFORMATION IN ALL SEISMIC PROCESSING ALGORITHMS

The inverse scattering series represents the potential to achieve all processing goals directly in terms of recorded data, and without any need, in principle or practice, to provide any subsurface information, whatsoever. Therefore, it is natural that we would look to the inverse scattering series to provide new algorithms that avoid the need for subsurface information and can provide new and effective methods, to fill that gap when conventional methods fail when their required subsurface information is beyond our reach. For example, given an accurate velocity model the classic downward continuation and imaging concept directly produces a structure map. The inverse scattering series states that the same accurate structure map is able to be directly output from an algorithm that only inputs the recorded data.

We have become familiar with this type of magical behavior in the removal of free surface multiples. Data with primaries, internal multiples and free surface multiples is input, and data with primaries and internal multiples and without free surface multiples is output. Absolutely nothing about the earth is required as input, and nothing about the earth is ever determined, approximated, needed, used or output, implicitly or explicitly, and without searching, model matching or optimization. Data goes in with free surface multiples and data comes out without free surface multiples. That's it.

There are different ways to derive the free surface multiple removal algorithm, and among these different ways, one derivation comes from the inverse scattering series. However, the unique and critically important message delivered by the inverse scattering series, and by only the inverse

scattering series, is that ALL processing goals are achievable in the same way as the free surface multiples are removed, and can be achieved directly in terms of data, and without the need for subsurface information. Among other processing goals that have the potential of being achieved directly in terms of data, and without subsurface information, are: internal multiple removal, depth imaging, non-linear direct target identification and Q compensation without Q. Each of these goals has a project within M-OSRP and this report describes the progress and plans, for each of these initiatives. We also have launched a new project specific to on-shore issues and application, and a first report by Shih-Ying Hsu et al is in this Annual Report.

Since the free surface multiple removal algorithm is a simplest realization of the potential of the inverse scattering series, and serves as a template for more ambitious processing goals, understanding how it operates is a central lesson for both achieving other goals, and understanding how the ISS differs and stands apart in terms of its promise and potential from all other comprehensive high ambition processing and inversion strategies and approaches.

The methods and algorithms that derive from the inverse scattering series are neither mystical nor mysterious. They simply use the seismic recorded data, and the information contained within that entire set of events in a collective rather than in an isolated event fashion. In general, for example, if a method for predicting multiples or depth imaging primaries, has adequate subsurface information to separate or model those events, then the time of a single multiple is sufficient to remove it, and the time of a single primary is sufficient to directly image it correctly in depth. The inverse scattering series(ISS) agrees with that conclusion.

However, in the absence of subsurface information the inverse scattering series assumes another attitude and sits on a higher superseding perch, and states that achieving goals that with subsurface information operate on an isolated event, now require a collective interaction of events in your data, with the use of both the amplitude and time of those events to achieve progressing objectives. The amplitude of the event means the amplitude of what you record when the event arrives in your phone, removing only the source signature in water.

Please note that it is definitely not requiring reflection coefficient amplitude or anything like a reflection coefficient amplitude associated with primary events. That collective amplitude and phase information is what the inverse scattering free surface multiple removal method requires, and all other seismic objectives that derive from the inverse scattering series operate in that same manner. The success of the inverse scattering free surface multiple removal algorithm, (e.g., SRME) speaks to that event phase and amplitude information being directly or indirectly achievable in practice, and that is the one and the same source signature needed for all ISS applications for removing free surface and internal multiples (F. A. Araujo et al, A. C. Ramirez et al), direct Q compensating primaries without knowing or determining Q (Kris Innanen and Jose Eduardo Lira et al), and depth imaging primaries, (S. Shaw, D. Foster, K. Matson, F. Liu, K. Innanen, J. Zhang, A. Ramirez, S. Jiang and Z. Wang et al) and non-linear direct AVO (H. Zhang and Xu Li).

Progress for these projects is described in this Annual Report and will be presented at the Annual Meeting.

It is worth noting that the free surface multiple removal algorithm doesnt change i.e., the code doesnt change in any way, not a slightest change in even one single line, if you happen to decide the earth is acoustic, elastic, anisotropic or anelastic. The method does not care about subsurface

properties, and it doesnt even care about the type of earth model you imagine is governing subsurface wave propagation in the real earth. That is what we mean when we say an algorithm is model-type independent and that is a truly amazing property, already shared by the inverse scattering free surface and internal multiple removal codes pioneered by P. M. Carvalho, F. V. Araujo, and A. C. Ramirez, and coded and documented by S. Kaplan, E. Otnes, A. C. Ramirez and K. A. Innanen and distributed in M-OSRP. The 3D free surface code is being tested and evaluated by Innanen, and Kaplan, and a team at ConocoPhillips led by Simon Shaw and Paul Valasek prior to distribution to our sponsors (please see the status report by Innanen et al).

Now please try to imagine an accurate depth imaging algorithm with that shared property. Thats what we are after, and thats one of our goals. We have come part way towards that prize and the first 3D field data tests with Fang Liu's closed form imaging algorithm are planned, separately with Scott Morton at Hess (with data jointly owned by Hess, BHP and Repsol) and Doug Foster and Fernanda Araujo at ConocoPhillips. These 3D field data imaging tests are scheduled to begin this summer. We are enormously grateful and appreciative for this invaluable sponsor support on progressing the testing and distribution of the 3D Free Surface Multiple code and the 3D imaging algorithms. Those test results will be shared with all sponsors, and will be included in a technical note and subsequent code distribution.

3D CLOSED FORM IMAGING PLUS NEW AND FURTHER AND EXCLUSIVELY MULTI-DIMENSIONAL IMAGING CAPTURE

In this report and in our presentations: (1) Fang Liu will present his three D closed form imaging algorithm, and separately his new and further capture beyond his latter closed form, now addressing distinct multi-dimensional imaging challenges that have no counterpart in a one dimensional earth, and (2) Shansong Jiang and A. B. Weglein will describe further developed concepts and algorithms to move the Fang Liu imaging capture to more complicated earth models and realism and towards model type independence. Early tests of Fang Liu's new and exclusively multi-D imaging capture will be shown at the Annual Meeting, May 28, 29.

Please note that Fang Liu's new imaging capture is no longer computer time free, and M-OSRP will be requiring and arranging for significantly increased compute power, with much appreciated assistance and support from Tom McClure, Michael Perrone and Earl Dodd of IBM, and Nicola Bienati and the M-OSRP HPC Committee. The anticipated M-OSRP research need for a bigger boat (computer) for our imaging research has definitely arrived. A set of tests for the new imaging capture is planned for the coming year.

This inverse scattering series can be counterintuitive, in general, and is especially so for depth imaging without the velocity. It runs opposite to conventional established wisdom and the entire evolution of seismic imaging, where increased capability and completeness in the imaging method and migration algorithm always had an immediate and concomitant increase in the demand for more accurate velocity information. In addition to the need for adequate subsurface information, such as velocity, required with all current leading-edge depth imaging algorithms, there are also additional innate assumptions and limitations for current imaging methods themselves, given perfect velocity information, that the inverse scattering series also has the potential to address.

DOES SCATTERING THEORY EVER AGREE WITH ANYONE OR ANYTHING THAT IS REASONABLE, INTUITIVE AND THAT WE ALREADY FIRMLY UNDERSTAND, BELIEVE AND CAN RIGOROUSLY PROVE AND KNOW TO BE ABSOLUTELY TRUE?

Scattering theory agrees with all modeling methods. It agrees that a precise description of each and every detail of all subsurface physical properties is essential and unavoidable to generate a wave-field inside and on the boundary of any medium, and that precise information is needed to create and predict primaries and multiples.

Linear approximate forward scattering and linear approximate inverse scattering, called the Born and inverse Born approximation, respectively, each assume that to approximately model data, or to approximately invert data, requires an adequate estimate of medium properties, as well. It also typically assumes the input data consists of only primaries. This latter linear approximate concept is behind all current migration and migration-inversion methods, regardless of their wave or asymptotic nature, and underpins the industry common wisdom and dogma that to determine depth requires an adequate estimate of velocity. That need today can be either direct or indirect through a proxy or other indirect expression of that need. It is somewhat disingenuous for methods that seek a proxy or assumed aligned objective to an input velocity model, and hence in principle need a velocity, to label themselves as velocity independent depth imaging. The approximate linear inverse scattering framework behind current imaging methods also explains the common view that migration and modeling are the flip sides of the same coin, and hence share the same requirements. Furthermore, if you go further in the forward scattering series to more accurately model data, you still need the exact subsurface properties to precisely predict primaries and multiples.

The refrain, din and chorus on the need for subsurface information to directly achieve seismic processing objectives comes up against a totally new and alternate viewpoint and compelling mathematical physics logic only when moving beyond a truncated approximate first term inverse scattering theory, or an iterative linear inverse of that first term, and when we examine and understand the entirety of the inverse scattering series, and specifically the message contained in the terms beyond the first and linear term. The input data can be primaries and all free surface and internal multiples and the unique and delivered message is that all processing objectives concerned with removing multiples, and for primaries , Q compensating, depth imaging and inversion can be achieved directly in terms of data and without actual physical properties that govern wave propagation in the subsurface being required or needed or predicted in principle and practice. We emphasize the words ‘in principle’ as a key and critical message. The need for a velocity model to directly and accurately depth image seismic data from the ISS is non-existent. The ISS imaging methods are direct and no optimization, search algorithms , or proxies, or stacking over weighted trajectories or flat common image gather criteria are ever called upon or needed. Direct, period.

The inverse scattering series has this unique message, and that is not a message shared with any other current processing methodology including all other non-linear methods such as : iterative linear inversion, model-matching, Bremmer series, and the feedback loop techniques. It represents and remains the unique promise and potential of the inverse scattering series.

DIRECT AND INDIRECT INVERSION: THE FUNDAMENTAL NEED FOR MULTI-COMPONENT ACQUISTION FOR TARGET IDENTIFICATION

The idea behind indirect methods begins by assuming that you have no direct way or path to solve a problem of interest. Therefore we will find an indirect aligned problem whose solution will eventually end up equivalent to a direct approach. This is not a bad idea, and there are times when it might be appropriate and necessary. For example, in Carvalho and Weglein (1994) there was a global search simulated annealing method to minimize energy for the purpose of estimating a wavelet, not readily available by other means, and necessary for the inverse scattering free surface multiple removal algorithm.

However, there are dangers in model matching or other indirect optimization approaches. There is great danger that the aligned objective is not really aligned, or adequate or accurate or sufficient. There are also a group of techniques around generalized inverse methods that have the sense of a method looking for a problem, or of the child with a hammer thinking that everything looks like a nail. The danger and problem is when searching and jumping around error surfaces and using search engine computational techniques becomes a push-button reflexive replacement for thinking and the fundamental physics of wave forward and inverse processes. The danger is often greatest when the application seems to be most 'reasonable'. To illustrate: consider PP data and non-linear AVO. Given PP data at a sufficient set of angles, it would seem reasonable to solve for linear estimates of changes in physical properties, and perhaps iteratively update. Or one might think of setting the Rpp equal to an exact Zoeppritz form in terms of those changes in earth properties, and perform a global search of values of those latter changes that would match the reflection data. What could be wrong?

The direct inversion of the elastic inverse scattering series, see e.g., the K. Matson and H. Zhang theses, communicates that PP data is fundamentally and intrinsically inadequate to achieve the above stated goal. PP data alone is as inadequate to achieve that goal from a fundamental and elementary physics point of view, as a single stacked trace can simultaneously and reliably invert for velocity and density as a function of depth. You could certainly search around and iteratively linear inverse, and find sensitivity matrices and optimize for a match. The searching and matching and iterating with PP data will never tell you have the wrong framework and starting point. The fundamental and clear meaning of an approximation linear in the data, needs to begin with clarity on what data you are talking about. The data needs to first be adequate to determine the actual sought after material property changes, and only a direct method can provide and communicate that data need. The directness of the elastic target identification solution provided only by the inverse scattering series, not only gives explicit direct forms to output those subsurface material properties, but perhaps as important tells you for the first time and unambiguously and precisely what data types will be needed to satisfy the need of the direct solution. That is what direct inverse provides. It takes a non-linear direct solution to define the very meaning of linear inverse.

A TERM IN THE SERIES ACTS ONLY AFTER IT DETERMINES THAT ITS SERVICE IS NEEDED AND CALLED UPON BY THE SPECIFIC DATA SET

There are other amazing and for me very impressive qualities that the inverse scattering series possesses, among them the ability to determine for a given data set whether a certain issue is present and will need to be addressed. The first term in a task specific subseries decides before it acts whether there is a need, and if there is no need it shuts down, and signals to those higher terms within that task specific subseries that they can relax and that this specific data set doesnt have that type of problem. On the other hand, if the first term in a task specific subseries determines that the data contains a certain issue, then it lights up, and alerts all of those beyond the first that their services will be called upon. That is amazing. We explicate and illustrate the latter property in our reports, SEG Abstracts and papers and in presentations at the meeting. The intelligence and data specific purposefulness, and certain model type independent goals and algorithms, all derives from the explicit inverse scattering series, and how it represents the not so simple way that changes in earth properties relate to changes in a wave-field.

FURTHER IMPORTANT ITEMS TO NOTE

Among other themes that are within this report and will be presented at our Annual Meeting are:

1. There is a difference between recognizing a specific potential and promise within the ISS and harvesting and capturing that potential.

2. Complex is complex, and imaging beneath a complex overburden and/or at a complex target is and remains that, complex. The ISS says it can replace the conventional simple imaging formula with a required complex ingredient (adequate complex overburden) with a complex sum with a simple ingredient (homogeneous overburden). The relevant question is achievability and effectiveness and impact. Closed forms for ISS imaging to-date provide much value and run at lightning speed, newer capture will need compute power.

3. The deterministic direct methods that we pursue have limits and requirements, and there is always reality beyond what we include in our physics, and the latter cannot be ignored if you are seeking practical solutions. Indirect methods are often employed in an attempt to accommodate the reality that is outside of our current physics model (e.g., cable feathering, instrument response, rough seas, ambient noise, and on-shore near surface variability), and we continue to progress that critical aspect of capability (e.g., recent Geophysics paper by Kaplan and Innanen). We encourage new criteria for adaptive methods that enhance and complement (rather than sometimes running at cross-purposes to) the deterministic methods they are meant to support.

4. We risk-manage our portfolio of objectives and manage expectations, e.g., our depth image will produce an accurate structure map, but not for migration-inversion at this juncture, and we progress and aim our non-linear direct AVO for development application. We provide an

umbrella to protect and nurture newer projects and ideas, e.g., the embryonic Q compensation without Q research, with a set of other projects that allow for different schedules of reporting and deliverables.

5. We warmly congratulate Drs. Adriana C. Ramirez and Jingfeng Zhang for completing their PhDs this past year, and wish them all the best of success in their careers at WesternGeco/Schlumberger and BP, respectively. They will present summaries of their important landmark contributions at the Annual Meeting.

6. The inverse scattering series does not provide methods to satisfy its own deterministic prerequisites, and requirements, such as deghosted data, a source signature, and adequate surface measurements. Green's theorem comes to the rescue, and Jingfeng Zhang and Adriana Ramirez will speak on those issues and their pioneering developments. A report is included here by Adriana C. Ramirez et al that provides a way to understand interferometric principles and theorems and virtual sources, and spurious multiples as all contained and derivable approximations or consequences within the Green's theorem (1828) framework. That Greens theorem framework also allows Ramirez to pursue and provide a systematic set of improvements that are compared with various interferometric algorithms for data extrapolation.

In summary: This has been another good and exciting year with much progress to report. We will be introducing our new, capable and energized group of graduate students to you, at the Annual Meeting, and they will each say a few words on the research projects they are pursuing. I look forward to seeing you at the Annual Technical Meeting.

Thanks for your encouragement and support.

Best regards,
Art

Arthur B. Weglein

Green's theorem as a comprehensive framework for seismic interferometry, data reconstruction and regularization, redatuming, wavefield separation and wavelet estimation

A. C. Ramírez[†]and A. B. Weglein
[†]Presently at WesternGeco

Abstract

It would be almost impossible to write a tutorial on Green's theorem (Green, 1828) that includes all its different applications in seismic exploration. Almost every single step in the set of methods and processing technology used in exploration seismology to process and obtain information from recorded data has been affected or influenced by Green's theorem whether or not it is explicitly acknowledged. Among the list of seismic processes that can be related to Green's theorem it is easy to find wavelet estimation, wavefield separation, multiple elimination, wavefield reconstruction, regularization, redatuming, imaging, wavefield deconvolution, deghosting, and interferometry. This tutorial aims to provide an overview of a set of Green's theorem based methods for addressing challenges in seismic exploration. In particular, the tutorial will focus on wavefield retrieval, using measurements at a given surface in a marine experiment. Wavefield reconstruction, interpolation and extrapolation methods based on Green's theorem are remarkable in their flexibility and ability of providing added value such as statics correction, regularization, wavefield separation and multiple removal. In the last decade, there have been an ever increasing attention within the energy industry and its concomitant representation in the published literature to methods dealing with wavefield retrieval through interferometry or virtual source techniques and their applications to different seismic exploration problems. This attention has brought about a renewed interest in Green's theorem because all the different approaches to what is called seismic interferometry (*e.g.*,techniques that synthesize the field propagating between two receivers by correlating the signals recorded at these two receivers) can be derived from this single theorem and unifying framework. In this tutorial, a derivation and explication of the limitations of interferometric techniques, as approximations to Green's theorem, will be provided. A definitive statement of the comprehensive framework and umbrella that Green's theorem provides to interferometry will be given, showing that the latter new *principles* are really directly understandable as simple approximations to Green's theorem. The artifacts and errors produced by these approximations will also be explained, and methods to improve upon the output of interferometry will be provided. The latter methods recognize their foundation on Green's theorem, and, thus, have a secure and firm mathematical-physics cornerstone to generate and recognize the assumptions behind distinct approximate solutions, and to guide the search for every more accurate and effective techniques

Introduction

Several of the subjects which concern the broad field of seismic exploration can be, and have been, solved by the application of Green's theorem using appropriate assumptions and specific functions such as Green's functions and measured values of pressure and/or elastic wavefields. Applications of Green's theorem,*i.e.*, Green's first and second identities, are known by many names: reciprocity

theorem, Kirchhoff integral, Helmholtz-Kirchhoff integral, etc. Extensions of the theorem are recognized as *e.g.,* Betti's and Rayleigh-Betti's reciprocity theorems. With all these names, confusion of the human being behind this great mathematical breakthrough is easily achieved. Geophysicist might be interested on knowing that these tools are the work of a self-taught mathematical genius with a premature death: George Green, the miller of Nottingham (Schwinger, 1993). As in many other scientific fields, seismic exploration utilizes the work of Green widely and plentiful. However, there are very few specific or direct references to George Green and his landmark work: *An Essay on the Applications of Mathematical Analysis to the Theory of Electricity and Magnetism* published by subscription in 1828. In this tutorial, we would like to acknowledge some of Green's contributions to seismic exploration, and, hence, to the betterment of our daily lives.

Green's theorem is one of the many jewels found in Green's original essay. Green's theorem provides a way of thinking, and a mathematical-physics framework that transcends the sum total of all the specific applications of that theorem to-date. To begin we state that a complete history of Green's theorem, and its immense scientific and technical contribution is far beyond the scope and purpose of this paper. This tutorial will merely focus on a few general themes and contributions within that very broad topic of Green's theorem. The selected contributions directly relate to the parochial interests of this tutorial: wavefield reconstruction or retrieval and interferometry.

In the next section Green's theorem will be introduced, and an overview of the impact of Green's theorem on seismic exploration will be provided.

Waves, and the information they contain: The Isaac Newton, Karl F. Gauss and George Green legacy for understanding and progressing seismic interferometry and wavefield retrieval

Seismic waves are widely used to study the Earth's structure and material properties by means of measurements on, or close to, its surface. Seismic waves can be produced through seismic experiments in which a source, such as a dynamite shot, generates acoustic or elastic vibrations that travel into the Earth, propagate through the subsurface and return to the surface to be recorded or acquired as seismic data. The goal of seismic exploration is to locate hydrocarbon (oil and gas) reservoirs in the Earth's subsurface in economically producible quantities. Hence, seismic exploration makes inferences from surface recorded wavefield measurements that are relevant and useful for locating and producing hydrocarbons.

The wavefield character at any point in space and at any instant of time, is determined by the entirety of experiences it has undergone, from the moment it was created at the source, until the time it is recorded. The wavefield due to a localized source is measured during a predefined length of time. During that period of time, there is a specific extent of the subsurface properties that contribute to the wave character measured at the receivers. The part of the subsurface that was experienced by the recorded part of the wavefield is restricted to a volume in space determined by how far in the subsurface the wave could reach, get reflected, and return to be recorded at the measurement surface during that time length; the volume in space is also governed by the Earth's subsurface properties and by causality. In the temporal frequency domain, the properties of the recorded wavefield depend on all subsurface properties.

Given that the seismic exploration/processing purpose is to extract subsurface properties from recorded data, it is natural to examine and to develop methods that relate surface recorded measurements to subsurface properties. There are three central purposes in this tutorial:
(1) Provide some sense of the breadth and scope of Green's theorem for addressing type of undertaking.
(2) Show how Green's theorem provides not only a comprehensive framework for all seismic interferometry techniques, but also a platform for developing a systematic set of improvements upon current methods and practice.
(3) Show how Green's theorem can be used to perform tasks of wavefield retrieval and wavefield separation.

Green's theorem is a critically important cornerstone for seismic theory, concepts and algorithms with a distinct contribution that supersedes the abilities of causality and linear superposition. It can match and go beyond the limits of causality and superposition constructs in wavefield theory. It is an integral formulation. Hence, it relates to integral equations, which incorporate the differential equation governing wave propagation with *any and all* necessary boundary and initial conditions. In contrast to a differential equation, the integral formulation includes all specifics that prescribe the actual particular physical experiment and realization.

Wavefields care about all the medium properties the wave has experienced. Linear superposition and causality provide a solution in all space and time. Linear superposition and causality are sufficient when all sources and medium properties are explicitly known, and included in their formulation. If the objective is to reconstruct the wavefield in a restricted region of space and time, Green's theorem provides a solution that calls for explicit inclusion of medium's properties and source's characteristics within that restricted portion of space and time, and an implicit but precise inclusion of medium and source influences outside that space region and interval of time, through boundary contributions in space and time.

Among the plethora of Green's theorem contributions, we provide a short list from seismic applications: (1) It can separate wavefields due to sources on different sides of a boundary, *i.e.*, the extinction theorem. (2) It can predict wavefields explicitly from surface measurements; a basic ingredient in wave theory migration and tomography. (3) It provides a fully quantitative and complete description of Huygens principle, and predicts and includes the famous obliquity factor. (4) It is a method for determining the source signature and radiation pattern. (5) It provides a way to remove ghosts, and free-surface multiples.

Green's theorem is an integral method. When discussing integral methods, it is useful to begin with Isaac Newton's fundamental theorem of the integral calculus, which relates something summed over an interval to something else evaluated at the endpoints of the interval. The fundamental theorem of integral calculus provides the foundation for solving a problem within a bounded region when the boundary is known: if $f'(x)$ is continuous on the closed interval $[a, b]$ and $f(x)$ is the antiderivative of $f'(x)$ (*i.e.*, $f'(x) = \dfrac{df(x)}{dx}$) on $[a, b]$, then

$$\int_a^b f'(x)dx = f(x)|_a^b. \tag{1}$$

This important result connects the purely algebraic indefinite integral with the analytic (or geometric) definite integral; the area under the curve $f'(x)$ within a region $[a, b]$ is analogous to evaluating the function $f(x)$ at the endpoints, $f(x)|_a^b$. The multidimensional extension of this theorem is found in the divergence or Gauss's theorem: Given a vector $\boldsymbol{A}$, which is continuous at the surface S and whose divergence is integrable,

$$\int_V \boldsymbol{\nabla} \cdot \boldsymbol{A} \; d\boldsymbol{x} = \oint_S \boldsymbol{A} \cdot \boldsymbol{n} \; d\boldsymbol{S} \tag{2}$$

is obtained, where $\boldsymbol{x}$ is a three dimensional vector (x_1, x_2, x_3) characterizing the volume V enclosed by the surface S, and $\boldsymbol{n}$ is the unit vector normal to this surface. The integral of the divergence of $\boldsymbol{A}$ over the whole volume contained by S is equivalent to the normal outflow integral of this vector (Morse and Feshbach, 1953). Letting $\boldsymbol{A} = u\boldsymbol{\nabla}\nu - \nu\boldsymbol{\nabla}u$, Green's theorem or Green's second identity is obtained (Green, 1828),

$$\int_V [u\nabla^2\nu - \nu\nabla^2 u] d\boldsymbol{x} = \oint_S [u\boldsymbol{\nabla}\nu - \nu\boldsymbol{\nabla}u] \cdot \boldsymbol{n} d\boldsymbol{s}. \tag{3}$$

This result provides a mathematical tool to evaluate a volume integral of the the quantity $[u\nabla^2\nu - \nu\nabla^2 u]$ using only boundary values at the surface of integration given by the normal component of the vector $[u\boldsymbol{\nabla}\nu - \nu\boldsymbol{\nabla}u]$. This elegant mathematical identity is simple and powerful. It can be used with any pair of scalar functions that have normal derivatives at the surface S and Laplacians in V, hence, resulting in an unconstrained amount of possible combinations and applications.

Thus, it is possible to think of Green's theorem as a generalization of Gauss's theorem[1], and the latter as a generalization of the fundamental theorem of integral calculus, which provides a foundation to solving problems within a limited region or interval. All of these theorems[2] provide a cumulative effect or sum of what is inside to something else summed on the boundary.

When Green's theorem is applied to seismic waves, what happens is that two wavefields are considered at once, one being the actual wavefield of interest and the other chosen entirely for convenience, called the auxiliary wavefield, and chosen entirely to achieve a specific purpose or objective. The auxiliary wavefield is totally a mathematical entity, it may or may not have any relationship with the physics of the actual problem. For example, if the conveniently chosen auxiliary wavefield has a localized Dirac delta function as its source, then the interplay between the actual wavefield and the auxiliary wavefield will sift the integral over the volume, and rather than producing a sum, it will produce the value of the actual wavefield at a point within the volume (*i.e.*, at the center of the Dirac delta function). A different example is when the actual wavefield is the marine wavefield and contains free-surface multiples and ghosts, and the auxiliary wave field is the wavefield without free-surface associated events. Green's theorem then provides an integral equation whose solution represents free surface multiple removal; see for example, Fokkema and van den Berg (1993).

In the case of Green's theorem applied to source signature estimation, one field is the actual entire wavefield and the auxiliary is the causal Green's function for a half space of water. In migration,

[1]However, it most be noted that George Green formulated and published his theorem more than ten years ahead of Johann Carl Friedrich Gauss (Kline, 1974).

[2]Stoke's theorem also obeys this explanation.

one wavefield is the actual scattered wavefield (reflection data) and the auxiliary is the anticausal Green's function assumed to govern propagation in the region above the sought after reflector target. These few examples are in fact a small sampling of choices of auxiliary wavefields for different Green's theorem applications.

Now we are in a position to introduce the specific forms of Green's theorem that are relevant for the objectives in this tutorial.

Using Green's theorem in seismic exploration

The objective of this tutorial is to study and analyze some specific applications of Green's theorem to seismic exploration. For those different applications, there will be different choices of the volume and functions u and ν introduced to satisfy equation 3. These different choices are the foundation for applications dealing with

- data reconstruction (including regularization and redatuming),
- seismic interferometry and virtual source method,
- wavefield separation,
- wavelet estimation, and
- wavefield deconvolution.

(This list of applications is not intended to be complete.) These applications are connected by the same framework and their differences rely on the specific functions and boundary conditions imposed upon Green's theorem as well as the approximations that some of these applications make to avoid certain requirements of the theory. Throughout this tutorial, the first function in equation 3, u, will be selected to be the pressure field P corresponding to recorded values of the pressure field in a marine seismic experiment. The second function ν will be selected depending on the application that will be derived.

In the section concerning seismic interferometry, a form of wavefield retrieval, an anticausal Green's function satisfying the same Helmholtz operator as the pressure field is selected as the second function, ν, in equation 3 (see for example Weaver and Lobkis (2004); Wapenaar (2004); Korneev and Bakulin (2006); Wapenaar and Fokkema (2006) and references within). In a marine experiment, the pressure field satisfies the Helmholtz operator for a medium consisting of a half space of air, the water column and the Earth's subsurface. Two points have to be considered:
First, to provide an analytic form of this Green's function, requires knowledge of the medium's properties (velocity, density, etc.) that produced the pressure field. In general, that medium is unknown. It is then not possible to solve for this anticausal Green's function, nevertheless it can be approximated by the conjugate of a second pressure field produced by the same medium but by a different source.
Second, this choice of functions in Green's theorem requires dual measurements (pressure data and

its normal derivative). Since the normal derivative of the pressure field is not always measured, approximations have to be introduced to seismic interferometry. The consequence is that the synthesized wavefield has errors, the so-called spurious events.

Next we consider another form of wavefield retrieval, using a reference Green's function[3] and Green's theorem to create a more effective seismic interferometry method (Ramírez et al., 2007). This is found by selecting the function ν as a causal or anticausal reference Green's function satisfying the Helmholtz operator for two homogeneous half spaces separated by a zero pressure surface (such as the air-water surface in a marine experiment)(Weglein and Secrest, 1990; Weglein and Devaney, 1992; Ramírez and Weglein, 2007). Both choices will provide algorithms to retrieve the wavefield within a specified volume, requiring measurements of the pressure field and its normal derivative at the volume's surface. We will show that a high frequency approximation of the pressure field's normal derivative is more forgiving when an anticausal reference Green's function is used in situations when two-way wavefield exist.

The choice of a causal reference Green's function as the second function ν in equation 3, will also provide an algorithm for wavelet estimation and for the scattered field that depends on dual measurements (Weglein and Secrest, 1990; Weglein and Devaney, 1992). A different choice for ν that removes the requirement of the wavefield's normal derivative is a Green's function that vanishes at two surfaces, which is going to be referred to as Dirichlet Green's function (Osen et al., 1998; Tan, 1999). The two surfaces where the Dirichlet boundary conditions are imposed are the air-water surface and the measurement surface in a marine experiment (see figure 1). This choice of functions in Green's theorem gives a formalism for wavelet estimation that does not require the wavefield's normal derivative. With this choice of functions, another form of wavefield retrieval is derived. The latter requires only measured pressure data and it can be applied to marine surface seismic acquisitions (Weglein et al., 2000; Ramírez et al., 2007).

The last application is wavefield deconvolution, a theory applied to the removal of overburden effects (overburden refers to the medium above the receiver or measurement plane), *e.g.* removal of free-surface multiples (events due to the existence of the air-water surface) and source effects (due to a source exploding above the location of interest). For this purpose, the function ν is selected to be a Green's function produced by the same medium as the pressure field, but without the existence of a zero-pressure boundary condition at the free surface (Amundsen, 1999, 2001; Holvik and Amundsen, 2005). The algorithm derived with this choice will remove all the free-surface multiples and the source wavelet from the pressure field, and it will retrieve the deconvolved wavefield at the receiver location (coincident source and receiver), effectively creating a source at the receiver location. An analogous method for wavefield deconvolution, which requires the source wavelet, was derived by Ziolkowski et al. (1998) and Johnston and Ziolkowski (1999). We will show that wavefield deconvolution is related to the virtual source method (which is an interferometry method and an approximation to Green's theorem).

[3]In marine applications, when a towed streamer or OBS acquisition is considered, the reference Green's function can be selected to satisfy a homogeneous medium with water velocity with or without a free surface. Therefore, in these situations, the reference Green's function is analogous to the source-wavelet deconvolved direct wave in the experiment. The direct wave in a VSP acquisition is not equal to the reference Green's function.

We are going to start this analysis with a selection of a pressure field and a causal Green's function as u and ν in equation 3. First we chose a causal reference Green's function to obtain the general Weglein and Secrest (1990) result; this form of Green's theorem is commonly referred to as the Kirchhoff-Helmholtz integral representation (Weglein and Devaney, 1992; Osen et al., 1994). This selection will also permit to obtain an equation to compute the scattered field within a volume with dual measurements at the surface. The results will be analyzed and the next choice of functions and applications will be introduced. Throughout this tutorial, the medium satisfied by the Green's function strictly inside the volume is going to be assumed to be equal to the medium satisfied by the pressure field within that same volume; the boundary conditions are not always going to be equal for both wavefields, the same flexibility will be considered for the medium outside the volume.

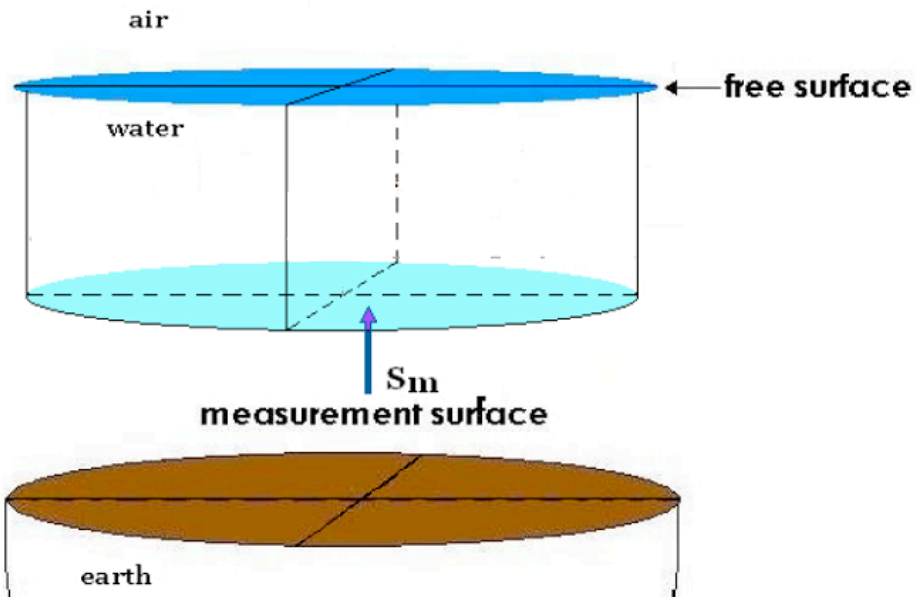

Figure 1: *Volume bounded by the free-surface and the measurement surface.*

Green's Theorem

The power of Green's theorem resides in the flexibility and arbitrariness and remaining valid independent of the choice of volumes, and evaluation points, and the interplay of the actual and fit for purpose chosen auxiliary function, and the auxiliary function boundary conditions.

In the following, Green's theorem is used to derive an integral representation of the pressure field P, which satisfies the inhomogeneous Helmholtz equation for a velocity distribution $c(\boldsymbol{x})$ and constant density

$$\left(\nabla^2 + \frac{\omega^2}{c^2(\boldsymbol{x})}\right) P(\boldsymbol{x}|\boldsymbol{x_a};\omega) = s(\boldsymbol{x},\omega), \tag{4}$$

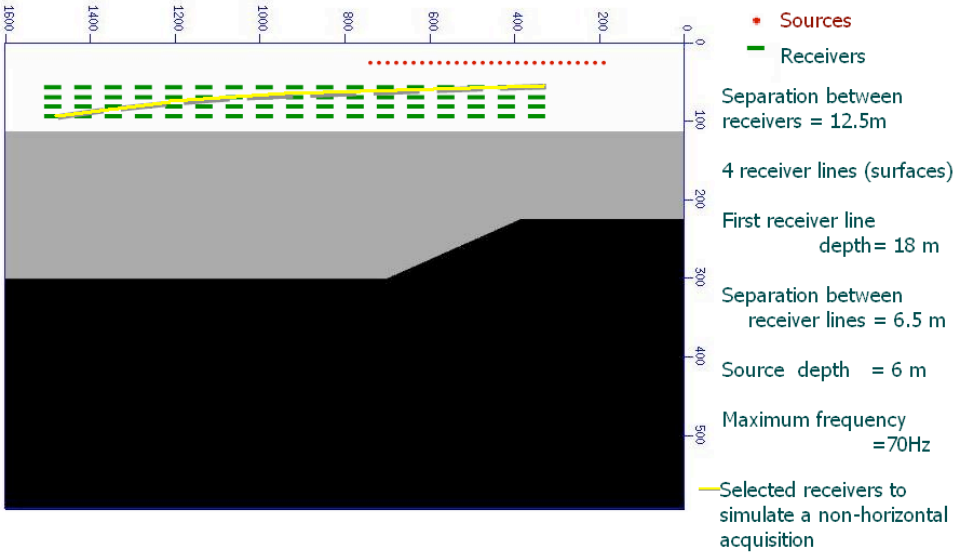

Figure 2: *2D Model.*

where $s(\boldsymbol{x},\omega)$ is the source function. For simplicity, the source $s(\boldsymbol{x},\omega)$ in equation 4 is selected to be

$$s(\boldsymbol{x},\omega) = A(\omega)\delta(\boldsymbol{x}-\boldsymbol{x_a}), \tag{5}$$

which represents an impulsive source at $x = x_a$ with signature $A(\omega)$, producing the pressure field $P(\boldsymbol{x}|\boldsymbol{x_a};\omega)$. The source representation as a convolution of an impulsive source and a wavelet or source signature is reasonable for seismic experiments, which are performed with localized and controlled sources.

The Green's function, or impulse response, for the Helmholtz operator satisfies

$$\left(\nabla^2 + \frac{\omega^2}{c^2(\boldsymbol{x})}\right) G(\boldsymbol{x}|\boldsymbol{x_b};\omega) = \delta(\boldsymbol{x}-\boldsymbol{x_b}), \tag{6}$$

where the impulsive source is centered at a position $\boldsymbol{x} = \boldsymbol{x_b}$ and the velocity distribution is given by $c(\boldsymbol{x})$. The solutions for equations 4 and 6 can be causal or anticausal with outgoing or ingoing boundary conditions, respectively. The causal and anticausal waves are denoted by a $+$ and a $-$ superscript, respectively. The pressure field is assumed to correspond to the measured data, hence, its physical or causal solution is the only one that will be considered. However, for the Green's function, different selections in terms of causality and boundary conditions will be made to derive the different applications of Green's theorem in seismic exploration presented in this tutorial.

Substituting the wavefield $P(\boldsymbol{x}|\boldsymbol{x_a};\omega)$ and the causal Green's function $G(\boldsymbol{x}|\boldsymbol{x_b};\omega)$ into Green's theorem, equation 3, as u and ν, and using equations 6 and 4 in the volume integral, gives

$$\int_V (P(\boldsymbol{x}|\boldsymbol{x_a};\omega)[-\frac{\omega^2}{c(\boldsymbol{x})^2}G(\boldsymbol{x}|\boldsymbol{x_b};\omega) + \delta(\boldsymbol{x}-\boldsymbol{x_b})]$$

$$-G(\boldsymbol{x}|\boldsymbol{x_b};\omega)[-\frac{\omega^2}{c(\boldsymbol{x})^2}P(\boldsymbol{x}|\boldsymbol{x_a};\omega)+A(\omega)\delta(\boldsymbol{x}-\boldsymbol{x_a})])d\boldsymbol{x}$$
$$=\oint_S[P(\boldsymbol{x}|\boldsymbol{x_a};\omega)\boldsymbol{\nabla}G(\boldsymbol{x}|\boldsymbol{x_b};\omega)-G(\boldsymbol{x}|\boldsymbol{x_b};\omega)\boldsymbol{\nabla}P(\boldsymbol{x}|\boldsymbol{x_a};\omega)]\cdot\boldsymbol{n}\ d\boldsymbol{s}, \tag{7}$$

which simplifies to

$$\int_V(P(\boldsymbol{x}|\boldsymbol{x_a};\omega)\delta(\boldsymbol{x}-\boldsymbol{x_b})-G(\boldsymbol{x}|\boldsymbol{x_b};\omega)A(\omega)\delta(\boldsymbol{x}-\boldsymbol{x_a}))\ d\boldsymbol{x}$$
$$=\oint_S[P(\boldsymbol{x}|\boldsymbol{x_a};\omega)\boldsymbol{\nabla}G(\boldsymbol{x}|\boldsymbol{x_b};\omega)-G(\boldsymbol{x}|\boldsymbol{x_b};\omega)\boldsymbol{\nabla}P(\boldsymbol{x}|\boldsymbol{x_a};\omega)]\cdot\boldsymbol{n}\ d\boldsymbol{s}. \tag{8}$$

This solution is the most general form of Green's theorem that will be encountered in this tutorial.

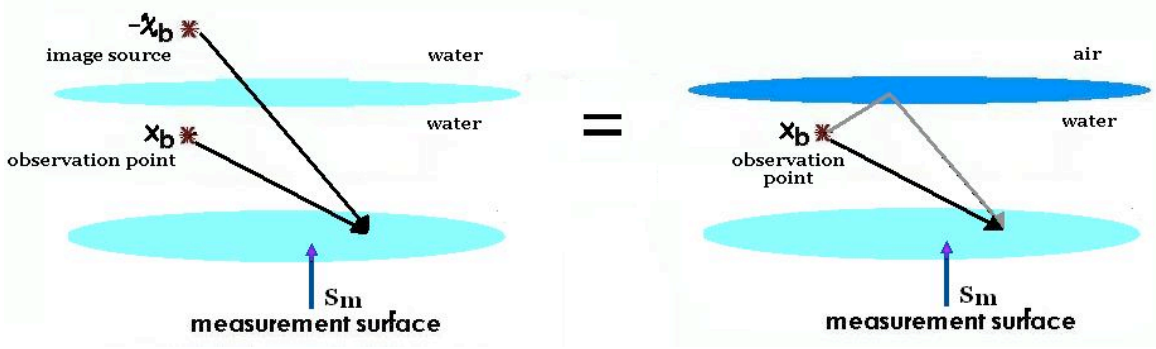

Figure 3: *Green's function for an experiment with a free surface. On the left hand side, the method of images is illustrated. The right hand side shows the actual reference Green's function for a source and receiver below the zero pressure surface.*

Green's Theorem with a causal Green's function

In this section, two seismic applications using Green's theorem will be derived: wavelet estimation, and wavefield retrieval. Both methods are applied to a marine seismic experiment. An analysis and discussion of the results will be performed at the end of the section. This analysis will serve as motivation for the applications of Green's theorem discussed and derived in section .

If the Green's function, G, in equation 8 is selected to be a causal Green's function, G^+, we obtain

$$\int_V\left(P(\boldsymbol{x}|\boldsymbol{x_a};\omega)\delta(\boldsymbol{x}-\boldsymbol{x_b})-G^+(\boldsymbol{x}|\boldsymbol{x_b};\omega)A(\omega)\delta(\boldsymbol{x}-\boldsymbol{x_a})\right)\ d\boldsymbol{x}$$
$$=\oint_S[P(\boldsymbol{x}|\boldsymbol{x_a};\omega)\boldsymbol{\nabla}G^+(\boldsymbol{x}|\boldsymbol{x_b};\omega)-G^+(\boldsymbol{x}|\boldsymbol{x_b};\omega)\boldsymbol{\nabla}P(\boldsymbol{x}|\boldsymbol{x_a};\omega)]\cdot\boldsymbol{n}\ d\boldsymbol{s}, \tag{9}$$

which corresponds to the Kirchhoff-Helmholtz integral representation (see, e.g., Morse and Feshbach (1953); Weglein and Secrest (1990); Weglein and Devaney (1992)).

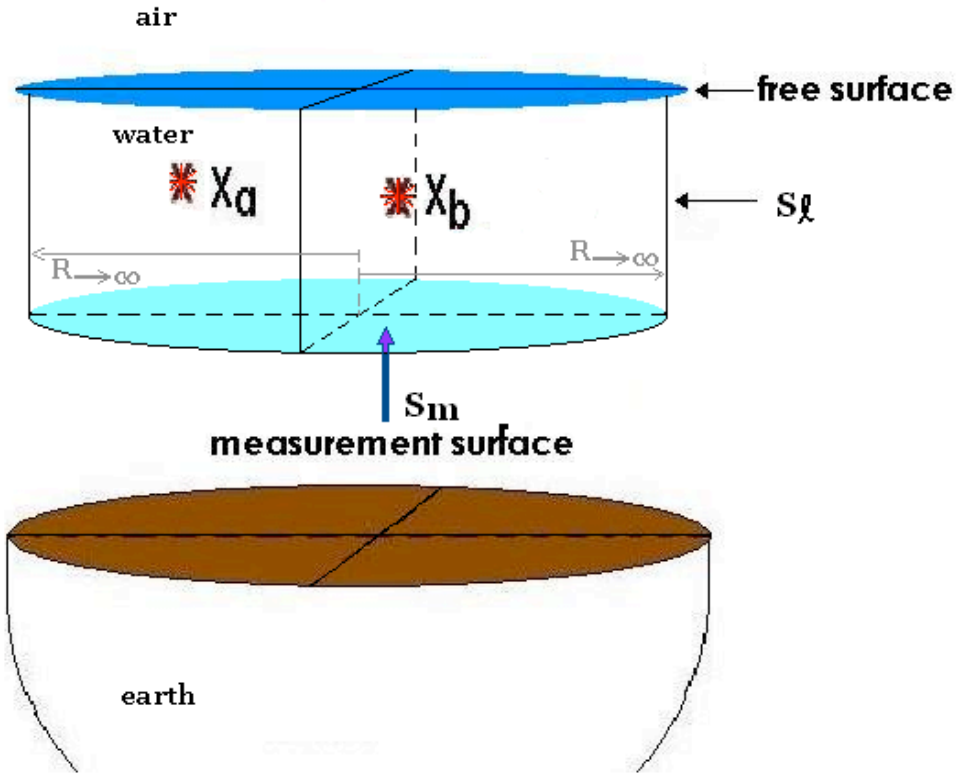

Figure 4: *The cylindrical volume shown is bounded by the free surface and the measurement surface. The lateral surface of the cylinder is assumed to be at infinity.*

1^{st} Scenario: The medium parameters for both fields are equal everywhere

Probably the simplest case that can be considered is the one in which the Green's function is the impulse response for the same Helmholtz operator as the measured pressure field everywhere. If the medium parameters, $c(\boldsymbol{x})$, for the pressure field (satisfying equation 4) and the reference Green's function (satisfying equation 6) are identical not only throughout the volume enclosed by S, but everywhere, then, the pressure field obeys the relation $P = A(\omega)G^{+}$. This relation helps analyzing the output of Green's theorem in equation 9 in the present scenario. The surface integral in Green's theorem requires the knowledge or measurement of the pressure field, the Green's function and their normal derivatives at the boundary.

The volume integral contains delta functions. Hence, the output of this integral depends on whether the source position, $\boldsymbol{x_a}$, and the observation point (the position of the Green's function's source), $\boldsymbol{x_b}$, are or not enclosed by the mathematical surface defined by S. Therefore, there exist three possibilities for the evaluation of the volume integral.

$$\int_V \left(P(\boldsymbol{x}|\boldsymbol{x_a};\omega)\ \delta(\boldsymbol{x}-\boldsymbol{x_b}) - G^{+}(\boldsymbol{x}|\boldsymbol{x_b};\omega)\ A(\omega)\ \delta(\boldsymbol{x}-\boldsymbol{x_a}) \right)\ d\boldsymbol{x}$$

$$= \begin{cases} P(\boldsymbol{x_a}|\boldsymbol{x_b};\omega) - A(\omega)G^+(\boldsymbol{x_a}|\boldsymbol{x_b};\omega) = 0 & \text{if both sources are strictly inside } S \\ P(\boldsymbol{x_a}|\boldsymbol{x_b};\omega) & \text{if only the observation point } \boldsymbol{x_b} \text{ lies within } V \\ -A(\omega)G^+(\boldsymbol{x_a}|\boldsymbol{x_b};\omega) = -P(\boldsymbol{x_a}|\boldsymbol{x_b};\omega) & \text{if only the source } \boldsymbol{x_a} \text{ lies within } V, \end{cases} \tag{10}$$

where the principle of source-receiver reciprocity has been used, and

$$\int_V \left(P(\boldsymbol{x}|\boldsymbol{x_a};\omega)\delta(\boldsymbol{x}-\boldsymbol{x_b}) - G^+(\boldsymbol{x}|\boldsymbol{x_b};\omega)A(\omega)\delta(\boldsymbol{x}-\boldsymbol{x_a})\right)\, d\boldsymbol{x}$$
$$= \oint_S [P(\boldsymbol{x}|\boldsymbol{x_a};\omega)\boldsymbol{\nabla}G^+(\boldsymbol{x}|\boldsymbol{x_b};\omega) - G^+(\boldsymbol{x}|\boldsymbol{x_b};\omega)\boldsymbol{\nabla}P(\boldsymbol{x}|\boldsymbol{x_a};\omega)] \cdot \boldsymbol{n}\, d\boldsymbol{s}. \tag{11}$$

When both sources lie within V (first case in equation 10) a functional relationship between P and its normal gradient on S is found,

$$0 = \oint_S [P(\boldsymbol{x}|\boldsymbol{x_a};\omega)\boldsymbol{\nabla}G^+(\boldsymbol{x}|\boldsymbol{x_b};\omega) - G^+(\boldsymbol{x}|\boldsymbol{x_b};\omega)\boldsymbol{\nabla}P(\boldsymbol{x}|\boldsymbol{x_a};\omega)] \cdot \boldsymbol{n}\, d\boldsymbol{s}, \tag{12}$$

meaning that the pressure field and its normal derivative cannot be prescribed independently (Amundsen, 1994; Visser et al., 1998). This functional relationship was used by Amundsen (1994) to develop an inverse wavefield extrapolation method that allows reconstruction of the wavefield within the subsurface to create a structural image by extrapolating the field from the measurement surface through each one of the different Earth layers and applying boundary conditions at each interface before continuing extrapolation through the next layer. The medium between the different interfaces must be known (a smoothly varying approximation of the medium can be used) and dual measurements of the pressure field are necessary. In general, imaging with Green's theorem requires knowledge of the medium. Therefore, its effectiveness depends on the accuracy of the Earth model used (in particular, is highly dependent on the quality of the velocity model). Another important example of inverse wavefield extrapolation (migration) using the framework of Green's theorem is given by the work of Schneider (1978), in which data containing primaries only and an anticausal Green's function are used.

Due to the fact that $P = A(\omega)G^+$, the output of Green's theorem when only one of the points $\boldsymbol{x_a}$ or $\boldsymbol{x_b}$ lie strictly within S, is roughly equivalent for either experiment. The results in the second and third case in equation 10 are equivalent within a (-1) factor indicating whether the observation point is inside or outside the volume. Both produce the physical pressure field for a medium with velocity $c(x)$ and constant density between two points, $\boldsymbol{x_a}$ and $\boldsymbol{x_b}$; one point being located anywhere inside the mathematical volume V and the other one outside. In these two cases, boundary conditions (*i.e.* measurements of the wavefields and their normal derivative at the closed surface S) produce the total wavefield for a source inside the volume enclosed by S and a receiver outside, as well as the reciprocal experiment.

Green's theorem for two functions, P and G^+, satisfying the same medium parameters everywhere results in a formalism for inverse wavefield extrapolation, or migration, which depends on the knowledge or ability to accurately estimate the subsurface properties. This form of the theorem also provides two reciprocal and analogous formulations to predict the wavefield produced by a source

lying within a closed surface, where dual measurements are available, and a receiver outside that volume. The Green's function required for this configuration is, in realistic situations, not available since the medium parameters (in this case $c(x)$) that created it are unknown. Furthermore, if regularizing data to a grid with coincident sources and receivers is the purpose of doing wavefield extrapolation, then, the results in this section can not be the method of choice. To create coincident sources and receivers, it is necessary to have both the source and observation point surrounded by the closed surface. The output of the surface integral in this scenario is zero (see first case). To overcome this situation, a possibility would be to select a Green's function that only satisfies the same medium as the pressure field within the volume and a different medium outside it.

2^{nd} Scenario: The medium parameters for both fields are only equal at the boundary S and within the volume V

When the medium parameters for the pressure field and the Green's function are equal only throughout V, the volume integral or left hand side of Green's theorem, with a causal Green's function for the medium within V, becomes

$$l.h.s. = \begin{cases} P(\boldsymbol{x_b}|\boldsymbol{x_a};\omega) - A(\omega)G^+(\boldsymbol{x_a}|\boldsymbol{x_b};\omega) & \text{if both sources are strictly inside } S \\ P(\boldsymbol{x_b}|\boldsymbol{x_a};\omega) & \text{if only the observation point } \boldsymbol{x_b} \text{ lies within } V \\ -A(\omega)G^+(\boldsymbol{x_a}|\boldsymbol{x_b};\omega) & \text{if only the source } \boldsymbol{x_a} \text{ lies within } V, \end{cases} \quad (13)$$

depending on the position of the source and observation point, and

$$l.h.s. = \oint_S [P(\boldsymbol{x}|\boldsymbol{x_a};\omega)\boldsymbol{\nabla}G^+(\boldsymbol{x}|\boldsymbol{x_b};\omega) - G^+(\boldsymbol{x}|\boldsymbol{x_b};\omega)\boldsymbol{\nabla}P(\boldsymbol{x}|\boldsymbol{x_a};\omega)] \cdot \boldsymbol{n}\, d\boldsymbol{s}. \quad (14)$$

The medium parameters for the Green's function and the pressure field are not equal everywhere, so $P \neq A(\omega)G^+$.

For a volume in which P and G^+ satisfy the same Helmholtz operator, the source for the pressure field lies outside the volume and the observation point lies inside (third case in equation 13), Green's theorem gives

$$-A(\omega)G^+(\boldsymbol{x_a}|\boldsymbol{x_b};\omega) = \oint_S [P(\boldsymbol{x}|\boldsymbol{x_a};\omega)\boldsymbol{\nabla}G^+(\boldsymbol{x}|\boldsymbol{x_b};\omega) - G^+(\boldsymbol{x}|\boldsymbol{x_b};\omega)\boldsymbol{\nabla}P(\boldsymbol{x}|\boldsymbol{x_a};\omega)] \cdot \boldsymbol{n}\, d\boldsymbol{s}. \quad (15)$$

The left hand side is the wavefield produced by all the sources inside V. The surface integral acts as a filter for the effects of the sources lying outside the volume. The wavefield $A(\omega)G^+(\boldsymbol{x_a}|\boldsymbol{x_b};\omega)$ is the reference wavefield, produced by all sources enclosed by S and propagating in a wholespace satisfying the medium parameters in V. Equation 15 can be used to estimate the source wavelet in a marine seismic experiment; it was first proposed and derived by Weglein and Secrest (1990) and Weglein and Devaney (1992).

For a marine application, a convenient volume within the water column bounded by the measurement surface and the air-water interface, or free surface, is considered (see figure 4). The medium parameter $c(x)$ in V is the constant water velocity c_0, or reference velocity. The pressure field and

the Green's function satisfy the Helmholtz equation for a medium with constant velocity, c_0, within the volume V, and share the same boundary condition at the free surface.

The Green's function is chosen to propagate in a homogeneous half space bounded by a free-surface S_0 at depth $z = 0$. In order to impose the Dirichlet boundary condition at $z = 0$, required by the free-surface, the Helmholtz equation is expressed using a real source at $\boldsymbol{x_b} = (x_{1b}, x_{2b}, x_{3b})$ and an image source with negative amplitude at $-\boldsymbol{\chi_b} = (x_{1b}, x_{2b}, -x_{3b})$ (see figure 3), where x_3 is the vertical direction and it is zero at the free surface. Thus,

$$\left(\nabla^2 + \frac{\omega^2}{c_0^2}\right) \mathcal{G}_0^+(\boldsymbol{x}|\boldsymbol{x_b};\omega) = \delta(\boldsymbol{x} - \boldsymbol{x_b}) - \delta(\boldsymbol{x} + \boldsymbol{\chi_b}) \tag{16}$$

is the Helmholtz equation.

The causal reference Green's function $\mathcal{G}_0^+$ includes the wave that propagates directly from the source at $\boldsymbol{x_b}$ to the receiver, $\mathcal{G}_0^{d+}$, and the wave that propagates directly from the image source at $-\boldsymbol{\chi_b}$ to the receiver, $\mathcal{G}_0^{d'+}$,

$$\mathcal{G}_0^+(\boldsymbol{x}|\boldsymbol{x_b};\omega) = \mathcal{G}_0^{d+}(\boldsymbol{x}|\boldsymbol{x_b};\omega) - \mathcal{G}_0^{d'+}(\boldsymbol{x}|-\boldsymbol{\chi_b};\omega). \tag{17}$$

In this experiment, both P and $\mathcal{G}_0^+$ vanish at the free-surface. Therefore, the upper boundary of V gives zero contribution to the integral. If the measurement surface extend towards infinity, only the measurement surface (S_m in figure 4) contributes to the surface integral, the lateral surface contribution, S_l, will vanish according to the Sommerfeld radiation condition (Sommerfeld, 1954). Selecting the actual source for the pressure field to be inside V, and the observation point, $\boldsymbol{x_b}$, outside the medium, below the measurement surface, equation 15 becomes

$$-A(\omega)\mathcal{G}_0^+(\boldsymbol{x_a}|\boldsymbol{x_b};\omega) = \int_{S_m} [P(\boldsymbol{x}|\boldsymbol{x_a};\omega)\boldsymbol{\nabla}\mathcal{G}_0^+(\boldsymbol{x}|\boldsymbol{x_b};\omega) - \mathcal{G}_0^+(\boldsymbol{x}|\boldsymbol{x_b};\omega)\boldsymbol{\nabla}P(\boldsymbol{x}|\boldsymbol{x_a};\omega)] \cdot \boldsymbol{n}\ d\boldsymbol{s}. \tag{18}$$

This equation reproduces the result first obtained by Weglein and Secrest (1990). Equation 18 is used to estimate the source wavelet in a marine experiment (the method has been extended to include a source array and to accommodate an experiment produced by an elastic Earth (Weglein and Secrest, 1990; Weglein and Devaney, 1992)). The surface integral effectively filters the scattered wavefield and produces the reference Green's function multiplied by the source wavelet, which, in this example, corresponds to the direct wave. This technique relies on dual measurements (pressure field and its normal derivative). Traditionally, the gradient of the pressure field has not always been available, representing a challenge and an impediment to take full advantage of this theory. In recent years, new acquisitions techniques with dual measurements have surfaced and the promise of this theory can be tested and used in practice.

Using the reference Green's function in equation 16 and allowing the observation point and the actual source to be inside the medium, a formalism for the prediction or reconstruction of the scattered field is obtained. It is given by the **first case** in the present section (equation 13),

$$P(\boldsymbol{x_b}|\boldsymbol{x_a};\omega) - A(\omega)\mathcal{G}_0^+(\boldsymbol{x_a}|\boldsymbol{x_b};\omega) = \int_{S_m} [P(\boldsymbol{x}|\boldsymbol{x_a};\omega)\boldsymbol{\nabla}\mathcal{G}_0^+(\boldsymbol{x}|\boldsymbol{x_b};\omega) - \mathcal{G}_0^+(\boldsymbol{x}|\boldsymbol{x_b};\omega)\boldsymbol{\nabla}P(\boldsymbol{x}|\boldsymbol{x_a};\omega)] \cdot \boldsymbol{n}\ d\boldsymbol{s}. \tag{19}$$

Using the principle of source-receiver reciprocity and the fact that the scattered field is the difference between the total pressure field and the direct wave or reference field, $P_s(\boldsymbol{x_a}|\boldsymbol{x_b};\omega) = P(\boldsymbol{x_a}|\boldsymbol{x_b};\omega) - A(\omega)\mathcal{G}_0^+(\boldsymbol{x_a}|\boldsymbol{x_b};\omega)$, results in

$$P_s(\boldsymbol{x_a}|\boldsymbol{x_b};\omega) = \int_{S_m} [P(\boldsymbol{x}|\boldsymbol{x_a};\omega)\boldsymbol{\nabla}\mathcal{G}_0^+(\boldsymbol{x}|\boldsymbol{x_b};\omega) - \mathcal{G}_0^+(\boldsymbol{x}|\boldsymbol{x_b};\omega)\boldsymbol{\nabla}P(\boldsymbol{x}|\boldsymbol{x_a};\omega)], \cdot\boldsymbol{n}\ d\boldsymbol{s}. \qquad (20)$$

This is an output with important practical implications for seismic exploration. It retrieves the total wavefield in new locations and removes the direct wave $A(\omega)\mathcal{G}_0^+(\boldsymbol{x_a}|\boldsymbol{x_b};\omega)$. The output is the scattered field.

With both sources inside the volume, the surface integral effectively filters the reference field and retrieves the scattered field between the sources (as if one source was a receiver: virtual receiver). The retrieved scattered field is the total wavefield due to all sources being outside the volume. This method was tested with $2D$ finite difference data modeled at Statoil Research Center. using the model shown in figure 2. The data was modeled for five receiver lines at increasing depths, starting at $11.5m$ with an increment of $6.5m$, the sources were located at $6m$ depth, the maximum frequency in the data is 70hz and the time interval between measurements is $0.004s$. The input data corresponds to receivers from the four deeper surfaces (yellow line in figure 2), an example of the input data is displayed in figure 5. The calculations were done with an analytic Green's function $\mathcal{G}_0^+$ computed for a source at $11.5m$ and the same receivers used in the input data. Hence, the reconstructed scattered field corresponds to a source at $6m$ and receivers at $11.5m$. An example of the reconstructed scattered field (near offsets in this example) is displayed in figure 6. Note that the reconstructed scattered field contains a small direct wave residual. According to the theory, the algorithm given by equation 20 must retrieve the scattered field and filter the direct wave. However, this theory assumes infinite aperture in space and time. When applied to data with limited aperture, the method effectively retrieves the scattered field, but the direct wave is not completely filtered. If the near offsets are provided, the screening of the direct wave can be improved.

The second case in equation 13, places the actual source outside and the observation point inside V. The result is the total wavefield between the source outside and the observation point inside V. Since there is no physical source within the volume, only the observation point, then the extrapolated wavefield is the total wavefield,

$$P(\boldsymbol{x_b}|\boldsymbol{x_a};\omega) = \int_{S_m} [P(\boldsymbol{x}|\boldsymbol{x_a};\omega)\boldsymbol{\nabla}\mathcal{G}_0^+(\boldsymbol{x}|\boldsymbol{x_b};\omega) - \mathcal{G}_0^+(\boldsymbol{x}|\boldsymbol{x_b};\omega)\boldsymbol{\nabla}P(\boldsymbol{x}|\boldsymbol{x_a};\omega)] \cdot \boldsymbol{n}\ d\boldsymbol{s}. \qquad (21)$$

Green's theorem retrieves the total wavefield due to all sources outside the volume. The first and second case are both good relations to retrieve the wavefield between two sources, where one source acts as a virtual receiver.

The filtering effect provided by the surface integral in this application of Green's theorem, is also known as extinction theorem. The application of the extinction theorem, will screen the scattered field if the observation point is outside V and the source inside (third case); it will screen the reference field for all actual sources inside the volume if the observation point lies inside V (second and third case).

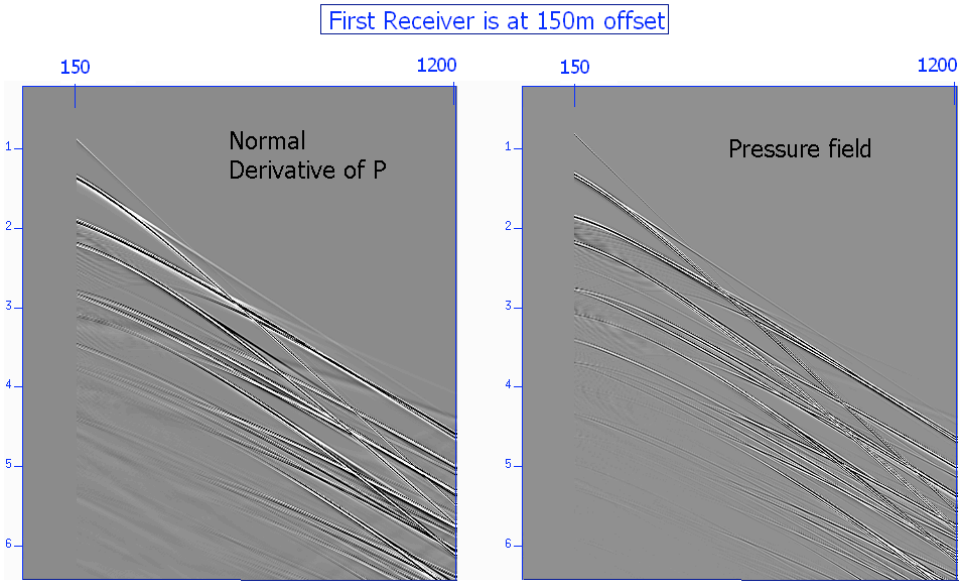

Figure 5: *Input data: pressure field (right) and its normal derivative (left). Near offsets from* $0-150m$ *are assumed not to be recorded.*

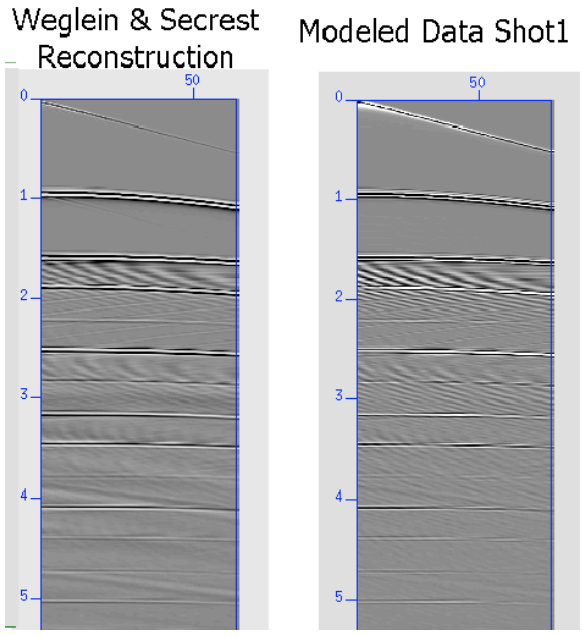

Figure 6: *Reconstructed scattered field compared with modeled data.*

Analysis

Using causal Green's functions, Green's theorem provides formalisms for wavelet estimation, seismic interferometry and inverse wavefield extrapolation. All of these applications require the availability

of the pressure field and its normal derivative. Within specific choices of Green's functions, the actual medium properties were also required.

In seismic exploration, probably the most desired method for seismic interferometry, or wavefield retrieval, is the one that considers both sources within the medium and that would allow for extrapolation to coincident source and receiver positions (in a regular grid). Therefore, Green's theorem, with a causal reference impulse response, as described by equation 20, seems to be the more convenient result. It can be readily applied to applications such as wavefield extrapolation, interpolation, and regularization in a surface seismic experiment. Green's theorem with a causal reference field provides a method to extrapolate data into a regular grid of coincident sources and receivers in a 3D experiment. The latter is performed by using an analytic Green's function $\mathcal{G}_0^+(\boldsymbol{x}|\boldsymbol{x_b};\omega)$ calculated for the actual receiver positions $\boldsymbol{x}$ and placing the observation point at the desired output locations within the volume enclosed by the receivers. With this choice of source and virtual receiver positions, the algorithm performs wavefield separation and outputs only the scattered part of the field (it outputs the unperturbed field when the observation point is outside V). It is an exact method. Accordingly, it requires measurements of the pressure field and its normal derivative at the surface.

For situations when the normal derivative is not measured and an estimate is not always available, approximations are often used. In the seismic interferometry derivation, Wapenaar (2004) proposed to use an asymptotic approximation to the pressure field's normal derivative,

$$\boldsymbol{\nabla} P(\boldsymbol{x}|\boldsymbol{x_a};\omega)] \cdot \boldsymbol{n} \approx ikP(\boldsymbol{x}|\boldsymbol{x_a};\omega), \tag{22}$$

where $k = \frac{\omega}{c_0}$. This is a very poor approximation for scenarios in which two-way wavefield exist, such as a marine experiment (the free-surface reflects all the upgoing wavefield). It is a high frequency and one-way wave approximation taken at a location where two-way waves exist. Asymptotic approximations, although often useful, are never equivalent to the original form. In appendix , we show that the approximation in equation 22, changes completely the output of the surface integral in the form of Green's theorem studied in this section. The output of the surface integral, with this approximation, becomes zero independent of the source and virtual receiver location relative to the surface of integration.

There are different ways of addressing this situation. The first, and more reliable one, is to provide all the ingredients required by Green's theorem by measuring the wavefield's normal derivative, or by measuring the pressure field at a second surface parallel to the measurement surface and calculating the gradient between the fields. The second solution is to find a better approximation for the normal component of the particle velocity, we refer the interested reader to Amundsen et al. (1995), Guo et al. (2005) and references within. A third solution is to use an anticausal Green's function in the calculations (Weaver and Lobkis, 2004; Wapenaar, 2004; Korneev and Bakulin, 2006; Draganov et al., 2006; Ramírez et al., 2007) and use approximations, as explained and discussed in the next section. Last, but not least, it is possible to use a different Green's function that annihilates the requirement of the wavefield's normal derivative, *i.e.* using a Green's function with Dirichlet boundary conditions at the free surface and at the measurement surface (Osen et al., 1998; Tan, 1999; Weglein et al., 2000; Zhang and Weglein, 2006; Ramírez et al., 2007). This is explained in section .

Green's theorem with an anticausal Green's function

In this section, anticausal solutions for the Helmholtz operator will be used to derive standard seismic interferometry and direct wave interferometry with crosscorrelations. An analysis and discussion of these applications will be provided at the end of the section. The limitations and errors of these forms of Green's theorem and interferometry applications, due to assumptions that will be explained, will serve as motivation for section .

The Helmholtz equation can have a causal solution or an anticausal solution. The anticausal Green's function, $G^-(\boldsymbol{x}|\boldsymbol{x_b};\omega)$, is the complex conjugate of the causal one, $G^+(\boldsymbol{x}|\boldsymbol{x_b};\omega)$, and $P^-(\boldsymbol{x}|\boldsymbol{x_b};\omega)$ is the complex conjugate of $P^+(\boldsymbol{x}|\boldsymbol{x_b};\omega)$. An anticausal pressure field is a non physical solution.

The anticausal Green's function is defined by

$$G^-(\boldsymbol{x}|\boldsymbol{x_b};\omega) = \int_{-\infty}^{\infty} e^{-i\omega t} G^+(\boldsymbol{x}|\boldsymbol{x_b};-t)dt. \tag{23}$$

Green's theorem applied to the pressure field and an anticausal Green's function, when both wavefields satisfy the same medium parameters within the mathematical volume, V, enclosed by the surface S, becomes

$$\begin{aligned}&\int_V \left(P(\boldsymbol{x}|\boldsymbol{x_a};\omega)\delta(\boldsymbol{x}-\boldsymbol{x_b}) - G^-(\boldsymbol{x}|\boldsymbol{x_b};\omega)A(\omega)\delta(\boldsymbol{x}-\boldsymbol{x_a})\right)\, d\boldsymbol{x}\\ &= \oint_S [P(\boldsymbol{x}|\boldsymbol{x_a};\omega)\boldsymbol{\nabla} G^-(\boldsymbol{x}|\boldsymbol{x_b};\omega) - G^-(\boldsymbol{x}|\boldsymbol{x_b};\omega)\boldsymbol{\nabla} P(\boldsymbol{x}|\boldsymbol{x_a};\omega)]\cdot \boldsymbol{n}\, d\boldsymbol{s}.\end{aligned} \tag{24}$$

In the next sections, we analyze the inner workings of this equation with different choices of Green's functions.

1^{st} Scenario: The medium parameters for both fields are equal everywhere

The medium parameters for the pressure field and the anticausal Green's function are chosen to be identical everywhere. Using the principle of source-receiver reciprocity, the pressure field, P, and the anticausal Green's function, G^-, in Green's theorem, the volume integral (left hand side of equation 24) becomes

$$l.h.s. = \begin{cases} 2i\Im[P(\boldsymbol{x_a}|\boldsymbol{x_b};\omega)] & \text{if both sources are strictly inside } S\\ P(\boldsymbol{x_b}|\boldsymbol{x_a};\omega) & \text{if only observation point } \boldsymbol{x_b} \text{ lies within } V\\ -P^-(\boldsymbol{x_a}|\boldsymbol{x_b};\omega) = -A(\omega)G^-(\boldsymbol{x_a}|\boldsymbol{x_b};\omega) & \text{if only the source at } \boldsymbol{x_a} \text{ lies within } V, \end{cases} \tag{25}$$

where $\Im[P]$ refers to the imaginary part of the pressure field, and

$$l.h.s. = \oint_S [P(\boldsymbol{x}|\boldsymbol{x_a};\omega)\boldsymbol{\nabla} G^-(\boldsymbol{x}|\boldsymbol{x_b};\omega) - G^-(\boldsymbol{x}|\boldsymbol{x_b};\omega)\boldsymbol{\nabla} P(\boldsymbol{x}|\boldsymbol{x_a};\omega)]\cdot \boldsymbol{n}\, d\boldsymbol{s}. \tag{26}$$

For application on marine data, a volume bounded by the free-surface and the measurement surface is selected. Since the medium for G^- is the same as the one that P satisfies everywhere, the measurement surface is not restricted to the water column.

The configuration leading to the result for the first case in 25 can be used to derive the traditional seismic interferometry equation. This configuration assumes that the physical source and the observation point lie within V. This equation,

$$2i\Im P(\boldsymbol{x_a}|\boldsymbol{x_b};\omega) = \oint_S [P(\boldsymbol{x}|\boldsymbol{x_a};\omega)\boldsymbol{\nabla} G^-(\boldsymbol{x}|\boldsymbol{x_b};\omega) - G^-(\boldsymbol{x}|\boldsymbol{x_b};\omega)\boldsymbol{\nabla} P(\boldsymbol{x}|\boldsymbol{x_a};\omega)] \cdot \boldsymbol{n}\ d\boldsymbol{s}, \tag{27}$$

is used as the starting point for common approaches to seismic interferometry. In these approaches, the normal derivatives are approximated with a far-field and one-way wave approximation shown in equation 22. After applying the one-way wave and high frequency approximation in equation 22 and simple mathematical manipulation, an equation for wavefield retrieval or seismic interferometry (Wapenaar, 2004; Wapenaar and Fokkema, 2006) is obtained (see appendix),

$$2i\Im\left[P(\boldsymbol{x_b}|\boldsymbol{x_a};\omega)\right] \approx \int_{S_m} -2ik\ P(\boldsymbol{x}|\boldsymbol{x_a};\omega)G^-(\boldsymbol{x}|\boldsymbol{x_b};\omega)\ d\boldsymbol{x}. \tag{28}$$

This equation requires the knowledge of the medium everywhere. The Green's function G^- satisfies the same medium properties as the pressure field.

In general, the actual medium is unknown. Hence, G^- is substituted by the complex conjugate of a second pressure field $\overline{P}$, defining $P^- = \overline{P}^*$. Complex conjugation is indicated by a $*$ superscript. The pressure field $\overline{P}$ is assumed to satisfy the same wave equation as P (equation 4); it is also assumed to be measured at the same receiver positions as P, but generated by a different source location, x_b, within the volume. The source producing the anticausal Green's function is assumed to be $s(\boldsymbol{x},\omega) = B(\omega)\delta(\boldsymbol{x}-\boldsymbol{x_b})$, where $B(\omega)$ is the source signature for P^-. Using these two pressure fields in Green's theorem, multiplies the output by an extra source wavelet,

$$\begin{aligned}&\int_V \left(P(\boldsymbol{x}|\boldsymbol{x_a};\omega)B(\omega)\delta(\boldsymbol{x}-\boldsymbol{x_b}) - P^-(\boldsymbol{x}|\boldsymbol{x_b};\omega)A(\omega)\delta(\boldsymbol{x}-\boldsymbol{x_a})\right)\ d\boldsymbol{x}\\ &= \oint_S [P(\boldsymbol{x}|\boldsymbol{x_a};\omega)\boldsymbol{\nabla} P^-(\boldsymbol{x}|\boldsymbol{x_b};\omega) - P^-(\boldsymbol{x}|\boldsymbol{x_b};\omega)\boldsymbol{\nabla} P(\boldsymbol{x}|\boldsymbol{x_a};\omega)] \cdot \boldsymbol{n}\ d\boldsymbol{s}.\end{aligned} \tag{29}$$

For simplicity we can assume that $A(\omega) = B(\omega)$. Considering the first case in equation 25, Green's theorem simplifies to

$$2iB(\omega)\Im\left[P(\boldsymbol{x_b}|\boldsymbol{x_a};\omega)\right] \approx \int_{S_m} -2ik\ P(\boldsymbol{x}|\boldsymbol{x_a};t)P^-(\boldsymbol{x}|\boldsymbol{x_b};\omega)\ d\boldsymbol{x}, \tag{30}$$

after solving the volume integrals and approximating the normal derivatives. In the frequency domain the real and imaginary parts of the Fourier transform of a causal function are said to be Hilbert transforms of each other. In other words, the Fourier transform of the odd and even parts of a causal function constitute a Hilbert transform pair (Costain and Coruh, 2004). Since only the imaginary part of the field is reconstructed, a Hilbert transform is used to calculate the real part of the field (Robinson and Treitel, 1980).

Using two measured wavefields to construct new data instead of a measured wavefield and a Green's function, introduces an extra factor of the source wavelet multiplying the reconstructed data. The fact that the Green's function G^- is not calculated analytically and is replaced by a second measured pressure field P^-, constrains the reconstructed wavefield to locations where actual sources or receivers exist. If the anticausal Green's function, satisfying the same medium properties as the actual pressure field, is calculated, the extra source signature does not appear in the output (Wapenaar, 2004). This particular Green's function could be calculated by deconvolving the wavelet of the pressure field in a preprocessing step, or as an extra step during the computation of seismic interferometry as proposed by Vasconcelos and Snieder (2006). Wavelet deconvolution is a very sensitive step and often introduces more errors and artifacts.

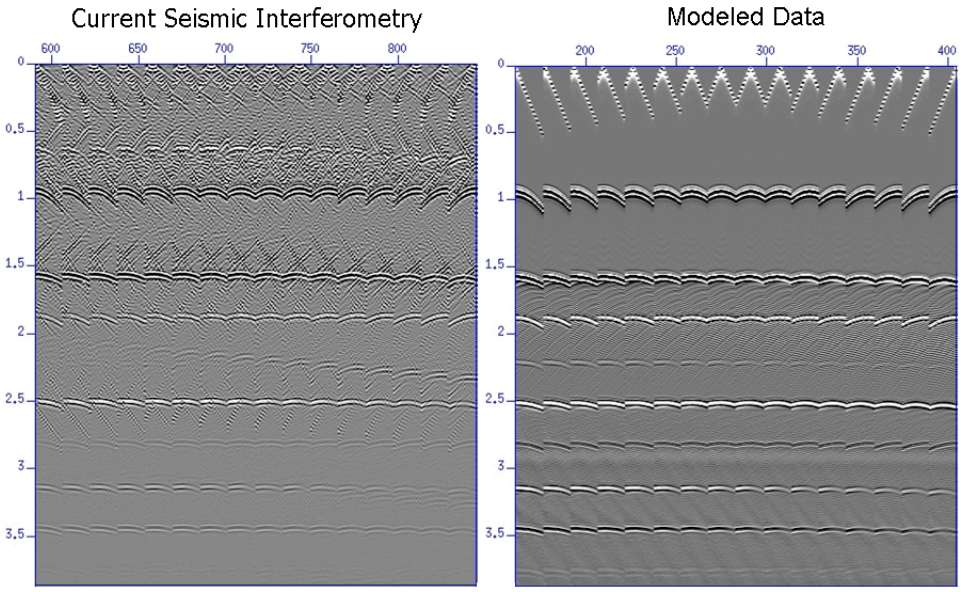

Figure 7: *Reconstructed data with current seismic interferometry compared with modeled data.*

Traditional seismic interferometry requires two approximations to the exact theory (one for each normal derivative in equation 29). Seismic interferometry (equations 28 and 30) is a compromised form of Green's theorem and, hence, gives rise to spurious events. The normal derivative information required by Green's theorem, avoided by using far field approximations, would have combined nonlinearly to cancel the so-called spurious multiples by using differences in sign that identify opposite directions of the wavefield. Directivity is a part of the wavefield's normal derivative. The fact that equation 30 is compromising the theory was also discussed by Korneev and Bakulin (2006) in their derivation of the virtual source method. To test traditional seismic interferometry, the $2D$ finite difference pressure data for the model in figure 2 was used. The normal derivative was approximated with the high frequency and one-way wave approximation used to derive equation 30. In the test, the data used were modeled with finite differences for a receiver line with 200 receivers separated $12.5m$ from each other and 16 sources with a $25m$ separation. The 16 source gathers were used to calculate P and P^- and introduced into the algorithm described by equation 30. Hence, the output traces correspond to 16 sources separated $25m$ from each other and 16 receivers separated

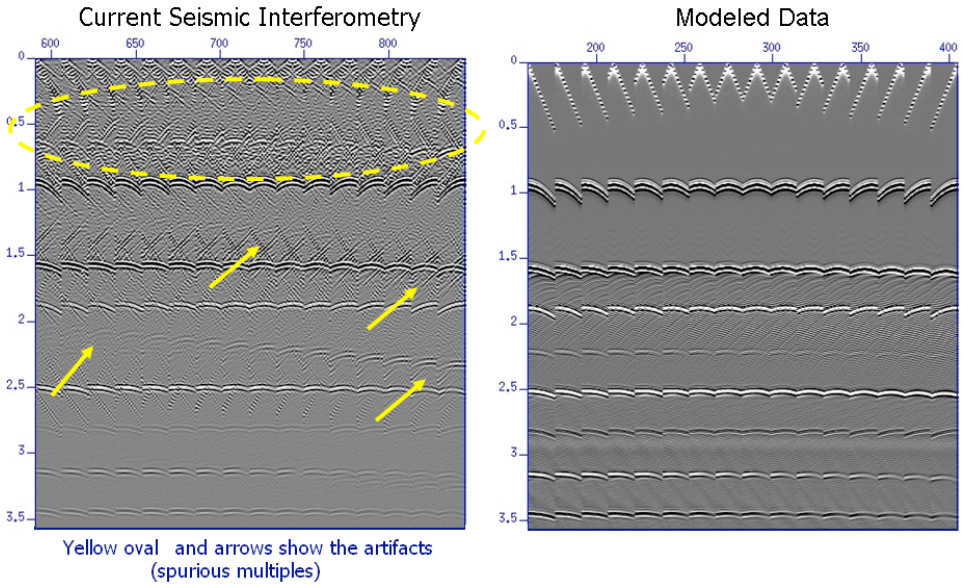

Figure 8: *The spurious multiples produced by current seismic interferometry are highlighted.*

$25m$ from each other. The reconstructed data is shown on the left of figure 7. The modeled data is shown on the right hand side for comparison. In figure 8, the spurious multiples are highlighted.

2^{nd} Scenario: The medium parameters for both fields are equal inside the volume V and different outside

In this section, we chose an anticausal Green's function and a causal pressure field, both corresponding to the same medium properties only at the surface, S, and throughout the volume, V. Again, the output of the volume integral in Green's theorem (equation 24) will depend on the location of the physical source and the observation point.

The evaluation of volume integral, or the left hand side, in Green's theorem gives

$$l.h.s. = \begin{cases} P(\boldsymbol{x_b}|\boldsymbol{x_a};\omega) - A(\omega)G^-(\boldsymbol{x_a}|\boldsymbol{x_b};\omega) & \text{if both sources are strictly inside } S \\ P(\boldsymbol{x_b}|\boldsymbol{x_a};\omega) & \text{if only the observation point } \boldsymbol{x_b} \text{ lies within } V \\ -A(\omega)G^-(\boldsymbol{x_a}|\boldsymbol{x_b};\omega) & \text{if only the source at } \boldsymbol{x_a} \text{ lies within } V, \end{cases} \quad (31)$$

and

$$l.h.s. = \oint_S [P(\boldsymbol{x}|\boldsymbol{x_a};\omega)\boldsymbol{\nabla}G^-(\boldsymbol{x}|\boldsymbol{x_b};\omega) - G^-(\boldsymbol{x}|\boldsymbol{x_b};\omega)\boldsymbol{\nabla}P(\boldsymbol{x}|\boldsymbol{x_a};\omega)] \cdot \boldsymbol{n}\, d\boldsymbol{s}. \quad (32)$$

For a marine application (towed streamer and OBC acquisitions), a volume within the water column, bounded by the free-surface and the measurement surface is selected. When the volume is bounded by the free-surface and the measurement surface, the surface integral in Green's theorem has no

contribution from the upper boundary of V. Letting the measurement surface extend towards infinity, and using causal wavefields, the contribution from the lateral surface S_l vanishes according to the Sommerfeld radiation condition (Sommerfeld, 1954). The anticausal waves, on the other hand, have a contribution at infinity, so there will have a small error due to lack of measurements at the cylinder's wall S_l. The measurement surface (S_m in figure 4) will be the only contribution considered in the surface integral.

For a medium with a free surface, the anticausal version (or the complex conjugate) of the causal reference Green's function, G_0^+, in equation 16 will be considered. Introducing the anticausal reference Green's function into the first case in equation 31, we find an equation for wavefield retrieval that assumes a source within the volume and predicts the wavefield anywhere inside that volume,

$$P(\boldsymbol{x_a}|\boldsymbol{x_b};\omega) - A(\omega)\mathcal{G}_0^-(\boldsymbol{x_a}|\boldsymbol{x_b};\omega) = \int_{S_m} [P(\boldsymbol{x}|\boldsymbol{x_a};\omega)\boldsymbol{\nabla}\mathcal{G}_0^-(\boldsymbol{x}|\boldsymbol{x_b};\omega) - \mathcal{G}_0^-(\boldsymbol{x}|\boldsymbol{x_b};\omega)\boldsymbol{\nabla}P(\boldsymbol{x}|\boldsymbol{x_a};\omega)] \cdot \boldsymbol{n}\ d\boldsymbol{s}, \tag{33}$$

in agreement with the result derived by Ramírez et al. (2007). Introduce $P(\boldsymbol{x_a}|\boldsymbol{x_b};\omega) = P^0(\boldsymbol{x_a}|\boldsymbol{x_b};\omega) + P^s(\boldsymbol{x_a}|\boldsymbol{x_b};\omega)$ into equation 33, where $P^0 = A(\omega)\mathcal{G}_0^+(\boldsymbol{x_a}|\boldsymbol{x_b};\omega)$ is the reference field and P^s is the scattered field. The left hand side becomes

$$P^s(\boldsymbol{x_a}|\boldsymbol{x_b};\omega) + A(\omega)\left[\mathcal{G}_0^+(\boldsymbol{x_a}|\boldsymbol{x_b};\omega) - \mathcal{G}_0^-(\boldsymbol{x_a}|\boldsymbol{x_b};\omega)\right] = P^s(\boldsymbol{x_a}|\boldsymbol{x_b};\omega) + 2i\ A(\omega)\ \Im\left[\mathcal{G}_0^+(\boldsymbol{x_a}|\boldsymbol{x_b};\omega)\right]. \tag{34}$$

Thus, in equation 33, the total scattered field plus the imaginary part of the direct wave between a source at $\boldsymbol{x_a}$ and an observation point at $\boldsymbol{x_b}$ is reconstructed. This result is less desirable than the one obtained with a causal Green's function, where the surface integral effectively screened all the contribution of the direct or reference wavefield. Using an anticausal Green's function the direct wave is not screened by the surface integral; only the real part of the direct wave is filtered. If a measurement or good estimate of the pressure field's normal derivative is available, then, a causal reference Green's function is the best choice.

If the normal derivative can not be obtained, and a high frequency approximation is used, then, choosing an anticausal reference impulse response (rather than a causal one) is a better solution. The reason is that when the normal particle velocity of a two-way wavefield is approximated by a factor of ik times the original wavefield, and used in Green's theorem, the output of the surface integral with a causal reference Green's function vanishes (see appendix). As it is explained in the following lines, and demonstrated by numerical examples, this does not happen with the anticausal Green's function.

Ramírez et al. (2007) assumed that the normal derivative of the pressure field is not measured and selected a high frequency approximation to satisfy, with a single compromise, Green's theorem. In other words, the approximation described by equation 22 was used in equation 34, to obtain direct wave seismic interferometry

$$P(\boldsymbol{x_a}|\boldsymbol{x_b};\omega) \approx \oint_S [P(\boldsymbol{x}|\boldsymbol{x_a};\omega)\boldsymbol{\nabla}\mathcal{G}_0^-(\boldsymbol{x}|\boldsymbol{x_b};\omega)$$

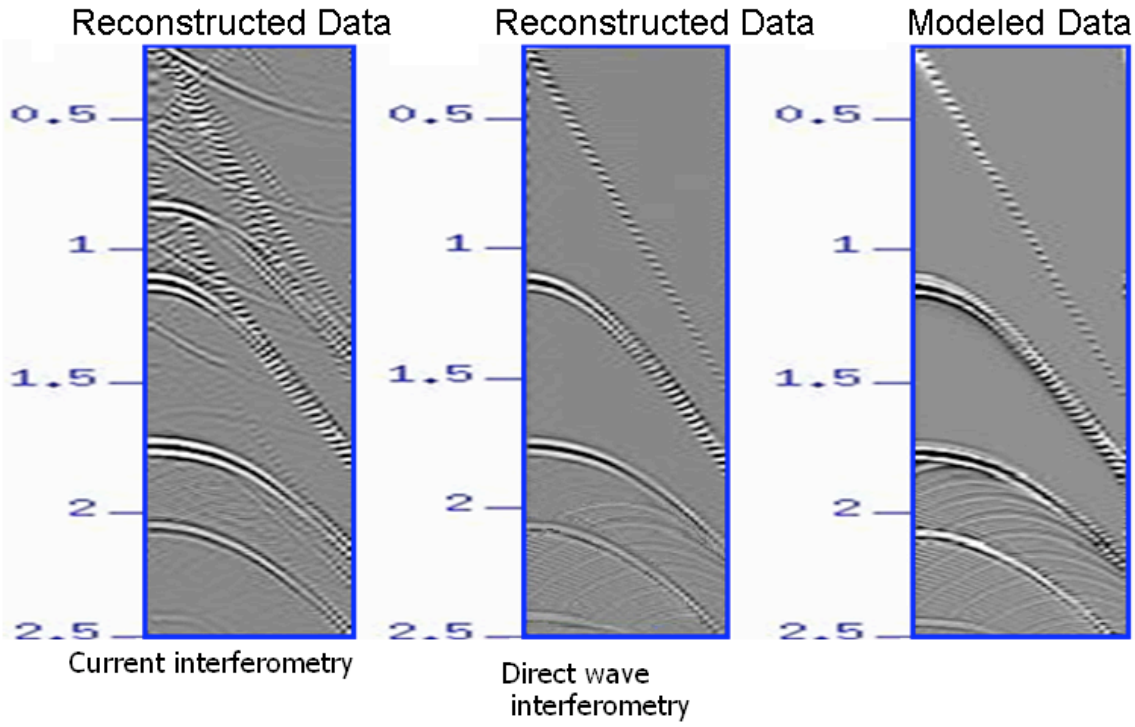

Figure 9: *Comparison between direct wave interferometry (Green's theorem + a single approximation), current seismic interferometry and modeled data.*

$$- ikP(\boldsymbol{x}|\boldsymbol{x_a};\omega)\mathcal{G}_0^-(\boldsymbol{x}|\boldsymbol{x_b};\omega)] \cdot \boldsymbol{n}\ d\boldsymbol{s}, \tag{35}$$

or

$$P^s(\boldsymbol{x_a}|\boldsymbol{x_b};\omega) + 2i\ A(\omega)\ \Im\left[\mathcal{G}_0^+(\boldsymbol{x_a}|\boldsymbol{x_b};\omega)\right] \approx \oint_S [P(\boldsymbol{x}|\boldsymbol{x_a};\omega)\boldsymbol{\nabla}\mathcal{G}_0^-(\boldsymbol{x}|\boldsymbol{x_b};\omega) - ikP(\boldsymbol{x}|\boldsymbol{x_a};\omega)\mathcal{G}_0^-(\boldsymbol{x}|\boldsymbol{x_b};\omega)] \cdot \boldsymbol{n}\ d\boldsymbol{s}. \tag{36}$$

The output is approximately equal to the scattered field and the imaginary part of the direct wave. This result is very accurate compared to other seismic interferometry methods, when applied to the surface seismic experiment. The improvement is illustrated with the 2 numerical example shown in figure 9, where the input data corresponds to the pressure field modeled and used in the previous sections of this tutorial.

Direct wave seismic interferometry, equation 36, was also tested using elastic finite difference $3D$ surface seismic marine data(Ramírez et al., 2007). The Earth model consists of 3 layers, a free surface, and a set of random point diffractors. The data was modeled by Ketil Hokstad and Roger Sollie at Statoil Research Center. The modeled data consist of 10 source lines with 12 shots per line. The source and receiver spacing in the numerical modeling was $25m$ in both (inline and crossline) directions. The configuration is shown in figure 10. Direct wave seismic interferometry was applied to 20 receiver lines with 121 receivers per line, $25m$ inline separation and $100m$ crossline

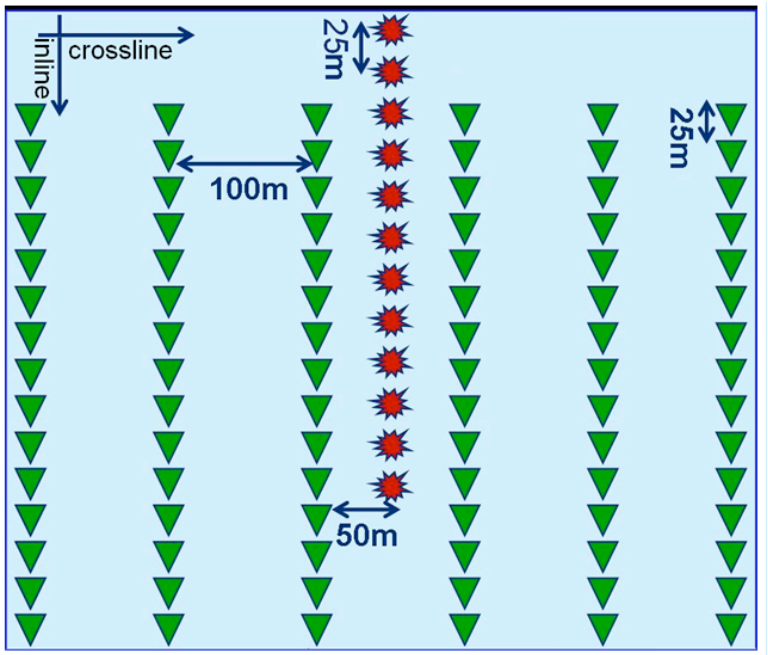

Figure 10: *Configuration for zero-crossline offset data reconstruction.*

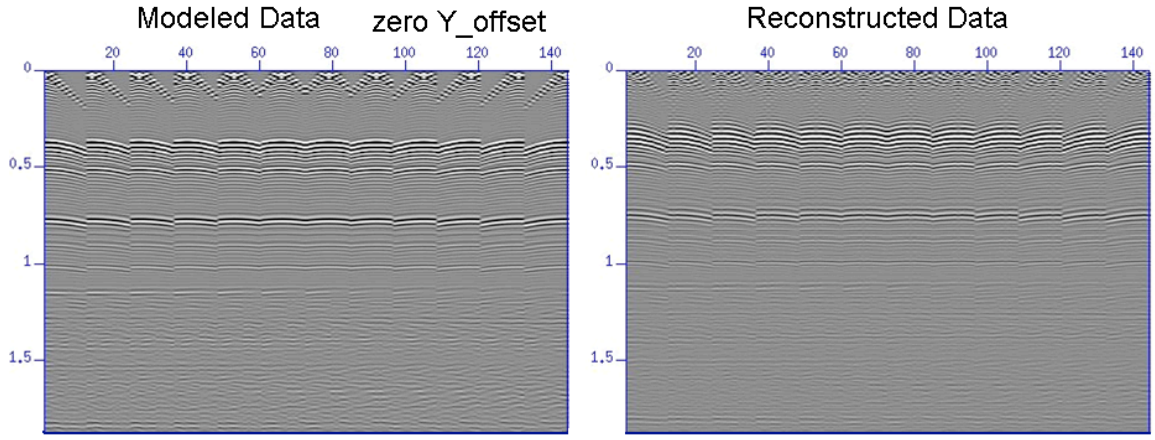

Figure 11: *Reconstructed data (direct wave seismic interferometry) and modeled data.*

separation. A simulated source line (12 sources) with $25m$ source interval overlay each receiver line, as illustrated in figure 10 (sources are marked by red stars and receivers by green triangles). The minimum distance to the receivers in both inline and crossline direction is 50 m in the selected shot gathers. This data subset was put into equation 36 with an analytic anticausal reference Green's function. This Green's function was calculated for 12 sources in a line with $25m$ source interval and located at $0m$ crossline offset from the source line in the input data. In other words, the 12 sources for the anticausal reference Green's function shared the same position as the sources for the

input pressure field. The numerical test was repeated calculating the anticausal reference Green's function for 12 sources located at $100m$ crossline offset away from the source line in the input data. The configuration for the second test is shown in figure 12. The goal is to reconstruct coincident sources and receivers at the source line location, for the first experiment and to reconstruct the receiver line at 100 meter away from the source line in the crossline direction (marked by the dashed line in figure 12) for the second experiment. The retrieved Green's function corresponds to:
Experiment 1.- A line with coincident sources and receivers (source line in figure 10) displayed in figure 11. The reconstructed data is shown on the right and modeled data is shown on the left for comparison.
Experiment 2.- A line consisting of 12 sources at zero crossline offset, sources from the input data, and 12 receivers in a line at 100 m crossline offset (dashed line in figure 12). Figure 13 shows the extrapolated data using direct wave seismic interferometry on the right. The modeled data is shown on the left hand side of figure 13 for comparison.

Thee output of direct wave seismic interferometry has all the events correctly predicted and there are no spurious multiples in the predicted data. The difference between the modeled data and the direct wave seismic interferometry result is due to the high frequency approximation and a bandlimited reference Green's function used in the calculations. Also remember that this algorithm has an effect on the output of the direct wave, as discussed in this section.

Analysis

Using the anticausal Green's function, it is possible to find a formalism that permits an approximate retrieval of the pressure field between two sources (or receivers, using reciprocity principles) as if one of them was a receiver. Two methods were explained and both of them have compromises to the exact theory. The first one, standard seismic interferometry (Schuster, 2001; Derode et al., 2003; Roux and Fink, 2003; Wapenaar et al., 2002) uses the measured wavefield and its complex conjugate, making two approximations. These two approximations introduces the spurious events and squares the output source signature. In most surface seismic situations, the spurious multiple can damage the retrieved data significantly since their amplitudes are comparable to the ones of the reconstructed primaries. The second one, direct wave interferometry using Green's theorem (Ramírez et al., 2007), uses an analytic anticausal Green's function and only makes one approximation. The output of this method is a close approximation to the total scattered field plus the imaginary part of the direct wave.

The result provided by traditional seismic interferometry (equation 30) is often used as the starting point for further analysis and applications. Some applications even assume that the normal derivative of P^+ and P^- is P and $-P$, respectively. A considerable part of seismic interferometry analysis and related publications, aims to address the issues created by the compromises made to the exact theory and framework. This theory aims to fix the weaknesses of interferometry, such as the extra power of the source wavelet and the spurious multiples. For example, Snieder et al. (2006) studied the appearance of spurious multiples and proposed types of sources and acquisition geometries that would help diminish it. Snieder et al. (2006) introduced the term spurious multiples to refer to artifacts created by interferometry. In particular, their analysis was performed

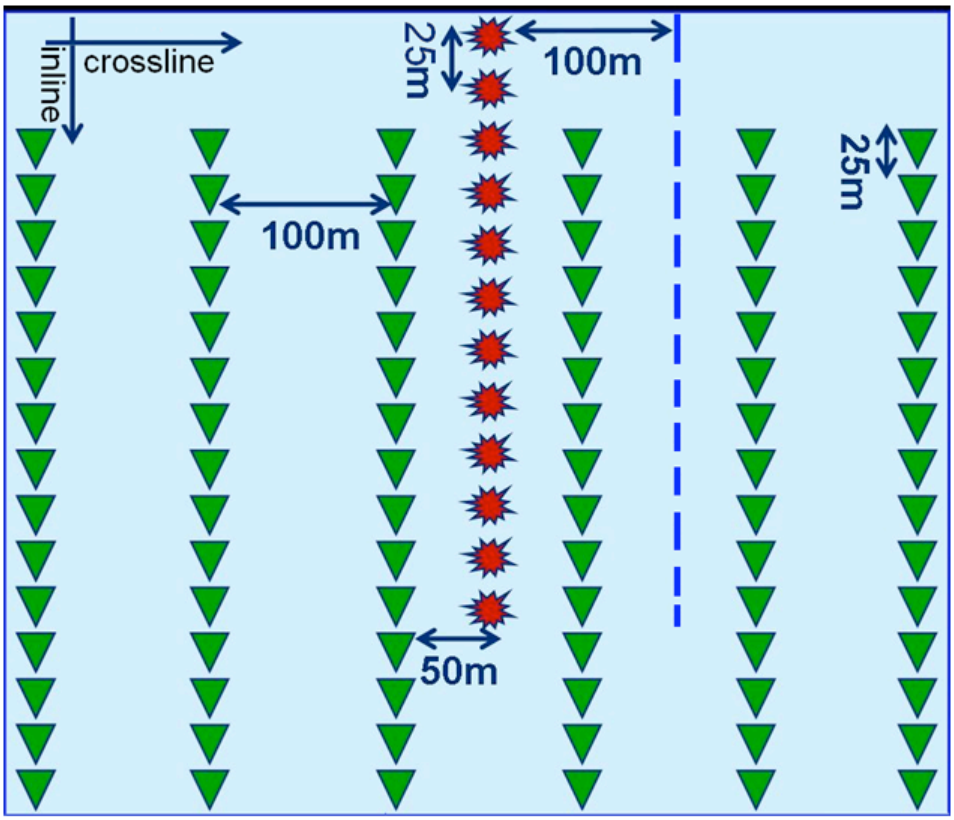

Figure 12: *Configuration for zero-crossline offset data reconstruction.*

on data containing only singly reflected events. They showed, through analytic examples, how the kinematics of singly reflected waves propagating between two receivers can be reproduced by correlating the primaries produced by all sources and recorded by these two receivers. They also showed that the correlation of primaries generated at different reflectors produce artifacts, which they call spurious multiples. These artifacts are not true multiples. The reason to use the word multiples was that these artifacts are the product of two amplitudes (reflection coefficients) due to two different recorded primaries. In seismic interferometry any two events contained in the total wavefields of two receiver or shot gathers will have a nonzero contribution. This contribution will be the product of the two amplitudes corresponding to the pair of events being correlated and the subtraction of their corresponding times, regardless of the amount of reflections the event had experienced. Hence, all events (primaries, direct wave, multiples, ghosts) are synthesized analogously and they all have the opportunity to produce artifacts when being correlated with each other. In an attempt to understand the nature of these artifacts, Snieder et al. (2006) give a heuristic argument that interpret spurious multiples as the effect of aperture limitations and correlated sources; they propose the idea that uncorrelated sources will eliminate these errors. This idea was later used and extended by Wapenaar (2006).

Spurious multiples are the direct effect of theoretical approximations. Furthermore, spurious multi-

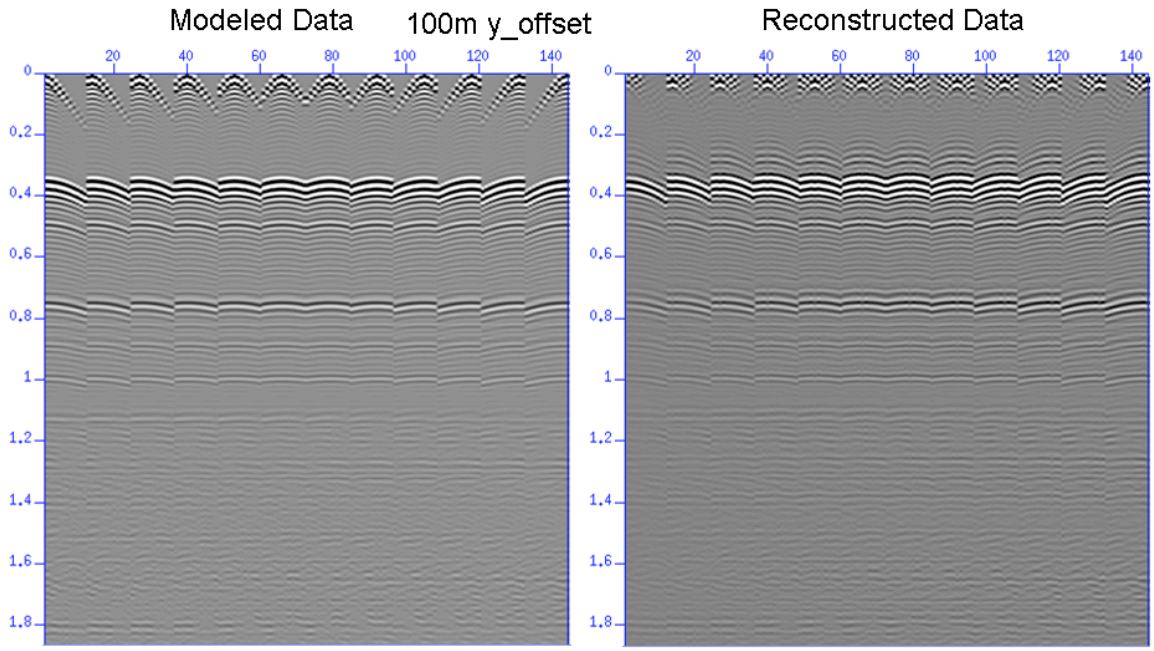

Figure 13: *Reconstructed data (direct wave seismic interferometry) and modeled data.*

ples are not a direct consequence of aperture limitations and/or interactions between specific events such as primaries in the data, but the outcome of the far-field approximations compromising the effectiveness of Greens theorem Ramírez Pérez (2007); Ramírez and Weglein (2008). The analysis and new theory launched from seismic interferometry often ignored the fact that approximations were made. It is necessary to understand that asymptotic analysis has, in fact, two steps: (1) an asymptotic approximation (*e.g.*, a high frequency and one-way wave approximation) and (2) an analysis, and a set of conclusions reached from the result of the first step. The very reason for performing asymptotic approximation is to alter algorithms and their underlying assumptions, properties, and requirements. An approximation is never equivalent to the original form.

We are not claiming that analyzing and using the result in standard seismic interferometry to develop new theory, understanding or applications is a bad path to follow, but there exists a danger of forgetting the assumptions and requirements of the original theory. In many situations, the new tools are effective and on target. For example, Otnes et al. (2006) derived a data-driven free surface demultiple algorithm for WVSP data. The method was derived by using seismic interferometry and applied to a real WVSP experiment to effectively construct surface seismic data, which was convolved with the WVSP data to achieve its goal of removing the free-surface multiples without any subsurface information.

Another strategy is to understand that the errors in the synthesized wavefield are an effect of the assumptions applied to satisfy Green's theorem, as well as the functions used in its derivation (Ramírez et al., 2007). Hence, direct wave interferometry appears to be a better approximation for surface seismic experiments where an analytic Green's function is available and fewer assumptions provide more accuracy and effectiveness. Furthermore, using an analytic reference Green's function,

data can be extrapolated to positions where no receivers or sources were located. The synthesized data would have a single source signature and almost no artifacts are created. Thus, direct wave interferometry provides an improvement over traditional approaches.

Anticipating the consequences due to the compromises made, allows us to look at the original framework and attempt to find better ways to meet its requirements. If the vertical component of the pressure field is the weakness, then we can find ways to avoid that requirement. An example of this approach is accomplished by introducing another form of Green's theorem in which a two-surface Dirichlet boundary condition to the reference Green's function is imposed. This method does not require the normal component of the particle velocity. It is explained in the next part of this tutorial.

Green's theorem with different boundary conditions imposed

In this section we introduce different boundary conditions imposed to the functions u and ν used in Green's theorem (equation 3). It will be shown that, for the applications discussed in the previous sections, an improvement can be found in the framework given by Green's theorem.

Dirichlet boundary conditions: The medium parameters for both fields are equal inside the volume V and different at and below the measurement surface

A Green's function that vanishes on both the free and measurement surfaces, eliminates the data requirement of the normal derivative in Green's theorem (Weglein and Devaney, 1992; Tan, 1992; Osen et al., 1998). This boundary condition can be fulfilled by the method of images or by adding a particular solution that contains the desired boundary conditions to the homogeneous solution for the Helmholtz equation (Morse and Feshbach, 1953).

The double-surface Dirichlet Green's function cannot be measured in a seismic experiment, since the actual medium only has one zero pressure surface. This Green's function does not represent a physical wavefield; it is a convenient mathematical construction. It needs to be calculated analytically. We consider a homogeneous medium within the volume and the source point for the Green's function located inside V.

Use the configuration shown in figure 4, where the selected volume lies entirely in a homogeneous medium and is bounded by the air-water surface and the measurement surface. These two surfaces are the ones on which the Dirichlet boundary conditions will be imposed for the Green's function calculation.

If we describe the two-surface Dirichlet Green's function $\mathcal{G}_0^D$ by the method of images (see figure 14), it will include the wave that propagates directly from the real source to the receiver and the wave that propagates directly from each image source to the receiver. Introducing P and $\mathcal{G}_0^D(\boldsymbol{x}|\boldsymbol{x_b};\omega)$ into equation 3 as u and ν, and assuming the medium parameters for both fields are equal within the volume V (where V is the volume in figure 4), we obtain

$$\int_V \left(P(\boldsymbol{x}|\boldsymbol{x_a};\omega)\delta(\boldsymbol{x}-\boldsymbol{x_b}) - \mathcal{G}_0^D(\boldsymbol{x}|\boldsymbol{x_b};\omega)A(\omega)\delta(\boldsymbol{x}-\boldsymbol{x_a})\right)\, d\boldsymbol{x}$$

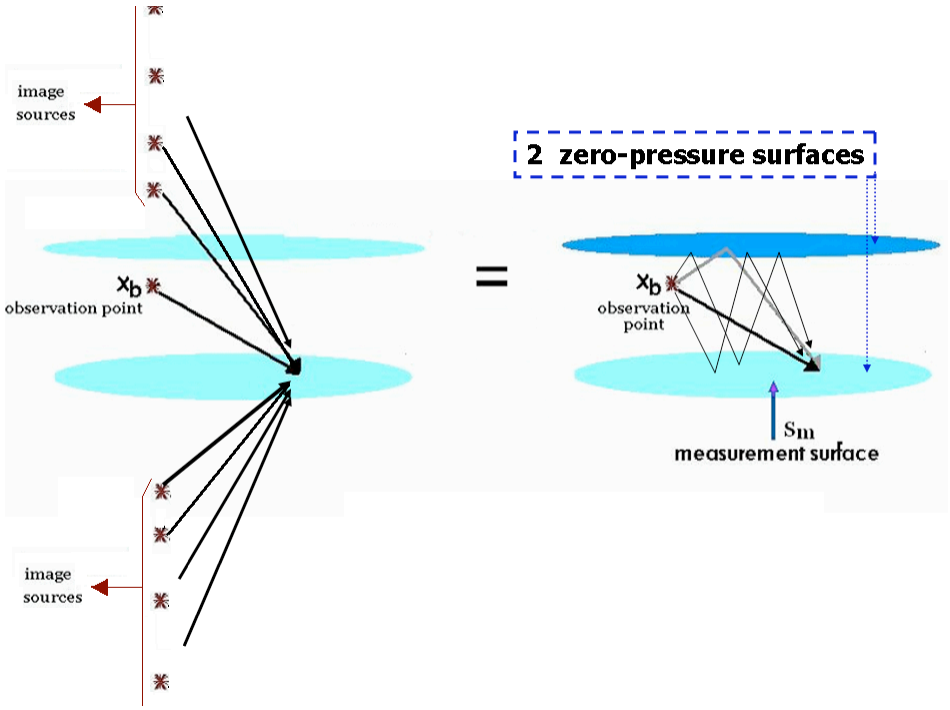

Figure 14: *The method of images is used to mathematically describe the two-surface Dirichlet Green's function.*

$$= \int_{S_m} P(\boldsymbol{x}|\boldsymbol{x_a};\omega)\boldsymbol{\nabla}\mathcal{G}_0^D(\boldsymbol{x}|\boldsymbol{x_b};\omega)\cdot\boldsymbol{n}d\boldsymbol{s}, \tag{37}$$

where we have taken into account the boundary conditions. The left hand side gives

$$l.h.s. = \begin{cases} P(\boldsymbol{x_b}|\boldsymbol{x_a};\omega) - A(\omega)\mathcal{G}_0^D(\boldsymbol{x_a}|\boldsymbol{x_b};\omega) & \text{if both sources are strictly inside } S \\ P(\boldsymbol{x_b}|\boldsymbol{x_a};\omega) & \text{if only the observation point } \boldsymbol{x_b} \text{ lies within } V. \end{cases} \tag{38}$$

The source for the Dirichlet Green's function must be inside the volume to satisfy the boundary conditions.

The first case in equation 38,

$$P(\boldsymbol{x_a}|\boldsymbol{x_b};\omega) - A(\omega)\mathcal{G}_0^D(\boldsymbol{x_a}|\boldsymbol{x_b};\omega) = \int_{S_m} P(\boldsymbol{x}|\boldsymbol{x_a};\omega)\boldsymbol{\nabla}\mathcal{G}_0^D(\boldsymbol{x}|\boldsymbol{x_b};\omega)\cdot\boldsymbol{n}\ d\boldsymbol{s}, \tag{39}$$

shows a method to determine the wavefield above the measurement surface and below the free surface from measured pressure on a typical surface.

The algorithm described by equation 39 does not require the normal derivative of the pressure field. This method for wavefield retrieval or extrapolation was proposed by Weglein et al. (2000) and Ramírez et al. (2007). However, it has an error of $-A(\omega)\mathcal{G}_0^D(\boldsymbol{x_a}|\boldsymbol{x_b};\omega)$, which, according to Tan (1992) and Weglein et al. (2000), for the typical surface seismic exploration source-receiver configurations and frequency content is small.

Equation 39 also has applications in source signature estimation (Osen et al., 1998; Tan, 1999) and deghosting(Amundsen et al., 2005; Zhang and Weglein, 2005, 2006). The result for wavelet estimation, as well as the analogous results in the previous sections using different Green's function, shows that when the receiver level is below the sources, there exists a triangle relationship between the pressure, its normal derivative, and the source wavelet. In order to theoretically calculate any one of these quantities, the other two must be known (Weglein and Secrest, 1990; Amundsen, 2001). Green's theorem with a Dirichlet Green's function apparently overcomes the need of a third quantity, the normal component of the particle velocity. However, it does not break the triangle relationship, since an extra pressure measurement at any point above the measurement surface and below the free-surface is needed. The extra measurement is, in general, not available and a possible solution is to introduce an approximation that alters equation 39 as described in Guo et al. (2005).

If an estimate of the wavelet is available, or obtainable, the error in equation 39 for seismic interferometry can be easily removed, by adding a factor of $A(\omega)\mathcal{G}_0^D(\boldsymbol{x_a}|\boldsymbol{x_b};\omega)$. This will give an exact equation. The only limitation for a 'perfect' output would the effect of the aperture limitations in the recorded pressure data. The rest of the ingredients required by Green's function would be fulfilled analytically.

When the wavelet is not available and it is possible to separate the direct wave from the scattered field (*e.g.* in a deep water experiment), we can find an exact equation for reconstructing scattered field that does not need the source wavelet. It is given by the **second case** in equation 38. Substituting $P^s(\boldsymbol{x_a}|\boldsymbol{x_b};\omega)$, the scattered field, into Green's theorem (instead of the total wavefield), and using the two surface Dirichlet Green's function as the second function,

$$P^s(\boldsymbol{x_a}|\boldsymbol{x_b};\omega) = \int_{S_m} P^s(\boldsymbol{x}|\boldsymbol{x_a};\omega)\boldsymbol{\nabla}\mathcal{G}_0^D(\boldsymbol{x}|\boldsymbol{x_b};\omega)\cdot\boldsymbol{n}\ d\boldsymbol{s}, \tag{40}$$

is obtained. This is possible because the scattered field satisfies the wave equation without a source function,

$$\left(\nabla^2 + \frac{\omega^2}{c^2(\boldsymbol{x})}\right) P^s(\boldsymbol{x}|\boldsymbol{x_a};\omega) = 0. \tag{41}$$

Hence, only the observation point lies within the volume V. This form of Green's theorem does not require the normal derivative of the pressure field, nor the source signature. It only asks for the scattered field, or the pressure field due to sources outside the medium, and an analytic Green's function that vanishes at the measurement and air-water surface.

The $3D$ data used to test direct wave seismic interferometry in section , was also used to test Green's theorem with a two-surface Dirichlet Green's function. The second configuration, figure 12, was used. Two different tests were made. The first one, used total pressure field as input data to equation 39. The second test used scattered field as input to equation 40. The output is shown in figure 15. The reconstructed data, for both examples corresponds to a line consisting of 12 sources at zero crossline offset, sources from the input data, and 12 receivers in a line at 100 m crossline offset (dashed line in figure 12). The reconstructed data on the left represent the second test and the data in the middle correspond to the first test. Modeled data is displayed on the right hand side of figure 15 for comparison.

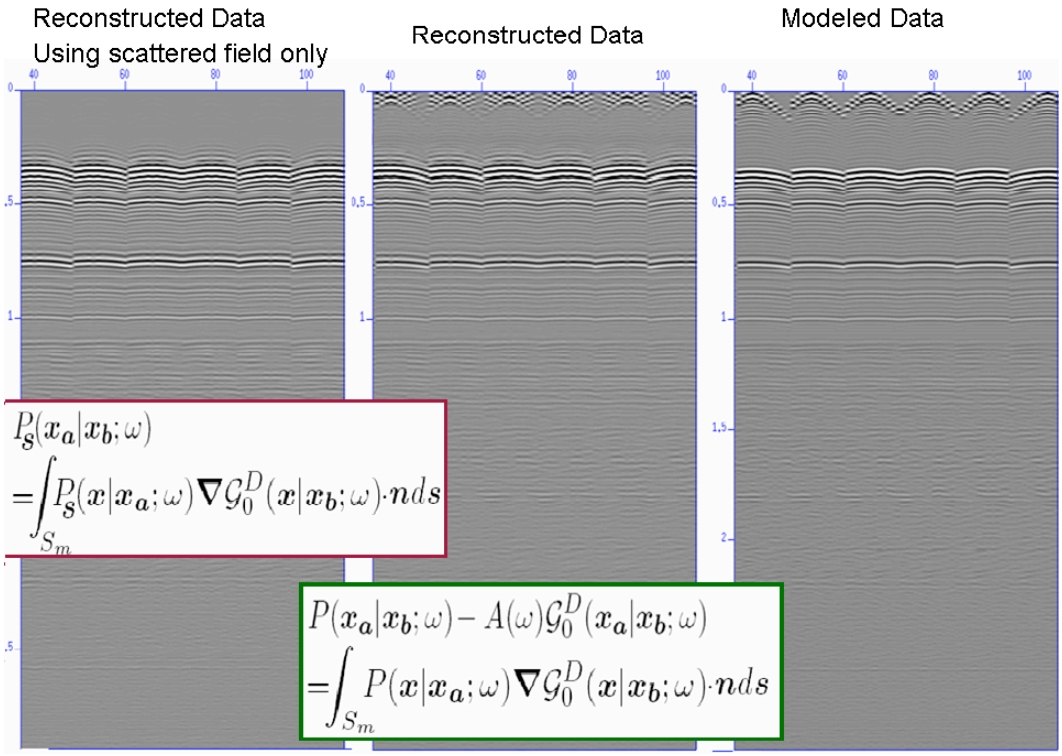

Figure 15: *Green's theorem with a double Dirichlet Green's function. The input for the figure on the left was scattered field. The input for the middle figure is total wave field. The figure on the right is modeled data.*

In this section, it was shown that certain choices of functions and boundary conditions in Green's theorem can help to avoid specific requirements and assumptions made by other methods with similar purposes. An example of this requirement, is the pressure field's normal derivative required to satisfy the methods for wavefield retrieval and wavelet estimation discussed in the previous sections in this tutorial. The wavefield's normal derivative was approximated twice for standard seismic interferometry and once for direct wave seismic interferometry. Using a Dirichlet boundary condition imposed upon the Green's function used in Green's theorem, the approximation is not necessary, and a wavefield reconstruction method is achieved, only requiring measurements of the pressure field. For the calculation of the Dirichlet Green's function, the volume and its boundaries must be located within a known medium. Hence, this theory is ideal for marine surface seismic acquisitions, where pressure measurements exist within the water column. However, this is a very special situation. There are circumstances when Green's function with a Dirichlet boundary condition is not available (or it cannot be calculated analytically). Hence, it is not possible to overcome a requirement of the pressure field's normal derivative when the medium inside the volume is unknown. An example of this situation is in the derivation of the virtual source method by Bakulin and Calvert (2004) and Korneev and Bakulin (2006) as well as in the derivation of wavefield deconvolution by Amundsen (2001).

Wavefield deconvolution and the virtual source method

In this section we discuss two methods to retrieve the wavefield between two receivers located at the water bottom or beneath the subsurface in a seismic experiment. These methods are wavefield deconvolution and the virtual source method. Both methods are based on Green's theorem and, in principle, both of them require dual measurements. In practice, the first method, wavefield deconvolution, is applied using both the pressure and its normal derivative measured in a seismic experiment (*e.g.* in OBC acquisitions). On the other hand, virtual source method is applied using only the pressure field, in clear analogy with other common seismic interferometry methods.

Besides the approximations and their effect on the retrieved wavefield, virtual source has another important difference with wavefield deconvolution: virtual source aims to retrieve the total wavefield between two receivers located beneath the subsurface while wavefield deconvolution retrieves the deconvolved wavefield for a coincident source-receiver experiment at the receiver location. Deconvolution refers to the removal of overburden effects and overburden refers to the medium above the receiver or measurement plane. In the following we are going to discuss the wavefield deconvolution method and then relate it to the virtual source method.

As discussed in the introduction for this dissertation, in a marine experiment there exist events that owe their existence to the presence of the air-water surface. These events are known a ghosts and free-surface multiples. In general, these events are removed from the data since they are not used for further processing. Imposing a specific selection of boundary conditions upon the pressure field and the Green's function, used in Green's theorem, we can find a formalism that eliminates the free-surface multiples and the wavelet from the pressure field (Amundsen, 2001; Holvik and Amundsen, 2005).

In wavefield deconvolution, two mediums are selected:

1) A medium corresponding to a physical seismic experiment in a marine setting (shown on the left hand side of figure 16), it consists of the Earth, a layer of water and a half space of air. The position x_s denotes the location of the source (a source array could also be chosen) and x_r is the receiver location.

2) A medium corresponding to a hypothetical experiment (shown on the left hand side of figure 16), it consists of the Earth and a half space of water (no free-surface). The position x_s is the receiver location and x_r is the source location.

The pressure field, P, propagates in the first medium and a second pressure wavefield P' propagates in the second or ideal medium. Both pressure fields satisfy equation 4. A Dirichlet boundary condition is imposed to P. The volume selected to evaluate Green's theorem is shown in figure 16. It is bounded by the surface S_0 (where the different boundary conditions are imposed) and the surface S_R which is assumed to be at infinity (due to the Sommerfeld radiation condition, receives at S_r give zero contribution to the surface integral in Green's theorem). Using the pressure fields P and P' as u and ν in Green's theorem, equation 3, gives

$$\int_V \left(P(\boldsymbol{x_r}|\boldsymbol{x_s};\omega) A'(\omega) \delta(\boldsymbol{x}-\boldsymbol{x_s}) - P'(\boldsymbol{x_s}|\boldsymbol{x_r};\omega) A(\omega) \delta(\boldsymbol{x}-\boldsymbol{x_r}) \right) \, d\boldsymbol{x}$$

$$= \int_{S_0} [-P'(\boldsymbol{x}|\boldsymbol{x_r};\omega)\boldsymbol{\nabla} P(\boldsymbol{x}|\boldsymbol{x_s};\omega)] \cdot \boldsymbol{n}\ d\boldsymbol{s}.$$

Evaluating the volume integral, we obtain an integral relation describing the relation between the experiments with and without a free-surface:

$$A'(\omega)P(\boldsymbol{x_r}|\boldsymbol{x_s};\omega) - A(\omega)P'(\boldsymbol{x_s}|\boldsymbol{x_r};\omega) = -\int_{S_0} P'(\boldsymbol{x}|\boldsymbol{x_r};\omega)\boldsymbol{\nabla} P(\boldsymbol{x}|\boldsymbol{x_s};\omega) \cdot \boldsymbol{n}\ d\boldsymbol{s}. \tag{42}$$

This integral equation has been derived and used for free-surface elimination by Fokkema and van den Berg (1993) and Amundsen (2001), among others. In contrast to the previous solutions of Green's theorem derived in this work, the relation described by equation 42 is not a relation that can be readily applied to retrieve a useful result. The solution of the problem is the wavefield P' and it cannot be retrieved from the previous equation unless more mathematical manipulations are done. There are different mathematical manipulations that have been used to exploit equation 42 (the interested reader is referred to Fokkema and van den Berg (1993); Amundsen (2001) and references within). The method selected by Amundsen (2001), assumes that the pressure field is a sum of upgoing and downgoing waves,

$$P(\boldsymbol{x_r}|\boldsymbol{x_s};\omega) = u(\boldsymbol{x_r}|\boldsymbol{x_s};\omega) + d(\boldsymbol{x_r}|\boldsymbol{x_s};\omega) \tag{43}$$

and introduces the relations

$$u(\boldsymbol{k_r}, z_r|\boldsymbol{x_s};\omega) = \frac{1}{2}\left(P(\boldsymbol{k_r}, z_r|\boldsymbol{x_s};\omega) - \frac{\rho\omega}{k_z}\boldsymbol{\nabla} P(\boldsymbol{k_r}, z_r|\boldsymbol{x_s};\omega) \cdot \boldsymbol{n}\right), \tag{44}$$

and

$$d(\boldsymbol{k_r}, z_r|\boldsymbol{x_s};\omega) = \frac{1}{2}\left(P(\boldsymbol{k_r}, z_r|\boldsymbol{x_s};\omega) + \frac{\rho\omega}{k_z}\boldsymbol{\nabla} P(\boldsymbol{k_r}, z_r|\boldsymbol{x_s};\omega) \cdot \boldsymbol{n}\right) \tag{45}$$

where u and d refer to upgoing and downgoing, respectively, $\boldsymbol{k_r}$ is the horizontal wavenumber conjugate to the horizontal coordinates (x_{1r}, x_{2r}), k_z is the vertical wavenumber conjugate to z, and $z_r = x_{3r}$ is the receiver depth. Equation 42 requires the normal derivative of the pressure field P at the free-surface. Amundsen (2001) redatumed the normal derivative of P in the wavenumber domain, to obtain its values at the free-surface, and introduced the relations in equations $43 - 45$, to obtain a second integral equation:

$$A'(\omega)P(\boldsymbol{x_r}|\boldsymbol{x_s};\omega) = -\frac{1}{2\pi^2}\int_{-\infty}^{\infty} (ik_z)P'(-\boldsymbol{k}, z_r|\boldsymbol{x_r};\omega)d(\boldsymbol{k}, z_r|\boldsymbol{x_s};\omega) \cdot \boldsymbol{n}\ d\boldsymbol{s}.$$

where the integral is taken over the horizontal wavenumber $\boldsymbol{k}$. This result is a Fredholm integral equation of the first kind. This is an equation difficult to solve and in general it is ill-conditioned (Amundsen, 2001). However, when the medium is 1D (horizontally layered), a much simpler solution is found,

$$P'(-\boldsymbol{k}, z_r|\boldsymbol{\chi_s} = 0, z_r;\omega) = \frac{-A(\omega)}{2ik_z}\frac{P(-\boldsymbol{k}, z_r|\boldsymbol{\chi_s} = 0, z_r;\omega)}{d(-\boldsymbol{k}, z_r|\boldsymbol{\chi_s} = 0, z_s;\omega)}, \tag{46}$$

or

$$P'_r(-\boldsymbol{k}, z_r|\boldsymbol{\chi_s} = 0, z_r; \omega) = \frac{-A(\omega)}{2ik_z} \frac{u(-\boldsymbol{k}, z_r|\boldsymbol{\chi_s} = 0, z_r; \omega)}{d(-\boldsymbol{k}, z_r|\boldsymbol{\chi_s} = 0, z_s; \omega)} \tag{47}$$

where $\boldsymbol{\chi_s}$ denotes the horizontal coordinates for the source position. It is set to zero because the medium is laterally invariant. P' is the wavefield corresponding to an hypothetical experiment without a free surface, and P'_r is the scattered field in that experiment. Hence, it is assumed that P' can be separated in a direct arrival P'_0 and a scattered field P'_r.

The right hand side of equation 47 contains a wavelet factor of $A(\omega)$, this wavelet can be selected to be different from the original. Furthermore, $A(\omega)$ can be set to be equal to unity, and the retrieved wavefield won't have any source signature, it will be the pressure wavefield due to an impulsive point source.

The final result retrieves a wavefield without overburden effects, and with coincident source and receiver positions. The wavefield retrieval is performed by deconvolving the total pressure field P with the downgoing part of P at the receiver location $\boldsymbol{x_r}$. It retrieves the wavefield for coincident source and receiver locations at $\boldsymbol{x_r}$. Hence, it effectively creates a virtual source at x_r. This method can be applied to image beneath complex structures when receivers are locating within the Earth. In those cases the removal of free-surface multiples will be extended to the removal of all overburden effects in the retrieved wavefield. It is accurate when dual measurements exist at the receiver location. It has been extended for an elastic medium by Holvik and Amundsen (2005).

As discussed earlier, wavefield deconvolution has similarities with the virtual source method derived by Bakulin and Calvert (2004) and Korneev and Bakulin (2006), whose equation is given by a simplification of equation 30. To derive the virtual source method, two pressure wavefields P and P^- are used as the functions u and ν in Green's theorem, equation 3. The medium parameters for both wavefields are assumed to be equal everywhere (see section 2.2 and 2.3), and the selected volume is a halfspace in a seismic experiment, as shown in figure 17. The volume is bounded by a surface S_0 where the sources explode (which is not assumed to be a zero-pressure surface) and the surface S_r that is assumed to be at infinity. This surface does not vanish when anticausal or time-reversed wavefields are used (in this case we are using the conjugate or time-reversed pressure field), but it is not possible to have sources or measurements along this surface, hence its contribution is ignored. Evaluating Green's theorem with this choice of functions and boundary conditions, gives

$$2iA(\omega)\Im\left[P(\boldsymbol{x_a}|\boldsymbol{x_b}; \omega)\right] \approx \int_{S_0} \left[P(\boldsymbol{x_a}|\boldsymbol{x}; \omega)\boldsymbol{\nabla} P^-(\boldsymbol{x_b}|\boldsymbol{x}; \omega) - P^-(\boldsymbol{x_b}|\boldsymbol{x}; \omega)\boldsymbol{\nabla} P(\boldsymbol{x_a}|\boldsymbol{x}; \omega)\right] \cdot \boldsymbol{n}\ d\boldsymbol{s}, \tag{48}$$

where the sum is performed over source locations $\boldsymbol{x}$.

This equation is analogous to equation 29 derived in section 2.3. The differences are in the selected volume and surfaces taken into account and the location of the receivers. In virtual source method, the receivers are assumed to be below a complex overburden.

As in the traditional seismic interferometry, discussed in section 2.3, the wavefield's normal derivatives are assumed not to be available, and a one-way wave high frequency approximation is applied,

$$2iA(\omega)\Im\left[P(\boldsymbol{x_b}|\boldsymbol{x_a}; \omega)\right] \approx \int_{S_m} -2ik\ P(\boldsymbol{x}|\boldsymbol{x_a}; t)P^-(\boldsymbol{x}|\boldsymbol{x_b}; \omega)\ d\boldsymbol{x}. \tag{49}$$

The seismic interferometry equation is further approximated by assuming $\boldsymbol{\nabla} P \cdot \boldsymbol{n} \approx P$ and $\boldsymbol{\nabla} P^{-} \cdot \boldsymbol{n} \approx -P^{-}$, which results in

$$2iA(\omega)\Im\left[P(\boldsymbol{x_b}|\boldsymbol{x_a};\omega)\right] \approx \int_{S_m} P(\boldsymbol{x}|\boldsymbol{x_a};t)P^{-}(\boldsymbol{x}|\boldsymbol{x_b};\omega)\ d\boldsymbol{x}. \tag{50}$$

This equation is a compromise to Green's theorem, as explained by Korneev and Bakulin (2006). Hence, errors and artifacts are anticipated.

Using the virtual source method an approximate wavefield retrieval at the receiver level is achieved. In contrast to the more complete method (wavefield deconvolution), the overburden effects are not removed. In fact, an extra power of the source signature multiplies the retrieved wavefield. The advantage of the virtual source method is that it can be applied in the absence of the pressure field's normal derivative and an approximate wavefield is retrieved between two receivers located below a complex overburden. The synthesized wavefield will contain useful phase information.

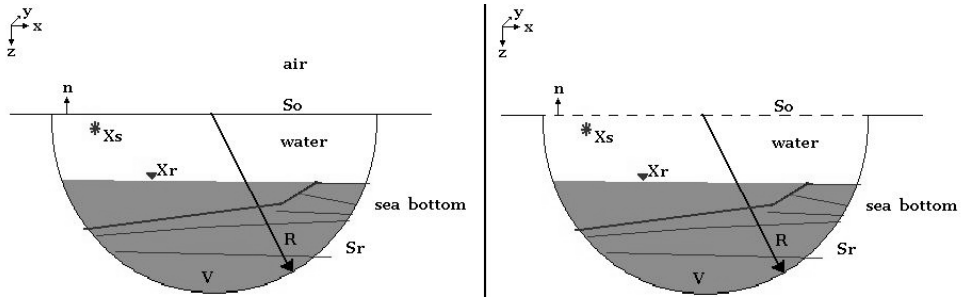

Figure 16: *Volumes used in wavefield deconvolution.*

Analysis

Certain choices of functions and boundary conditions in Green's theorem provide a formalism to avoid certain requirements and assumptions made by other methods and that are not always satisfied. When an assumption is not satisfied, the method can have shortcomings. For example, current seismic interferometry makes two assumptions. The consequence is the creation of artifacts. Direct wave seismic interferometry only make one approximation and its output is a clear improvement over current seismic interferometry. Using a two-surface Dirichlet boundary condition imposed upon the Green's function used in Green's theorem, a theory and algorithm for data reconstruction is derived without the need for the pressure field's normal derivative. There are no approximation and the only limitation to the theory comes from practical circumstances such as limited data. However, the method was tested with limited aperture data and it showed robustness. There is one extra limitation, though, the two-surface Dirichlet Green's function decays exponentially. Hence, the reconstruction is limited to distances within the range of $0 - 200m$ approximately. This is

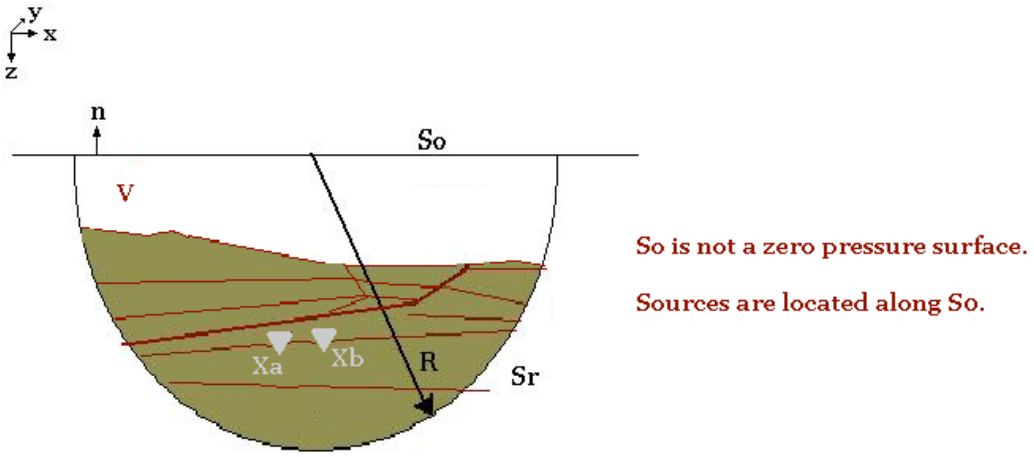

Figure 17: *Volume used in the virtual source method.*

considering the seismic processing standard single precision calculations. This theory also requires knowledge of the medium where the Green's function is calculated. It is ideal for marine surface seismic acquisitions, where pressure measurements exist within the water column. On the other hand, there are circumstances when Green's function with a two-surface Dirichlet boundary condition is not available (or it cannot be calculated analytically), but dual measurements exist. Such is the case of the wavefield deconvolution theory. Wavefield deconvolution removes all the overburden effects and retrieves coincident sources and receivers at the receiver location. The method was compared to the virtual source method, which is very similar to current seismic interferometry in the sense that it does not use the normal derivative of the pressure field, but a severe approximation.

Having a framework, allows us to review it and anticipate that things are not going to be as accurate as we would like when we make compromises to the theory. This knowledge provides the opportunity to correct the weaknesses (when possible) of any approximate method by going back to first principles and attempting to better satisfy the framework instead of trying to create new theory to correct the compromised output. With this understanding, Weglein et al. (2000) and Ramírez et al. (2007) proposed a method for seismic interferometry that overcomes the need for approximations. It requires only the pressure field at the measurement surface. It is exact if the scattered field is provided. Otherwise, an estimate of the wavelet would be necessary to decrease the occurrence of a small error in the synthesized wavefield.

Remarks

Most of the original, somewhat intuitive, interferometry methods were originally formulated to work on passive data (Schuster, 2001). The closed surface boundary was formed by sources (*i.e.* Earthquakes or ambient fluctuations) far away from the receivers (Shapiro and Campillo, 2004; Sabra et al., 2005; Larose et al., 2006). Wavefield crosscorrelations were applied to pairs of receiver

gathers and a noisy Green's function was retrieved from that passive data originally seen as noise. The theory that evolved from approximations to Green's theorem or to the principle of time reversal came later to explain what was being reconstructed with crosscorrelations. (Derode et al., 2003; Roux and Fink, 2003; Wapenaar et al., 2002; Weaver and Lobkis, 2004). New applications, analysis, and results were obtained along the way, *e.g.* the virtual source method (Bakulin and Calvert, 2004), VSP and WVSP applications (Schuster and Zhou, 2006; Otnes et al., 2006), connections with energy principles (Snieder et al., 2007), imaging, multiple removal, etc. Nowadays, seismic interferometry also considers the work by Claerbout (1968), which provided a formalism for wavefield reconstruction in horizontally layered media, as an early interferometric formulation. Lobkis and Weaver (2001) extended Claerbout's early theory to allow for a 3D heterogeneous media of nite extent (discrete frequency spectrum). Schuster (2001) gave the name *seismic interferometry* to all the processing tools that perform wave field reconstruction through correlation. Derode et al. (2003) and Roux and Fink (2003) proposed an alternative formulation for this technology using the principle of time reversal. Wapenaar et al. (2002) overcame the need for nite media with the one-way propagation representation theorem. Wapenaar (2004) and Weaver and Lobkis (2004) gave an equivalent formulation for seismic interferometry using high frequency and one-way wave approximations of the general representation theorem, which is a form of Green's Theorem.

On the side of Green's theorem, Weglein et al. (2000) proposed to use this mathematical theorem to retrieve the total two-way wavefield anywhere above a typical towed streamer using measurements of only the pressure field along the cables and imposing Dirichlet boundary conditions on the reference Green's function. This method does not make any approximations. Ramírez et al. (2007), (2007b) and Ramírez and Weglein (2007) showed that the foundations of interferometry and virtual source methods are found in Green's theorem, explained the so-called spurious multiples as errors produced by the approximations made by these methods, and extended those methods by proposing the use of specific Green's functions in Green's theorem that require less or no approximations to the framework. These more accurate formulations for Green's function or wavefield retrieval include the formulation originally proposed by Weglein et al. (2000) and successfully used by Zhang and Weglein (2005, 2006) to reconstruct the normal derivative of the pressure field (using only pressure measurements) and to subsequently perform pressure wavefield deghosting.

Conclusion

Green's theorem (equation 3) is the theoretical basis that unifies a broad class of interferometry approaches. This mathematical relation was derived by George Green in 1828 and has been widely used during the past and present century in all kind of applications including almost any processing step in seismic exploration (*e.g.* wavelet estimation, wavefield retrieval, imaging, wavefield deconvolution, etc.). The attention given by the energy industry and the literature to methods dealing with wavefield retrieval, or seismic interferometry, and its applications to different seismic exploration problems, has brought about a renewed interest in Green's theorem. The reason for this is that all the different approaches to what we call seismic interferometry can be derived from this single unifying framework: Green's theorem (and its extensions by Betti (1872) and Rayleigh (1873)).

Throughout this tutorial, Green's theorem was used to: 1) provide an overview of a broad set of seismic applications that recognize Green's theorem as the starting point of their theory and algorithms;
2) show that Green's theorem provides a platform and unifying principle for the field of seismic interferometry;
3) explain artifacts, or spurious multiples, (in certain interferometry approaches) as fully anticipated errors and as violations of the theory, rather than as some mystery or numerical manifestation that ought to be explained with physics; 4) provide a systematic approach to understanding, comparing and improving upon many current concepts, approximations and compromises.

In this tutorial, we presented a unifying framework for a broad class of interferometry techniques using Green's theorem. This framework and starting point serves several important purposes. One purpose and benefit is that much of what has been published as breakthrough new "interferometric principles" and "fundamental new theorems" and new "virtual sources" are really much less than profound new concepts and theories, but rather simply explained as approximate forms of Green's theorem. Furthermore artifacts observed and labeled as mysterious spurious multiples are neither mysterious nor spurious. They are simply errors in properly applying Green's theorem. That sounds a lot less impressive. Green's theorem and apparent inadvertent compromises that are violating Green's theorem in certain interferometric methods leads to those fully anticipated and precisely predicted errors. Hence, recognizing Green's theorem as a foundation allows errors and artifacts that occur in certain compromised interferometry approaches to be anticipated and fully explained as a consequence of approximations made within Green's theorem. Green's theorem provides a solid and classic mathematical-physics foundation, well understood in the literature, to also systematically, confidently and consistently step out from that cornerstone of clarity and clear derivation. With Green's theorem to point the way in this paper we develop a set of progressively improved and practical approximate interferometric methods, that are then tested and demonstrated with added-value and good effect in comparison with various standard interferometric forms and methods.

Appendix

High frequency and one-way wave approximation

The one-way and high frequency approximation proposed by Wapenaar (2004) to avoid the need of the pressure field's normal component could damage and change seriously the output of Green's theorem. This happens, for example, when we use Green's theorem with a causal reference Green's function, $\mathcal{G}_0^+$, and a measured pressure field, P, (section). If we use the approximation

$$\boldsymbol{\nabla} P(\boldsymbol{x}|\boldsymbol{x_a};\omega)] \cdot \boldsymbol{n} \approx ikP(\boldsymbol{x}|\boldsymbol{x_a};\omega) \tag{51}$$

in the surface integral required by Green's theorem, we find a zero result independent of the position of the source and observation point. This can be shown in a $1D$ situation, using equation 51 to approximate the normal derivative in the surface integral of Green's theorem, and a $1D$ reference Green's function for an experiment with a free surface,

$$\mathcal{G}^+(z|z_b,\omega) = \frac{e^{ik|z-z_b|}}{2ik} - \frac{e^{ik(z+z_b)}}{2ik}, \tag{52}$$

obtaining

$$\int_{S_m} [P(\boldsymbol{x}|\boldsymbol{x_a};\omega)\boldsymbol{\nabla}\mathcal{G}_0^+(\boldsymbol{x}|\boldsymbol{x_b};\omega) - \mathcal{G}_0^+(\boldsymbol{x}|\boldsymbol{x_b};\omega)\boldsymbol{\nabla}P(\boldsymbol{x}|\boldsymbol{x_a};\omega)] \cdot \boldsymbol{n}\ d\boldsymbol{s}$$
$$\approx \int_{S_m} [P(\boldsymbol{x}|\boldsymbol{x_a};\omega)\boldsymbol{\nabla}\mathcal{G}_0^+(\boldsymbol{x}|\boldsymbol{x_b};\omega) \cdot \boldsymbol{n} - \mathcal{G}_0^+(\boldsymbol{x}|\boldsymbol{x_b};\omega)ikP(\boldsymbol{x}|\boldsymbol{x_a};\omega)]\ d\boldsymbol{s}. \quad (53)$$

Evaluating the normal derivative of the reference Green's function with the approximation gives zero,

$$\int_{S_m} [P(\boldsymbol{x}|\boldsymbol{x_a};\omega)ik\mathcal{G}_0^+(\boldsymbol{x}|\boldsymbol{x_b};\omega) - \mathcal{G}_0^+(\boldsymbol{x}|\boldsymbol{x_b};\omega)ikP(\boldsymbol{x}|\boldsymbol{x_a};\omega)]\ d\boldsymbol{s} = 0, \quad (54)$$

independent of the positions $\boldsymbol{x_a}$ and $\boldsymbol{x_b}$ relative to the volume enclosed by S. Numerical tests in 3D also confirm this result.

Appendix

Seismic interferometry

The original equation derived by Wapenaar (2004) for seismic interferometry used the reciprocal experiment of the one presented in this dissertation. In their derivation, two receivers inside the volume were surrounded by sources at S. Using source-receiver reciprocity, the standard interferometry equation is

$$2i\Im\left[P(\boldsymbol{x_b}|\boldsymbol{x_a};\omega)\right] \approx \int_{S_m} -2ik\ P(\boldsymbol{x_a}|\boldsymbol{x};\omega)G^-(\boldsymbol{x_b}|\boldsymbol{x};\omega)\ d\boldsymbol{x}, \quad (55)$$

where $\boldsymbol{x_a}$ and $\boldsymbol{x_b}$ are receiver positions, and $\boldsymbol{x}$ corresponds to source positions at the surface S_m. To be consistent with the rest of this work, we will continue with the previous notation where $\boldsymbol{x_a}$ and $\boldsymbol{x_b}$ represent source locations and the surface integral is taken over receiver locations $\boldsymbol{x}$ at the measurement surface.

References

Amundsen, L. "The propagator matrix related to the Kirchhoff-Helmholtz integral in inverse wavefield extrapolation." *Geophysics* 59 (1994): 1902–1910.

Amundsen, L. "Elimination of free-surface related multiples without need of the source wavelet." *SEG Technical Program Expanded Abstracts* 18 (1999): 1064–1067.

Amundsen, L. "Elimination of free-surface related multiples without need of the source wavelet." *Geophysics* 66 (2001): 327–341.

Amundsen, L., B. Secrest, and B. Arnsten. "Extraction of the normal component of the particle velocity from marine pressure data." *Geophysics* 60 (1995): 212–222.

Amundsen, L., T. R. Sten, J. O. A. Robertsson, and E. Kragh. "Rough-sea deghosting of streamer data using pressure gradient approximations." *Geophysics* 50 (2005): 1–9.

Bakulin, A. and R. Calvert. "Virtual source: new method for imaging and 4D below complex overburden." *SEG Expanded Abstracts* 23 (2004): 2477–2480.

Betti, E. "Teoria dell'elasticitá: Il Nuovo Cimento." *Sezione 6* (1872): no. 7–8, 87–97.

Claerbout, J. F. "Synthesis of a layered medium from its acoustic transmission response.." *Geophysics* 33 (1968): 264–269.

Costain, J.K. and C. Coruh. *Basic Theory of Exploration Seismology*. Ed. Klaus Helbig and Sven Treitel. Volume 1 . Oxford, UK: Elsevier, 2004.

Derode, A., E. Larose, M. Tanter, J. de Rosny, a. Tourin, M. Campillo, and M. Fink. "Recovering the Green's function for a heterogeneous medium between two passive sensors? Application to acoustic waves." *Applied Physics Letter* 83 (2003): 3054–3056.

Draganov, D., K. A. Wapenaar, and J. Thorbecke. "Seismic interferometry: Reconstructing the Earth's reflection response." *Geophysics* 71 (2006): S161–S170.

Fokkema, J. T. and P. M. van den Berg. *Seismic applications of acoustic reciprocity*. New York: Elsevier Science Publ., 1993.

Green, G. *An essay on the application of mathematical analysis to the theories of electricity and magnetism*. Nottingham, London: privately published, 1828.

Guo, Z., A. B. Weglein, and T. H. Tan. "Using pressure data on the cable to estimate the seismic wavelet." *SEG Technical Program Expanded Abstracts* 24 (2005): 2390–2393.

Holvik, E. and L. Amundsen. "Elimination of the overburden response from multicomponent source and receiver seismic data, with source designature and decomposition into PP-, PS-, SP-, and SS-wave responses." *Geophysics* 70 (2005): S43–S59.

Johnston, Rodney and Anton Ziolkowski. "Benefits of source signature measurements for multiple removal in streamer and OBC data." *SEG Expanded Abstracts* 23 (1999): 1346–1349.

Kline, M. *Mathematical thought from ancient to modern times*. Bull. Amer. Math. Soc. - 80. New York: Oxford University Press, 1974.

Korneev, V. and A. Bakulin. "On the fundamentals of the virtual source method." *Geophysics* 71 (2006): A13–A17.

Larose, E., L. Margerin, A. Derode, B. van Tiggelen, M. Campillo, N. Shapiro, A. Paul, L. Stehly, and M. Tanter. "Correlation of random wavefields: An interdisciplinary review." *Geophysics* 71 (2006): SI11–SI21.

Lobkis, O. I. and R. L. Weaver. "On the emergence of the Green's function in the crosscorrelations of a diffuse field." *Journal of the Acoustic Society of America* 110 (2001): 3011–3017.

Morse, P. M. and H. Feshbach. *Methods of Theoretical Physics*. International Series in Pure and Applied Physics. (Div. of McGraw-Hill, Inc.): McGraw-Hill Book Co., 1953.

Osen, A., L. Amundsen, and B.G. Secrest. "Source signature estimation in the seismic experiment." *64th Ann. Internat. Mtg., Soc. Expl. Geophys., Expanded Abstracts* 13 (1994): 767–770.

Osen, A., B.G. Secrest, L. Amundsen, and A. Reitan. "Wavelet estimation from marine pressure measurements." *Geophysics* 63 (1998): 2108–2119.

Otnes, E., K. Hokstad, G. Rønholt, and S.-K. Foss. "Data-driven surface related multiple elimination on walkaway VSP data." *Extended Abstracts of the 68th Annual International Meeting of the EAGE* (2006).

Ramírez, A. C., K. Hokstad, and E. Otnes. "Data driven regularization/extrapolation." *EAGE 69^{th} Conference & Exhibition London, UK* (2007): B032.

Ramírez, A. C. and A. B. Weglein. "Remarks on Green's Theorem for seismic interferometry." *Technical Report, M-OSRP annual meeting.* 6 (2007): 15–39.

Ramírez, A. C. and A. B. Weglein. "Deriving, explicating, and extending interferometric methods using Green's theorem." *SEG Technical Program Expanded Abstracts* (2008): (Submitted).

Ramírez, A. C., A. B. Weglein, E. Otnes, and K. Hokstad. "The role of the direct wave and Green's Theorem in seismic interferometry and spurious multiples." *SEG Technical Program Expanded Abstracts* 26 (2007): 2471–2475.

Ramírez Pérez, A. C. *I.- Inverse scattering subserioes for removal of internal multiples and depth imaging primaries; II.- Green's theorem as the foundation of interferometry and guiding new practical methods and applications.* PhD thesis, University of Houston, Houston, Tx., USA, 2007.

Rayleigh, Lord. "Some general theorems related to vibrations." *Proc. Lond. Math. Soc.* 4 (1873): 366368.

Robinson, Enders A. and Sven Treitel. *Geophysical Signal Analysis*. NJ, USA: Prentice-Hall Signal Processing Seri, 1980.

Roux, P. and Fink. "Green's function estimation using secondary sources in a shallow water environment." *Journal of the Acoustic Society of America* 113 (2003): 1406–1416.

Sabra, K. G., P. Gerstoft, P. Roux, and W. A. Kuperman. "Extracting time-domain Green's function estimates from ambient seismic noise." *Geophysics Research Letters* 32, L03310 (2005): doi:10.1029/2004GL021862.

Schneider, W. A. "Integral formulation for migration in two-dimensions and three-dimensions." *Geophysics* 43 (1978): 4976.

Schuster, G. T. "Theory of daylight/interferometric imaging: tutorial." *Extended Abstracts of the 63rd Annual Meeting Conference and Exhibition, EAGE* A32 (2001).

Schuster, G. T. and M. Zhou. "A theoretical overview of model-based and correlation-based redatuming methods." *Geophysics* 4 (2006): SI103–SI110.

Schwinger, Julian. "The Greening of Quantum Field Theory: George and I." *University of California, Los Angeles*. 1993.

Shapiro, N. M. and M. Campillo. "Emergence of broadband Rayleigh waves from correlations of the ambient seismic noise." *Geophysics Research Letters* 31, L07614 (2004): doi10.1029/2004GL019491.

Snieder, R., K. Wapenaar, and K. Larner. "Spurious multiples in seismic interferometry of primaries." *Geophysics* 71 (2006): SI111–SI124.

Snieder, R., K. Wapenaar, and U. Wegler. "Unified Green's function retrieval by cross-correlation; connection with energy principles." *Physical review E* 75 (2007): 036103–1 – 036103–14.

Sommerfeld, A. *Optics*. New York: Academic Press, 1954.

Tan, T. H. *Source signature estimation*. Moscow, Russia: Presented at the Internat. Conf. and Expo. of Expl. and Development Geophys., 1992.

Tan, T. H. "Wavelet spectrum estimation." *Geophysics* 64 (1999): 1836–1846.

Vasconcelos, I. and R. Snieder. "Interferometric imaging by deconvolution: Theory and numerical examples." *SEG Technical Program Expanded Abstracts* 25 (2006): 2416–2420.

Visser, T. D., P. S. Carney, and E. Wolf. "Remarks on boundary conditions for scalar scattering." *Physics letters A* 249 (1998): 243–247.

Wapenaar, K. "Retrieving the elastodynamic Green's function of an arbitrary inhomogeneous medium by cross correlation." *Phys. Rev. Lett.* 93(25) (2004): 254301–1 –254301–4.

Wapenaar, K. "Seismic interferometry for passive and exploration data: Reconstruction of internal multiples." *SEG Expanded Abstracts* 25 (2006): 2981–2985.

Wapenaar, K., D. Draganov, J. Thorbecke, and J. Fokkema. "Theory of acoustic daylight imaging revisited." *72nd Annual International Meeting, SEG, Expanded Abstracts* 21 (2002): 2269–2272.

Wapenaar, K. and J. Fokkema. "Green's function representations for seismic interferometry." *Geophysics* 71 (2006): SI33–SI46.

Weaver, R. L. and O. I. Lobkis. "Diffuse fields in open systems and the emergence of the Green's function." *Journal of the Acoustic Society of America* 116 (2004): 2731–2734.

Weglein, A. B. and A. J. Devaney. "The inverse source problem in the presence of external sources." *Proc. SPIE* 1767 (1992): 170176.

Weglein, A. B. and B.G. Secrest. "Wavelet estimation for a multidimensional acoustic or elastic Earth." *Geophysics* 55 (1990): 1975–1989.

Weglein, A. B., T. H. Tan, S. A. Shaw, K. H. Matson, and D. J. Foster. "Prediction of the wavefield anywhere above an ordinary towed streamer: Application to source waveform estimation, demultiple, deghosting, data reconstruction and imaging." *70th Annual Internat. Mtg., Soc. Expl. Geophys., Expanded Abstracts* 19 (2000): 2413–2415.

Zhang, J. and A. B. Weglein. "Extinction theorem deghosting method using towed streamer pressure data: analysis of the receiver array effect on deghosting and subsequent free surface multiple removal." *SEG Expanded Abstracts* 24 (2005): 2095–2098.

Zhang, J. and A. B. Weglein. "Application of extinction theorem deghosting method on ocean bottom data." *SEG/New Orleans 2006 Expanded Abstracts* 25 (2006): 2674–2678.

Ziolkowski, A.M., D.B. Taylor, and R.G.K. Johnston. "Multiple wavefields: separating incident from scattered, up from down, and primaries from multiples." *8th Ann. Internat. Mtg., Soc. Expl. Geophys., Expanded Abstracts* 6 (1998): 1499–1502.

3D free-surface multiple elimination implementation project status

K. A. Innanen, S. A. Shaw[†]and A. B. Weglein
[†]ConocoPhillips

Abstract

We report on the ongoing 3D free-surface multiple elimination code implementation project. We are at the stage of testing and validation of the code. The effort has been collaborative, involving data used by permission from WesternGeco and Statoil-Hydro and Lawrence Livermore National Lab, and computing knowledge and resources from ConocoPhillips.

Background

In 2006 an early-stage 3D implementation of the free-surface multiple elimination algorithm (Carvalho, 1992; Weglein et al., 1997), was written by Sam Kaplan, extending the previous M-OSRP 2D implementation (Kaplan et al., 2005). Through a set of collaborative efforts, we are in the process of validating and testing the code in preparation for distribution to the sponsors. In aid of this effort, WesternGeco, through Bill Dragoset, has facilitated our use of a 3D synthetic data set co-owned by Statoil-Hydro and Lawrence Livermore National Lab to be used in the validation and testing. ConocoPhillips, through Paul Valasek, Brian Macy and Phil Anno, has put computing knowledge and resources to the testing and validation. We have benefited greatly from, and are very grateful for, the efforts that have been expended in this ongoing project.

Status and plan

When its pre-requisites are in place, the free-surface multiple elimination (FSME) algorithm predicts the exact phase and amplitude of all orders of free-surface multiple in 3D seismic reflection data (Weglein et al., 1997). If the data contain ghosts or the source wavelet, the phase of the predicted multiples will be correct, but the amplitudes will be affected. The synthetic data set, meanwhile, is 2.5D, meaning it is constructed with point sources and point receivers placed above a medium that is invariant in one lateral dimension. As such, it contains 3D multiples, but we point out that with a specific re-sorting of the data that simulates sail lines at an angle to the subsurface variations, the "3D-ness" of these multiples can be greatly enhanced. Finally, the data contain ghosts and a source wavelet.

These facts lead to a natural hierarchy of testing and validation goals. Arranged in order of increasing ambition:

1. Leaving the data in its current (actual) geometry and leaving the wavelet and ghosts in the data, demonstrate the correct prediction of the phase of the 2.5D multiples.

2. Simulating sail lines at an angle to the subsurface variations, and leaving the wavelet and ghosts intact, demonstrate the correct prediction of the phase of the "maximally 3D" multiples.

3. Leaving the data in its current (actual) geometry and removing the wavelet and ghosts, demonstrate the correct prediction of the phase and amplitude of the first-order multiples.

4. Simulating sail lines at an angle to the subsurface variations, and removing the wavelet and ghosts, demonstrate the correct prediction of the phase and amplitude of the first-order "maximally 3D" multiples.

We are currently completing item 1. above. A small example follows. In Figure 1 we illustrate some receiver lines extracted from the full synthetic data set. For each shot location we extract a patch of receivers (72 in the in-line dimension, by 3 in the cross-line dimension). We repeat this for a patch of shots (72 in the in-line dimension, by 3 in the cross-line dimension). The cross-line sampling is 12.5m, and the in-line sampling is 25m. In Figure 2 we illustrate the corresponding predictions. In Figure 3 we illustrate side-by-side detail. The small but noticeable time difference between the predicted and the actual is a consequence of the wavelet.

This is a tentative confirmation of goal 1; we have encountered some issues as the size of the extracted data grows, related to the parallel (MPI) sorting component of the code. A larger, more complete data set will be tested subsequently to complete this phase.

References

Carvalho, P. M. *Free-surface multiple reflection elimination method based on nonlinear inversion of seismic data*. PhD thesis, Universidade Federal da Bahia, 1992.

Kaplan, S. T., K. A. Innanen, and A. B. Weglein. "Updates to M-OSRP internal and free surface multiple coding projects." *Mission-Oriented Seismic Research Program (M-OSRP) Annual Report*. 2005.

Weglein, A. B., F. A. Gasparotto, P. M. Carvalho, and R. H. Stolt. "An Inverse-Scattering Series Method for Attenuating Multiples in Seismic Reflection Data." *Geophysics* 62 (November-December 1997): 1975–1989.

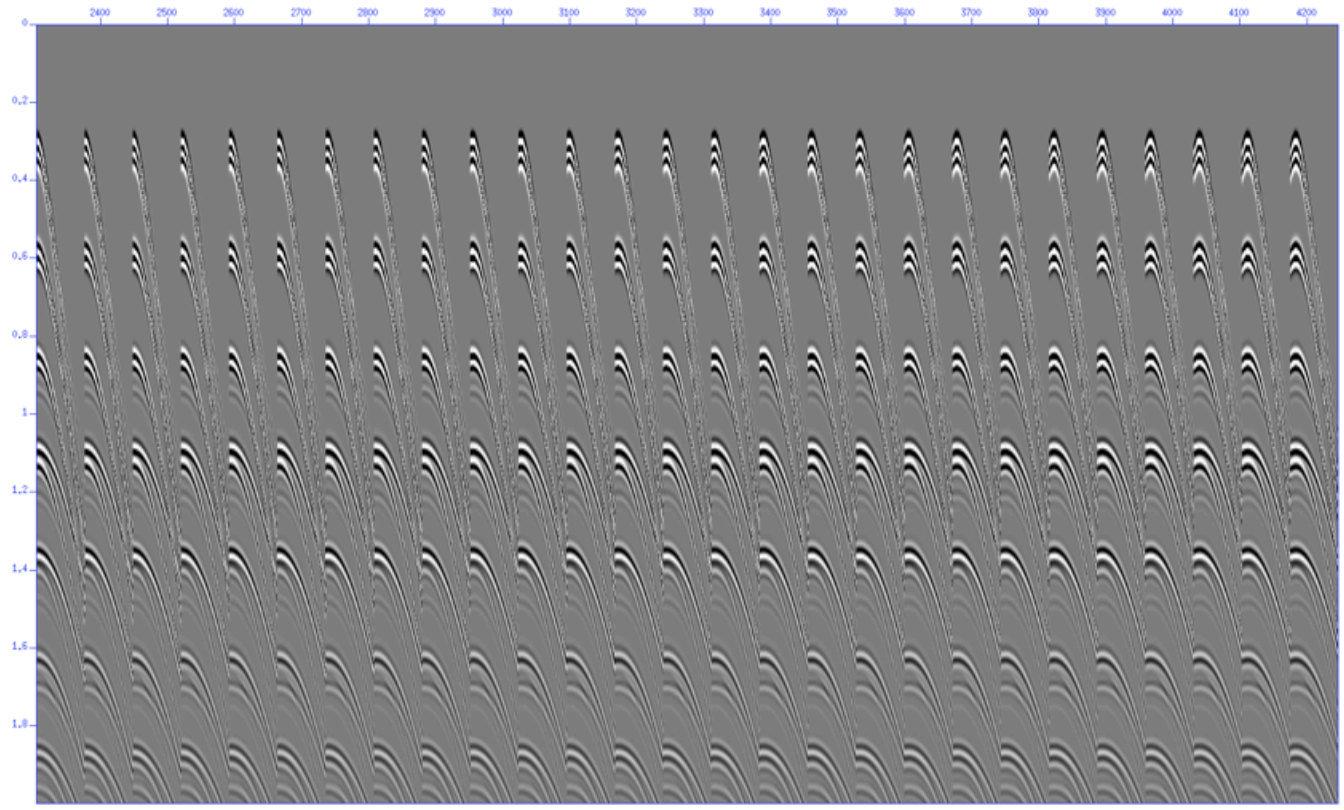

Figure 1: *Extraction from the synthetic data set.*

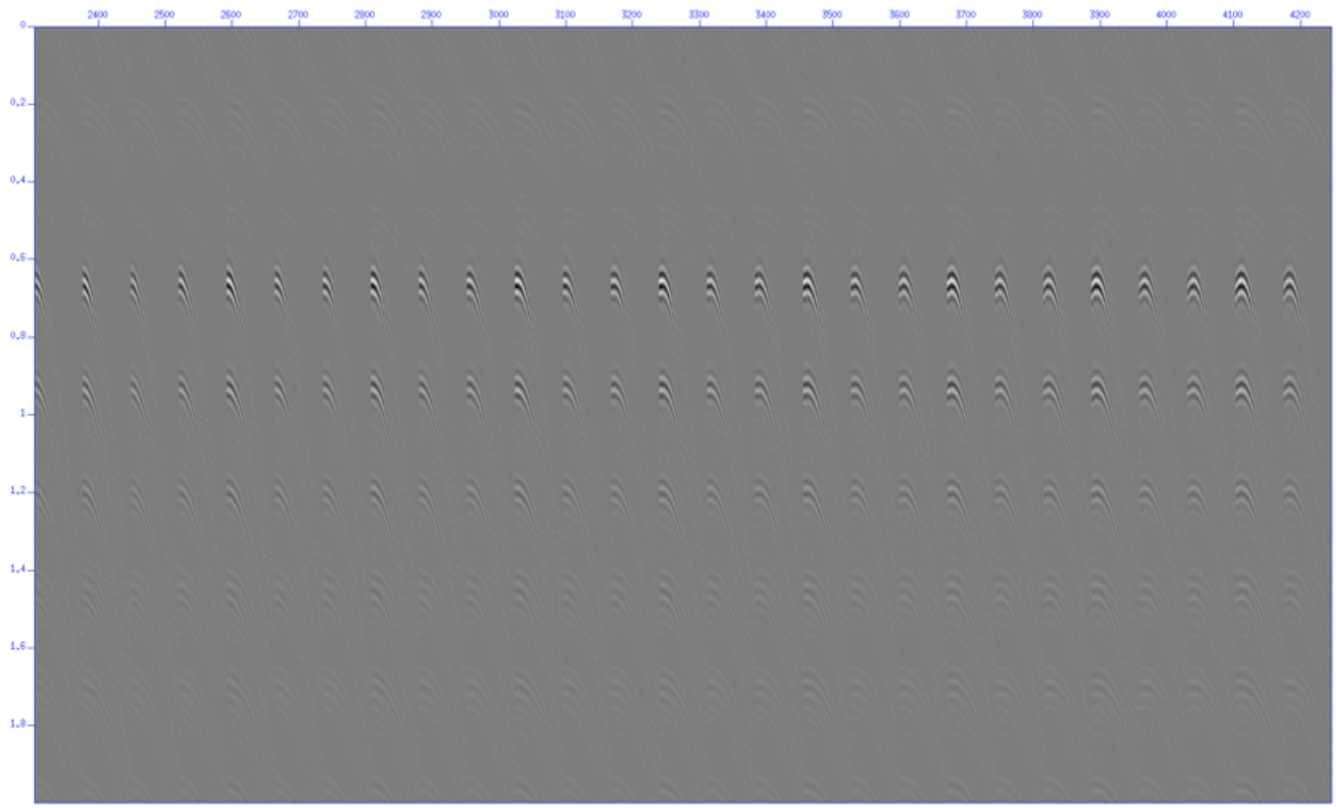

Figure 2: *Prediction result.*

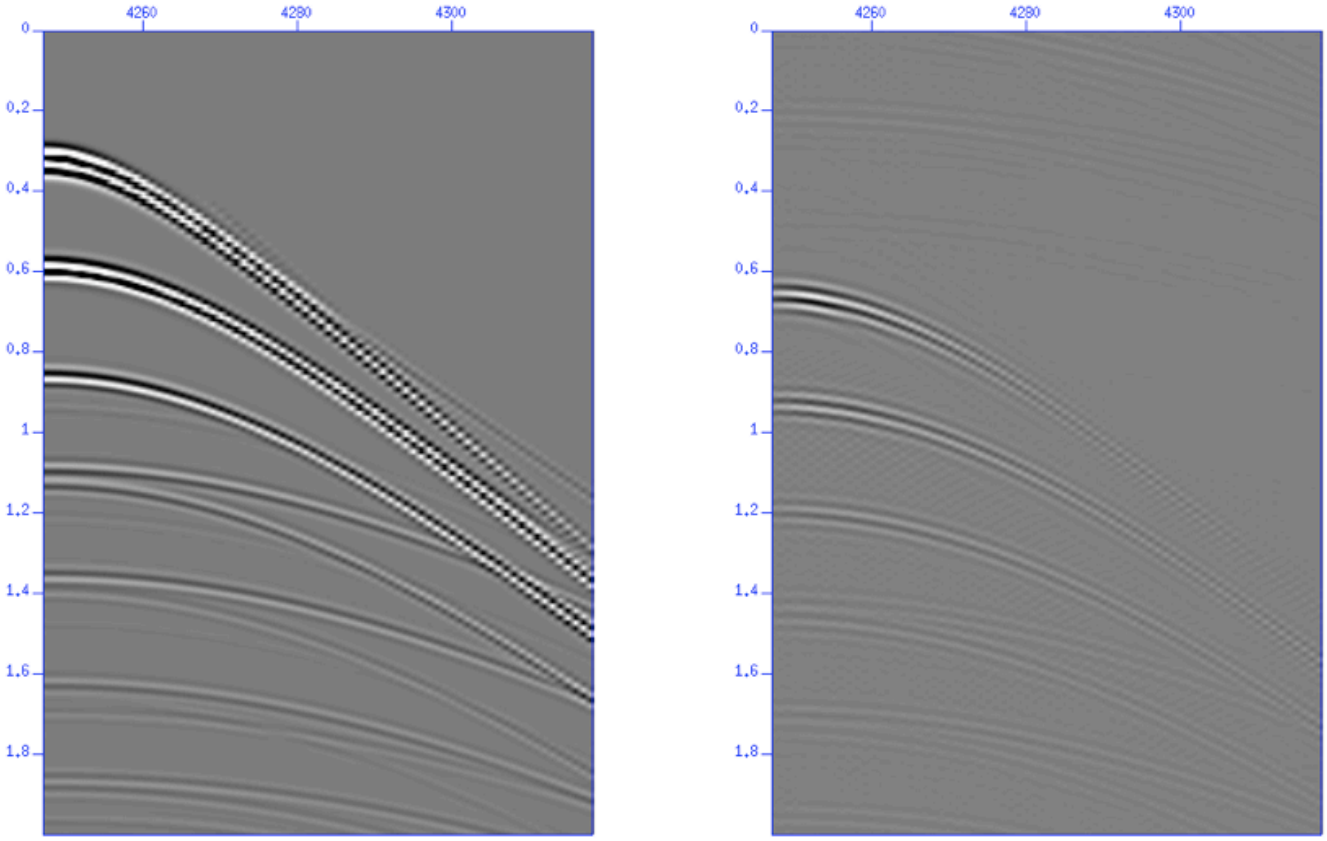

Figure 3: *Comparison of synthetic data and prediction.*

A framework for correction of reflected seismic primary amplitudes for transmission through an unknown overburden using internal multiples

J. E. Lira, K. A. Innanen, A. B. Weglein and A. C. Ramírez[†]
[†]Presently at WesternGeco

Abstract

Primaries are the main source of subsurface information in seismic exploration. The ability to estimate and remove overburden transmission effects on these events determines the level of realistic ambition in extracting such information concerning the target reflection at depth. In this paper we address this primary amplitude correction problem, using internal multiples. The inverse scattering series internal multiple attenuation algorithm suppresses internal multiples to within an amplitude error that is determined by plane wave transmission losses down to, and across, the reflector where the first order internal multiple experiences its downward reflection. This may be exploited to remove those overburden transmission effects; the impact is particularly striking for absorptive media. We demonstrate the construction of primary amplitude correction operators using combinations of multiples and their respective predictions with simple synthetic examples. We identify fundamental research into the amplitudes of the internal multiple predictions in 2D and 3D media as a pre-requisite to field data application of this concept-level algorithm.

1 Introduction

A primary is a recorded seismic event with one upward reflection. This event is considered the source of subsurface information for structural mapping, parameter estimation, and, ultimately, petroleum delineation at the target. In all current leading-edge processing of primaries, the ability to infer useful information at depth critically depends upon the ability to estimate and to remove the effect of the overburden on the character of the wave during propagation. The ability to effectively estimate (and remove) these effects determines the level of realistic ambition in subsequent processing of primaries. In this paper we propose an approach to this problem that involves the prediction and attenuation of internal multiples.

The problem we address is conceptually straightforward. Most primaries of interest (Figure 1) have amplitudes characterized by both the contrast in material properties at the point of reflection (via the reflection coefficient), and the downward and upward legs of propagation through the overburden. Roughly put:

$$\text{Primary} = [\text{Transmission Down}] \times [\text{Reflection}] \times [\text{Transmission Up}].$$

Methods for determination of material properties at depth (via, e.g., some form of AVO analysis) are helped by the former and hindered by the latter. We seek a corrective operator,

$$\text{Corrective Operator} = ([\text{Transmission Down}] \times [\text{Transmission Up}])^{-1},$$

such that, when it is applied to the raw primary, leaves only the local reflection coefficient intact, and prepares the event for further inverse processing:

$$\text{Corrected Primary} = [\text{Reflection}].$$

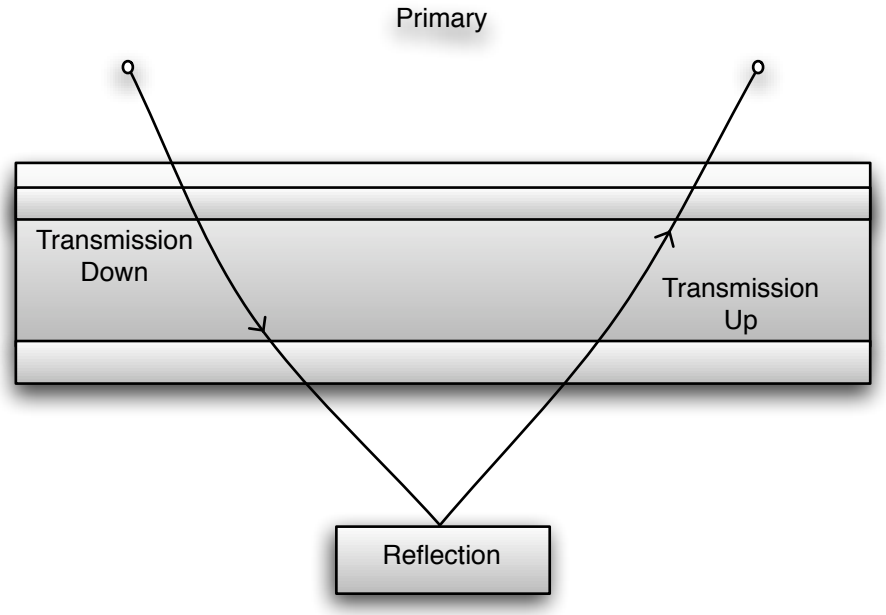

Figure 1: *Sketch of a primary. Amplitudes are determined by the material property contrast at the point of reflection, and propagation down and back through the overburden.*

We will provide a framework for determining such operators using an algorithm for the attenuation of multiples. The inverse scattering series has provided a set of algorithms for the removal of all orders of free-surface and internal multiples (Weglein et al., 1997, 2003). Within the overall class of events referred to as internal multiples, events are further catalogued by order, i.e., the number of downward reflections experienced. The algorithm of Araújo (1994) and Weglein et al. (1997) is a series for the attenuation of all orders of internal multiples, the first term of which attenuates the first-order event. It is to this first term that we direct our current attention. In practice, this component of the full algorithm has often been fully adequate. However, there are occasions when an elimination rather than attenuation algorithm would provide distinct added value. Ramirez and Weglein (2005a) have provided a closed-form *elimination* algorithm for the first-order internal multiple to fill this requirement. Concurrently the algorithm has been refined (Nita et al., 2004) and efficiently implemented in multiple dimensions for large data sets (Kaplan et al., 2005). These two algorithms (attenuation and elimination), and the known properties of the former (Weglein et al., 1997; Weglein and Matson, 1998; Ramirez and Weglein, 2005b), may be exploited to address the problem we have posed above.

The key is that the amplitude discrepancy between the actual first-order internal multiple and the output of the attenuator is a direct expression of plane wave transmission loss down to and across a particular reflector. The information provided by the internal multiple algorithm is, in fact, inherently a correcting factor for certain primaries associated with that reflector. The logical development in this paper is entirely geared towards performing the slight manipulations necessary to carry out the correction. The results are particularly striking if the overburden corrupting the amplitude of the primary in question is absorptive.

Let us be more specific about the motivation for pursuing an amplitude corrector of this kind. The ambitious goal of separation and extraction of a well-located and accurate angle-dependent reflection coefficient at depth is typically hindered by the experience of the primary wavefield as it propagates through an unknown overburden, which conceals the event with spurious amplitude changes. Contemporary methodologies to counter these effects are generally inconsistent with wave theoretic processing, and rarely go forward without a well-tie. There are additional potential benefits. First, the information is a byproduct of an existing part of the wave-theoretic processing flow–the de-multiple phase–and comes at no additional cost. Second, this information becomes available at a convenient point during processing, just prior to its likely use in primary processing/inversion. Third, it is consistent with wave-theoretic processing. Fourth, it is not restricted to a production setting, but is also applicable in reconnaissance and exploration settings.

This paper presents and illustrates these concepts in the following way. In Section 2, we review the internal multiple attenuation algorithm, and the existing results characterizing the amplitude of the prediction, and extend those results to incorporate absorptive media. In Section 3 we manipulate these expressions of the prediction error, demonstrating that, when combined recursively, they produce correction operators of the kind we describe, ready for multiplicative application to specific primaries, which will have to be separated out in the data. In particular we distinguish between the correction procedures necessary in acoustic/elastic vs. absorptive media. In Section 4 we illustrate the procedure on synthetic data for the absorptive case, examining the form and effect of the correction operators. Finally we conclude with remarks on a path forward for making this conceptual approach practical.

2 Amplitudes predicted by the multiple attenuation algorithm

The inverse scattering series internal multiple attenuation algorithm (IMAA) (Araujo et al., 1994; Araújo, 1994; Weglein et al., 1997, 2003) acts non-linearly on reflection seismic data to calculate the exact phase and approximate amplitude of all orders of internal multiples:

$$\begin{aligned} b_{3IM}(k_g,k_s,q_g+q_s) &= \frac{1}{(2\pi)^2}\int_{-\infty}^{\infty}dk_1 e^{-iq_1(z_g-z_s)}\int_{-\infty}^{\infty}dk_2 e^{iq_2(z_g-z_s)} \\ &\times \left[\int_{-\infty}^{\infty}dz_1' b_1(k_g,k_1,z_1')e^{i(q_g+q_1)z_1'}\right. \\ &\times \left.\int_{-\infty}^{z_1'-\epsilon}dz_2' b_1(k_1,k_2,z_2')e^{-i(q_1+q_2)z_2'}\right. \end{aligned}$$

$$\times \quad \int_{z_2'+\epsilon}^{\infty} dz_3' b_1(k_2, k_s, z_3') e^{i(q_2+q_s)z_3'} \Bigg], \tag{1}$$

where $q_g = \text{sgn}(\omega)\sqrt{(\frac{\omega}{c_0})^2 - (k_g)^2}$, $q_s = \text{sgn}(\omega)\sqrt{(\frac{\omega}{c_0})^2 - (k_s)^2}$, k_g and k_s are the horizontal wavenumbers conjugate to receiver and source coordinates (x_g, x_s), and ϵ is a small positive quantity. The input for the IMAA is b_1, which is created from the pre-stack reflection seismic data. It is constructed as follows. The surface recorded data, deghosted and without free surface multiples, $D(x_g, x_s, t)$, is Fourier transformed over all variables, to produce $D(k_g, k_s, \omega)$. A change of variables is made, to $D(k_g, k_s, q_g + q_s)$, after which b_1 is defined as $b_1(k_g, k_s, q_g + q_s) = D(k_g, k_s, q_g + q_s)(2iq_s)^{-1}$, and inverse Fourier transformed over $q_g + q_s$ to pseudo-depth. The result, $b_1(k_g, k_s, z)$, is used as input in equation (1), and the output, b_{3IM}, is the predicted internal multiple data set, produced without knowledge of earth material properties or structure and it accommodating all earth model types that satisfy the convolutional model (Ramirez and Weglein, 2005b).

2.1 The relationship between the predicted and the actual multiple amplitude

Weglein and Matson (1998) and Ramirez and Weglein (2005b) examined the difference between the actual amplitudes of internal multiples and those of the IMAA predictions. This discrepancy, which the latter authors described in terms of an *amplitude factor*, is related to the transmission coefficients down to and across the multiple generator interface, and can be understood intuitively by considering the way the algorithm predicts multiples. Consider Figure 2. On the left panel we sketch an internal multiple and the three primaries that are used in the algorithm to predict it. The generator is interface 2. The multiple has the path $abcdijkl$. The algorithm predicts the multiple by multiplying the amplitudes of the three primaries, adding the phases of the deeper two, $abcdef$ and $ghijkl$, and subtracting the phase of the shallower, $ghef$. The phase of the actual multiple and the predicted multiple are therefore identical. However, the amplitude of the actual multiple,

$$T_{ab}T_{bc}R_{cd}(-R_{he})R_{ij}T_{jk}T_{kl},$$

and the multiplied amplitudes of the primaries in the prediction,

$$[T_{ab}T_{bc}R_{cd}T_{de}T_{ef}] \times [T_{gh}R_{he}T_{ef}] \times [T_{gh}T_{hi}R_{ij}T_{jk}T_{kl}],$$

clearly differ in that the actual multiple does not experience the transmission history of the shallower primary. That is, the terms T_{de}, T_{ef}, T_{gh}, T_{hi} in the prediction are extraneous. We note that this includes transmission across the generating interface. This is the source of the amplitude error in the algorithm.

Let us next depart from schematics and consider the general accounting of this behavior for predicted multiples within an arbitrary stack of layers by Ramirez and Weglein (2005b). Figure 3 shows a 1-D acoustic model consisting of three reflectors, the lower two of which have associated reflection coefficients R_1 and R_2, and layer velocities c_0, c_1 and c_2. The transmission coefficient from layer i to layer j is T_{ij}. For example, a multiple generated at interface 1 in Figure 3 has an amplitude

$$M_1 = [T_{01}T_{12}R_2(-R_1)R_2T_{21}T_{10}]. \tag{2}$$

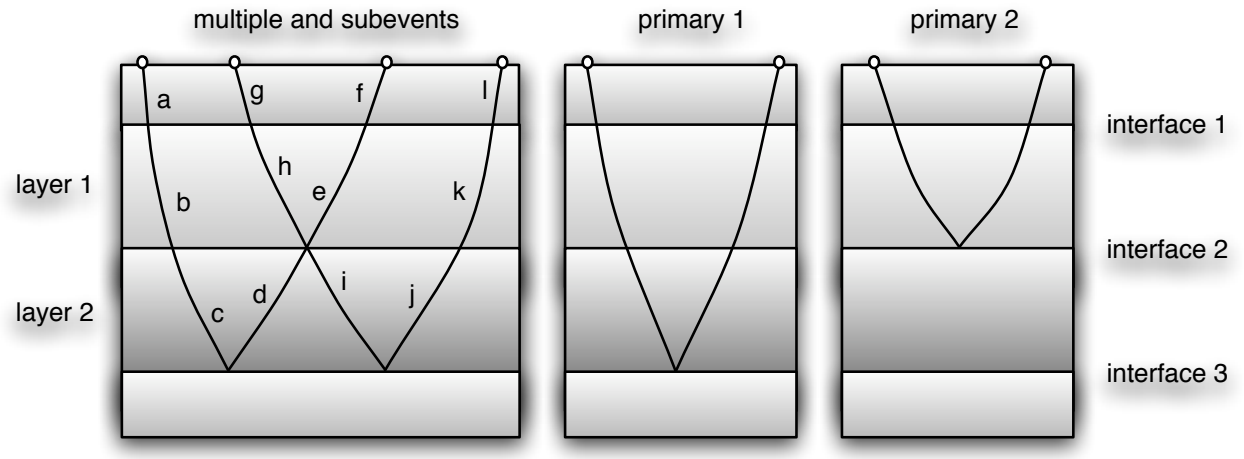

Figure 2: *Schematic diagram of primaries and internal multiples in a stratified medium. Left panel: an internal multiple and the primary subevents used to predict it. Middle and right panels: associated primaries whose amplitudes may be corrected using the discrepancy between the amplitudes of the predicted and actual multiple on the right.*

The predicted multiple amplitude is:

$$M_1^{\mathrm{PRED}} = [T_{01}T_{12}R_2(-R_1)R_2T_{21}T_{10}][(T_{01}T_{10})^2(T_{12}T_{21})]. \tag{3}$$

Comparing equations (2) and (3) we see that their ratio, as we now intuitively expect, carries information about the transmission coefficients down to and across the multiple generator interface. Ramirez and Weglein (2005b) refer to this ratio as the amplitude factor AF:

$$\mathrm{AF}_2 = \frac{M_1^{\mathrm{PRED}}}{M_1} = [T_{01}T_{10}]^2[T_{12}T_{21}]. \tag{4}$$

The index 2 anticipates our later use of this factor for corrective purposes, and signifies that the second interface is the generator. With this terminology the amplitude factor expressing the discrepancy between the predicted and actual amplitudes of an internal multiple generated at the j'th interface in a stack of layers is

$$\mathrm{AF}_j = \begin{cases} T_{01}T_{10} & \text{for j=1;} \\ \prod_{i=1}^{j-1}(T_{i,i-1}^2T_{i-1,i}^2)T_{j,j-1}T_{j-1,j} & \text{for } 1 < j < J, \end{cases} \tag{5}$$

where J is the total number of interfaces in the model. Presently we will manipulate this factor to become a correction operator for primary amplitudes.

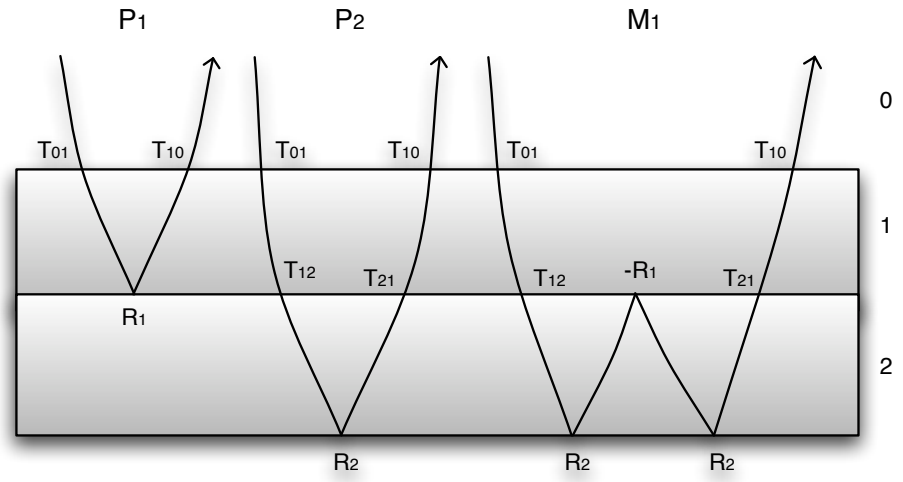

Figure 3: *A further multiple and subevent schematic suitable for general description of the amplitude properties of the internal multiple attenuation algorithm.*

2.2 Extension of the amplitude analysis to absorptive media

Ramirez and Weglein (2005b) assume an acoustic medium, in which plane-wave transmission losses are local, occurring at the point at which the wave crosses a contrast in material properties. For an absorptive stack of layers, in which transmission loss occurs over the entire course of propagation, a slight extension of their results is required. In later sections we will see that this minor theoretical alteration leads to major practical differences when the predicted-actual amplitude discrepancy is exploited.

In order to study the transmission coefficients in an anelastic medium we select an intrinsic attenuation model to describe amplitude and phase alterations in a wave due to friction. These alterations are modeled by a generalization of the wavefield phase velocity to a complex, frequency-dependent quantity parameterized in terms of Q. A reasonably well-accepted Q model (Aki and Richards, 2002) alters the scalar propagation constant of the j'th layer, $k_j = \omega/c_j(z)$, to

$$k_j = \frac{\omega}{c_j(z)}\left[1 + \frac{F(\omega)}{Q_j(z)}\right], \tag{6}$$

where $F(\omega) = \frac{i}{2} - \frac{1}{\pi}\log(\omega/\omega_0)$. The reference frequency ω_0 may be considered a parameter to be estimated, or assumed to be the largest frequency available to a given experiment. The model divides propagation into three parts: a propagation component, an attenuation component, and a dispersion component.

With this new definition of k_j, and assuming that in Figure 3 the two bottom layers are anelastic, we again construct the prediction. It is convenient to re-define the transmission coefficient of a given interface to incorporate absorptive amplitude loss within the layer *above* that interface. For

instance, the coefficients T_{12} and T_{21} of the previous section are altered to become

$$\mathcal{T}_{12} = \left[\frac{2c_2 \left(1 + \frac{F(\omega)}{Q_2}\right)^{-1}}{c_1 \left(1 + \frac{F(\omega)}{Q_1}\right)^{-1} + c_2 \left(1 + \frac{F(\omega)}{Q_2}\right)^{-1}} \right] \overbrace{e^{-\frac{\omega}{2Q_1 c_1}(z_1 - z_0)}}^{Q \text{ in overlying layer}} e^{\frac{i\omega}{\pi Q_1 c_1} \log(\frac{\omega}{\omega_0})(z_1 - z_0)} \tag{7}$$

$$\mathcal{T}_{21} = \left[\frac{2c_1 \left(1 + \frac{F(\omega)}{Q_1}\right)^{-1}}{c_2 \left(1 + \frac{F(\omega)}{Q_2}\right)^{-1} + c_1 \left(1 + \frac{F(\omega)}{Q_1}\right)^{-1}} \right] \underbrace{e^{-\frac{\omega}{2Q_1 c_1}(z_1 - z_0)}}_{Q \text{ in overlying layer}} e^{\frac{i\omega}{\pi Q_1 c_1} \log(\frac{\omega}{\omega_0})(z_1 - z_0)}. \tag{8}$$

We make particular note of the dependence (via the attenuation component) of this definition of transmission coefficients on the thickness of the layer *overlying* the interface in question.

With this extension, we have essentially the same amplitude factor, for instance AF_2, in the anelastic case as we did in the elastic case. By analogy with equation (4):

$$\mathrm{AF}_2 = [T_{01} T_{10}]^2 \mathcal{T}_{12} \mathcal{T}_{21}. \tag{9}$$

Provided that this re-definition of the absorptive transmission coefficients is adopted, the amplitude factors and internal multiple attenuation error analysis for the general absorptive stack of layers at normal incidence is given again by equation (5).

3 Correction of primary amplitudes using internal multiples

Let us make two comments about the amplitude error analysis above. First, we see that the discrepancy between the predicted and the actual multiple for a given generator is directly related to the transmission losses experienced by a primary associated with that generator. Second, we note that the discrepancy, characterized by the amplitude factor AF, is available directly from the data and the output of the IMAA. In this section we use the information in the various AF factors as a direct means to correct the amplitude of the primary associated with the generator for transmission effects, in the sense we have put forward in the introduction.

Next we define what will become the primary correction operator, PCO, to be built recursively from the data-determined AFs:

$$\mathrm{PCO}_n \equiv \frac{\mathrm{PCO}_{n-1}}{\mathrm{AF}_n}, \tag{10}$$

with the terminating definition

$$\mathrm{PCO}_0 = 1. \tag{11}$$

Expanding this operator over several orders n clarifies that it will indeed act as a correction operator when applied to a primary whose upward reflection has occurred near the n'th interface. We find that *precisely which* primary is best corrected with the n'th operator depends on whether we believe the medium is or is not absorptive. In delineating this, we find it useful to index primaries from 0 upward. In the scheme in Figure 2, the 0'th primary reflects upward at interface 1.

3.1 Correction of primaries in acoustic/elastic media

Consider once again the multiple sketched in Figure 2, whose generator is interface 2. Setting $n = 2$, expanding equation (10), and employing the alphabetical indices we used in the figure, we have

$$\mathrm{PCO}_2 = \frac{1}{T_{gh}T_{hi}T_{de}T_{ef}}. \tag{12}$$

If the medium is acoustic/elastic, we note that for the primary depicted in the middle panel of Figure 2, the last overburden effect on the event before the reflection at interface 3 is the transmission through interface 2, and the first overburden effect on the event after the reflection is again transmission through interface 2. Consequently, PCO_2 is exactly appropriate as an operator to correct this (middle panel of Figure 2) primary. More generally, in the acoustic/elastic case, the operator PCO_n in equation (10) corrects the n'th primary, leaving the n'th reflection coefficient "bare", and suitable as input to other inverse procedures:

$$R_n = \mathrm{PCO}_n \times P_n. \tag{13}$$

3.2 Correction of primaries in absorptive media

Next, let us suppose that the medium in Figure 2 is absorptive, and again consider PCO_2. Recall that we may maintain the same form for the amplitude discrepancy between predicted and actual multiples in absorptive media, and thereby this operator PCO_2, provided we alter the transmission coefficients of a given interface to include absorptive propagation through the layer *above* that interface.

With this arrangement PCO_2 is evidently no longer appropriate as an operator to correct primary 2, i.e., the primary depicted in the middle panel of Figure 2, because it does not account for absorptive propagation through the layer between the reflection and the multiple generator.

To maintain the usefulness of the operator, we instead make an approximation. We state that in an absorptive medium, the effect of the local transmission coefficient at a boundary on the amplitude of a primary is dwarfed by the effect of absorptive propagation. With that assumption we may simply change the primary being corrected by PCO_2 to the one depicted in the right panel of Figure 2. This statement is true to within the combined local transmission coefficient down and up across interface 2. More generally, in the absorptive case, the (now frequency-dependent) operator PCO_n in equation (10) corrects the $n-1$'th primary:

$$R_{n-1}(\omega) = \mathrm{PCO}_n(\omega) \times P_{n-1}(\omega). \tag{14}$$

4 Synthetic examples

In this section, we illustrate with simple synthetic examples the steps necessary to correct a primary for absorptive transmission losses, using a multiple and the IMA algorithm prediction. We generate

zero-offset traces from three layered models with the geometry of the model in Figure 3, assuming the waves behave in accordance with the propagation constant in equation (6), and using layer parameter values in Table 1. We include the two primaries and the first order internal multiple. The traces are wavelet deconvolved, and bandlimited (3–50 Hz). Figure 4 shows the traces generated for each model, which differ in their Q values, ranging from relatively low attenuation to relatively high attenuation. The arrival times of the two primaries and the multiple are approximately 1.5s, 2.3s and 2.9s, respectively.

Depth (m)	c (m/s)	Q_1	Q_2	Q_3
000-300	1500	∞	∞	∞
300-480	2200	200	100	50
480-855	2800	100	50	25
855-∞	3300	50	25	10

Table 1. *Absorptive Earth models.*

With the knowledge that the medium is absorptive, and in accordance with our arguments in the previous section, we use the predicted multiples to correct the amplitude of the shallower primary. We do so as follows.

1. We use each trace as input to the internal multiple attenuation algorithm, generating predictions of the internal multiples.
2. We isolate and calculate the spectra of each internal multiple and its prediction.
3. We take the reciprocal of the ratio between the spectra of each internal multiple and its prediction. By equation (10), this is the appropriate correction operator PCO.
4. We isolate the shallower primary, and apply the operator to its spectrum of the primary.

We compare the result to an equivalent primary which we model in the absence of all transmission through the overburden.

Figure 5 illustrates the uncorrected, shallower primary from each of the three models. We predict the multiple with the attenuation algorithm, and isolate both this prediction and the original multiple from the trace, and compute their spectra (Figure 6). The prediction spectra evidently have experienced a greater level of attenuation in comparison to the actual multiple spectra. This is in agreement with the extra transmission paths involved in the prediction, as discussed above, and the frequency dependence of this discrepancy will form the basis for the correction of the shallower primary, which will have a distinct Q-compensation flavor. Figure 7 illustrates the spectra of the primary correction operators derived from these quantities, and Figure 8 illustrates the spectra of the shallower primaries for each model, before and after the correction. The recovery of high frequencies is notable. In Figure 9, we illustrate the corrected primaries after inverse Fourier transforming to the time domain, and compare the results against their idealized counterparts constructed without transmission losses. Figures 10 to 12 illustrate in close succession the original primary in the data (top panel), the corrected primary (middle panel) and the idealized primary

(bottom panel), for all models. We point out that the discrepancy between the corrected primaries and idealized primaries is of a form and magnitude expected given the approximation associated with correcting primaries in an absorptive medium (Section 3).

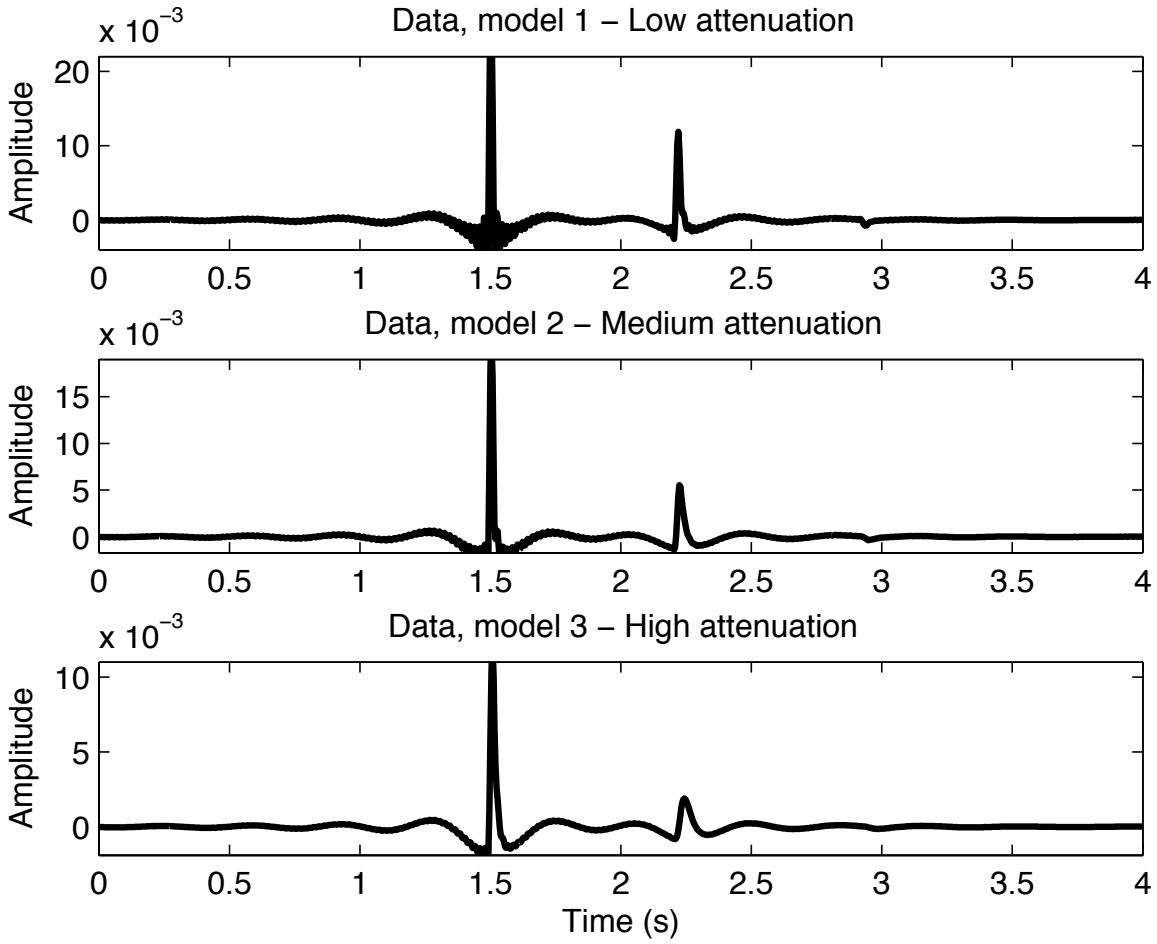

Figure 4: *Data generated for the numerical tests comprised of two primaries and one multiple for all models.*

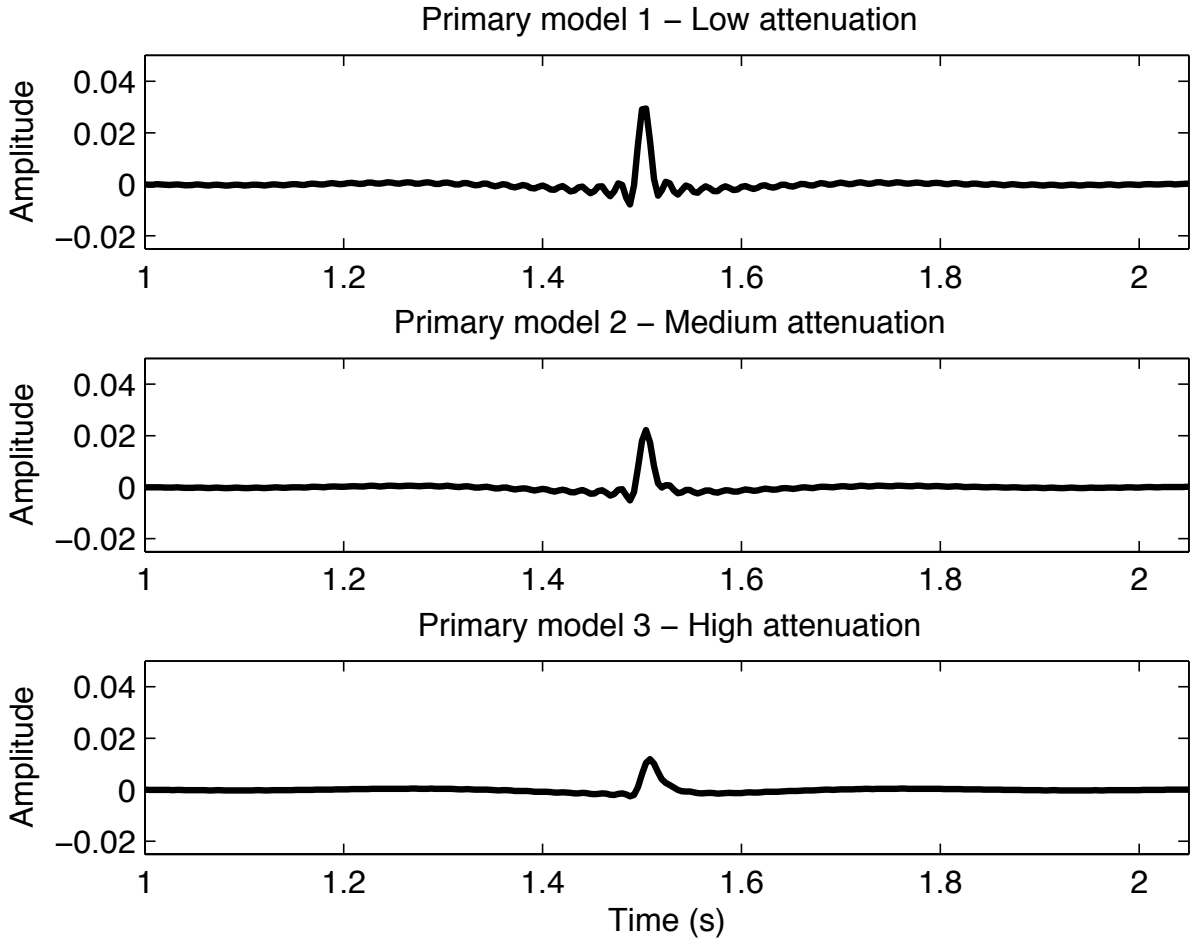

Figure 5: *Primary generated at interface* 1 *for all models. These are the events to be corrected for transmission losses using the discrepancy between the actual multiple generated at interface* 1 *and its prediction.*

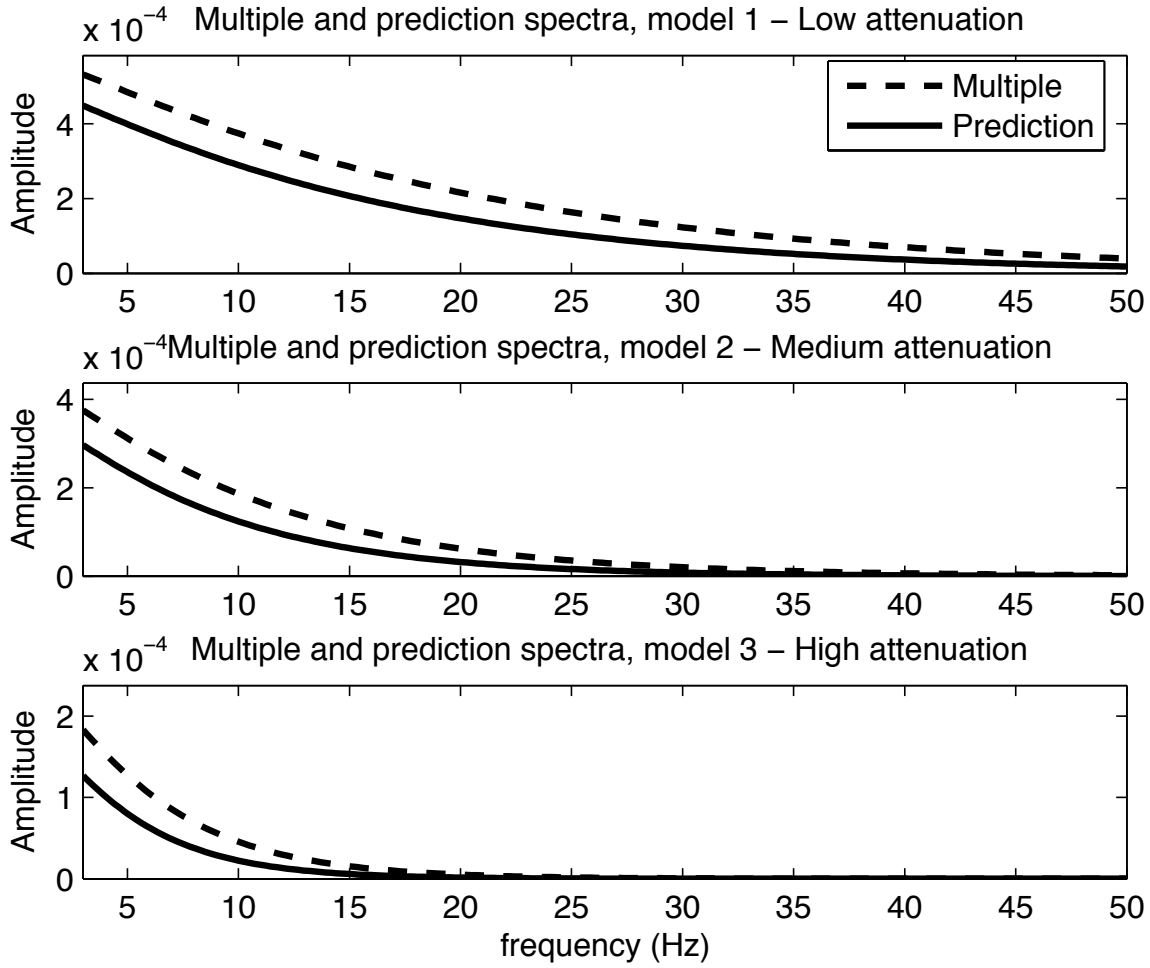

Figure 6: *The spectra of the multiple and its prediction from the IMA algorithm. The ratio of each pair of curves will be used for creating an operator for correcting the primaries for their transmission losses.*

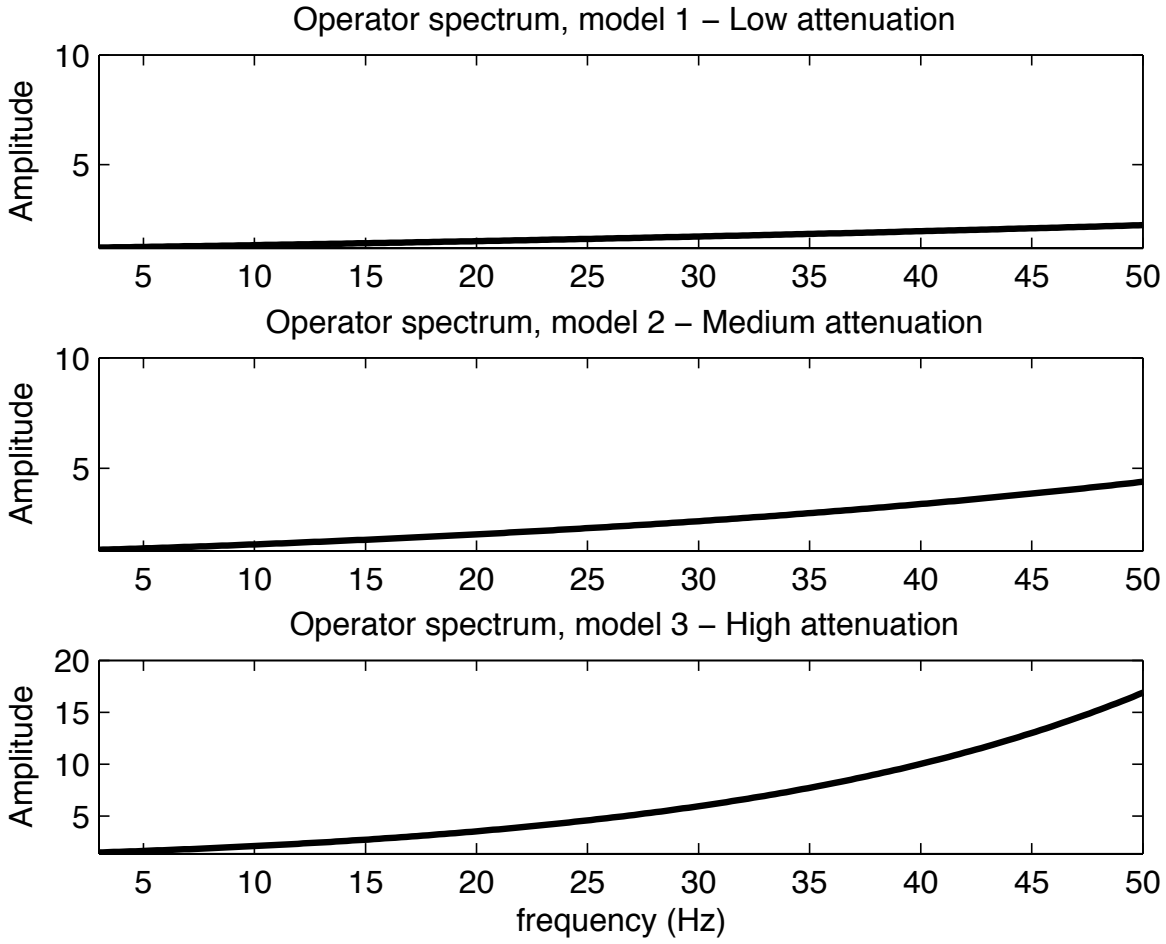

Figure 7: *Operators for correction of the primaries for transmission losses, generated by taking the ratio between the spectrum of the actual multiple and its prediction in Figure 6.*

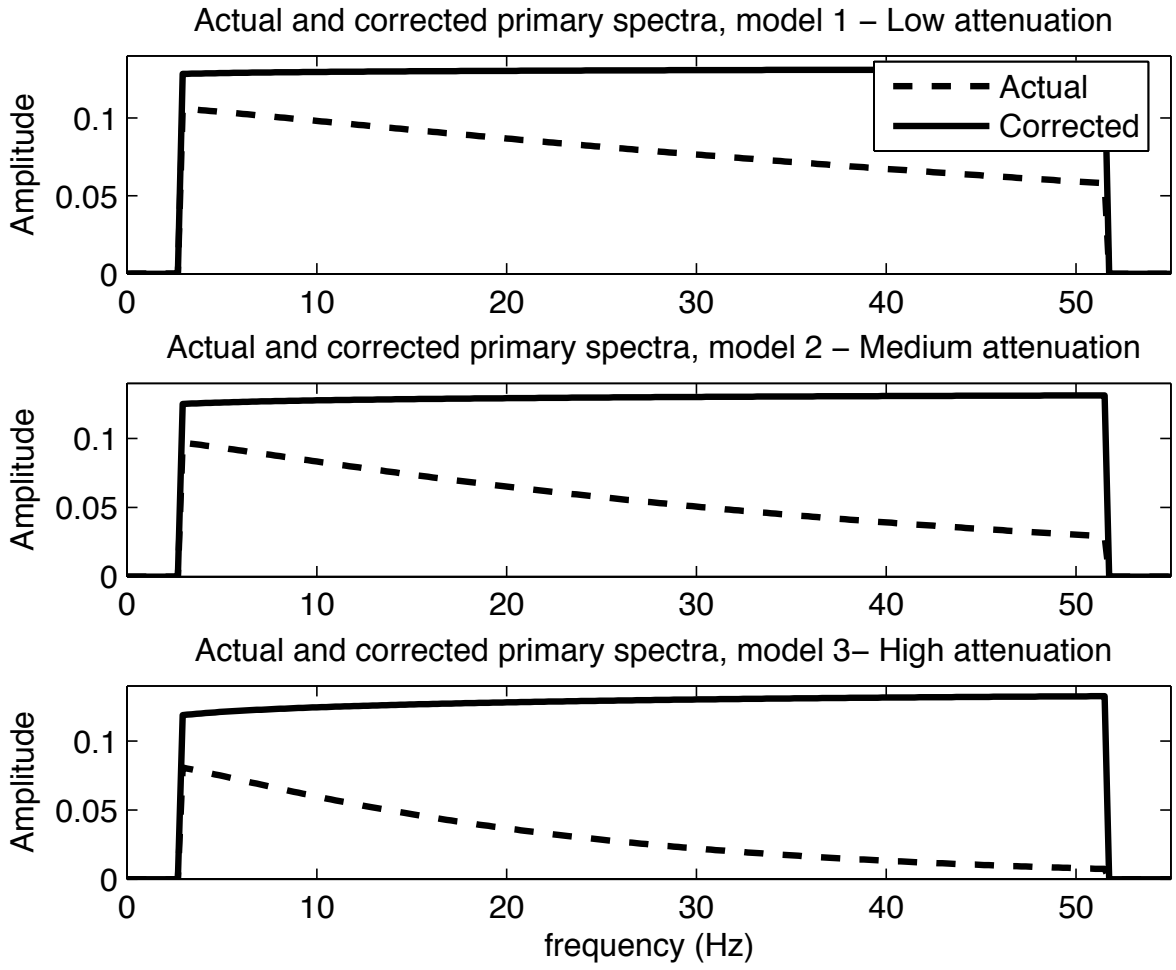

Figure 8: *Spectra of the original primaries and the corrected primaries for each model. The corrections were accomplished using the operators depicted in Figure 7.*

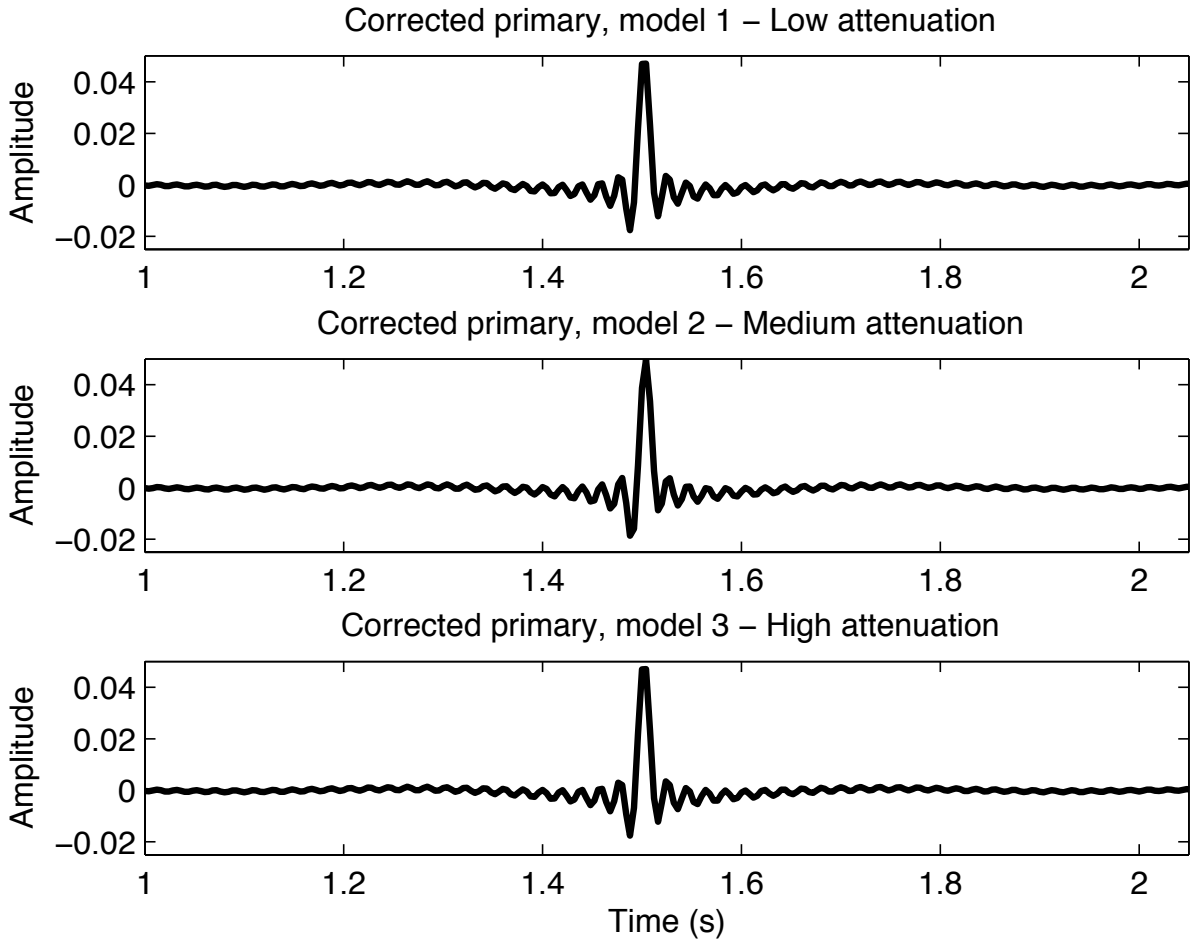

Figure 9: *The corrected primaries.*

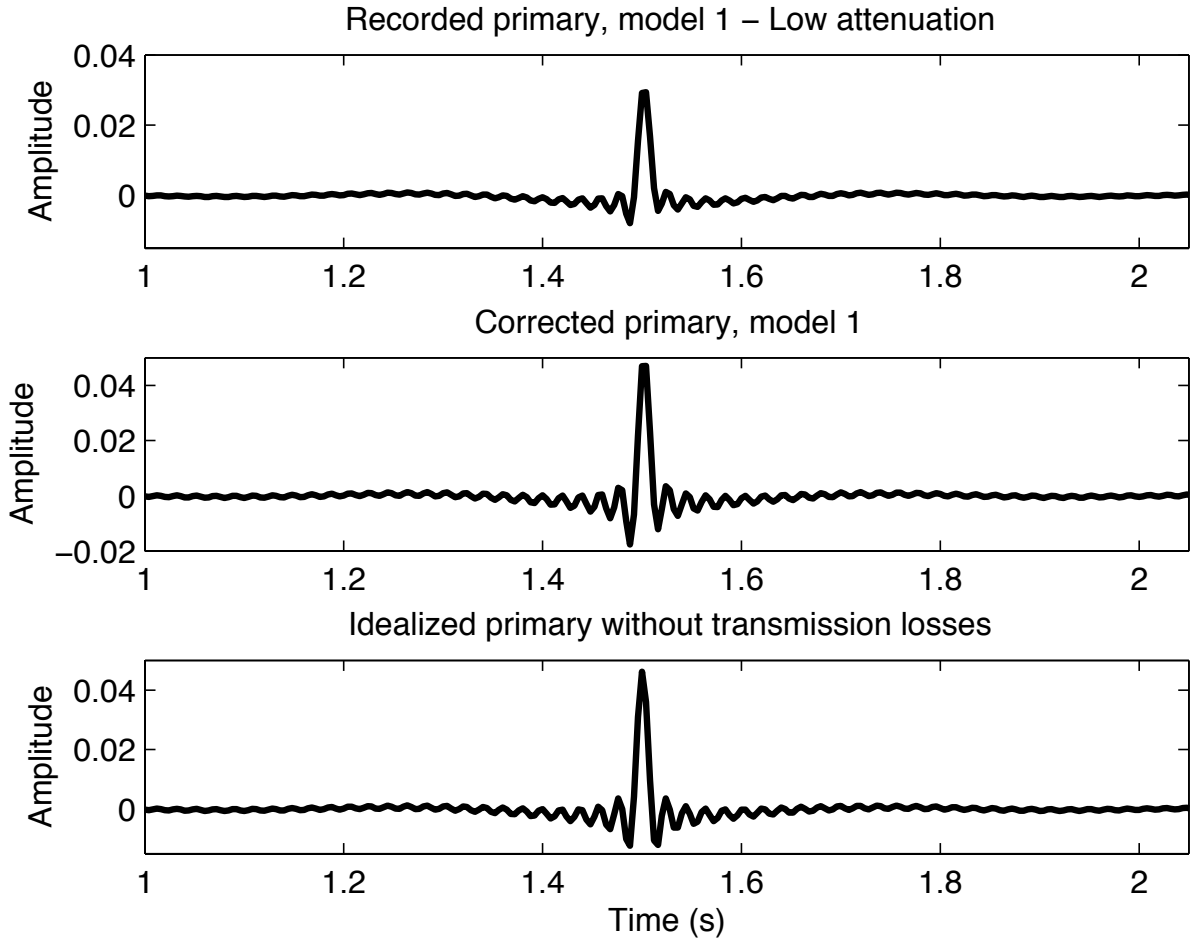

Figure 10: *Correction results for the low attenuation case ($Q = 200$). Original primary (top panel), corrected primary (middle panel), idealized result (bottom panel).*

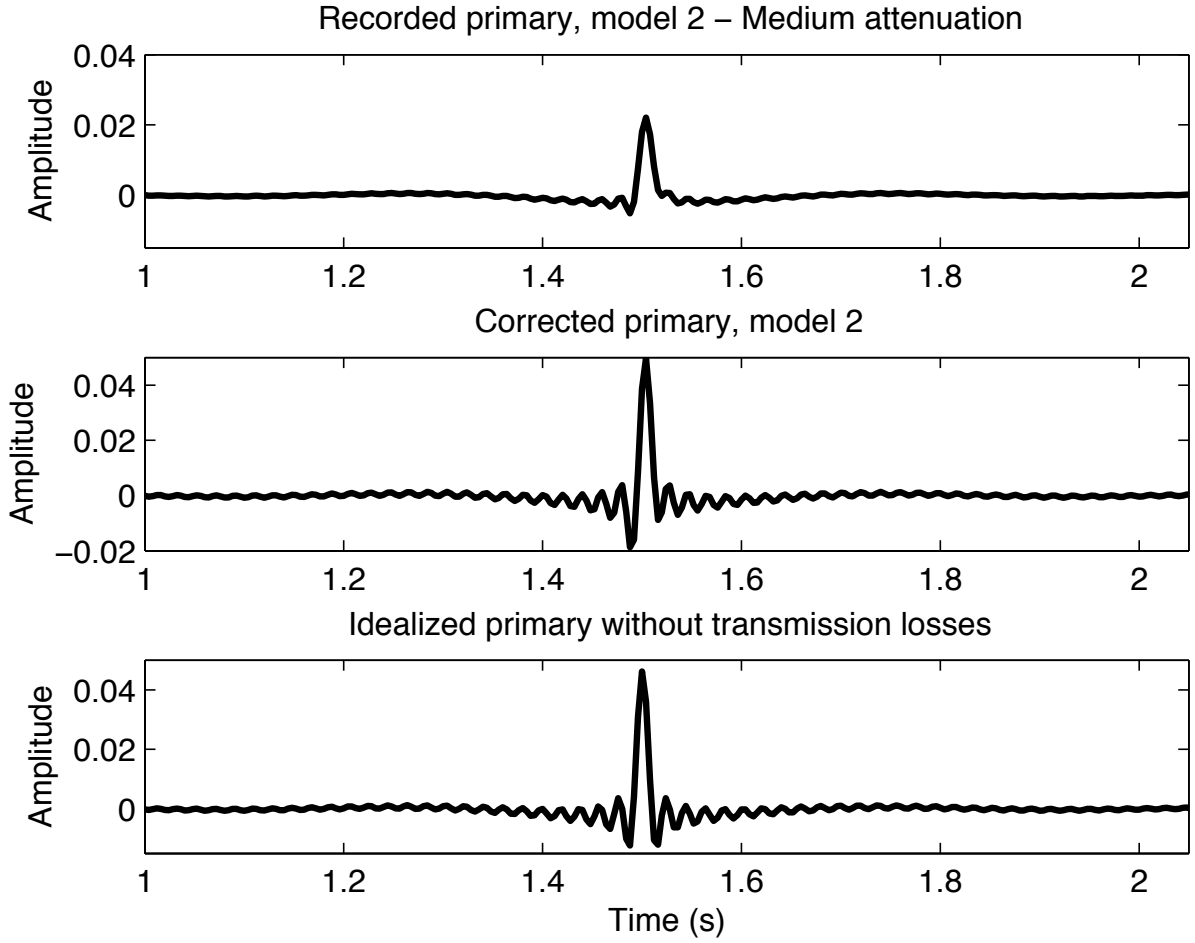

Figure 11: *Correction results for the medium attenuation case ($Q = 100$). Original primary (top panel), corrected primary (middle panel), idealized result (bottom panel).*

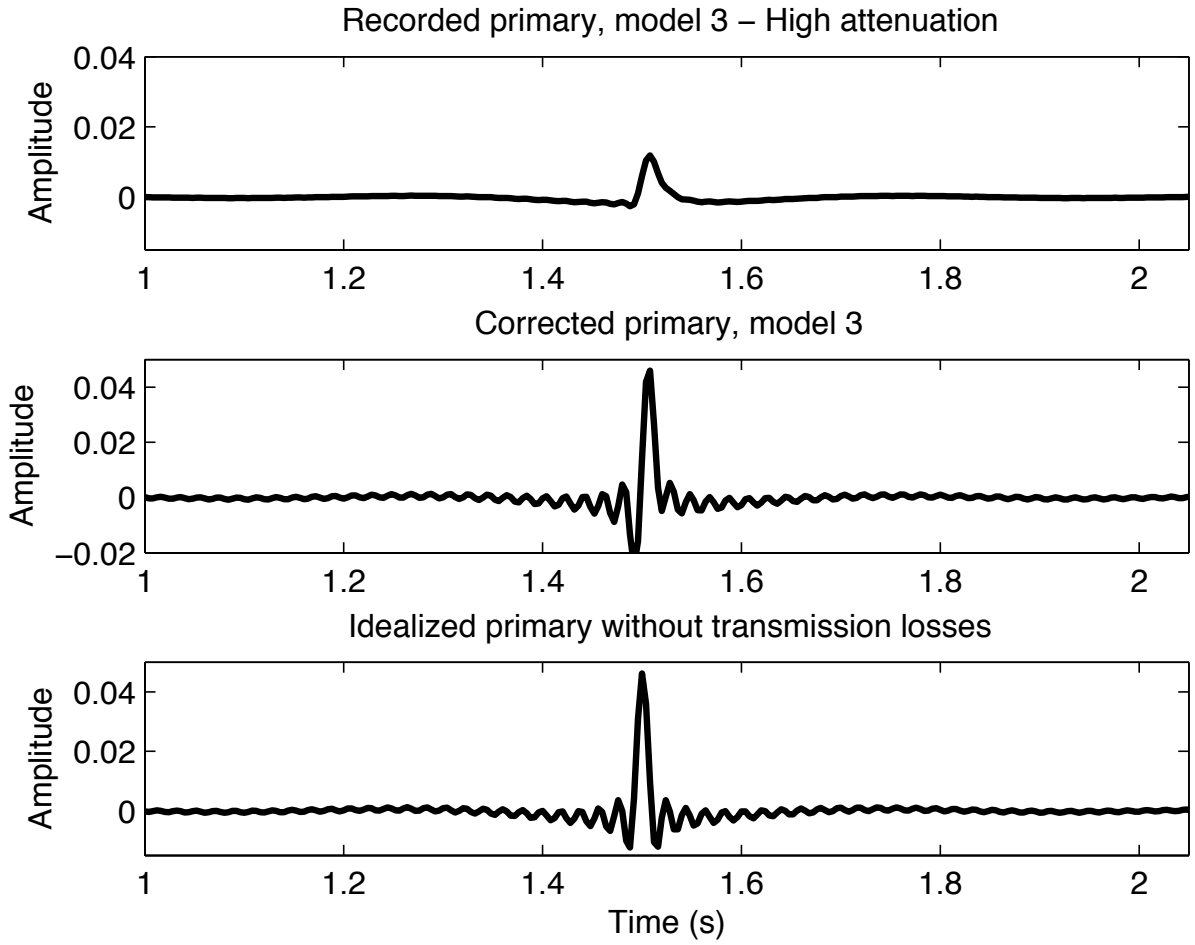

Figure 12: *Correction results for the high attenuation case ($Q = 50$). Original primary (top panel), corrected primary (middle panel), idealized result (bottom panel).*

5 Conclusions

In this paper we have presented a procedure for correcting a primary for transmission losses using internal multiples and the output of the inverse scattering series internal multiple attenuation algorithm.

We have made particular mention and use of the a priori distinction between situations involving significant absorption and situations that are largely acoustic or elastic. In spite of this broad categorization (that we have found to be practically important), one of the strengths of the approach is that it will act to correct transmission losses *whatever* their physical origin or mechanism, without requiring a precise model. In this sense the approach is truly data-driven – the events in the data, in comparison to one another, "decide" what the transmission loss must be.

Our simple numerical results are encouraging and motivate examination of the approach in the presence of more complex media, both absorptive and otherwise. The main tool in this approach, the internal multiple algorithm, is immediately applicable in multiple dimensions, and since the amplitude error is in terms of plane wave transmission coefficients, a plane wave decomposition of 2D and/or 3D data will likely suffice to extend the method. Nevertheless, detailed extension of the approach stands as ongoing and future research. For these reasons in particular, we identify field data testing as a medium-term to long-term goal, contingent on the fundamental study of the internal multiple attenuation amplitudes in multiple dimensions.

6 Acknowledgments

The support of the M-OSRP sponsors is gratefully acknowledged.

References

Aki, K. and P. G. Richards. *Quantitative Seismology.* 2nd edition. University Science Books, 2002.

Araújo, F. V. *Linear and non-linear methods derived from scattering theory: backscattered tomography and internal multiple attenuation.* PhD thesis, Universidade Federal da Bahia, 1994.

Araujo, F. V., A. B. Weglein, P. M. Carvalho, and R. H. Stolt. "Internal multiple attenuation." *56th Mtg., Assoc. Expl. Geophys. Session H036.* . 1994.

Kaplan, Sam T., Billy Robinson, and Kristopher A. Innanen. "Optimizing internal multiple attenuation algorithms for large distributed computing systems." *Mission-Oriented Seismic Research Program (M-OSRP) Annual Report.* 2005.

Nita, B. G., K. H. Matson, and A. B. Weglein. "Forward scattering series and seismic events: Far field approximations, critical and postcritical events." *SIAM Journal of Applied Mathematics* 64 (2004): 2167–2185.

Ramirez, A. C. and A. B. Weglein. "An inverse scattering internal multiple elimination method: Beyond attenuation, a new algorithm and initial tests." *SEG Expanded Abstracts.* (2005): 2115–2118.

Ramirez, A. C. and A.B. Weglein. "Progressing the analysis of the phase and amplitude prediction properties of the inverse scattering internal multiple attenuation algorithm.." *J. of Seismic Expl.* 13 (2005): 283–301.

Weglein, A. B. and K. H. Matson. "Inverse Scattering Internal Multiple Attenuation: An Analytic Example and Subevent interpretation." *SPIE Conference on Mathematical Methods in Geophysical Imaging.* 1998, 108–117.

Weglein, Arthur B., Fernanda V. Araújo, Paulo M. Carvalho, Robert H. Stolt, Kenneth H. Matson, Richard T. Coats, Dennis Corrigan, Douglas J. Foster, Simon A. Shaw, and Haiyan Zhang. "Inverse Scattering Series and Seismic Exploration." *Inverse Problems* (2003): R27–R83.

Weglein, Arthur B., Fernanda Araújo Gasparotto, Paulo M. Carvalho, and Robert H. Stolt. "An Inverse-Scattering Series Method for Attenuating Multiples in Seismic Reflection Data." *Geophysics* 62 (November-December 1997): 1975–1989.

On shore project report I
Reference velocity sensitivity for the marine internal multiple attenuation algorithm: analytic examples

S. Y. Hsu and A. B. Weglein

Abstract

In this note, we present a review of the inverse scattering series internal multiple attenuation algorithm for land data (Matson, 1997). In particular, we look at internal multiple attenuation since it is a dominant issue when processing land data. The requirements of four-component data and reference velocity for a 2D earth is shown. Effects due to velocity errors includes artifacts in the (P, S) data (Matson, 1997) and the algorithm's sensitivity to reference velocity. Two analytic examples for 1D normal incidence (Weglein and Matson, 1998) and 1D non-normal incidence (Nita and Weglein, 2005) are used to demonstrate the inner working of this algorithm. We extend their analysis to investigate velocity sensitivity. In conclusion, accurate near surface reference velocities are essential to properly predict internal multiples except for the 1-D normal incidence case.

Introduction

In seismic processing, primaries are considered signal. All other events, such as ghosts, free surface multiples, and internal multiples, need to be removed. Many conventional methods have been developed to remove multiples but most of them assume at least one of the following: (1) the earth is 1D, (2) the velocity is known, or (3) primaries are random and multiples are periodic (Weglein et al., 2003). When earth properties agree with these assumptions, the conventional methods are effective. However, these assumptions are not always satisfied and hence the conventional methods may be ineffective.

To overcome the limitations of these conventional methods, Carvalho (1992), Araújo (1994) and Weglein et al. (1997) developed methods to perform free surface multiple removal and internal multiple suppression using the inverse scattering series. These methods do not require earth model and leave primaries untouched. Their independence from subsurface information make these methods effective while the conventional methods fail. Following previous work in the marine case, Matson (1997) adapted the inverse scattering internal multiple attenuation algorithm from marine to multi-component land data. Note that for marine data, the air-water interface can be viewed as a perfect reflector; therefore, the free surface multiples dominate and need to be removed. On the contrary, the interactions that take place at the air-land interface are mostly refraction-like rather than reflection-like scattering. Hence, the internal multiples become dominant in the land date and need to be removed.

As a preliminary step in considering inverse scattering series processing for land data, we present a review of the elastic internal multiple attenuation algorithm (Matson, 1997), followed by two

analytic examples of the attenuation algorithm. Matson's work shows that the data requirements for elastic internal multiple attenuation are line sources, four components, regularly sampled data, known wavelets, and near surface velocities. The near surface velocity errors will have a noticeable effect on the (P, S) decomposition (Matson, 1997). Another effect due to the velocity errors comes form the algorithm's sensitivity to reference velocity. In this note, two analytic examples are used to demonstrate this issue. The 1-D normal incidence case will show that the inverse scattering internal multiple attenuation algorithm is capable of predicting travel time and estimating amplitude without actual velocity. In the non-normal incidence case, we demonstrate that using a wrong reference velocity to predict internal multiples may not precisely obtain the total travel time. For this reason, it is important to obtain accurate reference velocities to better perform the inverse scattering internal multiple attenuation algorithm.

Background

We consider a set of elastic wave equations in the displacement domain,

$$\mathcal{L}\mathbf{u} = \mathbf{f}, \tag{1}$$
$$\mathcal{L}_0\mathbf{u} = \mathbf{f}, \tag{2}$$
$$\mathcal{L}\mathcal{G} = \delta, \tag{3}$$
$$\mathcal{L}_0\mathcal{G}_0 = \delta. \tag{4}$$

where $\mathcal{L}, \mathcal{L}_0, \mathcal{G}$, and $\mathcal{G}_0$ are the actual and reference differential operators and Green's functions, respectively, and $\mathbf{u}$ and $\mathbf{f}$ are the corresponding displacement and source terms.
The perturbation is defined as $\mathcal{V} \equiv \mathcal{L}_0 - \mathcal{L}$; the elastic Lippmann-Schwinger equation is

$$\mathcal{G} = \mathcal{G}_0 + \mathcal{G}_0\mathcal{V}\mathcal{G}, \tag{5}$$

which can be expanded in a forward series

$$\mathcal{G} = \mathcal{G}_0 + \mathcal{G}_0\mathcal{V}\mathcal{G}_0 + \mathcal{G}_0\mathcal{V}\mathcal{G}_0\mathcal{V}\mathcal{G}_0 + \cdots . \tag{6}$$

We define $\mathcal{D}$ as the measurement of the scattered field. Therefore

$$\mathcal{D} = \mathcal{G} - \mathcal{G}_0 = \mathcal{G}_0\mathcal{V}\mathcal{G}_0 + \mathcal{G}_0\mathcal{V}\mathcal{G}_0\mathcal{V}\mathcal{G}_0 + \cdots . \tag{7}$$

The solution for $\mathcal{V}$ is in the form of a series,

$$\mathcal{V} = \mathcal{V}_1 + \mathcal{V}_2 + \mathcal{V}_3 + \cdots , \tag{8}$$

where $\mathcal{V}_n$ is nth order in the measurement data, $\mathcal{D}$. The expansion gives the elastic inverse scattering series in displacement domain,

$$\mathcal{D} \;=\; \mathcal{G}_0\mathcal{V}_1\mathcal{G}_0, \tag{9}$$

$$
\begin{aligned}
0 &= \mathcal{G}_0\mathcal{V}_2\mathcal{G}_0 + \mathcal{G}_0\mathcal{V}_1\mathcal{G}_0\mathcal{V}_1\mathcal{G}_0, && (10)\\
0 &= \mathcal{G}_0\mathcal{V}_3\mathcal{G}_0 + \mathcal{G}_0\mathcal{V}_2\mathcal{G}_0\mathcal{V}_1\mathcal{G}_0 + \mathcal{G}_0\mathcal{V}_1\mathcal{G}_0\mathcal{V}_2\mathcal{G}_0 + \mathcal{G}_0\mathcal{V}_1\mathcal{G}_0\mathcal{V}_1\mathcal{G}_0\mathcal{V}_1\mathcal{G}_0, && (11)\\
&\vdots
\end{aligned}
$$

The scattering series in the elastic case has similar form as that in the acoustic case (Weglein et al., 2003). However, in the elastic world the wave propagations are more complicated. In acoustic reference medium only P waves can propagate. In the two dimensional elastic medium, the incident P waves can give rise to P as well as S waves and vise versa, after interacting with the elastic interface. Therefore, the displacement data usually consist of P and S waves. For convenience, we transform the displacement into P and S wave potentials and decompose the displacement operators (Green's functions as well as perturbations) into the (P, S) domain (Weglein and Stolt, 1995; Matson, 1997).

We make use of decomposition

$$
\begin{aligned}
\mathcal{G}_0 &= \Pi^{-1}\Gamma_0^{-1}G_0\Pi, && (12)\\
V &= \Pi\mathcal{V}\Pi^{-1}\Gamma_0^{-1}, && (13)
\end{aligned}
$$

where

$$
G_0 = \begin{pmatrix} G_{0P} & 0 \\ 0 & G_{0S} \end{pmatrix} \quad , \Gamma_0 = \begin{pmatrix} \gamma_0 & 0 \\ 0 & \mu_0 \end{pmatrix} \quad , \Gamma_0^{-1} = \begin{pmatrix} 1/\gamma_0 & 0 \\ 0 & 1/\mu_0 \end{pmatrix}, \tag{14}
$$

$$
V = \begin{pmatrix} V_{PP} & V_{PS} \\ V_{SP} & V_{SS} \end{pmatrix} \quad , \Pi = \begin{pmatrix} \partial_x & \partial_z \\ -\partial_z & \partial_x \end{pmatrix} \quad , \Pi^{-1} = \frac{1}{\nabla^2}\begin{pmatrix} \partial_x & \partial_z \\ -\partial_z & \partial_x \end{pmatrix}. \tag{15}
$$

Here, G_{0P} and G_{0S} are pure P and S wave Green's functions, and γ_0 and μ_0 are the strain modulus and shear modulus, respectively. The Green's functions G_{0P} and G_{0S} satisfy the scalar wave equations

$$
\begin{aligned}
(\nabla^2 + \frac{\omega^2}{\alpha_0^2})G_{0P}(x_g, z_g|x_s, z_s; \omega) &= \delta(x_g - x_s)\delta(z_g - z_s),\\
(\nabla^2 + \frac{\omega^2}{\beta_0^2})G_{0S}(x_g, z_g|x_s, z_s; \omega) &= \delta(x_g - x_s)\delta(z_g - z_s)
\end{aligned} \tag{16}
$$

where $\alpha_0 = (\gamma_0/\rho)^{1/2}$ is the reference P wave velocity and $\beta_0 = (\mu_0/\rho)^{1/2}$ is the reference S wave velocity. The solution for G_{0P} and G_{0S} are

$$
\begin{aligned}
G_{0P}(x_g, z_g|x_s, z_s; \omega) &= \frac{1}{2\pi}\int_{-\infty}^{\infty}\frac{1}{2i\nu}e^{ik(x_g - x_s)}e^{i\nu|z_s - z_g|}dk,\\
G_{0S}(x_g, z_g|x_s, z_s; \omega) &= \frac{1}{2\pi}\int_{-\infty}^{\infty}\frac{1}{2i\eta}e^{ik(x_g - x_s)}e^{i\eta|z_s - z_g|}dk
\end{aligned} \tag{17}
$$

where $\nu = \text{sign}(\omega)(\omega^2/\alpha_0^2 - k^2)^{1/2}$ and $\eta = \text{sign}(\omega)(\omega^2/\beta_0^2 - k^2)^{1/2}$ are vertical wavenumbers for P and S waves, respectively.

The data in the (P,S) domain is

$$\begin{aligned} D = G_0 V_1 G_0 &= \begin{pmatrix} G_{0P} & 0 \\ 0 & G_{0S} \end{pmatrix} \begin{pmatrix} V^1_{PP} & V^1_{PS} \\ V^1_{SP} & V^1_{SS} \end{pmatrix} \begin{pmatrix} G_{0P} & 0 \\ 0 & G_{0S} \end{pmatrix} \\ &= \begin{pmatrix} D_{PP} & D_{PS} \\ D_{SP} & D_{SS} \end{pmatrix}. \end{aligned} \tag{18}$$

The subscripts PP represents pure P waves, coming from the source, that are scattered into further P waves which then propagate to the receiver. Similarly, the subscripts PS represents incoming S waves, that are scattered and converted into P waves, propagating to the receiver.

Note that velocity errors have an effect on the (P,S) decomposition since it depends on derivatives in the displacement space. In Fourier transform space, the horizontal derivative is a multiplication by the horizontal wavenumber ik. The vertical derivative is a multiplication by $i\nu$ or $i\eta$ which corresponds to the reference P wave velocity, α_0, or the reference S wave velocity, β_0, respectively (Matson, 1997).

Elastic internal multiple attenuation

After decomposition, we now move to the internal multiple attenuation. Unlike the free surface multiple removal, we cannot isolate the portion in the direct wave Green's function G_0^d that exists when the internal multiples are present and disappears when internal multiples are absent (Weglein et al., 1997).

Evaluating the forward series in equation (7), the first two terms do not contribute to internal multiples since there are less than three interactions between waves and reflectors. To begin to construct internal multiples, the wave propagation has to be altered at least three times. Hence, the first order internal multiple starts with the third term in the forward series. In general, the $(2n+1)$th term in forward series is the leading term of the nth order internal multiple.

Similarly, the first two terms in the inverse series do not remove multiples. The internal multiple attenuation starting with the third term in the inverse series, that is

$$\begin{aligned} G_0^d V_3 G_0^d &= -G_0^d V_1 G_0^d V_1 G_0^d V_1 G_0^d - G_0^d V_1 G_0^d V_2 G_0^d - G_0^d V_2 G_0^d V_1 G_0^d \\ &= G_0^d (V_{33} + V_{32} + V_{31}) G_0^d \end{aligned} \tag{19}$$

where

$$V_{31} = -V_2 G_0^d V_1, \tag{20}$$

$$V_{32} = -V_1 G_0^d V_2, \tag{21}$$

$$V_{33} = -V_1 G_0^d V_1 G_0^d V_1. \tag{22}$$

$G_0^d V_{33} G_0^d$, the first term in (19), is defined as a reflection-like inverse scattering if it changes propagation direction with respect to the measurement point after being altered by V_1. Note that for

reflection-like scattering the geometric relationship between scatterers must be lower-higher-lower. The remaining two terms in (19) are refraction-like scattering associated with primaries but not internal multiples since they do not satisfy the lower-higher-lower relationship between scatterers (Weglein et al., 2003).

Following the method developed by Weglein et al. (1997) and Araújo (1994), the equation for first order internal multiples in 2-D acoustic data is

$$\begin{aligned} b_{3IM}(k_g,k_s,q_g+q_s) = \frac{1}{(2\pi)^2}\int_{-\infty}^{\infty} dk_1 e^{-iq_1(z_g-z_s)} \int_{-\infty}^{\infty} dz_1' b_1(k_g,k_1,z_1') e^{i(q_g+q_1)z_1'} \\ \cdot \int_{-\infty}^{\infty} dk_2 e^{iq_2(z_g-z_s)} \int_{-\infty}^{z_1'-\epsilon} dz_2' b_1(k_1,k_2,z_2') e^{-i(q_1+q_2)z_2'} \\ \cdot \int_{z_2'+\epsilon}^{\infty} dz_3' b_1(k_2,k_s,z_3') e^{i(q_2+q_s)z_3'} \end{aligned} \tag{23}$$

where $b_1(z)$ represents the recorded seismic data in pseudo depth. The parameter $\epsilon > 0$ ensures $z_1' > z_2'$ and $z_3' > z_2'$ which satisfy the geometric relationship between reflections of internal multiples (lower-higher-lower). b_1 is defined in terms of the original prestack data without free surface multiples. The data can be written as

$$D(k_g,k_s,\omega) = (-2iq_s)^{-1} b_1(k_g,k_s,q_g+q_s). \tag{24}$$

The adaption elastic version of (23) given by Matson (1997) is

$$\begin{aligned} B_{ij}^{3IM}(k_1,k_2,\theta_{1i}+\theta_{2j}) = \frac{1}{(2\pi)^2}\int_{-\infty}^{\infty} dk_3 e^{-i\theta_{3l}(z_g-z_s)} \int_{-\infty}^{\infty} B_{il}(k_1,k_3,z_1) e^{i(\theta_{1i}+\theta_{3l})z_1} dz_1 \\ \cdot \int_{-\infty}^{\infty} dk_4 e^{i\theta_{4m}(z_g-z_s)} \int_{-\infty}^{z_1-\epsilon} B_{lm}(k_3,k_4,z_2) e^{-i(\theta_{3l}+\theta_{4m})z_2} dz_2 \\ \cdot \int_{z_2+\epsilon}^{\infty} B_{mj}(k_4,k_2,z_3) e^{i(\theta_{4m}+\theta_{2j})z_3} dz_3 \end{aligned} \tag{25}$$

where θ_{1i} indicates P and S vertical wavenumber for $i = P$ and S, respectively.

Similarly, B_{ij} is defined in terms of the original pre-stack data, that is

$$D_{ij}(k_1,k_2,\omega) = (-2i\theta_{2j})^{-1} B_{ij}(k_g,k_s,\theta_{1i}+\theta_{2j}). \tag{26}$$

Hence,

$$D_{PP}(k_1,k_2,\omega) = (-2i\theta_{2P})^{-1} B_{PP}(k_g,k_s,\theta_{1P}+\theta_{2P}), \tag{27}$$

$$D_{PS}(k_1,k_2,\omega) = (-2i\theta_{2S})^{-1} B_{PS}(k_g,k_s,\theta_{1P}+\theta_{2S}), \tag{28}$$

$$D_{SP}(k_1,k_2,\omega) = (-2i\theta_{2P})^{-1} B_{SP}(k_g,k_s,\theta_{1S}+\theta_{2P}), \tag{29}$$

$$D_{SS}(k_1,k_2,\omega) = (-2i\theta_{2S})^{-1} B_{SS}(k_g,k_s,\theta_{1S}+\theta_{2S}). \tag{30}$$

One can see that if the converted waves do not exist, equation (25) becomes equation (23), which is the first order internal multiple attenuator in acoustic form.

Evaluating the expression of B_{PP}^{3IM}, we have

$$\begin{aligned}
B_{PP}^{3IM}(k_1,k_2,\theta_{1P}+\theta_{2P}) = & \frac{1}{(2\pi)^2}\int_{-\infty}^{\infty} dk_3 e^{-i\theta_{3P}(z_g-z_s)} \int_{-\infty}^{\infty} \underline{B_{PP}}(k_1,k_3,z_1) e^{i(\theta_{1P}+\theta_{3P})z_1} dz_1 \\
& \cdot \int_{-\infty}^{\infty} dk_4 e^{i\theta_{4P}(z_g-z_s)} \int_{-\infty}^{z_1-\epsilon} \underline{B_{PP}}(k_3,k_4,z_2) e^{-i(\theta_{3P}+\theta_{4P})z_2} dz_2 \\
& \cdot \int_{z_2+\epsilon}^{\infty} \underline{B_{PP}}(k_4,k_2,z_3) e^{i(\theta_{4P}+\theta_{2P})z_3} dz_3 \\
& + \frac{1}{(2\pi)^2}\int_{-\infty}^{\infty} dk_3 e^{-i\theta_{3P}(z_g-z_s)} \int_{-\infty}^{\infty} \underline{B_{PP}}(k_1,k_3,z_1) e^{i(\theta_{1P}+\theta_{3P})z_1} dz_1 \\
& \cdot \int_{-\infty}^{\infty} dk_4 e^{i\theta_{4S}(z_g-z_s)} \int_{-\infty}^{z_1-\epsilon} \underline{B_{PS}}(k_3,k_4,z_2) e^{-i(\theta_{3P}+\theta_{4S})z_2} dz_2 \\
& \cdot \int_{z_2+\epsilon}^{\infty} \underline{B_{SP}}(k_4,k_2,z_3) e^{i(\theta_{4S}+\theta_{2P})z_3} dz_3 \\
& + \frac{1}{(2\pi)^2}\int_{-\infty}^{\infty} dk_3 e^{-i\theta_{3S}(z_g-z_s)} \int_{-\infty}^{\infty} \underline{B_{PS}}(k_1,k_3,z_1) e^{i(\theta_{1P}+\theta_{3S})z_1} dz_1 \\
& \cdot \int_{-\infty}^{\infty} dk_4 e^{i\theta_{4S}(z_g-z_s)} \int_{-\infty}^{z_1-\epsilon} \underline{B_{SS}}(k_3,k_4,z_2) e^{-i(\theta_{3S}+\theta_{4S})z_2} dz_2 \\
& \cdot \int_{z_2+\epsilon}^{\infty} \underline{B_{SP}}(k_4,k_2,z_3) e^{i(\theta_{4S}+\theta_{2P})z_3} dz_3 \\
& + \frac{1}{(2\pi)^2}\int_{-\infty}^{\infty} dk_3 e^{-i\theta_{3S}(z_g-z_s)} \int_{-\infty}^{\infty} \underline{B_{PS}}(k_1,k_3,z_1) e^{i(\theta_{1P}+\theta_{3S})z_1} dz_1 \\
& \cdot \int_{-\infty}^{\infty} dk_4 e^{i\theta_{4P}(z_g-z_s)} \int_{-\infty}^{z_1-\epsilon} \underline{B_{SP}}(k_3,k_4,z_2) e^{-i(\theta_{3S}+\theta_{4P})z_2} dz_2 \\
& \cdot \int_{z_2+\epsilon}^{\infty} \underline{B_{PP}}(k_4,k_2,z_3) e^{i(\theta_{4P}+\theta_{2P})z_3} dz_3.
\end{aligned} \tag{31}$$

Equation (31) shows that the four-component data, ie. B_{PP}, B_{PS}, B_{SP}, and B_{SS}, are coupled in the calculation of B_{PP}^{3IM}. If the converted waves do not exist, equation (31) will simplify to the acoustic form. However, for land data, the converted waves are not negligible. In order to better perform the internal multiple attenuation algorithm, four components of data are needed. Another requirement is the known reference elastic properties. As mentioned perviously, velocity errors will produce artifacts in the (P,S) data which will affect the internal multiple estimation (Matson, 1997). Besides the (P,S) decomposition issue, the algorithm's sensitivity to the reference properties will cause errors when predicting the total traveltimes of internal multiples. We will use two analytic examples to demonstrate this issue in the following section.

A 1-D analytic example of internal multiple attenuation

In this section, we use an analytic example given by Weglein and Matson (1998) and Weglein et al. (2003) to show the working of inverse scattering internal multiple attenuation algorithm and its

sensitivity to reference velocity. We considered a one dimensional normal incidence case. The first term of the internal multiple sub-series given by Araújo (1994) and Weglein et al. (1997) is

$$b_{3IM}(k_z) = \int_{-\infty}^{\infty} dz_1' b_1(z_1') e^{ik_z z_1'} \int_{-\infty}^{z_1'-\epsilon} dz_2' b_1(z_2') e^{-ik_z z_2'} \int_{z_2'+\epsilon}^{\infty} dz_3' b_1(z_3') e^{ik_z z_3'} \tag{32}$$

The model consists of two reflectors located at depths Z_1 and Z_2 with the corresponding reflection coefficients R_1 and R_2. The reflected data due to the normal incident plane wave source is

$$b_1(t) = R_1\delta(t-t_1) + R_2T_1T_1'\delta(t-t_2) + \text{internal multiples.} \tag{33}$$

where t_1 and t_2 are the arrival times of the first and second primaries; and T_1 and T_1' are the transmission coefficients corresponding to the first reflector for incoming and outgoing waves, respectively.

To simplify the calculation, we use only primaries as the input data. Fourier transforming (33) into the frequency domain gives

$$\begin{aligned} b_1(\omega) &= R_1 e^{i\omega t_1} + R_2T_1T_1' e^{i\omega t_2} \\ &= R_1 e^{i(2\omega/c_0)(c_0t_1/2)} + R_2T_1T_1' e^{i(2\omega/c_0)(c_0t_2/2)} \\ &= R_1 e^{ik_z z_1} + R_2T_1T_1' e^{ik_z z_2} \end{aligned} \tag{34}$$

where c_0 is the reference velocity (the water speed for the marine case). The vertical wavenumber is defined as $k_z = 2\omega/c_0$ and the pseudo depths of the first and second reflectors are defined as $z_1 = c_0t_1/2$ and $z_2 = c_0t_2/2$, respectively.

In order to input data into (32), we Fourier transform (34) into pseudo depth

$$b_1(z) = R_1\delta(z-z_1) + R_2T_1T_1'\delta(z-z_2). \tag{35}$$

The actual first order internal multiple of this model is

$$IM_{actual}(t) = -R_1R_2^2T_1T_1'\delta(t-(2t_2-t_1)). \tag{36}$$

Fourier transforming equation (36) into frequency domain gives

$$IM_{actual}(\omega) = -R_1R_2^2T_1T_1' e^{i\omega(2t_2-t_1))}, \tag{37}$$

and the predicted first order internal multiple shown by Weglein and Matson (1998) is

$$IM_{est}(\omega) = R_1R_2^2T_1^2T_1'^2 e^{i\omega(2t_2-t_1))}. \tag{38}$$

Comparing this result to the actual internal multiple (36), one can see that the internal multiple algorithm correctly predicts the total travel time and properly estimates the amplitude. The amplitude of the estimation has a T_1T_1' factor which is less than but close to 1.

Suppose we choose the wrong reference velocity c_0'. The new vertical wave number becomes $k_z' = 2\omega/c_0'$, and the new pseudo depths are $z_a = c_0' t_1/2$ and $z_b = c_0' t_2/2$.

Equation (35) can be rewritten as

$$b_1(z) = R_1\delta(z - z_a) + R_2 T_1 T_1' \delta(z - z_b). \tag{39}$$

Substituting (44) into the third integral of (32), we have

$$\begin{aligned}&\int_{z_2'+\epsilon}^{\infty} dz_3' e^{ik_z' z_3'}[R_1\delta(z_3' - z_a) + R_2 T_1 T_1' \delta(z_3' - z_b)] \\ &= R_1 e^{ik_z' z_a} H(z_a - (z_2' + \epsilon)) + R_2 T_1 T_1' e^{ik_z' z_b} H(z_b - (z_2' + \epsilon)),\end{aligned} \tag{40}$$

where H is the Heaviside function. The second integral becomes

$$\begin{aligned}&\int_{-\infty}^{z_1'-\epsilon} dz_2' e^{-ik_z' z_2'}[R_1\delta(z_2' - z_a) + R_2 T_1 T_1' \delta(z_2' - z_b)] \\ &\qquad \cdot [R_1 e^{ik_z' z_a} H(z_a - (z_2' + \epsilon)) + R_2 T_1 T_1' e^{ik_z' z_b} H(z_b - (z_2' + \epsilon))] \\ &\qquad = R_1^2 e^{ik_z'(z_a - z_a)} \underline{H(z_a - (z_a + \epsilon))} H((z_1' - \epsilon) - z_a) \\ &\qquad + R_1 R_2 T_1 T_1' e^{ik_z'(z_a - z_b)} \underline{H(z_a - (z_b + \epsilon))} H(z_1' - \epsilon - z_b) \\ &\qquad + R_1 R_2 T_1 T_1' e^{ik_z'(z_b - z_a)} H(z_b - (z_a + \epsilon)) H(z_1' - \epsilon - z_a) \\ &\qquad + R_2^2 T_1^2 {T_1'}^2 e^{ik_z'(z_b - z_b)} \underline{H(z_b - (z_b + \epsilon))} H(z_1' - \epsilon - z_b).\end{aligned} \tag{41}$$

The underlined Heaviside function in (41) are zero due to $H(< 0) = 0$. The remaining third term is

$$R_1 R_2 T_1 T_1' e^{ik_z'(z_b - z_a)} H(z_b - (z_a + \epsilon)) H(z_1' - \epsilon - z_a). \tag{42}$$

Therefore,

$$\begin{aligned}b_{3IM}(k_z') &= \int_{-\infty}^{\infty} dz_1' e^{ik_z' z_1'}[R_1\delta(z_1' - z_a) + R_2 T_1 T_1' \delta(z_1' - z_b)] \\ &\quad \cdot [R_1 R_2 T_1 T_1' e^{ik_z'(z_b - z_a)} H(z_b - (z_a + \epsilon)) H(z_1' - \epsilon - z_a)] \\ &= R_1^2 R_2 T_1 T_1' e^{ik_z'(z_b - z_a + z_a)} H(z_b - (z_a + \epsilon)) \underline{H(z_a - \epsilon - z_a)} \\ &\quad + R_1 R_2^2 T_1^2 {T_1'}^2 e^{ik_z'(z_b - z_a + z_b)} H(z_b - (z_a + \epsilon)) H(z_b - \epsilon - z_a) \\ &= R_1 R_2^2 T_1^2 {T_1'}^2 e^{ik_z'(2z_b - z_a)} \\ &= R_1 R_2^2 T_1^2 {T_1'}^2 e^{i(2\omega/c_0')(2c_0' t_2/2 - c_0' t_1/2)} \\ &= R_1 R_2^2 T_1^2 {T_1'}^2 e^{i\omega(2t_2 - t_1)}.\end{aligned} \tag{43}$$

Note that the underlined term $H(-\epsilon) = 0$, and $H(> 0) = 1$.

The result of (43) agrees with the estimation that uses true reference velocity (see equation (38). One can see that the internal multiple estimation is independent of reference velocity. The different reference velocities will change the pseudo depths and the corresponding vertical wavenumbers but the total time of the predicted multiple remain accurate. In other words, even if we use a wrong reference velocity to perform this algorithm, the internal multiples will be properly predicted. However, the independence from the reference velocity is only true for the 1-D normal incidence case. In the next section, we will show that using inaccurate reference velocity to process the internal multiple algorithm may cause errors in the non-normal incidence case.

A 1.5D analytic example of internal multiple attenuation

We consider a 2-D layering model given by Nita and Weglein (2005) (see Figure 1). The velocity changes across the interfaces located at $z = z_a$ and $z = z_b$ where the velocities are c_0, c_1, and c_2, respectively. The sources and receivers are located at the measurement surface where the depth $z = 0$.

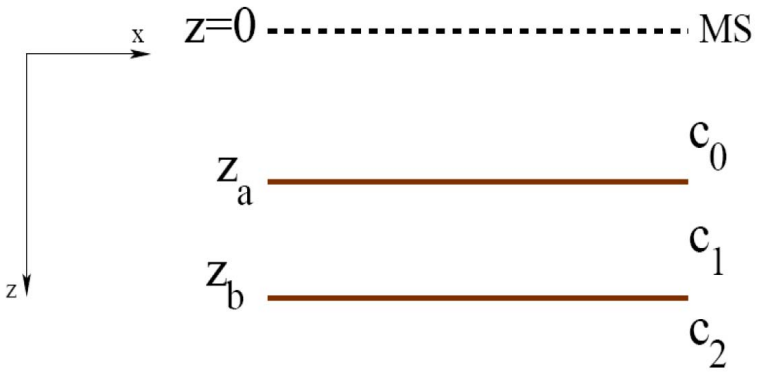

Figure 1: The model for the 1.5D example

The data in the frequency ω domain can be written as

$$D(x_h, 0; \omega) = \frac{1}{2\pi} \int_{-\infty}^{\infty} dk_h \frac{R_1 + T_1 R_2 T_1' e^{i\nu_1(z_b - z_a)} + \cdots}{iq_s} e^{ik_z z_a} e^{ik_h x_h}. \tag{44}$$

where $k_z = q_g + q_s$, $k_h = k_g - k_s$, $x_h = (x_g - x_s)/2$, and $\nu_1 = q_{1g} + q_{1s}$.

For the first primary (see Figure 2), we have

$$q_s = \frac{\omega}{c_0} cos\theta. \tag{45}$$

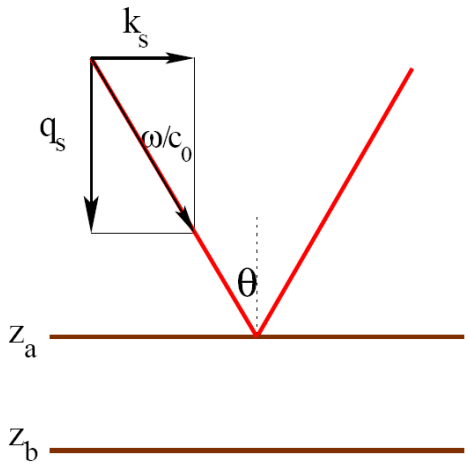

Figure 2: The geometry of the first primary in the data

The reference vertical speed is defined as

$$c_v = \frac{c_0}{cos\theta}, \tag{46}$$

the reference horizontal speed is defined as

$$c_h = \frac{c_0}{sin\theta}. \tag{47}$$

and the horizontal travel time is

$$t_h = \frac{x_g - x_s}{c_h} = \frac{2x_h}{c_h}, \tag{48}$$

The pseudo depths of the first and second reflectors become

$$z_1 = c_v t_{v1}/2, \tag{49}$$
$$z_2 = c_v t_{v2}/2. \tag{50}$$

where t_{v1} and t_{v2} are the vertical travel times for the first and second primaries, respectively.

Therefore, the total travel times for the first and second primaries are $T_1 = t_{v1}+t_h$ and $T_2 = t_{v2}+t_h$, respectively.

The reflected data due to the incident plane wave source is

$$b_1(t) = R_1\delta(t - T_1) + R_2T_1T_1'\delta(t - T_2). \tag{51}$$

Fourier transforming into the frequency ω domain gives

$$\begin{aligned} b_1(\omega) &= R_1 e^{i\omega T_1} + R_2 T_1 T_1' e^{i\omega T_2} \\ &= R_1 e^{i\omega(t_{v1}+t_h)} + R_2 T_1 T_1' e^{i\omega(t_{v_2}+t_h)} \\ &= [R_1 e^{i(\frac{2\omega}{c_v})(\frac{c_v t_{v1}}{2})} + R_2 T_1 T_1' e^{i(\frac{2\omega}{c_v})(\frac{c_v t_{v2}}{2})}] e^{i(\frac{2\omega}{c_h})(\frac{c_h t_h}{2})}. \end{aligned} \tag{52}$$

Equation (52) can be rewritten as

$$b_1(k_h, k_z) = [R_1 e^{ik_z z_1} + R_2 T_1 T_1' e^{ik_z z_2}] e^{ik_h x_h}. \tag{53}$$

Fourier transforming b_1 over x_h, we find

$$b_1(k_h, k_z) = [R_1 e^{ik_z z_1} + R_2 T_1 T_1' e^{ik_z z_2}] \delta(k_g - k_s). \tag{54}$$

Inverse Fourier transforming equation (53) over k_z gives

$$b_1(k_h, z) = [R_1 \delta(z - z_1) + R_2 T_1 T_1' \delta(z - z_2)] \delta(k_g - k_s) \tag{55}$$

Substituting equation (55) into the third integral of equation (23), we have

$$\begin{aligned} &\int_{z_2'+\epsilon}^{\infty} dz_3' e^{ik_z z_3'} [R_1 \delta(z_3' - z_1) + R_2 T_1 T_1' \delta(z_3' - z_2)] \delta(k_2 - k_s) \\ &= [R_1 e^{ik_z z_1} H(z_1 - (z_2' + \epsilon)) + R_2 T_1 T_1' e^{ik_z z_2} H(z_2 - (z_2' + \epsilon))] \delta(k_2 - k_s). \end{aligned} \tag{56}$$

The second integral is

$$\begin{aligned} &\int_{-\infty}^{z_1'-\epsilon} dz_2' e^{-ik_z z_2'} [R_1 \delta(z_2' - z_1) + R_2 T_1 T_1' \delta(z_2' - z_2)] \delta(k_1 - k_2) \\ &\quad \cdot [R_1 e^{ik_z z_1} H(z_1 - (z_2' + \epsilon)) + R_2 T_1 T_1' e^{ik_z z_2} H(z_2 - (z_2' + \epsilon))] \delta(k_2 - k_s) \\ &\quad = R_1^2 e^{ik_z(z_1 - z_1)} \underline{H(z_1 - (z_1 + \epsilon))} H((z_1' - \epsilon) - z_1) \delta(k_1 - k_2) \delta(k_2 - k_s) \\ &\quad + R_1 R_2 T_1 T_1' e^{ik_z(z_1 - z_2)} \underline{H(z_1 - (z_2 + \epsilon))} H((z_1' - \epsilon) - z_2) \delta(k_1 - k_2) \delta(k_2 - k_s) \\ &\quad + R_1 R_2 T_1 T_1' e^{ik_z(z_2 - z_1)} H(z_2 - (z_1 + \epsilon)) H((z_1' - \epsilon) - z_1) \delta(k_1 - k_2) \delta(k_2 - k_s) \\ &\quad + R_2^2 T_1^2 T_1'^2 e^{ik_z(z_2 - z_2)} \underline{H(z_2 - (z_2 + \epsilon))} H((z_1' - \epsilon) - z_2) \delta(k_1 - k_2) \delta(k_2 - k_s). \end{aligned} \tag{57}$$

The underline Heaviside functions are zero. The remaining third term is

$$[R_1 R_2 T_1 T_1' e^{ik_z(z_2 - z_1)} H(z_2 - (z_1 + \epsilon)) H((z_1' - \epsilon) - z_1)] \delta(k_1 - k_2) \delta(k_2 - k_s). \tag{58}$$

Therefore,

$$\begin{aligned} b_3(k_h, k_z) &= \int_{-\infty}^{\infty} dz_1' e^{-ik_z z_1'} [R_1 \delta(z_1' - z_1) + R_2 T_1 T_1' \delta(z_1' - z_2)] \delta(k_g - k_1) \\ &\quad \cdot [R_1 R_2 T_1 T_1' e^{ik_z(z_2 - z_1)} H(z_2 - (z_1 + \epsilon)) H((z_1' - \epsilon) - z_1)] \delta(k_1 - k_2) \delta(k_2 - k_s) \\ &\quad = R_1^2 R_2 T_1 T_1' e^{ik_z(z_2 - z_1 + z_1)} H(z_2 - (z_1 + \epsilon)) \underline{H((z_1 - \epsilon) - z_1)} \delta(k_g - k_1) \delta(k_1 - k_2) \delta(k_2 - k_s) \\ &\quad + R_1 R_2^2 T_1^2 T_1'^2 e^{ik_z(z_2 - z_1 + z_2)} H(z_2 - (z_1 + \epsilon)) H(z_2 - \epsilon - z_1) \delta(k_g - k_1) \delta(k_1 - k_2) \delta(k_2 - k_s) \\ &\quad = R_1 R_2^2 T_1^2 T_1'^2 e^{ik_z(2z_2 - z_1)} \delta(k_g - k_1) \delta(k_1 - k_2) \delta(k_2 - k_s) \end{aligned} \tag{59}$$

where the underline term is zero.

The result for the b_3 is

$$\begin{aligned} b_3(k_h,k_z) &= \int_{-\infty}^{\infty} dk_1 \int_{-\infty}^{\infty} dk_2 R_1 R_2^2 T_1^2 T_1'^2 e^{ik_z(2z_2-z_1)} \delta(k_g-k_1)\delta(k_1-k_2)\delta(k_2-k_s) \\ &= R_1 R_2^2 T_1^2 T_1'^2 e^{ik_z(2z_2-z_1)} \delta(k_g-k_s) \\ &= R_1 R_2^2 T_1^2 T_1'^2 e^{i2(\omega/c_v)(2c_v t_{v2}/2 - c_v t_{v1}/2)} e^{i(2\omega/c_h)(c_h t_h/2)} \\ &= R_1 R_2^2 T_1^2 T_1'^2 e^{i\omega(2t_{v2}-t_{v1})} e^{i\omega t_h} \end{aligned} \tag{60}$$

One can see that the result of equation (59) agrees with the expression of the actual internal multiple,

$$IM_{actual} = R_1 R_2^2 T_1 T_1' e^{i\omega(2t_{v2}-t_{v1})} e^{i\omega t_h}, \tag{61}$$

except for the extra factor of $T_1 T_1'$, which is always less than but close to 1.

If we pick a wrong reference velocity, c_0', to perform the internal multiple algorithm, the new vertical and horizontal velocities become $c_v' = \frac{c_0'}{cos\theta}$ and $c_h' = \frac{c_0'}{sin\theta}$, respectively. The new pseudo depths are

$$z_1' = c_v' t_{v1}/2, \tag{62}$$

$$z_2' = c_v' t_{v2}/2. \tag{63}$$

where t_{v1} and t_{v2} are the vertical travel times for first and second primaries, respectively.

The horizontal travel time becomes

$$t_h' = \frac{x_g - x_s}{c_h'} = \frac{2x_h}{c_h'}. \tag{64}$$

Subsituting equations (62), (63) and (64) into equation (59), we have

$$IM_{est} = R_1 R_2^2 T_1^2 T_1'^2 e^{i\omega(2t_{v2}-t_{v1})} e^{i\omega t_h'}. \tag{65}$$

Comparing equation (65) to (61), one can see that the pseudo depths varies when we choose a wrong reference velocity, but the vertical traveltimes t_{v1} and t_{v2} remain unchanged. However, the horizontal traveltime changes if we use a wrong reference velocity since the horizontal distance between source and receiver is fixed. In other words, the error due to the wrong velocity occurs in the horizontal direction so the total traveltime ($T = (2t_{v2} - t_{v1}) + t_h'$) may not be precisely predicted.

From the 1.5D analytic example, we find the inverse scattering series internal multiple algorithm is sensitive to the reference velocity. In the marine case, the reference velocity, namely water speed, is well-known so we have no problem predicting the correct timing of internal multiples. However, in elastic internal multiple attenuation, the sensitivity to reference velocity becomes an important issue. In order to properly perform the attenuation algorithm, an accurate reference velocity is necessary.

Conclusion and Future Plan

This study showed that the inverse scattering series is a direct and effective method to predict internal multiples without any information below the measurement surface. However, four-component data are needed to perform this algorithm effectively. Another requirement, the known reference velocities, has effects on (P, S) decomposition and predicting the total traveltimes of internal multiples. We followed the analysis of Weglein and Matson (1998) and Nita and Weglein (2005) to further investigate reference velocity sensitivity issue. The result revealed that velocity errors may have an effect on predicting the correct timing of the interanl multiples for the 1D normal incidence case. Therefore, this study will focus on the issue of reference velocity so that we can optimize the performance of internal multiple attenuation for land data.

Acknowledgments

We are grateful to all M-OSRP sponsors for supporting our research. We also thank all the members in M-OSRP for reviewing this manuscript and valuable discussions.

References

Araújo, F. V. *Linear and non-linear methods derived from scattering theory: backscattered tomography and internal multiple attenuation.* PhD thesis, Universidade Federal da Bahia, 1994.

Carvalho, P. M. *Free-surface multiple reflection elimination method based on nonlinear inversion of seismic data.* PhD thesis, Universidade Federal da Bahia, 1992.

Matson, K. H. *An inverse-scattering series method for attenuating elastic multiples from multicomponent land and ocean bottom seismic data.* PhD thesis, University of British Columbia, 1997.

Nita, Bogdan G. and Arthur B. Weglein. Inverse scattering internal multiple attenuation algorithm in complex multi-d media. Technical report, Mission-Oriented Seismic Research Project, University of Houston, 2005.

Weglein, A. B., F. V. Araújo, P. M. Carvalho, R. H. Stolt, K. H. Matson, R. T. Coates, D. Corrigan, D. J. Foster, S. A. Shaw, and H. Zhang. "Inverse Scattering Series and Seismic Exploration." *Inverse Problems* (2003): R27–R83.

Weglein, A. B., F. A. Gasparotto, P. M. Carvalho, and R. H. Stolt. "An Inverse-Scattering Series Method for Attenuating Multiples in Seismic Reflection Data." *Geophysics* 62 (November-December 1997): 1975–1989.

Weglein, A. B. and R. H. Stolt. *I. The wave physics of downward continuation, wavelet estimation and volume and surface scattering. II. Approaches to linear and non-linear migration inversion.* Mathematical Frontiers in Reflection Seismology. SEG/SIAM, 1995.

Weglein, Arthur B. and Ken H. Matson. "Inverse scattering internal multiple attenuation: an analytic example and subevent interpretation." SPIE, 1998, 108–117.

Inverse scattering series with lateral variations in 3D

F. Liu and A. B. Weglein

Abstract

This articles represents one part of the integrated efforts in M-OSRP for velocity independent seismic imaging algorithms, it focuses on the 3D nature of wave propagation in the field acquisition. In this stage, we assume sifficient data coverage to allow a full wave-theoretical treatment. Simultaneously, Wang and Weglein (2007) developed asymptotic method to deal with sparse sampling in the cross-line direction. In the progresive development of the inverse scattering series, this article represents the first two terms of the inverse scattering series (Weglein et al., 2003) with lateral variations, and is an exnension of the 2D seismic imaging algorithm detailed in Liu (2006) into 3D. It brings the velocity independent imaging algorithm one step closer to the field-data test. A compact vector notation is identified to make our 3D formalism very similar to its 2D predecessor, simplifying the 3D upgrade of the our existing 2D computer programs. New structures of the algorithms specific to 3D, for example, vectorized partial derivatives over lateral coordinates and their interaction in the inverse scattering series, are also identified and documented.

1 Introduction

This article studies the inverse scattering series (ISS) as it pertains to imaging in a laterally- and vertically-varying acoustic medium in 3D.

The notations and derivation strategies are specifically tailored so that the extended formalism resembles the procedure of Liu (2006) as much as possible. After expressing the horizontal coordinates in a single vector notation, our method in 3D shows remarkable resemblance with its 2D counterpart in Liu (2006), especially the 1D generalizable term in equation 33, which is essentially the same as Shaw (2005). Compared with many current seismic imaging methods, the extension from 2D to 3D is very straightforward in the inverse scattering series: good news for for upgrading our existing 2D code to 3D. One of 3D-specific structure of the algorithms is that, if we define the partial derivatives over the laterial coordinates as vectors, the simple product in the 2D algorithm simply become dot products between vectors in our 3D algorithm, for example equation 34.

In this article, portions of the first and second order terms in the ISS are derived. Each term is separated into "1D generalized" terms vs. terms "without 1D analogy". The "1D generalized" portion (equation (33)) of these terms is demonstrated to sum to closed form (equation (39)).

Sections 3–4 contain sequential presentations of the derived forms (full and/or partial) for the 1^{st}–2^{nd} order terms, of a wavespeed perturbation that is permitted variation in both lateral and vertical coordinates. Section 5 describes the organization and summation of subsets of the previously derived terms.

Although presented concisely in this chapter, these derivations contain relatively involved mathematics; much of the detail is included (along with several useful notations and conventions) in an extensive set of appendices. Please refer to relevant appendices for technical detail.

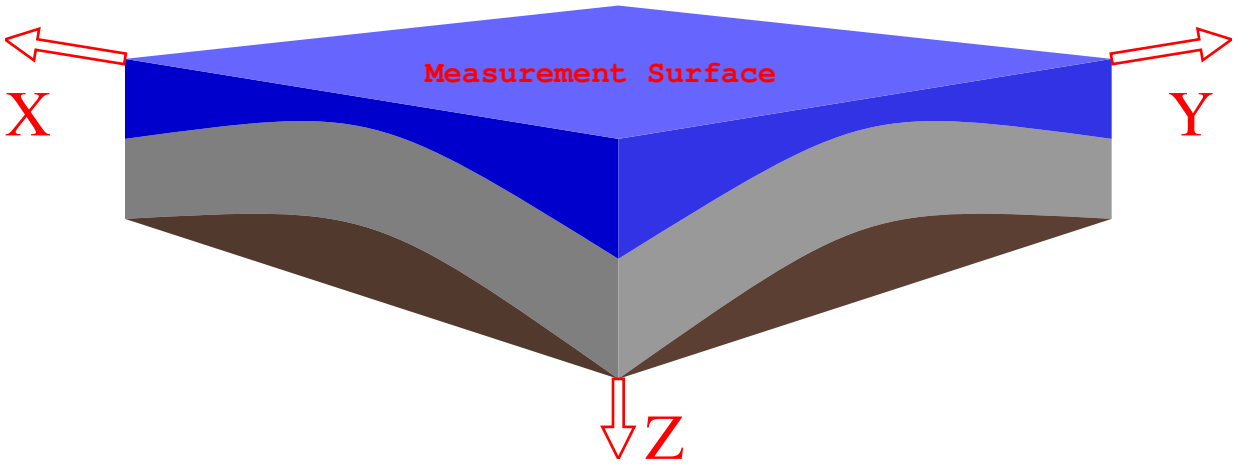

Figure 1: Seismic exploration problem in 3D. The horizontal coordinates are denoted as $\vec{x}$ and y, respectively. The vertical coordinate is denoted as z. In this example, the measurement surface is chosen as $z_g = z_s = 0$, which means both sources and receivers are located at $z = 0$, very typical for reflection seismology.

2 Seismic imaging problems in 3D

Let us consider a simplified seismic experiment in 3D where the elevation of the sources z_s and receivers z_g is fixed (see Fig. 1). In this case, the seismic data should be considered as a function of three variables: the horizontal coordinates of the sources $\vec{x}_s = (x_s, y_s)$, the horizontal coordinates of the receivers $\vec{x}_g = (x_g, y_g)$, and time t: totally five degree of freedom.

In many formalisms for seismic imaging, a certain model (often much simplified) is assumed for the derivation of the algorithm. For example, in the most popular constant-density acoustic model, only the velocity is assumed to be varying. If velocity is the only objective function, the Earth has only three degrees of freedom: the horizontal coordinates $\vec{x} = (x, y)$ and the vertical coordinate z. There are two more degrees of freedom in the data than the objective function. The extra freedom must be reduced to reach an answer. In this article, a constant vector of angles $\vec{\theta} = (\theta_x, \theta_y)$ is chosen to make a consistent reduction; for the detail of the angle-vector $\vec{\theta}$, see equation (27). Physically, $\vec{\theta}$ represents the incidence angle of synthesized plane-wave.

For a constant-density acoustic model, the mathematical description of the wave-propagation problem is,

$$\left(\frac{\partial^2}{\partial x^2}+\frac{\partial^2}{\partial y^2}+\frac{\partial^2}{\partial z^2}+\frac{\omega^2}{c^2(x,y,z)}\right)P(x,y,z,x_s,y_s,z_s,\omega)=\delta(x-x_s)\delta(y-y_s)\delta(z-z_s)A(\omega), \quad (1)$$

where ω is the temporary frequency (the Fourier conjugate of time t), $P(x, y, z, x_s, y_s, z_s, \omega)$ is the wave-field, $A(\omega)$ is the **source signature** (or **wavelet**), the function $c(x, y, z)$ is the velocity field governing the wave propagation in the subsurface. If the wavelet is known and its effect had been

compensated for, we can use $A(\omega) = 1$, and the corresponding wave-field is called the **Green's function** (or **impulse response**) in the medium $c(x, y, z)$,

$$\left(\frac{\partial^2}{\partial x^2} + \frac{\partial^2}{\partial y^2} + \frac{\partial^2}{\partial z^2} + \frac{\omega^2}{c^2(x, y, z)}\right) G(x, y, z, x_s, y_s, z_s, \omega) = \delta(x - x_s)\delta(y - y_s)\delta(z - z_s). \quad (2)$$

The inverse scattering series (ISS) is a procedure to construct the medium property $c(x, y, z)$ using a reference velocity c_0 [1] and its corresponding Green's function G_0,

$$\left(\frac{\partial^2}{\partial x^2} + \frac{\partial^2}{\partial y^2} + \frac{\partial^2}{\partial z^2} + \frac{\omega^2}{c_0^2}\right) G_0(x, y, z, x_s, y_s, z_s, \omega) = \delta(x - x_s)\delta(y - y_s)\delta(z - z_s). \quad (3)$$

The major reason to choose the constant reference velocity is the availability of the analytic solution for its Green's function and exact analytic inverse for the corresponding integral equation.

For constant velocity c_0, the reference Green's function G_0 can be obtained by applying the following Fourier transforms on both sides of equation (3),

$$\int_{-\infty}^{\infty} dx \int_{-\infty}^{\infty} dy e^{-i(k_x x + k_y y)}. \quad (4)$$

We have,

$$\left(\frac{\partial^2}{\partial z^2} + q^2\right) \widetilde{G_0}(k_x, k_y, z, x_s, y_s, z_s, \omega) = \delta(z - z_s) e^{-i(k_x x_s + k_y y_s)}, \quad (5)$$

where,

$$q^2 = \frac{\omega^2}{c_0^2} - k_x^2 - k_y^2$$
$$q = \mathrm{sgn}(\omega)\sqrt{\frac{\omega^2}{c_0^2} - k_x^2 - k_y^2}$$

and,

$$\widetilde{G_0}(k_x, k_y, z, x_s, y_s, z_s, \omega) = \int_{-\infty}^{\infty} dx \int_{-\infty}^{\infty} dy e^{-i(k_x x + k_y y)} G_0(x, y, z, x_s, y_s, z_s, \omega). \quad (6)$$

[1] in this article, the reference velocity is chosen as a constant

Throughout this article, the function sgn is defined as the sign of its argument:

$$\mathrm{sgn}(x) = \begin{cases} 1 & (x > 0) \\ 0 & (x = 0) \\ -1 & (x < 0) \end{cases} \tag{7}$$

Equation (5) is a wave-equation in 1D, its casual solution can be obtained by multiplying the solution of 1D Green's function with an extra factor $e^{-i(k_x x_s + k_y y_s)}$:

$$\widetilde{G_0}(k_x, k_y, z, x_s, y_s, z_s, \omega) = e^{-i(k_x x_s + k_y y_s)} \frac{e^{iq|z-z_s|}}{2iq}. \tag{8}$$

The Fourier transform in equation (4) has a corresponding inverse Fourier transform,

$$\frac{1}{4\pi^2} \int_{-\infty}^{\infty} dk_x \int_{-\infty}^{\infty} dk_y e^{i(k_x x + k_y y)}. \tag{9}$$

Using the inverse Fourier transform in equation (9), we transform the solution in equation (8) to the solution of equation (3),

$$\widetilde{G_0}(x, y, z, x_s, y_s, z_s, \omega) = \frac{1}{4\pi^2} \int_{-\infty}^{\infty} dx \int_{-\infty}^{\infty} dy e^{i(k_x[x-x_s] + k_y[y-y_s])} \frac{e^{iq|z-z_z|}}{2iq}. \tag{10}$$

If we use the vector notation: $\vec{k} = (k_x, k_y)$, $k^2 = |\vec{k}|^2 = k_x^2 + k_y^2$, $\vec{x} = (x, y)$, $\vec{x}_s = (x_s, y_s)$, and define: $\vec{\int} d\vec{x}$ as $\vec{\int} d\vec{x} = \int_{-\infty}^{\infty} \int_{-\infty}^{\infty} dx dy$, equation (10) can be further simplified,

$$G_0(\vec{x}, z, \vec{x}_s, z_s, \omega) = \frac{1}{4\pi^2} \int_{-\infty}^{\infty} dx \int_{-\infty}^{\infty} dy e^{i\vec{k}\bullet(\vec{x}-\vec{x}_s)} \frac{e^{iq|z-z_z|}}{2iq} = \frac{1}{4\pi^2} \vec{\int} d\vec{x} e^{i\vec{k}\bullet(\vec{x}-\vec{x}_s)} \frac{e^{iq|z-z_z|}}{2iq}. \tag{11}$$

Using a constant reference velocity will result in larger perturbation since the Earth should be much better approximated by a reference velocity that varies with depth. Although a larger perturbation decelerates the convergence rate of the ISS (Shaw et al., 2003), this problem is solved by the availability of fast closed-form solutions (for example, equation (39)) which collapse an infinite number of terms.

The input data D (available only on the measurement surface where $z_g = z_s = 0$) for the inverse scattering series is the difference between the Green's function in the actual and reference medium:

$$D(x_g, y_g, z_g, x_s, y_s, z_s, \omega) = G(x_g, y_g, z_g, x_s, y_s, z_s, \omega) - G_0(x_g, y_g, z_g, x_s, y_s, z_s, \omega) \tag{12}$$

We can denote two horizontal variables: (x, y) with a single vector $\vec{x}$: $\vec{x} = (x, y)$, and similarly $\vec{x}_g = (x_g, y_g)$, $\vec{x}_g = (x_s, y_s)$, $\vec{x}' = (x', y')$, $\vec{x}'' = (x'', y'')$, $\vec{x}''' = (x''', y''')$.

The data in the inverse scattering series can also be considered as the recorded wave-field G with the direct arrival G_0 being removed.

With the data defined in equation (12), the first 3 terms of the inverse series can be iteratively computed in an order-by-order fashion via (Weglein et al., 2003, equation *(11)*∼*(13)*) [2],

$$D(\vec{x}_g, z_g, \vec{x}_s, z_s, \omega) = \int_{-\infty}^{\infty} dz' \vec{\int} d\vec{x}' G_0(\vec{x}_g, z_g, \vec{x}', z', \omega) V_1(\vec{x}', z') G_0(\vec{x}', z', \vec{x}_s, z_s, \omega), \tag{13}$$

at first order,

$$\begin{aligned} 0 = & \int_{-\infty}^{\infty} dz' \vec{\int} d\vec{x}' G_0(\vec{x}_g, z_g, \vec{x}', z', \omega) V_2(\vec{x}', z') G_0(\vec{x}', z', \vec{x}_s, z_s, \omega) \\ & + \int_{-\infty}^{\infty} dz' \vec{\int} d\vec{x}' G_0(\vec{x}_g, z_g, \vec{x}', z', \omega) V_1(\vec{x}', z') \\ & \int_{-\infty}^{\infty} dz'' \vec{\int} d\vec{x}'' G_0(\vec{x}', z', \vec{x}'', z'', \omega) V_1(\vec{x}'', z'') G_0(\vec{x}'', z'', \vec{x}_s, z_s, \omega), \end{aligned} \tag{14}$$

at the second order,

$$\begin{aligned} 0 = & \int_{-\infty}^{\infty} dz' \vec{\int} d\vec{x}' G_0(\vec{x}_g, z_g, \vec{x}', z', \omega) V_3(\vec{x}', z') G_0(\vec{x}', z', \vec{x}_s, z_s, \omega) \\ & + \int_{-\infty}^{\infty} dz' \vec{\int} d\vec{x}' G_0(\vec{x}_g, z_g, \vec{x}', z', \omega) V_1(\vec{x}', z') \\ & \int_{-\infty}^{\infty} dz'' \vec{\int} d\vec{x}'' G_0(\vec{x}', z', \vec{x}'', z'', \omega) V_2(\vec{x}'', z'') G_0(\vec{x}'', z'', \vec{x}_s, z_s, \omega) \\ & + \int_{-\infty}^{\infty} dz' \vec{\int} d\vec{x}' G_0(\vec{x}_g, z_g, \vec{x}', z', \omega) V_2(\vec{x}', z') \\ & \int_{-\infty}^{\infty} dz'' \vec{\int} d\vec{x}'' G_0(\vec{x}', z', \vec{x}'', z'', \omega) V_1(\vec{x}'', z'') G_0(\vec{x}'', z'', \vec{x}_s, z_s, \omega) \\ & + \int_{-\infty}^{\infty} dz' \vec{\int} d\vec{x}' G_0(\vec{x}_g, z_g, \vec{x}', z', \omega) V_1(\vec{x}', z') \\ & \int_{-\infty}^{\infty} dz'' \vec{\int} d\vec{x}'' G_0(\vec{x}', z', \vec{x}'', z'', \omega) V_1(\vec{x}'', z'') \\ & \int_{-\infty}^{\infty} dz''' \vec{\int} d\vec{x}''' G_0(\vec{x}'', z'', \vec{x}''', z''', \omega) V_1(\vec{x}''', z''') G_0(\vec{x}''', z''', \vec{x}_s, z_s, \omega), \end{aligned} \tag{15}$$

[2] Each equation is explicitly written in the integral form rather than the operator form in the reference.

at third order, etc., in which

$$V_n(\vec{x},z) = \frac{\omega^2}{c_0^2}\alpha_n(\vec{x},z), \tag{16}$$

and $\alpha_n(\vec{x},z)$ is the n-th order component of the wavespeed perturbation $\alpha(\vec{x},z) = \sum_{n=1}^{\infty}\alpha_n(\vec{x},z)$, whose reconstruction is the aim of the inverse scattering series.

This definition of perturbation V is valid for the constant-density acoustic wave equation. In this case, the perturbation is defined as $V = \omega^2\alpha/c_0^2$ where $\alpha(\vec{x},z) = 1 - c_0^2/c^2(\vec{x},z)$. For more details about how the perturbation is defined in the inverse scattering series, interested readers may refer to (Weglein et al., 2003, page-R32).

3 Inversion result of the first term

Changing $\vec{x}$ to $\vec{x}_g$, and $\vec{k}$ to $\vec{k}_g$, the Green's function in equation (11) can also be written as,

$$G_0(\vec{x}_g,z_g,\vec{x}_s,z_s,\omega) = \frac{1}{4\pi^2}\vec{\int} d\vec{k}_g \frac{e^{i\vec{k}_g\bullet(\vec{x}_g-\vec{x}_s)}e^{iq_g|z_g-z_s|}}{2iq_g}, \tag{17}$$

where $\vec{k}_g$ is the Fourier conjugate to $\vec{x}_g$, $q_g = \mathrm{sgn}(\omega)\sqrt{(\omega/c_0)^2 - k_g^2}$, $k_g^2 = |\vec{k}_g|^2$. $(\vec{x}_g,z_g)$ and $(\vec{x}_s,z_s)$ denote the spatial coordinates of the receivers and sources, respectively.

With the Green's function defined in equation (17), equation (13) can be elegantly solved by applying two nested Fourier transforms [3]: $\vec{\int}d\vec{x}_g\vec{\int}d\vec{x}_s e^{i\vec{k}_s\bullet\vec{x}_s - i\vec{k}_g\bullet\vec{x}_g}$, over the lateral source and receiver coordinates to obtain α_1. After the Fourier transform above, the left-hand side of equation (13) become the triple Fourier of the data: $\vec{\vec{\vec{D}}}\left(\vec{k}_g,\vec{k}_s,\omega\right)$, the nested integral on the right-hand-side of equation (13) is reduced to a simple product:

$$\begin{aligned}
&\vec{\int}d\vec{x}'\int_{-\infty}^{\infty}dz'\vec{\int}d\vec{x}_g G_0(\vec{x}_g,z_g,\vec{x}',z',\omega)e^{-i\vec{k}_g\bullet\vec{x}_g}\vec{\int}d\vec{x}_s G_0(\vec{x}',z',\vec{x}_s,z_s,\omega)e^{i\vec{k}_s\bullet\vec{x}_s}\frac{\omega^2}{c_0^2}\alpha_1(\vec{x}',z') \\
=&\vec{\int}d\vec{x}'\int_{-\infty}^{\infty}dz'\frac{\omega^2}{c_0^2}\alpha_1(\vec{x}',z')\vec{\int}d\vec{x}_g G_0(\vec{x}_g,z_g,\vec{x}',z',\omega)e^{-i\vec{k}_g\bullet\vec{x}_g}\vec{\int}d\vec{x}_s G_0(\vec{x}_s,z_s,\vec{x}',z',\omega)e^{i\vec{k}_s\bullet\vec{x}_s}
\end{aligned} \tag{18}$$

The last step in the derivation above using the reciprocity: for acoustic medium the Green's function is the same if you exchange the source and receiver locations. Please notice that the two innermost

[3] Note that the "sign convention" of the Fourier transform is different for the source and geophone coordinates. See Clayton and Stolt (1981) for detail of this choice of Fourier transform.

integral in the equation above, namely the $\vec{\int} d\vec{x}_g$ and $\vec{\int} d\vec{x}_s$ integral, is actually in the same form as equation (6). Since equation (6) can be written in vector form as

$$\widetilde{G_0}(\vec{k}, z, \vec{x}, z_s, \omega) = \vec{\int} d\vec{x} e^{-i\vec{k}\bullet\vec{x}} G_0(\vec{x}, z, \vec{x}_s, z_s, \omega). \tag{19}$$

its ansnwer, given in equation (8), can be written in vector form as,

$$\widetilde{G_0}(\vec{k}, z, \vec{x}_s, z_s, \omega) = e^{-i\vec{k}\bullet\vec{x}_s} \frac{e^{iq|z-z_s|}}{2iq}. \tag{20}$$

And consequently, equation (18) can be written as,

$$\begin{aligned}
&\vec{\int} d\vec{x}' \int_{-\infty}^{\infty} dz' \frac{\omega^2}{c_0^2} \alpha_1(\vec{x}', z') e^{-i\vec{k}_g\bullet\vec{x}'} \frac{e^{iq_g|z_g-z'|}}{2iq_g} e^{i\vec{k}_s\bullet\vec{x}'} \frac{e^{iq_s|z_s-z'|}}{2iq_s} \\
=&\vec{\int} d\vec{x}' \int_{-\infty}^{\infty} dz' \frac{\omega^2}{c_0^2} \alpha_1(\vec{x}', z') e^{-i\vec{k}_g\bullet\vec{x}'} \frac{e^{iq_g(z'-z_g)}}{2iq_g} e^{i\vec{k}_s\bullet\vec{x}'} \frac{e^{iq_s(z'-z_s)}}{2iq_s} \\
=&\vec{\int} d\vec{x}' \int_{-\infty}^{\infty} dz' \frac{\omega^2}{c_0^2} \alpha_1(\vec{x}', z') e^{-i(\vec{k}_g-\vec{k}_s)\bullet\vec{x}'} \frac{e^{i(q_g+q_s)z'}}{-4q_gq_s} \\
=&-\frac{\omega/c_0}{4q_gq_s} \vec{\int} d\vec{x}' e^{-i(\vec{k}_g-\vec{k}_s)\bullet\vec{x}'} \int_{-\infty}^{\infty} dz' e^{i(q_g+q_s)z'} \alpha_1(\vec{x}', z') = -\frac{\omega/c_0}{4q_gq_s} \widetilde{\widetilde{\alpha_1}}(\vec{k}_g-\vec{k}_s, q_g+q_s)
\end{aligned} \tag{21}$$

So we have:

$$\widetilde{\widetilde{\widetilde{D}}}\left(\vec{k}_g, \vec{k}_s, \omega\right) = -\frac{\omega^2}{4q_gq_sc_0^2} \widetilde{\widetilde{\alpha}}_1(\vec{k}_g-\vec{k}_s, q_g+q_s), \tag{22}$$

where $\widetilde{\widetilde{\alpha}}_1$ is the double Fourier transform of $\alpha_1(\vec{x}, z)$:

$$\widetilde{\widetilde{\alpha}}_1(\vec{k}_m, k_z) = \vec{\int} d\vec{x} e^{-i\vec{k}_m\bullet\vec{x}} \int_{-\infty}^{\infty} dz e^{ik_zz} \alpha_1(\vec{x}, z),$$

and $q_g = \text{sgn}(\omega)\sqrt{(\omega/c_0)^2 - k_g^2}$, $q_s = \text{sgn}(\omega)\sqrt{(\omega/c_0)^2 - k_s^2}$, $k_g^2 = |\vec{k}_g|^2$, $k_s^2 = |\vec{k}_s|^2$. $\widetilde{\widetilde{\widetilde{D}}}$ is the triple Fourier transform of the data $D(\vec{x}_g, \vec{x}_s, t)$:

$$\widetilde{\widetilde{D}}\left(\vec{k}_g,\vec{k}_s,\omega\right)=\int d\vec{x}_g e^{i\vec{k}_g\bullet\vec{x}_g}\int d\vec{x}_s e^{-i\vec{k}_s\bullet\vec{x}_s}\int_{-\infty}^{\infty}dt e^{i\omega t}D(\vec{x}_g,x_s,t).$$

Equation (22) can be rearranged as:

$$\widetilde{\widetilde{\alpha}}_1(\vec{k}_g-\vec{k}_s,q_g+q_s)=-4\frac{q_g q_s}{\omega^2/c_0^2}\widetilde{\widetilde{D}}\left(\vec{k}_g,\vec{k}_s,\omega\right), \tag{23}$$

For convenience, let me summarize all the variables and their corresponding Fourier conjugates in the table below:

Physical meaning	Variable name	Fourier conjugate
Horizontal coordinate of the receiver	$\vec{x}_g$	$\vec{k}_g$
Horizontal coordinate of the source	$\vec{x}_s$	$\vec{k}_s$
Time	t	ω
Horizontal coordinate of the mid-point	$\vec{x}_m=0.5(\vec{x}_g+\vec{x}_s)$	$\vec{k}_m=\vec{k}_g-\vec{k}_s=(k_{mx},k_{my})$
Offset	$\vec{x}_h=\vec{x}_g-\vec{x}_s$	$\vec{k}_h=\vec{k}_g+\vec{k}_s=(k_{hx},k_{hy})$

By a simple transformation of coordinates, the data can be transformed to the mid-point $\vec{x}_m$ and offset $\vec{x}_h$ coordinate,

$$\vec{x}_m=\frac{\vec{x}_g+\vec{x}_s}{2}\qquad\qquad \vec{x}_h=\vec{x}_g-\vec{x}_s. \tag{24}$$

Equation (23) can be written in an equivalent form,

$$\widetilde{\widetilde{\alpha}}_1(\vec{k}_m,k_z)=-4\frac{q_g q_s}{\omega^2/c_0^2}\widetilde{\widetilde{D}}\left(\vec{k}_m,\vec{k}_h,k_z\right). \tag{25}$$

In equation (25), $\widetilde{\widetilde{\alpha}}_1(\vec{k}_m,k_z)$ (in the left-side of equation) has three degree of freedom, but $\widetilde{\widetilde{D}}\left(\vec{k}_m,\vec{k}_h,k_z\right)$ (in the right-side of equation) has five degree of freedom. The five-degree of freedom in the right-hand side has to be reduced to three-degree of freedom in the left-hand side. To consistently make such a reduction, we define a vector of two fixed angles $\vec{\theta}=(\theta_x,\theta_y)$, and denote $\sin\vec{\theta}$ as:

$$\sin\vec{\theta}=(\sin\theta_x,\sin\theta_y) \tag{26}$$

With the definition above, we require,

$$\vec{k}_h=\vec{k}_g+\vec{k}_s=2\tfrac{\omega}{c_0}\sin\vec{\theta}\qquad\qquad \vec{k}_g-\vec{k}_s=\vec{k}_m\ . \tag{27}$$

One important reason to choose angle $\vec{\theta}$ as our parameterization is that parameter inversion is normally done as a function of angle, very popular in seismic imaging.

For an arbitrary angle $\vec{\theta}$, we will solve equation (23) under the constraint of equation (27). Consequently, for each k_m and ω, the corresponding vertical wave-number k_z can be calculated by:

$$\begin{aligned} k_z = q_g + q_s = \operatorname{sgn}(\omega)\sqrt{\left(\frac{\omega}{c_0}\right)^2 - \left(\frac{\omega}{c_0}\sin(\theta_x) + \frac{k_{mx}}{2}\right)^2 - \left(\frac{\omega}{c_0}\sin(\theta_y) + \frac{k_{my}}{2}\right)^2} \\ + \operatorname{sgn}(\omega)\sqrt{\left(\frac{\omega}{c_0}\right)^2 - \left(\frac{\omega}{c_0}\sin(\theta_x) - \frac{k_{mx}}{2}\right)^2 - \left(\frac{\omega}{c_0}\sin(\theta_y) - \frac{k_{my}}{2}\right)^2}. \end{aligned}$$

For fixed $\vec{k}_m$ and $\vec{\theta}$, let us consider the equation above as a function of ω:

$$k_z = \kappa(\omega). \tag{28}$$

For the same fixed $\vec{k}_m$ and $\vec{\theta}$, the relation above can be inverted to express ω as a function of k_z:

$$\omega = \kappa^{-1}(k_z) = \frac{c_0 k_z}{2}\sqrt{\frac{k_z^2 + k_m^2}{k_z^2\left[\cos^2\theta_x + \cos^2\theta_y\right] - \left[\vec{k}_m \bullet \sin\vec{\theta}\right]^2}}, \tag{29}$$

where $k_m^2 = |\vec{k}_m|^2 = k_{mx}^2 + k_{my}^2$.

With ω being defined in equation (29), our generalized formalism can be expressed as:

$$\begin{aligned} \widetilde{\widetilde{\alpha}}_1\left(\vec{k}_m, k_z\right) &= -\frac{4q_g q_s}{\omega^2/c_0^2}\widetilde{\widetilde{D}}\left(\frac{\omega\sin\vec{\theta}}{c_0} + \frac{\vec{k}_m}{2}, \frac{\omega\sin\vec{\theta}}{c_0} - \frac{\vec{k}_m}{2}, \omega\right) \\ &= -\frac{4q_g q_s}{\omega^2/c_0^2}\int_{-\infty}^{\infty} d\vec{x}_g e^{-i\vec{k}_g \bullet \vec{x}_g}\int_{-\infty}^{\infty} d\vec{x}_s e^{i\vec{k}_s \bullet \vec{x}_s}\int_{-\infty}^{\infty} dt e^{i\omega t} D\left(\vec{x}_g, \vec{x}_s, t\right). \end{aligned} \tag{30}$$

Let us change the integration variable from ($\vec{x}_g$,$\vec{x}_s$) to ($\vec{x}_m = 0.5(\vec{x}_g + \vec{x}_s)$, $\vec{x}_h = \vec{x}_g - \vec{x}_s$):

$$
\begin{aligned}
&-\frac{4q_gq_s}{\omega^2/c_0^2}\vec{\int}d\vec{x}_m\vec{\int}d\vec{x}_h e^{-i\vec{k}_g\bullet[\vec{x}_m+0.5\vec{x}_h]}e^{i\vec{k}_s\bullet[\vec{x}_m-0.5\vec{x}_h]}\int_{-\infty}^{\infty}dte^{i\omega t}D\left(\vec{x}_m+0.5\vec{x}_h,\vec{x}_m-0.5\vec{x}_h,t\right)\\
&=-\frac{4q_gq_s}{\omega^2/c_0^2}\vec{\int}d\vec{x}_m e^{-i(\vec{k}_g-\vec{k}_s)\bullet\vec{x}_m}\vec{\int}d\vec{x}_h e^{-i(\vec{k}_g+\vec{k}_s)\bullet\vec{x}_h/2}\int_{-\infty}^{\infty}dte^{i\omega t}D\left(\vec{x}_m+0.5\vec{x}_h,\vec{x}_m-0.5\vec{x}_h,t\right)\\
&=-\frac{4q_gq_s}{\omega^2/c_0^2}\vec{\int}d\vec{x}_m e^{-i\vec{k}_m\bullet\vec{x}_m}\vec{\int}d\vec{x}_h e^{-i\frac{\omega\sin\vec{\theta}}{c_0}\bullet\vec{x}_h}\int_{-\infty}^{\infty}dte^{i\omega t}D\left(\vec{x}_m+0.5\vec{x}_h,\vec{x}_m-0.5\vec{x}_h,t\right)\\
&=-\frac{4q_gq_s}{\omega^2/c_0^2}\vec{\int}d\vec{x}_m e^{-i\vec{k}_m\bullet\vec{x}_m}\int_{-\infty}^{\infty}dt\vec{\int}d\vec{x}_h e^{i\omega\left[t-\frac{\sin(\vec{\theta})\bullet\vec{x}_h}{c_0}\right]}D\left(\vec{x}_m+0.5\vec{x}_h,\vec{x}_m-0.5\vec{x}_h,t\right)
\end{aligned}
$$

With another change of the integration variable from t to $(\tau = t - \frac{\sin(\vec{\theta})\bullet\vec{x}_h}{c_0})$, the expression above can be written as:

$$
\begin{aligned}
&-\frac{4q_gq_s}{\omega^2/c_0^2}\vec{\int}d\vec{x}_m e^{-i\vec{k}_m\bullet\vec{x}_m}\int_{-\infty}^{\infty}e^{i\omega\tau}d\tau\vec{\int}d\vec{x}_h D\left(\vec{x}_m+0.5\vec{x}_h,\vec{x}_m-0.5\vec{x}_h,\tau+\frac{\sin(\vec{\theta})\bullet\vec{x}_h}{c_0}\right)\\
&=-\frac{4q_gq_s}{\omega^2/c_0^2}\vec{\int}d\vec{x}_m e^{-i\vec{k}_m\bullet\vec{x}_m}\int_{-\infty}^{\infty}d\tau e^{i\omega\tau}D^{\tau p}\left(\vec{x}_m,\tau\right)
\end{aligned}
$$

where $D^{\tau p}$ is simply the linear Radon transform of all traces within a **CMP** gather [4]:

$$
D^{\tau p}\left(\vec{x}_m,\tau\right)=\vec{\int}d\vec{x}_h D\left(\vec{x}_m+\frac{\vec{x}_h}{2},\vec{x}_m-\frac{\vec{x}_h}{2},\tau+\frac{\sin(\vec{\theta})\bullet\vec{x}_h}{c_0}\right). \tag{31}
$$

The equation above is defined for the expression of α_1 :

$$
\widetilde{\widetilde{\alpha}}_1\left(\vec{k}_m,k_z\right)=-\frac{4q_gq_s}{\omega^2/c_0^2}\vec{\int}d\vec{x}_m e^{-i\vec{k}_m\bullet\vec{x}_m}\int_{-\infty}^{\infty}d\tau e^{i\omega\tau}D^{\tau p}\left(\vec{x}_m,\tau\right). \tag{32}
$$

[4] CMP means "common mid-point". A **CMP**-gather is the set of seismic data sharing the same mid-point $\vec{x}_m$.

The advantages of expressing data in this form are: (1) an easier cut of the direct-arrivals, and (2), very straightforward control over the amplitude and waveform [5]. Similar slant-stacking idea can be found in (Shaw, 2005, equation *3.12* and *3.13*).

There are also pre-processing procedures that can be more easily and quickly done in the $\tau - p$ domain (the data after slant stacking) than in the original domain; the computation cost can be greatly reduced since the freedom of the data is reduced.

4 Inversion result of the second term

In the previous section, α_1 is derived in a general form where the angle θ can be an arbitrary constant [6]. From now on, the derivation of α_2 and later terms is only the special case $\theta = 0$.

In the derivation of α_2 (see, for instance, Liu (2006)), there begins to arise some of the complexity characteristics of this multidimensional Earth problem. Only the result is presented here, interested readers may refer to Appendix C for a complete analysis (see also Appendix A and B for an introduction to the derivation and analytical strategy used.). The second-order term α_2 is computed using α_1 via equation (14). In the final result, α_2 is split into 3 parts: $\alpha_2 = \alpha_{2,1} + \alpha_{2,2} + \alpha_{2,3}$. The first two terms are 1D-generalizable and can be expressed in the $(\vec{x}, z)$ domain as

$$\alpha_{2,1}(\vec{x}, z) = -\frac{1}{2}\alpha_1^2(\vec{x}, z) - \frac{1}{2}\frac{\partial \alpha_1(\vec{x}, z)}{\partial z} \int_{-\infty}^{z} \alpha_1(\vec{x}, u) du, \tag{33}$$

and

$$\alpha_{2,2}(\vec{x}, z) = \frac{1}{2}\frac{\partial \alpha_1(\vec{x}, z)}{\partial \vec{x}} \bullet \int_{-\infty}^{z} du \int_{-\infty}^{u} dv \frac{\partial \alpha_1(\vec{x}, v)}{\partial \vec{x}}. \tag{34}$$

Equation (33) is identical to the α_2 equation obtained by Shaw (2005) and Liu (2006), except for the lateral variable $\vec{x}$. From a mechanical point of view, we recall from the interpretation of Shaw that the presence in the inverse scattering series of the weighted n-th partial derivative of α_1 with respect to z was indicative of the n-th term in a series to correct the location of a reflector in depth. In equation (33), the z-corrective behavior is clearly seen in the multidimensional case also. What appears in this analysis for the first time is a weighted first partial derivative [7] with respect to $\vec{x}$,

[5] The sources in seismic exploration are localized in space, which produce reflection data with varying waveform for different offsets even for the simplest horizontal reflectors. But after applying the linear Radon transform, which can be easily implemented, we have a physical problem with plane-wave incidence. For a horizontal reflector, the reflection responses to an incident plan-wave share the same waveform for different incident angles.

[6] Of course, in the actual computation, the value of θ should not be so big that post-critical phenomena occurs.

[7] In this case, since $\vec{x}$ is a vector $\vec{x} = (x, y)$, $\frac{\partial}{\partial \vec{x}}$ is defined as the following vector $\left(\frac{\partial}{\partial x}, \frac{\partial}{\partial y}\right)$. And in this article "$\bullet$" is the dot product of two vectors.

in equation (34). This term, being a low order derivative with respect to the lateral coordinate of α_1, should be regarded as a low order term in the construction of a laterally corrective function. It is intriguing to note that the coefficient of this lateral corrector involves integrals over *depth* z.

Equation 34 can be considered as the derivative with respect to $\vec{x}$ of the first term in the 1D inverse series α_1, multiplied by (in an inner-product sense) one-half of the following newly defined factor:

$$F(\vec{x},z)=\int_{-\infty}^{z}du\int_{-\infty}^{u}dv\frac{\partial\alpha_1(\vec{x},v)}{d\vec{x}}dv \tag{35}$$

The last component of α_2 is expressed in the $(\vec{k}_m,z)$ domain because its equivalent expression in the $(\vec{x}_m,z)$ domain is much more complicated:

$$\begin{aligned}\widetilde{\alpha}_{2,3}(\vec{k}_m,z)=\frac{1}{8\pi^2}\vec{\int}d\vec{k}_1\int_{-\infty}^{\infty}dz_1\widetilde{\alpha}_1\left(0.5\vec{k}_m-\vec{k}_1,z_1\right)\int_{-\infty}^{z_1}dz_2\widetilde{\alpha}_1\left(\vec{k}_1+0.5\vec{k}_m,z_2\right)\\ \widetilde{\xi}_2\left(\vec{k}_m,\vec{k}_1,\frac{z_1+z_2}{2}-z,\frac{z_1-z_2}{2}\right),\end{aligned} \tag{36}$$

where $\widetilde{\xi}_2$ is defined as follows:

$$\begin{aligned}&\widetilde{\xi}_2\left(\vec{k}_m,\vec{k}_1,\varepsilon_0,\varepsilon_1\right)=\int_{-\infty}^{\infty}e^{i(\varepsilon_0+\varepsilon_1)k_z}dk_z\left(i\frac{k_z^2+k_m^2}{u_1}e^{i\triangle\psi}-ik_z+\frac{\varepsilon_1a_1}{2}\right)\\ &a_1=k_m^2-4k_1^2\qquad u_1=\mathrm{sgn}(k_z)\sqrt{k_z^2+a_1}\qquad\triangle\psi=\varepsilon_1(u_1-k_z).\end{aligned} \tag{37}$$

Please notice that the $\widetilde{\xi}_2$ in equation 37 is exactly the same as the $\widetilde{\xi}_2$ expression in equaton (2.28) in terms of k_m^2 and k_1^2.

Neither $\alpha_{2,2}$ nor $\alpha_{2,3}$ have no 1D analogy and both will vanish if the Earth has no lateral variation.

5 Patterns and closed-forms

In this section, the sets of terms that have aggregate meaning in light of our understanding of the 1D imaging subseries are accumulated. As stated above, there is a complete recurrence of the depth-sensitive terms found in the 1D/1.5D analysis [8].

Generally our approach has been to explicitly manipulate and compute terms in the inverse scattering series until patterns emerge that permit the prediction of certain subclasses of subsequent

[8] for reference, see Shaw et al. (2003)

series terms. At present however, with second and third order components of α computed, there is sufficient information to identify and move forward with a set of patterns. These patterns and the closed-forms are itemized below:

A closed form for "1D-generalized" terms

In α_2 inversion result appear terms (see equation (33)) that are in essence identical to expressions obtained under the 1D Earth assumption (The only difference is an extra lateral variable $\vec{x}$). As a result, the leading-order imaging subseries in a 1D Earth (see equation (17) in Shaw et al. (2003)) can be trivially extended for a multi-dimensional Earth by simply adding a lateral variable $\vec{x}$ as:

$$\alpha^{LOIS}(\vec{x},z)=\alpha_1\left(\vec{x},z-\frac{1}{2}\int\limits_{-\infty}^{z}\alpha_1(\vec{x},u)du\right),$$

the superscript LOIS in the equation above means "Leading order imaging subseries".

The first- and higher-order lateral corrector terms (involving lateral derivatives as discussed above), when collapsed in the correct way may be added to this term.

A closed form for part of the 1st order lateral corrector

Notice that the first term of $\alpha_{2,2}$ involve a depth integral of the lateral rate of change of α_1, multiplied by the first derivative (with respect to $\vec{x}$) of a growing set of terms akin to the 1D depth imaging series. It seems that the part of a first-order lateral correction will occur given a summation over these depth terms. Calling that quantity $A(\vec{x},z)$, a term of the form

$$\frac{1}{2}\frac{\partial A(\vec{x},z)}{\partial\vec{x}}\bullet\int\limits_{-\infty}^{z}du\int\limits_{-\infty}^{v}dv\frac{\partial\alpha_1(\vec{x},v)}{\partial\vec{x}}$$

is the corresponding closed-form with 1st order lateral correction.

Incorporating non-LOIS imaging components

The leading order imaging subseries is not the entire imaging subseries. There are higher order terms left out which will be more pronounced for larger contrasts. Let us look at the 1D leading order imaging subseries (Shaw et al., 2003, equation (17)):

$$\alpha^{LOIS}(z)=\sum_{n=0}^{\infty}\frac{(-1/2)^n}{n!}\frac{d^n\alpha_1(z)}{dz^n}\left(\int\limits_{-\infty}^{z}du\alpha_1(u)\right)^n=\alpha_1\left(z-\frac{1}{2}\int\limits_{-\infty}^{z}du\alpha_1(u)\right)\qquad(38)$$

The higher-order imaging subseries used in the numerical examples of this article is,

$$\alpha^{HOIS}\left(\vec{x}, z+\frac{1}{2}\int\limits_{-\infty}^{z} du \frac{\alpha_1(\vec{x},u)}{1-\frac{1}{4}\alpha_1(\vec{x},u)}\right)=\alpha_1(\vec{x},z). \tag{39}$$

If the lateral variable $\vec{x}$ is ignored, equation (39) becomes,

$$\alpha^{HOIS}\left(z+\frac{1}{2}\int\limits_{-\infty}^{z} du \frac{\alpha_1(u)}{1-\frac{1}{4}\alpha_1(u)}\right)=\alpha_1(z). \tag{40}$$

Equation (40) is identical to the simultaneous imaging and inversion subseries proposed in (Innanen, 2005, equation (3)) in terms of moving reflectors spatially. The only difference is the fact that equation (39) keeps the amplitude of the reflector unchanged.

For a more general choice of data, i.e., for $\vec{\theta}\neq\vec{0}$, which is defined in equation (27), the higher-order imaging subseries in equation (39) can be generalized as,

$$\alpha^{HOIS}\left(\vec{x}, z+\frac{1}{2}\int\limits_{-\infty}^{z} du \frac{\alpha_1(\vec{x},u)}{\cos^2\theta_x+\cos^2\theta_y-\frac{1}{4}\alpha_1(\vec{x},u)}\right)=\alpha_1(\vec{x},z). \tag{41}$$

.

6 Conclusions

In the effort to push the seismic imaging subseries one more step closer to the field-data testing, we presented a seismic imaging formalism in 3D, keeping maximal resemblance with our corresponding 2D algorithm summarized in Liu (2006) to minimize the modification to our existing 2D code for the future 3D extension. The extension from 2D to 3D is found to be very straightforward in most situations: simply extend the scalar lateral variable to a vector. This similarity is very encouraging in M-OSRP's effort for future field data test.

New structures in our 3D seismic imaging algorithm which is missing in the 2D counterpart are also identified: for example, in equation (34): the partial derivatives over the laterial variables can be viewed as a vector, and the product between laterial derivatives in the 2D algorithm can be extended as a dot product between vectors.

Future test, either of numerical- or field-data, will be carried out to verify the effectiveness of our velocity-independent seismic imaging algorithms.

7 Acknowledgments

The authors would like to thank GX Technology for granting Fang 2006-2007 GXT fellowship. We felt indebted to all M-OSRP members for informative discussions and MOSRP sponsors for their support. This work has been partially funded by NSFCMG award DMS-0327778 and DOE Basic Energy Sciences award DE-FG02-05ER15697.

References

Clayton, R. W. and R. H. Stolt. "A Born-WKBJ inversion method for acoustic reflection data." *Geophysics* 46 (1981): 1559–1567.

Innanen, K. A. "Reflector location using high-order inverse scattering series terms." *M-OSRP Annual Report* 4 (2005): 264–270.

Liu, Fang. *Multi-dimensional depth imaging without an adequate velocity model*. PhD thesis, University of Houston, 2006.

Shaw, S. A., A. B. Weglein, D. J. Foster, K. H. Matson, and R. G. Keys. "Convergence properties of a leading order depth imaging series." *73rd Annual Internat. Mtg., Soc. Expl. Geophys., Expanded Abstracts*. . Soc. Expl. Geophys., 2003. 937–940.

Shaw, Simon. A. *An inverse scattering series algorithm for depth imaging of reflection data from a layered acoustic medium with an unknown velocity model*. PhD thesis, University of Houston, 2005.

Wang, Z. and A. B Weglein. "Preparing data with sparse cross-line sampling and aperture for input to 3D non-linear imaging algorithms." *M-OSRP Annual Report* 6 (2007).

Weglein, A. B., F. V. Araújo, P. M. Carvalho, R. H. Stolt, K. H. Matson, R. T. Coates, D. Corrigan, D. J. Foster, S. A. Shaw, and H. Zhang. "Inverse scattering series and seismic exploration." *Inverse Problems* 19 (2003): R27–R83.

Appendix A: Notations and conventions

In this appendix, we present a detailed derivation of the inverse series up to the second order. We use $\vec{x}$ and z to denote the lateral and vertical coordinates in space, respectively. t is used to denote the time. The Fourier conjugate of t is ω. Fourier transform between $\vec{x}$ and its Fourier conjugate $\vec{k}_m$ is defined as:

$$\widetilde{f}(\vec{k}_m) = \int d\vec{x} e^{-i\vec{k}_m \bullet \vec{x}} f(\vec{x}) \qquad\qquad f(\vec{x}) = \frac{1}{4\pi^2} \int d\vec{k}_m e^{i\vec{k}_m \bullet \vec{x}} \widetilde{f}(\vec{k}_m) \tag{42}$$

The Fourier transform between z and its Fourier conjugate k_z is defined as:

$$\widetilde{f}(k_z) = \int_{-\infty}^{\infty} dz e^{ik_z z} f(z) \qquad\qquad f(z) = \frac{1}{2\pi} \int_{-\infty}^{\infty} dk_z e^{-ik_z z} \widetilde{f}(k_z) \tag{43}$$

We use the tilde sign on top of a function to denote its Fourier transform throughout this note. Single tilde sign means that this expression is in $(\vec{k}_m, z)$ domain, double tilde sign means that this expression is in $(\vec{k}_m, k_z)$. Because α_1 is a function of $(\vec{x}, z)$, time is not explicitly present in α_1 and higher order terms $\alpha_2, \alpha_3, \cdots$. The only place where time is involved is when α_1 is calculated from measured data, which is a function of time.

A very useful concept to simplify inverse scattering terms are permutation sum. It will be defined as follows:

For a function of two variables, like $f(A, B)$, we define the permutation sum $\sum^{\odot}$ as:

$$\begin{aligned} \sum^{\odot} f(A, A) &= f(A, A) \\ \sum^{\odot} f(A, B) &= f(A, B) + f(B, A) \qquad\qquad A \neq B \end{aligned} \tag{44}$$

For a function of three variables, like $f(A, B, C)$, we define the permutation sum $\sum^{\odot}$ as (assuming A, B, C are mutually distinct):

$$\begin{aligned} \sum^{\odot} f(A, A, A) &= f(A, A, A) \\ \sum^{\odot} f(A, A, B) &= f(A, A, B) + f(A, B, A) + f(B, A, A) \\ \sum^{\odot} f(A, B, C) &= f(A, B, C) + f(B, C, A) + f(C, A, B) \\ &\quad + f(A, C, B) + f(B, A, C) + f(C, B, A) \end{aligned} \tag{45}$$

Lots of derivatives and integrals over $\vec{x}$ and z will be used in inverse scattering series. The following notations are suggested for conciseness: $\alpha^x \stackrel{\text{def}}{=} \frac{\partial \alpha}{\partial \vec{x}}$ (which is actually the vector $\left(\frac{\partial \alpha}{\partial x}, \frac{\partial \alpha}{\partial y}\right)$), $\alpha^z \stackrel{\text{def}}{=} \frac{\partial \alpha}{\partial z}$, $\alpha^{x+z} \stackrel{\text{def}}{=} \frac{\partial^2 \alpha}{\partial \vec{x} \partial z}$, $\alpha^{-z} = \int_{-\infty}^{z} du \alpha(\vec{x}, u)$, $\alpha^{-2z} = \int_{-\infty}^{z} du \int_{-\infty}^{u} dv \alpha(\vec{x}, v)$. The reason to use these notations above is that most of the integrals in the derivation are expressible in the form mentioned above. The much more powerful usual notations are not necessary to carry all the physics.

Using superscripts to denote derivatives will cause confusion with powers. That is why in the many places in the derivation procedure, the square of A is often written as AA rather than the popular A^2.

Assuming both A B, and C are functions of $\vec{x}$ and z, the fact that $\frac{\partial (AB)}{\partial z} = \frac{\partial A}{\partial z} B + A \frac{\partial B}{\partial z}$ can be expressed in the short hand notation as:

$$[AB]^z = A^z B + A B^z. \tag{46}$$

Likewise $\frac{\partial (AB)}{\partial \vec{x}} = \frac{\partial A}{\partial \vec{x}} B + A \frac{\partial B}{\partial \vec{x}}$ can be expressed as:

$$[AB]^x = A^x B + A B^x. \tag{47}$$

With integration by parts, we can easily reach the following identity $\int_{-\infty}^{z} A(u) B(u) du = \left(\int_{-\infty}^{z} A(u) du\right) B(z) - \int_{-\infty}^{z} \left(\int_{-\infty}^{z} A(v) dv\right) B'(u) du$, it can be very conveniently expressed in the following short-hand-notation:

$$[AB]^{-z} = A^{-z} B - \left[A^{-z} B^z\right]^{-z}. \tag{48}$$

Of course, there is another way to do the integration by parts, which can be expressed in ordinary notation as,

$$\int_{-\infty}^{z} A(u) B(u) du = A(z) \left(\int_{-\infty}^{z} B(u) du\right) - \int_{-\infty}^{z} A'(u) \left(\int_{-\infty}^{z} B(v) dv\right) du.$$

It can be expressed in our short-hand notation as,

$$[AB]^{-z} = A B^{-z} - \left[A^z B^{-z}\right]^{-z}. \tag{49}$$

A very useful equation is:

$$\left[A \left[A^{-z}\right]^m\right]^{-z} = \frac{1}{m+1} \left[A^{-z}\right]^{m+1} \tag{50}$$

This means: $\int\limits_{-\infty}^{z} A(u) \left(\int_{-\infty}^{u} A(v) dv\right)^m du = \frac{1}{m+1} \left(\int_{-\infty}^{z} A(u) du\right)^{m+1}$. It can be proved by carrying out the $\frac{\partial}{\partial z}$ operation on both sides, both left- and right-hand-side will end up with: $A(z) \left(\int_{-\infty}^{z} A(u) du\right)^m$.

Another useful simplification of integrals is the following:

$$\left[AB^{-z}\right]^{-z} + \left[A^{-z}B\right]^{-z} = A^{-z}B^{-z} \tag{51}$$

which can be easily proved by taking the partial derivative over z on both sides.

Several popular rules for integration over δ-functions are summarized below:

$$\int_{-\infty}^{\infty} f(z)\delta(z - z_0) = f(z_0) \tag{52}$$

$$\int_{-\infty}^{\infty} f(z)\delta'(z - z_0) = -f'(z_0) \tag{53}$$

$$\int_{-\infty}^{\infty} f(z)\delta''(z - z_0) = f''(z_0) \tag{54}$$

Rules mentioned above will be used over and over again in the derivation process. In order to make clear which rule is used, I use the following notation:

$$\cdots = \overrightarrow{(54)} = \cdots$$

to denote the simplification rule specified in equation (54) is used to justify the equivalence between the left and right-hand side.

But some integrals cannot be expressed in the form above, for example, the integral in internal multiple removal. we choose to define any new form of integral by short-hand notations. we define some integrals involved the higher-lower-higher relation (w-diagram), which is critical in the internal multiple algorithm in the inverse scattering series:

$$\mathbb{IM}_1(A, B, C) = \int_{-\infty}^{z} duA(u) \int_{-\infty}^{z} dvC(v)B(u + v - z) \tag{55}$$

$$\mathbb{IM}_2(A, B, C) = \int_{-\infty}^{z} duA(u) \int_{-\infty}^{z} dv(z - v)C(v)B(u + v - z) \tag{56}$$

$$\mathbb{IM}_3(A, B, C) = \int_{-\infty}^{z} duA(u) \int_{-\infty}^{z} dv(z - v)^2C(v)B(u + v - z) \tag{57}$$

$$\mathbb{IM}_{3X}(A,B,C) = \int_{-\infty}^{z} du \frac{\partial^2 A(\vec{x},u)}{\partial \vec{x}^2} \frac{\partial^2}{\partial x^2} \int_{-\infty}^{z} dv (z-v)^2 C(\vec{x},v) B(\vec{x},u+v-z) \tag{58}$$

$$\mathbb{IM}_{4}(A,B,C) = \int_{-\infty}^{z} du (z-u) A(u) \int_{-\infty}^{z} dv (z-v) C(v) B(u+v-z) \tag{59}$$

$$\mathbb{IM}_{4X}(A,B,C) = \int_{-\infty}^{z} du (z-u) \frac{\partial A(u)}{\partial \vec{x}} \frac{\partial}{\partial x} \int_{-\infty}^{z} dv (z-v) C(v) B(u+v-z) \tag{60}$$

Appendix B: Derivation strategies

The mathematics involved in computation of the multidimensional inverse scattering series is complicated, and can be made much more straightforward with some simple conventions. This section provides an overview and intuitive introduction to a particular and useful derivation convention.

Let us begin by reviewing the first order portions of the inverse scattering series, closely following the development of, e.g., Weglein et al. (2003). The desired scattering potential V, which for our purposes describes perturbations of wavespeed away from a constant background wavespeed c_0:

$$V(\vec{x}, z, \omega) = \frac{\omega^2}{c_0^2}\alpha(\vec{x}, z),$$

(in which $\alpha(\vec{x}, z) = 1 - c_0^2/c^2(\vec{x}, z)$ for a true wavespeed distribution $c(\vec{x}, z)$), can be expressed in terms which are first, second, third, ... order in data : $\alpha(\vec{x}, z) = \sum_{n=1}^{\infty} \alpha_n(\vec{x}, z)$. The relationship between various part of V, and corresponding part of α, can be summarized as:

$$V_n(\vec{x}, z, \omega) = \frac{\omega^2}{c_0^2}\alpha_n(\vec{x}, z), \qquad (n = 1, 2, 3, \cdot \cdot \cdot \cdot \cdot)$$

The first order (linear) portion of the inverse scattering series is an exact relationship between V_1 and the scattered field evaluated on a measurement surface (i.e. the data D). In the operator form, this relationship is

$$\mathbf{G_0 V_1 G_0 = D = G - G_0}. \tag{61}$$

Next, consider the well-known α_2 equation:

$$\mathbf{G_0 V_2 G_0 = -G_0 V_1 G_0 V_1 G_0}$$

With $n \geq 3$, the portion of α which is n-th order in data will contain considerably more terms. For example, α_3 contains three pieces:

$$\mathbf{G_0 V_3 G_0 = -G_0 V_1 G_0 V_1 G_0 V_1 G_0 - G_0 V_2 G_0 V_1 G_0 - G_0 V_1 G_0 V_2 G_0}.$$

Generally speaking, for an arbitrary positive integer m, the number of corresponding m-th order terms in the inverse series will depend on how many ways m can be expressed in terms of the sum of smaller positive integers. For example, if $m = 4$, 4 can be expressed in seven different ways: $4 = 1+1+1+1 = 1+1+2 = 1+2+1 = 2+1+1 = 2+2 = 1+3 = 3+1$. That means α_4 will have seven pieces:

$$\begin{aligned}\mathbf{G_0 V_4 G_0 =} & \mathbf{- G_0 V_1 G_0 V_1 G_0 V_1 G_0 V_1 G_0 - G_0 V_1 G_0 V_1 G_0 V_2 G_0 - G_0 V_1 G_0 V_2 G_0 V_1 G_0} \\ & \mathbf{- G_0 V_2 G_0 V_1 G_0 V_1 G_0 - G_0 V_2 G_0 V_2 G_0 - G_0 V_1 G_0 V_3 G_0 - G_0 V_3 G_0 V_1 G_0}.\end{aligned}$$

In order to make clear where each piece comes from, we denote each piece differently. One approach is to use newly defined functions. For example, we define $k = \omega/c_0$, and define the solution of the following problem:

$$G_0 k^2 F G_0 = -G_0 k^2 A_1 G_0 k^2 A_2 G_0$$

as

$$F = \mathcal{SC}_2 (A_1, A_2)$$

In this general formulism, both A_1 and A_2 can be α_1, α_2, α_3, $\cdots$. For example, the simplest case in the ISS: $A_1 = A_2 = \alpha_1$, can be expressed as: $\alpha_2 = \mathcal{SC}_2 (\alpha_1, \alpha_1)$.

Likewise, we define the solution of the following equation:

$$G_0 k^2 F G_0 = -G_0 k^2 A_1 G_0 k^2 A_2 G_0 k^2 A_3 G_0$$

as

$$F = \mathcal{SC}_3 (A_1, A_2, A_3)$$

Generally speaking, for an integer $n \geq 2$, we define the solution of the following equation:

$$G_0 k^2 F G_0 = -G_0 k^2 A_1 G_0 k^2 A_2 \cdots k^2 A_n G_0$$

as

$$F = \mathcal{SC}_n (A_1, A_2, \cdots, A_n)$$

The definitions above can be used to express the first four terms in the inverse scattering series:

$$\begin{aligned}
\alpha_2 =& \mathcal{SC}_2 (\alpha_1, \alpha_1) \\
\alpha_3 =& \mathcal{SC}_3 (\alpha_1, \alpha_1, \alpha_1) + \mathcal{SC}_2 (\alpha_1, \alpha_2) + \mathcal{SC}_2 (\alpha_2, \alpha_1) \\
\alpha_4 =& \mathcal{SC}_4 (\alpha_1, \alpha_1, \alpha_1, \alpha_1) + \mathcal{SC}_3 (\alpha_1, \alpha_1, \alpha_2) + \mathcal{SC}_3 (\alpha_1, \alpha_2, \alpha_1) + \mathcal{SC}_3 (\alpha_2, \alpha_1, \alpha_1) \\
& + \mathcal{SC}_2 (\alpha_2, \alpha_2) + \mathcal{SC}_2 (\alpha_1, \alpha_3) + \mathcal{SC}_2 (\alpha_3, \alpha_1)
\end{aligned}$$

These functions not only differentiate terms, they also shorten the derivation process. For example, $\mathcal{SC}_2$ can be derived once, and used repeatedly later.

One might notice that, for example, in the α_4 term, all different permutations of $(\alpha_1, \alpha_1, \alpha_2)$ are involved. It is natural to ask if the sum of these similar looking terms possess some symmetry not manifested in each individual term? The answer is yes, especially for the portion which is 1D generalizable (the only surviving term if the Earth is indeed horizontal).

We define the permutation sum of $\mathcal{SC}$ as $\mathbb{SC}$, for example, in the case of $\mathcal{SC}_2$, we define:

$$\mathbb{SC}_2\left(A_1, A_2\right) = \sum^{\odot} \mathcal{SC}_2\left(A_1, A_2\right)$$

where the permutation sum acting on a function of two variables is defined in equation (44).

In the case of $\mathcal{SC}_3$, if A_1 A_2 , and A_3 are different from each other, we define:

$$\mathbb{SC}_3\left(A_1, A_2, A_3\right) = \sum^{\odot} \mathcal{SC}_3\left(A_1, A_2, A_3\right)$$

where the permutation sum acting on a function of three variables is defined in equation (45).

Strictly speaking, $\mathcal{SC}_2$ is a function of (A_1, A_2), and can be expressed in $(\vec{x}, z)$, $(\vec{k}_m, z)$, or $(\vec{k}_m, k_z)$ domain. In this note, $\mathcal{SC}_3$ (without tilde above) means the representation in the $(\vec{x}, z)$ domain. $\widetilde{\mathcal{SC}}_2$ (with single tilde above) means the representation in the $(\vec{k}_m, z)$ domain. $\widetilde{\widetilde{\mathcal{SC}}}_2$ (with double tilde above) means the representation in the $(\vec{k}_m, k_z)$ domain. If not specified, $\mathcal{SC}_2$ is assumed as the function of (A_1, A_2).

For $\mathcal{SC}_3$, we use tilde sign to explicitly denote its domain, just like the case for $\mathcal{SC}_2$. If not specified, $\mathcal{SC}_3$ is assumed as a function of (A_1, A_2, A_3).

Very similar logic is applied to later functions.

With definitions above, α_4 can written as:

$$\alpha_4 = \mathbb{SC}_4\left(\alpha_1, \alpha_1, \alpha_1, \alpha_1\right) + \mathbb{SC}_3\left(\alpha_1, \alpha_1, \alpha_2\right) + \mathbb{SC}_2\left(\alpha_1, \alpha_3\right) + \mathbb{SC}\left(\alpha_2, \alpha_2\right) \tag{62}$$

Within one index n, especially when n is large, there remain many very different terms. We differentiate those terms further. Here we introduce another index m, with $n \geq m \geq 1$, to denote how fast each term grows with respect to k_z. The reason behind this is that, in the equation to invert for $\mathcal{SC}_n$, we will obtain a distribution behave like k_z^{n-1} asymptotically in the k_z domain. If the Earth is 1D, only the portion of the distribution which is of the order of k_z^{n-1} is needed, the other portions will be discarded by the sifting property of the δ-function (see Liu et. al. 2004). If the Earth is not 1D, the other portions, which will be separated into lower powers of k_z as: $k_z^{n-2}, k_z^{n-3}, \cdots, k_z^0$. We use $1 \leq m \leq n$ to denote the piece associated with k_z^{n-m}. We use $m = n+1$ to denote the remaining parts.

Inside each (n, m), there are still very different looking terms. For example, in the internal multiple removal, only the part of the third term in which the three scatters satisfy the higher-lower-higher relation is necessary: $z_1 \geq z_2 \leq z_3$. How many high-low relations exist between n scatters: $z_1, z_2, \cdots, z_n$? There are 2^{n-1} of them because there two possible relations between two adjacent scatters z_j and z_{j+1}, either $z_j \geq z_{j+1}$ or $z_j \leq z_{j+1}$. That is why we introduce a third index l, $1 \leq l \leq 2^{n-1}$ to further differentiate the terms. In the current classification scheme, the equation to calculate the index l is:

$$l = (d_1 d_2 \cdots d_{n-1})_b + 1 \tag{63}$$

where $(d_1 d_2 \cdots d_{n-1})_b$ is an integer in binary representation, its j-th digit, d_j is either 0 or 1 depending whether or not $z_j \geq z_{j+1}$.

In summary, we systematically classify the function $\mathcal{SC}_n$ into $\mathcal{SC}_{n,m,l}$, where $1 \leq m \leq n+1$ denotes the asymptotic power of the term in terms of k_z, with $m = 1$ denotes the highest power. The last index $1 \leq l \leq 2^{n-1}$ denotes where he high-low relationship between adjacent scatters.

Appendix C: Derivation of $\mathcal{SC}_2$

In this section, we solve for: $F = \mathcal{SC}_2\,(A_1, A_2)$, or equivalently:

$$\mathbf{G_0}k^2 F\mathbf{G_0} = -\mathbf{G_0}k^2 A_1\mathbf{G_0}A_2\mathbf{G_0}. \tag{64}$$

Expressing equation (64) explicitly in the actual integral form,

$$\begin{aligned}
&\vec{\int} d\vec{x}_1 \int_{-\infty}^{\infty} dz_1 G_0(\vec{x}_g, z_g, \vec{x}_1, z_1, \omega)\left(\frac{\omega}{c_0}\right)^2 F(\vec{x}_1, z_1) G_0(\vec{x}_1, z_1, \vec{x}_s, z_s, \omega) \\
&= -\vec{\int} d\vec{x}_1 \int_{-\infty}^{\infty} dz_1 G_0(\vec{x}_g, z_g, \vec{x}_1, z_1, \omega)\left(\frac{\omega}{c_0}\right)^2 A_1(\vec{x}_1, z_1) \\
&\vec{\int} d\vec{x}_2 \int_{-\infty}^{\infty} dz_2 G_0(\vec{x}_1, z_1, \vec{x}_2, z_2, \omega)\left(\frac{\omega}{c_0}\right)^2 A_2(\vec{x}_2, z_2) G_0(\vec{x}_2, z_2, \vec{k}_s, z_s, \omega).
\end{aligned} \tag{65}$$

We next Fourier transform over lateral geophone and shot coordinates: $\vec{\int} d\vec{x}_g \vec{\int} d\vec{x}_s e^{i\vec{k}_s\vec{x}_s - i\vec{k}_g\vec{x}_g}$, and express the Green's function in the middle of the right-hand-side of equation (65) as

$$G_0(\vec{x}_1, z_1, \vec{x}_2, z_2, \omega) = \frac{1}{4\pi^2}\vec{\int} d\vec{k}_1 \frac{e^{i\vec{k}_1\bullet(\vec{x}_1 - \vec{x}_2)} e^{iq_1|z_1 - z_2|}}{2iq_1},$$

in which $\vec{k}_1$ is conjugate to $\vec{x}_1$, and $q_1 = \mathrm{sgn}(\omega)\sqrt{(\omega/c_0)^2 - k_1^2}$.

This results in

$$\begin{aligned}
&-\frac{1}{4c_0^2}\frac{\omega^2}{q_g q_s}\widetilde{\widetilde{F}}(\vec{k}_g - \vec{k}_s, k_z) e^{-i(q_g z_g + g_s z_s)} = -\frac{i}{32\pi^2 c_0^4}\vec{\int} d\vec{k}_1 \frac{\omega^4}{q_g q_1 q_s}\int_{-\infty}^{\infty} dz_1 \widetilde{A_1}(\vec{k}_g - \vec{k}_1, z_1) \\
&\int_{-\infty}^{\infty} dz_2 \widetilde{A_2}(\vec{k}_1 - \vec{k}_s, z_2) e^{i[q_g(z_1 - z_g) + q_1|z_2 - z_1| + q_s(z_2 - z_s)]}.
\end{aligned} \tag{66}$$

The quantity

$$\widetilde{A_1}(\vec{k}_m, z) = \frac{1}{2\pi}\int_{-\infty}^{\infty} dk_z e^{-ik_z z}\widetilde{\widetilde{A_1}}(\vec{k}_m, k_z)$$

is the Fourier transform of $A_1(\vec{x}_m, z)$, and $\widetilde{\widetilde{F}}(\vec{k}_m, k_z)$ is the Fourier transform of $F(\vec{x}_m, z)$ over both $\vec{x}_m$ and z.

We next compute F in the $(\vec{k}_m, z)$ domain: we apply the inverse Fourier transform,

$$\frac{1}{2\pi}\int_{-\infty}^{\infty} e^{-ik_z z}dk_z,$$

to equation (66). The intemediate result is,

$$\begin{aligned}\widetilde{F}(\vec{k}_g-\vec{k}_s,z) =& \frac{1}{16\pi^3 c_0^2}\int_{-\infty}^{\infty} d\vec{k}_1\int_{-\infty}^{\infty} dz_1\int_{-\infty}^{\infty} dz_2\int_{-\infty}^{\infty} dk_z \\ & \frac{i\omega^2}{q_1}\widetilde{A_1}(\vec{k}_g-\vec{k}_1,z_1)\widetilde{A_2}(\vec{k}_1-\vec{k}_s,z_2)e^{i[q_g(z_1-z)+q_1|z_2-z_1|+q_s(z_2-z)]}.\end{aligned} \tag{67}$$

The innermost integral of equation (67) contains $\widetilde{A_1}$ and $\widetilde{A_2}$, which depends on the measurement of the wave field; it can be taken out of this integral (with respect to k_z) if the data are parameterized such that the Fourier conjugate k_h of the lateral offset coordinate to be 0. See Clayton and Stolt (1981) for a more detailed discussion. Making this choice, we have:

$$\begin{aligned}&\vec{k}_h = \vec{k}_g+\vec{k}_s = 0,\\ &\frac{\omega}{c_0} = \frac{1}{2}\mathrm{sgn}(k_z)\sqrt{k_z^2+k_m^2},\\ &\vec{k}_g = -\vec{k}_s = 0.5\vec{k}_m,\end{aligned} \tag{68}$$

which results in a simplified expression for $\widetilde{F}(\vec{k}_m,z)$:

$$\widetilde{F}(\vec{k}_m,z) = \frac{1}{32\pi^3}\int d\vec{k}_1\int_{-\infty}^{\infty} dz_1\widetilde{A_1}(\frac{\vec{k}_m}{2}-\vec{k}_1,z_1)\int_{-\infty}^{\infty} dz_2\widetilde{A_2}(\vec{k}_1+\frac{\vec{k}_m}{2},z_2)\widetilde{\gamma}_2(\vec{k}_m,\vec{k}_1;\varepsilon_0,\varepsilon_1), \tag{69}$$

where

$$\widetilde{\gamma}_2(\vec{k}_m,\vec{k}_1;\varepsilon_0,\varepsilon_1) = \int_{-\infty}^{\infty} dk_z i\frac{k_z^2+k_m^2}{u_1}e^{i[\varepsilon_0 k_z+\varepsilon_1 u_1]} = \int_{-\infty}^{\infty} dk_z i\frac{k_z^2+k_m^2}{u_1}e^{i\triangle\psi}e^{i[\varepsilon_0+\varepsilon_1]k_z}, \tag{70}$$

and where we have defined:

$$\begin{aligned}&\varepsilon_0 = 0.5(z_1+z_2)-z\\ &\varepsilon_1 = 0.5|z_1-z_2|\\ &u_1 = 2q_1 = \mathrm{sgn}(k_z)\sqrt{k_z^2+a_1}\\ &a_1 = k_m^2-4k_1^2\\ &\triangle\psi = \varepsilon_1(u_1-k_z).\end{aligned} \tag{71}$$

Notice that the expression $\widetilde{\gamma}_2(\vec{k}_m,\vec{k}_1;\varepsilon_0,\varepsilon_1)$ does not depend on the measured data; it may be computed once and used repeatedly, saving on computation.

Evaluation of $F = \mathcal{SC}_2\left(A_1, A_2\right)$ in the $(\vec{k}_m, z)$ domain

From equation (70), it is easy to tell that $\widetilde{\gamma}_2$ is not an ordinary function because $\lim\limits_{k_z\to\infty}\frac{u_1}{k_z} = 1$, so the integrand $(k_z^2 + k_m^2)/(u_1)$ approaches k_z as $k_z \to \infty$. We decompose $ie^{i\triangle\psi}(k_z^2 + k_m^2)/(u_1)$ as follows:

$$\begin{aligned} i\frac{k_z^2 + k_m^2}{u_1}e^{i\triangle\psi} &= ik_z - \frac{\varepsilon_1 a_1}{2} + \widetilde{\widetilde{\xi}}_2 \\ \widetilde{\widetilde{\xi}}_2 &= i\frac{k_z^2 + k_m^2}{u_1}e^{i\triangle\psi} - ik_z + \frac{\varepsilon_1 a_1}{2} \end{aligned} \tag{72}$$

Decomposition above is based on the fact that, after put into the integral of inverse Fourier transform $\int_{-\infty}^{\infty} dk_z e^{i(\varepsilon_0+\varepsilon_1)k_z}$, the first term k_z will result in a singular distribution:

$$\int_{-\infty}^{\infty} ik_z e^{i(\varepsilon_0+\varepsilon_1)k_z}dk_z = \frac{\partial\int_{-\infty}^{\infty} e^{i(\varepsilon_0+\varepsilon_1)k_z}dk_z}{\partial(\varepsilon_0+\varepsilon_1)} = (2\pi)\delta'(\varepsilon_0+\varepsilon_1)$$

Likewise another singular distribution is produced by the second term:

$$\int_{-\infty}^{\infty} -\frac{\varepsilon_1 a_1}{2}e^{i(\varepsilon_0+\varepsilon_1)k_z}dk_z = -\pi\varepsilon_1 a_1\delta(\varepsilon_0+\varepsilon_1)$$

But the distribution produced by the third term:

$$\int_{-\infty}^{\infty} \widetilde{\widetilde{\xi}}_2 e^{i(\varepsilon_0+\varepsilon_1)k_z}dk_z$$

is regular because $\lim\limits_{k_z\mapsto\infty}\widetilde{\widetilde{\xi}}_2 k_z = \frac{ik_m^2}{2} + 2k_1^2 - \frac{\varepsilon_1^2 a_1^2}{8}$, which is a finite constant. For the purpose of short notation, let us denote the numerically expressible function as $\widetilde{\xi}_2$:

$$\widetilde{\xi}_2(\vec{k}_m, \vec{k}_1; \varepsilon_0, \varepsilon_1) = \int_{-\infty}^{\infty} \widetilde{\widetilde{\xi}}_2 e^{i(\varepsilon_0+\varepsilon_1)k_z}dk_z \tag{73}$$

So we decompose $\widetilde{\gamma}_2(\vec{k}_m, \vec{k}_1; \varepsilon_0, \varepsilon_1)$ into 2 singular distributions and 1 regular distribution:

$$\widetilde{\gamma}_2(\vec{k}_m, \vec{k}_1; \varepsilon_0, \varepsilon_1) = (2\pi)\delta'(\varepsilon_0+\varepsilon_1) - \pi\varepsilon_1 a_1\delta(\varepsilon_0+\varepsilon_1) + \widetilde{\xi}_2(\vec{k}_m, \vec{k}_1; \varepsilon_0, \varepsilon_1). \tag{74}$$

From equation (69) and equation (70), the explicit expression of the phase term $\varepsilon_0 + \varepsilon_1$ depends on $z_1 \geq z_2$ or $z_1 \leq z_2$, and in the first case $\varepsilon_0 + \varepsilon_1 = z_1 - z$. So equation (74) can be further expressed as:

$$\widetilde{\gamma}_2(\vec{k}_m, \vec{k}_1; \varepsilon_0, \varepsilon_1) = (2\pi)\delta'(z_1 - z) - \pi\varepsilon_1 a_1\delta(z_1 - z) + \widetilde{\xi}_2\left(\vec{k}_m, \vec{k}_1; \frac{z_1+z_2}{2} - z, \frac{z_1 - z_2}{2}\right) \tag{75}$$

In the second case $\varepsilon_0 + \varepsilon_1 = z_2 - z$. So equation (74) can be further expressed as:

$$\widetilde{\gamma}_2(\vec{k}_m, \vec{k}_1; \varepsilon_0, \varepsilon_1) = (2\pi)\delta'(z_2 - z) - \pi\varepsilon_1 a_1 \delta(z_2 - z) + \widetilde{\xi}_2\left(\vec{k}_m, \vec{k}_1; \frac{z_1 + z_2}{2} - z, \frac{z_2 - z_1}{2}\right) \tag{76}$$

Substituting equation (75) or equation (76) into equation (69), depending on $z_1 \geq z_2$ or $z_1 \leq z_2$, we can decompose F into three terms:

$$\begin{aligned}
&\widetilde{F}(\vec{k}_m, z) = \frac{1}{32\pi^3}\vec{\int} d\vec{k}_1 \\
&\left(\begin{array}{c}
\int_{-\infty}^{\infty} dz_1 \widetilde{A_1}\left(\frac{\vec{k}_m}{2} - \vec{k}_1, z_1\right) \int_{-\infty}^{z_1} dz_2 \widetilde{A_2}\left(\vec{k}_1 + \frac{\vec{k}_m}{2}, z_2\right) \widetilde{\gamma}_2\left(\vec{k}_m, \vec{k}_1; \frac{z_1+z_2}{2} - z, \frac{z_1-z_2}{2}\right) \\
+ \\
\int_{-\infty}^{\infty} dz_2 \widetilde{A_1}\left(\vec{k}_1 + \frac{\vec{k}_m}{2}, z_2\right) \int_{-\infty}^{z_2} dz_1 \widetilde{A_2}\left(\vec{k}_1 + \frac{\vec{k}_m}{2}, z_1\right) \widetilde{\gamma}_2\left(\vec{k}_m, \vec{k}_1; \frac{z_1+z_2}{2} - z, \frac{z_2-z_1}{2}\right)
\end{array}\right) \\
&= \widetilde{\mathcal{SC}}_{2,1} + \widetilde{\mathcal{SC}}_{2,2} + \widetilde{\mathcal{SC}}_{2,3},
\end{aligned} \tag{77}$$

The split above is based on the classification idea described in the equation (63). For the first case: $z_1 \geq z_2$, the binary expression for this relation is 0, its corresponding index is $l = 0 + 1 = 1$. For the second case: $z_1 \leq z_2$, the binary expression for this relation is 1, its corresponding index is $l = 1 + 1 = 2$.

The first term $\widetilde{\mathcal{SC}}_{2,1}$ is further decomposed as:

$$\widetilde{\mathcal{SC}}_{2,1} = \widetilde{\mathcal{SC}}_{2,1,1} + \widetilde{\mathcal{SC}}_{2,1,2} \tag{78}$$

$$\widetilde{\mathcal{SC}}_{2,1,1} = \frac{1}{32\pi^3}\vec{\int} d\vec{k}_1 \int_{-\infty}^{\infty} dz_1 \delta'(z_1 - z)\widetilde{A_1}(0.5\vec{k}_m - \vec{k}_1, z_1) \int_{-\infty}^{z_1} dz_2 \widetilde{A_2}(\vec{k}_1 + 0.5\vec{k}_m, z_2)(2\pi).$$

Using equation (53), we have,

$$\begin{aligned}
&= -\frac{1}{16\pi^2}\vec{\int} d\vec{k}_1 \frac{\partial \widetilde{A_1}(0.5\vec{k}_m - \vec{k}_1, z)}{\partial z} \int_{-\infty}^{z} dz_2 \widetilde{A_2}(\vec{k}_1 + 0.5\vec{k}_m, z_2) \\
&\quad - \frac{1}{16\pi^2}\vec{\int} d\vec{k}_1 \widetilde{A_1}(0.5\vec{k}_m - \vec{k}_1, z)\widetilde{A_2}(\vec{k}_1 + 0.5\vec{k}_m, z) \\
\widetilde{\mathcal{SC}}_{2,1,2} &= \frac{2\pi}{32\pi^3}\vec{\int} d\vec{k}_1 \int_{-\infty}^{\infty} dz_2 \delta'(z_2 - z)\widetilde{A_2}\left(\vec{k}_1 + \frac{\vec{k}_m}{2}, z_2\right) \int_{-\infty}^{z_2} dz_1 \widetilde{A_1}\left(\frac{\vec{k}_m}{2} - \vec{k}_1, z_1\right)
\end{aligned}$$

Using equation (53), we have,

$$= -\frac{1}{16\pi^2}\vec{\int} d\vec{k}_1 \frac{\partial \widetilde{A_2}(\vec{k}_1 + 0.5\vec{k}_m, z)}{\partial z} \int_{-\infty}^{z} dz_2 \widetilde{A_1}(0.5\vec{k}_m - \vec{k}_1, z_2)$$
$$- \frac{1}{16\pi^2}\vec{\int} d\vec{k}_1 \widetilde{A_1}(0.5\vec{k}_m - \vec{k}_1, z)\widetilde{A_2}(\vec{k}_1 + 0.5\vec{k}_m, z)$$

So we split $\widetilde{\mathcal{SC}}_{2,1,1}$ and $\widetilde{\mathcal{SC}}_{2,1,2}$ into two parts by integration by parts (which is used to get the last step in the derivation above). In each case, the first part contains the first two terms in the right-hand-side of the last equal sign above, they are purely responsible for imaging in the special case of $A_1 = A_2 = \alpha_1$. The last term is responsible for parameter inversion in the special case mentioned above. Only $\mathcal{SC}_{2,1}$ will not vanish if we indeed have a 1D Earth.

$$\widetilde{\mathcal{SC}}_{2,2} = \frac{1}{32\pi^3}\vec{\int} d\vec{k}_1$$
$$\left(\begin{array}{l} \int_{-\infty}^{\infty} dz_1 \widetilde{A_1}(0.5\vec{k}_m - \vec{k}_1, z_1) \int_{-\infty}^{z_1} dz_2 \widetilde{A_2}(\vec{k}_1 + 0.5\vec{k}_m, z_2)(-\pi\varepsilon_1 a_1)\delta(z_1 - z) \\ \int_{-\infty}^{\infty} dz_2 \widetilde{A_2}(\vec{k}_1 + 0.5\vec{k}_m, z_2) \int_{-\infty}^{z_2} dz_1 \widetilde{A_1}(0.5\vec{k}_m - \vec{k}_1, z_1)(-\pi\varepsilon_1 a_1)\delta(z_2 - z) \end{array} \right)$$
$$= \widetilde{\mathcal{SC}}_{2,2,1} + \widetilde{\mathcal{SC}}_{2,2,2}$$

The split above is based on the high-low relation between z_1 and z_2. For the first case: $z_1 \geq z_2$, the binary expression for this relation is 0, its corresponding index is $l = 0 + 1 = 1$. For the second case: $z_1 \leq z_2$, the binary expression for this relation is 1, its corresponding index is $l = 1 + 1 = 2$.

$$\widetilde{\mathcal{SC}}_{2,2} = \widetilde{\mathcal{SC}}_{2,2,1} + \widetilde{\mathcal{SC}}_{2,2,2}$$
$$\widetilde{\mathcal{SC}}_{2,2,1} = -\frac{1}{64\pi^2}\vec{\int} d\vec{k}_1 \, (k_m^2 - 4k_1^2)\widetilde{A_1}(0.5\vec{k}_m - \vec{k}_1, z) \int_{-\infty}^{z} du(z-u)\widetilde{A_2}(\vec{k}_1 + 0.5\vec{k}_m, u)$$
$$\widetilde{\mathcal{SC}}_{2,2,2} = -\frac{1}{64\pi^2}\vec{\int} d\vec{k}_1 \, (k_m^2 - 4k_1^2)\widetilde{A_2}(0.5\vec{k}_m + \vec{k}_1, z) \int_{-\infty}^{z} du(z-u)\widetilde{A_1}(0.5\vec{k}_m - \vec{k}_1, u).$$

$\widetilde{\mathcal{SC}}_{2,2}$ will vanish if we have a 1D Earth. Even for geological model with lateral variations, $\widetilde{\mathcal{SC}}_{2,2}$ is very clean for the portion where the Earth is horizontal. $\widetilde{F_2}$ is strong where the model is laterally varying.

The third term is regular, and can be literally implemented as the form in equation (69). Because $\widetilde{\xi}_2(\vec{k}_m, \vec{k}_1; \varepsilon_0, \varepsilon_1)$ is regular, no integration by parts is needed.

$$\widetilde{\mathcal{SC}}_{2,3} = \widetilde{\mathcal{SC}}_{2,3,1} + \widetilde{\mathcal{SC}}_{2,3,2}$$

where:

$$\begin{aligned}
\widetilde{\mathcal{SC}}_{2,3,1} = \frac{1}{32\pi^3} \vec{\int} d\vec{k}_1 \int_{-\infty}^{\infty} dz_1 \widetilde{A_1}(0.5\vec{k}_m - \vec{k}_1, z_1) \int_{-\infty}^{z_1} dz_2 \\
\widetilde{A_2}(\vec{k}_1 + 0.5\vec{k}_m, z_2) \widetilde{\xi}_2 \left(\vec{k}_m, \vec{k}_1; \frac{z_1 + z_2}{2} - z, \frac{z_1 - z_2}{2} \right) \\
\widetilde{\mathcal{SC}}_{2,3,2} = \frac{1}{32\pi^3} \vec{\int} d\vec{k}_1 \int_{-\infty}^{\infty} dz_2 \widetilde{A_2}(0.5\vec{k}_m + \vec{k}_1, z_2) \int_{-\infty}^{z_2} dz_1 \\
\widetilde{A_2}(0.5\vec{k}_m - \vec{k}_1, z_1) \widetilde{\xi}_2 \left(\vec{k}_m, \vec{k}_1; \frac{z_1 + z_2}{2} - z, \frac{z_2 - z_1}{2} \right),
\end{aligned} \tag{79}$$

where $\widetilde{\xi}_2$ is defined in equation (73)

The further classification is based on the relative high-low relation between z_1 and z_2.

Evaluation of $F = \mathcal{SC}_2(A_1, A_2)$ in the $(\vec{x}, z)$ domain

The suggestion of transforming the results in the previous subsection into space domain, came from Arthur Weglein.

We then go a step further by applying the inverse Fourier transform $(1/4\pi^2) \vec{\int} d\vec{k}_m e^{i\vec{k}_m \bullet \vec{x}}$ to the results above to have:

$$\begin{aligned}
\mathcal{SC}_{2,1,1}(\vec{x}, z) &= \frac{1}{4\pi^2} \vec{\int} d\vec{k}_m e^{i\vec{k}_m \bullet \vec{x}} \widetilde{\mathcal{SC}}_{2,1,1}(\vec{k}_m, z) \\
&= -\frac{1}{64\pi^4} \vec{\int} d\vec{k}_1 \vec{\int} e^{i\vec{k}_m \bullet \vec{x}} d\vec{k}_m \frac{\partial \widetilde{A_1}(0.5\vec{k}_m - \vec{k}_1, z)}{\partial z} \int_{-\infty}^{z} dz_2 \widetilde{A_2}(\vec{k}_1 + 0.5\vec{k}_m, z_2) \\
&\quad - \frac{1}{64\pi^4} \vec{\int} d\vec{k}_1 \vec{\int} e^{i\vec{k}_m \bullet \vec{x}} d\vec{k}_m \widetilde{A_1}(0.5\vec{k}_m - \vec{k}_1, z) \widetilde{A_2}(\vec{k}_1 + 0.5\vec{k}_m, z).
\end{aligned}$$

Using equation (88), we have,

$$\mathcal{SC}_{2,1,1}(\vec{x},z) = -\frac{1}{4}\left(\frac{\partial A_1(\vec{x},z)}{\partial z}\int_{-\infty}^{z} du A_2(\vec{x},u) \;+\; A_1(\vec{x},z)A_2(\vec{x},z)\right) \tag{80}$$

$$\begin{aligned}\mathcal{SC}_{2,1,2}(\vec{x},z) &= \frac{1}{4\pi^2}\vec{\int} d\vec{k}_m e^{i\vec{k}_m\bullet\vec{x}}\,\widetilde{\mathcal{SC}}_{2,1,2}(\vec{k}_m,z)\\ &= -\frac{1}{64\pi^4}\vec{\int} d\vec{k}_1\vec{\int} e^{i\vec{k}_m\bullet\vec{x}}\,d\vec{k}_m\frac{\partial\widetilde{A_2}(\vec{k}_1+0.5\vec{k}_m,z)}{\partial z}\int_{-\infty}^{z} dz_1\widetilde{A_1}(0.5\vec{k}_m-\vec{k}_1,z_1)\\ &\quad -\frac{1}{64\pi^4}\vec{\int} d\vec{k}_1\vec{\int} e^{i\vec{k}_m\bullet\vec{x}}\,d\vec{k}_m\widetilde{A_1}(0.5\vec{k}_m-\vec{k}_1,z)\widetilde{A_2}(\vec{k}_1+0.5\vec{k}_m,z).\end{aligned}$$

Using equation (88), we have,

$$\mathcal{SC}_{2,1,2}(\vec{x},z) = -\frac{1}{4}\left(\frac{\partial A_2(\vec{x},z)}{\partial z}\int_{-\infty}^{z} du A_1(\vec{x},u) \;+\; A_1(\vec{x},z)A_2(\vec{x},z)\right) \tag{81}$$

We sum the two equations above to have:

$$\begin{aligned}\mathcal{SC}_{2,1}(\vec{x},z) &= \mathcal{SC}_{2,1,1}(\vec{x},z)+\mathcal{SC}_{2,1,2}(\vec{x},z)\\ &= -\frac{1}{4}\left(\frac{\partial A_1(\vec{x},z)}{\partial z}\int_{-\infty}^{z} du A_2(\vec{x},u) \;+\; \frac{\partial A_2(\vec{x},z)}{\partial z}\int_{-\infty}^{z} du A_1(\vec{x},u) \;+\; 2A_1(\vec{x},z)A_2(\vec{x},z)\right)\end{aligned}$$

$$\begin{aligned}\mathcal{SC}_{2,2,1}(\vec{x},z) &= \frac{1}{4\pi^2}\vec{\int} d\vec{k}_m e^{i\vec{k}_m\bullet\vec{x}}\,\widetilde{\mathcal{SC}}_{2,2,1}(\vec{k}_m,z)\\ &= -\frac{1}{256\pi^4}\vec{\int} d\vec{k}_1\vec{\int} d\vec{k}_m e^{i\vec{k}_m\bullet\vec{x}}\,(k_m^2-4k_1^2)\widetilde{A_1}(0.5\vec{k}_m-\vec{k}_1,z)\\ &\qquad\qquad \int_{-\infty}^{z} dz_2(z-z_2)\widetilde{A_2}(\vec{k}_1+0.5\vec{k}_m,z_2)\end{aligned} \tag{82}$$

$$\overrightarrow{(89)} \quad = \frac{1}{4}\frac{\partial A_1(\vec{x},z)}{\partial x}\int_{-\infty}^{z} du\frac{\partial A_2(\vec{x},u)}{\partial\vec{x}}(z-u)$$

$$\overrightarrow{(85)} \quad = \frac{1}{4}\frac{\partial A_1(\vec{x},z)}{\partial x}\int_{-\infty}^{z} du\int_{-\infty}^{u} dv\frac{\partial A_2(\vec{x},v)}{\partial\vec{x}}$$

$$
\begin{aligned}
\mathcal{SC}_{2,2,2}(\vec{x},z) &= \frac{1}{4\pi^2}\vec{\int} d\vec{k}_m e^{i\vec{k}_m\bullet\vec{x}}\,\widetilde{\mathcal{SC}}_{2,2,2}(\vec{k}_m,z) \\
&= -\frac{1}{256\pi^4}\vec{\int} d\vec{k}_1\vec{\int} d\vec{k}_m e^{i\vec{k}_m\bullet\vec{x}}\,(k_m^2-4k_1^2)\widetilde{A_2}(0.5\vec{k}_m-\vec{k}_1,z) \\
&\qquad\qquad \int_{-\infty}^{z} dz_1(z-z_2)\widetilde{A_1}(\vec{k}_1+0.5\vec{k}_m,z_2) \\
\overrightarrow{(89)} &= \frac{1}{4}\frac{\partial A_2(\vec{x},z)}{\partial x}\int_{-\infty}^{z} du\frac{\partial A_1(\vec{x},u)}{\partial\vec{x}}(z-u) \\
\overrightarrow{(85)} &= \frac{1}{4}\frac{\partial A_2(\vec{x},z)}{\partial x}\int_{-\infty}^{z} du\int_{-\infty}^{u} dv\frac{\partial A_1(\vec{x},v)}{\partial\vec{x}}
\end{aligned}
\tag{83}
$$

We sum the two equations above to have:

$$
\begin{aligned}
&\mathcal{SC}_{2,2}(\vec{x},z) = \mathcal{SC}_{2,2,1}(\vec{x},z)+\mathcal{SC}_{2,2,2}(\vec{x},z) \\
&= \frac{1}{4}\frac{\partial A_1(\vec{x},z)}{\partial x}\int_{-\infty}^{z} du\int_{-\infty}^{u} dv\frac{\partial A_2(\vec{x},v)}{\partial\vec{x}} \quad + \quad \frac{1}{4}\frac{\partial A_2(\vec{x},z)}{\partial x}\int_{-\infty}^{z} du\int_{-\infty}^{u} dv\frac{\partial A_1(\vec{x},v)}{\partial\vec{x}}
\end{aligned}
\tag{84}
$$

In the derivation process above, the relation below was used to make the expression more symmetrical. For convenience, let us define: $B(\vec{x},z)=\int_{-\infty}^{z} duA(\vec{x},u)$, $dB(\vec{x},z)=A(\vec{x},z)dz$, we have:

$$
\begin{aligned}
&\int_{-\infty}^{z} duA(\vec{x},u)(z-u) = \int_{-\infty}^{z}(z-u)dB(\vec{x},u) \\
&= [(z-u)B(\vec{x},u)]_{u=-\infty}^{u=z} - \int_{-\infty}^{z} B(\vec{x},u)d(z-u) \\
&= \int_{-\infty}^{z} B(\vec{x},u)du = \int_{-\infty}^{z} du\int_{-\infty}^{u} A(\vec{x},v)dv
\end{aligned}
\tag{85}
$$

Simplification and clarification in physical interpretations have occured after Fourier transformation of the singular terms $\mathcal{SC}_{2,1}$ and $\mathcal{SC}_{2,2}$. However, in the regular term $\mathcal{SC}_{2,3}$, no simplification and clarification have been found in this manner.

We summarize various parts of $\mathcal{SC}_2(A_1,A_2)$ in the short-hand notation as:

	$\mathcal{SC}_2(A_1,A_2)$	$\mathcal{SC}_2(A_2,A_1)$
$\mathcal{SC}_{2,1,1}$	$-\frac{1}{4}\left(A_1^z A_2^{-z}+A_1A_2\right)$	$-\frac{1}{4}\left(A_2^z A_1^{-z}+A_1A_2\right)$
$\mathcal{SC}_{2,1,2}$	$-\frac{1}{4}\left(A_2^z A_1^{-z}+A_1A_2\right)$	$-\frac{1}{4}\left(A_1^z A_2^{-z}+A_1A_2\right)$
$\mathcal{SC}_{2,2,1}$	$-\frac{1}{4}A_1^x A_2^{x-2z}$	$-\frac{1}{4}A_2^x A_1^{x-2z}$
$\mathcal{SC}_{2,2,2}$	$-\frac{1}{4}A_2^x A_1^{x-2z}$	$-\frac{1}{4}A_1^x A_2^{x-2z}$
$\mathcal{SC}_{2,3,1}$	$\mathcal{SC}_{2,3,1}(A_1,A_2)$	$\mathcal{SC}_{2,3,2}(A_1,A_2)$
$\mathcal{SC}_{2,3,2}$	$\mathcal{SC}_{2,3,2}(A_1,A_2)$	$\mathcal{SC}_{2,3,1}(A_1,A_2)$

In the general case of $A_1 \neq A_2$, we have:

$$\begin{aligned}
&\mathbb{SC}_2(A_1,A_2) = \mathcal{SC}_2(A_1,A_2) + \mathcal{SC}_2(A_2,A_1) \\
&= -\frac{1}{2}\left(2A_1A_2 + A_1^z A_2^{-z} + A_2^z A_1^{-z}\right) + \frac{1}{2}A_1^x A_2^{x-2z} + \frac{1}{2}A_2^x A_1^{x-2z} \\
&+ 2\mathcal{SC}_{2,3,1}(A_1,A_2) + 2\mathcal{SC}_{2,3,1}(A_2,A_1)
\end{aligned} \tag{86}$$

In the special case of $A_1 = A_2 = A$, we have:

$$\mathbb{SC}_2(A,A) = \mathcal{SC}_2(A,A) = -\frac{1}{2}\left(A^2 + A^z A^{-z}\right) + \frac{1}{2}A^x A^{x-2z} + 2\mathcal{SC}_{2,3,1}(A,A) \tag{87}$$

Or in the simplest case: $A_1 = A_2 = \alpha_1$, we have α_2:

$$\alpha_2 = \mathbb{SC}_2(\alpha_1,\alpha_1) = \mathcal{SC}_2(\alpha_1,\alpha_1) = -\frac{1}{2}\left(\alpha_1^2 + \alpha_1^z \alpha_1^{-z}\right) + \frac{1}{2}\alpha_1^x \bullet \alpha_1^{x-2z} + 2\mathcal{SC}_{2,3,1}(\alpha_1,\alpha_1)$$

where $Sc_{2,3,1}$ is implemented in the $(\vec{k}_m, z)$ domain as defined in equation (79)

Appendix D: Several useful Fourier integrals over the lateral wave-numbers

If we define:

$$\widetilde{f}_1\left(\vec{k}\right) = \int d\vec{x}\, e^{i\vec{k}\bullet\vec{x}}\, f_1(\vec{x}) \qquad\qquad \widetilde{f}_2\left(\vec{k}\right) = \int d\vec{x}\, e^{i\vec{k}\bullet\vec{x}}\, f_2(\vec{x})$$

then we have,

$$\int d\vec{k}_1 \int e^{i\vec{k}_m\bullet\vec{x}}\, d\vec{k}_m \widetilde{f}_1(0.5\vec{k}_m - \vec{k}_1)\widetilde{f}_2(\vec{k}_1 + 0.5\vec{k}_m) = 16\pi^4 f_1(\vec{x})f_2(\vec{x}), \tag{88}$$

and

$$\int d\vec{k}_1 \int e^{i\vec{k}_m\bullet\vec{x}}\, d\vec{k}_m \left(k_m^2 - 4k_1^2\right) \widetilde{f}_1(0.5\vec{k}_m - \vec{k}_1)\widetilde{f}_2(\vec{k}_1 + 0.5\vec{k}_m) = -64\pi^4 \frac{\partial f_1(\vec{x})}{\partial\vec{x}} \bullet \frac{\partial f_2(\vec{x})}{\partial\vec{x}}. \tag{89}$$

For the proof of equation (88) and (89), let's define: $\vec{h}_1 = 0.5\vec{k}_m - \vec{k}_1$ and $\vec{h}_2 = 0.5\vec{k}_m + \vec{k}_1$, we have: $\vec{k}_m = \vec{h}_1 + \vec{h}_2$, $k_m^2 - 4k_1^2 = 4\vec{h}_1 \bullet \vec{h}_2$, and the following integration relation after changing integration variables from $(\vec{k}_1, \vec{k}_m)$ to $(\vec{h}_1, \vec{h}_2)$:

$$\int d\vec{k}_1 \int d\vec{k}_m = \int d\vec{h}_1 \int d\vec{h}_2 \quad . \tag{90}$$

Let us further rewrite,

$$\begin{aligned} \widetilde{f}_1(0.5\vec{k}_m - \vec{k}_1) = \widetilde{f}_1(\vec{h}_1) &= \int d\vec{x}'\, f_1(\vec{x}')e^{-i\vec{h}_1\bullet\vec{x}'}, \\ \widetilde{f}_2(\vec{k}_1 + 0.5\vec{k}_m) = \widetilde{f}_1(\vec{h}_2) &= \int d\vec{x}'\, f_2(\vec{x}'')e^{-i\vec{h}_2\bullet\vec{x}''}. \end{aligned} \tag{91}$$

Using equation (90) and (91), we can rewrite the left-hand-side of equation (88) as,

$$
\begin{aligned}
&\int d\vec{h}_1 \int d\vec{h}_2 e^{i(\vec{h}_1+\vec{h}_2)\bullet\vec{x}} \int d\vec{x}'\, f_1(\vec{x}') e^{-i\vec{h}_1\bullet\vec{x}'} \int d\vec{x}''\, f_2(\vec{x}'') e^{-i\vec{h}_2\bullet\vec{x}''} \\
&= \int d\vec{h}_1 \int d\vec{h}_2 \int d\vec{x}'\, f_1(\vec{x}') e^{-i\vec{h}_1\bullet\vec{x}'} e^{i\vec{h}_1\bullet\vec{x}} \int d\vec{x}''\, f_2(\vec{x}'') e^{-i\vec{h}_2\bullet\vec{x}''} e^{i\vec{h}_2\bullet\vec{x}} \\
&= \int d\vec{h}_1 \int d\vec{h}_2 \int d\vec{x}'\, f_1(\vec{x}') e^{i\vec{h}_1\bullet(\vec{x}-\vec{x}')} \int d\vec{x}''\, f_2(\vec{x}'') e^{i\vec{h}_2\bullet(\vec{x}-\vec{x}'')} \\
&= \int d\vec{x}'\, f_1(\vec{x}') \int d\vec{h}_1 e^{i\vec{h}_1\bullet(\vec{x}-\vec{x}')} \int d\vec{x}''\, f_2(\vec{x}'') \int d\vec{h}_2 e^{i\vec{h}_2\bullet(\vec{x}-\vec{x}'')} \\
&= \int d\vec{x}'\, f_1(\vec{x}')(4\pi^2)\delta(\vec{x}-\vec{x}') \int d\vec{x}''\, f_2(\vec{x}'')(4\pi^2)\delta(\vec{x}-\vec{x}'') = 16\pi^4 f_1(\vec{x}) f_2(\vec{x})
\end{aligned}
$$

Similarly, using the fact that: $k_m^2 - 4k_1^2 = 4\vec{h}_1 \bullet \vec{h}_2$, equation (90) and equation (91), we can rewrite the left-hand-side of equation (89) as,

$$
\begin{aligned}
&\int d\vec{h}_1 \int d\vec{h}_2 \left(4\vec{h}_1 \bullet \vec{h}_2\right) e^{i(\vec{h}_1+\vec{h}_2)\bullet\vec{x}} \int d\vec{x}'\, f_1(\vec{x}') e^{-i\vec{h}_1\bullet\vec{x}'} \int d\vec{x}''\, f_2(\vec{x}'') e^{-i\vec{h}_2\bullet\vec{x}''} \\
&= \int d\vec{h}_1 \int d\vec{h}_2 \left(-4\left[i\vec{h}_1\right] \bullet \left[i\vec{h}_2\right]\right) \int d\vec{x}'\, f_1(\vec{x}') e^{-i\vec{h}_1\bullet\vec{x}'} e^{i\vec{h}_1\bullet\vec{x}} \int d\vec{x}''\, f_2(\vec{x}'') e^{-i\vec{h}_2\bullet\vec{x}''} e^{i\vec{h}_2\bullet\vec{x}} \\
&= -4 \int d\vec{h}_1 \int d\vec{h}_2 \left(\left[i\vec{h}_1\right] \bullet \left[i\vec{h}_2\right]\right) \int d\vec{x}'\, f_1(\vec{x}') e^{i\vec{h}_1\bullet(\vec{x}-\vec{x}')} \int d\vec{x}''\, f_2(\vec{x}'') e^{i\vec{h}_2\bullet(\vec{x}-\vec{x}'')} \\
&= -4 \int d\vec{x}'\, f_1(\vec{x}') \int d\vec{h}_1 \left[i\vec{h}_1\right] e^{i\vec{h}_1\bullet(\vec{x}-\vec{x}')} \bullet \int d\vec{x}''\, f_2(\vec{x}'') \int d\vec{h}_2 \left[i\vec{h}_2\right] e^{i\vec{h}_2\bullet(\vec{x}-\vec{x}'')} \\
&= -4 \int d\vec{x}'\, f_1(\vec{x}')(4\pi^2)\delta'(\vec{x}-\vec{x}') \bullet \int d\vec{x}''\, f_2(\vec{x}'')(4\pi^2)\delta'(\vec{x}-\vec{x}'') = -64\pi^4 \frac{\partial f_1(\vec{x})}{\partial \vec{x}} \bullet \frac{\partial f_2(\vec{x})}{\partial \vec{x}}
\end{aligned}
$$

Deriving an imaging algorithm for a laterally invariant multi-parameter acoustic medium from the inverse scattering series

S. Jiang and A. B. Weglein

Abstract

Imaging challenges in a complex earth can be a significant obstacle to seismic effectiveness. The purpose of the research presented here is to extend the velocity only varying acoustic leading and higher order imaging methods of F. Liu to a multi-parameter earth, and thereby towards model type independence. A conjectured imaging candidate algorithm using inverse scattering series, appropriate for a 1D two-parameter (density and velocity variation) acoustic medium, was proposed by Weglein in 2007, and thereafter further extended by Weglein to multi-D multi-parameter acoustic/elastic media. The conjectured imaging algorithm for the 1D acoustic two-parameter medium is derived and examined in this report. The calculation of the inverse scattering series (*ISS*) third order term leads to the identification of an imaging sub-series for the 1D two-parameter acoustic medium. Because it is a partial capture of the imaging series in the *ISS*, this imaging sub-series is called the leading order imaging sub-series (*LOIS*). It can be expressed in a closed form which justifies the conjectured imaging algorithm. The two parameters of the medium are imaged together as a composite linear to a data set. The imaging result can be expressed as a shifted seismic data set in the pseudo-depth domain. This method has the promise of imaging P-P data in an acoustic or isotropic multi-D elastic medium. The image is a structure map, not suited for subsequent AVO analysis. Tests on multi-parameter acoustic and elastic media are planned.

Introduction

Many pressing challenges in current seismic exploration can be addressed by using the inverse scattering series (*ISS*) (Weglein, 1985; Weglein et al., 1997, 2003). For instance, depth imaging using *ISS* proceeds without knowing any subsurface information (subsurface velocity fields, for example). The development of depth imaging algorithm at M-OSRP is proceeding in stages:
Stage (1) - for a 1D one parameter (velocity variation only) acoustic medium, a leading order imaging sub-series (*LOIS*) is identified and tested in Weglein et al. (2000); Shaw et al. (2002); Shaw and Weglein (2003); Shaw (2005). It works for a layered medium with small velocity contrasts, because this imaging series is a partial capture of the whole imaging series. The *LOIS* can be written as a closed form.

Stage (2) - for a multi-D one parameter (velocity variation only) acoustic medium, a laterally variant acoustic medium with large velocity contrasts is considered. The calculation of the *ISS* terms in the multi-D medium leads to more imaging terms identified in which there are imaging terms without analog in the 1D medium. These terms deal with the lateral variations of the medium. By capturing more imaging terms than the *LOIS* in the 1D acoustic case, a higher order imaging

sub-series (*HOIS*) and corresponding closed form are identified and numerically tested on a salt model with lateral variation and large velocity contrasts (Liu et al., 2004, 2005; Liu, 2006). The encouraging numerical test result indicates the *HOIS* imaging algorithm works very well for a multi-dimensional acoustic medium with velocity variation only. The logic connection and understanding between the *LOIS* and *HOIS* closed forms for depth imaging have been analyzed in Zhang et al. (2007).

Stage (3) - To advance the *ISS* imaging algorithm application to the real earth which is a multi-parameter medium generally, it is necessary to derive a multi-parameter (velocity, density variation etc.) *ISS* imaging algorithm. In this stage, starting with the simplest model, a multi-parameter 1D acoustic medium is studied. An imaging-only term is identified in Zhang and Weglein (2005) for a layered acoustic medium with both velocity and density variations. Following the philosophy of identifying the *LOIS* and *HOIS* algorithm, a conjectured imaging algorithm for the 1D two-parameter acoustic medium, was proposed by Weglein in 2007, and then further extended to multi-D multi-parameter acoustic/elastic cases. The extension is straightly done by substituting the integral in the imaging-only term of the one-parameter case with the integral of the imaging-only term under the multi-parameter case. But the final expression of the imaging formula for a multi-parameter medium (either acoustic or elastic) is expressed as a shifted data-set scaled by a constant subjected to the imaged seismic model. For example, for the 1D two-parameter acoustic medium, the conjectured imaging algorithm indicates that the two parameters will be imaged together as a composite form, in other words, the imaging task does not distinguish which parameter, either velocity or density, should be recognized to image, but recognize them as a combined form linear to the measured data set - a "composite". If there is no variation of the velocity parameter in the medium, then the imaging algorithm will shut down automatically and immediately. To justify the conjectured imaging algorithm, higher *ISS* terms need to be calculated so that higher order imaging-only terms can be identified and collected to develop an imaging algorithm in the multi-parameter case.

Stage (4) - for a multi-D multi-parameter acoustic medium, stage (5) - for a 1D/multi-D multi-parameter elastic medium and stage (6) - for a model type independent depth imaging algorithm. The imaging algorithm development for the former two stages will be continued following stage (3) in the way to justify Weglein's imaging conjectures. The last stage is the ultimate objective to develop the *ISS* imaging algorithm - the model type independent *ISS* imaging algorithm which means to image the medium by using the same algorithm without considering whether the underlying imaged medium is acoustic, elastic, inelastic or whatever kind of medium.

It is important to mention that all of the imaging algorithms have been developed or will be developed without knowing any priori information of the subsurface – to image directly the subsurface medium only using the data set collected on the measurement surface and the chosen reference wavefield (Weglein et al., 2003).

This paper presents an effort to advance research within stage (3). As a starting point, a laterally invariant acoustic medium with both velocity and density variation (two parameters) will be con-

sidered and studied here. Section (1) is a brief description of *ISS* imaging algorithm development history within M-OSRP and the future stages to achieve the ultimate *ISS* imaging algorithm. Section (2) is an introduction to the inverse scattering theory and series. The study on a two-parameter 1D acoustic medium starts from section (3) in which the work in Zhang and Weglein (2005) is introduced and a series of conjectured imaging algorithms proposed by Dr. Weglein are presented. The logic behind those conjectures will also be stated in this section. To justify the conjectured imaging algorithm for the 1D two-parameter acoustic medium, some calculation results on the *ISS* higher order (3^{rd} order) term are shown and examined in section (4), and an *LOIS* imaging algorithm (which is exactly the conjectured imaging algorithm) is derived at the end of the section (4). Some discussion and conclusions are described in the last section.

Inverse scattering theory and series

Scattering theory is a form of perturbation analysis. Generally speaking, it describes how a perturbation in the properties of a medium relates to a wavefield that experiences that perturbed medium. Consider the two differential equations governing wave propagation in these media (Weglein et al., 2003):

$$LG = \delta(\mathbf{r} - \mathbf{r_s}), \tag{1}$$

$$L_0 G_0 = \delta(\mathbf{r} - \mathbf{r_s}). \tag{2}$$

where L, L_0 and G, G_0 are the actual and reference differential operators and Green's functions, respectively, for a single temporal frequency, ω, and $\delta(\mathbf{r} - \mathbf{r_s})$ is a Dirac delta function. $\mathbf{r}$ and $\mathbf{r_s}$ are the field point and source location, respectively.

Lippmann-Schwinger equation

The Lippmann-Schwinger equation is an integral solution to the wave equation (1) by using the reference wave equation (2) and defining a perturbation operator as $V = L_0 - L$,

$$\Psi_s = G - G_0 = G_0 V G. \tag{3}$$

where Ψ_s is the scattered field.

The total scattered field is related to the earth perturbation and the reference wave field (generally using water as reference background for marine seismic exploration) by the above recursive integral Lippmann-Schiwinger equation. It is a direct solution to the real wave equation.

Forward scattering series

Expanding equation (3) by iterating itself (Taylor, 1972), a forward scattering series is obtained,

$$\Psi_s = G_0 V G_0 + G_0 V G_0 V G_0 + \cdots \tag{4}$$

$$= \quad (\Psi_s)_1 + (\Psi_s)_2 + \cdots, \tag{5}$$

where $(\Psi_s)_n$ is the portion of Ψ_s that is the n^{th} order in V. The measured value of Ψ_s is the data, D, where $D = (\Psi_s)_{ms} = (\Psi_s)_{\text{on the measurement surface}}$.

The forward scattering series provides an ability of modeling the data since the perturbation V underneath the measurement surface has been assumed known in the forward problem.

Inverse scattering series

Expanding the perturbation operator V in orders of data D yields,

$$V = V_1 + V_2 + V_3 + \cdots \tag{6}$$

where V_n is the n^{th} order of the data D.

An inverse scattering series is obtained by setting the same order of the data equal on both sides of equation (4) at the measurement surface,

$$\begin{aligned}
D &= [G_0 V_1 G_0]_{ms}, && (7)\\
0 &= [G_0 V_2 G_0]_{ms} + [G_0 V_1 G_0 V_1 G_0]_{ms}, && (8)\\
0 &= [G_0 V_3 G_0]_{ms} + [G_0 V_1 G_0 V_2 G_0]_{ms} \\
&+ [G_0 V_2 G_0 V_1 G_0]_{ms} + [G_0 V_1 G_0 V_1 G_0 V_1 G_0]_{ms}, && (9)\\
&\vdots
\end{aligned}$$

The inverse scattering series provides a direct method to obtain the subsurface information by inverting the series order by order to solve the perturbation V, only using the measured data D and a reference wave field G_0.

1D two-parameter acoustic medium

To study a 1D two-parameter acoustic medium, let us first consider the 3D acoustic wave equations in the actual and reference medium (Zhang and Weglein, 2005),

$$\begin{aligned}
\left[\frac{\omega^2}{K(\vec{r})} + \nabla \cdot \frac{1}{\rho(\vec{r})}\nabla\right] G(\vec{r}, \vec{r_s}; \omega) &= \delta(\vec{r} - \vec{r_s}),\\
\left[\frac{\omega^2}{K_0(\vec{r})} + \nabla \cdot \frac{1}{\rho_0(\vec{r})}\nabla\right] G_0(\vec{r}, \vec{r_s}; \omega) &= \delta(\vec{r} - \vec{r_s}).
\end{aligned} \tag{10}$$

where G and G_0 are the actual and reference Green's functions, or wavefields, respectively, for a single temporal frequency, ω. $K = c^2\rho$, is P-bulk modulus, c is P-wave velocity and ρ is the density.

The quantities with subscript "0" are in the reference medium, otherwise, they are in the actual medium.

The perturbation operator is therefore defined as,

$$V = L_0 - L = \frac{\omega^2 \alpha}{K_0(\vec{r})} + \nabla \cdot \frac{\beta}{\rho_0(\vec{r})} \nabla, \tag{11}$$

where $\alpha = 1 - \frac{K_0}{K}$, $\beta = 1 - \frac{\rho_0}{\rho}$.

Similar to operator V, we also expand α and β in orders of the data, considering a 1D acoustic medium,

$$\begin{aligned} \alpha(z) &= \alpha_1(z) + \alpha_2(z) + ... \\ \beta(z) &= \beta_1(z) + \beta_2(z) + ... \end{aligned} \tag{12}$$

Results of the first two *ISS* terms

Using the expansions of α and β, and inserting equation (11) into the *ISS*, equation (7) and equation (8), yield the 1^{st} order and 2^{nd} order approximations to the two parameters (Zhang and Weglein, 2005):

$$D(z,\theta) = -\frac{\rho_0}{4}\left[\frac{1}{\cos^2\theta}\alpha_1(z) + \left(1 - \tan^2\theta\right)\beta_1(z)\right], \tag{13}$$

and,

$$\begin{aligned} &\frac{1}{\cos^2\theta}\alpha_2(z) + \left(1 - \tan^2\theta\right)\beta_2(z) \\ &= -\frac{1}{2}\frac{1}{\cos^4\theta}\alpha_1^2(z) - \frac{1}{2}\left(\tan^4\theta + 1\right)\beta_1^2(z) + \frac{\tan^2\theta}{\cos^2\theta}\alpha_1(z)\beta_1(z) \\ &- \frac{1}{2}\frac{1}{\cos^4\theta}{\alpha_1}'(z)\int_{-\infty}^{z}\left[\alpha_1(z') - \beta_1(z')\right]dz' + \frac{1}{2}\left(\tan^4\theta - 1\right){\beta_1}'(z)\int_{-\infty}^{z}\left[\alpha_1(z') - \beta_1(z')\right]dz'. \end{aligned} \tag{14}$$

Here we have already made an inverse Fourier transform with respect to $-2q_g$ from the original equation, and set $z_g = z_s = 0$ for simplicity. For the two parameters case, the imaging-only terms were identified in equation (14) as the integral terms in Zhang and Weglein (2005).

Conjectured multi-parameter imaging algorithms

In this section, a series of conjectured imaging algorithms, proposed by Weglein, for both acoustic and elastic multi-parameter media are introduced, and the logic behind the development of those algorithms is described.

Let us take a retrospect on the *LOIS* imaging algorithm development of the 1D velocity-only acoustic medium at normal incidence (Weglein et al., 2000; Shaw et al., 2002; Shaw and Weglein, 2003;

Shaw, 2005). The first three orders imaging-only terms captured in the *LOIS* imaging algorithm are respectively,

$$\alpha_1(z), \quad -\frac{1}{2}\frac{d\alpha_1(z)}{dz}\int_{-\infty}^{z}\alpha_1(z')dz', \quad \frac{1}{8}\frac{d^2\alpha_1(z)}{dz^2}\left[\int_{-\infty}^{z}\alpha_1(z')dz'\right]^2.$$

In the above three terms, the z is a pseudo-depth obtained by re-scaling time with a reference velocity (for example water speed). The derivatives outside the integrals are analyzed as "*attention-needed terms*", and the integrals are "*attention-provided terms*"(proposed and discussed by Weglein in 2005/2006 M-OSRP annual reports). The attention-needed term indicates the local amplitude variation of the imaged parameter with respect to depth z (The parameter is the velocity for the 1D acoustic medium considered above, for instance.). This local amplitude variation examination will show the local medium property variations (including real velocity change) of the seismic model. If the local properties changed, this term would turn the attention light on. If and only if the reference velocity used to locate the parameter to the pseudo-depth z is different from the real velocity in the seismic model, then the "attention-provided term" will be turned on to correct the migration effect by using the wrong reference velocity. And the correction will be accumulated from the above medium down to the current pseudo-depth z by doing the integral of the velocity difference in the 1^{st} order. For example, in the above three terms, $\alpha_1(z)$ is the 1^{st} order of the velocity parameter. The derivative of $\alpha_1(z)$ indicates at pseudo-depth z the velocity parameter needs "attention" by comparing the local velocity with the reference velocity. If the local velocity is different from the reference velocity used in the inverse scattering series, then, the integral term will provide "attention" by summing together the velocity difference down to the current pseudo-depth z. In other words, if the used reference velocity is exactly the velocity of the underlying imaged medium, then, the integral term shuts down and therefore no imaging task is needed: the imaging result is correct by using reference velocity.

By adding together all of the leading order imaging-only terms like the above three terms in the higher order *ISS* terms, the leading order imaging sub-series closed form was obtained,

$$\alpha^{LOIS}(z) = \alpha_1\left(z - \frac{1}{2}\int_{-\infty}^{z}\alpha_1(z')dz'\right). \tag{15}$$

The closed form above is a shifted "attention-needed term" by a quantity of the "attention-provided term".

Now let us take a look at the imaging-only term for the multi-parameter acoustic medium in equation (14). Rewrite it as the following form:

$$-\frac{1}{2}\frac{1}{\cos^2\theta}\left[\frac{1}{\cos^2\theta}\alpha_1(z) + \left(1-\tan^2\theta\right)\beta_1(z)\right]\int_{-\infty}^{z}\left[\alpha_1(z') - \beta_1(z')\right]dz'$$

The "*attention-needed terms*" turn out to be the combination term of the two parameters $\alpha_1(z)$ and $\beta_1(z)$ in the bracket, and the corresponding "*attention-provided term*" is the integral of $\alpha_1(z)-\beta_1(z)$ which only takes care of the velocity change (Zhang and Weglein, 2005). If there is no velocity change in the medium, the integral shuts down and the imaging task is not needed. The logic here

is following the same way as we stated in the above 1D one-parameter acoustic medium case. So, Weglein intuitively proposed the following conjectured imaging algorithm for the 1D two-parameter acoustic medium:

$$\begin{aligned} LOIS = & \frac{1}{\cos^2\theta}\alpha_1\left(z - \frac{1}{2}\frac{1}{\cos^2\theta}\int_{-\infty}^{z}\alpha_1(z')dz'\right) \\ & + \left(1-\tan^2\theta\right)\beta_1\left(z - \frac{1}{2}\frac{1}{\cos^2\theta}\int_{-\infty}^{z}\alpha_1(z')dz'\right). \end{aligned} \tag{16}$$

Following the same philosophy and logic of the "*attention-needed terms*" and the "*attention-provided term*", the above conjecture was extended by Weglein to a multi-D multi-parameter acoustic medium and 1D/multi-D elastic multi-parameter medium, by directly substituting the original one-parameter "*attention-provided term*" with the multi-parameter "*attention-provided term*" expressed in the multi-parameter shifted "*attention-needed term*". Jingfeng Zhang justified this conjecture on the the 1^{st} order and 2^{nd} order approximations in the 1D multi-parameter elastic medium where imaging-only terms have been identified in Zhang and Weglein (2006).

To justify the above conjectured imaging algorithm for the 1D two-parameter acoustic medium, more imaging-only terms should be identified by calculating higher order *ISS* terms. Due to an exponential increase in the complexity of calculation for higher and higher *ISS* terms, a good way is to calculate as few *ISS* terms as possible, and identify a similar mathematical pattern in higher order terms, then conclude an imaging sub-series/closed form from those similar terms. The following sections are based on this idea and examine the conjectured imaging algorithm for the two-parameter acoustic medium.

Multi-parameter imaging algorithm

This section aims to identify a multi-parameter imaging algorithm by calculating and capturing some imaging-only terms hidden in the higher order *ISS* terms.

Calculation of the third order *ISS* term

We start with the calculation of the *ISS* third term, equation (9),

$$-G_0V_3G_0 = G_0V_2G_0V_1G_0 + G_0V_1G_0V_2G_0 + G_0V_1G_0V_1G_0V_1G_0.$$

where,

$$G_0V_3G_0 = \iint_{-\infty}^{\infty} dx'dz'G_0(x_g,z_g;x',z')\hat{V}_3(x',z')G_0(x',z';x_s,z_s), \tag{17}$$

$$\begin{aligned} G_0V_2G_0V_1G_0 = & \iint_{-\infty}^{\infty} dx'dz' \iint_{-\infty}^{\infty} dx''dz''G_0(x_g,z_g;x',z')\hat{V}_2(x',z')G_0(x',z';x'',z'') \\ & \cdot \hat{V}_1(x'',z'')G_0(x'',z'';x_s,z_s), \end{aligned} \tag{18}$$

$$G_0V_1G_0V_2G_0 = \iint_{-\infty}^{\infty} dx'dz' \iint_{-\infty}^{\infty} dx''dz'' G_0(x_g, z_g; x', z')\hat{V}_1(x', z')G_0(x', z'; x'', z'') \quad (19)$$
$$\cdot \quad \hat{V}_2(x'', z'')G_0(x'', z''; x_s, z_s),$$
$$G_0V_1G_0V_1G_0V_1G_0 = \iint_{-\infty}^{\infty} dx'dz' \iint_{-\infty}^{\infty} dx''dz'' \iint_{-\infty}^{\infty} dx'''dz''' G_0(x_g, z_g; x', z')\hat{V}_1(x', z') \quad (20)$$
$$\cdot \quad G_0(x', z'; x'', z'')\hat{V}_1(x'', z'')G_0(x'', z''; x''', z''')\hat{V}_1(x''', z''')G_0(x''', z'''; x_s, z_s).$$

For the 1D two-parameter acoustic medium, the perturbation defined in equation (11) becomes,

$$\hat{V}_n(x', z') = \frac{\omega^2}{K_0}\alpha_n(z') + \frac{\beta_n(z')}{\rho_0}\frac{\partial^2}{\partial x'^2} + \frac{1}{\rho_0}\frac{\partial}{\partial z'}\beta_n(z')\frac{\partial}{\partial z'} \qquad n = 1, 2, 3... \quad (21)$$

and a 2D Green's function bilinear form is used in calculation, which is defined as,

$$G_0(x', z'; x'', z'') = \frac{\rho_0}{(2\pi)^2} \iint_{-\infty}^{\infty} dk_x'dk_z' \frac{e^{ik_x'(x'-x'')}e^{ik_z'(z'-z'')}}{k^2 - \left(k_x'^2 + k_z'^2\right)}. \quad (22)$$

After mathematical calculation, the third term turns out to be,

$$
\begin{aligned}
&\frac{1}{\cos^2\theta}\alpha_3(z) + \left(1-\tan^2\theta\right)\beta_3(z) \\
&= -\frac{1}{\cos^4\theta}\left[\alpha_1(z)-\beta_1(z)\right]\left[\alpha_2(z)-\beta_2(z)\right] + \frac{1}{4}\frac{1}{\cos^2\theta}\beta_1^2(z)\left[\alpha_1(z)-\beta_1(z)\right] \\
&+ \frac{1}{8}\frac{1}{\cos^4\theta}\beta_1(z)\left[\alpha_1(z)-\beta_1(z)\right]^2 - \frac{5}{16}\frac{1}{\cos^6\theta}\left[\alpha_1(z)-\beta_1(z)\right]^3 \\
&- \frac{1}{2}\frac{1}{\cos^4\theta}{\alpha_1}'(z)\int_{-\infty}^{z}\left[\alpha_2(z')-\beta_2(z')\right]dz' \\
&- \frac{1}{2}\frac{1}{\cos^4\theta}{\alpha_2}'(z)\int_{-\infty}^{z}\left[\alpha_1(z')-\beta_1(z')\right]dz' \\
&+ \frac{1}{2}\left(\tan^4\theta-1\right){\beta_1}'(z)\int_{-\infty}^{z}\left[\alpha_2(z')-\beta_2(z')\right]dz' \\
&+ \frac{1}{2}\left(\tan^4\theta-1\right){\beta_2}'(z)\int_{-\infty}^{z}\left[\alpha_1(z')-\beta_1(z')\right]dz' \\
&- \frac{1}{8}\frac{1}{\cos^6\theta}{\alpha_1}''(z)\left[\int_{-\infty}^{z}(\alpha_1(z')-\beta_1(z'))dz'\right]^2 \\
&- \frac{1}{8}\frac{1}{\cos^4\theta}\left(1-\tan^2\theta\right){\beta_1}''(z)\left[\int_{-\infty}^{z}(\alpha_1(z')-\beta_1(z'))dz'\right]^2 \\
&- \frac{1}{4}\frac{3}{\cos^6\theta}\alpha_1(z){\alpha_1}'(z)\int_{-\infty}^{z}\left[\alpha_1(z')-\beta_1(z')\right]dz' \\
&+ \frac{1}{4}\frac{3}{\cos^6\theta}\beta_1(z){\alpha_1}'(z)\int_{-\infty}^{z}\left[\alpha_1(z')-\beta_1(z')\right]dz' \\
&+ \frac{1}{4}\frac{1}{\cos^4\theta}\left(3\tan^2\theta+1\right)\alpha_1(z){\beta_1}'(z)\int_{-\infty}^{z}\left[\alpha_1(z')-\beta_1(z')\right]dz' \\
&+ \frac{1}{4}\frac{1}{\cos^4\theta}\left(3\tan^2\theta-1\right)\beta_1(z){\beta_1}'(z)\int_{-\infty}^{z}\left[\alpha_1(z')-\beta_1(z')\right]dz' \\
&- \frac{1}{4}\frac{1}{\cos^4\theta}{\beta_1}'(z)\int_{-\infty}^{z}\left[\alpha_1(z')-\beta_1(z')\right]^2dz' \\
&- \frac{1}{8}\frac{1}{\cos^6\theta}\left[{\alpha_1}'(z)-{\beta_1}'(z)\right]\int_{-\infty}^{z}\left[\alpha_1(z')-\beta_1(z')\right]^2dz' \\
&+ MUL.
\end{aligned}
\tag{23}
$$

where $MUL.$ term is the multiple-related term expressed as the following equation,

$$
\begin{aligned}
MUL. = &-\frac{1}{16}\frac{1}{\cos^6\theta}\int_{-\infty}^{z}\alpha_1{}'(z')\int_{-\infty}^{z}\alpha_1{}'(z'')\alpha_1(z'+z''-z)dz''dz' \\
&-\frac{1}{8}\left(\frac{1}{\cos^4\theta}-\frac{1}{2}\frac{1}{\cos^6\theta}\right)\int_{-\infty}^{z}\alpha_1{}'(z')\int_{-\infty}^{z}\alpha_1{}'(z'')\beta_1(z'+z''-z)dz''dz' \\
&-\frac{1}{4}\left(\frac{1}{\cos^4\theta}-\frac{1}{2}\frac{1}{\cos^6\theta}\right)\int_{-\infty}^{z}\alpha_1{}'(z')\int_{-\infty}^{z}\beta_1{}'(z'')\alpha_1(z'+z''-z)dz''dz' \\
&-\frac{1}{4}\left(\frac{2}{\cos^2\theta}-\frac{2}{\cos^4\theta}+\frac{1}{2}\frac{1}{\cos^6\theta}\right)\int_{-\infty}^{z}\alpha_1{}'(z')\int_{-\infty}^{z}\beta_1{}'(z'')\beta_1(z'+z''-z)dz''dz' \\
&-\frac{1}{4}\left(\frac{1}{\cos^2\theta}-\frac{1}{\cos^4\theta}+\frac{1}{4}\frac{1}{\cos^6\theta}\right)\int_{-\infty}^{z}\beta_1{}'(z')\int_{-\infty}^{z}\beta_1{}'(z'')\alpha_1(z'+z''-z)dz''dz' \\
&+\frac{1}{4}\left(\frac{3}{\cos^2\theta}-\frac{3}{2}\frac{1}{\cos^4\theta}+\frac{1}{4}\frac{1}{\cos^6\theta}\right)\int_{-\infty}^{z}\beta_1{}'(z')\int_{-\infty}^{z}\beta_1{}'(z'')\beta_1(z'+z''-z)dz''dz'.
\end{aligned}
\tag{24}
$$

where the $'$ means a derivative of the argument in that function.

Examination on the one-parameter case

Now we have already obtained the complicated mathematical expression for the 3^{rd} *ISS* term. How good is the calculation? Let us check the 3^{rd} term result under a 1D acoustic medium with velocity variation only at normal incidence case.

Under the above assumptions,

$$\beta_1 = 0, \qquad \theta = 0 \ (then,\ \cos\theta = 1 \ and \ \tan\theta = 0).$$

By using the above two values, we can further simplify the 3^{rd} term,

$$L.H.S. = \alpha_3(z).$$

$$
\begin{aligned}
R.H.S. = &-\alpha_1(z)\alpha_2(z) - \frac{5}{16}{\alpha_1}^3(z) \\
&-\frac{1}{2}\alpha_1{}'(z)\int_{-\infty}^{z}\alpha_2(z')dz' - \frac{1}{2}\alpha_2{}'(z)\int_{-\infty}^{z}\alpha_1(z')dz' \\
&-\frac{1}{8}\alpha_1{}''(z)\left[\int_{-\infty}^{z}\alpha_1(z')dz'\right]^2 + \frac{3}{4}\alpha_1(z)\alpha_1{}'(z)\int_{-\infty}^{z}\left(-\alpha_1(z')\right)dz' \\
&-\frac{1}{16}\int_{-\infty}^{z}\alpha_1{}'(z')\int_{-\infty}^{z}\alpha_1{}'(z'')\alpha_1(z'+z''-z)dz''dz'.
\end{aligned}
\tag{25}
$$

To get the final expression of R.H.S. term, we will substitute into the above equation the expression of α_2 in Shaw et al. (2002) for the one-parameter case.

$$\alpha_2(z) = -\frac{1}{2}\left[{\alpha_1}^2(z) + \alpha_1{}'(z)\int_{-\infty}^{z}\alpha_1(z')dz'\right]. \tag{26}$$

Substituting equation (26) back into equation (25), we find,

$$\begin{aligned} R.H.S. =& \frac{1}{2}\alpha_1(z)\left[{\alpha_1}^2(z)+{\alpha_1}'(z)\int_{-\infty}^{z}\alpha_1(z')dz'\right]-\frac{5}{16}{\alpha_1}^3(z) \\ &+\frac{1}{4}{\alpha_1}'(z)\int_{-\infty}^{z}dz'\left[{\alpha_1}^2(z')+{\alpha_1}'(z')\int_{-\infty}^{z'}\alpha_1(z'')dz''\right] \\ &+\frac{1}{4}\frac{d}{dz}\left[{\alpha_1}^2(z)+{\alpha_1}'(z)\int_{-\infty}^{z}\alpha_1(z')dz'\right]\int_{-\infty}^{z}\alpha_1(z')dz'-\frac{1}{8}{\alpha_1}''(z)\left[\int_{-\infty}^{z}\alpha_1(z')dz'\right]^2 \\ &-\frac{3}{4}\alpha_1(z){\alpha_1}'(z)\int_{-\infty}^{z}\alpha_1(z')dz'-\frac{1}{16}\int_{-\infty}^{z}{\alpha_1}'(z')\int_{-\infty}^{z}{\alpha_1}'(z'')\alpha_1(z'+z''-z)dz''dz'. \end{aligned} \tag{27}$$

After collecting the same terms and using some simple algebra, and letting the R.H.S. equal the L.H.S., we obtain,

$$\begin{aligned} \alpha_3(z) =& \frac{3}{16}{\alpha_1}^3(z)+\frac{3}{4}\alpha_1(z)\frac{d\alpha_1(z)}{dz}\int_{-\infty}^{z}\alpha_1(z'))dz' \\ &+\frac{1}{8}\frac{d^2\alpha_1(z)}{dz^2}\left[\int_{-\infty}^{z}\alpha_1(z')dz'\right]^2-\frac{1}{8}\frac{d\alpha_1(z)}{dz}\int_{-\infty}^{z}{\alpha_1}^2(z')dz' \\ &-\frac{1}{16}\int_{-\infty}^{z}{\alpha_1}'(z')\int_{-\infty}^{z}{\alpha_1}'(z'')\alpha_1(z'+z''-z)dz''dz'. \end{aligned} \tag{28}$$

Equation (28) is exactly $\alpha_3(z)$ for the 1D one-parameter acoustic medium at normal incidence case in Shaw (2005), which indicates the calculation of the 3^{rd} order term is effective.

Leading order imaging sub-series

In the following calculation, we try to further simplify some integrals in equation (23) by collecting some similar terms and using the 2^{nd} term result equation (14).

We consider the following two integrals in equation (23),

$$\begin{aligned} &-\frac{1}{2}\frac{1}{\cos^4\theta}{\alpha_2}'(z)\int_{-\infty}^{z}\left[\alpha_1(z')-\beta_1(z')\right]dz'+\frac{1}{2}\left(\tan^4\theta-1\right){\beta_2}'(z)\int_{-\infty}^{z}\left[\alpha_1(z')-\beta_1(z')\right]dz' \\ &=-\frac{1}{2}\frac{1}{\cos^2\theta}\left(\tan^2\theta+1\right){\alpha_2}'(z)\int_{-\infty}^{z}\left[\alpha_1(z')-\beta_1(z')\right] \\ &\quad+\frac{1}{2}\frac{1}{\cos^2\theta}\left(\tan^2\theta-1\right){\beta_2}'(z)\int_{-\infty}^{z}\left[\alpha_1(z')-\beta_1(z')\right]dz' \\ &=-\frac{1}{2}\frac{1}{\cos^2\theta}\frac{d}{dz}\left[\frac{1}{\cos^2\theta}\alpha_2(z)+\left(1-\tan^2\theta\right)\beta_2(z)\right]\int_{-\infty}^{z}\left[\alpha_1(z')-\beta_1(z')\right]dz'. \end{aligned} \tag{29}$$

where we notice that the total derivative part outside the integral is exactly the ISS 2^{nd} term equation (14).

Now substituting equation (14) into equation (29),

$$\begin{aligned}
&-\frac{1}{2}\frac{1}{\cos^4\theta}\alpha_2{}'(z)\int_{-\infty}^{z}\left[\alpha_1(z')-\beta_1(z')\right]dz' \\
&+\frac{1}{2}\left(\tan^4\theta-1\right)\beta_2{}'(z)\int_{-\infty}^{z}\left[\alpha_1(z')-\beta_1(z')\right]dz' \\
&=\frac{3}{4}\frac{1}{\cos^4\theta}\left[\alpha_1(z)-\beta_1(z)\right]\frac{d\mathcal{D}(z,\theta)}{dz}\int_{-\infty}^{z}\left[\alpha_1(z')-\beta_1(z')\right]dz' \\
&+\frac{1}{2}\frac{1}{\cos^2\theta}\beta_1(z)\frac{d\mathcal{D}(z,\theta)}{dz}\int_{-\infty}^{z}\left[\alpha_1(z')-\beta_1(z')\right]dz' \\
&-\frac{1}{2}\frac{1}{\cos^4\theta}\left[\alpha_1(z)-\beta_1(z)\right]\frac{d\beta_1(z)}{dz}\int_{-\infty}^{z}\left[\alpha_1(z')-\beta_1(z')\right]dz' \\
&+\frac{1}{4}\frac{1}{\cos^4\theta}\frac{d^2\mathcal{D}(z,\theta)}{dz^2}\left[\int_{-\infty}^{z}(\alpha_1(z')-\beta_1(z'))dz'\right]^2.
\end{aligned} \tag{30}$$

where we define a new quantity $\mathcal{D}(z,\theta)$ in the above result, called the"imaging composite" and expressed as,

$$\mathcal{D}(z,\theta)\equiv\frac{1}{\cos^2\theta}\alpha_1(z)+\left(1-\tan^2\theta\right)\beta_1(z). \tag{31}$$

This new quantity $\mathcal{D}(z,\theta)$ is the linear term, equation (13), except for a constant.

Similarly, we also notice the following integrals in equation (23),

$$\begin{aligned}
&-\frac{1}{8}\frac{1}{\cos^6\theta}\alpha_1{}''(z)\left[\int_{-\infty}^{z}(\alpha_1(z')-\beta_1(z'))dz'\right]^2 \\
&+\frac{1}{8}\frac{1}{\cos^4\theta}\left(\tan^2\theta-1\right)\beta_1{}''(z)\left[\int_{-\infty}^{z}(\alpha_1(z')-\beta_1(z'))dz'\right]^2 \\
&=-\frac{1}{2}\frac{1}{\cos^4\theta}\frac{d^2\mathcal{D}(z,\theta)}{dz^2}\left[\int_{-\infty}^{z}(\alpha_1(z')-\beta_1(z'))dz'\right]^2.
\end{aligned} \tag{32}$$

and,

$$\begin{aligned}
&-\frac{1}{4}\frac{1}{\cos^4\theta}\beta_1{}'(z)\int_{-\infty}^{z}\left[\alpha_1(z')-\beta_1(z')\right]^2dz' \\
&-\frac{1}{8}\frac{1}{\cos^6\theta}\left[\alpha_1{}'(z)-\beta_1{}'(z)\right]\int_{-\infty}^{z}\left[\alpha_1(z')-\beta_1(z')\right]^2dz' \\
&=-\frac{1}{\cos^4\theta}\frac{d\mathcal{D}(z,\theta)}{dz}\int_{-\infty}^{z}\left[\alpha_1(z')-\beta_1(z')\right]^2dz'.
\end{aligned} \tag{33}$$

Substituting all of the above equations back into the equation (23) and combining similar terms, we obtain the 3^{rd} term in terms of the new defined imaging composite $\mathcal{D}(z,\theta)$,

$$
\begin{aligned}
&\frac{1}{\cos^2\theta}\alpha_3(z) + \left(1-\tan^2\theta\right)\beta_3(z) \\
&= -\frac{1}{\cos^4\theta}\left[\alpha_1(z)-\beta_1(z)\right]\left[\alpha_2(z)-\beta_2(z)\right] + \frac{1}{4}\frac{1}{\cos^2\theta}{\beta_1}^2(z)\left[\alpha_1(z)-\beta_1(z)\right] \\
&+ \frac{1}{8}\frac{1}{\cos^4\theta}\beta_1(z)\left[\alpha_1(z)-\beta_1(z)\right]^2 - \frac{5}{16}\frac{1}{\cos^6\theta}\left[\alpha_1(z)-\beta_1(z)\right]^3 \\
&- \frac{1}{2}\frac{1}{\cos^2\theta}\frac{d\mathcal{D}(z,\theta)}{dz}\int_{-\infty}^{z}\left[\alpha_2(z')-\beta_2(z')\right]dz' \\
&+ \frac{3}{4}\frac{1}{\cos^4\theta}\left[\alpha_1(z)-\beta_1(z)\right]\frac{d\mathcal{D}(z,\theta)}{dz}\int_{-\infty}^{z}\left[\alpha_1(z')-\beta_1(z')\right]dz' \\
&+ \frac{1}{2}\frac{1}{\cos^2\theta}\beta_1(z)\frac{d\mathcal{D}(z,\theta)}{dz}\int_{-\infty}^{z}\left[\alpha_1(z')-\beta_1(z')\right]dz' \\
&- \frac{1}{8}\frac{1}{\cos^4\theta}\frac{d\mathcal{D}(z,\theta)}{dz}\int_{-\infty}^{z}\left[\alpha_1(z')-\beta_1(z')\right]^2dz' \\
&+ \frac{1}{8}\frac{1}{\cos^4\theta}\frac{d^2\mathcal{D}(z,\theta)}{dz^2}\left[\int_{-\infty}^{z}\left(\alpha_1(z')-\beta_1(z')\right)dz'\right]^2 \\
&- \frac{1}{2}\frac{1}{\cos^4\theta}\left[\alpha_1(z)-\beta_1(z)\right]\frac{d\beta_1(z)}{dz}\int_{-\infty}^{z}\left[\alpha_1(z')-\beta_1(z')\right]dz' \\
&+ \frac{1}{4}\frac{1}{\cos^4\theta}\left(3\tan^2\theta+1\right)\alpha_1(z)\frac{d\beta_1(z)}{dz}\int_{-\infty}^{z}\left[\alpha_1(z')-\beta_1(z')\right]dz' \\
&+ \frac{1}{4}\frac{1}{\cos^4\theta}\left(3\tan^2\theta-1\right)\beta_1(z)\frac{d\beta_1(z)}{dz}\int_{-\infty}^{z}\left[\alpha_1(z')-\beta_1(z')\right]dz' \\
&- \frac{3}{4}\frac{1}{\cos^6\theta}\alpha_1(z)\frac{d\alpha_1(z)}{dz}\int_{-\infty}^{z}\left[\alpha_1(z')-\beta_1(z')\right]dz' \\
&+ \frac{3}{4}\frac{1}{\cos^6\theta}\beta_1(z)\frac{d\alpha_1(z)}{dz}\int_{-\infty}^{z}\left[\alpha_1(z')-\beta_1(z')\right]dz' \\
&+ MUL.
\end{aligned}
\tag{34}
$$

where the multiple-related term *MUL.* is expressed in equation (24).

The examination on the imaging-only terms shown in the 2^{nd} order results (Zhang and Weglein, 2005) indicates that only the integral terms of the difference between the two parameters, in the 3^{rd} order *ISS* term, will contribute to the imaging algorithm. And the philosophy of collecting similar but higher order imaging-only terms leads to the consideration of the following term in equation (34):

$$
\frac{1}{8}\frac{1}{\cos^4\theta}\frac{d^2\mathcal{D}(z,\theta)}{dz^2}\left[\int_{-\infty}^{z}\left(\alpha_1(z')-\beta_1(z')\right)dz'\right]^2
$$

Similarly, we can rewrite equation (13) and the 2^{nd} order imaging-only term in equation (14) in terms of the defined imaging composite $\mathcal{D}(z,\theta)$:

$$
-\frac{4}{\rho_0}D(z,\theta) = \mathcal{D}(z,\theta). \tag{35}
$$

$$-\frac{1}{2}\frac{1}{\cos^2\theta}\frac{d\mathcal{D}(z,\theta)}{dz}\int_{-\infty}^{z}\left[\alpha_1(z')-\beta_1(z')\right]dz'$$

The above three terms are imaging terms identified from the first three *ISS* terms that are going to be collected and taken as the basis to identify the following imaging sub-series. An observation through the first three imaging terms provides a mathematical pattern, called as "leading order imaging sub-series" (*LOIS*):

$$\mathcal{D}^{LOIS}=\sum_{n=0}^{\infty}\frac{\left(-\frac{1}{2}\frac{1}{\cos^2\theta}\right)^n}{n!}\frac{d^n\mathcal{D}(z,\theta)}{dz^n}\left[\int_{-\infty}^{z}\left(\alpha_1(z')-\beta_1(z')\right)dz'\right]^n. \tag{36}$$

Every term in this *LOIS* is an imaging-only term and appears in the higher *ISS* terms with increasing n.

Leading order imaging closed form

Employing the same mathematical procedure as Shaw (2005), the *LOIS* is a Taylor expansion series of the following imaging function, called as "leading order imaging closed form":

$$\begin{aligned}&\sum_{n=0}^{\infty}\frac{\left(-\frac{1}{2}\frac{1}{\cos^2\theta}\right)^n}{n!}\frac{d^n\mathcal{D}(z,\theta)}{dz^n}\left[\int_{-\infty}^{z}\left(\alpha_1(z')-\beta_1(z')\right)dz'\right]^n\\&=\mathcal{D}\left(z-\frac{1}{2}\frac{1}{\cos^2\theta}\int_{-\infty}^{z}\left(\alpha_1(z')-\beta_1(z')\right)dz'\right).\end{aligned} \tag{37}$$

Noticing the quantity $\mathcal{D}$ defined in equation (31), the above leading order imaging closed form is exactly the conjectured imaging algorithm proposed by Weglein in equation (16).

Discussion

Shutting down the density variation, namely, letting $\beta(z)=0$, and therefore, $\beta_1(z)=0$, equation (37) will be simplified as,

$$\begin{aligned}&\sum_{n=0}^{\infty}\frac{\left(-\frac{1}{2}\frac{1}{\cos^2\theta}\right)^n}{n!}\frac{d^n\alpha_1(z)}{dz^n}\left[\int_{-\infty}^{z}\alpha_1(z')dz'\right]^n\\&=\alpha_1\left(z-\frac{1}{2}\frac{1}{\cos^2\theta}\int_{-\infty}^{z}\alpha_1(z')dz'\right).\end{aligned} \tag{38}$$

This equation is exactly the leading order imaging sub-series and closed form for the 1D velocity-only changed acoustic medium (Shaw et al., 2002; Shaw, 2005). For the one parameter case, the imaging algorithm recognizes the one parameter (velocity) as the imaging object, and the shifted quantity in the $\alpha_1(z)$ depends on the integral of the 1^{st} order approximation of the velocity parameter to the uncorrected location.

Unlike the one parameter case, there are two parameters to be imaged for the acoustic medium with both density and velocity variations. So which one should be imaged? or, should both be imaged, in the way as the above one parameter case? The leading order imaging closed form, equation (37), answers these questions: it recognizes the imaging of the two parameters as a imaging composite $\mathcal{D}(z,\theta)$. In fact, the imaging composite $\mathcal{D}(z,\theta)$ is related with the seismic data in the pseudo-depth domain, presenting in equation (35). Therefore, the closed form can be further identified as a shifted seismic data set in the re-scaled time domain using reference velocity, called as pseudo-depth domain, i.e.,

$$\begin{aligned}&\mathcal{D}\left(z-\frac{1}{2}\frac{1}{\cos^2\theta}\int_{-\infty}^{z}\left(\alpha_1(z')-\beta_1(z')\right)dz'\right)\\&=-\frac{4}{\rho_0}D\left(z-\frac{1}{2}\frac{1}{\cos^2\theta}\int_{-\infty}^{z}\left(\alpha_1(z')-\beta_1(z')\right)dz'\right).\end{aligned}\tag{39}$$

This imaging result is valuable and indicates that for multi-parameter medium imaging, the algorithm itself will recognize the existence of different parameters in the medium, since reflection happens when medium properties change, i.e. medium parameters change. The inverse scattering imaging algorithm captures the medium property changes as a composite change, in other words, it images the medium structure in the composite when medium property changes occur. Meanwhile, the shifted quantity in the above imaging algorithm is expressed as the integral of the difference between the 1^{st} order approximations of the two parameters, which is only taking care of the velocity change (Zhang and Weglein, 2005). It will be automatically shut down when there is no velocity variation in the medium (then there is no imaging necessity). This indicates the fact that inverse scattering theory is a purposeful perturbation theory – tasks will be 'waken up' only when needed by the medium. Another surprising capability of the *ISS* imaging algorithm is that it will shut down each imaging term at the first step when it knows there is no velocity change, i.e. when $\alpha_1(z)-\beta_1(z)=0$, and hence each imaging term related with the integral of the difference will be dead to zero immediately. This indicates the *ISS* is an instantly responsive series.

Conclusion

In this report, a leading order imaging algorithm has been derived for a 1D acoustic two-parameter medium, which justifies the logic of the imaging conjectures proposed by Weglein in 2007. The derived imaging algorithm can be expressed as a shifted seismic data set. The shifted quantity is an integral of the difference between the two first order approximations of the two parameters in the medium, which is integrated to zero when there is no velocity variation in the medium. The examination and justification of the logic developed by Weglein in his imaging conjectures by deriving the leading order imaging algorithm in this report presents a framework to develop the ultimate *ISS* model-type independent imaging algorithm step by step. The logic steps are: For a specific model, find the "attention-needed term" which linearly relates with the measured seismic data set, then the "attention-needed term" provides the multi-parameter imaging composite which is migrated with an *ISS* reference velocity and will be shifted in the final imaging algorithm with a quantity of the "attention-provided term"–an integral of the difference among the first order

approximations of the multi-parameters in that medium, which only takes care of the velocity variation of that medium. The imaging algorithm developed here and the conjectured imaging algorithms extended to multi-D and multi-parameter acoustic/elastic media are a structure mapping (using phase information to image the medium structure where reflectors reside), not suited for subsequent AVO analysis because the amplitudes are not correct in the imaging algorithms.

To implement the imaging algorithm (39), the research and related numerical tests are carrying on within M-ORSP. The imaging algorithm developed in this report will also be extended to the multi-D multi-parameter acoustic/elastic media using the logic described in this report and related numerical tests will be planned.

Acknowledgments

Shansong Jiang would like to thank Kristopher Innanen for his valuable discussions during this research. All M-OSRP colleagues are thanked for reviewing this report. The authors would also like to acknowledge the sponsors of M-OSRP for the encouragement and support on this research program. NSF-CMG (award DMS-0327778) and U.S. DOE-BES (Grant No. DOE-De-FG02-05ER15697) are also thanked for their support of fundamental seismic research.

References

Liu, F., B. G. Nita, A. B. Weglein, and K. A. Innanen. "Inverse Scattering Series in the presence of lateral variations." *M-OSRP Annual Report* 3 (2004).

Liu, F., A.B. Weglein, K.A. Innanen, and B.G Nita. "Extension of the non-linear depth imaging capability of the inverse scattering series to multidimensional media: strategies and numerical results." 2005.

Liu, Fang. *Multi-Dimensional Depth Imaing without an Adequate Velocity model*. PhD thesis, University of Houston, 2006.

Shaw, S. A. *An inverse scattering series algorithm for depth imaging of reflection data from a layered acoustic medium with an unknown velocity model*. PhD thesis, University of Houston, 2005.

Shaw, S. A. and A. B. Weglein. "Imaging seismic reflection data at the correct depth without specifying an accurate velocity model: Initial examples of an inverse scattering subseries." *Frontiers of remote sensing information processing*. Ed. C. H. Chen. World Scientific Publishing Company, 2003. chapter 21, 469–484.

Shaw, Simon A., A. B. Weglein, K. H. Matson, and D. J. Foster. "Cooperation of the leading order terms in an inverse-scattering subseries for imaging: 1-D analysis and evaluation.." *SEG Technical Program Expanded Abstracts* (2002): 2277–2280.

Taylor, J. R. *Scattering theory: the quantum theory of nonrelativistic collisions*. John Wiley & Sons, Inc., 1972.

Weglein, A. B. "The inverse scattering concept and its seismic application." *Developments in geophysical exploration methods*. Ed. A.A. Fitch. Volume 6 . Elsevier Applied Science, 1985. 111–138.

Weglein, A. B., F. V. Araújo, P. M. Carvalho, R. H. Stolt, K. H. Matson, R. T. Coates, D. Corrigan, D. J. Foster, S. A. Shaw, and H. Zhang. "Inverse Scattering Series and Seismic Exploration." *Inverse Problems* (2003): R27–R83.

Weglein, A. B., F. A. Gasparotto, P. M. Carvalho, and R. H. Stolt. "An Inverse-Scattering Series Method for Attenuating Multiples in Seismic Reflection Data." *Geophysics* 62 (November-December 1997): 1975–1989.

Weglein, A. B., K. H. Matson, D. J. Foster, P. M. Carvalho, D. Corrigan, and S. A. Shaw. "Imaging and inversion at depth without a velocity model: Theory, concepts and initial evaluation." *70th Annual Internat. Mtg., Soc. Expl. Geophys., Expanded Abstracts*. . Soc. Expl. Geophys., 2000. 1016–1019.

Zhang, H. and A.B. Weglein. "The inverse scattering series for tasks associated with primaries: depth imaging and direct non-linear inversion of 1D variable velocity and density acoustic media." *SEG Technical Program Expanded Abstracts*. 2005, 1705–1708.

Zhang, H. and A.B. Weglein. "Direct non-linear inversion of multi-parameter 1D elastic media using the inverse scattering series." *M-OSRP 2005 Annual Meeting*. 2006, 284–311.

Zhang, J., F. Liu, K. A. Innanen, and A. B. Weglein. "Comprehending and analyzing the leading order and higher order imaging closed forms derived from inverse scattering series." *SEG Technical Program Expanded Abstracts*. 2007.

Preparing data with finite cross-line aperture for input to 3D non-linear imaging algorithms

Z. Wang, A. B. Weglein and F. Liu

Abstract

Seismic imaging methods input measurements on the earth's surface to make inference about subsurface reflectors' locations. When a source generates a wave into a medium, the wave is ubiquitous, including to all points on the measurement surface. Wave theoretic propagation and imaging methods require measurements on the measurement surface where wave theory predicts it will arrive, i.e., everywhere on the measurement surface. When data collection is limited by economic and/or practical considerations, a compromise to wave theory using asymptotic analysis can be used to image limited data with a compromised theory.

In this note, we assume data is adequately sampled in the in-line direction but has a serious aperture limitation in the cross-line direction. Our objective is to provide a wave theory imaging in the direction that has adequate collecion and asymptotic migration in the cross-line limited aperture direction. This is deriving an imaging algorithm that will allow the near-future anticipated less than full cross-line coverage and adequate in-line acquistion to be input into the velocity independent inverse scattering imaging algorithm pioneered by Liu et al. (2007).

1 Introduction

The inverse scattering series, a multidimensional direct inversion method, has been used to derive candidate direct nonlinear imaging algorithms that do not require the actual propagation velocity. Weglein et al. (2001) isolated an imaging sub-series out from the whole inverse scattering seires. Shaw et al. (2004) and Shaw and Weglein (2004) successfully isolated the leading order imaging subseries (LOIS) in the laterally invariant acoustic medium and presented its closed form, which makes the series truncation unnecessary. Liu et al. (2005) and Liu et al. (2007) extended it with the higher order imaging subseries (HOIS) in the laterally variant 2D and 3D acoustic medium. All of the algorithms above are functions of α_1, which derives directly from the collected data. So calculating α_1 from the data D is a prerequisite step for the use of the algorithms.

Currently, data collection is often adequate in the in-line direction but has a serious aperture limitation in the cross-line direction, because of economic and/or practical considerations. So the wave theoretic algorithm stated in Liu et al. (2007), which requires full data collection in both directions, does not suit this case well. In Stolt and Benson (1986) Chapter 3, they developed a method to do 2.5D finite-aperture migration. We will extend their method to 3D.

In this note, first, we use the inverse scattering theory to review the derivation of α_1 in a 3D constant-density acoustic medium. Then an algorithm that can fully use the data to calculate α_1, which is a wave theory imaging in the direction that has adequate collecion and asymptotic migration in the cross-line limited aperture direction, is provided. This prepares data with sparse cross-line sampling and aperture for input to the velocity independent inverse scattering imaging algorithm provided in Liu et al. (2007).

2 α_1 in a 3D constant-density acoustic medium

For a 3D constant-density acoustic medium, the wave equations for the actual and reference wavefield are expressed by:

$$(\frac{\partial^2}{\partial x^2}+\frac{\partial^2}{\partial y^2}+\frac{\partial^2}{\partial z^2}+\frac{\omega^2}{c^2(x,y,z)})G(x_g,y_g,z_g,x_s,y_s,z_s,\omega)=\delta(x-x_s)\delta(y-y_s)\delta(z-z_s), \quad (1)$$

$$(\frac{\partial^2}{\partial x^2}+\frac{\partial^2}{\partial y^2}+\frac{\partial^2}{\partial z^2}+\frac{\omega^2}{c_0^2(x,y,z)})G_0(x_g,y_g,z_g,x_s,y_s,z_s,\omega)=\delta(x-x_s)\delta(y-y_s)\delta(z-z_s). \quad (2)$$

The scattered wavefield is defined by the difference between the total wavefield and the direct arrival wavefield:

$$D(x_g,y_g,z_g,x_s,y_s,z_s,\omega)=G(x_g,y_g,z_g,x_s,y_s,z_s,\omega)-G_0(x_g,y_g,z_g,x_s,y_s,z_s,\omega). \quad (3)$$

If the reference medium is chosen to be an acoustic wholespace with constant velocity c_0, then the scattering potential is:

$$V(x,y,z)=\frac{\omega^2}{c_0^2}-\frac{\omega^2}{c^2(x,y,z)}=\frac{\omega^2}{c_0^2}\alpha(x,y,z), \quad (4)$$

where

$$\alpha(x,y,z)=1-\frac{c_0^2}{c^2(x,y,z)}. \quad (5)$$

As shown by Weglein et al. (2003), the scattering potential can be expressed in orders of the scattered wavefield. At first order, the relationship is:

$$\begin{aligned}D(x_g,y_g,z_g,x_s,y_s,z_s,\omega)=&\int_{-\infty}^{\infty}dx_1\int_{-\infty}^{\infty}dy_1\int_{-\infty}^{\infty}dz_1G_0(x_g,y_g,z_g,x_1,y_1,z_1,\omega)\\&V_1(x_1,y_1,z_1)G_0(x_1,y_1,z_1,x_s,y_s,z_s,\omega),\end{aligned} \quad (6)$$

where V_1 is the linear approximation of V, i.e. the first order in measurements of the scattered wavefield,

$$V_1(x,y,z)=\frac{\omega^2}{c_0^2}\alpha_1(x,y,z), \quad (7)$$

and $\alpha_1(x,y,z)$ is the first order of $\alpha(x,y,z)$ in terms of the data D. Fourier transforming on $x_g,\ y_g,\ x_s$ and y_s:

$$\frac{1}{(2\pi)^4}\int_{-\infty}^{\infty}dx_g\int_{-\infty}^{\infty}dy_g\int_{-\infty}^{\infty}dx_s\int_{-\infty}^{\infty}dy_s\,e^{ik_{sx}x_s+ik_{sy}y_s-ik_{gx}x_g-ik_{gy}y_g},$$

we get:

$$\begin{aligned}&D(k_{gx},k_{gy},k_{sx},k_{sy},\omega)\\&=\int_{-\infty}^{\infty}dx_1\int_{-\infty}^{\infty}dy_1\int_{-\infty}^{\infty}dz_1G(k_{gx},k_{gy},z_g,x_1,y_1,z_1,\omega)\frac{\omega^2}{c_0^2}\alpha_1(x_1,y_1,z_1)G(x_1,y_1,z_1,k_{sx},k_{sy},z_s,\omega)\end{aligned}$$

$$= \int_{-\infty}^{\infty} dx_1 \int_{-\infty}^{\infty} dy_1 \int_{-\infty}^{\infty} dz_1 \frac{1}{(2\pi)^2} \frac{e^{-i(k_{gy}y_1 + k_{gx}x_1)} e^{ik_{gz}|z_g - z_1|}}{2ik_{gz}} \frac{\omega^2}{c_0^2} \alpha_1(x_1, y_1, z_1) \frac{1}{(2\pi)^2} \frac{e^{i(k_{sy}y_1 + k_{sx}x_1)} e^{ik_{sz}|z_1 - z_s|}}{2ik_{sz}}$$

$$= -\frac{1}{2\pi} \frac{\omega^2}{4k_{gz}k_{sz}c_0^2} \alpha_1(k_{gx} - k_{sx}, k_{gy} - k_{sy}, k_{gz} + k_{sz}). \quad (8)$$

Here we have chosen $z_g = z_s = 0$. Or equivalently,

$$\alpha_1(k_{mx}, k_{my}, q_z) = -2\pi \frac{4k_{gz}k_{sz}c_0^2}{\omega^2} D(k_{gx}, k_{gy}, k_{sx}, k_{sy}, \omega). \quad (9)$$

The quantities k_{mx}, k_{my}, q_z used here, and k_{hx}, k_{hy}, to be used later, are defined as follows:

$$k_{mx} = k_{gx} - k_{sx}, \qquad k_{hx} = k_{gx} + k_{sx},$$

$$k_{my} = k_{gy} - k_{sy}, \qquad k_{hy} = k_{gy} + k_{sy}, \qquad q_z = k_{gz} + k_{sz}.$$

Equation (9) is an exact, simple relationship between α_1 and the data. If we have enough data, we can inverse Fourier transform it back to the space domain, which is done in Liu et al. (2007). In this note, we assume that data is adequately sampled in the in-line direction but has a serious aperture limitation in the cross-line direction. So we can not do the inverse Fourier transform in the cross-line direction. Next we will provide a possible route around this problem, involving an asymtotic approximation developed in Stolt and Benson (1986) Chapter 3.

3 Stationary phase approximation in cross-line direction

In equation (9), there are three variables on the left hand side of the equation but there are five variables on the right hand side, which means that there are two extra degrees of freedom (in the 2D case there is one). We will use the extra degree of freedom in the cross-line domain to compensate for the change of the integration range in this direction from infinite to a finite aperture. Also, Liu et al. (2006) has demonstrated that, although the extra degree of freedom will influence the imaging result of α_n ($n = 1, 2, ..$), it affects the closed form little when we use the HOIS. This is consistent with the fact that α represents the real medium and doesn't depend on what method we use, as long as our result is exact. So for simplicity, we can eliminate the other extra degree of freedom by fixing one variable.

Suppose the y direction is the cross-line direction. We can eliminate the extra degree of freedom in the x direction by fixing

$$k_{hx} = 0 \Rightarrow k_{gx} = -k_{sx} = 0.5k_{mx}.$$

Then

$$D(0.5k_{mx}, k_{gy}, -0.5k_{mx}, k_{sy}, \omega) = -\frac{1}{2\pi} \frac{\omega^2}{4k_{gz}k_{sz}c_0^2} \alpha_1(k_{mx}, k_{my}, q_z). \quad (10)$$

In the following, we will follow the finite-aperture migration method stated in Stolt and Benson (1986) Chapter 3 in $y - z$ domain. Because we are considering the 3D case and k_{mx} is on both sides of equation (10), some small changes to the formulas are made.

In general, the inversion will be such that α_1 is estimated as a linear combination of the data D:

$$\alpha_1(k_{mx}, k_{my}, q_z) = \int_{-\infty}^{+\infty} dk_{hy} L(k_{mx}, k_{my}, k_{hy}, q_z) D(0.5k_{mx}, k_{gy}, -0.5k_{mx}, k_{sy}, \omega). \tag{11}$$

Using equations (10) and (11) together, we can see that L must be an arbitrary normalized function that satisfies:

$$1 = -\int_{-\infty}^{+\infty} dk_{hy} L(k_{mx}, k_{my}, k_{hy}, q_z) \frac{1}{2\pi} \frac{\omega^2/c_0^2}{4k_{gz}k_{sz}}. \tag{12}$$

One can choose many different forms for L, and this flexibility makes the compensation for the limited cross-line aperture possible. Fourier transforming from the k_{my}, q_z domain to the y, z domain:

$$\begin{aligned}\alpha_1(k_{mx}, y, z) = &\int_{-\infty}^{+\infty} dk_{my} \int_{-\infty}^{+\infty} dq_z \int_{-\infty}^{+\infty} dk_{hy} e^{i(k_{my}y - q_z z)} L(k_{mx}, k_{my}, k_{hy}, q_z) \\ &\frac{1}{(2\pi)^2} \int_{-\infty}^{+\infty} dy_g \int_{-\infty}^{+\infty} dy_s e^{i(k_{sy}y_s - k_{gy}y_g)} D(0.5k_{mx}, y_g, -0.5k_{mx}, y_s, \omega).\end{aligned} \tag{13}$$

Changing the integration variables from (k_{my}, k_{hy}, q_z) to (k_{gy}, k_{sy}, ω), and the order of integration,

$$dk_{my}dk_{hy}dq_z = dk_{gy}dk_{sy}dw \; 2wq_z/(c^2 k_{gz}k_{sz}), \tag{14}$$

$$\alpha_1(k_{mx}, y, z) = \int_{-\infty}^{+\infty} dy_g \int_{-\infty}^{+\infty} dy_s \int_{-\infty}^{+\infty} dw \, I(k_{mx}, y, z | y_g, y_s, \omega) D(0.5k_{mx}, y_g, -0.5k_{mx}, y_s, \omega), \tag{15}$$

where

$$I = \frac{1}{2\pi^2} \int_{-\infty}^{+\infty} dk_{gy} e^{ih_g} \int_{-\infty}^{+\infty} dk_{sy} e^{ih_s} \frac{\omega q_z}{c^2 k_{gz} k_{sz}} L(k_{mx}, k_{my}, k_{hy}, q_z). \tag{16}$$

The phase factors h_g and h_s are defined as follows:

$$h_g = -[k_{gy}(y_g - y) + k_{gz}z], \; h_s = -[k_{sy}(y - y_s) + k_{sz}z].$$

By assuming that the weighting function L is slowly varying compared to the phase factors, we can approximate the integration by using the method of stationary phase. At the stationary points of the two integrals, $k_{gy} = \hat{k}_{gy}$ and $k_{sy} = \hat{k}_{sy}$,

$$\frac{dh_g}{dk_g}|_{k_g = \hat{k}_g} = 0 \quad and \quad \frac{dh_s}{dk_s}|_{k_s = \hat{k}_s} = 0.$$

So the stationary points are:

$$\hat{k}_{gy} = \frac{k'(y_g - y)}{r_g}, \qquad \hat{k}_{sy} = \frac{k'(y - y_s)}{r_s}, \tag{17}$$

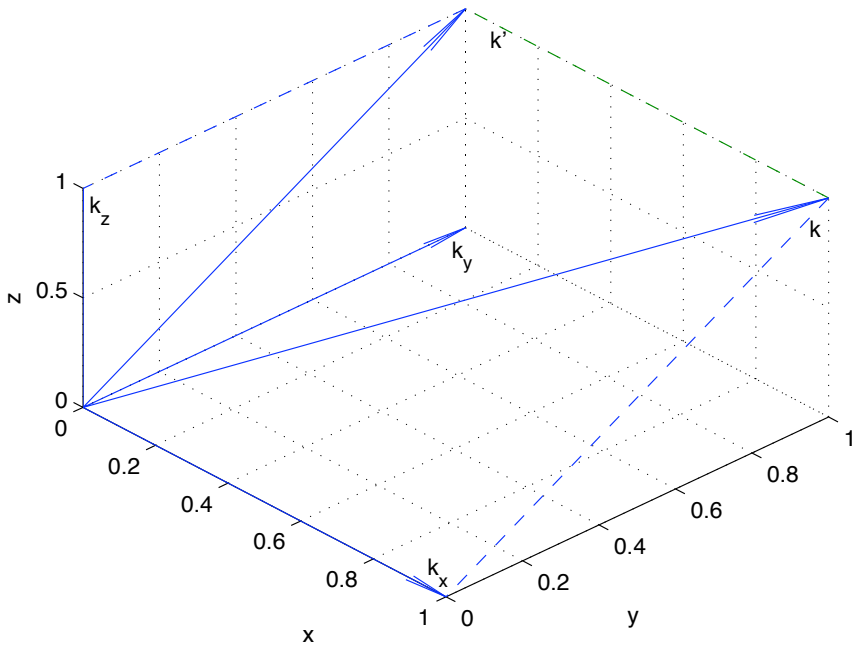

Figure 1: *Relationship between* $k = \frac{\omega}{c}$ *and* k'

where

$$r_g = \sqrt{z^2 + (y_g - y)^2}, \qquad r_s = \sqrt{z^2 + (y - y_s)^2}, \qquad k' = \sqrt{(\frac{\omega}{c})^2 - (0.5k_{mx})^2}.$$

They are the projections of distances and frequency onto the y-z plane (as shown in Figure 1), while in Stolt and Benson (1986) they are the total distances and frequency. This is because here we leave the x domain unchanged and consider the problem in the y-z plane. So the total distances and frequency here should be the projection of distances and frequency onto the y-z plane. For depth wavenumbers k_{gz} and k_{sz}

$$\hat{k}_{gz} = \frac{k'z}{r_g}, \qquad \hat{k}_{sz} = \frac{k'z}{r_s}, \qquad \hat{q}_z = \frac{k'z}{r_g} + \frac{k'z}{r_s} = k'\frac{zr}{r_g r_s}, \tag{18}$$

where $r = r_g + r_s$. It is interesting to note that:

$$\tan\theta_g = \frac{\hat{k}_{gy}}{\hat{k}_{gz}} = \frac{y_g - y}{z}, \qquad and \qquad \tan\theta_s = \frac{\hat{k}_{sy}}{\hat{k}_{sz}} = \frac{y - y_s}{z},$$

which means that, in the $y - z$ plane, the directions of wave vectors are the same as the connecting lines between the start points and the end points. So the wave propagation in the $y - z$ plane can be explained by using ray theory. In the $r_g - x$ plane or the $r_s - x$ plane, the wave vectors k_x and

k', which are the Fourier conjugates of x and r_g or r_s, are continuous. The propagations act as a 2D propagating wave, and can be explained by using wavefield theory. These wave propagations are illustrated in Figure 2. Because the amplitudes of $\hat{k}_{gy}$, $\hat{k}_{sy}$, $\hat{k}_{gz}$, and $\hat{k}_{sz}$ depend on the value of k_{mx}, they are coupled together.

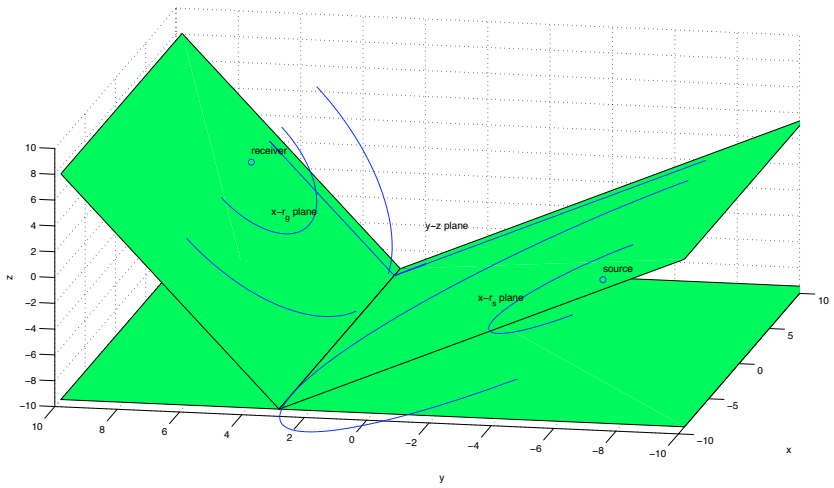

Figure 2: *Illustration of the wave propagation.*

Continuing with the approximation:

$$\hat{h}_g = -k' r_g, \qquad \hat{h}_s = -k' r_s. \tag{19}$$

The second derivatives at the stationary point are:

$$\hat{h}_g'' = \frac{r_g^3}{z^2 k'}, \qquad \hat{h}_s'' = \frac{r_s^3}{z^2 k'}. \tag{20}$$

Midpoint and offset frequencies become:

$$\hat{k}_{my} = k'\left(\frac{y_g - y}{r_g} - \frac{y - y_s}{r_s}\right), \qquad \hat{k}_{hy} = k'\left(\frac{y_g - y}{r_g} + \frac{y - y_s}{r_s}\right). \tag{21}$$

Making the stationary point approximation:

$$\begin{aligned} I =& \frac{1}{2\pi^2} \frac{2i\pi}{\sqrt{\hat{h}_g'' \hat{h}_s''}} e^{i(\hat{h}_g + \hat{h}_s)} \frac{\omega \hat{k}_z}{c^2 \hat{k}_{gz} \hat{k}_{sz}} L(k_{mx}, \hat{k}_{my}, \hat{k}_{hy}, \hat{q}_z) \\ =& \frac{iw}{\pi c^2} e^{-ik'(r_g + r_s)} \frac{zr}{(r_g r_s)^{\frac{3}{2}}} L(k_{mx}, \hat{k}_{my}, \hat{k}_{hy}, \hat{q}_z), \end{aligned} \tag{22}$$

where the frequencies k', $\hat{k}_{my}$, and $\hat{k}_{hy}$ are all functions of ω, k_{mx} and other space variables. In order to separate the frequency variables ω and k_{mx} from the space variables, we can restrict L to be of the form:

$$L(k_{mx}, \hat{k}_{my}, \hat{k}_{hy}, \hat{q}_z) = S(\beta, \gamma) F(k_{mx}, \omega), \tag{23}$$

where

$$\beta = \hat{k}_{my}/\hat{q}_z \quad and \quad \gamma = \hat{k}_{hy}/\hat{q}_z. \tag{24}$$

So equation (15) becomes:

$$\begin{aligned}\alpha_1(k_{mx}, y, z) &= \int_{-\infty}^{+\infty} dy_g \int_{-\infty}^{+\infty} dy_s \int_{-\infty}^{+\infty} dw\, I(k_{mx}, y, z|y_g, y_s, \omega) D(0.5k_{mx}, y_g, -0.5k_{mx}, y_s, \omega) \\ &= \frac{2z}{c} \int_{-\infty}^{+\infty} dy_g \int_{-\infty}^{+\infty} dy_s \frac{r}{(r_g r_s)^{\frac{3}{2}}} S(\beta, \gamma) P_F, \end{aligned} \tag{25}$$

where P_F is a frequency-filtered version of the data:

$$P_F = \frac{1}{2\pi} \int_{-\infty}^{+\infty} dw e^{-ik'(r_g + r_s)} \frac{iw}{c} F(k_{mx}, \omega) D(0.5k_{mx}, y_g, -0.5k_{mx}, y_s, \omega). \tag{26}$$

As stated above, we don't have sufficient data. We must control the offset in the cross-line direction. This control can be achieved by adding a "boxcar" function to S:

$$S(\beta, \gamma) = B(h_1, h_2; y_h) T(\beta, \gamma). \tag{27}$$

Here $B(h_1, h_2; y_h)$ is the Boxcar function:

$$B(h_1, h_2; y_h) = \begin{cases} 1 & if\ y_g - y_s = y_h \in (h_1, h_2) \\ \\ 0 & otherwise. \end{cases} \tag{28}$$

Applying all of these limitations to the restriction function (12),

$$1 = -\int_{-\infty}^{+\infty} dk_{hy} F(k_{mx}, \omega) B(h1, h2; y_h) T(\beta, \gamma) \frac{1}{2\pi} \frac{\omega^2/c_0^2}{q_z^2(1 - \frac{\hat{k}_{my}^2 \hat{k}_{hy}^2}{q_z^4})}. \tag{29}$$

About q_z, it satisfies:

$$q_z = \frac{2k'}{\sqrt{(1+\beta^2)(1+\gamma^2)}}. \tag{30}$$

So the restriction is:

$$-2\pi = \frac{\omega^2}{c_0^2} \frac{F(k_{mx}, \omega)}{2k'} \int_{\gamma_1}^{\gamma_2} d\gamma T(\beta, \gamma) \frac{\sqrt{(1+\beta^2)(1+\gamma^2)}}{1 - \beta^2\gamma^2}. \tag{31}$$

For simplicity, we choose (as Wang (1990))

$$F(k_{mx}, \omega) = -\frac{4\pi k'}{\omega^2/c_0^2}. \tag{32}$$

$$T(\beta, \gamma) = \frac{1 - \beta^2\gamma^2}{(1+\beta^2)(1+\gamma^2)} \frac{1}{\gamma_2 - \gamma_1}. \tag{33}$$

So

$$\begin{aligned}\alpha_1(k_{mx},y,z) &= \frac{2z}{c}\int_{-\infty}^{+\infty}dy_g\int_{-\infty}^{+\infty}dy_s\frac{r}{(r_g r_s)^{\frac{3}{2}}}S(\beta,\gamma)P_F \\ &= \frac{2z}{c}\int_{-\infty}^{+\infty}dy_s\int_{y_s+h_1}^{y_s+h_2}dy_g\frac{r}{(r_g r_s)^{\frac{3}{2}}}\frac{1-\beta^2\gamma^2}{(1+\beta^2)(1+\gamma^2)}\frac{1}{\gamma_2-\gamma_1}P_F.\end{aligned} \tag{34}$$

Transforming k_{mx} back to space domain, we obtain the inversion result for the first term α_1:

$$\alpha_1(x,y,z) = \frac{2z}{c}\int_{-\infty}^{+\infty}e^{ik_{mx}x}dk_{mx}\int_{-\infty}^{+\infty}dy_s\int_{y_s+h_1}^{y_s+h_2}dy_g\frac{r}{(r_g r_s)^{\frac{3}{2}}}\frac{1-\beta^2\gamma^2}{(1+\beta^2)(1+\gamma^2)}\frac{1}{\gamma_2-\gamma_1}P_F, \tag{35}$$

where

$$\begin{aligned}P_F &= \frac{1}{2\pi}\int_{-\infty}^{+\infty}dw\ e^{-ik'(r_g+r_s)}\frac{iw}{c_0}F(k_{mx},\omega)D(0.5k_{mx},y_g,-0.5k_{mx},y_s,\omega) \\ &= -\frac{1}{2\pi}\int_{-\infty}^{+\infty}dw\ e^{-ik'(r_g+r_s)}\frac{4\pi ik'}{\omega/c_0}D(0.5k_{mx},y_g,-0.5k_{mx},y_s,\omega).\end{aligned} \tag{36}$$

We can see that Equation (35) represents a wave propagation the in in-line direction and a finite-aperture integration in the cross-line direction. All of the collected data is used.

Substituting the result into the leading order or higher order closed form in Liu et al. (2007):

$$\alpha^{LOIS}(\vec{x},z) = \alpha_1\left(\vec{x},z-\frac{1}{2}\int_{-\infty}^{z}\alpha_1(\vec{x},u)du\right), \tag{37}$$

$$\alpha^{HOIS}\left(\vec{x},z+\frac{1}{2}\int_{-\infty}^{z}du\frac{\alpha_1(\vec{x},u)}{\cos^2\theta_x+\cos^2\theta_x-\frac{1}{4}\alpha_1(\vec{x},u)}\right) = \alpha_1(\vec{x},z), \tag{38}$$

we can get the imaging result. Note that, in equation (38), $\theta_x = 0$, because we have made the assumption that $k_{hx} = 0$.

4 Summary

In this paper, according to the assumption that the data is adequately sampled in in-line direction but has a serious aperture limitation in cross-line direction, which is often the case, we used an finite-aperture algorithm which utilizes wave theoretic method in in-line direction and asymptotic method in cross-line limited aperture direction to calculate α_1. This algorithm is compromised

because we don't collect data over all of the measurement surface. The algorithm does imaging using all of the collected data. Then the velocity independent inverse scattering imaging algorithm in Liu et al. (2007) can be carried out.

The work is not yet complete. We will continue to extend the result without fixing $k_{hx} = 0$, in order to use it in other more complicated models than the constant-density acoustic medium. Another aspect we are going to focus on is using numercial tests to evaluate the quality of this approximation and improve it.

5 Acknowledgements

All M-OSRP sponsors are gratefully acknowledged for their support in the research. This work has been partially funded by NSF-CMG (award DMS-0327778) and U.S. DOE-BES (Grant No. DOE-De-FG02-05ER15697)

References

Liu, F., A. B. Weglein, and K. A. Innanen. "Inverse scattering series with lateral variations in 3D." *Mission-Oriented Seismic Research Program (M-OSRP) Annual Report*. 2007.

Liu, F., A. B. Weglein, K. A. Innanen, B. G. Nita, and J. Zhang. "Direct horizontal common imaging gathers without the velocity of "ironing"." *Mission-Oriented Seismic Research Program (M-OSRP) Annual Report*. 2006.

Liu, F., A. B. Weglein, B. G. Nita, and K. A. Innanen. "Investigating the Grouping of Inverse Scattering Series Terms: Simultaneous Imaging and Inversion I(Theory)." *Mission-Oriented Seismic Research Program (M-OSRP) Annual Report*. 2005.

Shaw, S. A. and A. B. Weglein. "A leading order imaging series for prestack data acquired over a laterally invariant acoustic medium. Part I: Derivation and preliminary analysis." *M-OSRP Annual Report* 3 (2004).

Shaw, S. A., A. B. Weglein, D. J. Foster, K. H. Matson, and R. G. Keys. "Isolation of a leading order depth imaging series and analysis of its convergence properties." *Journal of Seismic Exploration* 2 (November 2004): 157–195.

Stolt, Robert H. and Alvin K. Benson. *Seismic Migration: Theory and Practice*. Ed. Klaus Helbig and Sven Treitel. Volume 5 of Seismic Exploration. Geophysical Press, 1986.

Wang, D. *Recovery of Zero-offset Reflectivity from Constant Velocity Aperture-Compensated Migration/Inversion Method*. PhD thesis, University of Wyoming, 1990.

Weglein, A. B., F. V. Araújo, P. M. Carvalho, R. H. Stolt, K. H. Matson, R. T. Coates, D. Corrigan, D. J. Foster, S. A. Shaw, and H. Zhang. "Inverse Scattering Series and Seismic Exploration." *Inverse Problems* (2003): R27–R83.

Weglein, A. B., D. J. Foster, K. H. Matson, S. A. Shaw, P. M. Carvalho, and D. Corrigan. "An inverse-scattering sub-series for predicting the spatial location of reflectors without the precise reference medium and wave velocity." *71st Annual Internat. Mtg., Soc. Expl. Geophys., Expanded Abstracts*. . Soc. Expl. Geophys., 2001. 2108–2111.

What are α_1 and α_2?

J. D. Mayhan, D. W. Fisher, X. Li, J. E. Lira, and Z. Wang

Abstract

The first author, a first year graduate student in M-OSRP, describes the research he plans to begin this summer. The research is aimed at improving our understanding of the roles of α_1 and α_2 in the Inverse Scattering Series. α_1 and α_2 are the linear and quadratic terms, respectively, in the expansion of α, the perturbation in the index of refraction, in orders of the measured data.

Background

Where does the first author fit into the "big picture"?

Interpreting a seismic experiment can be done using the Inverse Scattering Series (ISS), which is broken down into task-specific subseries, one of which is the imaging subseries ("migration"). Ongoing research in M-OSRP on the imaging subseries is being conducted by F. Liu, S. Jiang, Z. Wang, and J. D. Mayhan[1]. S. A. Shaw (2005) imaged 1D variable velocity acoustic media, F. Liu (2006) extended imaging to 2D variable velocity acoustic media, and Z. Wang and the first author plan to extend imaging to 3D variable velocity acoustic media. To begin his work, the first author will critically examine the roles of α_1 and α_2 in F. Liu's imaging results.

What is the ISS?

Recall that the starting point for the ISS is the Lippmann-Schwinger equation (an operator identity) (Weglein et al., 2003):

$$G = G_0 + G_0 V G, \tag{1}$$

where G is the Green's function (impulse response) in the medium of interest, G_0 is the Green's function in the reference medium, and $V = L - L_0$ is the perturbation operator, the difference between the differential operators governing wavefield propagation through the medium of interest (L) and the reference medium (L_0). The Lippmann-Schwinger equation is solved via (i) iteration:

$$G - G_0 = G_0 V G_0 + G_0 V G_0 V G_0 + \ldots, \tag{2}$$

(ii) expanding V in orders of the measured data:

$$V = V_1 + V_2 + V_3 + \ldots, \tag{3}$$

[1]Liu, Wang, and Mayhan are pronounced Lou, Wong, and May-hand, respectively.

(iii) substituting equation (3) into equation (2), and (iv) collecting equal orders in the data. The result is a set of equations which can be sequentially solved for V_n (n = 1, 2, 3,...) using only measured data D and the reference medium G_0^+ where the "+" indicates use of a causal Green's function:

$$\begin{aligned}
(G_0^+ V_1 G_0^+)_m &= D, && (4)\\
(G_0^+ V_2 G_0^+)_m &= -(G_0^+ V_1 G_0^+ V_1 G_0^+)_m, && (5)\\
(G_0^+ V_3 G_0^+)_m &= -(G_0^+ V_1 G_0^+ V_2 G_0^+)_m - (G_0^+ V_2 G_0^+ V_1 G_0^+)_m - (G_0^+ V_1 G_0^+ V_1 G_0^+ V_1 G_0^+)_m, && (6)
\end{aligned}$$

and so forth. In equation (4) D $(= G - G_0)$ is the recorded wavefield at the measurement surface m.

Collecting equal orders in the data is justified because orders/powers of the measured data are linearly independent. Hence the expansion can equal zero only if each order equals zero. For example, if $a_0 + a_1 x + a_2 x^2 = 0$ for all x, then $a_0 = a_1 = a_2 = 0$.

In variable velocity acoustic media, the perturbation $V = (\omega^2/c_0^2)\alpha^2$ is characterized by the perturbation α in the index of refraction:

$$\frac{1}{c^2(\vec{r})} = \frac{1}{c_0^2}(1 - \alpha(\vec{r})), \tag{7}$$

where $c(\vec{r})$ = the wave velocity in the medium of interest, c_0 = the wave velocity in the reference medium, and α (like V) is expanded in orders of the measured data:

$$\alpha = \alpha_1 + \alpha_2 + \alpha_3 + \ldots, \tag{8}$$

i.e., α_n is nth order in the data required to solve for α. For example, in his thesis F. Liu derived α_2 and α_3 for a 2D variable velocity acoustic medium.

Future Plan

The first author's initial research will build on F. Liu's thesis (Liu, 2006) and has the following goals:

Better understand α_1.

Recall that α is the perturbation in the index of refraction, and α_1 is the linear term in the expansion of α in orders of the measured data.

In traditional imaging methods, the source of challenge is the complexity inherent in determining the actual velocity. In contrast, the ISS neither requires nor explicitly determines actual velocity. The ISS begins the process of imaging by generating reference velocity images with fidelity (i.e., the ISS "expects the wrong thing to be done right"). The ISS then interrogates the resulting images in a non-linear fashion using derivatives and integrals of α_1. "Non-linear" means the data

comprising each image is multiplied by itself up to several orders, and pairs, triples, etc. of data are compared. As a result of this non-linear data interrogation, the images are migrated from their reference velocity positions closer to their actual positions.

Higher order terms in the ISS are expressed using derivatives and integrals of α_1, therefore it is important that we better understand α_1, e.g., its properties, what it does, what each of its various derivatives do, what $\partial\alpha_1/\partial z$ can handle, when $\partial\alpha_1/\partial x$ kicks in, etc.

The first author will define imaging challenges and their corresponding responses by studying the simplest incarnation of each issue. Given a medium configuration, when an ISS term "lights up" signals its purpose. For example, F. Liu imaged several synthetic models in his thesis, including a complex salt model provided by ExxonMobil (Fig. 1 in the Appendix). The first author plans to track the numeric values of α_1 and $\partial\alpha_1/\partial z$ as they cross reflectors. This technique may enable understanding of precisely what happens when the integral relating α_1 and data (equation (13) in the Appendix) crosses a reflector. What happens when the integral crosses a boundary helps define what higher order terms are looking at. For example, F. Liu has shown the first author how to move the cursor over the "soft copy" versions of the above images and simultaneously view the numeric values of α_1 and $\partial\alpha_1/\partial z$ underlying the images. It is hoped that such detailed study of the images will shed some light on the detailed behavior of α_1 and $\partial\alpha_1/\partial z$ as functions of medium geometry/physical properties.

Suppose we have an inclined boundary separating two homogeneous media. If we evaluate $\int dz \frac{\partial\alpha_1(x,z)}{\partial x}$ along a vertical line that crosses the inclined boundary, the integral may be non-zero only at the intersection because $\alpha_1(x,z)$ would have non-zero lateral variation only when it crosses the inclined boundary. The first author will try to use these kinds of analysis to develop templates which indicate which physical configurations in the medium cause which terms in the ISS to "light up".

Better understand $\alpha_{2,3}$.

Recall that α_2 is the quadratic term in the expansion of α in orders of the measured data. F. Liu's derivation of α_2 for a 2D variable v acoustic medium resulted in three components: $\alpha_{2,1}$, $\alpha_{2,2}$, and $\alpha_{2,3}$. The first subscript indicates order in the data required to solve for α (in this case 2), and the second subscript indicates how fast the term grows with k_z, the Fourier conjugate of depth z. The expression for $\alpha_{2,1}$ contains two terms:

$$\alpha_{2,1}(x,z) = -\frac{1}{2}\,\alpha_1^2(x,z) - \frac{1}{2}\,\frac{\partial\alpha_1(x,z)}{\partial z}\int_{-\infty}^{z} du\,\alpha_1(x,u). \tag{9}$$

α_1^2 acts to correct the amplitude of α_1 towards α, and the product of $\partial\alpha_1/\partial z$ and $\int du\,\alpha_1$ acts to shift the mislocated reflector in α_1 towards its correct location (where the shift takes place in depth z). The expression for $\alpha_{2,2}$ contains one term:

$$\alpha_{2,2}(x,z) = \frac{1}{2}\,\frac{\partial\alpha_1(x,z)}{\partial x}\int_{-\infty}^{z} du \int_{-\infty}^{u} dv\,\frac{\partial\alpha_1(x,v)}{\partial x}. \tag{10}$$

The product of $\partial\alpha_1/\partial x$ and $\int du \int dv\, \partial\alpha_1/\partial x$ acts to shift the mislocated reflector in α_1 towards its correct location (where the shift is lateral in x). The expression for $\alpha_{2,3}$ is much more complex than $\alpha_{2,1}$ and $\alpha_{2,2}$, even though it contains only one term:

$$\begin{aligned}\widetilde{\alpha}_{2,3}(k_m,z) =& \frac{1}{8\pi^2}\int_{-\infty}^{\infty} dk_1 \int_{-\infty}^{\infty} dz_1\, \widetilde{\alpha}_1(0.5k_m - k_1, z_1) \int_{-\infty}^{z_1} dz_2\, \widetilde{\alpha}_1(0.5k_m + k_1, z_2) \\ & \widetilde{\xi}_2(k_m, k_1, 0.5(z_1+z_2) - z, 0.5(z_1 - z_2)),\end{aligned} \tag{11}$$

where

$$\begin{aligned}\widetilde{\xi}_2(k_m,k_1,\epsilon_0,\epsilon_1) &= \int_{-\infty}^{\infty} dk_z \exp\left(i(\epsilon_1+\epsilon_0)k_z\right)\left(\frac{i}{u_1}(k_z^2+k_m^2)\exp\left(i\Delta\Psi\right) - ik_z + \frac{1}{2}\epsilon_1 a_1\right), \\ a_1 &= k_m^2 - 4k_1^2, \\ u_1 &= sgn(k_z)\sqrt{k_z^2 + a_1}, \\ \Delta\Psi &= \epsilon_1(u_1 - k_z).\end{aligned} \tag{12}$$

k_1 is the Fourier conjugate of x_1, where x_1 is the lateral coordinate of the first V_1 in equation (5), and k_z is the Fourier conjugate of depth z. z_1 is the depth coordinate of the first V_1 in equation (5), z_2 is the depth coordinate of the second V_1 in equation (5), and a tilde over a variable indicates a Fourier transformed variable. As a first step in interpreting $\alpha_{2,3}$, the first author has derived what may be a simpler form of $\alpha_{2,3}$ that combines its forms in the space-time and double Fourier domains.

Recalling that the goal is to interpret $\alpha_{2,1}$, $\alpha_{2,2}$, and $\alpha_{2,3}$ (i.e., what physics are they expressing?), can one tell from looking at α_1 and its different derivatives what $\alpha_{2,1}$, $\alpha_{2,2}$, and $\alpha_{2,3}$ are doing? What specifically is being addressed in a 2D earth by $\alpha_{2,2}$ and $\alpha_{2,3}$ that's not being captured by $\alpha_{2,1}$? In addition, tieing $\alpha_{2,3}$ back to scattering diagrams (which encode the physics) may shed some light on its physical interpretation.

F. Liu's image of the ExxonMobil model using α_1 (Fig. 2 in the Appendix) shows diffraction below the ends of the salt (the false shadows). Diffraction exists in 2D and 3D, not in 1D, and $\alpha_{2,2}$ and $\alpha_{2,3}$ have no 1D analogue. Is this a clue that $\alpha_{2,2}$ and $\alpha_{2,3}$ touch diffraction? Imaging a flat reflector can be done with α_1, but imaging a rugose surface probably requires $\alpha_{2,2}$ and $\alpha_{2,3}$ (terms with no 1D analogue) because incident and reflected rays may traverse both media (above and below the surface) due to the surface's roughness.

Wrap Up

When the first author worked for a major oil, gas, and petrochemical company, one executive began meetings with the question, "why are we wasting our time and the shareholders' money by having this meeting?" It is hoped that this note has convinced M-OSRP's sponsors that the first author's research will waste neither the sponsors' time nor their shareholders' money.

References

Liu, Fang. *Multi-Dimensional Depth Imaing without an Adequate Velocity model.* PhD thesis, University of Houston, 2006.

Weglein, A. B., F. V. Araújo, P. M. Carvalho, R. H. Stolt, K. H. Matson, R. T. Coates, D. Corrigan, D. J. Foster, S. A. Shaw, and H. Zhang. "Inverse Scattering Series and Seismic Exploration." *Inverse Problems* (2003): R27–R83.

Appendix: Referenced equations and figures from F. Liu's thesis

F. Liu's integral relating α_1 and measured data is:

$$\begin{aligned} \widetilde{\widetilde{\alpha}}_1(k_m, k_z) &= \frac{-4q_g q_s}{(\omega^2/c_0^2)} \int_{-\infty}^{\infty} dx_m \exp(-ik_m x_m) \int_{-\infty}^{\infty} d\tau \exp(i\omega\tau) D^{\tau p}(x_m, \tau) \\ D^{\tau p}(x_m, \tau) &= \int_{-\infty}^{\infty} dx_h D(x_m + 0.5\, x_h, x_m - 0.5\, x_h, \tau + x_h \sin\theta/c_0) \end{aligned} \tag{13}$$

where c_0 = the wave velocity in the reference medium,
$D^{\tau p}(x_m, \tau)$ = the linear Radon transform of all traces within a common mid-point gather,
k_g = the Fourier conjugate of the x-coordinate of the receiver,
$k_m = k_g - k_s$ = the Fourier conjugate of the x-coordinate of the mid-point,
k_s = the Fourier conjugate of the x-coordinate of the source,
k_z = the Fourier conjugate of depth z,
ω = the Fourier conjugate of time t,
$p = \sin\theta/c_0$ = the horizontal slowness,
$q_g = sgn(\omega)\sqrt{(\omega/c_0)^2 - k_g^2}$,
$q_s = sgn(\omega)\sqrt{(\omega/c_0)^2 - k_s^2}$,
$\tau = t - x_h \sin\theta/c_0$ = a time-like integration variable,
θ = angle of incidence of the plane wave,
$x_h = x_g - x_s$ = x-coordinate of the offset,
and $x_m = 0.5(x_g + x_s)$ = x-coordinate of the mid-point.

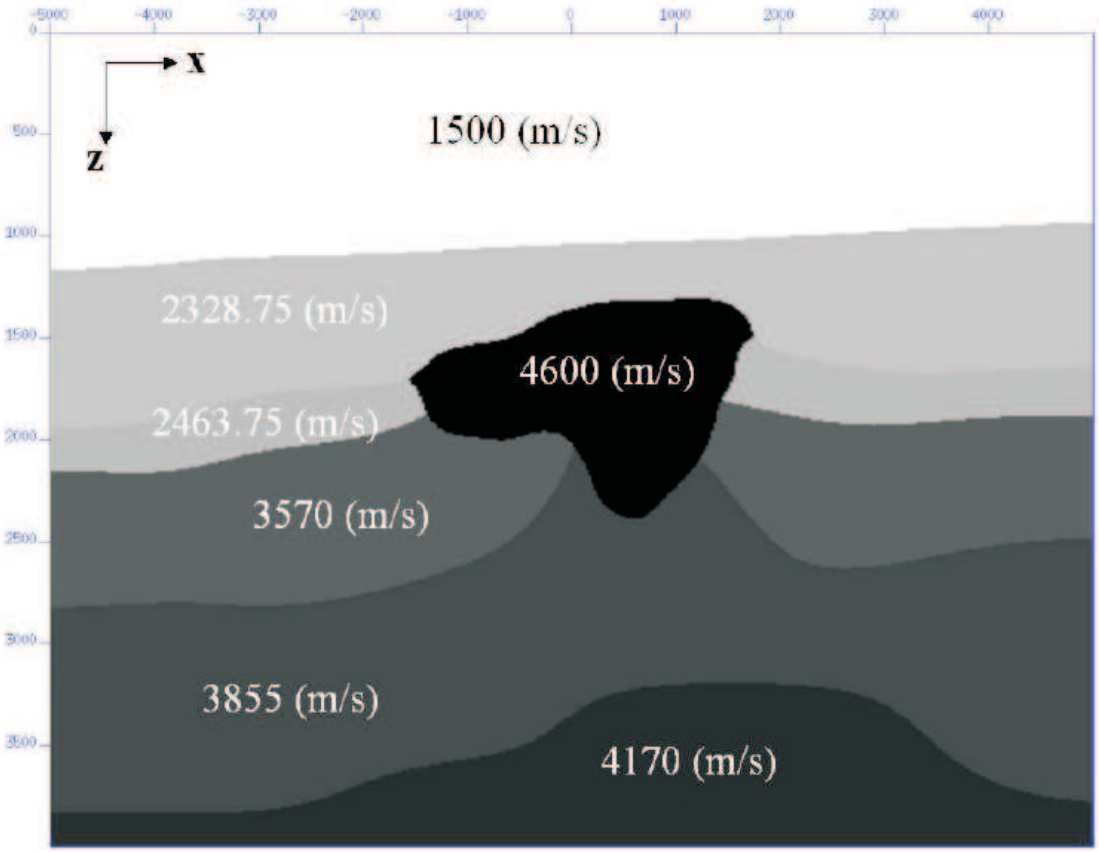

Figure 1: *The geometry and velocity of each layer in the salt model.*

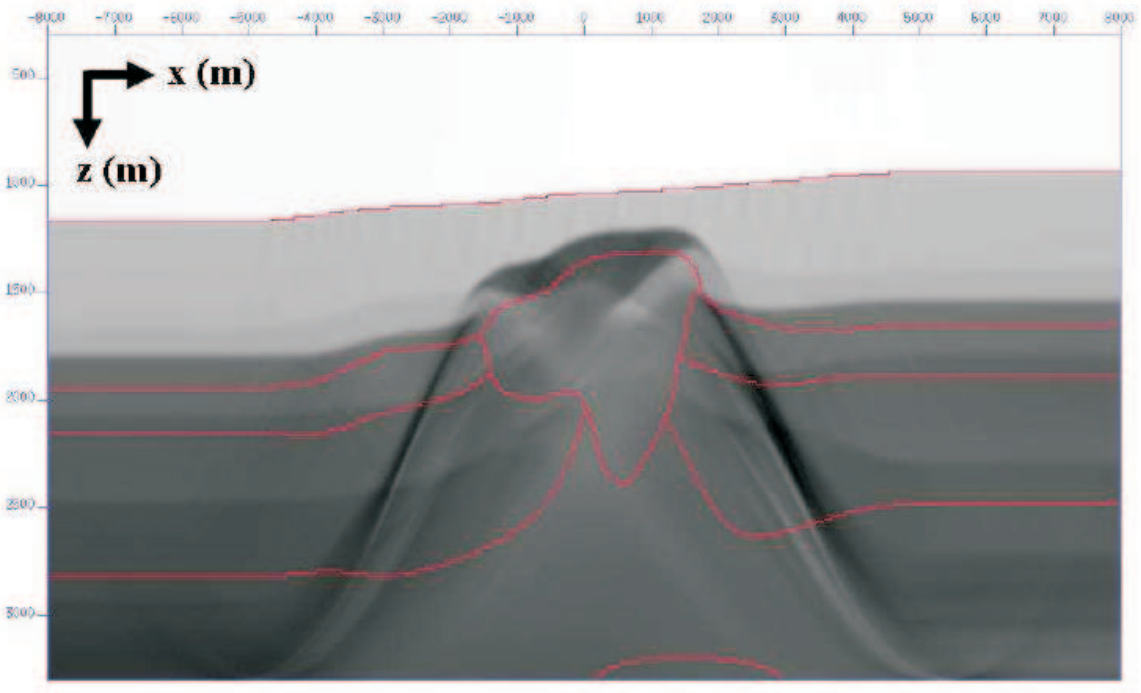

Figure 2: *Linear imaging results for the salt model.*

Conservation of cumulative reflection coefficients

F. Liu and A. B. Weglein

Abstract

This article presents a simplified relationship after grouping the amplitude of seismic events with similar propagation history: for layered acoustic medium, the cumulative reflection coefficient (i.e., the total amplitude of the events that had never propagated through a target), depends only on the acoustic property below the target and the first layer, and does not depend on any other overburden property of the middle layers above the target. One significance of the cumulative reflection coefficient is its direct impact on direct non-linear imaging: if it is utilized by the current higher-order siesmic imaging algorithm (Liu, 2006, equation *2.33* and *2.34*), we can achieve accurate depth for all the reflectors with a constant, unchanged migration velocity. This observation has the potential to become a procedure for the full seismic imaging subseries proposed in Weglein et al. (2003). Similar approach, i.e., removing the overburden effects on primaries with the help of the internal multiples, had already been studied in Lira et al. (2006).

1 Introduction

As defined in Weglein et al. (2003), an **event** in the seismic data is a distinct arrival of wave energy. Seismic data consists of many kinds of events with very different types of history from their creation at the source to their measurement at the receiver. **Primaries** are events that experienced one upward reflection (Figure 1 (a) and (b)), whereas multiply reflected events or **multiples** have experienced more than one upward reflection (see Figure 1 (c), (d), and (e)).

Even for very simple idealized layered models, every event carries information about its propagation history: the acoustic properties of the layers it had propagated through. This article presents a neat conservation relationship stating the opposite: after grouping the complicated information in events with similar propagation history, the final result "forget" their propagation history.

To be more specific, for a layered medium containing $N+1$ layers, each layer consists of acoustic medium with velocity c_n ($n = 0, 1, \cdots, N$), its **cumulative reflection coefficient** (denoted as $\mathbb{R}_{N-1}$), defined as "the total amplitude of all the events that never penetrate c_{N-1}/c_N interface", is $\mathbb{R}_{N-1} = \frac{c_N - c_0}{c_N + c_0}$. If we consider the last reflector (the c_{N-1}/c_N reflector) as the target, its cumulative reflection coefficient does not depend on the overburden information $c_1, \cdots, c_{N-1}$, it only depends on the velocity of the first layer c_0, and the velocity below the target c_N.

One interesting observation is that, if the amplitude of the n'th primaries is modefied to the difference between the cumulative reflection coefficients of two adjacent layers: $\mathbb{R}_n - \mathbb{R}_{n-1}$, our current higher-order imaging series achieves the accurate depth of all reflectors using a constant, unchanged migration velocity. This modification, although not an automatic procedure in the current stage, provides us with valuable insights to go beyond our current higher-order imaging subseries and reach the goal of the full seismic imaging subseries.

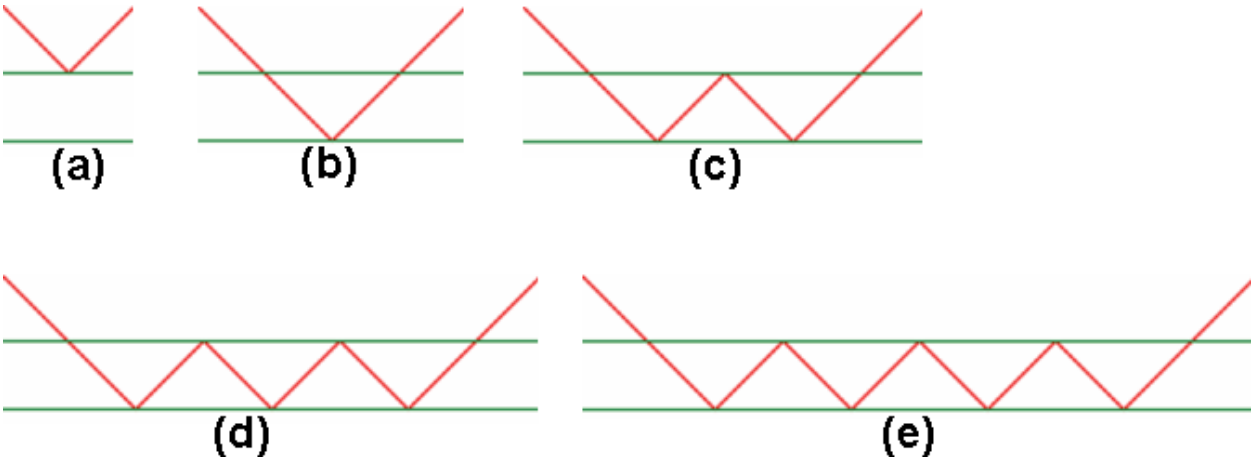

Figure 1: The earliest five events from the model defined in equation (1): (a) Primary from the first reflector; (b) primary from the second reflector; (c) first-order internal multiple; (d) second-order internal multiple; (e) third-order internal multiple.

2 Theory

For simplicity, we restrict our discussion to layered model without laterial variation, with piecewise-constant velocity function depending only on depth (z),

$$c(z) = \begin{cases} c_0 & z < d_0 \\ c_1 & d_0 \le z < d_1 \\ c_2 & d_1 \le z \end{cases} . \tag{1}$$

There are two reflectors in this model: (1) the reflector associated with the c_0/c_1 interface, according to Weglein et al. (2003), its reflection coefficient is $r_0 = \frac{c_1-c_0}{c_1+c_0}$; (2) the reflector associated with the c_1/c_2 interface, its reflection coefficient is $r_1 = \frac{c_2-c_1}{c_2+c_1}$. In Figure 1, a plane-wave normal incidence experiment and the propagation history of its earliest events are illustrated (for display purpose, the propagation is shown with a slope, since if strictly shown with up or down propagation, the propagation pathes overlap with each other, and we cannot tell how the wave propagates).

From Weglein et al. (2003), it's easy to deduce that the n^{th}-order internal multiple is $(-1)^n(1 - r_0^2)r_0^n r_1^{n+1}$, where $n = 1, 2, 3, \cdots$. The amplitude of n^{th}-order transmission event is $(-1)^{n-1}(1 + r_0)(1 + r_1)(r_0 r_1)^{n-1}$.

The reflection data recorded at $z = 0$ include the primaries and the n^{th}-order internal multiple ($n = 1, 2, 3, \cdots$), the sum of their amplitude (denoted as $\mathbb{R}_1$) is:

$$\begin{aligned} \mathbb{R}_1 &= r_0 + \sum_{n=0}^{\infty} (-1)^n \left(1 - r_0^2\right) r_1 \left(r_0 r_1\right)^n \\ &= r_0 + \frac{(1 - r_0^2)r_1}{1 + r_0 r_1} = \frac{r_0 + r_1}{1 + r_0 r_1} . \end{aligned} \tag{2}$$

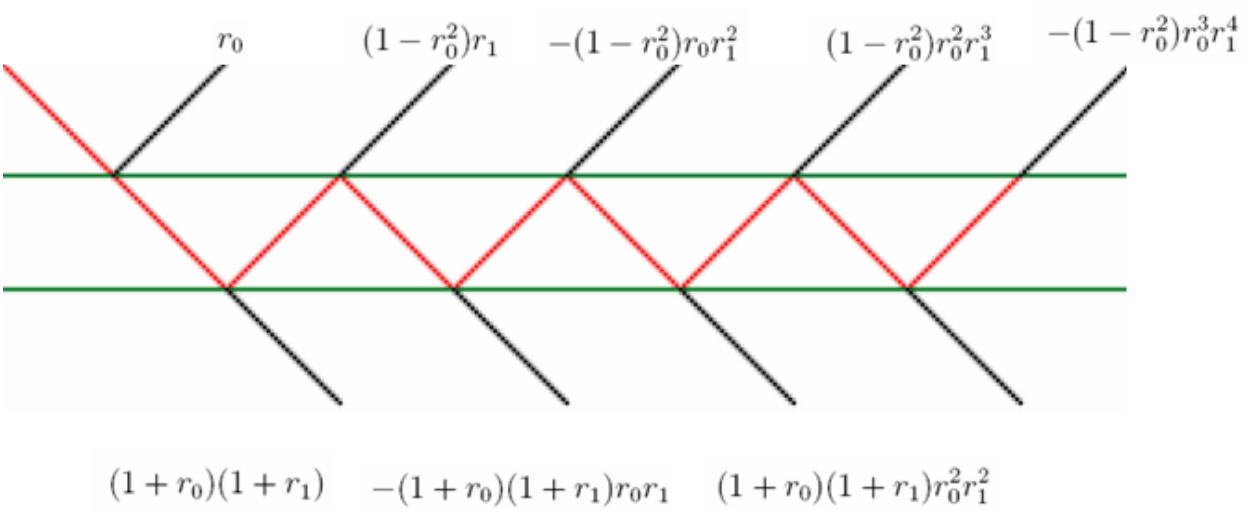

Figure 2: Events with their amplitudes labeled. We focused on the black colored events. The upward black events are reflection data (from left to right): (1) primary from the first reflector; (2) primary from the second reflector; (3) the 1^{st}-order internal multiple from the second reflector; (4) the 2^{nd}-order internal multiple from the second reflector; $\cdots$. Those upward events will never come back. The downward black events are transmission events (from left to right): (1) the 1^{st} transmission event; (2) the 2^{nd} transmission event; (3) the 3^{rd} transmission event, $\cdots$. Like the upward events mentioned before, those downward events will never return.

On the other hand, the total transmission strength (i.e., the sum of the amplitude of all transmission events, denoted as $\mathbb{T}_1$) is,

$$\begin{aligned}\mathbb{T}_1 &= \sum_{n=0}^{\infty}(-1)^n(1+r_0)(1+r_1)\,(r_0r_1)^n \\ &= \frac{(1+r_0)(1+r_1)}{1+r_0r_1} = \frac{1+r_0r_1+r_0+r_1}{1+r_0r_1} \\ &= 1+\frac{r_0+r_1}{1+r_0r_1} = 1+\mathbb{R}_1\ .\end{aligned} \tag{3}$$

What is significant about $\mathbb{R}_1$ in equation (2)? It turns out to be the reflection coefficient for a single reflector with c_0 above, and c_2 below, as if the middle layer with velocity c_1 does not exist. The presence of the medium in between (with velocity c_1) can be removed by a simple summing. This can be shown in the equation below,

$$\mathbb{R}_1 = \frac{r_0+r_1}{1+r_0r_1} = \frac{\frac{c_1-c_0}{c_1+c_0}+\frac{c_2-c_1}{c_2+c_1}}{1+\frac{c_1-c_0}{c_1+c_0}\frac{c_2-c_1}{c_2+c_1}} = \frac{c_2-c_0}{c_2+c_0}. \tag{4}$$

Similarly, $\mathbb{T}_1$ is the transmission coefficient of the same effective medium (with reflection coefficient $\mathbb{R}_1$) since $\mathbb{T}_1 = 1+\mathbb{R}_1$.

Let's consider a layered medium consisting of n reflectors, with depth-varying velocity function below,

$$c(z) = \begin{cases} c_0 & z < d_0 \\ c_n & d_n \le z < d_{n+1} \\ c_{N+1} & d_{N+1} \le z \end{cases} \quad (n = 1, 2, \cdots, N). \tag{5}$$

The model defined in equation (1) can be considered as a special case of the model defined in equation (5) where $N = 1$. For a much simpler 2-reflector model where $N = 1$, and for the 1-reflector model where $N = 0$. The following propositions are true: **Proposition I**, the up-going reflection events recorded in the medium c_0 can be expressed as a set of events with cumulative amplitude of $\mathbb{R}_N = \frac{c_{N+1}-c_0}{c_{N+1}+c_0}$; **Proposition II**, the transmission events recorded in the medium c_{N+1} can be expressed as a set of events with cumulative amplitude $\mathbb{T}_N = 1 + \mathbb{R}_N$.

In the induction proof, we assume the two propositions are true for $N = 1, 2, \cdots, n-1$. We consider a model with $N = n - 1$ (it will be refered to as $\texttt{model}_{n-1}$, We now add another velocity layer c_{n+1}, and consequently we have a model for $N = n$, see Fig. (3). Lets assume a single wave packet $\psi(t)$ incident from medium c_0, as indicated by the solid black arrow at the upper-left corner of Fig. (3). According to our inductive proposation, $\texttt{model}_{n-1}$ will produce two groups of events: (1) the up-going group $U^{(0)}$ with cumulative amplitude $\frac{c_n-c_0}{c_n+c_0}$ (it will be denoted as $\mathbb{R}_{n-1}$); and (2) the down-going group $A^{(0)}$ with cumulative amplitude $1 + \mathbb{R}_{n-1}$.

Let's define the cumulative amplitude of a group of events, denote as $\mathcal{A}$, its argument is a set of events of the form $\{A(i)\psi(t - t_i) : i = 0, 1, 2, \cdots\}$ [1], and defined as,

$$\mathcal{A}(\{A_i\psi(t - t_i) : i = 0, 1, 2, \cdots\}) = \sum_{i=0}^{\infty} A_i \quad . \tag{6}$$

Please notice that, in the definition $\mathcal{A}$, only A_i (the amplitude term of each event) is effective, t_i (the phase or the lag time of each event) is totally irrelavent.

$$\mathcal{A}(\{A_i : i = 0, 1, 2, \cdots\}) = \sum_{i=0}^{\infty} A_i \quad . \tag{7}$$

An event in the group $A^{(0)}$, propagates down first, and then will reflect back and transmit through the c_n/c_{n+1} interface, whose reflection coefficient is denoted as $r_n = \frac{c_{n+1}-c_n}{c_{n+1}+c_n}$. If we assume the amplitude of this event is S, it will produce an up-going reflection event with amplitude Sr_n, and a down-going transmission event with amplitude $S(1 + r_n)$. Consequently, the group $A^{(0)}$ will produce a group of reflection events denoted by $B^{(0)}$, and a group of transmission events denoted

[1] For a plane-wave normal incident upon a layered medium, seismic data recorded in a fixed location consist of many events, each event share the same temporary variation as the incident wave-packet $\psi(t)$ with an additional amplitude A_i and phase term t_i.

by $D^{(0)}$. It is obvious that the cumulative amplitude of the events in group $B^{(0)}$ is $r_n\mathbb{R}_{n-1}$, and the cumulative amplitude of the events in group $D^{(0)}$ is $(1+r_n)\mathbb{R}_{n-1}$,

$$\mathcal{A}(B^{(0)}) = r_n\mathbb{R}_{n-1} \qquad \mathcal{A}(D^{(0)}) = (1+r_n)\mathbb{R}_{n-1}\ .$$

The events in group $D^{(0)}$ will never return, and can be ignored for further discussion. Only the events in group $B^{(0)}$ are still inside the model.

Any event in the group $B^{(0)}$, which propagates upward towards the down side of $\texttt{model}_{n-1}$, will propagate toward a model which is the reversal of $\texttt{model}_{n-1}$, i.e., a model with first layer velocity c_n, the second layer velocity c_{n-1}, the third layer velocity c_{n-2}, $\cdots$, and the last layer velocity c_0; let's denote it by $\texttt{model}^{\texttt{reversal}}_{n-1}$.

Since $\texttt{model}^{\texttt{reversal}}_{n-1}$ is a model with $N = n-1$, from our inductive assumptions, it has a cumulative reflection coefficient determined by its first layer velocity c_n, and last layer velocity c_0: $\frac{c_0-c_n}{c_0+c_n} = -\frac{c_n-c_0}{c_n+c_0} = -\mathbb{R}_{n-1}$, and cumulative transmission coefficient $1+(-\mathbb{R}_{n-1}) = 1-\mathbb{R}_{n-1}$. As a result, an event in $B^{(0)}$, denoted as e_1, will produce a group of transmission events (denoted as G_1) propagating into c_0 and will never return, and a group of reflection events (denoted as H_1) propagating back into c_n. Another event in $B^{(0)}$, denoted as e_2, will produce a different group of transmission events G_2 and a different group of reflection events H_2. Since $\texttt{model}^{\texttt{reversal}}_{n-1}$ is a model with $N = n-1$, according to our inductive assumptions, it is obvious the cumulative amplitude of G_1 is proportional to the amplitude of e_1, the cumulative amplitude of G_2 is proportional to the amplitude of e_2, with the same proportional factor $1-\mathbb{R}_{n-1}$; the cumulative amplitude of H_1 is proportional to the amplitude of e_1, the cumulative amplitude of H_2 is proportional to the amplitude of e_2, with the same proportional factor $-\mathbb{R}_{n-1}$,

$$\begin{aligned}
&\mathcal{A}(G_1) = (1-\mathbb{R}_{n-1})\mathcal{A}(e_1) \qquad \mathcal{A}(G_2) = (1-\mathbb{R}_{n-1})\mathcal{A}(e_2),\\
&\mathcal{A}(H_1) = (-\mathbb{R}_{n-1})\mathcal{A}(e_1) \qquad \mathcal{A}(H_2) = (-\mathbb{R}_{n-1})\mathcal{A}(e_2).
\end{aligned}$$

In Fig. (3), G_1 and G_2 are two sub-groups of the event group $U^{(1)}$, H_1 and H_2 are two sub-groups of the event group $A^{(1)}$. The cumulative amplitude of group $U^{(1)}$ is $r_n(1-\mathbb{R}_{n-1})^2$ since,

$$\begin{aligned}
\mathcal{A}(U^{(1)}) &= \sum_{i=0}^{\infty}\mathcal{A}(G_i) = (1-\mathbb{R}_{n-1})\sum_{i=0}^{\infty}\mathcal{A}(e_i)\\
&= (1-\mathbb{R}_{n-1})\mathcal{A}(B^{(0)}) = (1-\mathbb{R}_{n-1})r_n(1+\mathbb{R}_{n-1})\\
&= r_n(1-\mathbb{R}^2_{n-1}).
\end{aligned}$$

$$\begin{aligned}
\mathcal{A}(A^{(1)}) &= \sum_{i=0}^{\infty}\mathcal{A}(H_i) = (-\mathbb{R}_{n-1})\sum_{i=0}^{\infty}\mathcal{A}(e_i)\\
&= (-\mathbb{R}_{n-1})\mathcal{A}(B^{(0)}) = -r_n\mathbb{R}_{n-1}(1+\mathbb{R}_{n-1}).
\end{aligned}$$

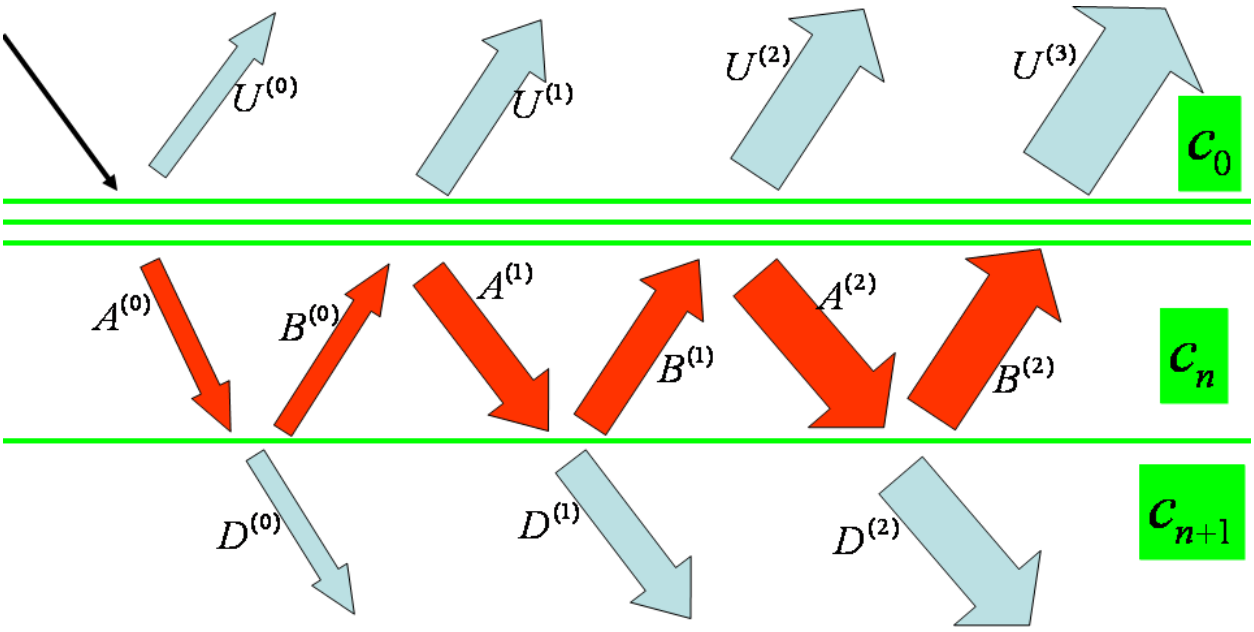

Figure 3: A model with one more reflector constructed by introducing another velocity c_{n+1}

	$U^{(k)}$	$A^{(k)}$
$k=0$	$\mathbb{R}_{n-1}$	$1+\mathbb{R}_{n-1}$
$k=1$	$r_n(1-\mathbb{R}_{n-1}^2)$	$(1+\mathbb{R}_{n-1})(-r_n\mathbb{R}_{n-1})$
$k=2$	$r_n(1-\mathbb{R}_{n-1}^2)(-r_n\mathbb{R}_{n-1})$	$(1+\mathbb{R}_{n-1})(-r_n\mathbb{R}_{n-1})^2 i$

	$B^{(k)}$	$D^{(k)}$
$k=0$	$r_n(1+\mathbb{R}_{n-1})$	$(1+r_n)(1+\mathbb{R}_{n-1}$
$k=1$	$r_n(1+\mathbb{R}_{n-1})(-r_n\mathbb{R}_{n-1})$	$(1+r_n)(1+\mathbb{R}_{n-1}$
$k=2$	$r_n(1+\mathbb{R}_{n-1})(-r_n\mathbb{R}_{n-1})^2$	$(1+r_n)(1+\mathbb{R}_{n-1}$

Since the events in group $U^{(1)}$ propagate into c_0 and will never return, they can be ignored for further discussion. The only group of events we should consider is $A^{(1)}$. We can repeat the previous analysis to obtain the reflection events and transmission events produced by the group $A^{(0)}$ and the previous arguments follows exactly the same manner. In summary, the cumulative amplitude of each group of events are listed in the table below.

The reflection data recorded at $z=0$ include the following group, $U^{(0)}$, $U^{(1)}$, $U^{(2)}$, $\cdots$, the sum of their amplitude is:

$$\begin{aligned}\mathbb{R}_n &= \mathbb{R}_{n-1} + \sum_{k=0}^{\infty}(-1)^k\left(1-\mathbb{R}_{n-1}^2\right) r_n \left(\mathbb{R}_{n-1}r_n\right)^k \\ &= \mathbb{R}_{n-1} + \frac{(1-\mathbb{R}_{n-1}^2)r_n}{1+\mathbb{R}_{n-1}r_n} \\ &= \frac{\mathbb{R}_{n-1}+r_n}{1+\mathbb{R}_{n-1}r_n}.\end{aligned} \tag{8}$$

On the other hand, the total transmission strength (i.e., the sum of the amplitude of $D^{(0)}$, $D^{(1)}$, $D^{(2)}$, $\cdots$) is,

$$\begin{aligned}\mathbb{T}_n &= \sum_{k=0}^{\infty}(-1)^k(1+\mathbb{R}_{n-1})(1+r_n)\left(\mathbb{R}_{n-1}r_n\right)^k \\ &= \frac{(1+\mathbb{R}_{n-1})(1+r_n)}{1+\mathbb{R}_{n-1}r_n} = \frac{1+\mathbb{R}_{n-1}r_n+\mathbb{R}_{n-1}+r_n}{1+\mathbb{R}_{n-1}r_n} \\ &= 1+\frac{\mathbb{R}_{n-1}+r_n}{1+\mathbb{R}_{n-1}r_n} = 1+\mathbb{R}_n.\end{aligned} \tag{9}$$

What is special about $\mathbb{R}_n$ in equation (8)? It turns out to be the reflection coefficient for a single reflector with c_0 above, and c_{n+1} below, as if the middle layers with velocity $c_1, c_2, \cdots, c_n$ do not exist. The presence of those layers can be removed by a simple summing. This can be shown in the equation below,

$$\mathbb{R}_n = \frac{\mathbb{R}_{n-1}+r_n}{1+\mathbb{R}_{n-1}r_n} = \frac{\frac{c_n-c_0}{c_n+c_0}+\frac{c_{n+1}-c_n}{c_{n+1}+c_n}}{1+\frac{c_n-c_0}{c_n+c_0}\frac{c_{n+1}-c_n}{c_{n+1}+c_n}} = \frac{c_{n+1}-c_0}{c_{n+1}+c_0}\,. \tag{10}$$

Similarly, $\mathbb{T}_n$ is the transmission coefficient of the same effective medium (with reflection coefficient $\mathbb{R}_n$) since $\mathbb{T}_n = 1+\mathbb{R}_n$.

From equation (8) and equation (9), the claims in our two propositions about the cumulative amplitude are true also for the next N value $N = n$. Then it is clear that **Proposation I** and **Proposation II** are true for 1D acoustic models with any number of layers. The simplification stated in the introduction of this article is simply **Proposation I**.

A layered model, for example, the one defined in equation (5), will produce many events. We further define Ω_n as the set of events that had been reflected by, but no transmitted through, the $N+1^{\texttt{th}}$ reflector. It can be equivalently defined as the group of events with deepest reflection point at the $N+1^{\texttt{th}}$ reflector. Several observations can be reached immediately,

1. From the definition, the union $\bigcup_{n=0}^{N}\Omega_n$ contains all the events reflected from the model.
2. The sets in the union are mutually exclusive. For example, if $m < n \le N$, it is easy to verify that any event in Ω_n does not belong to Ω_m; and any event in Ω_m does not belong to Ω_n.
3. A partial union of the form $\bigcup_{n=0}^{M}\Omega_n$ (where $M \le N$) consists of all the events from the simpler model with M reflectors. The cumulative amplitude of the reflection data from this model, according to our proposition, is $\mathcal{A}(\bigcup_{n=0}^{M}\Omega_n) = \frac{c_{M+1}-c_0}{c_{M+1}+c_0}$.
4. Each Ω_n contains only one primary, i.e., the primary from the n^{th} reflector. The other events are multiples.

5. The cumulative amplitude of each Ω_n is: $\mathcal{A}(\Omega_0) = \frac{c_1-c_0}{c_1+c_0}$, $\mathcal{A}(\Omega_n) = \frac{c_{n+1}-c_0}{c_{n+1}+c_0} - \frac{c_n-c_0}{c_n+c_0}$, $n = 1, 2, \cdots, N$.

6. For 1D acoustic medium with density variation, our previous argument is also valid if velocity is replaced by impedance (the product of velocity and density). In this case, although the reflection and transmission coefficients are determined by impedance contrast, instead of velocity contrast, the equations determining the cummulative reflection and transmission strength are the same if impedance is used instead of velocity.

3 Numerical example

For 1D layered acoustic model, the amplitude of each event can be analytically obtained, allowing the numerical example (see Figure 4) below to be designed and tested in the frame-work of this article.

This example shows that, after the removal of multiples, and adding the amplitude of all the internal multiples to the primary that reflects from the same deepest reflection location as the multiples, then our current higher-order imaging subseries (Liu, 2006) achieved accurate depth for all the primaries.

4 Conclusions

A simplication had been reached after grouping seismic events with similar propagation history. This simplification provides us with additional insight about how to fully realize the depth-imaging potential of the inverse scattering series that achieves accurate depth with a constant, unchanged reference medium. To be more specific,

1. The current higher-order seismic imaging subseries, although very effective and robust for large contrast geological models, is still not the full seismic imaging seubseries. The **first** interesting fact is that, if we modify the amplitude of each primary to the difference between two adjacent cumulative reflection coefficients, the current higher-order imaging subseries will indeed achieve accurate depth for all reflectors, as demonstrated by a numerical example in section 3.

2. The **second** interesting fact is that: almost all the overburden information was cleared from cumulative reflection coefficients.

3. The **third** interesting fact is that, the relationship in this article hold *not only* for velocity-only acoustic mdeium, *but also* for acoustic medium with velocity and density variations. An procedure, capable of reaching cumulative reflection coefficient for velocity-only acoustic medium, will be equally effective to remove the overburden effect for acoustic medium with velocity and density variation. It will certainly give better chance for parameter inversion.

Further research is needed to obtain a procedure to realize the concept in this article.

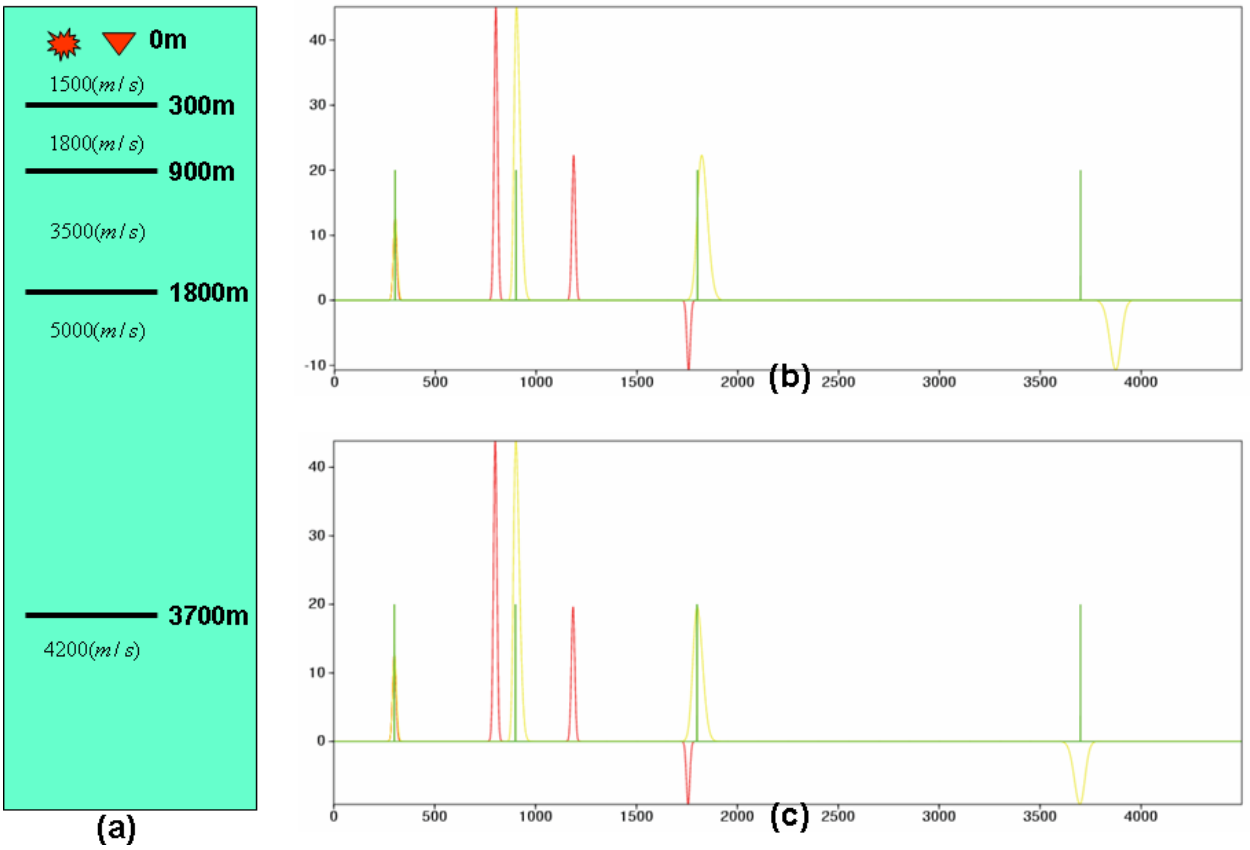

Figure 4: (a): A geological model with four reflectors. (b): The input data (displayed in red) includes primaries and the corresponding higher-order imaging result (displayed in yellow). (c): in red is the input data that each primary's amplitudes changed to the total amplitude of group of events with deepest reflection point at that primary's reflection depth, in yellow is the corresponding higher-order imaging result. It is clear that with the modification in (c), the current higher-order imaging subseries achieved accurate depth for all reflectors.

5 Acknowledgments

The authors would like to thank GX Technology for granting Fang 2006-2007 GXT fellowship. We felt indebted to all M-OSRP members for informative discussions and MOSRP sponsors for their support. This work has been partially funded by NSFCMG award DMS-0327778 and DOE Basic Energy Sciences award DE-FG02-05ER15697.

References

Lira, J. E., A. B. Weglein, and A. C. Ramirez. "Estimating plane-wave transmission loss with the inverse scattering internal multiple attenuation algorithm: concept and an application to Q estimation." *M-OSRP Annual Report* 5 (2006): 45–57.

Liu, Fang. *Multi-dimensional depth imaging without an adequate velocity model.* PhD thesis, University of Houston, 2006.

Weglein, A. B., F. V. Araújo, P. M. Carvalho, R. H. Stolt, K. H. Matson, R. T. Coates, D. Corrigan, D. J. Foster, S. A. Shaw, and H. Zhang. "Inverse scattering series and seismic exploration." *Inverse Problems* 19 (2003): R27–R83.

Note on multi-component elastic direct nonlinear target identification

X. Li, H. Zhang and A. B. Weglein

Abstract

In this note, firstly, we will review the prior research on multi-component elastic direct nonlinear inversion (Zhang, 2006). Based on the inverse scattering task-specific subseries (Weglein et al., 2003), a multi-component direct nonlinear inversion framework for 1D two parameter (velocity and density variation with depth) acoustic case was developed and extended to 1D three parameter (P-wave velocity, S-wave velocity, and density variation with depth) elastic case. Because it is a direct non-linear method, we can solve for the medium properties explicitly and directly without global searching, and this procedure has the potential to give more accurate and reliable estimation of earth property changes for small and large contrast targets.

Zhang provided the direct non-linear inversion formulas for medium properties for the simplest 1D elastic earth using line sources and receivers. The unambiguous message was that a full set of multicomponent data, D^{PP}, D^{PS}, D^{SP} and D^{SS} (Zhang and Weglein, 2005) was needed to achieve the objective. Although synthetic tests using only D^{PP} have been done and which provided consistent value-added results, never the less D^{PP} is intrinsically inadequate.

Secondly, in order to better understand the derivation and the algorithm for the elastic case in Zhang's thesis, we examine some specific calculations involving the operator $\frac{1}{\nabla^2}$. $\frac{1}{\nabla^2}$ appears in the perturbation $\hat{V}$ when we transform from the displacement domain to the P and S potential (PS) domain (Weglein and Stolt, 1992; Matson, 1997; Zhang and Weglein, 2005). Ambiguity occurs when $\frac{1}{\nabla^2}$ acts on different Green's functions in the nonlinear term. In this note, we confirm Zhang's elastic derivation and results from a different point of view and present a further explanation on this issue.

H. Zhang (2006) studied the important and standard marine towed streamer case where only D^{PP} is available.The required D^{PS}, D^{SP}, and D^{SS} data is approximately synthesized using D^{PP}. The non-linear results with this towed streamer data demonstrated added-value in comparison with linear results for a suite of tests for each of several different target types. There were cases where the goal was to distinguish between two target regimes with very close change in elastic properties and density, and different underlying rock fluid and pressure characteristics. We plan to test the actual rather than approximate synthesized data components, and to compare that called for data with linear and non-linear synthesized data.

Introduction

Seismic data processing is an inverse method during which measured data are inverted for Earth properties. The inverse scattering series promises to produce a direct non-linear inversion procedure in terms of only recorded data and reference information (Weglein et al., 2003). Scattering theory relates the perturbation (the difference between the reference and actual medium properties) to the scattered wave field (the difference between reference and actual wave field). It recognizes that when you perturb anything in a medium the associated perturbation in the wavefield is always non-linearly related to that change.

Research has been done to seek isolated convergent subseries which perform individual tasks (Weglein et al., 2003): 1. Free surface multiple removal; 2. Internal multiple removal; 3. Imaging (positioning reflectors at the correct spacial locations), and 4. Target Identification (inverting reflectivity for changes in Earth parameters). The order in which these steps are carried out is very important because the algorithms assume that the data have been processed by the previous steps. On her way to the direct non-linear inversion solution, Zhang, assumed that the unperturbed medium is a homogeneous wholespace; the free surface multiples and internal multiples have already been removed. When reduced to the special case of a single horizontal reflector, the exact location of the reflector and the reference medium down to the reflector are known, and the goal is to determine the medium properties below the reflector which have a nonlinear relationship with the recorded data.

Current parameter inversion methods 1. assume a linear relationship between the amplitude of a primary and the mechanical property change across the reflector, which can be violated in practice and result in erroneous predictions; or 2. assume a nonlinear relationship but use an indirect model-matching method to seek the solution, which often has a significant computation effort and also has reported ambiguous results. The direct multi-parameter non-linear inversion is direct and non-linear without making a small contrast assumption. The directness and explicitness of the ISS provides not only the precise framework but also a much greater clarity, for the meaning of "linear in the data", and precisely what data collection will be required to achieve classic processing goals, for example, in a 2D problem, it needs to solve for a 2×2 matrix V, from a 2×2 matrix data, D^{PP}, D^{PS}, D^{SP} and D^{SS}, where previously only anecdotal experience provided a hint.

Research has proceeded in stages: We started by analyzing a one parameter (only velocity varying in depth) 1D acoustic constant density medium and 1D normal incidence (Weglein et al., 2002; Shaw et al., 2004). Zhang examined the two parameter (velocity and density varying in depth) 1D acoustic case and extended to three parameter (P-wave velocity, S-wave velocity, and density varying in depth) 1D elastic case (Zhang, 2006) which is a further important stage towards realism for target identification. Zhang has demonstrated, for the first time, 1. an explicit and direct set of equations for improving upon linear estimates of the changes in those elastic properties; 2. the absolutely clear data requirements: all four components of data, $\hat{D}^{PP}$, $\hat{D}^{PS}$, $\hat{D}^{SP}$ and $\hat{D}^{SP}$ (Zhang and Weglein, 2005) are needed for determining the three parameters: a_ρ, relative change in density; a_γ, relative change in bulk modulus; a_μ, relative change in shear modulus. If started using only D^{PP} to solve for linear estimates of changes in medium properties and obtain every form of generalized inverse by minimizing the objective function, people would never realize that the whole framework is intrinsically inadequate. Although, mathematically, solving three independent equations for three unknowns sounds pretty reasonable, it does not represent the correct linear relationship of the changes in the medium properties in terms of the data that can determine the quantities. This problem is only pointed by the direct nonlinear solution only provided by ISS.

The following section is a brief review about the multi-parameter direct non-linear inversion for 1D elastic medium. We then provide a further discussion about the calculation of the non-linear terms.

Research Review

In this section, a review of multi-component direct nonlinear inversion for 1D elastic medium (Zhang, 2006) is presented. The direct method shows how the message of explicit data requirements for direct nonlinear parameter estimation was delivered by inverse scattering series.

The inverse scattering series, in the PS domain (Weglein and Stolt, 1992; Matson, 1997) is

$$\hat{V} = \hat{V}_1 + \hat{V}_2 + \hat{V}_3 + ..., \tag{1}$$

and

$$\hat{D} = \hat{G}_0\hat{V}_1\hat{G}_0, \tag{2}$$

$$\hat{G}_0\hat{V}_2\hat{G}_0 = -\hat{G}_0\hat{V}_1\hat{G}_0\hat{V}_1\hat{G}_0, \tag{3}$$

where the perturbation is given by $\hat{V} = \begin{pmatrix} \hat{V}^{PP} & \hat{V}^{PS} \\ \hat{V}^{SP} & \hat{V}^{SS} \end{pmatrix}$, the Green's operator by $\hat{G}_0 = \begin{pmatrix} \hat{G}^P & 0 \\ 0 & \hat{G}^S \end{pmatrix}$, and the data by $\hat{D} = \begin{pmatrix} \hat{D}^{PP} & \hat{D}^{PS} \\ \hat{D}^{SP} & \hat{D}^{SS} \end{pmatrix}$.

Linear inversion of 1D elastic medium

Equation (2) leads to four equations:

$$\hat{D}^{PP} = \hat{G}_0^P\hat{V}_1^{PP}\hat{G}_0^P, \tag{4}$$

$$\hat{D}^{PS} = \hat{G}_0^P\hat{V}_1^{PS}\hat{G}_0^S, \tag{5}$$

$$\hat{D}^{SP} = \hat{G}_0^S\hat{V}_1^{SP}\hat{G}_0^P, \tag{6}$$

$$\hat{D}^{SS} = \hat{G}_0^S\hat{V}_1^{SS}\hat{G}_0^S. \tag{7}$$

These equations describe how $\hat{V}_1^{PP}$ relates to $\hat{D}^{PP}$, $\hat{V}_1^{PS}$ relates to $\hat{D}^{PS}$, and so on. For example, in equation (4), an incoming P-wave interacts with $\hat{V}_1$ and leaves as a P-wave; and in equation (6), an incoming P-wave interacts with $\hat{V}_1$ but leaves as a S-wave, and so forth.

Take $\hat{D}^{PP} = \hat{G}_0^P\hat{V}_1^{PP}\hat{G}_0^P$, as an example, in the $(k_s, z_s; k_g, z_g; \omega)$ domain, assuming $z_s = z_g = 0$, we have:

$$\widetilde{D}^{PP}(k_g, 0; -k_g, 0; w) = -\frac{1}{4}(1 - \frac{{k_g}^2}{{\nu_g}^2})\tilde{a}_\rho^{(1)}(-2\nu_g) - \frac{1}{4}(1 + \frac{{k_g}^2}{{\nu_g}^2})\tilde{a}_\gamma^{(1)}(-2\nu_g) + \frac{2{k_g}^2{\beta_0}^2}{({\nu_g}^2 + {k_g}^2){\alpha_0}^2}\tilde{a}_\mu^{(1)}(-2\nu_g), \tag{8}$$

where $k_g^2 + \nu_g^2 = \frac{\omega^2}{\alpha_0^2}$. And there are three other equations for $\widetilde{D}^{PS}$, $\widetilde{D}^{SP}$ and $\widetilde{D}^{SS}$ (Appendix A). We can see that, even for the linear case, the solutions are much more complicated than those for the acoustic case.

For the P-wave incidence case, using $k_g^2/\nu_g^2 = \tan^2\theta$ and $k_g^2/(\nu_g^2 + k_g^2) = \sin^2\theta$, where θ is the P-wave incident angle (Appendix B), equation (8) becomes

$$\widetilde{D}^{PP}(\nu_g, \theta) = -\frac{1}{4}(1 - \tan\theta^2)\tilde{a}_\rho^{(1)}(-2\nu_g) - \frac{1}{4}(1 + \tan\theta^2)\tilde{a}_\gamma^{(1)}(-2\nu_g) + \frac{2\sin\theta^2{\beta_0}^2}{{\alpha_0}^2}\tilde{a}_\mu^{(1)}(-2\nu_g). \tag{9}$$

Non-linear inversion of 1D elastic medium for 2D experiment

We next write equation (3) in matrix form:

$$\begin{aligned}
&\begin{pmatrix} \hat{G}^P & 0 \\ 0 & \hat{G}^S \end{pmatrix} \begin{pmatrix} \hat{V}_2^{PP} & \hat{V}_2^{PS} \\ \hat{V}_2^{SP} & \hat{V}_2^{SS} \end{pmatrix} \begin{pmatrix} \hat{G}^P & 0 \\ 0 & \hat{G}^S \end{pmatrix} \\
= \; &-\begin{pmatrix} \hat{G}^P & 0 \\ 0 & \hat{G}^S \end{pmatrix} \begin{pmatrix} \hat{V}_1^{PP} & \hat{V}_1^{PS} \\ \hat{V}_1^{SP} & \hat{V}_1^{SS} \end{pmatrix} \begin{pmatrix} \hat{G}^P & 0 \\ 0 & \hat{G}^S \end{pmatrix} \begin{pmatrix} \hat{V}_1^{PP} & \hat{V}_1^{PS} \\ \hat{V}_1^{SP} & \hat{V}_1^{SS} \end{pmatrix} \begin{pmatrix} \hat{G}^P & 0 \\ 0 & \hat{G}^S \end{pmatrix}, \quad (10)
\end{aligned}$$

which leads to four equations:

$$\hat{G}_0^P \hat{V}_2^{PP} \hat{G}_0^P = -\hat{G}_0^P \hat{V}_1^{PP} \hat{G}_0^P \hat{V}_1^{PP} \hat{G}_0^P - \hat{G}_0^P \hat{V}_1^{PS} \hat{G}_0^S \hat{V}_1^{SP} \hat{G}_0^P, \quad (11)$$

$$\hat{G}_0^P \hat{V}_2^{PS} \hat{G}_0^S = -\hat{G}_0^P \hat{V}_1^{PP} \hat{G}_0^P \hat{V}_1^{PS} \hat{G}_0^S - \hat{G}_0^P \hat{V}_1^{PS} \hat{G}_0^S \hat{V}_1^{SS} \hat{G}_0^S, \quad (12)$$

$$\hat{G}_0^S \hat{V}_2^{SP} \hat{G}_0^P = -\hat{G}_0^S \hat{V}_1^{SP} \hat{G}_0^P \hat{V}_1^{PP} \hat{G}_0^P - \hat{G}_0^S \hat{V}_1^{SS} \hat{G}_0^S \hat{V}_1^{SP} \hat{G}_0^P, \quad (13)$$

$$\hat{G}_0^S \hat{V}_2^{SS} \hat{G}_0^S = -\hat{G}_0^S \hat{V}_1^{SP} \hat{G}_0^P \hat{V}_1^{PS} \hat{G}_0^S - \hat{G}_0^S \hat{V}_1^{SS} \hat{G}_0^S \hat{V}_1^{SS} \hat{G}_0^S. \quad (14)$$

Here we have already encountered one advantage of direct inversion: it determines data requirements for parameter estimation. Since $\hat{V}_1^{PP}$ relates to $\hat{D}^{PP}$, $\hat{V}_1^{PS}$ relates to $\hat{D}^{PS}$, and so on, the four components of the data will be coupled for the non-linear elastic inversion. We cannot perform the direct non-linear inversion without knowing all components of the data. In comparing with the previous work on the two parameter acoustic case, we point out that this elastic extension is not just adding another parameter, but involves more issues. For example, four different sets of linear parameter estimates are produced from each component of the data. Also, generally four distinct reflector mislocations arise from the two reference velocities (P-wave velocity and S-wave velocity).

The three parameters we are seeking to determine, a_ρ, a_γ and a_μ are to be expanded as a series in the data which is needed to determine those three quantities. The required data are

$$D = \begin{pmatrix} \hat{D}^{PP} & \hat{D}^{PS} \\ \hat{D}^{SP} & \hat{D}^{SS} \end{pmatrix},$$

for a 2D earth and a 3×3 matrix for a 3D earth with SH and SV shear waves.
The 2D message is delivered in equation (10), equation (11)-(14) which are the first non-linear contribution to a_ρ, a_γ, a_μ requires that data; and, hence the exact determination of those elastic quantities also require that data.

$$\begin{pmatrix} V^{PP} & V^{PS} \\ V^{SP} & V^{SS} \end{pmatrix} = \begin{pmatrix} V_1^{PP} & V_1^{PS} \\ V_1^{SP} & V_1^{SS} \end{pmatrix} + \begin{pmatrix} V_2^{PP} & V_2^{PS} \\ V_2^{SP} & V_2^{SS} \end{pmatrix} + \cdots$$

In some cases like the towed streamer case, all components of data are unavailable. A particular non-linear approach – using only $\hat{D}^{PP}$ has been chosen to address our typical lack of four components of elastic data. Synthetic tests are encouraging and show significant improvement by adding the second term (the first nonlinear term) (Zhang and Weglein, 2006) to the linear term. However, inverting only $\hat{D}^{PP}$ for the linear term of the properties ${a_\rho}^{(1)}$, ${a_\gamma}^{(1)}$, and ${a_\mu}^{(1)}$ is basically an injured linear estimate. It has the inherent deficiency in the very beginning – inverting the insufficient data D^{PP} for the linear term of medium properties. The ISS and task specific subseries need to treat the linear term as the linear term and then let the higher order terms carry out their purpose.

The operator $\frac{1}{\nabla^2}$ acting on G_0

$\frac{1}{\nabla^2}$ appears in the perturbation $\hat{V}$ when transforming from the displacement domain to the PS domain (Weglein and Stolt, 1992; Matson, 1997; Zhang and Weglein, 2005). The notation $\frac{1}{\nabla^2}$ is the inverse of the differential operator ∇^2. Therefore, it is an integral operator. In the nonlinear term, for example $\hat{G}_0\hat{V}\hat{G}_0\hat{V}\hat{G}_0$, the source and receiver side Green's functions are different from the middle Green's function because of the relative positions of scattering points. Ambiguity will occur when $\hat{V}$ acts on different Green's functions. In this section we will present mathematic details about some calculations involving the operator $\frac{1}{\nabla^2}$, so as to better understand the derivation and algorithm for the elastic case in Zhang's thesis.

Considering the term: $\hat{G}_0^P\frac{1}{\nabla^2}\hat{G}_0^P\frac{1}{\nabla^2}\hat{G}_0^P$, and number this $(*)$. Let us see what happens when we evaluate it. Firstly, we give the bilinear form of the Green's function $\hat{G}_0{}^P$ in 2D. Starting with the wave equation, the reference operator, L_0, satisfies

$$L_0G_0 = (\nabla'^2 + \frac{\omega^2}{c_0^2})G_0(x', z', x'', z''; \omega) = -\delta(x' - x'')\delta(z' - z''). \tag{15}$$

Fourier transforming (15) with respect to x' and z', we find

$$[k^2 - k_x'^2 - k_z'^2]G_0(k_x', k_z', x'', z''; \omega) = -e^{-ik_x'x''}e^{-ik_z'z''}, \tag{16}$$

where $k^2 = \frac{\omega^2}{c_0^2}$, thus,

$$G_0(x', z'; x'', z''; \omega) = -\frac{1}{(2\pi)^2}e^{-ik_x'x''}\iint dk_x'dk_z'\frac{e^{ik_z'(z'-z'')}}{k^2 - k_x'^2 - k_z'^2}. \tag{17}$$

Since the sources and receivers are always above the non-reference medium, for the outside Green's function we have

$$G_0(k_x, z; x_s, z_s; \omega) = \frac{e^{-ik_xx_s}}{2iq}e^{iq(z-z_s)},$$

$(q = \sqrt{k^2 - k_x^2})$ where there are no absolute value bars; likewise, for the middle Green's function

$$G_0(k_x', z'; x'', z''; \omega) = \frac{e^{-ik_x'x''}}{2iq}e^{iq|z'-z''|},$$

the relative locations of the two scattering points could change, so the absolute value bars remain.

Writing equation $(*)$ in integral form, and calling the result I, we have

$$\begin{aligned} I \;=\; & \tfrac{1}{(2\pi)^6}\iiiint dx'dx''dz'dz''\iint dk_x'dk_z'\tfrac{e^{ik_x'(x_g-x')}e^{ik_z'(z_g-z')}}{k^2-k_x'^2-k_z'^2} \\ & \times\tfrac{1}{\nabla'^2}\iint dk_x''dk_z''\tfrac{e^{ik_x''(x'-x'')}e^{ik_z''(z'-z'')}}{k^2-k_x''^2-k_z''^2} \\ & \times\tfrac{1}{\nabla''^2}\iint dk_x'''dk_z'''\tfrac{e^{ik_x'''(x''-x_s)}e^{ik_z'''(z''-z_s)}}{k^2-k_x'''^2-k_z'''^2}. \end{aligned} \tag{18}$$

Fourier transforming over x_s and x_g, multiplying by $\frac{1}{(2\pi)^2}\iint dx_g dx_s e^{-ik_g x_g} e^{ik_s x_s}$ on both sides, then integrating over k'_x and k'''_x, and calling the result $\tilde{I}$, we have

$$\begin{aligned}\tilde{I} &= \tfrac{1}{(2\pi)^6}\iiiint dx'dx''dz'dz''e^{-ik_g x'}\int dk'_z \tfrac{e^{ik'_z(z_g-z')}}{\nu_g^2-{k'_z}^2}\tfrac{1}{\nabla'^2}\\ &\quad\times\iint dk''_x dk''_z \tfrac{e^{ik''_x(x'-x'')}e^{ik''_z(z'-z'')}}{k^2-{k''_x}^2-{k''_z}^2}\tfrac{1}{\nabla''^2}e^{ik_s x''}\int dk'''_z \tfrac{e^{ik'''_z(z''-z_s)}}{\nu_s^2-{k'''_z}^2}.\end{aligned} \tag{19}$$

Integrating over k'_z and k'''_z,

$$\begin{aligned}\tilde{I} &= \tfrac{1}{(2\pi)^6}\iiiint dx'dx''dz'dz''e^{-ik_g x'}(-i\pi)\tfrac{e^{i\nu_g(z'-z_g)}}{\nu_g}\tfrac{1}{\nabla'^2}\\ &\quad\times\iint dk''_x dk''_z \tfrac{e^{ik''_x(x'-x'')}e^{ik''_z(z'-z'')}}{k^2-{k''_x}^2-{k''_z}^2}\tfrac{1}{\nabla''^2}e^{ik_s x''}(-i\pi)\tfrac{e^{i\nu_s(z''-z_s)}}{\nu_s},\end{aligned} \tag{20}$$

where $\nu_g^2 = k^2 - k_g^2$ and $\nu_s^2 = k^2 - k_s^2$. For the outside G_0 term, we have

$$\nabla''^2 e^{ik_s x''}\frac{e^{i\nu_s(z''-z_s)}}{\nu_s} = (-k_s^2-\nu_s^2)e^{ik_s x''}\frac{e^{i\nu_s(z''-z_s)}}{\nu_s},$$

so,

$$\frac{1}{\nabla''^2}e^{ik_s x''}\frac{e^{i\nu_s(z''-z_s)}}{\nu_s} = \frac{1}{(-k_s^2-\nu_s^2)}e^{ik_s x''}\frac{e^{i\nu_s(z''-z_s)}}{\nu_s}. \tag{21}$$

Hence after integrating over x'', then over k''_x and k''_z in equation (20), we have

$$\begin{aligned}\tilde{I} &= 2\pi^4 i\tfrac{1}{2\pi^6}\iiint dx'dz'dz''e^{-ik_g x'}\tfrac{e^{i\nu_g(z'-z_g)}}{\nu_g}\tfrac{1}{\nabla'^2}\\ &\quad\times\tfrac{e^{ik_s x'}e^{i\nu_s|z'-z''|}}{\nu_s}\tfrac{1}{(-k_s^2-\nu_s^2)}\tfrac{e^{i\nu_s(z''-z_s)}}{\nu_s}.\end{aligned} \tag{22}$$

For the middle Green's function term, we note that

$$\begin{aligned}\nabla'^2\tfrac{e^{ik_s x'}}{\nu_s}e^{i\nu_s|z'-z''|} &= -k_s^2\tfrac{e^{ik_s x'}}{\nu_s}e^{i\nu_s|z'-z''|} + \partial'^2_z[e^{i\nu_s(z'-z'')}H(z'-z'')+e^{i\nu_s(z''-z')}H(z''-z')]\tfrac{e^{ik_s x'}}{\nu_s}\\ &= -k_s^2\tfrac{e^{ik_s x'}}{\nu_s}e^{i\nu_s|z'-z''|} + \partial'_z[i\nu_s e^{i\nu_s(z'-z'')}H(z'-z'')-i\nu_s e^{i\nu_s(z''-z')}H(z''-z')]\tfrac{e^{ik_s x'}}{\nu_s}\\ &= (-k_s^2-\nu_s^2+2i\nu_s\delta(z'-z''))\tfrac{e^{ik_s x'}}{\nu_s}e^{i\nu_s|z'-z''|}.\end{aligned} \tag{23}$$

A δ function appears in the mathematics, which prevents us from doing what we did in equation (21). Zhang used a trick when dealing with this issue by exchanging the order of the integration and the $\frac{1}{\nabla'^2}$ acting on the middle G_0 (Zhang, 2006).
But what will happen if we change the order of calculation for the outer G_0? Will we produce the same result as in equation (21) which kept the original order?

Going back to equation (19), we put $\frac{1}{\nabla''^2}$ inside $\int dk'''_z$, resulting in

$$\begin{aligned}\tilde{I}' &= \tfrac{1}{(2\pi)^6}\iiiint dx'dx''dz'dz''e^{-ik_g x'}\int dk'_z\tfrac{e^{ik'_z(z_g-z')}}{\nu_g^2-{k'_z}^2}\tfrac{1}{\nabla'^2}\\ &\quad\times\iint dk''_x dk''_z\tfrac{e^{ik''_x(x'-x'')}e^{ik''_z(z'-z'')}}{k^2-{k''_x}^2-{k''_z}^2}\int dk'''_z\tfrac{1}{\nabla''^2}e^{ik_s x''}\tfrac{e^{ik'''_z(z''-z_s)}}{\nu_s^2-{k'''_z}^2}\\ &= \tfrac{1}{(2\pi)^6}\iiiint dx'dx''dz'dz''e^{-ik_g x'}\int dk'_z\tfrac{e^{ik'_z(z_g-z')}}{\nu_g^2-{k'_z}^2}\tfrac{1}{\nabla'^2}\\ &\quad\times\iint dk''_x dk''_z\tfrac{e^{ik''_x(x'-x'')}e^{ik''_z(z'-z'')}}{k^2-{k''_x}^2-{k''_z}^2}e^{ik_s x''}\int dk'''_z\tfrac{e^{ik'''_z(z''-z_s)}}{(-k_s^2-{k'''_z}^2)(\nu_s^2-{k'''_z}^2)}.\end{aligned} \tag{24}$$

For the last term, in the complex plane

$$\begin{aligned} I' &= \int dk_z''' \frac{e^{ik_z'''(z''-z_s)}}{(-k_s^2-k_z'''^2)(\nu_s^2-k_z'''^2)}, \\ &= \lim_{\epsilon\to 0}\int dk_z''' \frac{e^{ik_z'''(z''-z_s)}}{(k_s^2+k_z'''^2)[k_z'''^2-(\nu_s+i\epsilon)^2]}, \end{aligned}$$

for $\nu_s > 0$, $k_s > 0$ and $z'' > z_s$. Computing the residues

$$Resf(k_z''' = \nu_s + i\epsilon) = \frac{e^{i(\nu_s+i\epsilon)(z''-z_s)}}{[(\nu_s+i\epsilon)^2+k_s^2][2(\nu_s+i\epsilon)]},$$

$$Resf(k_z''' = ik_s) = \frac{e^{i(ik_s)(z''-z_s)}}{2ik_s[-k_s^2-(\nu_s+i\epsilon)^2]},$$

we have,

$$\begin{aligned} I' &= \lim_{\epsilon\to 0}\int dk_z''' \frac{e^{ik_z'''(z''-z_s)}}{(k_s^2+k_z'''^2)[k_z'''^2-(\nu_s+i\epsilon)^2]} \\ &= 2\pi i \lim_{\epsilon\to 0^+}[Resf(k_z''' = \nu_s+i\epsilon) + Resf(k_z''' = ik_s)] \\ &= \frac{-\pi i}{-k_s^2-\nu_s^2}[\frac{e^{i\nu_s(z''-z_s)}}{\nu_s} - \frac{e^{-k_s(z''-z_s)}}{ik_s}]. \end{aligned}$$

Substituting the above results into equation (24) and integrating over k_z', x'', k_x'' and k_z'' we finally have

$$\begin{aligned} \tilde{I'} &= 2\pi^4 i \frac{1}{2\pi^6}\iiint dx'dz'dz'' e^{-ik_g x'}\frac{e^{i\nu_g(z'-z_g)}}{\nu_g}\frac{1}{\nabla'^2} \\ &\quad \times \frac{e^{ik_s x'}e^{i\nu_s|z'-z''|}}{\nu_s} e^{ik_s x'}\frac{-\pi i}{-k_s^2-\nu_s^2}[\frac{e^{i\nu_s(z''-z_s)}}{\nu_s} - \frac{e^{-k_s(z''-z_s)}}{ik_s}]. \end{aligned} \tag{25}$$

Comparing equation (22) with equation (25), we see that changing the order of integration has produced different results for the outer G_0. Then, which way should $\frac{1}{\nabla^2}$ act on a Green's function? To answer this, we must further examine the operator $\frac{1}{\nabla^2}$. It is the inverse operator of ∇^2, an integral operator. We think of Poisson's equation in 2D:

$$\nabla^2\varphi(x,z) = \rho(x,z), \tag{26}$$

applying $\frac{1}{\nabla^2}$ on both sides of the Poisson's equation, we have

$$\frac{1}{\nabla^2}\cdot\nabla^2\varphi(x,z) = \varphi(x,z) = \frac{1}{\nabla^2}\rho(x,z). \tag{27}$$

That is to say, if we are looking for $\frac{1}{\nabla^2}\rho(x,z)$, we can solve the Poisson's equation for $\varphi(x,z)$. And the Green's function for Poisson's equation satisfies:

$$\nabla^2 G_0(x,z;x',z') = \delta(x-x')\delta(z-z'). \tag{28}$$

Fourier transforming over x and z,

$$(-k_x^2-k_z^2)\widetilde{G_0}(k_x,k_z;x',z') = e^{-ik_x x'}e^{-ik_z z'}, \tag{29}$$

and the Green's function for Poisson's equation is

$$G_0(x,z;x',z') = \frac{1}{(2\pi)^2}\iint dk_x dk_z \frac{e^{ik_x(x-x')}e^{ik_z(z-z')}}{-k_x^2-k_z^2}, \tag{30}$$

so,

$$\begin{aligned}\frac{1}{\nabla^2}\rho(x,z) &= \varphi(x,z) = \iint dx'dz' G_0(x,z;x',z')\rho(x',z') \\ &= \frac{1}{(2\pi)^2}\iiiint dx'dz'dk_x dk_z \frac{e^{ik_x(x-x')}e^{ik_z(z-z')}}{-k_x^2-k_z^2}\rho(x',z'). \end{aligned}\tag{31}$$

This is an explicit expression of $\frac{1}{\nabla^2}$ acting on ρ. We next apply this to the outer Green's function in equation (21), resulting in

$$\frac{1}{\nabla''^2}e^{ik_s x''}\frac{e^{i\nu_s(z''-z_s)}}{\nu_s},$$

which is equivalent to solving the following equation

$$\nabla''^2\varphi(x'',z'',z_s) = e^{ik_s x''}\frac{e^{i\nu_s(z''-z_s)}}{\nu_s}, \tag{32}$$

and,

$$\varphi(x'',z'',z_s) = \frac{1}{(2\pi)^2}\iiiint dx'dz'dk_x''dk_z''\frac{e^{ik_x''(x''-x')}e^{ik_z''(z''-z')}}{-k_x''^2-k_z''^2}e^{ik_s x'}\frac{e^{i\nu_s(z'-z_s)}}{\nu_s}. \tag{33}$$

Integrating over x' and then k_x'', we have

$$\varphi(x'',z'',z_s) = \frac{1}{2\pi}\iint dz'dk_z''\frac{e^{ik_z''(z''-z')}}{-{k_s}^2-k_z''^2}\frac{e^{i\nu_s(z'-z_s)}}{\nu_s}e^{ik_s x''}. \tag{34}$$

Integrating over z' and then k_z'', we finally have

$$\begin{aligned}\frac{1}{\nabla''^2}e^{ik_s x''}\frac{e^{i\nu_s(z''-z_s)}}{\nu_s} &= \varphi(x'',z'',z_s) \\ &= \frac{1}{-{k_s}^2-{\nu_s}^2}e^{ik_s x''}\frac{e^{i\nu_s(z''-z_s)}}{\nu_s}, \end{aligned}\tag{35}$$

which is consistent with what we have in equation (21).
We now deal with the middle Green's function term, in equation (22). We have

$$\frac{1}{\nabla'^2}\frac{e^{ik_s x'}e^{i\nu_s|z'-z''|}}{\nu_s}.$$

According to the previous explanation, this is equivalent to solving the equation

$$\nabla'^2\varphi(x',z',z'') = \frac{e^{ik_s x'}e^{i\nu_s|z'-z''|}}{\nu_s}. \tag{36}$$

For the purpose of integration, renaming the variable z'' as z_0,

$$\varphi(x',z',z_0)=\frac{1}{(2\pi)^2}\iiiint dx''dz''dk'_xdk'_z\frac{e^{ik'_x(x'-x'')}e^{ik'_z(z'-z'')}}{-{k'_x}^2-{k'_z}^2}\frac{e^{ik_sx''}e^{i\nu_s|z''-z_0|}}{\nu_s}. \tag{37}$$

Integrating over x'' and then k'_x,

$$\varphi(x',z',z_0)=\frac{1}{2\pi}\iint dz''dk'_z\frac{e^{ik'_z(z'-z'')}}{-k_s^2-{k'_z}^2}\frac{e^{ik_sx'}e^{i\nu_s|z''-z_0|}}{\nu_s}, \tag{38}$$

and integrating over k'_z using residue theorem,

$$\begin{aligned}
\varphi(x',z',z_0) &= -i\int dz''\frac{e^{-k_s|z'-z''|}e^{i\nu_s|z''-z_0|}}{2ik_s\nu_s}e^{ik_sx'}\\
&= -\frac{e^{ik_sx'}}{2k_s\nu_s}\int dz''e^{-k_s|z'-z''|}e^{i\nu_s|z''-z_0|}\\
&= -\frac{e^{ik_sx'}}{2k_s\nu_s}\int dz''[e^{-k_s(z'-z'')}H(z'-z'')+e^{-k_s(z''-z')}H(z''-z')]\\
&\quad\times[e^{i\nu_s(z''-z_0)}H(z''-z_0)+e^{i\nu_s(z_0-z'')}H(z_0-z'')]\\
&= -\frac{e^{ik_sx'}}{2k_s\nu_s}[e^{-k_sz'-i\nu_sz_0}\int dz''e^{(k_s+i\nu_s)z''}H(z'-z'')H(z''-z_0)\\
&\quad+e^{-k_sz'+i\nu_sz_0}\int dz''e^{(k_s-i\nu_s)z''}H(z'-z'')H(z_0-z'')\\
&\quad+e^{k_sz'-i\nu_sz_0}\int dz''e^{(-k_s+i\nu_s)z''}H(z''-z')H(z''-z_0)\\
&\quad+e^{k_sz'+i\nu_sz_0}\int dz''e^{(-k_s-i\nu_s)z''}H(z''-z')H(z_0-z'')].
\end{aligned} \tag{39}$$

We calculate the four terms separately without the coefficient, for the first term, calling which I_1, $z'>z''>z_0$,

$$\begin{aligned}
I_1 &= e^{-k_sz'-i\nu_sz_0}\int_{z_0}^{z'}dz''e^{(k_s+i\nu_s)z''}\\
&= e^{-k_sz'-i\nu_sz_0}\frac{e^{k_sz'+i\nu_sz'}-e^{k_sz_0+i\nu_sz_0}}{k_s+i\nu_s}\\
&= \frac{1}{k_s+i\nu_s}[e^{i\nu_s(z'-z_0)}-e^{-k_s(z'-z_0)}],
\end{aligned} \tag{40}$$

since $z'>z_0$, we can write

$$I_1=\frac{1}{k_s+i\nu_s}[e^{i\nu_s(z'-z_0)}-e^{-k_s(z'-z_0)}]H(z'-z_0).$$

For the fourth term, calling which I_4, $z_0>z''>z'$,

$$I_4 = e^{k_sz'+i\nu_sz_0}\int_{z'}^{z_0}dz''e^{(-k_s-i\nu_s)z''}$$

$$
\begin{aligned}
&= e^{k_s z' + i\nu_s z_0} \frac{e^{-k_s z_0 - i\nu_s z_0} - e^{-k_s z' - i\nu_s z'}}{-k_s - i\nu_s} \\
&= \frac{1}{k_s + i\nu_s}[e^{i\nu_s(z_0 - z')} - e^{-k_s(z_0 - z')}], \qquad (41)
\end{aligned}
$$

since $z_0 > z'$, we can write

$$
I_4 = \frac{1}{k_s + i\nu_s}[e^{i\nu_s(z_0 - z')} - e^{-k_s(z_0 - z')}]H(z_0 - z').
$$

Then,

$$
I_1 + I_4 = \frac{1}{k_s + i\nu_s}[e^{i\nu_s|z' - z_0|} - e^{-k_s|z' - z_0|}]. \qquad (42)
$$

Next, we calculate the second term (I_2)and the third term (I_3) together

$$
\begin{aligned}
I_2 + I_3 &= H(z' - z_0)[e^{-k_s z' + i\nu_s z_0} \int_{-\infty}^{z_0} dz'' e^{(k_s - i\nu_s)z''} + e^{k_s z' - i\nu_s z_0} \int_{z'}^{\infty} dz'' e^{(-k_s + i\nu_s)z''}] \\
&\quad + H(z_0 - z')[e^{-k_s z' + i\nu_s z_0} \int_{-\infty}^{z'} dz'' e^{(k_s - i\nu_s)z''} + e^{k_s z' - i\nu_s z_0} \int_{z_0}^{\infty} dz'' e^{(-k_s + i\nu_s)z''}] \\
&= H(z' - z_0)[e^{-k_s z' + i\nu_s z_0} \frac{e^{(k_s - i\nu_s)z_0}}{k_s - i\nu_s} + e^{k_s z' - i\nu_s z_0} \frac{e^{-(k_s - i\nu_s)z'}}{k_s - i\nu_s}] \\
&\quad + H(z_0 - z')[e^{-k_s z' + i\nu_s z_0} \frac{e^{(k_s - i\nu_s)z'}}{k_s - i\nu_s} + e^{k_s z' - i\nu_s z_0} \frac{e^{-(k_s - i\nu_s)z_0}}{k_s - i\nu_s}] \\
&= \frac{1}{k_s - i\nu_s}[H(z' - z_0)(e^{-k_s(z' - z_0)} + e^{i\nu_s(z' - z_0)}) + H(z_0 - z')(e^{-k_s(z_0 - z')} + e^{i\nu_s(z_0 - z')})] \\
&= \frac{1}{k_s - i\nu_s}[e^{i\nu_s|z' - z_0|} + e^{-k_s|z' - z_0|}]. \qquad (43)
\end{aligned}
$$

Changing the variable z_0 back to z'', and collecting the four terms,

$$
\begin{aligned}
\frac{1}{\nabla'^2} \frac{e^{ik_s x'} e^{i\nu_s|z' - z''|}}{\nu_s} &= \varphi(x', z', z'') = I_1 + I_2 + I_3 + I_4 \\
&= -\frac{e^{ik_s x'}}{2k_s\nu_s}[\frac{1}{k_s + i\nu_s}(e^{i\nu_s|z' - z''|} - e^{-k_s|z' - z''|}) \\
&\quad + \frac{1}{k_s - i\nu_s}(e^{i\nu_s|z' - z''|} + e^{-k_s|z' - z''|})] \\
&= -\frac{e^{ik_s x'}}{k_s^2 + \nu_s^2}[\frac{e^{i\nu_s|z' - z''|}}{\nu_s} - \frac{e^{-k_s|z' - z''|}}{ik_s}]. \qquad (44)
\end{aligned}
$$

We obtained the same result as Zhang had for the operator $\frac{1}{\nabla^2}$ acting on the middle $\hat{G}_0$ (Zhang, 2006). This further analysis provides another perspective and confirms the previous elastic derivation and results as well.

Conclusion and Future plan

In this note, 1. we made a brief summary of the previous work involving 1D three parameter elastic medium by Zhang; for the first time, Zhang provided an explicit and direct set of equations for the non-linear estimates, which clearly express the requirements for all four components of data to do the inversion. 2. we also studied and discussed the integral operator $\frac{1}{\nabla^2}$ acting on Green's function for the non-linear terms, and provided a further understanding and explication.

Different media may have small differences in their medium properties, which if not correctly estimated, can affect adversely the decision to drill. Linear terms may not be able to calculate small changes accurately enough. Therefore non-linear terms play a significant role in better estimating these medium properties. As we were led by Zhang to the first non-linear direct equations for the 1D three parameter elastic case, further progress on solving the equations for the non-linear terms is going to be carried out. Mathematically, there could be many ways to solve these equations, but we are trying to find a solution which is guided by the inverse scattering series. Although the previous work is mainly on 1D media, the procedure can be extended to multi-D. The future work will also examine the multi-D generalization.

Acknowledgements

We are grateful to all M-OSRP sponsors for long-term encouragement and support in this research. All members in M-OSRP are thanked for the help of finishing this paper and valuable discussions in this research program.

Appendix A

$\widetilde{D}^{PS}$,$\widetilde{D}^{SP}$ and $\widetilde{D}^{SS}$ in the $(k_s, z_s; k_g, z_g; \omega)$ domain; and the coefficients before every linear quantity $(a_\gamma^{(1)}, a_\rho^{(1)}, a_\mu^{(1)})$– different incidence angle θ

$$\widetilde{D}^{PS}(\nu_g,\eta_g) = -\frac{1}{4}(\frac{k_g}{\nu_g}+\frac{k_g}{\eta_g})\tilde{a}_\rho^{(1)}(-\nu_g-\eta_g) - \frac{{\beta_0}^2}{2\omega^2}k_g(\nu_g+\eta_g)(1-\frac{{k_g}^2}{\nu_g\eta_g})\tilde{a}_\mu^{(1)}(-\nu_g-\eta_g), \tag{45}$$

where,

$$k_g = \frac{\omega}{\beta_0}\sin\theta^{PS},$$
$$\nu_g = \frac{\omega}{\alpha_0}\sqrt{1-\frac{\alpha_0^2}{\beta_0^2}\sin\theta^{PS}},$$
$$\eta_g = \frac{\omega}{\beta_0}\cos\theta^{PS},$$

$$\widetilde{D}^{SP}(\nu_g,\eta_g) = \frac{1}{4}(\frac{k_g}{\nu_g}+\frac{k_g}{\eta_g})\tilde{a}_\rho^{(1)}(-\nu_g-\eta_g) + \frac{{\beta_0}^2}{2\omega^2}k_g(\nu_g+\eta_g)(1-\frac{{k_g}^2}{\nu_g\eta_g}\tilde{a}_\mu^{(1)}(-\nu_g-\eta_g), \tag{46}$$

where,

$$k_g = \frac{\omega}{\alpha_0}\sin\theta^{SP},$$
$$\nu_g = \frac{\omega}{\alpha_0}\cos\theta^{SP},$$
$$\eta_g = \frac{\omega}{\beta_0}\sqrt{1-\frac{\beta_0^2}{\alpha_0^2}\sin\theta^{SP}},$$

$$\widetilde{D}^{SS}(k_g,\eta_g) = -\frac{1}{4}(1-\frac{{k_g}^2}{{\eta_g}^2})\tilde{a}_\rho^{(1)}(-2\nu_g) - (\frac{{\eta_g}^2+{k_g}^2}{4{\eta_g}^2} - \frac{{k_g}^2}{{\eta_g}^2+{k_g}^2}\tilde{a}_\mu^{(1)}(-2\eta_g). \tag{47}$$

where,

$$k_g = \frac{\omega}{\beta_0}\sin\theta^{SS},$$
$$\nu_g = \frac{\omega}{\beta_0}\cos\theta^{SS}.$$

Appendix B

Response of incident compressional wave on a planar elastic interface

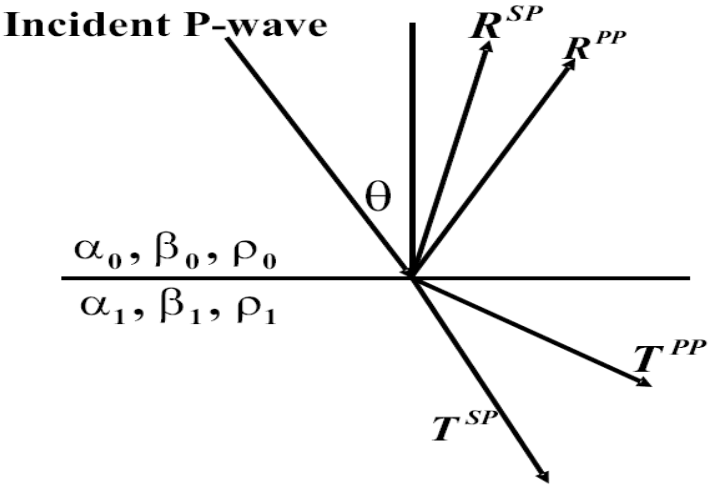

Figure 1: *α_0, β_0 and ρ_0 are the compressional wave velocity, shear wave velocity and density of the upper layer, respectively; α_1, β_1 and ρ_1 denote the compressional wave velocity, shear wave velocity and density of the lower layer, R^{PP}, R^{SP}, T^{PP} and T^{SP} denote the coefficients of the reflected compressional wave, the reflected shear wave, the transmitted compressional wave and the transmitted shear wave,respectively (Foster et al., 1997).*

Appendix C

The perturbation V

In the actual medium, the 2D elastic wave equation is (Weglein and Stolt, 1992)

$$L\vec{u} \equiv [\rho\omega^2 \begin{pmatrix} 1 & 0 \\ 0 & 1 \end{pmatrix} + \begin{pmatrix} \partial_1\gamma\partial_1 + \partial_2\mu\partial_2 & \partial_1(\gamma - 2\mu)\partial_2 + \partial_2\mu\partial_1 \\ \partial_2(\gamma - 2\mu)\partial_1 + \partial_1\mu\partial_2 & \partial_2\gamma\partial_2 + \partial_1\mu\partial_1 \end{pmatrix}] \begin{bmatrix} u_1 \\ u_2 \end{bmatrix} = \vec{f},$$

$\vec{u}$ = displacement
ρ = density,
γ = bulk modulus ($\equiv \rho\alpha^2$ where $alpha$ = P-wave velocity),
μ = shear modulus ($\equiv \rho\beta^2$ where $alpha$ = S-wave velocity),
ω temporal frequency (angular), ∂_1 and ∂_2 denote the derivative over x and z, respectively, and $\vec{f}$ is the source term.

$$\begin{aligned} V &\equiv L_0 - L \\ &= -\rho_0 \begin{bmatrix} a_\rho\omega^2 + \alpha_0^2 a_\gamma\partial_1^2 + \beta_0^2\partial_2 a_\mu\partial_2 & (\alpha_0^2 a_\gamma - 2\beta_0^2 a_\mu)\partial_1\partial_2 + \beta_0^2\partial_2 a_\mu\partial_1 \\ \partial_2(\alpha_0^2 a_\gamma - 2\beta_0^2 a_\mu)\partial_1 + \beta_0^2 a_\mu\partial_1\partial_2 & a_\rho\omega^2 + \alpha_0^2\partial_2 a_\gamma\partial_2 + \beta_0^2 a_\mu\partial_1^2 \end{bmatrix}. \end{aligned}$$

In PS domain:

$$\hat{V} = \Pi V \Pi^{-1}\Gamma_0^{-1} = \begin{pmatrix} \hat{V}^{PP} & \hat{V}^{PS} \\ \hat{V}^{SP} & \hat{V}^{SS} \end{pmatrix}.$$

$$\hat{V}_1^{PP} = -\nabla^2 a_\gamma^{(1)} - \frac{\omega^2}{alpha_0^2}(a_\rho^{(1)}\partial_1^2 + \partial_2 a_\rho^{(1)}\partial_2)\frac{1}{\nabla^2} - [-2\partial_2^2 a_{mu}^{(1)}\partial_1^2 - 2\partial_1^2 a_{mu}^{(1)}\partial_2^2 + 4\partial_1^2\partial_2 a_{mu}^{(1)}\partial_2]\frac{1}{\nabla^2},$$

$$\hat{V}_1^{PS} = \frac{alpha_0^2}{\beta_0^2}[\frac{\omega^2}{alpha_0^2}(\partial_1 a_\rho^{(1)}\partial_2 - \partial_2 a_\rho^{(1)}\partial_1) + 2\partial_1\partial_2 a_{mu}^{(1)}(\partial_2^2 - \partial_1^2) - 2(\partial_2^2 - \partial_1^2)a_{mu}^{(1)}\partial_2\partial_1]\frac{1}{\nabla^2},$$

$$\hat{V}_1^{SP} = -[\frac{\omega^2}{alpha_0^2}(\partial_1 a_\rho^{(1)}\partial_2 - \partial_2 a_\rho^{(1)}\partial_1) + 2\partial_1\partial_2 a_{mu}^{(1)}(\partial_2^2 - \partial_1^2) - 2(\partial_2^2 - \partial_1^2)a_{mu}^{(1)}\partial_2\partial_1]\frac{1}{\nabla^2},$$

$$\hat{V}_1^{SS} = -\frac{alpha_0^2}{\beta_0^2}[\frac{\omega^2}{alpha_0^2}(a_\rho^{(1)}\partial_1^2 + \partial_2 a_\rho^{(1)}\partial_2) + (\partial_2^2 - \partial_1^2)a_{mu}^{(1)}(\partial_2^2 - \partial_1^2) - \partial_1\partial_2 a_{mu}^{(1)}\partial_1\partial_2]\frac{1}{\nabla^2}.$$

References

Foster, D. J., R. G. Keys, and D. P. Schmitt. "Detecting subsurface hydrocarbons with elastic wavefields." *Inverse Problems in Wave Propagation* Volume 90 of the IMA Volumes in Mathematics and its Application (1997): 195–217.

Matson, K. H. *An inverse-scattering series method for attenuating elastic multiples from multicomponent land and ocean bottom seismic data.* PhD thesis, University of British Columbia, 1997.

Shaw, S. A., A. B. Weglein, D. J. Foster, K. H. Matson, and R. G. Keys. "Isolation of a leading order depth imaging series and analysis of its convergence properties." *Journal of Seismic Exploration* 2 (November 2004): 157–195.

Weglein, A. B., F. V. Araújo, P. M. Carvalho, R. H. Stolt, K. H. Matson, R. T. Coates, D. Corrigan, D. J. Foster, S. A. Shaw, and H. Zhang. "Inverse Scattering Series and Seismic Exploration." *Inverse Problems* (2003): R27–R83.

Weglein, A. B., D. J. Foster, K. H. Matson, S. A. Shaw, P. M. Carvalho, and D. Corrigan. "Predicting the correct spatial location of reflectors without knowing or determining the precise medium and wave velocity: initial concept, algorithm and analytic and numerical example." *Journal of Seismic Exploration* 10 (2002): 367–382.

Weglein, Arthur B. and R.H. Stolt. "Approaches on linear and non-linear migration-inversion. Personal Communication." (1992).

Zhang, H. *Direct non-linear acoustic and elastic inversion: Towards fundamentally new comprehensive and realistic target identification.* PhD thesis, University of Houston, 2006.

Zhang, H. and A.B. Weglein. "The inverse scattering series for tasks associated with primaries: depth imaging and direct non-linear inversion of 1D variable velocity and density acoustic media." *SEG Technical Program Expanded Abstracts.* 2005, 1705–1708.

Zhang, H. and A.B. Weglein. "Direct non-linear inversion of multi-parameter 1D elastic media using the inverse scattering series." *SEG/Houston 2005 Annual Meeting.* 2006, 284–311.

Direct non-linear inversion of 1D acoustic media using inverse scattering subseries

H. Zhang[†]and A B. Weglein
[†]Presently at ConocoPhillips

Abstract

A task specific multi-parameter [1] direct non-linear inversion subseries of the inverse scattering series is derived and tested for a velocity and density varying 1D acoustic medium. There are various linear estimate solutions in the literature (e.g., Raz, 1981, Clayton and Stolt, 1981, Stolt and Weglein, 1985) that assume an adequate estimate of medium properties above any given target reflector. However, this is the first seismic inversion method that: (1) neither assumes nor requires an adequate estimate of medium properties above any reflector, and (2) does not assume that the changes in physical properties satisfies a linear relationship to the reflection data at the target, and (3) the most importantly the method stands alone in being a direct inversion. The meaning of direct is that there are formulas that explicitly solve for and directly output these physical properties, without e.g., search algorithms and optimization schemes, and proxies that typically characterize indirect methods. Numerical test results indicate that one term beyond linear provides added value beyond standard linear techniques and common practice for estimating changes in physical properties at a target. Imaging and inversion for a two parameter medium directly in terms of data and reference properties is much more complicated than that of the one parameter case. The message delivered from this study extends and progresses beyond the earlier one communicated in a one parameter velocity only medium, and serves as a necessary and critical step in, and guide for, the development of the yet more complicated and realistic elastic isotropic direct depth imaging and non-linear parameter estimation. Three important issues are identified and/or further progressed within the multi-parameter acoustic context and scope of this paper: (1) the concept of purposeful perturbation, (2) how the inverse series addresses the phenomena in linear inversion known as leakage, and (3) special parameter for linear inversion that is immune to linear inversion leakage, and the very significant implication of the latter result for direct depth imaging without the velocity model, are presented and discussed by analyzing these new two parameter non-linear direct inversion formulas and methods.

Introduction

The objective of seismic exploration is to determine the location (imaging) and mechanical properties (inversion) of subsurface targets to identify hydrocarbon resources in the earth using recorded data. The inverse scattering series has a tremendous generality and comprehensiveness allowing many distinct traditional processing objectives to be achieved within a single framework, but without the traditional need to provide information about the properties that govern actual wave propagation in the earth. It begins with scattering theory, which is the relationship between the

[1]Within the context and scope of this paper, a multi-parameter medium is an acoustic medium where the velocity and/or density can vary.

perturbation or alteration in a medium's properties and the concomitant perturbation or change in the wave field. The relationship between those two changes is always non-linear. Any change in a medium will result in a change in the wave-field that is non-linearly related to that physical property change.

In this paper we examine the relationship between the perturbation in a medium and the perturbation in a wave field for the case of a 1D variable velocity and variable density acoustic medium. We assume the original unperturbed medium is a homogeneous whole-space. We further assume that free surface and internal multiples have been removed (see, e.g., Weglein et al., 2003). And we assume that we are recording primaries, and our objectives are to: (1) locate reflectors and (2) determine medium properties of the actual medium. In this paper we present: (1) the first derivation of equations to directly achieve those two distinct objectives for a one dimensional velocity and density varying acoustic medium, and (2) we then reduce this general formalism to the special case of a single horizontal reflector, where the acoustic medium above the reflector is known, but the objective is to determine the acoustic properties of the half-space below the reflector. For the latter single reflector case, the recorded data have a non-linear relationship with the property changes across this reflector. Current inversion methods include: (1) the linear approximation (e.g., Clayton and Stolt, 1981; Weglein and Stolt, 1992) which is often useful, especially in the presence of small earth property changes across the boundary and/or small angle reflections, and (2) indirect model matching methods with global searching (e.g., Tarantola et al., 1984; Sen and Stoffa, 1995) which define an objective function assumed to be minimized when the best fitting model is obtained. The assumptions of the former methods (like the small contrast assumptions) are often violated in practice and can cause erroneous predictions; the latter category usually involves a significant and often daunting computation effort (especially in multi-D cases) and/or sometimes have reported erroneous or ambiguous results.

In this paper, a more comprehensive multi-parameter multi-dimensional direct non-linear inversion framework is developed based on the inverse scattering task-specific subseries (see, e.g., Weglein et al., 2003). In order to provide more accurate and reliable target identification especially with large contrast, large angle target geometry, we isolated the inverse scattering subseries responsible for non-linear amplitude inversion of data.

The original inverse scattering series research aimed at separating imaging and inversion tasks on primaries was developed for a 1D acoustic one parameter case (constant density medium, only velocity variable in depth) and a plane wave at normal incidence (Weglein et al., 2002; Shaw et al., 2003). In this paper we move a step closer to seismic exploration relevance by extending that earlier work to a multi-parameter case — two parameter case (velocity and density vary vertically in depth) and allowing for point sources and receivers over a 1D acoustic medium. Clayton and Stolt (1981) gave a two parameter *linear* inversion solution for *2D* acoustic media (velocity and density vary both vertically and laterally). In this paper, we use the same parameters but concentrate on *1D* acoustic media to derive the direct *non-linear* inversion solution. In the application of the direct *non-linear* inverse algorithm, we move one step each time (e.g., from one parameter 1D acoustic case to two parameter 1D acoustic case, or to one parameter 2D acoustic case, instead of 'jumping' directly to two parameter 2D acoustic case) so that we can solve the problem step by step and learn lessons from each step which would guide us to step further towards our goal of greater

realism and increased reliable prediction. For one parameter 1D and 2D acoustic media, some work on direct non-linear imaging with reference velocity is presented by Shaw (2005) and Liu et al. (2005). It has been shown in this paper that imaging and inversion for two parameter medium are much more complicated compared to one parameter case, although it seems like just simply adding one parameter. Examples of the new inverse issues that arise in a two parameter world (and needed responses) that have no one parameter analogue are leakage, purposeful perturbation for that issue, and the identification of the special parameter for inversion that avoids leakage, and the conceptual insights that this understanding provides for our campaign to address pressing imaging and inversion challenges.

For the direct non-linear inversion solution obtained in this paper, the tasks for imaging-only and inversion-only terms are separated. Tests with analytic data indicate significant added value for parameter predictions, beyond linear estimates, in terms of both the proximity to actual value and the increased range of angles over which the improved estimates are useful.

A closed form of the inversion terms for the one-interface case is also obtained. This closed form might be useful in predicting the precritical data using the postcritical data.

A special parameter Δc ($\Delta c = c - c_0$) (P-wave velocity change across an interface) is also found. Its Born inversion $(\Delta c)_1$ always has the right sign. That is, the sign of $(\Delta c)_1$ is always the same as that of Δc. In practice, it could be very useful to know whether the velocity increases or decreases across the interface. After changing parameters, from α (relative changes in P-wave bulk modulus) and β (relative changes in density) to velocity and β, another form of the non-linear solution is obtained. There is no leakage correction (please see details in the section on three important messages) in this solution. This new form clearly indicates that the imaging terms care only about velocity errors. The mislocation is due to the wrong velocity. This is suggestive of possible generalization to multi-D medium, and also of possible model-type independent imaging which only depends on velocity changes.

The following section is a brief introduction of the inverse scattering subseries. We then gave the one dimensional multi-parameter acoustic derivation in detail, and that is followed by the numerical tests for the single reflector case. We also provided a further discussion about the special physical non-leaking acoustic parameter.

Inverse scattering subseries

Scattering theory relates the perturbation (the difference between the reference and actual medium properties) to the scattered wave field (the difference between the reference medium's and the actual medium's wave field). It is therefore reasonable that in discussing scattering theory, we begin with the basic wave equations governing the wave propagation in the actual and reference medium, respectively [2],

$$LG = \delta, \tag{1}$$

[2]In this introductory math development, we follow closely Weglein et al. (1997); Weglein et al. (2002); Weglein et al. (2003).

$$L_0 G_0 = \delta, \tag{2}$$

where L and L_0 are respectively the differential operators that describe wave propagation in the actual and reference medium, and G and G_0 are the corresponding Green's operators. The δ on the right hand side of both equations is a Dirac delta operator and represents an impulsive source.

The perturbation is defined as $V = L_0 - L$. The Lippmann-Schwinger equation,

$$G = G_0 + G_0 V G, \tag{3}$$

relates G, G_0 and V (see, e.g., Taylor, 1972). Iterating this equation back into itself generates the forward scattering series

$$G = G_0 + G_0 V G_0 + G_0 V G_0 V G_0 + \cdots . \tag{4}$$

Then the scattered field $\psi_s \equiv G - G_0$ can be written as

$$\begin{aligned} \psi_s &= G_0 V G_0 + G_0 V G_0 V G_0 + \cdots \\ &= (\psi_s)_1 + (\psi_s)_2 + \cdots , \end{aligned} \tag{5}$$

where $(\psi_s)_n$ is the portion of ψ_s that is n^{th} order in V. The measured values of ψ_s are the data, D, where

$$D = (\psi_s)_{ms} = (\psi_s)_{\text{on the measurement surface}}.$$

In the inverse scattering series, expanding V as a series in orders of D,

$$V = V_1 + V_2 + V_3 + \cdots , \tag{6}$$

where the subscript "i" in V_i (i=1, 2, 3, ...) denotes the portion of V i-th order in the data. Substituting Eq. (6) into Eq. (5), and evaluating Eq. (5) on the measurement surface yields

$$D = [G_0(V_1 + V_2 + \cdots)G_0]_{ms} + [G_0(V_1 + V_2 + \cdots)G_0(V_1 + V_2 + \cdots)G_0]_{ms} + \cdots . \tag{7}$$

Setting terms of equal order in the data equal, leads to the equations that determine V_1, V_2, ... directly from D and G_0.

$$D = [G_0 V_1 G_0]_{ms}, \tag{8}$$

$$0 = [G_0 V_2 G_0]_{ms} + [G_0 V_1 G_0 V_1 G_0]_{ms}, \tag{9}$$

$$\begin{aligned} 0 =& [G_0 V_3 G_0]_{ms} + [G_0 V_1 G_0 V_2 G_0]_{ms} + [G_0 V_2 G_0 V_1 G_0]_{ms} \\ &+ [G_0 V_1 G_0 V_1 G_0 V_1 G_0]_{ms}, \end{aligned} \tag{10}$$

etc. Equations (8) $\sim$ (10) permit the sequential calculation of V_1, V_2, ..., and, hence, achieve full inversion for V (see Eq. 6) from the recorded data D and the reference wave field (i.e., the Green's operator of the reference medium) G_0. Therefore, the inverse scattering series is a multi-D inversion procedure that directly determines physical properties using only reflection data and reference medium information.

Derivation of α_1, β_1 and α_2, β_2

In this section, we will consider a 1D acoustic two parameter earth model (e.g. bulk modulus and density or velocity and density). We start with the 3D acoustic wave equations in the actual and reference medium (Clayton and Stolt, 1981; Weglein et al., 1997)

$$\left[\frac{\omega^2}{K(\mathbf{r})}+\nabla\cdot\frac{1}{\rho(\mathbf{r})}\nabla\right]G(\mathbf{r},\mathbf{r}_s;\omega)=\delta(\mathbf{r}-\mathbf{r}_s), \tag{11}$$

$$\left[\frac{\omega^2}{K_0(\mathbf{r})}+\nabla\cdot\frac{1}{\rho_0(\mathbf{r})}\nabla\right]G_0(\mathbf{r},\mathbf{r}_s;\omega)=\delta(\mathbf{r}-\mathbf{r}_s), \tag{12}$$

where $G(\mathbf{r},\mathbf{r}_s;\omega)$ and $G_0(\mathbf{r},\mathbf{r}_s;\omega)$ are respectively the free-space causal Green's functions that describe wave propagation in the actual and reference medium. $K=c^2\rho$, is P-wave bulk modulus, c is P-wave velocity and ρ is the density. The quantities with subscript "0" are for the reference medium, and those without the subscript are for the actual medium. The perturbation is

$$V=L_0-L=\frac{\omega^2\alpha}{K_0}+\nabla\cdot\frac{\beta}{\rho_0}\nabla, \tag{13}$$

where $\alpha=1-\frac{K_0}{K}$ and $\beta=1-\frac{\rho_0}{\rho}$ are the two parameters we choose to do the inversion. Assuming both ρ_0 and c_0 are constants, Eq. (12) becomes

$$\left(\frac{\omega^2}{c_0^2}+\nabla^2\right)G_0(\mathbf{r},\mathbf{r}_s;\omega)=\rho_0\delta(\mathbf{r}-\mathbf{r}_s). \tag{14}$$

For the 1-D case, the perturbation V has the following form

$$V(z,\nabla)=\frac{\omega^2\alpha(z)}{K_0}+\frac{1}{\rho_0}\beta(z)\frac{\partial^2}{\partial x^2}+\frac{1}{\rho_0}\frac{\partial}{\partial z}\beta(z)\frac{\partial}{\partial z}. \tag{15}$$

$V(z,\nabla)$, $\alpha(z)$ and $\beta(z)$ can be expanded respectively as

$$V(z,\nabla)=V_1(z,\nabla)+V_2(z,\nabla)+\cdots, \tag{16}$$

$$\alpha(z)=\alpha_1(z)+\alpha_2(z)+\cdots, \tag{17}$$

$$\beta(z)=\beta_1(z)+\beta_2(z)+\cdots. \tag{18}$$

Where the subscript "i" in V_i, α_i and β_i (i=1, 2, 3, ...) denote the portion of those quantities i-th order in the data.Then we have

$$V_1(z,\nabla)=\frac{\omega^2\alpha_1(z)}{K_0}+\frac{1}{\rho_0}\beta_1(z)\frac{\partial^2}{\partial x^2}+\frac{1}{\rho_0}\frac{\partial}{\partial z}\beta_1(z)\frac{\partial}{\partial z}, \tag{19}$$

$$V_2(z,\nabla)=\frac{\omega^2\alpha_2(z)}{K_0}+\frac{1}{\rho_0}\beta_2(z)\frac{\partial^2}{\partial x^2}+\frac{1}{\rho_0}\frac{\partial}{\partial z}\beta_2(z)\frac{\partial}{\partial z}, \tag{20}$$

$$\vdots$$

Substituting Eq. (19) into Eq. (8), we can get the linear solution for α_1 and β_1 in the frequency domain

$$\widetilde{D}(q_g,\theta,z_g,z_s) = -\frac{\rho_0}{4}e^{-iq_g(z_s+z_g)}\left[\frac{1}{\cos^2\theta}\widetilde{\alpha_1}(-2q_g) + (1-\tan^2\theta)\widetilde{\beta}_1(-2q_g)\right], \tag{21}$$

where the subscripts s and g denote source and receiver quantities respectively, and q_g, θ and $k = \omega/c_0$ shown in Fig. 1, have the following relations (Matson, 1997)

$$q_g = q_s = k\cos\theta,$$
$$k_g = k_s = k\sin\theta.$$

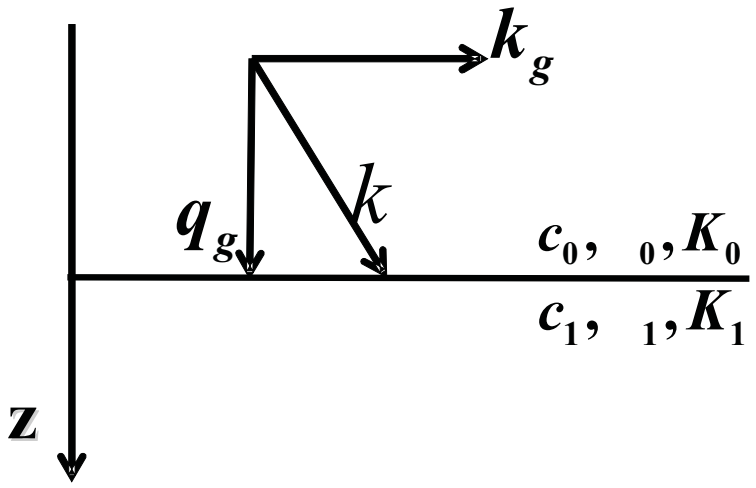

Figure 1: *The relationship between q_g, k_g and θ.*

Similarly, substituting Eq. (20) into Eq. (9), we can get the solution for $\alpha_2(z)$ and $\beta_2(z)$ as a function of $\alpha_1(z)$ and $\beta_1(z)$

$$\begin{aligned}\frac{1}{\cos^2\theta}\alpha_2(z) + (1-\tan^2\theta)\beta_2(z) = &-\frac{1}{2\cos^4\theta}\alpha_1^2(z) - \frac{1}{2}(1+\tan^4\theta)\beta_1^2(z) + \frac{\tan^2\theta}{\cos^2\theta}\alpha_1(z)\beta_1(z)\\ &-\frac{1}{2\cos^4\theta}\alpha_1'(z)\int_0^z dz'[\alpha_1(z') - \beta_1(z')]\\ &+\frac{1}{2}(\tan^4\theta - 1)\beta_1'(z)\int_0^z dz'[\alpha_1(z') - \beta_1(z')],\end{aligned} \tag{22}$$

where $\alpha_1'(z) = \frac{\mathrm{d}\alpha_1(\mathrm{z})}{\mathrm{dz}}$, $\beta_1'(z) = \frac{\mathrm{d}\beta_1(\mathrm{z})}{\mathrm{dz}}$.

The first two parameter direct non-linear inversion of 1D acoustic media for a 2D experiment has been obtained. As shown in Eq. (21) and Eq. (22), given two different angles θ, we can determine

α_1, β_1 and then α_2, β_2. For a single-interface example, it can be shown that only the first three terms on the right hand side contribute to parameter predictions, while the last two terms perform imaging in depth since they will be zero after the integration across the interface (see the section on three important messages). Therefore, in this solution, the tasks for imaging-only and inversion-only terms are separated.

For the $\theta = 0$ and constant density case, Eq. (22) reduces to the non-linear solution for 1D one parameter normal incidence case (e.g., Shaw, 2005)

$$\alpha_2(z) = -\frac{1}{2}\left[\alpha_1^2(z) + \alpha_1'(z)\int_{-\infty}^{z} dz'\alpha_1(z')\right]. \tag{23}$$

If another choice of free parameter other than θ (e.g., ω or k_h) is selected, then the functional form between the data and the first order perturbation Eq. (21) would change. Furthermore, the relationship between the first and second order perturbation Eq. (22) would, then, also be different, and new analysis would be required for the purpose of identifying specific task separated terms. Empirically, the choice of θ as free parameter (for a 1D medium) is particularly well suited for allowing a task separated identification of terms in the inverse series.

There are several important messages that exist in Eq. (21) and Eq. (22): (1) purposeful perturbation, (2) leakage, and (3) the special parameter for inversion. These three concepts will be discussed later in this paper. In Eq. (21), it seems simple and straightforward to use data at two angles in order to obtain α_1 and β_1. This is what we do in this paper. However, by doing this, it requires a whole new understanding of the definition of "the data". That is part of the discoveries of on-going research activities by Weglein et al. (2007). The imaging algorithm given by Liu et al. (2005) has been generalized to the two parameter case by Weglein et al. (2007) based on the understanding of Eq. (22).

A special case: one-interface model

In this section, we derive a closed form for the inversion-only terms. From this closed form, we can easily get the same inversion terms as those in Eqs. (21) and (22). We also show some numerical tests using analytic data. From the numerical results, we see how the corresponding non-linear terms contribute to the parameter predictions such as the relative changes in the P-wave bulk modulus $\left(\alpha = \frac{\Delta K}{K}\right)$, density $\left(\beta = \frac{\Delta\rho}{\rho}\right)$, impedance $\left(\frac{\Delta I}{I}\right)$ and velocity $\left(\frac{\Delta c}{c}\right)$.

Closed form for the inversion terms

1. Incident angle not greater than critical angle, i.e. $\theta \le \theta_c$

For a single interface example, the reflection coefficient has the following form (Keys, 1989)

$$R(\theta) = \frac{(\rho_1/\rho_0)(c_1/c_0)\sqrt{1-\sin^2\theta} - \sqrt{1-(c_1^2/c_0^2)\sin^2\theta}}{(\rho_1/\rho_0)(c_1/c_0)\sqrt{1-\sin^2\theta} + \sqrt{1-(c_1^2/c_0^2)\sin^2\theta}}. \tag{24}$$

After adding 1 on both sides of Eq. (24), we can get

$$1 + R(\theta) = \frac{2\cos\theta}{\cos\theta + (\rho_0/\rho_1)\sqrt{(c_0^2/c_1^2) - \sin^2\theta}}. \tag{25}$$

Then, using the definitions of $\alpha = 1 - \frac{K_0}{K_1} = 1 - \frac{\rho_0 c_0^2}{\rho_1 c_1^2}$ and $\beta = 1 - \frac{\rho_0}{\rho_1}$, Eq. (25) becomes

$$\frac{4R(\theta)}{(1+R(\theta))^2} = \frac{\alpha}{\cos^2\theta} + (1 - \tan^2\theta)\beta - \frac{\alpha\beta}{\cos^2\theta} + \beta^2\tan^2\theta, \tag{26}$$

which is the closed form we derived for the one interface two parameter acoustic inversion-only terms.

2. Incident angle greater than critical angle, i.e. $\theta > \theta_c$

For $\theta > \theta_c$, Eq. (24) becomes

$$R(\theta) = \frac{(\rho_1/\rho_0)(c_1/c_0)\sqrt{1-\sin^2\theta} - i\sqrt{(c_1^2/c_0^2)\sin^2\theta - 1}}{(\rho_1/\rho_0)(c_1/c_0)\sqrt{1-\sin^2\theta} + i\sqrt{(c_1^2/c_0^2)\sin^2\theta - 1}}. \tag{27}$$

Then, Eq. (25) becomes

$$1 + R(\theta) = \frac{2\cos\theta}{\cos\theta + i\,(\rho_0/\rho_1)\sqrt{\sin^2\theta - (c_0^2/c_1^2)}}, \tag{28}$$

which leads to the same closed form as Eq. (26)

$$\frac{4R(\theta)}{(1+R(\theta))^2} = \frac{\alpha}{\cos^2\theta} + (1 - \tan^2\theta)\beta - \frac{\alpha\beta}{\cos^2\theta} + \beta^2\tan^2\theta.$$

As we see, this closed form is valid for all incident angles.

In addition, for normal incidence ($\theta = 0$) and constant density ($\beta = 0$) media, the closed form Eq. (26) will be reduced to

$$\alpha = \frac{4R}{(1+R)^2}. \tag{29}$$

This represents the relationship between α and R for the one parameter 1D acoustic constant density medium and 1D normal incidence obtained in Innanen (2003). In this case, α becomes $1 - c_0^2/c_1^2$ and R becomes $(c_1 - c_0)/(c_1 + c_0)$.

3. Derivation of the inversion terms from the closed form

From the closed form Eq. (26), using Taylor expansion on the left hand side

$$\frac{1}{(1+R(\theta))^2} = \left[1 - R(\theta) + R^2(\theta) - \ldots\right]^2,$$

and setting the terms of equal order in the data equal, we have

$$\frac{\alpha_1}{\cos^2\theta} + (1 - \tan^2\theta)\beta_1 = 4R(\theta), \tag{30}$$

$$\frac{\alpha_2}{\cos^2\theta} + (1 - \tan^2\theta)\beta_2 = -\frac{1}{2}\frac{\alpha_1^2}{\cos^4\theta} - \frac{1}{2}(1 + \tan^4\theta)\beta_1^2 + \frac{\tan^2\theta}{\cos^2\theta}\alpha_1\beta_1. \tag{31}$$

For a one-interface example (in Fig. 2), Eqs. (21) and (22) will respectively reduce to the same form as Eqs. (30) and (31), which is shown below.

Assume the interface surface is at depth $z = a$, and suppose $z_s = z_g = 0$.

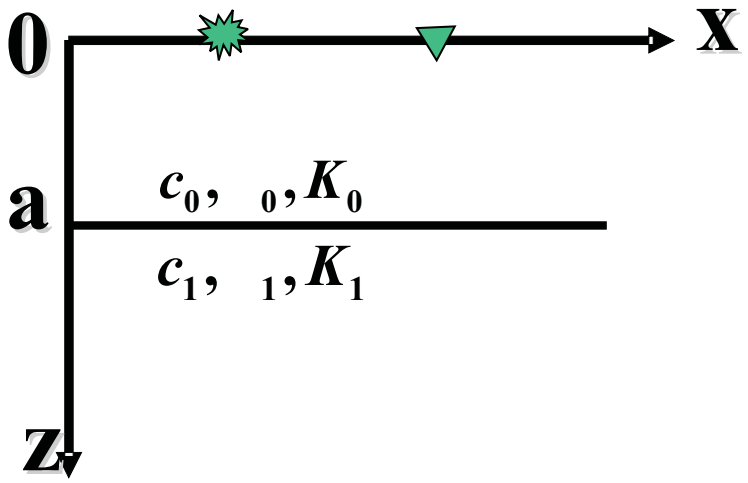

Figure 2: *1D one-interface acoustic model.*

Using the analytic data (Clayton and Stolt, 1981; Weglein et al., 1986),

$$\widetilde{D}(q_g, \theta) = \rho_0 R(\theta)\frac{e^{2iq_g a}}{4\pi i q_g}, \tag{32}$$

and substituting Eq. (32) into Eq. (21), after Fourier transformation over $2q_g$, for $z > a$ and fixed θ, we get

$$\frac{1}{\cos^2\theta}\alpha_1(z) + (1 - \tan^2\theta)\beta_1(z) = 4R(\theta)H(z - a). \tag{33}$$

Also, the non-linear solution Eq. (22) will reduce to

$$\begin{aligned}\frac{1}{\cos^2\theta}\alpha_2(z) + (1 - \tan^2\theta)\beta_2(z) = &-\frac{1}{2\cos^4\theta}\alpha_1^2(z) - \frac{1}{2}(1 + \tan^4\theta)\beta_1^2(z) \\ &+ \frac{\tan^2\theta}{\cos^2\theta}\alpha_1(z)\beta_1(z),\end{aligned} \tag{34}$$

The two equations Eqs. (33) and (34) agree with Eqs. (30) and (31), respectively.

Numerical tests

From Eq. (33), we choose two different angles to solve for α_1 and β_1

$$\beta_1(\theta_1,\theta_2) = 4\frac{R(\theta_1)\cos^2\theta_1 - R(\theta_2)\cos^2\theta_2}{\cos(2\theta_1)-\cos(2\theta_2)}, \tag{35}$$

$$\alpha_1(\theta_1,\theta_2) = \beta_1(\theta_1,\theta_2) + 4\frac{R(\theta_1)-R(\theta_2)}{\tan^2\theta_1-\tan^2\theta_2}. \tag{36}$$

Similarly, from Eq. (34), given two different angles we can solve for α_2 and β_2 in terms of α_1 and β_1

$$\begin{aligned}\beta_2(\theta_1,\theta_2) = \Bigg[&-\frac{1}{2}\alpha_1^2\left(\frac{1}{\cos^2\theta_1}-\frac{1}{\cos^2\theta_2}\right)+\alpha_1\beta_1\left(\tan^2\theta_1-\tan^2\theta_2\right)-\frac{1}{2}\beta_1^2\\ &\times\left(\cos^2\theta_1-\cos^2\theta_2+\frac{\sin^4\theta_1}{\cos^2\theta_1}-\frac{\sin^4\theta_2}{\cos^2\theta_2}\right)\Bigg]/\left[\cos(2\theta_1)-\cos(2\theta_2)\right],\end{aligned} \tag{37}$$

$$\begin{aligned}\alpha_2(\theta_1,\theta_2) =&\beta_2(\theta_1,\theta_2)+\Bigg[-\frac{1}{2}\alpha_1^2\left(\frac{1}{\cos^4\theta_1}-\frac{1}{\cos^4\theta_2}\right)+\alpha_1\beta_1\left(\frac{\tan^2\theta_1}{\cos^2\theta_1}-\frac{\tan^2\theta_2}{\cos^2\theta_2}\right)\\ &-\frac{1}{2}\beta_1^2\left(\tan^4\theta_1-\tan^4\theta_2\right)\Bigg]/\left(\tan^2\theta_1-\tan^2\theta_2\right);\end{aligned} \tag{38}$$

where α_1 and β_1 in Eqs. (37) and (38) denote $\alpha_1(\theta_1,\theta_2)$ and $\beta_1(\theta_1,\theta_2)$, respectively.

For a specific model, $\rho_0 = 1.0g/cm^3$, $\rho_1 = 1.1g/cm^3$, $c_0 = 1500m/s$ and $c_1 = 1700m/s$, in the following figures we give the results for the relative changes in the P-wave bulk modulus $\left(\alpha = \frac{\Delta K}{K}\right)$, density $\left(\beta = \frac{\Delta\rho}{\rho}\right)$, impedance $\left(\frac{\Delta I}{I}\right)$ and velocity $\left(\frac{\Delta c}{c}\right)$ corresponding to different pairs of θ_1 and θ_2.

From Fig. 3, we can see that when we add α_2 to α_1, the result is much closer to the exact value of α. Furthermore, the result is better behaved; i.e., the plot surface becomes flatter, over a larger range of precritical angles. Similarly, as shown in Fig. 4, the results of $\beta_1+\beta_2$ are much better than those of β_1. In addition, the sign of β_1 is wrong at some angles, while, the results for $\beta_1+\beta_2$ always have the right sign. So after including β_2, the sign of the density is corrected, which is very important in the earth identification, and also the results of $\frac{\Delta I}{I}$ (see Fig. 5) and $\frac{\Delta c}{c}$ (see Fig. 6) are much closer to their exact values respectively compared to the linear results.

Especially, the values of $\left(\frac{\Delta c}{c}\right)_1$ are always greater than zero, that is, the sign of $(\Delta c)_1$ is always positive, which is the same as that of the exact value Δc. We will further discuss this in the next section.

Three important messages

As mentioned before, in general, since the relationship between data and target property changes is non-linear, linear inversion will produce errors in target property prediction. When one actual

property change is zero, the linear prediction of the change can be non-zero. Also, when the actual change is positive, the predicted linear approximation can be negative. There is a special parameter for linear inversion of acoustic media, that never suffers the latter problem.

From Eq. (24) we can see that when $c_0 = c_1$, the reflection coefficient is independent of θ, then from the linear form Eq. (36), we have

$$\left(\frac{\Delta c}{c}\right)_1 = \frac{1}{2}(\alpha_1 - \beta_1) = 0 \text{ when } \Delta \text{c} = 0,$$

i.e., when $\Delta c = 0$, $(\Delta c)_1 = 0$. This generalizes to $(\Delta c)_1 > 0$ when $\Delta c > 0$, or $(\Delta c)_1 < 0$ when $\Delta c < 0$, as well. This can be shown mathematically (See Appendix B for details).

Therefore, we can, first, get the right sign of the relative change in P-wave velocity from the linear inversion $(\Delta c)_1$, then, get more accurate values by including non-linear terms.

Another interesting point is that the image does not move when the velocity does not change across an interface, i.e., $c_0 = c_1$, since, in this situation, the integrands of imaging terms $\alpha_1 - \beta_1$ in Eq. (22) are zero. We can see this more explicitly when we change the two parameters α and β to $\frac{\Delta c}{c}$ and β. Using the two relationships below (See details in Appendix A)

$$\left(\frac{\Delta c}{c}\right)_1 = \frac{1}{2}(\alpha_1 - \beta_1),$$

and

$$\left(\frac{\Delta c}{c}\right)_2 = \frac{1}{2}\left[\frac{1}{4}(\alpha_1 + \beta_1)^2 - \beta_1^2 + (\alpha_2 - \beta_2)\right],$$

rewriting Eq. (22) as

$$\begin{aligned}\frac{1}{\cos^2\theta}\left(\frac{\Delta c}{c}\right)_2(z) + \beta_2(z) =& \frac{\cos^2\theta - 2}{2\cos^4\theta}\left(\frac{\Delta c}{c}\right)_1^2(z) - \frac{1}{2}\beta_1^2(z) \\ &- \frac{1}{\cos^4\theta}\left(\frac{\Delta c}{c}\right)_1'(z)\int_0^z dz'\left(\frac{\Delta c}{c}\right)_1 \\ &- \frac{1}{\cos^2\theta}\beta_1'(z)\int_0^z dz'\left(\frac{\Delta c}{c}\right)_1. \end{aligned} \tag{39}$$

This equation indicates two important concepts. One is leakage: there is no leakage correction at all in this expression. Here the leakage means that, if the actual value of α (relative changes in P-wave bulk modulus) is zero, its linear approximation α_1 could be non-zero since α and β are coupled together (like the coupled term $\alpha_1\beta_1$ in Eq. 22) and α_1 could get leakage values from β_1. While in Eq. (39), no such coupled term is present at all and thus, if the actual changes in the velocity are zero, then its linear inversion $\left(\frac{\Delta c}{c}\right)_1$ would be zero and there would be no leakage from β_1. This leakage issue or coupled term has no analogue in the 1D one parameter acoustic case (Eq. 23) since in this case we only have one parameter and there is no other parameter to leak

into. In other words, in the one parameter (velocity) case, each 'jump' in the amplitude of the data (primaries only) corresponds to each wrong location with a wrong amplitude for the parameter predicted in the linear inverse step; while in the two parameter case of this paper, each 'jump' in the data no longer has the simple one-to-one relationship with the amplitude and location of the two parameters.

The other concept is purposeful perturbation. The integrand $\left(\frac{\Delta c}{c}\right)_1$ of the imaging terms clearly tells that if we have the right velocity, the imaging terms will automatically be zero even without doing any integration; otherwise, if we do not have the right velocity, these imaging terms would be used to move the interface closer to the right location from the wrong location. The conclusion from this equation is that the depth imaging terms depend only on the velocity errors.

Conclusion

In this paper, we derive the first two parameter direct non-linear inversion solution for 1D acoustic media with a 2D experiment. Numerical tests show that the terms beyond linearity in earth property identification subseries provide added value. Although the model we used in the numerical tests is simple, the potential within Eqs. (21) and (22) applies to more complex models since the inverse scattering series is a direct inversion procedure which inverts data directly without knowing the specific properties above the target.

As shown above, adding one parameter in the wave equation makes the problem much more complicated in comparison with the one parameter case. Three important concepts (purposeful perturbation, leakage and special parameter for inversion) have been discussed and how they relate to the linear and non-linear results for parameter estimation, addressing leakage, and imaging. Further progress on these issues is being carried out with on-going research.

The work presented in this paper is an important step forward for imaging without the velocity model, and target identification for the minimally acceptable elastic isotropic target. In this paper for the first time the general one-dimensional formalism for a depth varying acoustic medium is presented for depth imaging and direct parameter estimation, without needing to determine medium velocity properties that govern actual wave propagation for depth imaging, or what medium is above a target to be identified. The encouraging numerical results motivated us to move one step further — extension of our work to the isotropic elastic case (see, e.g., Boyse and Keller, 1986) using three parameters. The companion and sequel paper to this one provides that extension.

Acknowledgements

We thank all sponsors of M-OSRP and we are grateful that Robert Keys and Douglas Foster for valuable discussions.

Appendix A

In this appendix, we derive the expressions of $\left(\frac{\Delta c}{c}\right)_1$, $\left(\frac{\Delta c}{c}\right)_2$, $\left(\frac{\Delta I}{I}\right)_1$ and $\left(\frac{\Delta I}{I}\right)_2$ in terms of α_1, β_1 and α_2, β_2. Define $\Delta c = c - c_0$, $\Delta I = I - I_0$, $\Delta K = K - K_0$ and $\Delta\rho = \rho - \rho_0$.

Since $K = c^2\rho$, then we have

$$(c - \Delta c)^2 = \frac{K - \Delta K}{\rho - \Delta\rho}.$$

Divided by c^2, the equation above will become

$$2\left(\frac{\Delta c}{c}\right) - \left(\frac{\Delta c}{c}\right)^2 = \frac{\frac{\Delta K}{K} - \frac{\Delta\rho}{\rho}}{1 - \frac{\Delta\rho}{\rho}}.$$

Remember that $\alpha = \frac{\Delta K}{K}$ and $\beta = \frac{\Delta\rho}{\rho}$, the equation above can be rewritten as

$$2\left(\frac{\Delta c}{c}\right) - \left(\frac{\Delta c}{c}\right)^2 = \frac{\alpha - \beta}{1 - \beta}.$$

Then we have

$$2\left(\frac{\Delta c}{c}\right) - \left(\frac{\Delta c}{c}\right)^2 = (\alpha - \beta)(1 + \beta + \beta^2 + \cdots), \tag{40}$$

where the series expansion is valid for $|\beta| < 1$.

Similar to Eqs. (17) and (18), $\frac{\Delta c}{c}$ can be expanded as

$$\left(\frac{\Delta c}{c}\right) = \left(\frac{\Delta c}{c}\right)_1 + \left(\frac{\Delta c}{c}\right)_2 + \cdots. \tag{41}$$

Then substitute Eqs. (41), (17) and (18) into Eq. (40), and set those terms of equal order equal on both sides of Eq. (40), we can get

$$\left(\frac{\Delta c}{c}\right)_1 = \frac{1}{2}(\alpha_1 - \beta_1), \tag{42}$$

and

$$\left(\frac{\Delta c}{c}\right)_2 = \frac{1}{2}\left[\frac{1}{4}(\alpha_1 + \beta_1)^2 - \beta_1^2 + (\alpha_2 - \beta_2)\right]. \tag{43}$$

Similarly, using $I = c\rho$, we have

$$(I - \Delta I)^2 = (K - \Delta K)(\rho - \Delta\rho).$$

Divided by I^2, the equation above will become

$$2\left(\frac{\Delta I}{I}\right) - \left(\frac{\Delta I}{I}\right)^2 = \alpha + \beta - \alpha\beta. \tag{44}$$

Expanding $\frac{\Delta I}{I}$ as

$$\left(\frac{\Delta I}{I}\right) = \left(\frac{\Delta I}{I}\right)_1 + \left(\frac{\Delta I}{I}\right)_2 + \cdots, \tag{45}$$

and substitute Eqs. (45), (17) and (18) into Eq. (44), setting those terms of equal order equal on both sides of Eq. (44), we can get

$$\left(\frac{\Delta I}{I}\right)_1 = \frac{1}{2}(\alpha_1 + \beta_1), \tag{46}$$

and

$$\left(\frac{\Delta I}{I}\right)_2 = \frac{1}{2}\left[\frac{1}{4}(\alpha_1 - \beta_1)^2 + (\alpha_2 + \beta_2)\right]. \tag{47}$$

Appendix B

In this appendix, we show that $\left(\frac{\Delta c}{c}\right)_1$ has the same sign as Δc. For the single interface example, from Eqs. (36) and (42), we have

$$\left(\frac{\Delta c}{c}\right)_1 = 2\frac{R(\theta_1) - R(\theta_2)}{\tan^2\theta_1 - \tan^2\theta_2}.$$

The reflection coefficient is

$$R(\theta) = \frac{(\rho_1/\rho_0)(c_1/c_0)\sqrt{1-\sin^2\theta} - \sqrt{1-(c_1^2/c_0^2)\sin^2\theta}}{(\rho_1/\rho_0)(c_1/c_0)\sqrt{1-\sin^2\theta} + \sqrt{1-(c_1^2/c_0^2)\sin^2\theta}}.$$

Let

$$A(\theta) = (\rho_1/\rho_0)(c_1/c_0)\sqrt{1-\sin^2\theta},$$
$$B(\theta) = \sqrt{1-(c_1^2/c_0^2)\sin^2\theta}.$$

Then

$$R(\theta_1) - R(\theta_2) = 2\frac{A(\theta_1)B(\theta_2) - B(\theta_1)A(\theta_2)}{[A(\theta_1) + B(\theta_1)]\,[A(\theta_2) + B(\theta_2)]},$$

where the denominator is greater than zero. The numerator is

$$\begin{aligned} 2\,[A(\theta_1)B(\theta_2) - B(\theta_1)A(\theta_2)] =& 2(\rho_1/\rho_0)(c_1/c_0)\left[\sqrt{1-\sin^2\theta_1}\sqrt{1-(c_1^2/c_0^2)\sin^2\theta_2}\right. \\ & \left. -\sqrt{1-\sin^2\theta_2}\sqrt{1-(c_1^2/c_0^2)\sin^2\theta_1}\right]. \end{aligned}$$

Let

$$C = \sqrt{1-\sin^2\theta_1}\sqrt{1-(c_1^2/c_0^2)\sin^2\theta_2},$$
$$D = \sqrt{1-\sin^2\theta_2}\sqrt{1-(c_1^2/c_0^2)\sin^2\theta_1}.$$

Then,

$$C^2 - D^2 = \left(\frac{c_1^2}{c_0^2} - 1\right)(sin^2\theta_1 - sin^2\theta_2).$$

When $c_1 > c_0$ and $\theta_1 > \theta_2$, we have (Noticing that both C and D are positive.)

$$\left(\frac{c_1^2}{c_0^2} - 1\right)(sin^2\theta_1 - sin^2\theta_2) > 0,$$

so

$$R(\theta_1) - R(\theta_2) > 0;$$

Similarly, when $c_1 < c_0$ and $\theta_1 > \theta_2$, we have

$$\left(\frac{c_1^2}{c_0^2} - 1\right)(sin^2\theta_1 - sin^2\theta_2) < 0,$$

so

$$R(\theta_1) - R(\theta_2) < 0.$$

Remembering that $\left(\frac{\Delta c}{c}\right)_1 = 2\frac{R(\theta_1)-R(\theta_2)}{\tan^2\theta_1 - \tan^2\theta_2}$. So for $c_1 > c_0$, $(\Delta c)_1 > 0$ and for $c_1 < c_0$, $(\Delta c)_1 < 0$.

References

Boyse, W. E. and J. B. Keller. "Inverse elastic scattering in three dimensions." *J. Acoust. Soc. Am.* 79 (1986): 215–218.

Clayton, R. W. and R. H. Stolt. "A Born-WKBJ inversion method for acoustic reflection data." *Geophysics* 46 (1981): 1559–1567.

Innanen, Kristopher. A. *Methods for the treatment of acoustic and absorptive/dispersive wave field measurements.* PhD thesis, University of British Columbia, 2003.

Keys, R. G. "Polarity reversals in reflections from layered media." *Geophysics* 54 (1989): 900–905.

Liu, F., A. B. Weglein K. A. Innanen, and B. G. Nita. "Extension of the non-linear depth imaging capability of the inverse scattering series to multidimensional media: strategies and numerical results." *9th Ann. Cong. SBGf, Expanded Abstracts.* . SBGf, 2005.

Matson, K. H. *An inverse-scattering series method for attenuating elastic multiples from multi-component land and ocean bottom seismic data.* PhD thesis, University of British Columbia, 1997.

Raz, S. "Direct reconstruction of velocity and density profiles from scattered field data." *Geophysics* 46 (1981): 832–836.

Sen, M. and P. L. Stoffa. *Global Optimization Methods in Geophysical Inversion.* Amsterdam: Elsevier, 1995.

Shaw, S. A. *An inverse scattering series algorithm for depth imaging of reflection data from a layered acoustic medium with an unknown velocity model*. PhD thesis, University of Houston, 2005.

Shaw, S. A., A. B. Weglein, D. J. Foster, K. H. Matson, and R. G. Keys. "Isolation of a leading order depth imaging series and analysis of its convergence properties." *M-OSRP Annual Report* 2 (2003): 157–195.

Stolt, R. H. and A. B. Weglein. "Migration and inversion of seismic data." *Geophysics* 50 (1985): 2458–2472.

Tarantola, A., A. Nercessian, and O. Gauthier. "Nonlinear Inversion of Seismic Reflection Data." *54rd Annual Internat. Mtg., Soc. Expl. Geophys., Expanded Abstracts*. . Soc. Expl. Geophys., 1984. 645–649.

Taylor, J. R. *Scattering theory: the quantum theory on nonrelativistic collisions*. Wiley, New York, 1972.

Weglein, A. B., F. V. Araújo, P. M. Carvalho, R. H. Stolt, K. H. Matson, R. T. Coates, D. Corrigan, D. J. Foster, S. A. Shaw, and H. Zhang. "Inverse scattering series and seismic exploration." *Inverse Problems* 19 (2003): R27–R83.

Weglein, A. B., D. J. Foster, K. H. Matson, S. A. Shaw, P. M. Carvalho, and D. Corrigan. "Predicting the correct spatial location of reflectors without knowing or determining the precise medium and wave velocity: initial concept, algorithm and analytic and numerical example." *Journal of Seismic Exploration* 10 (2002): 367–382.

Weglein, A. B., F. A. Gasparotto, P. M. Carvalho, and R. H. Stolt. "An inverse-scattering series method for attenuating multiples in seismic reflection data." *Geophysics* 62 (1997): 1975–1989.

Weglein, A. B. and R. H. Stolt. 1992 "Approaches on linear and non-linear migration-inversion.". Personal Communication.

Weglein, A. B., P. B. Violette, and T. H. Keho. "Using multiparameter Born theory to obtain certain exact multiparameter inversion goals." *Geophysics* 51 (1986): 1069–1074.

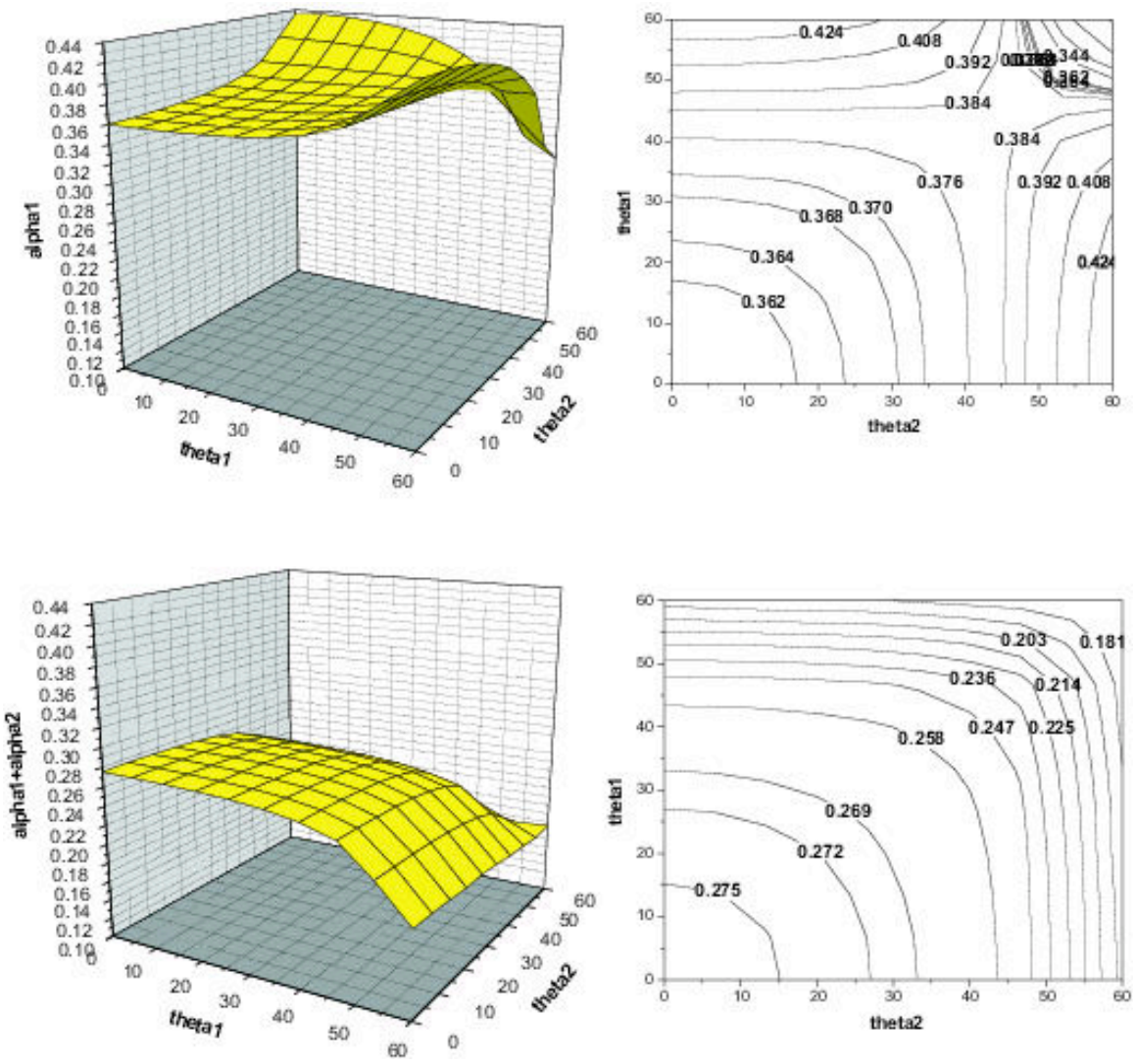

Figure 3: *α_1 (top) and $\alpha_1 + \alpha_2$ (bottom) displayed as a function of two different angles. The graphs on the right are the corresponding contour plots of the graphs on the left. In this example, the exact value of α is 0.292.*

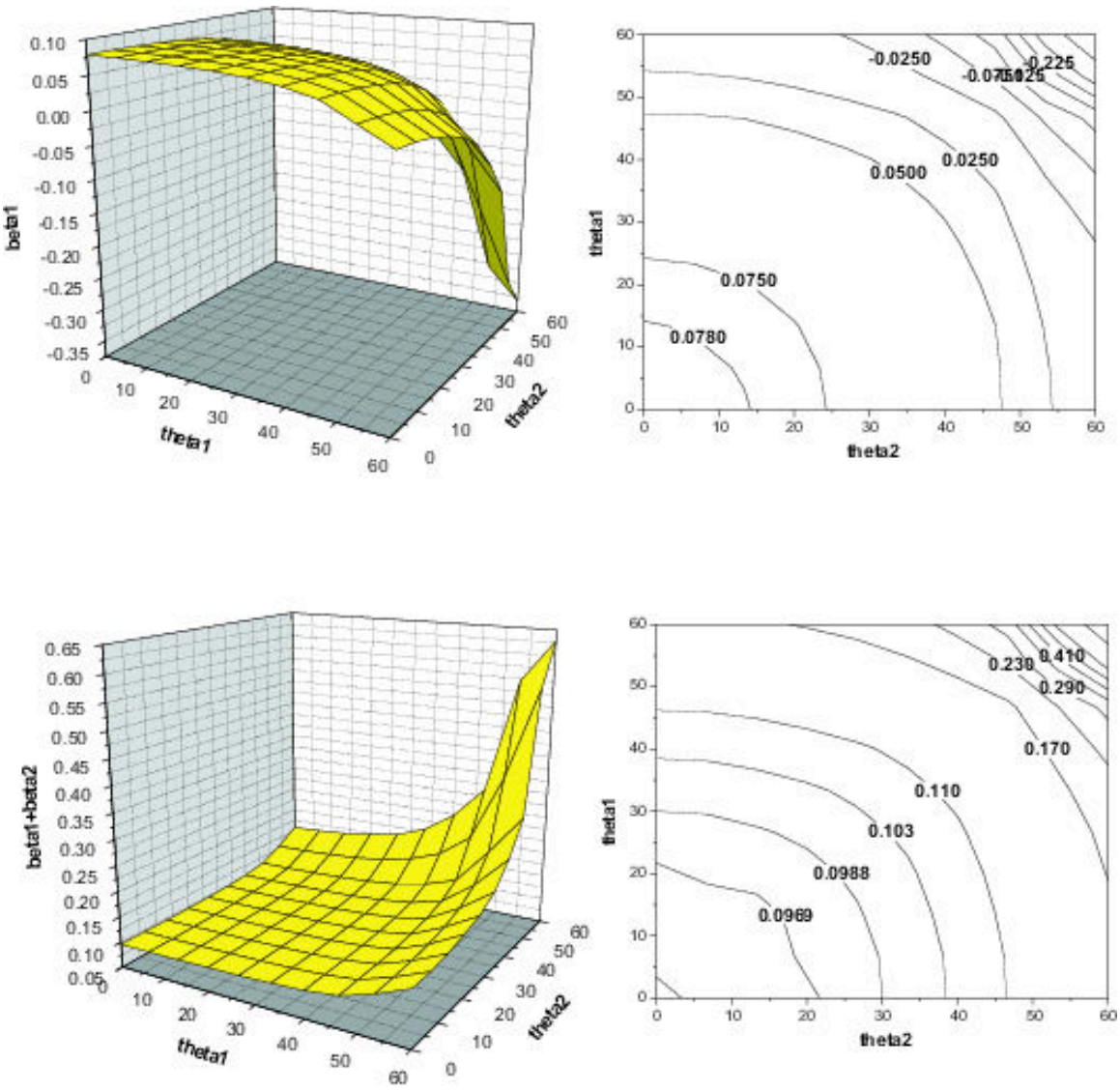

Figure 4: *β_1 (top) and $\beta_1 + \beta_2$ (bottom). In this example, the exact value of β is 0.09.*

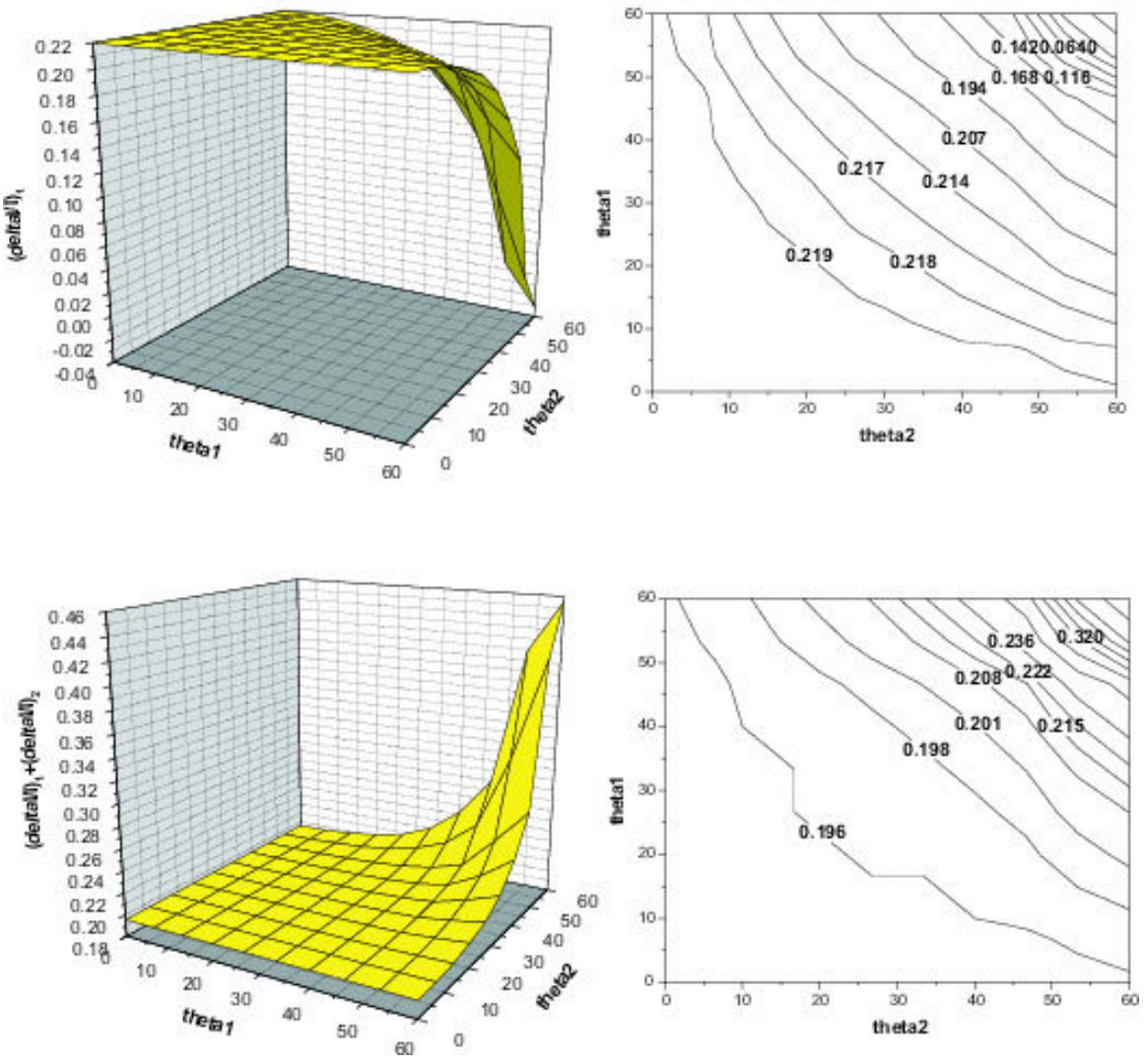

Figure 5: *Linear approximation to relative change in impedance (see details in Appendix A)* $\left(\frac{\Delta I}{I}\right)_1 = \frac{1}{2}(\alpha_1 + \beta_1)$ *(top). Sum of linear and first non-linear terms* $\left(\frac{\Delta I}{I}\right)_1 + \left(\frac{\Delta I}{I}\right)_2 = \left(\frac{\Delta I}{I}\right)_1 + \frac{1}{2}\left[\frac{1}{4}(\alpha_1 - \beta_1)^2 + (\alpha_2 + \beta_2)\right]$ *(bottom). In this example, the exact value of* $\frac{\Delta I}{I}$ *is 0.198.*

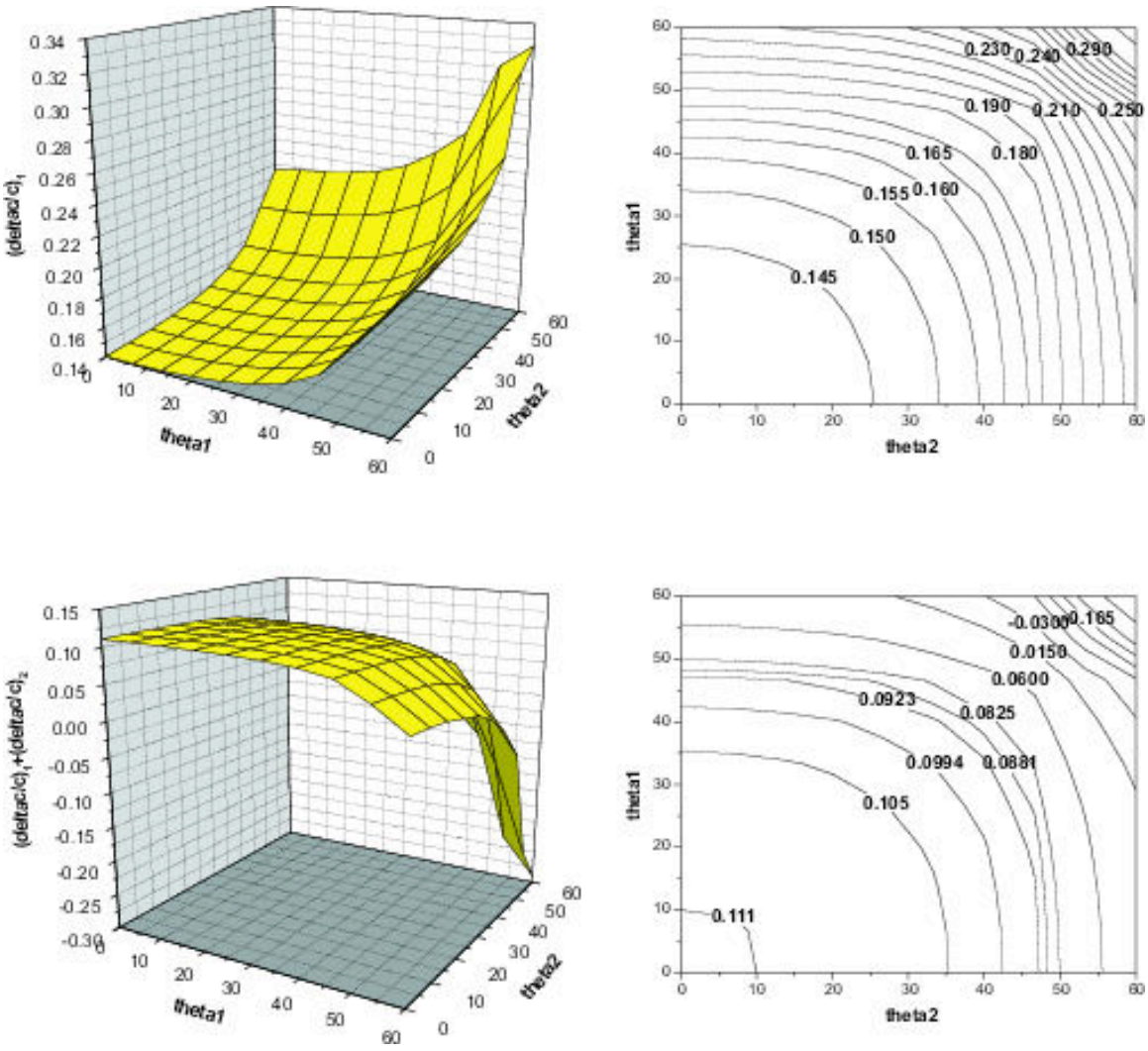

Figure 6: *Linear approximation to relative change in velocity (see details in Appendix A)* $\left(\frac{\Delta c}{c}\right)_1 = \frac{1}{2}(\alpha_1 - \beta_1)$ *(top). Sum of linear and first non-linear terms* $\left(\frac{\Delta c}{c}\right)_1 + \left(\frac{\Delta c}{c}\right)_2 = \left(\frac{\Delta c}{c}\right)_1 + \frac{1}{2}\left[\frac{1}{4}(\alpha_1 + \beta_1)^2 - \beta_1^2 + (\alpha_2 - \beta_2)\right]$ *(bottom). In this example, the exact value of* $\frac{\Delta c}{c}$ *is 0.118.*

Direct non-linear inversion of multi-parameter 1D elastic media using the inverse scattering series

H. Zhang[†]and A B. Weglein
[†]Presently at ConocoPhillips

Abstract

In this paper, we present the first non-linear direct target identification method and algorithm for 1D elastic media (P velocity, shear velocity and density vary in depth) from the inverse scattering series. Direct non-linear means that we provide explicit formulas that: (1) input data and directly output changes in material properties, without the use or need for any indirect procedures such as model matching, searching, optimization or other assumed aligned objectives or proxies, and (2) the algorithms recognize and directly invert the intrinsic non-linear relationship between changes in material properties and changes in the concomitant wave-field. The results clearly demonstrate that, in order to achieve full elastic inversion, all four components of data ($\hat{D}^{PP}$, $\hat{D}^{PS}$, $\hat{D}^{SP}$ and $\hat{D}^{SS}$) are needed. The method assumes that only data and reference medium properties are input, and terms in the inverse series for moving mislocated reflectors resulting from the linear inverse term, are separated from amplitude correction terms. Although in principle this direct inversion approach requires all four components of elastic data, synthetic tests indicate that a consistent value-added result may be achieved given only $\hat{D}^{PP}$ measurements, as long as the $\hat{D}^{PP}$ were used to approximately synthesize the $\hat{D}^{PS}$, $\hat{D}^{SP}$ and $\hat{D}^{SS}$ components. We can reasonably infer that further value would derive from actually measuring $\hat{D}^{PP}$, $\hat{D}^{PS}$, $\hat{D}^{SP}$ and $\hat{D}^{SS}$ as the method requires. For the case that all four components of data are available, we give one consistent method to solve for all of the second terms (the first terms beyond linear). The method's nonlinearity and directness provides this unambiguous data requirement message, and that unique clarity, and the explicit non-linear formulas casts doubts and reasonable concerns for indirect methods, in general, and their assumed aligned goals, e.g., using model matching objectives, that would never recognize the fundamental inadequacy from a basic physics point of view of using only PP data to perform elastic inversion. There are important conceptual and practical implications for the link between data acquisition and target identification goals and objectives.

Introduction

The ultimate objective of inverse problems is to determine medium and target properties from measurements external to the object under investigation. At the very first moment of problem definition, there is an immediate requirement and unavoidable expectation, that the model type of the medium be specified. In that step of model type specification, the number and type of parameters and dimension of spatial variation of those parameters are given, and carefully prescribed, and in that way you provide the inverse problem with clarity and meaning. Among the different model types used in exploration seismology are, e.g., acoustic, elastic, heterogeneous, anisotropic, and anelastic, and perhaps most important, the dimension of variability of the properties associated

with these model types. One would reasonably expect that the details of methods and algorithms for inversion objectives, and any tasks associated with achieving those ultimate objectives, would overall and each separately depend upon that starting assumption on model type. However, the ultimate objective of seismic inversion has never been achieved in a straight ahead single step manner directly from the seismic data, and that lack of success has not been due to a lack of computer power. The indirect model matching procedures have that computer power problem, especially in the applications to a multi-dimensional complex earth, where it is rare to have a reasonable proximal starting model. Those complex ill-defined geologic circumstances are the biggest impediments and challenges to current exploration and production seismic effectiveness.

The only direct multi-dimensional inversion procedure for seismic application, the inverse scattering series, does not require a proximal starting model and only assumes reference medium information. Of course, the whole inverse series has very limited application (Carvalho et al., 1992). What makes the inverse scattering series powerful is the so-called task isolated subseries which is a subset of the whole series that acts like only one task is performed for that subset (Weglein et al., 2003). All of these subseries act in a certain sequence so that the total seismic data can be processed accordingly. The order of processing is : (1) free-surface multiple removal, (2) internal multiple removal, (3) depth imaging without velocity, and (4) inversion or target identification. Since the entire process requires only reflection data and reference medium information, it is reasonable to assume that these intermediate steps, i.e., all of the derived subseries which are associated with achieving that objective, would also be attainable with only the reference medium and reflection data and no subsurface medium information is required.

The free surface multiple removal and internal multiple attenuation subseries have been presented by (Carvalho, 1992; Araújo, 1994; Weglein et al., 1997; Matson, 1997). Those two multiple procedures are model type independent, i.e., they work for acoustic, elastic and anelastic medium. Taking internal multiples from attenuation to elimination is being studied (Ramírez and Weglein, 2005). The task specific subseries associated with primaries (i.e., for imaging and inversion) have been progressed too: (1) imaging without the velocity for one parameter 1D and then 2D acoustic media (Weglein et al., 2002; Shaw and Weglein, 2003; Shaw et al., 2003a; Shaw et al., 2003b; Shaw et al., 2004; Shaw and Weglein, 2004; Liu and Weglein, 2003; Liu et al., 2004; Liu et al., 2005), and (2) direct non-linear inversion for multi-parameter 1D acoustic and then elastic media (Zhang and Weglein, 2005). Furthermore, recent work (Innanen and Weglein, 2004; Innanen and Weglein, 2005) suggests that some well-known seismic processing tasks associated with resolution enhancement (i.e., "Q-compensation") can be accomplished within the task-separated inverse scattering series framework. In this paper, we focus on item (2) above.

Compared with model type independent multiple removal procedures, there is a full expectation that tasks and algorithms associated with primaries will have a closer interest in model type. For example, there is no way to even imagine that medium property identification can take place without reference to a specific model type. Tasks and issues associated with structural determination, without knowing the medium, are also vastly different depending on the dimension of variation number of velocities that are required for imaging. Hence, a staged approach and isolation of tasks philosophy is essential in this yet tougher neighborhood, and even more in demand for seeking insights and then practical algorithms for these more complicated and daunting objectives. We

adopt the staged and isolation of issues approach for primaries. The isolated task achievement plan can often spin-off incomplete but useful intermediate objectives. The test and standard is not necessarily how complete the method is but rather how does it compare to, and improve upon, current best practice.

The stages within the strategy for primaries are as follows: (1) 1D earth, with one parameter, velocity as a function of depth, and a normal incidence wave, (2) 1D earth with one parameter subsurface and offset data, one shot record; (3) 2D earth with one parameter, velocity, varying in x and z, and a suite of shot records; (4) 1D acoustic earth with two parameters varying, velocity and density, one propagation velocity, and one shot record of PP data, and (5) 1D elastic earth, two elastic isotropic parameters and density, and two wave speeds, for P and S waves, and PP, PS, SP, and SS shot records data collected. This paper takes another step of direct non-linear inversion methodology, and task isolation and specifically for tasks associated with primaries, to the 1D elastic case, stage (5). The model is elastic and another paper in acoustic has been presented in Zhang and Weglein (2005). We take these steps and learn to navigate through this complexity and steer it towards useful and powerful algorithms.

However, more realism is more complicated with more issues involved. Following the task separation strategy, we ask the question what kind of tasks should we expect in this more complex, elastic, setting? In the acoustic case, for example, the acoustic medium only supports P-waves, and hence only one reference velocity (P-wave velocity) is involved. Therefore, when only one velocity is incorrect (i.e., poorly estimated), there exists only one "mislocation" for each parameter, and the imaging terms only need to correct this one mislocation. When we extend our previous work on the two parameter acoustic case to the present three parameter elastic case, there will be four mislocations because of the two reference velocities (P wave velocity and S velocity). Our reasoning is that the elastic medium supports both P- and S-wave propagation, and hence two reference velocities (P-wave velocity and S-wave velocity) are involved. When both of these velocities are incorrect, generally, there exist four mislocations due to each of four different combinations [1] of the two wrong velocities. Therefore, in non-linear elastic imaging-inversion, the imaging terms need to correct the four mislocations arising from linear inversion of any single mechanical property, such that a single correct location for the corresponding actual change in that property is determined.

In this paper, the first non-linear inversion term for three parameter 1D elastic medium is presented. It is demonstrated that under the inverse scattering series inversion framework, all four components of the data are needed in order to perform full elastic inversion. For the case that we don't have all four components data and only PP data are available, encouraging inversion results have been obtained by constructing other components of data from PP data. This means that we could perform elastic inversion only using pressure measurements, i.e. towed streamer data. For the case that all four components of data are available, a consistent method is provided. Further tests and evaluation of the four components of data.

The paper has the following structure: the next section is a brief introduction to the inverse

[1] The "four combinations" refers to PP, PS, SP and SS, where, for instance, PP means P-wave incidence, and P-wave reflection. Since P-waves non-normal incidence on an elastic interface can produce S-waves, or vice versa, which in those cases are known as converted waves (Aki and Richards, 2002), the elastic data generally contain four components: PP, PS, SP and SS.

scattering series and then presents, respectively, the derivations and numerical tests for elastic non-linear inversion when only PP data is available. A full non-linear elastic inversion method is also provided. Finally we will present some concluding remarks.

Background for 2D elastic inversion

In this section we consider the inversion problem in two dimensions for an elastic medium. We start with the displacement space, and then, for convenience (see e.g., (Weglein and Stolt, 1992); (Aki and Richards, 2002)), we change the basis and transform the equations to PS space. Finally, we do the elastic inversion in the PS domain.

In the displacement space

We begin with some basic equations in the displacement space (Matson, 1997):

$$L\mathbf{u} = \mathbf{f}, \tag{1}$$

$$L_0\mathbf{u} = \mathbf{f}, \tag{2}$$

$$LG = \delta, \tag{3}$$

$$L_0G_0 = \delta, \tag{4}$$

where L and L_0 are the differential operators that describe the wave propagation in the actual and reference medium, respectively, $\mathbf{u}$ and $\mathbf{f}$ are the corresponding displacement and source terms, respectively, and G and G_0 are the corresponding Green's operators for the actual and reference medium. In the following, the quantities with subscript "0" are for the reference medium, and those without the subscript are for the actual medium.

Following closely Weglein et al. (1997); Weglein et al. (2002) and Weglein et al. (2003), defining the perturbation $V = L_0 - L$, the Lippmann- Schwinger equation for the elastic media in the displacement space is

$$G = G_0 + G_0VG. \tag{5}$$

Iterating this equation back into itself generates the Born series

$$G = G_0 + G_0VG_0 + G_0VG_0VG_0 + \cdots . \tag{6}$$

We define the data D as the measured values of the scattered wave field. Then, on the measurement surface, we have

$$D = G_0VG_0 + G_0VG_0VG_0 + \cdots . \tag{7}$$

Expanding V as a series in orders of D we have

$$V = V_1 + V_2 + V_3 + \cdots . \tag{8}$$

Where the subscript "i" in V_i (i=1, 2, 3, ...) denotes the portion of V i-th order in the data. Substituting Eq. (8) into Eq. (7), evaluating Eq. (7), and setting terms of equal order in the data equal, the equations that determine V_1, V_2, ... from D and G_0 would be obtained.

$$D = G_0 V_1 G_0, \tag{9}$$

$$0 = G_0 V_2 G_0 + G_0 V_1 G_0 V_1 G_0, \tag{10}$$

$$\vdots$$

In the actual medium, the 2-D elastic wave equation is (Weglein and Stolt, 1992)

$$L\mathbf{u} \equiv \left[\rho\omega^2 \begin{pmatrix} 1 & 0 \\ 0 & 1 \end{pmatrix} + \begin{pmatrix} \partial_1\gamma\partial_1 + \partial_2\mu\partial_2 & \partial_1(\gamma - 2\mu)\partial_2 + \partial_2\mu\partial_1 \\ \partial_2(\gamma - 2\mu)\partial_1 + \partial_1\mu\partial_2 & \partial_2\gamma\partial_2 + \partial_1\mu\partial_1 \end{pmatrix}\right] \begin{bmatrix} u_1 \\ u_2 \end{bmatrix} = \mathbf{f}, \tag{11}$$

where

$\mathbf{u} = \begin{bmatrix} u_1 \\ u_2 \end{bmatrix}$ = displacement,

ρ = density,

γ = bulk modulus ($\equiv \rho\alpha^2$ where α = P-wave velocity),

μ = shear modulus ($\equiv \rho\beta^2$ where β = S-wave velocity),

ω = temporal frequency (angular), ∂_1 and ∂_2 denote the derivative over x and z, respectively, and $\mathbf{f}$ is the source term.

For constant $(\rho, \gamma, \mu) = (\rho_0, \gamma_0, \mu_0)$, $(\alpha, \beta) = (\alpha_0, \beta_0)$, the operator L becomes

$$L_0 \equiv \left[\rho_0\omega^2 \begin{pmatrix} 1 & 0 \\ 0 & 1 \end{pmatrix} + \begin{pmatrix} \gamma_0\partial_1^2 + \mu_0\partial_2^2 & (\gamma_0 - \mu_0)\partial_1\partial_2 \\ (\gamma_0 - \mu_0)\partial_1\partial_2 & \mu_0\partial_1^2 + \gamma_0\partial_2^2 \end{pmatrix}\right]. \tag{12}$$

Then,

$$\begin{aligned} V \equiv & L_0 - L \\ = & -\rho_0 \begin{bmatrix} a_\rho\omega^2 + \alpha_0^2\partial_1 a_\gamma\partial_1 + \beta_0^2\partial_2 a_\mu\partial_2 & \partial_1(\alpha_0^2 a_\gamma - 2\beta_0^2 a_\mu)\partial_2 + \beta_0^2\partial_2 a_\mu\partial_1 \\ \partial_2(\alpha_0^2 a_\gamma - 2\beta_0^2 a_\mu)\partial_1 + \beta_0^2\partial_1 a_\mu\partial_2 & a_\rho\omega^2 + \alpha_0^2\partial_2 a_\gamma\partial_2 + \beta_0^2\partial_1 a_\mu\partial_1 \end{bmatrix}, \end{aligned} \tag{13}$$

where $a_\rho \equiv \frac{\rho}{\rho_0} - 1$, $a_\gamma \equiv \frac{\gamma}{\gamma_0} - 1$ and $a_\mu \equiv \frac{\mu}{\mu_0} - 1$ are the three parameters we choose to do the elastic inversion. For a 1D earth (i.e. a_ρ, a_γ and a_μ are only functions of depth z), the expression above for V becomes

$$V = -\rho_0 \begin{bmatrix} a_\rho\omega^2 + \alpha_0^2 a_\gamma\partial_1^2 + \beta_0^2\partial_2 a_\mu\partial_2 & (\alpha_0^2 a_\gamma - 2\beta_0^2 a_\mu)\partial_1\partial_2 + \beta_0^2\partial_2 a_\mu\partial_1 \\ \partial_2(\alpha_0^2 a_\gamma - 2\beta_0^2 a_\mu)\partial_1 + \beta_0^2 a_\mu\partial_1\partial_2 & a_\rho\omega^2 + \alpha_0^2\partial_2 a_\gamma\partial_2 + \beta_0^2 a_\mu\partial_1^2 \end{bmatrix}. \tag{14}$$

Transforming to PS space

For convenience, we can change the basis from $\mathbf{u} = \begin{bmatrix} u_1 \\ u_2 \end{bmatrix}$ to $\begin{pmatrix} \phi^P \\ \phi^S \end{pmatrix}$ to allow L_0 to be diagonal,

$$\mathbf{\Phi} = \begin{pmatrix} \phi^P \\ \phi^S \end{pmatrix} = \begin{bmatrix} \gamma_0(\partial_1 u_1 + \partial_2 u_2) \\ \mu_0(\partial_1 u_2 - \partial_2 u_1) \end{bmatrix}, \tag{15}$$

also, we have

$$\begin{pmatrix} \phi^P \\ \phi^S \end{pmatrix} = \Gamma_0 \Pi \mathbf{u} = \begin{bmatrix} \gamma_0(\partial_1 u_1 + \partial_2 u_2) \\ \mu_0(\partial_1 u_2 - \partial_2 u_1) \end{bmatrix}, \tag{16}$$

where $\Pi = \begin{pmatrix} \partial_1 & \partial_2 \\ -\partial_2 & \partial_1 \end{pmatrix}$, $\Gamma_0 = \begin{pmatrix} \gamma_0 & 0 \\ 0 & \mu_0 \end{pmatrix}$. In the reference medium, the operator L_0 will transform in the new basis via a transformation

$$\hat{L}_0 \equiv \Pi L_0 \Pi^{-1} \Gamma_0^{-1} = \begin{pmatrix} \hat{L}_0^P & 0 \\ 0 & \hat{L}_0^S \end{pmatrix},$$

where $\hat{L}_0$ is L_0 transformed to PS space, $\Pi^{-1} = \begin{pmatrix} \partial_1 & -\partial_2 \\ \partial_2 & \partial_1 \end{pmatrix} \nabla^{-2}$ is the inverse matrix of Π, $\hat{L}_0^P = \omega^2/\alpha_0^2 + \nabla^2$, $\hat{L}_0^S = \omega^2/\beta_0^2 + \nabla^2$, and

$$\mathbf{F} = \Pi \mathbf{f} = \begin{pmatrix} F^P \\ F^S \end{pmatrix}. \tag{17}$$

Then, in PS domain, Eq. (2) becomes,

$$\begin{pmatrix} \hat{L}_0^P & 0 \\ 0 & \hat{L}_0^S \end{pmatrix} \begin{pmatrix} \phi^P \\ \phi^S \end{pmatrix} = \begin{pmatrix} F^P \\ F^S \end{pmatrix}. \tag{18}$$

Since $G_0 \equiv L_0^{-1}$, let $\hat{G}_0^P = \left(\hat{L}_0^P\right)^{-1}$ and $\hat{G}_0^S = \left(\hat{L}_0^S\right)^{-1}$, then the displacement G_0 in PS domain becomes

$$\hat{G}_0 = \Gamma_0 \Pi G_0 \Pi^{-1} = \begin{pmatrix} \hat{G}_0^P & 0 \\ 0 & \hat{G}_0^S \end{pmatrix}. \tag{19}$$

So, in the reference medium, after transforming from the displacement domain to PS domain, both L_0 and G_0 become diagonal.

Multiplying Eq. (5) from the left by the operator $\Gamma_0\Pi$ and from the right by the operator Π^{-1}, and using Eq. (19),

$$\begin{aligned} \Gamma_0 \Pi G \Pi^{-1} &= \hat{G}_0 + \hat{G}_0 \left(\Pi V \Pi^{-1} \Gamma_0^{-1}\right) \Gamma_0 \Pi G \Pi^{-1} \\ &= \hat{G}_0 + \hat{G}_0 \hat{V} \hat{G}, \end{aligned} \tag{20}$$

where the displacement Green's operator G is transformed to the PS domain as

$$\hat{G} = \Gamma_0 \Pi G \Pi^{-1} = \begin{pmatrix} \hat{G}^{PP} & \hat{G}^{PS} \\ \hat{G}^{SP} & \hat{G}^{SS} \end{pmatrix}. \tag{21}$$

The perturbation V in the PS domain becomes

$$\hat{V} = \Pi V \Pi^{-1} \Gamma_0^{-1} = \begin{pmatrix} \hat{V}^{PP} & \hat{V}^{PS} \\ \hat{V}^{SP} & \hat{V}^{SS} \end{pmatrix}, \tag{22}$$

where the left superscripts of the matrix elements represent the type of measurement and the right ones are the source type.

Similarly, applying the PS transformation to the entire inverse series gives

$$\hat{V} = \hat{V}_1 + \hat{V}_2 + \hat{V}_3 + \cdots . \tag{23}$$

It follows, from Eqs. (20) and (23) that

$$\hat{D} = \hat{G}_0 \hat{V}_1 \hat{G}_0, \tag{24}$$

$$\hat{G}_0 \hat{V}_2 \hat{G}_0 = -\hat{G}_0 \hat{V}_1 \hat{G}_0 \hat{V}_1 \hat{G}_0, \tag{25}$$

$$\vdots$$

where $\hat{D} = \begin{pmatrix} \hat{D}^{PP} & \hat{D}^{PS} \\ \hat{D}^{SP} & \hat{D}^{SS} \end{pmatrix}$ are the data in the PS domain.

In the displacement space we have, for Eq. (1),

$$\mathbf{u} = G\mathbf{f}. \tag{26}$$

Then, in the PS domain, Eq. (26) becomes

$$\mathbf{\Phi} = \hat{G}\mathbf{F}. \tag{27}$$

On the measurement surface, we have

$$\hat{G} = \hat{G}_0 + \hat{G}_0 \hat{V}_1 \hat{G}_0. \tag{28}$$

Substituting Eq. (28) into Eq. (27), and rewriting Eq. (27) in matrix form:

$$\begin{pmatrix} \phi^P \\ \phi^S \end{pmatrix} = \begin{pmatrix} \hat{G}_0^P & 0 \\ 0 & \hat{G}_0^S \end{pmatrix} \begin{pmatrix} F^P \\ F^S \end{pmatrix} + \begin{pmatrix} \hat{G}_0^P & 0 \\ 0 & \hat{G}_0^S \end{pmatrix} \begin{pmatrix} \hat{V}_1^{PP} & \hat{V}_1^{PS} \\ \hat{V}_1^{SP} & \hat{V}_1^{SS} \end{pmatrix} \begin{pmatrix} \hat{G}_0^P & 0 \\ 0 & \hat{G}_0^S \end{pmatrix} \begin{pmatrix} F^P \\ F^S \end{pmatrix}. \tag{29}$$

This can be written as the following two equations

$$\phi^P = \hat{G}_0^P F^P + \hat{G}_0^P \hat{V}_1^{PP} \hat{G}_0^P F^P + \hat{G}_0^P \hat{V}_1^{PS} \hat{G}_0^S F^S, \tag{30}$$

$$\phi^S = \hat{G}_0^S F^S + \hat{G}_0^S \hat{V}_1^{SP} \hat{G}_0^P F^P + \hat{G}_0^S \hat{V}_1^{SS} \hat{G}_0^S F^S. \tag{31}$$

We can see, from the two equations above, that for homogeneous media, (no perturbation, $\hat{V}_1 = 0$), there are only direct P and S waves and that the two kind of waves are separated. However, for inhomogeneous media, these two kinds of waves will be mixed together. If only the P wave is incident, $F^P = 1$, $F^S = 0$, then the two Eqs. (30) and (31) above are respectively reduced to

$$\phi^P = \hat{G}_0^P + \hat{G}_0^P \hat{V}_1^{PP} \hat{G}_0^P, \tag{32}$$

$$\phi^S = \hat{G}_0^S \hat{V}_1^{SP} \hat{G}_0^P. \tag{33}$$

Hence, in this case, there is only the direct P wave $\hat{G}_0^P$, and no direct wave S. But there are two kinds of scattered waves: one is the P-to-P wave $\hat{G}_0^P \hat{V}_1^{PP} \hat{G}_0^P$, and the other is the P-to-S wave $\hat{G}_0^S \hat{V}_1^{SP} \hat{G}_0^P$. For the acoustic case, only the P wave exists, and hence we only have one equation $\phi^P = \hat{G}_0^P + \hat{G}_0^P \hat{V}_1^{PP} \hat{G}_0^P$.

Similarly, if only the S wave is incident, $F^P = 0$, $F^S = 1$, and the two Eqs. (30) and (31) are, respectively, reduced to

$$\phi^P = \hat{G}_0^P \hat{V}_1^{PS} \hat{G}_0^S, \tag{34}$$

$$\phi^S = \hat{G}_0^S + \hat{G}_0^S \hat{V}_1^{SS} \hat{G}_0^S. \tag{35}$$

In this case, there is only the direct S wave $\hat{G}_0^S$, and no direct P wave. There are also two kinds of scattered waves: one is the S-to-P wave $\hat{G}_0^P \hat{V}_1^{PS} \hat{G}_0^S$, the other is the S-to-S wave $\hat{G}_0^S \hat{V}_1^{SS} \hat{G}_0^S$.

Linear inversion of a 1D elastic medium

Writing Eq. (24) in matrix form

$$\begin{pmatrix} \hat{D}^{PP} & \hat{D}^{PS} \\ \hat{D}^{SP} & \hat{D}^{SS} \end{pmatrix} = \begin{pmatrix} \hat{G}_0^P & 0 \\ 0 & \hat{G}_0^S \end{pmatrix} \begin{pmatrix} \hat{V}_1^{PP} & \hat{V}_1^{PS} \\ \hat{V}_1^{SP} & \hat{V}_1^{SS} \end{pmatrix} \begin{pmatrix} \hat{G}_0^P & 0 \\ 0 & \hat{G}_0^S \end{pmatrix}, \tag{36}$$

leads to four equations

$$\hat{D}^{PP} = \hat{G}_0^P \hat{V}_1^{PP} \hat{G}_0^P, \tag{37}$$

$$\hat{D}^{PS} = \hat{G}_0^P \hat{V}_1^{PS} \hat{G}_0^S, \tag{38}$$

$$\hat{D}^{SP} = \hat{G}_0^S \hat{V}_1^{SP} \hat{G}_0^P, \tag{39}$$

$$\hat{D}^{SS} = \hat{G}_0^S \hat{V}_1^{SS} \hat{G}_0^S. \tag{40}$$

For $z_s = z_g = 0$, in the $(k_s, z_s; k_g, z_g; \omega)$ domain, we get the following four equations relating the linear components (the "linear" is denoted by adding a superscript "(1)" on the three parameters) of the three elastic parameters and the four data types:

$$\begin{aligned} \widetilde{D}^{PP}(k_g, 0; -k_g, 0; \omega) = &-\frac{1}{4}\left(1 - \frac{k_g^2}{\nu_g^2}\right) \widetilde{a}_\rho^{(1)}(-2\nu_g) - \frac{1}{4}\left(1 + \frac{k_g^2}{\nu_g^2}\right) \widetilde{a}_\gamma^{(1)}(-2\nu_g) \\ &+ \frac{2k_g^2 \beta_0^2}{(\nu_g^2 + k_g^2)\alpha_0^2} \widetilde{a}_\mu^{(1)}(-2\nu_g), \end{aligned} \tag{41}$$

$$\widetilde{D}^{PS}(\nu_g, \eta_g) = -\frac{1}{4}\left(\frac{k_g}{\nu_g} + \frac{k_g}{\eta_g}\right) \widetilde{a}_\rho^{(1)}(-\nu_g - \eta_g) - \frac{\beta_0^2}{2\omega^2} k_g(\nu_g + \eta_g)\left(1 - \frac{k_g^2}{\nu_g \eta_g}\right) \widetilde{a}_\mu^{(1)}(-\nu_g - \eta_g), \tag{42}$$

$$\widetilde{D}^{SP}(\nu_g, \eta_g) = \frac{1}{4}\left(\frac{k_g}{\nu_g} + \frac{k_g}{\eta_g}\right) \widetilde{a}_\rho^{(1)}(-\nu_g - \eta_g) + \frac{\beta_0^2}{2\omega^2} k_g(\nu_g + \eta_g)\left(1 - \frac{k_g^2}{\nu_g \eta_g}\right) \widetilde{a}_\mu^{(1)}(-\nu_g - \eta_g), \tag{43}$$

$$\widetilde{D}^{SS}(k_g,\eta_g) = -\frac{1}{4}\left(1-\frac{k_g^2}{\eta_g^2}\right)\widetilde{a}_\rho^{(1)}(-2\eta_g) - \left[\frac{\eta_g^2+k_g^2}{4\eta_g^2} - \frac{2k_g^2}{\eta_g^2+k_g^2}\right]\widetilde{a}_\mu^{(1)}(-2\eta_g), \tag{44}$$

where

$$\nu_g^2 + k_g^2 = \frac{\omega^2}{\alpha_0^2},$$

$$\eta_g^2 + k_g^2 = \frac{\omega^2}{\beta_0^2},$$

For the P-wave incidence case (see Fig. 1), using $k_g^2/\nu_g^2 = \tan^2\theta$ and $k_g^2/(\nu_g^2+k_g^2) = \sin^2\theta$, where θ is the P-wave incident angle, Eq. (41) becomes

$$\widetilde{D}^{PP}(\nu_g,\theta) = -\frac{1}{4}(1-\tan^2\theta)\widetilde{a}_\rho^{(1)}(-2\nu_g) - \frac{1}{4}(1+\tan^2\theta)\widetilde{a}_\gamma^{(1)}(-2\nu_g) + \frac{2\beta_0^2\sin^2\theta}{\alpha_0^2}\widetilde{a}_\mu^{(1)}(-2\nu_g). \tag{45}$$

In this case, when $\beta_0 = \beta_1 = 0$, Eq. (45) reduces to the acoustic two parameter case Eq. (7) in Zhang and Weglein (2005) for $z_g = z_s = 0$.

$$\widetilde{D}(q_g,\theta) = -\frac{\rho_0}{4}\left[\frac{1}{\cos^2\theta}\widetilde{\alpha_1}(-2q_g) + (1-\tan^2\theta)\widetilde{\beta}_1(-2q_g)\right], \tag{46}$$

In Eq. (45), it seems straightforward that using the data at three angles to obtain the linear inversion of a_ρ, a_γ and a_μ, and this is what we do in this paper. However, by doing this it requires a whole new understanding of the definition of "the data". This point has been discussed by Weglein et al. (2007).

Direct non-linear inversion of 1D elastic medium

Writing Eq. (25) in matrix form:

$$\begin{aligned}
&\begin{pmatrix}\hat{G}_0^P & 0\\ 0 & \hat{G}_0^S\end{pmatrix}\begin{pmatrix}\hat{V}_2^{PP} & \hat{V}_2^{PS}\\ \hat{V}_2^{SP} & \hat{V}_2^{SS}\end{pmatrix}\begin{pmatrix}\hat{G}_0^P & 0\\ 0 & \hat{G}_0^S\end{pmatrix}\\
&= -\begin{pmatrix}\hat{G}_0^P & 0\\ 0 & \hat{G}_0^S\end{pmatrix}\begin{pmatrix}\hat{V}_1^{PP} & \hat{V}_1^{PS}\\ \hat{V}_1^{SP} & \hat{V}_1^{SS}\end{pmatrix}\begin{pmatrix}\hat{G}_0^P & 0\\ 0 & \hat{G}_0^S\end{pmatrix}\begin{pmatrix}\hat{V}_1^{PP} & \hat{V}_1^{PS}\\ \hat{V}_1^{SP} & \hat{V}_1^{SS}\end{pmatrix}\begin{pmatrix}\hat{G}_0^P & 0\\ 0 & \hat{G}_0^S\end{pmatrix},
\end{aligned} \tag{47}$$

leads to four equations

$$\hat{G}_0^P\hat{V}_2^{PP}\hat{G}_0^P = -\hat{G}_0^P\hat{V}_1^{PP}\hat{G}_0^P\hat{V}_1^{PP}\hat{G}_0^P - \hat{G}_0^P\hat{V}_1^{PS}\hat{G}_0^S\hat{V}_1^{SP}\hat{G}_0^P, \tag{48}$$

$$\hat{G}_0^P\hat{V}_2^{PS}\hat{G}_0^S = -\hat{G}_0^P\hat{V}_1^{PP}\hat{G}_0^P\hat{V}_1^{PS}\hat{G}_0^S - \hat{G}_0^P\hat{V}_1^{PS}\hat{G}_0^S\hat{V}_1^{SS}\hat{G}_0^S, \tag{49}$$

$$\hat{G}_0^S\hat{V}_2^{SP}\hat{G}_0^P = -\hat{G}_0^S\hat{V}_1^{SP}\hat{G}_0^P\hat{V}_1^{PP}\hat{G}_0^P - \hat{G}_0^S\hat{V}_1^{SS}\hat{G}_0^S\hat{V}_1^{SP}\hat{G}_0^P, \tag{50}$$

$$\hat{G}_0^S\hat{V}_2^{SS}\hat{G}_0^S = -\hat{G}_0^S\hat{V}_1^{SP}\hat{G}_0^P\hat{V}_1^{PS}\hat{G}_0^S - \hat{G}_0^S\hat{V}_1^{SS}\hat{G}_0^S\hat{V}_1^{SS}\hat{G}_0^S. \tag{51}$$

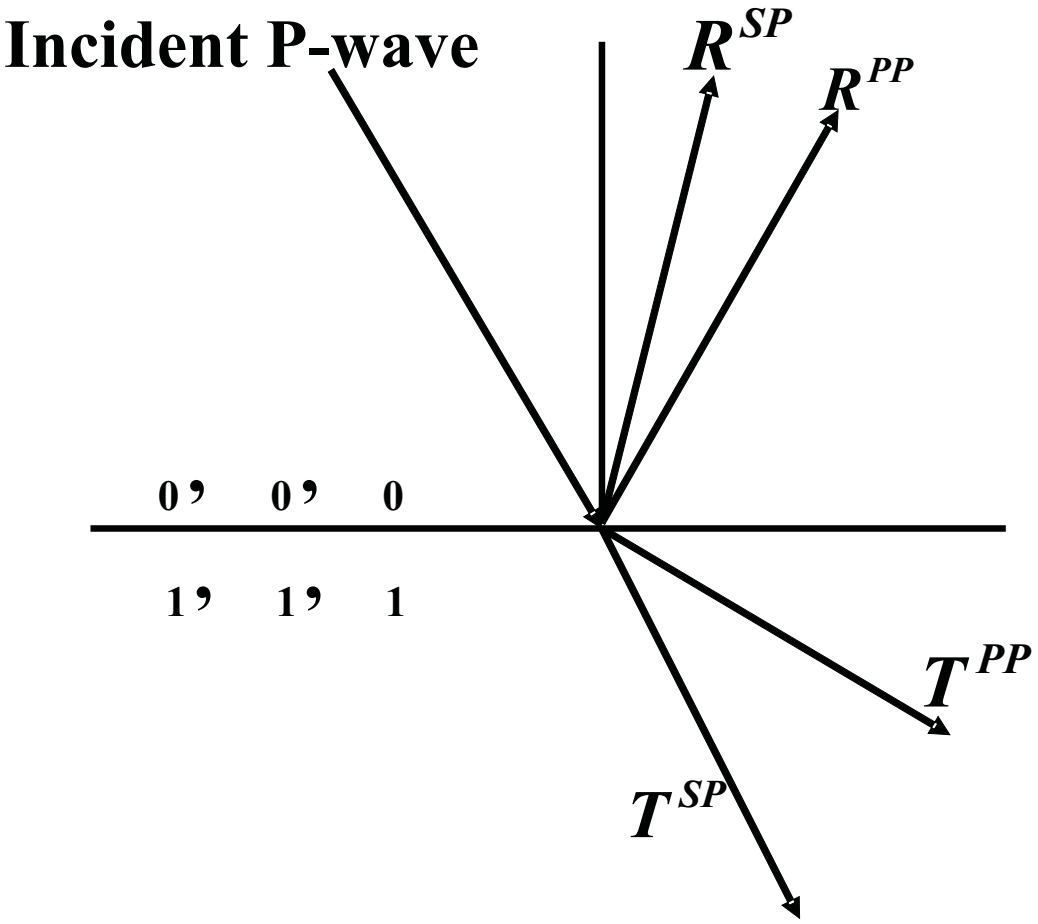

Figure 1: *Response of incident compressional wave on a planar elastic interface. α_0, β_0 and ρ_0 are the compressional wave velocity, shear wave velocity and density of the upper layer, respectively; α_1, β_1 and ρ_1 denote the compressional wave velocity, shear wave velocity and density of the lower layer. R^{PP}, R^{SP}, T^{PP} and T^{SP} denote the coefficients of the reflected compressional wave, the reflected shear wave, the transmitted compressional wave and the transmitted shear wave, respectively. (Foster et al., 1997)*

Since $\hat{V}_1^{PP}$ relates to $\hat{D}^{PP}$, $\hat{V}_1^{PS}$ relates to $\hat{D}^{PS}$, and so on, the four components of the data will be coupled in the non-linear elastic inversion. We cannot perform the direct non-linear inversion without knowing all components of the data. As shown in Zhang and Weglein (2005) and this chapter, when the work on the two parameter acoustic case is extended to the present three parameter elastic case, it is not just simply adding one more parameter, but there are more issues involved. Even for the linear case, the linear solutions found in (41) $\sim$ (44) are much more complicated than those of the acoustic case. For instance, four different sets of linear parameter estimates are produced

from each component of the data. Also, generally four distinct reflector mislocations arise from the two reference velocities (P-wave velocity and S-wave velocity).

However, in some situations like the towed streamer case, we do not have all components of data available. A particular non-linear approach to be presented in the next section, has been chosen to side-step a portion of this complexity and address our typical lack of four components of elastic data: using $\hat{D}^{PP}$ as the fundamental data input, and perform a reduced form of non-linear elastic inversion, concurrently asking: what beyond-linear value does this simpler framework add? We will see from the numerical tests presented in the following section.

Only using $\hat{D}^{PP}$ — a particular non-linear approach and the numerical tests

When assuming only $\hat{D}^{PP}$ are available, first, we compute the linear solution for $a_\rho^{(1)}$, $a_\gamma^{(1)}$ and $a_\mu^{(1)}$ from Eq. (41). Then, substituting the solution into the other three equations (42), (43) and (44), we synthesize the other components of data — $\hat{D}^{PS}$, $\hat{D}^{SP}$ and $\hat{D}^{SS}$. Finally, using the given $\hat{D}^{PP}$ and the synthesized data, we perform the non-linear elastic inversion, getting the following second order (first term beyond linear) elastic inversion solution from Eq. (48),

$$
\begin{aligned}
&\left(1-\tan^2\theta\right)a_\rho^{(2)}(z)+\left(1+\tan^2\theta\right)a_\gamma^{(2)}(z)-8b^2\sin^2\theta a_\mu^{(2)}(z)\\
=&-\frac{1}{2}\left(\tan^4\theta-1\right)\left[a_\gamma^{(1)}(z)\right]^2+\frac{\tan^2\theta}{\cos^2\theta}a_\gamma^{(1)}(z)a_\rho^{(1)}(z)\\
&+\frac{1}{2}\left[\left(1-\tan^4\theta\right)-\frac{2}{C+1}\left(\frac{1}{C}\right)\left(\frac{\alpha_0^2}{\beta_0^2}-1\right)\frac{\tan^2\theta}{\cos^2\theta}\right]\left[a_\rho^{(1)}(z)\right]^2\\
&-4b^2\left[\tan^2\theta-\frac{2}{C+1}\left(\frac{1}{2C}\right)\left(\frac{\alpha_0^2}{\beta_0^2}-1\right)\tan^4\theta\right]a_\rho^{(1)}(z)a_\mu^{(1)}(z)\\
&+2b^4\left(\tan^2\theta-\frac{\alpha_0^2}{\beta_0^2}\right)\left[2\sin^2\theta-\frac{2}{C+1}\frac{1}{C}\left(\frac{\alpha_0^2}{\beta_0^2}-1\right)\tan^2\theta\right]\left[a_\mu^{(1)}(z)\right]^2\\
&-\frac{1}{2}\left(\frac{1}{\cos^4\theta}\right)a_\gamma^{(1)\prime}(z)\int_0^z dz'\left[a_\gamma^{(1)}\left(z'\right)-a_\rho^{(1)}\left(z'\right)\right]\\
&-\frac{1}{2}\left(1-\tan^4\theta\right)a_\rho^{(1)\prime}(z)\int_0^z dz'\left[a_\gamma^{(1)}\left(z'\right)-a_\rho^{(1)}\left(z'\right)\right]\\
&+4b^2\tan^2\theta a_\mu^{(1)\prime}(z)\int_0^z dz'\left[a_\gamma^{(1)}\left(z'\right)-a_\rho^{(1)}\left(z'\right)\right]\\
&+\frac{2}{C+1}\frac{1}{C}\left(\frac{\alpha_0^2}{\beta_0^2}-1\right)\tan^2\theta\left(\tan^2\theta-C\right)b^2\int_0^z dz' a_\mu^{(1)}{}_z\left(\frac{(C-1)\,z'+2z}{(C+1)}\right)a_\rho^{(1)}\left(z'\right)\\
&-\frac{2}{C+1}\frac{2}{C}\left(\frac{\alpha_0^2}{\beta_0^2}-1\right)\tan^2\theta\left(\tan^2\theta-\frac{\alpha_0^2}{\beta_0^2}\right)b^4\int_0^z dz' a_\mu^{(1)}{}_z\left(\frac{(C-1)\,z'+2z}{(C+1)}\right)a_\mu^{(1)}\left(z'\right)\\
&+\frac{2}{C+1}\frac{1}{C}\left(\frac{\alpha_0^2}{\beta_0^2}-1\right)\tan^2\theta\left(\tan^2\theta+C\right)b^2\int_0^z dz' a_\mu^{(1)}\left(z'\right)a_\rho^{(1)}{}_z\left(\frac{(C-1)z'+2z}{(C+1)}\right)\\
&-\frac{2}{C+1}\frac{1}{2C}\left(\frac{\alpha_0^2}{\beta_0^2}-1\right)\tan^2\theta\left(\tan^2\theta+1\right)\int_0^z dz' a_\rho^{(1)}\left(z'\right)a_\rho^{(1)}{}_z\left(\frac{(C-1)\,z'+2z}{(C+1)}\right),
\end{aligned}
\tag{52}
$$

where $a_\rho^{(1)}{}_z\left(\frac{(C-1)z'+2z}{(C+1)}\right) = d\left[a_\rho^{(1)}\left(\frac{(C-1)z'+2z}{(C+1)}\right)\right]/dz$, $b = \frac{\beta_0}{\alpha_0}$ and $C = \frac{\eta_g}{\nu_g} = \frac{\sqrt{1-b^2\sin^2\theta}}{b\sqrt{1-\sin^2\theta}}$.

The first five terms on the right side of Eq. (52) are inversion terms; i.e., they contribute to parameter predictions. The other terms on the right side of the equation are imaging terms. The arguments for the remarks above are the same as in the acoustic case in (Zhang and Weglein, 2005). For one interface model, there is no imaging task. The only task is inversion. In this case, all of the integration terms on the right side of Eq. (52) are zero, and only the first five terms can be non-zero. Thus, we conclude that the integration terms (which care about duration) are imaging terms, and the first five terms are inversion terms. Both the inversion and imaging terms (especially the imaging terms) become much more complicated after the extension of acoustic case (Zhang and Weglein, 2005) to elastic case. The integrand of the first three integral terms is the first order approximation of the relative change in P-wave velocity. The derivatives $a_\gamma^{(1)\prime}$, $a_\rho^{(1)\prime}$ and $a_\mu^{(1)\prime}$ in front of those integrals are acting to correct the wrong locations caused by the inaccurate reference P-wave velocity. The other four terms with integrals will be zero as $\beta_0 \to 0$ since in this case $C \to \infty$.

In the following, we test this approach numerically.

For a single interface 1D elastic medium case, as shown in Fig. 1, the reflection coefficient R^{PP} has the following form (Foster et al., 1997)

$$R^{PP} = \frac{N}{D}, \tag{53}$$

where

$$\begin{aligned} N = &-(1+2kx^2)^2 b\sqrt{1-c^2x^2}\sqrt{1-d^2x^2} - (1-a+2kx^2)^2 bcdx^2 \\ &+ (a-2kx^2)^2 cd\sqrt{1-x^2}\sqrt{1-b^2x^2} \\ &+ 4k^2x^2\sqrt{1-x^2}\sqrt{1-b^2x^2}\sqrt{1-c^2x^2}\sqrt{1-d^2x^2} - ad\sqrt{1-b^2x^2}\sqrt{1-c^2x^2} \\ &+ abc\sqrt{1-x^2}\sqrt{1-d^2x^2}, \end{aligned} \tag{54}$$

$$\begin{aligned} D = &(1+2kx^2)^2 b\sqrt{1-c^2x^2}\sqrt{1-d^2x^2} + (1-a+2kx^2)^2 bcdx^2 \\ &+ (a-2kx^2)^2 cd\sqrt{1-x^2}\sqrt{1-b^2x^2} \\ &+ 4k^2x^2\sqrt{1-x^2}\sqrt{1-b^2x^2}\sqrt{1-c^2x^2}\sqrt{1-d^2x^2} + ad\sqrt{1-b^2x^2}\sqrt{1-c^2x^2} \\ &+ abc\sqrt{1-x^2}\sqrt{1-d^2x^2}, \end{aligned} \tag{55}$$

where $a = \rho_1/\rho_0$, $b = \beta_0/\alpha_0$, $c = \alpha_1/\alpha_0$, $d = \beta_1/\alpha_0$, $k = ad^2 - b^2$ and $x = \sin\theta$, and the subscripts "0" and "1" denote the reference medium and actual medium respectively. Similar to the acoustic case, using the analytic data (Clayton and Stolt, 1981; Weglein et al., 1986)

$$\widetilde{D}^{PP}(\nu_g, \theta) = R^{PP}(\theta)\frac{e^{2i\nu_g a}}{4\pi i\nu_g}, \tag{56}$$

where a is the depth of the interface. Substituting Eq.(56) into Eq.(45), Fourier transforming Eq.(45) over $2\nu_g$, and fixing $z > a$ and θ, we have

$$(1-\tan^2\theta)a_\rho^{(1)}(z) + (1+\tan^2\theta)a_\gamma^{(1)}(z) - 8\frac{\beta_0^2}{\alpha_0^2}\sin^2\theta a_\mu^{(1)}(z) = 4R^{PP}(\theta)H(z-a). \qquad (57)$$

In this section, we numerically test the direct inversion approach on the following four models:

Model 1: shale (0.20 porosity) over oil sand (0.10 porosity). $\rho_0 = 2.32g/cm^3$, $\rho_1 = 2.46g/cm^3$; $\alpha_0 = 2627m/s$, $\alpha_1 = 4423m/s$; $\beta_0 = 1245m/s$, $\beta_1 = 2939m/s$.

Model 2: shale over oil sand, 0.20 porosity. $\rho_0 = 2.32g/cm^3$, $\rho_1 = 2.27g/cm^3$; $\alpha_0 = 2627m/s$, $\alpha_1 = 3251m/s$; $\beta_0 = 1245m/s$, $\beta_1 = 2138m/s$.

Model 3: shale (0.20 porosity) over oil sand (0.30 porosity). $\rho_0 = 2.32g/cm^3$, $\rho_1 = 2.08g/cm^3$; $\alpha_0 = 2627m/s$, $\alpha_1 = 2330m/s$; $\beta_0 = 1245m/s$, $\beta_1 = 1488m/s$.

Model 4: oil sand over wet sand, 0.20 porosity. $\rho_0 = 2.27g/cm^3$, $\rho_1 = 2.32g/cm^3$; $\alpha_0 = 3251m/s$, $\alpha_1 = 3507m/s$; $\beta_0 = 2138m/s$, $\beta_1 = 2116m/s$.

To test and compare methods, the top of sand reflection was modeled for oil sands with porosities of 10, 20, and 30%. The three models used the same shale overburden. An oil/water contact model was also constructed for the 20% porosity sand.

The low porosity model (10%) represents a deep, consolidated reservoir sand. Pore fluids have little effect on the seismic response of the reservoir sand. It is difficult to distinguish oil sands from brine sands on the basis of seismic response. Impedance of the sand is higher than impedance of the shale.

The moderate porosity model (20%) represents deeper, compacted reservoirs. Pore fluids have a large impact on seismic response, but the fluid effect is less than that of the high porosity case. The overlying shale has high density compared to the reservoir sand, but the P-wave velocity of the oil sand exceeds that of the shale. As a result, impedance contrast is reduced, and shear wave information becomes more important for detecting the reservoir.

The high porosity model (30%) is typical of a weakly consolidated, shallow reservoir sand. Pore fluids have a large impact on the seismic response. Density, P-wave velocity, and the α/β ratio of the oil sand are lower than the density, P-wave velocity, and α/β ratio of the overlying shale. Consequently, there is a significant decrease in density and P-wave bulk modulus and an increase in shear modulus at the shale/oil sand interface.

The fourth model denotes an oil/water contact in a 20% porosity sand. At a fluid contact, both density and P-wave velocity increase in going from the oil zone into the wet zone. Because pore fluids have no affect on shear modulus, there is no change in shear modulus.

Using these four models, we can find the corresponding R^{PP} from Eq. (53). Then, choosing three different angles θ_1, θ_2 and θ_3, we can get the linear solutions for $a_\rho^{(1)}$, $a_\gamma^{(1)}$ and $a_\mu^{(1)}$ from Eq. (57) , and then get the solutions for $a_\rho^{(2)}$, $a_\gamma^{(2)}$ and $a_\mu^{(2)}$ from Eq. (52).

There are two plots in each figure. The left ones are the results for the first order, while the right ones are the results for the first order plus the second order. The red lines denote the corresponding actual values. In the figures, we illustrate the results corresponding to different sets of angles θ_1 and θ_2. The third angle θ_3 is fixed at zero.

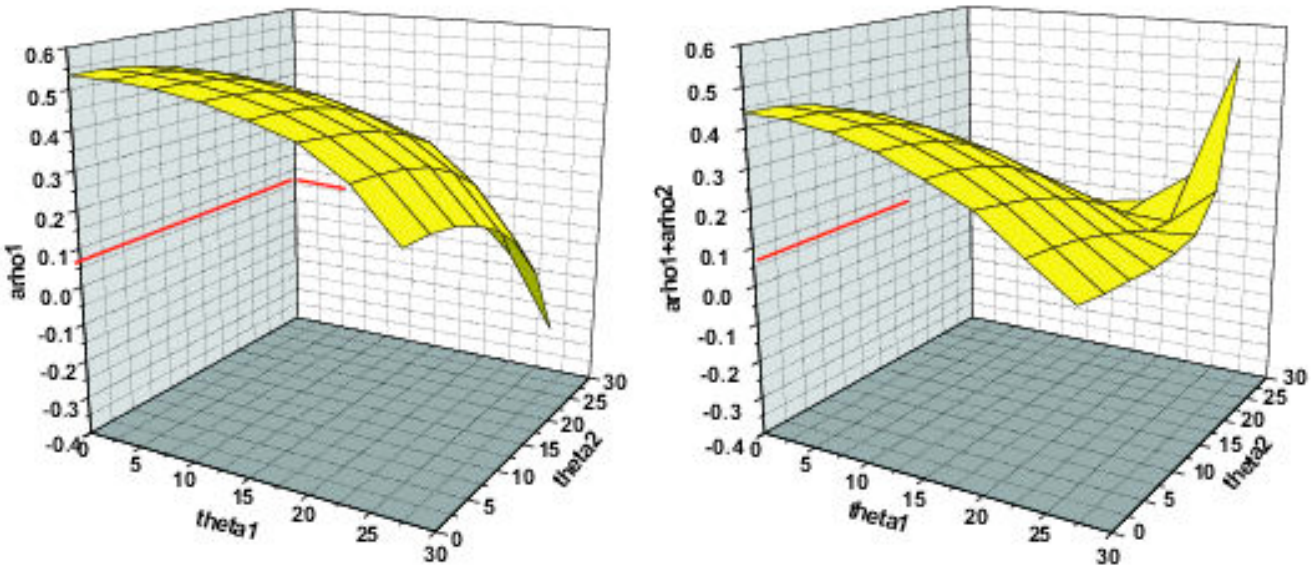

Figure 2: *Model 1: shale (0.20 porosity) over oil sand (0.10 porosity).* $\rho_0 = 2.32g/cm^3, \rho_1 = 2.46g/cm^3; \alpha_0 = 2627m/s, \alpha_1 = 4423m/s; \beta_0 = 1245m/s, \beta_1 = 2939m/s$. *For this model, the exact value of* a_ρ *is 0.06. The linear approximation* $a_\rho^{(1)}$ *(left) and the sum of linear and first non-linear* $a_\rho^{(1)} + a_\rho^{(2)}$ *(right).*

The numerical results indicate that all the second order solutions provide improvements over the linear solutions for all of the four models. When the second term is added to linear order, the results become much closer to the corresponding exact values and the surfaces become flatter in a larger range of angles. But the degrees of those improvements are different for different models. How accurately $\hat{D}^{PP}$ effectively synthesize $\hat{D}^{PS}$ and $\hat{D}^{SP}$ (as shown in Figs. 14 $\sim$ 17) determined the degree of benefit provided by the non-linear elastic approach. All of the "predicted" values in the figures are predicted using the linear results from $\hat{D}^{PP}$. And the "actual" values are calculated from the Zoeppritz' equations.

In principle, the elastic non-linear direct inversion in 2D requires all four components of data. However, in this section we introduce an approach which requires only $\hat{D}^{PP}$ and approximately synthesizes the other required components. Based on this approach, the first direct non-linear elastic inversion solution is derived. Value-added results are obtained from the non-linear inversion terms beyond linear. Although $\hat{D}^{PP}$ can itself provide useful non-linear direct inversion results, the implication of this research is that further value would derive from actually measuring $\hat{D}^{PP}$,

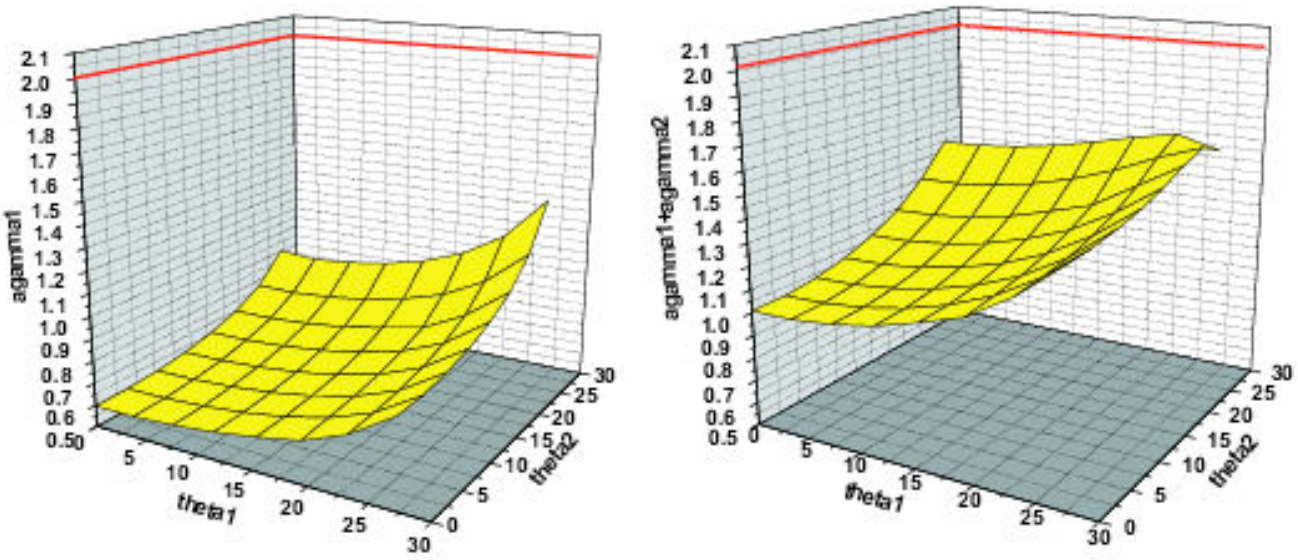

Figure 3: *Model 1: shale (0.20 porosity) over oil sand (0.10 porosity).* $\rho_0 = 2.32g/cm^3, \rho_1 = 2.46g/cm^3; \alpha_0 = 2627m/s, \alpha_1 = 4423m/s; \beta_0 = 1245m/s, \beta_1 = 2939m/s$. *For this model, the exact value of* a_γ *is 2.01. The linear approximation* $a_\gamma^{(1)}$ *(left) and the sum of linear and first non-linear* $a_\gamma^{(1)} + a_\gamma^{(2)}$ *(right).*

$\hat{D}^{PS}$, $\hat{D}^{SP}$ and $\hat{D}^{SS}$, as the method requires. In the following section, we give a consistent method and solve all of the second order Eqs. (48), (49), (50) and (51) with all four components of data available.

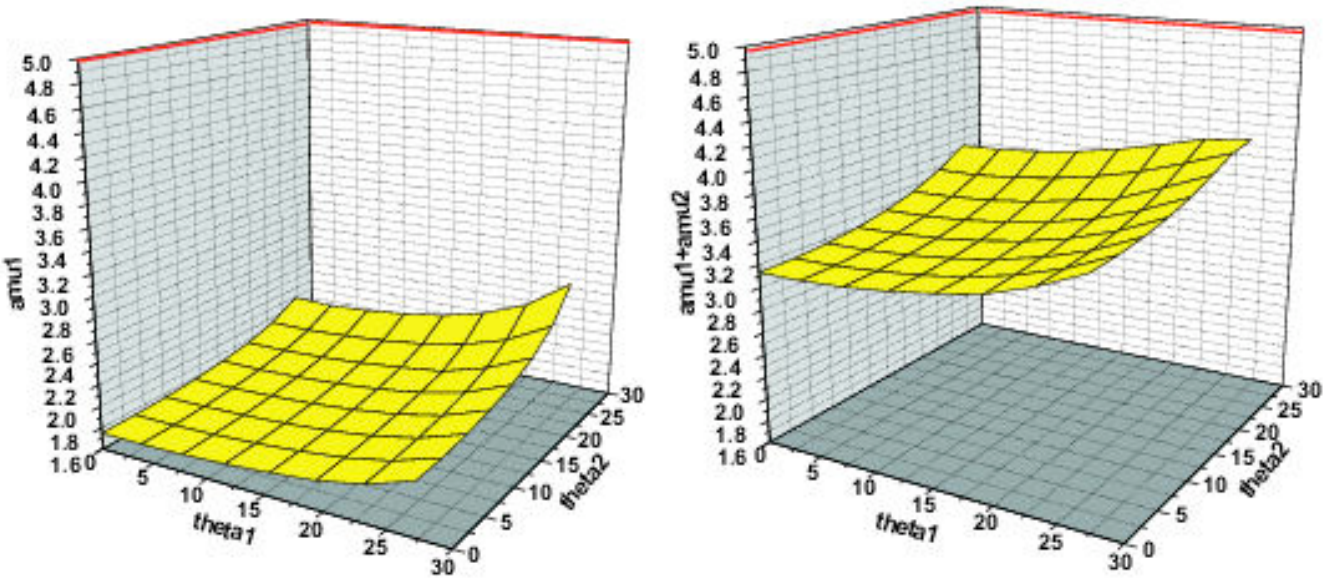

Figure 4: *Model 1: shale (0.20 porosity) over oil sand (0.10 porosity).* $\rho_0 = 2.32g/cm^3, \rho_1 = 2.46g/cm^3; \alpha_0 = 2627m/s, \alpha_1 = 4423m/s; \beta_0 = 1245m/s, \beta_1 = 2939m/s$. *For this model, the exact value of* a_μ *is 4.91. The linear approximation* $a_\mu^{(1)}$ *(left) and the sum of linear and first non-linear* $a_\mu^{(1)} + a_\mu^{(2)}$ *(right).*

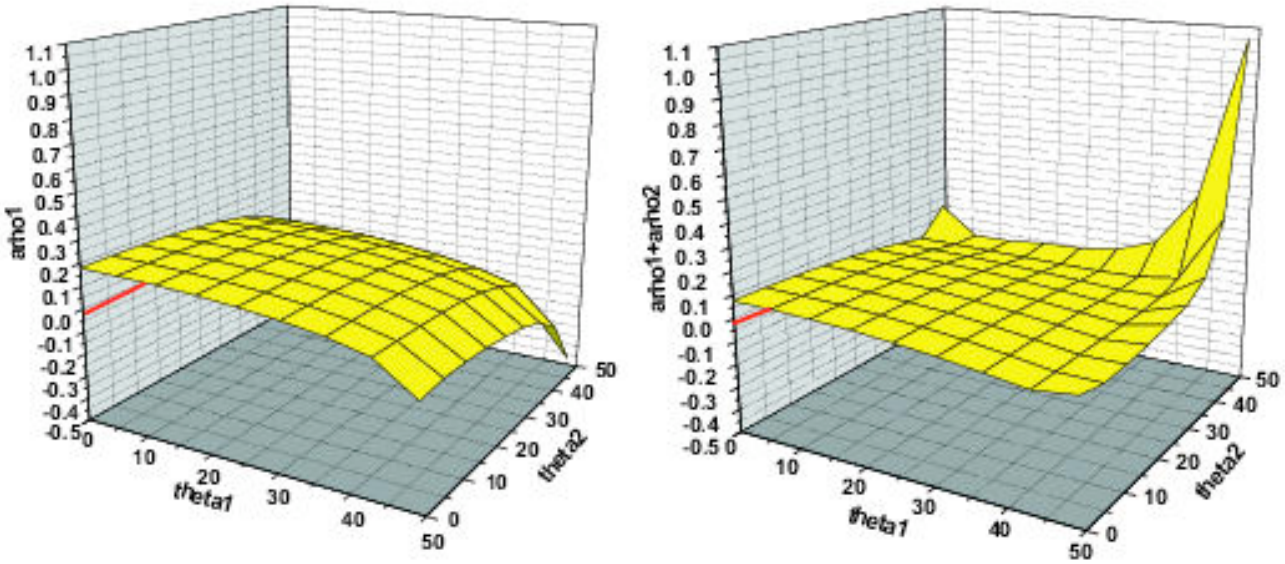

Figure 5: *Model 2: shale over oil sand, 0.20 porosity.* $\rho_0 = 2.32g/cm^3, \rho_1 = 2.27g/cm^3; \alpha_0 = 2627m/s, \alpha_1 = 3251m/s; \beta_0 = 1245m/s, \beta_1 = 2138m/s$. *For this model, the exact value of* a_ρ *is -0.022. The linear approximation* $a_\rho^{(1)}$ *(left) and the sum of linear and first non-linear* $a_\rho^{(1)} + a_\rho^{(2)}$ *(right).*

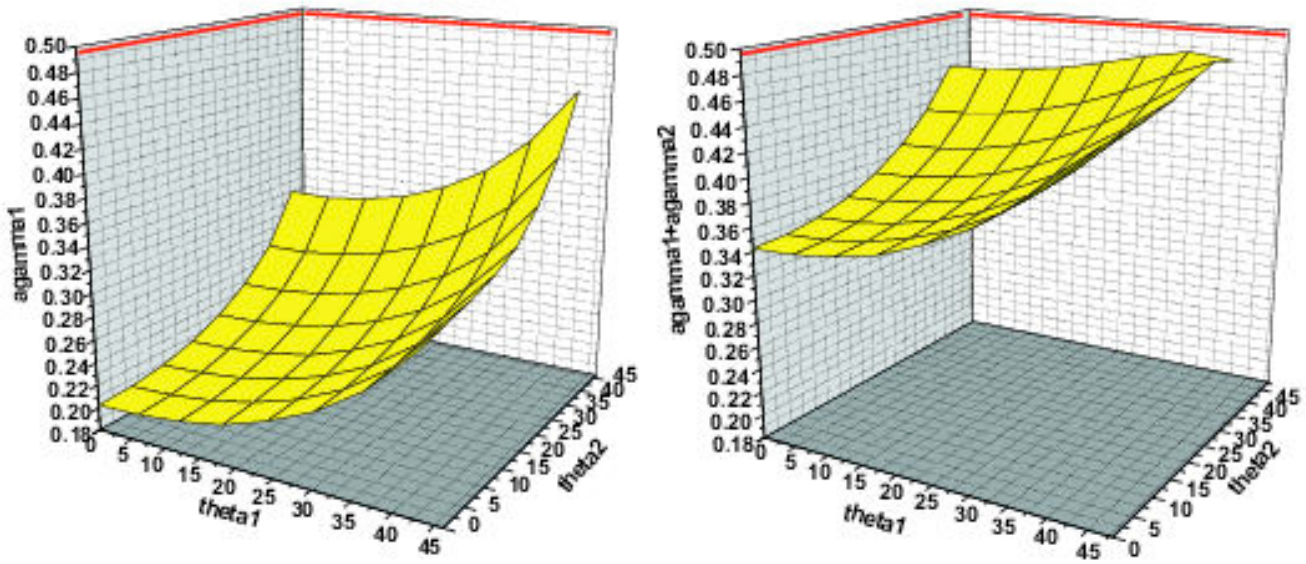

Figure 6: *Model 2: shale over oil sand, 0.20 porosity.* $\rho_0 = 2.32g/cm^3, \rho_1 = 2.27g/cm^3; \alpha_0 = 2627m/s, \alpha_1 = 3251m/s; \beta_0 = 1245m/s, \beta_1 = 2138m/s$. *For this model, the exact value of* a_γ *is 0.498. The linear approximation* $a_\gamma^{(1)}$ *(left) and the sum of linear and first non-linear* $a_\gamma^{(1)} + a_\gamma^{(2)}$ *(right).*

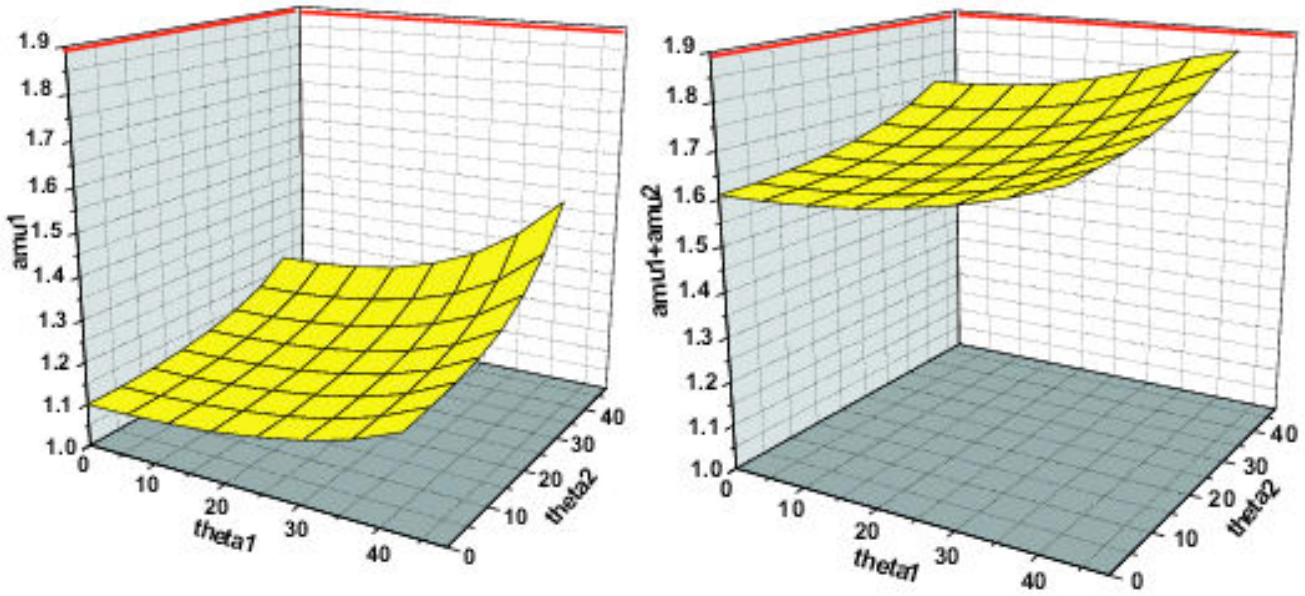

Figure 7: *Model 2: shale over oil sand, 0.20 porosity.* $\rho_0 = 2.32g/cm^3, \rho_1 = 2.27g/cm^3; \alpha_0 = 2627m/s, \alpha_1 = 3251m/s; \beta_0 = 1245m/s, \beta_1 = 2138m/s$. *For this model, the exact value of* a_μ *is 1.89. The linear approximation* $a_\mu^{(1)}$ *(left) and the sum of linear and first non-linear* $a_\mu^{(1)} + a_\mu^{(2)}$ *(right).*

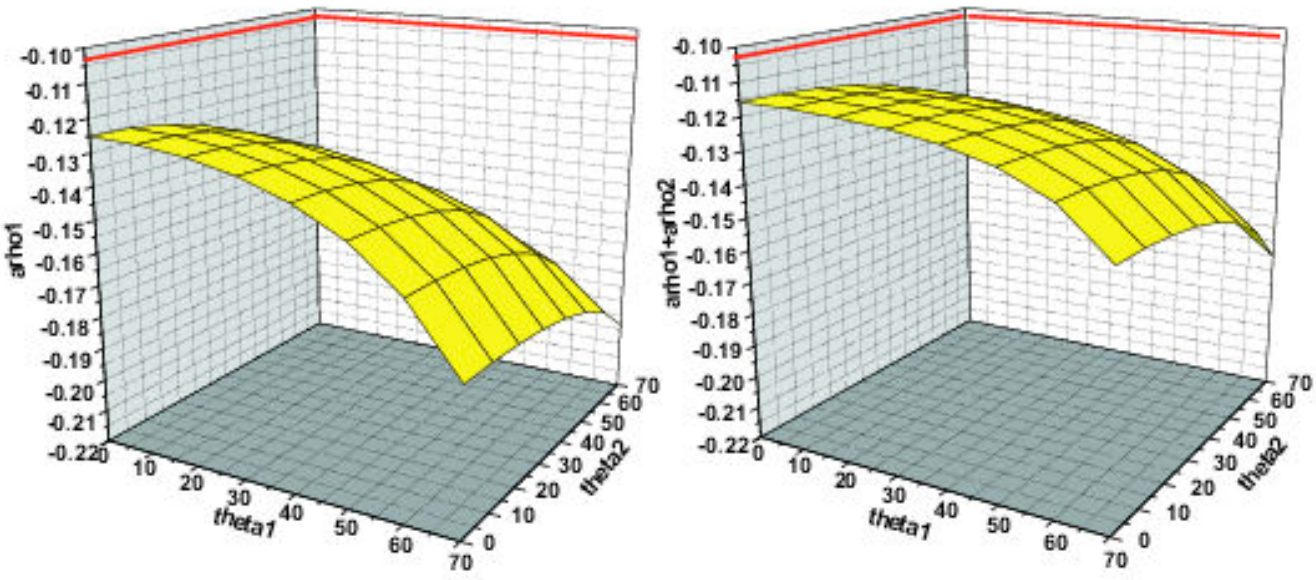

Figure 8: *Model 3: shale (0.20 porosity) over oil sand (0.30 porosity).* $\rho_0 = 2.32g/cm^3, \rho_1 = 2.08g/cm^3; \alpha_0 = 2627m/s, \alpha_1 = 2330m/s; \beta_0 = 1245m/s, \beta_1 = 1488m/s$. *For this model, the exact value of* a_ρ *is -0.103. The linear approximation* $a_\rho^{(1)}$ *(left) and the sum of linear and first non-linear* $a_\rho^{(1)} + a_\rho^{(2)}$ *(right).*

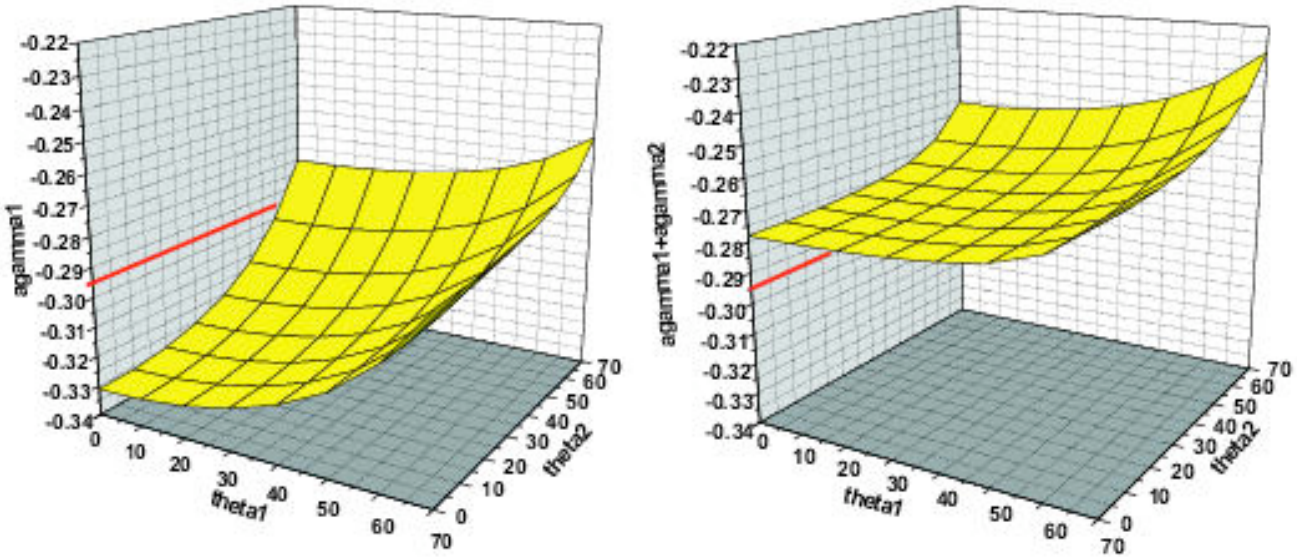

Figure 9: *Model 3: shale (0.20 porosity) over oil sand (0.30 porosity).* $\rho_0 = 2.32g/cm^3, \rho_1 = 2.08g/cm^3; \alpha_0 = 2627m/s, \alpha_1 = 2330m/s; \beta_0 = 1245m/s, \beta_1 = 1488m/s$. *For this model, the exact value of* a_γ *is -0.295. The linear approximation* $a_\gamma^{(1)}$ *(left) and the sum of linear and first non-linear* $a_\gamma^{(1)} + a_\gamma^{(2)}$ *(right).*

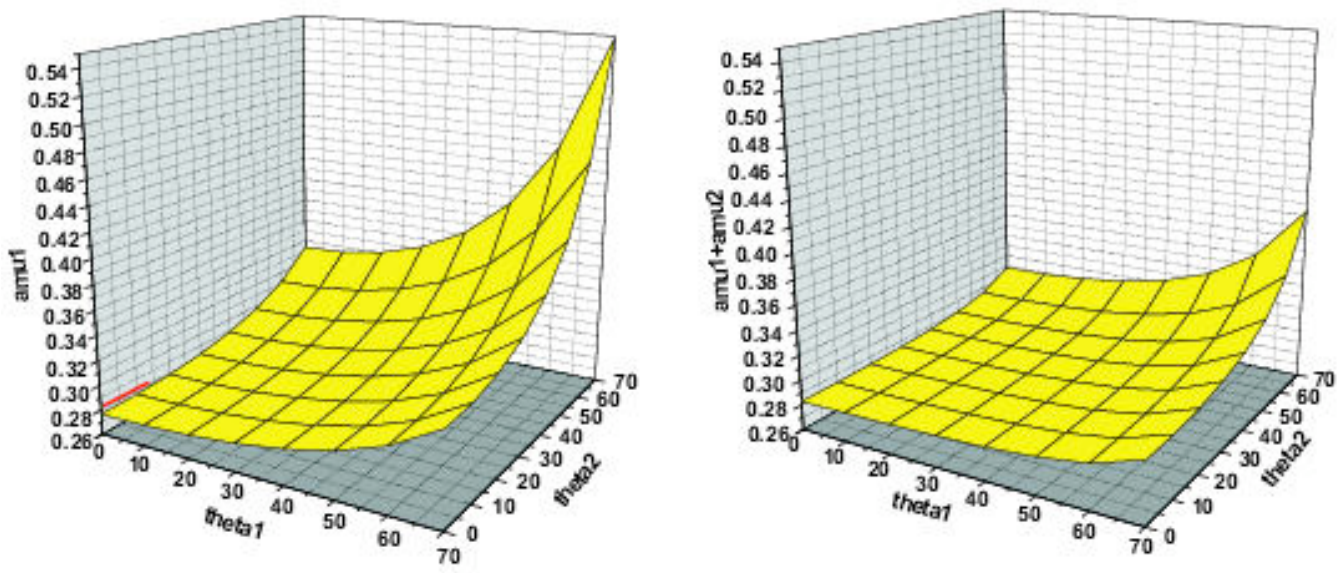

Figure 10: *Model 3: shale (0.20 porosity) over oil sand (0.30 porosity).* $\rho_0 = 2.32g/cm^3, \rho_1 = 2.08g/cm^3; \alpha_0 = 2627m/s, \alpha_1 = 2330m/s; \beta_0 = 1245m/s, \beta_1 = 1488m/s$. *For this model, the exact value of* a_μ *is 0.281. The linear approximation* $a_\mu^{(1)}$ *(left) and the sum of linear and first non-linear* $a_\mu^{(1)} + a_\mu^{(2)}$ *(right).*

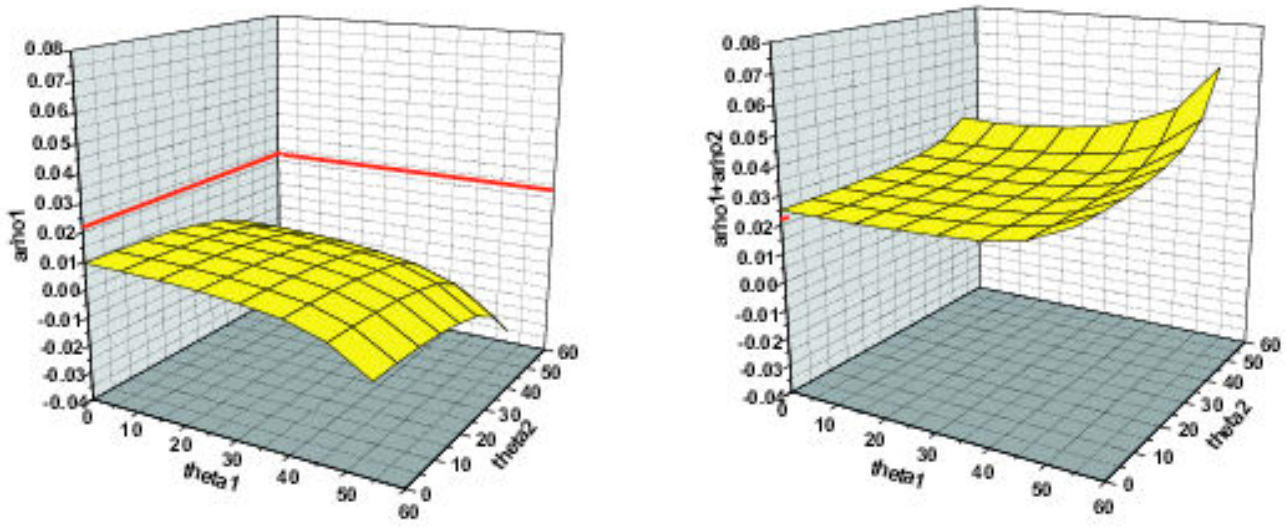

Figure 11: *Model 4: oil sand over wet sand, 0.20 porosity.* $\rho_0 = 2.27g/cm^3, \rho_1 = 2.32g/cm^3; \alpha_0 = 3251m/s, \alpha_1 = 3507m/s; \beta_0 = 2138m/s, \beta_1 = 2116m/s$. *For this model, the exact value of* a_ρ *is 0.022. The linear approximation* $a_\rho^{(1)}$ *(left) and the sum of linear and first non-linear* $a_\rho^{(1)} + a_\rho^{(2)}$ *(right).*

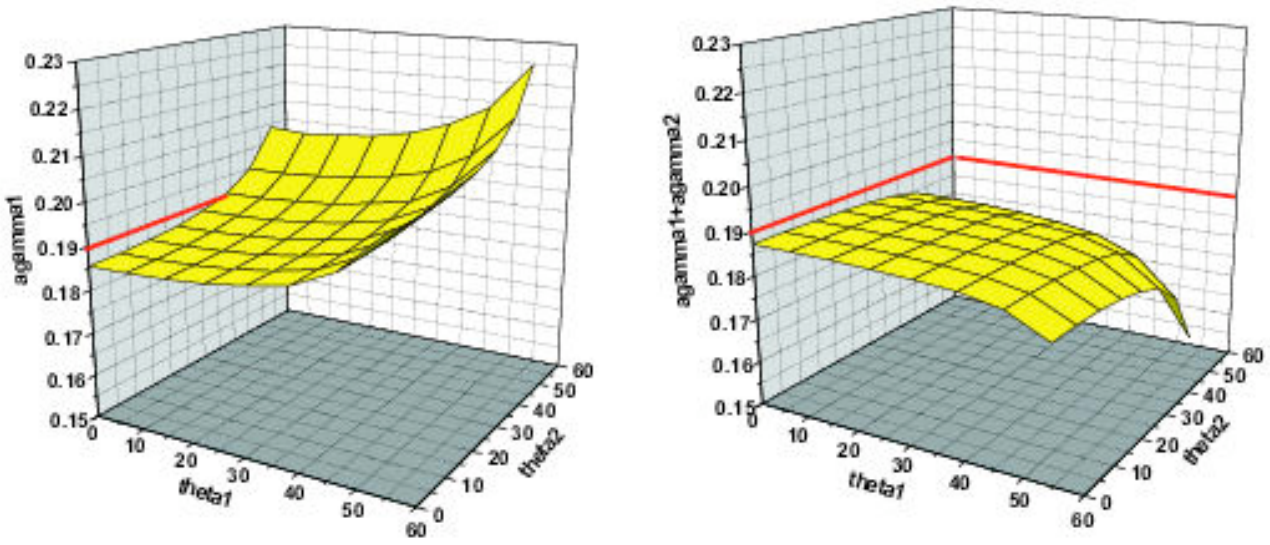

Figure 12: *Model 4: oil sand over wet sand, 0.20 porosity.* $\rho_0 = 2.27g/cm^3, \rho_1 = 2.32g/cm^3; \alpha_0 = 3251m/s, \alpha_1 = 3507m/s; \beta_0 = 2138m/s, \beta_1 = 2116m/s$. *For this model, the exact value of* a_γ *is 0.19. The linear approximation* $a_\gamma^{(1)}$ *(left) and the sum of linear and first non-linear* $a_\gamma^{(1)} + a_\gamma^{(2)}$ *(right).*

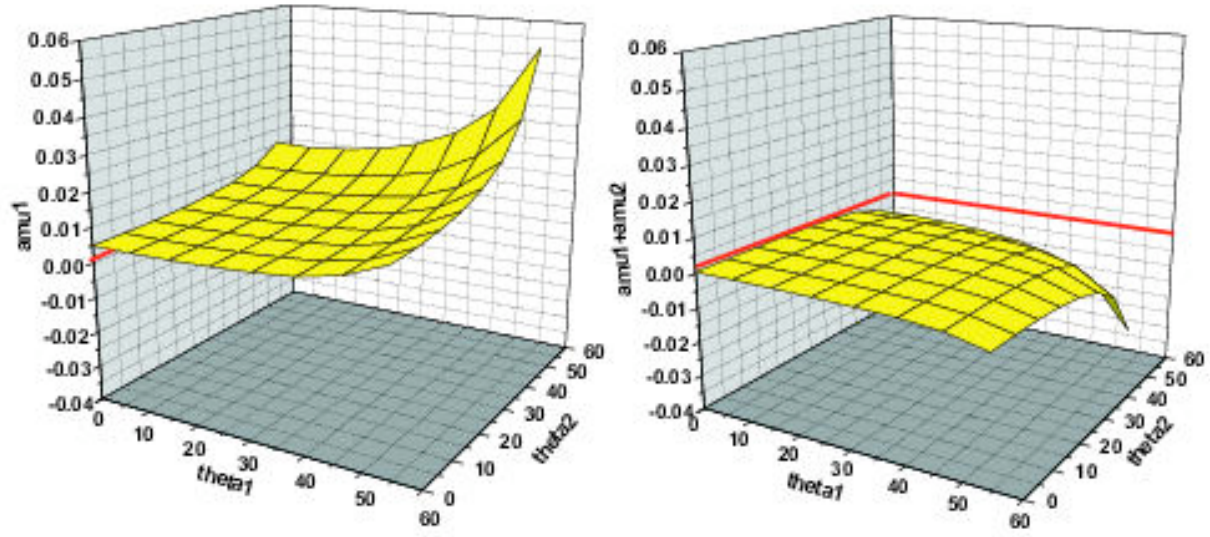

Figure 13: *Model 4: oil sand over wet sand, 0.20 porosity.* $\rho_0 = 2.27g/cm^3, \rho_1 = 2.32g/cm^3; \alpha_0 = 3251m/s, \alpha_1 = 3507m/s; \beta_0 = 2138m/s, \beta_1 = 2116m/s$. *For this model, the exact value of* a_μ *is 0.001. The linear approximation* $a_\mu^{(1)}$ *(left) and the sum of linear and first non-linear* $a_\mu^{(1)} + a_\mu^{(2)}$ *(right).*

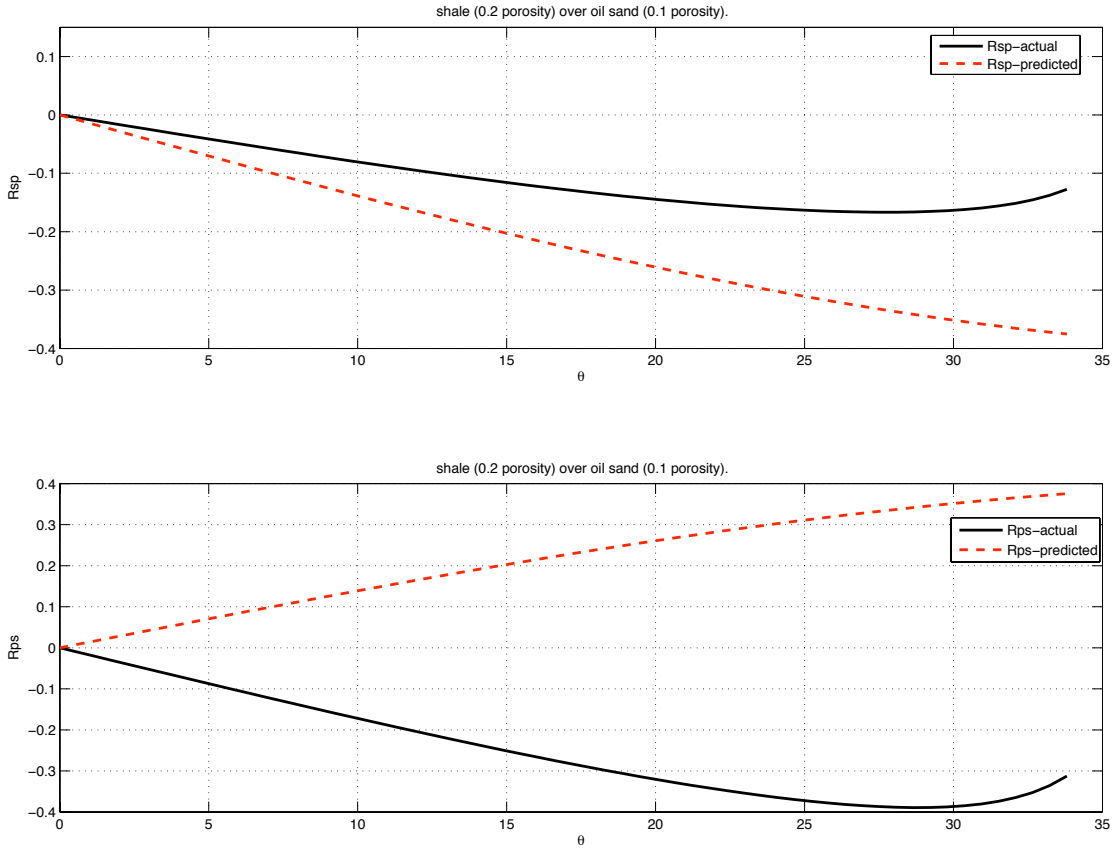

Figure 14: *The comparison between the synthesized values and the actual values of Rsp (top) and Rps (bottom) for Model 1: shale (0.20 porosity) over oil sand (0.10 porosity).* $\rho_0 = 2.32 g/cm^3, \rho_1 = 2.46 g/cm^3; \alpha_0 = 2627 m/s, \alpha_1 = 4423 m/s; \beta_0 = 1245 m/s, \beta_1 = 2939 m/s.$

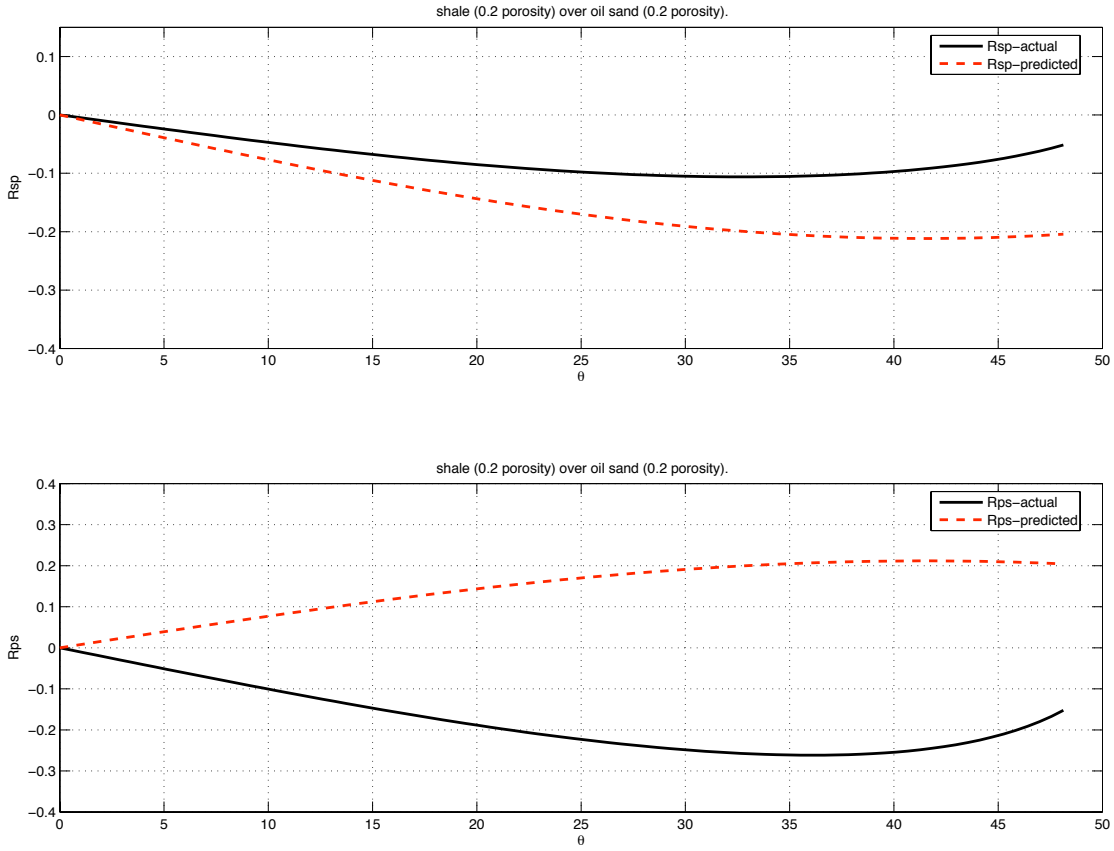

Figure 15: *The comparison between the synthesized values and the actual values of Rsp (top) and Rps (bottom) for Model 2: shale over oil sand, 0.20 porosity.* $\rho_0 = 2.32g/cm^3, \rho_1 = 2.27g/cm^3; \alpha_0 = 2627m/s, \alpha_1 = 3251m/s; \beta_0 = 1245m/s, \beta_1 = 2138m/s.$

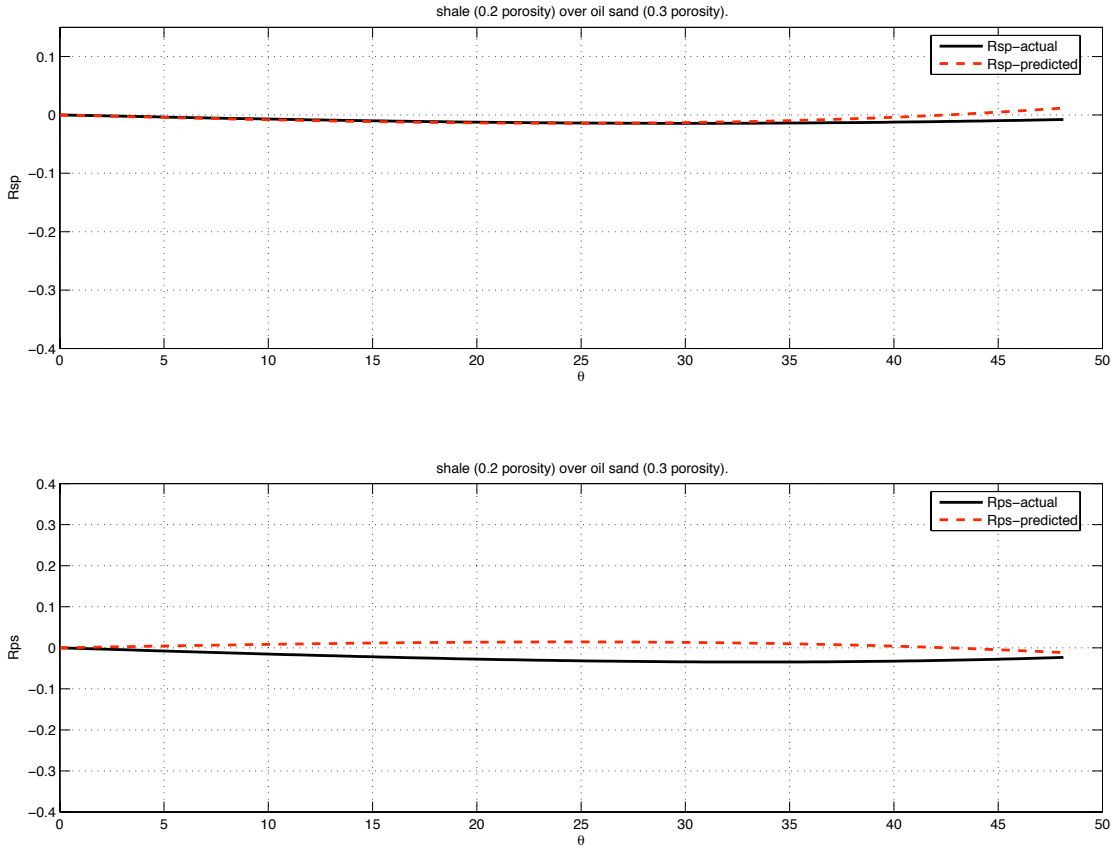

Figure 16: *The comparison between the synthesized values and the actual values of Rsp (top) and Rps (bottom) for Model 3: shale (0.20 porosity) over oil sand (0.30 porosity).* $\rho_0 = 2.32g/cm^3, \rho_1 = 2.08g/cm^3; \alpha_0 = 2627m/s, \alpha_1 = 2330m/s; \beta_0 = 1245m/s, \beta_1 = 1488m/s.$

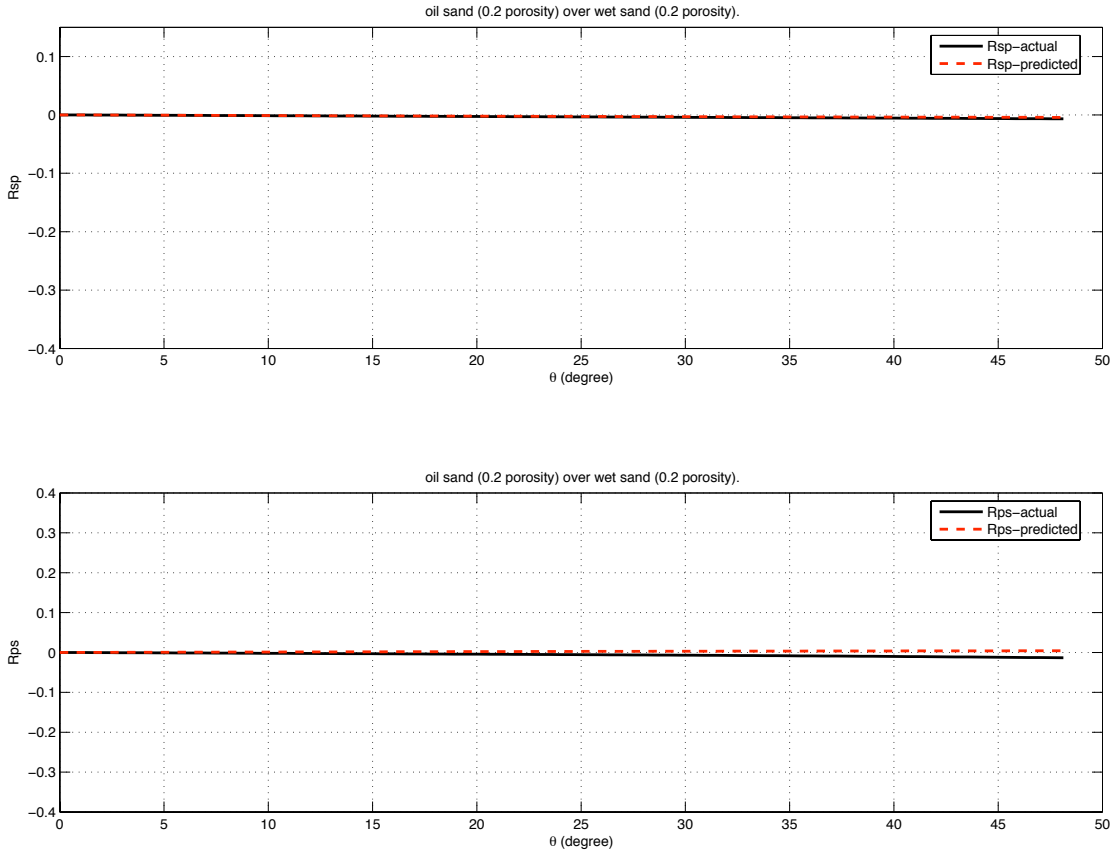

Figure 17: *The comparison between the synthesized values and the actual values of Rsp (top) and Rps (bottom) for Model 4: oil sand over wet sand, 0.20 porosity.* $\rho_0 = 2.27g/cm^3, \rho_1 = 2.32g/cm^3; \alpha_0 = 3251m/s, \alpha_1 = 3507m/s; \beta_0 = 2138m/s, \beta_1 = 2116m/s.$

Using all four components of data — full direct non-linear elastic inversion

Using four components of data, one consistent method to solve for the second terms is, first, using the linear solutions as shown in Eqs. (41), (42), (43) and (44), we can get the linear solution for $a_\rho^{(1)}$, $a_\gamma^{(1)}$ and $a_\mu^{(1)}$ in terms of $\hat{D}^{PP}, \hat{D}^{PS}, \hat{D}^{SP}$and $\hat{D}^{SS}$ through the following way

$$\begin{pmatrix} a_\rho^{(1)} \\ a_\gamma^{(1)} \\ a_\mu^{(1)} \end{pmatrix} = (O^T O)^{-1} O^T \begin{pmatrix} \hat{D}^{PP} \\ \hat{D}^{PS} \\ \hat{D}^{SP} \\ \hat{D}^{SS} \end{pmatrix}, \tag{58}$$

where the matrix O is

$$\begin{pmatrix} -\frac{1}{4}\left(1-\frac{k_g^{PP2}}{\nu_g^{PP2}}\right) & -\frac{1}{4}\left(1+\frac{k_g^{PP2}}{\nu_g^{PP2}}\right) & \frac{2\beta_0^2 k_g^{PP2}}{\alpha_0^2\left(\nu_g^{PP2}+k_g^{PP2}\right)} \\ -\frac{1}{4}\left(\frac{k_g^{PS}}{\nu_g^{PS}}+\frac{k_g^{PS}}{\eta_g^{PS}}\right) & 0 & -\frac{\beta_0^2}{2\omega^2}k_g^{PS}\left(\nu_g^{PS}+\eta_g^{PS}\right)\left(1-\frac{k_g^{PS2}}{\nu_g^{PS}\eta_g^{PS}}\right) \\ \frac{1}{4}\left(\frac{k_g^{SP}}{\nu_g^{SP}}+\frac{k_g^{SP}}{\eta_g^{SP}}\right) & 0 & \frac{\beta_0^2}{2\omega^2}k_g^{SP}\left(\nu_g^{SP}+\eta_g^{SP}\right)\left(1-\frac{k_g^{SP2}}{\nu_g^{SP}\eta_g^{SP}}\right) \\ -\frac{1}{4}\left(1-\frac{k_g^{SS2}}{\eta_g^{SS2}}\right) & 0 & -\left[\frac{k_g^{SS2}+\eta_g^{SS2}}{4\eta_g^{SS2}}-\frac{2k_g^{SS2}}{k_g^{SS2}+\eta_g^{SS2}}\right] \end{pmatrix}, \tag{59}$$

and O^T is the transpose of matrix O, the superscript -1 denotes the inverse of the matrix $O^T O$.

Let the arguments of $a_\rho^{(1)}$ and $a_\mu^{(1)}$ in Eqs. (41), (42), (43) and (44) equal, we need

$$-2\nu_g^{PP} = -\nu_g^{PS} - \eta_g^{PS} = -\nu_g^{SP} - \eta_g^{SP} = -2\eta_g^{SS},$$

which leads to (please see details in Appendix A)

$$\begin{aligned} 2\frac{\omega}{\alpha_0}\cos\theta^{PP} &= \frac{\omega}{\alpha_0}\sqrt{1-\frac{\alpha_0^2}{\beta_0^2}\sin^2\theta^{PS}} + \frac{\omega}{\beta_0}\cos\theta^{PS} = \frac{\omega}{\alpha_0}\cos\theta^{SP} + \frac{\omega}{\beta_0}\sqrt{1-\frac{\beta_0^2}{\alpha_0^2}\sin^2\theta^{SP}} \\ &= 2\frac{\omega}{\beta_0}\cos\theta^{SS}. \end{aligned}$$

From the expression above, given θ^{PP}, as shown in Fig. 18, we can find the corresponding angles θ^{PS}, θ^{SP} and θ^{SS} which appear in matrix O

$$\begin{aligned} \theta^{PS} &= \cos^{-1}\left[\frac{4b^2\cos^2\theta^{PP}+1-b^2}{4b\cos\theta^{PP}}\right], \\ \theta^{SP} &= \cos^{-1}\left[\frac{4b^2\cos^2\theta^{PP}-1+b^2}{4b^2\cos\theta^{PP}}\right], \\ \theta^{SS} &= \cos^{-1}\left(b\cos\theta^{PP}\right), \end{aligned}$$

where $b = \frac{\beta_0}{\alpha_0}$.

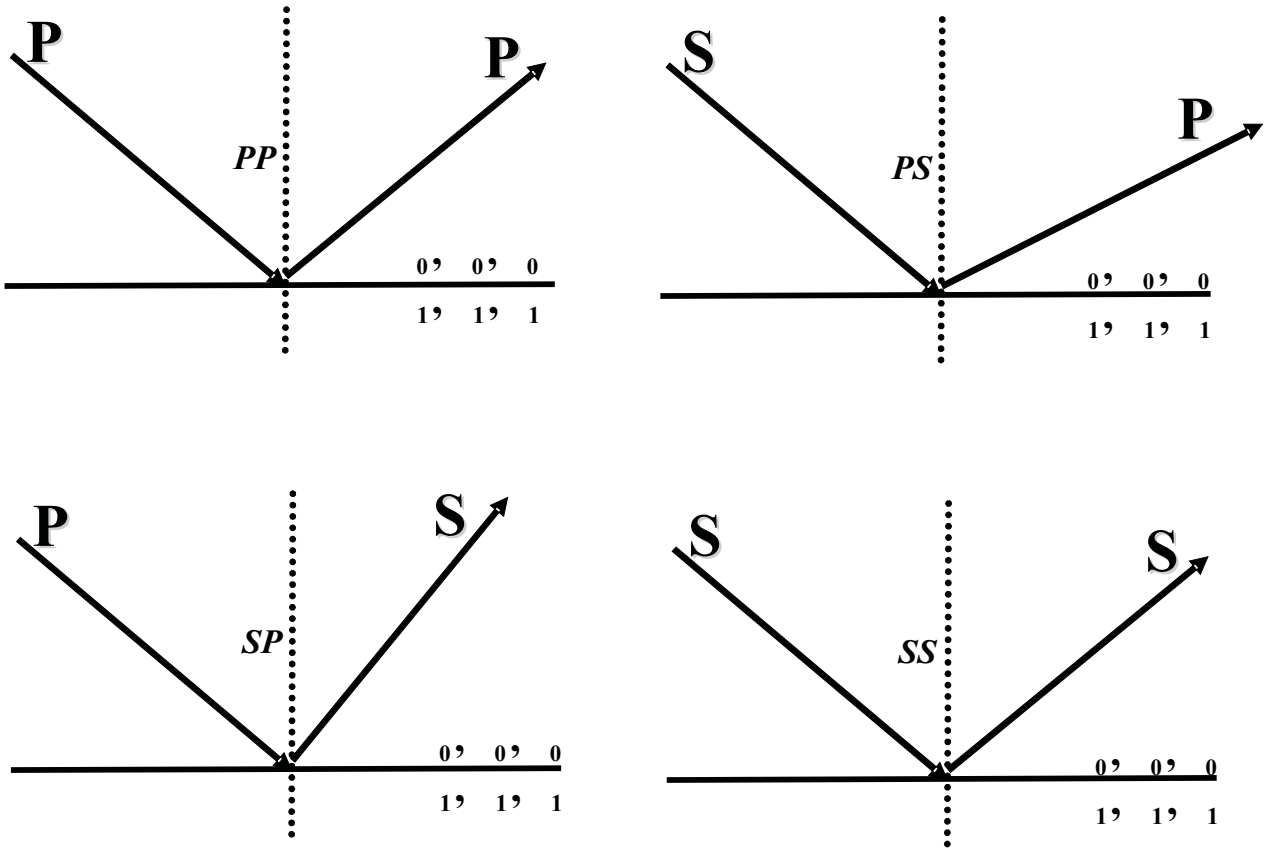

Figure 18: *Different incident angles.*

Then, through the similar way, we can get the solution for $a_\rho^{(2)}$, $a_\gamma^{(2)}$ and $a_\mu^{(2)}$ in terms of $a_\rho^{(1)}$, $a_\gamma^{(1)}$ and $a_\mu^{(1)}$

$$\begin{pmatrix} a_\rho^{(2)} \\ a_\gamma^{(2)} \\ a_\mu^{(2)} \end{pmatrix} = (O^T O)^{-1} O^T Q, \tag{60}$$

where the matrix Q is in terms of $a_\rho^{(1)}$, $a_\gamma^{(1)}$ and $a_\mu^{(1)}$.

Based on this idea, we get the following non-linear solutions for Eqs. (48), (49), (50) and (51) respectively.

The form of the solution for Eq. (48), i.e.,

$$\hat{G}_0^P \hat{V}_2^{PP} \hat{G}_0^P = -\hat{G}_0^P \hat{V}_1^{PP} \hat{G}_0^P \hat{V}_1^{PP} \hat{G}_0^P - \hat{G}_0^P \hat{V}_1^{PS} \hat{G}_0^S \hat{V}_1^{SP} \hat{G}_0^P ,$$

is the same as Eq. (52). In the $(k_s, z_s; k_g, z_g; \omega)$ domain, we get the the other three solutions respectively, for Eqs. (49), (50) and (51).

The solution for Eq. (49), i.e.,

$$\hat{G}_0^P \hat{V}_2^{PS} \hat{G}_0^S = -\hat{G}_0^P \hat{V}_1^{PP} \hat{G}_0^P \hat{V}_1^{PS} \hat{G}_0^S - \hat{G}_0^P \hat{V}_1^{PS} \hat{G}_0^S \hat{V}_1^{SS} \hat{G}_0^S,$$

is

$$\begin{aligned}
&-\frac{1}{4}\left(\frac{k_g}{\nu_g}+\frac{k_g}{\eta_g}\right)a_\rho^{(2)}(z)-\frac{\beta_0^2}{2\omega^2}k_g\left(\nu_g+\eta_g\right)\left(1-\frac{k_g^2}{\nu_g\eta_g}\right)a_\mu^{(2)}(z)\\
=&-\left[\left(\frac{1}{2}+\frac{1}{C+1}\right)\frac{1}{\eta_g\nu_g^2}\left(\frac{\beta_0^4}{\alpha_0^4}Ck_g^3-3\frac{\beta_0^2}{\alpha_0^2}Ck_g^5\frac{\beta_0^2}{\omega^2}-k_g^3\nu_g^2\frac{\beta_0^2}{\omega^2}+2k_g^5\nu_g^2\frac{\beta_0^4}{\omega^4}+2Ck_g^7\frac{\beta_0^4}{\omega^4}\right)\right.\\
&+\left(\frac{1}{2}-\frac{1}{C+1}\right)\frac{1}{\eta_g\nu_g^2}\left(\frac{\beta_0^2}{\alpha_0^2}Ck_g^3\nu_g^2\frac{\beta_0^2}{\omega^2}+2\frac{\beta_0^2}{\alpha_0^2}k_g^5\frac{\beta_0^2}{\omega^2}-2Ck_g^5\nu_g^2\frac{\beta_0^4}{\omega^4}-\frac{\beta_0^2}{\alpha_0^2}k_g^3+k_g^5\frac{\beta_0^2}{\omega^2}-2k_g^7\frac{\beta_0^4}{\omega^4}\right)\\
&+\left(\frac{1}{2C}+\frac{1}{C+1}\right)\frac{1}{4\eta_g^2\nu_g}\left(6k_g^3-12k_g^5\frac{\beta_0^2}{\omega^2}-k_g\frac{\omega^2}{\beta_0^2}+8k_g^7\frac{\beta_0^4}{\omega^4}+8C^3\nu_g^2k_g^5\frac{\beta_0^4}{\omega^4}\right.\\
&\left.-4\frac{\beta_0^2}{\alpha_0^2}C^3\nu_g^2k_g^3\frac{\beta_0^2}{\omega^2}\right)\\
&-\left(\frac{1}{2C}-\frac{1}{C+1}\right)\frac{1}{4\eta_g\nu_g^2}\left(4\frac{\beta_0^2}{\alpha_0^2}k_g^3-8k_g^5\frac{\beta_0^2}{\omega^2}-k_g\frac{\omega^2}{\alpha_0^2}+2k_g^3-4C\nu_g^2k_g^3\frac{\beta_0^2}{\omega^2}+8C\nu_g^2k_g^5\frac{\beta_0^4}{\omega^4}\right.\\
&\left.\left.-4\frac{\beta_0^2}{\alpha_0^2}k_g^5\frac{\beta_0^2}{\omega^2}+8k_g^7\frac{\beta_0^4}{\omega^4}\right)-\frac{\beta_0^2}{\alpha_0^2}\frac{k_g^3}{\nu_g}\frac{\beta_0^2}{\omega^2}+\frac{k_g}{2\eta_g}\left(2k_g^2\frac{\beta_0^2}{\omega^2}-1\right)\right]a_\mu^{(1)}(z)a_\mu^{(1)}(z)\\
&-\left[\left(\frac{1}{2}+\frac{1}{C+1}\right)\frac{k_g}{8\eta_g\nu_g^2}\left(Ck_g^2+\nu_g^2\right)-\left(\frac{1}{2}-\frac{1}{C+1}\right)\frac{k_g}{8\eta_g\nu_g^2}\left(k_g^2+C\nu_g^2\right)\right.\\
&\left.+\left(\frac{1}{2C}+\frac{1}{C+1}\right)\frac{k_g}{8\eta_g^2\nu_g}\left(C^3\nu_g^2+k_g^2\right)-\left(\frac{1}{2C}-\frac{1}{C+1}\right)\frac{k_g}{8\eta_g\nu_g^2}\left(k_g^2+C\nu_g^2\right)\right]a_\rho^{(1)}(z)a_\rho^{(1)}(z)\\
&-\left[\left(\frac{1}{2}+\frac{1}{C+1}\right)\frac{\beta_0^2}{\alpha_0^2}\frac{1}{4\nu_g^3}k_g\left(k_g^2-\nu_g^2\right)+\left(\frac{1}{2}-\frac{1}{C+1}\right)\frac{1}{4\eta_g\nu_g^2}\left(k_g\frac{\omega^2}{\alpha_0^2}-2\frac{\beta_0^2}{\alpha_0^2}k_g^3\right)+\frac{\beta_0^2}{\alpha_0^2}\frac{k_g}{2\nu_g}\right]\\
&\times a_\mu^{(1)}(z)a_\gamma^{(1)}(z)\\
&+\left[\left(\frac{1}{2}+\frac{1}{C+1}\right)\frac{k_g\left(k_g^2+\nu_g^2\right)}{8\nu_g^3}-\left(\frac{1}{2}-\frac{1}{C+1}\right)\frac{k_g\left(k_g^2+\nu_g^2\right)}{8\eta_g\nu_g^2}\right]a_\rho^{(1)}(z)a_\gamma^{(1)}(z)\\
&-\left[\left(\frac{1}{2}+\frac{1}{C+1}\right)\frac{1}{4\eta_g\nu_g^2}\left(3\frac{\beta_0^2}{\alpha_0^2}Ck_g^3+\nu_g^2k_g-4Ck_g^5\frac{\beta_0^2}{\omega^2}-4k_g^3\nu_g^2\frac{\beta_0^2}{\omega^2}\right)\right.\\
&-\left(\frac{1}{2}-\frac{1}{C+1}\right)\frac{1}{4\eta_g\nu_g^2}\left(\frac{\beta_0^2}{\alpha_0^2}C\nu_g^2k_g+k_g^3-4k_g^5\frac{\beta_0^2}{\omega^2}-4Ck_g^3\nu_g^2\frac{\beta_0^2}{\omega^2}+2\frac{\beta_0^2}{\alpha_0^2}k_g^3\right)\\
&+\left(\frac{1}{2C}+\frac{1}{C+1}\right)\frac{1}{4\eta_g^2\nu_g}\left(k_g^3-2k_g^5\frac{\beta_0^2}{\omega^2}+\frac{\beta_0^2}{\alpha_0^2}C^3\nu_g^2k_g-4C^3\nu_g^2k_g^3\frac{\beta_0^2}{\omega^2}-\frac{1}{2}k_g\frac{\omega^2}{\beta_0^2}\right.\\
&\left.+2C^2\nu_g^2k_g^3\frac{\beta_0^2}{\omega^2}\right)\\
&-\left(\frac{1}{2C}-\frac{1}{C+1}\right)\frac{1}{4\eta_g\nu_g^2}\left(C\nu_g^2k_g-2C\nu_g^2k_g^3\frac{\beta_0^2}{\omega^2}+\frac{\beta_0^2}{\alpha_0^2}k_g^3-2k_g^5\frac{\beta_0^2}{\omega^2}+2C^2\nu_g^2k_g^3\frac{\beta_0^2}{\omega^2}\right.
\end{aligned}$$

$$
\begin{aligned}
&-2C\nu_g^2 k_g^3 \frac{\beta_0^2}{\omega^2} - \frac{1}{2} k_g \frac{\omega^2}{\beta_0^2}\Bigg)\Bigg] \times a_\rho^{(1)}(z) a_\mu^{(1)}(z) \\
&- \frac{1}{\eta_g \nu_g^2}\left(\frac{\beta_0^4}{\alpha_0^4} C k_g^3 - 3\frac{\beta_0^2}{\alpha_0^2} C k_g^5 \frac{\beta_0^2}{\omega^2} - k_g^3 \nu_g^2 \frac{\beta_0^2}{\omega^2} + 2k_g^5 \nu_g^2 \frac{\beta_0^4}{\omega^4} + 2C k_g^7 \frac{\beta_0^4}{\omega^4}\right) \\
&\times \left[\frac{1}{2}\int_0^z dz' a_\mu^{(1)}{}_z\left(\frac{(C+1)z-(C-1)z'}{2}\right) a_\mu^{(1)}(z') + \frac{1}{C+1} a_\mu^{(1)'}(z) \int_0^z dz' a_\mu^{(1)}(z')\right] \\
&- \frac{1}{\eta_g \nu_g^2}\left(\frac{\beta_0^2}{\alpha_0^2} C k_g^3 \nu_g^2 \frac{\beta_0^2}{\omega^2} + 2\frac{\beta_0^2}{\alpha_0^2} k_g^5 \frac{\beta_0^2}{\omega^2} - 2C k_g^5 \nu_g^2 \frac{\beta_0^4}{\omega^4} - \frac{\beta_0^2}{\alpha_0^2} k_g^3 + k_g^5 \frac{\beta_0^2}{\omega^2} - 2k_g^7 \frac{\beta_0^4}{\omega^4}\right) \\
&\times \left[\frac{1}{2}\int_0^z dz' a_\mu^{(1)}{}_z\left(\frac{(C+1)z-(C-1)z'}{2}\right) a_\mu^{(1)}(z') - \frac{1}{C+1} a_\mu^{(1)'}(z) \int_0^z dz' a_\mu^{(1)}(z')\right] \\
&- \frac{1}{4\eta_g^2 \nu_g}\left(6k_g^3 - 12k_g^5 \frac{\beta_0^2}{\omega^2} - k_g \frac{\omega^2}{\beta_0^2} + 8k_g^7 \frac{\beta_0^4}{\omega^4} + 8C^3 \nu_g^2 k_g^5 \frac{\beta_0^4}{\omega^4} - 4\frac{\beta_0^2}{\alpha_0^2} C^3 \nu_g^2 k_g^3 \frac{\beta_0^2}{\omega^2}\right) \\
&\times \left[\frac{1}{2C}\int_0^z dz' a_\mu^{(1)}{}_z\left(\frac{(C+1)z+(C-1)z'}{2C}\right) a_\mu^{(1)}(z') + \frac{1}{C+1} a_\mu^{(1)'}(z) \int_0^z dz' a_\mu^{(1)}(z')\right] \\
&+ \frac{1}{4\eta_g \nu_g^2}\left(4\frac{\beta_0^2}{\alpha_0^2} k_g^3 - 8k_g^5 \frac{\beta_0^2}{\omega^2} - k_g \frac{\omega^2}{\alpha_0^2} + 2k_g^3 - 4C\nu_g^2 k_g^3 \frac{\beta_0^2}{\omega^2} + 8C\nu_g^2 k_g^5 \frac{\beta_0^4}{\omega^4} - 4\frac{\beta_0^2}{\alpha_0^2} k_g^5 \frac{\beta_0^2}{\omega^2} + 8k_g^7 \frac{\beta_0^4}{\omega^4}\right) \\
&\times \left[\frac{1}{2C}\int_0^z dz' a_\mu^{(1)}{}_z\left(\frac{(C+1)z+(C-1)z'}{2C}\right) a_\mu^{(1)}(z') - \frac{1}{C+1} a_\mu^{(1)'}(z) \int_0^z dz' a_\mu^{(1)}(z')\right] \\
&- \frac{k_g\left(Ck_g^2+\nu_g^2\right)}{8\eta_g \nu_g^2}\left[\frac{1}{2}\int_0^z dz' a_\rho^{(1)}{}_z\left(\frac{(C+1)z-(C-1)z'}{2}\right) a_\rho^{(1)}(z')\right. \\
&\left.+\frac{1}{C+1} a_\rho^{(1)'}(z) \int_0^z dz' a_\rho^{(1)}(z')\right] \\
&+ \frac{k_g\left(k_g^2+C\nu_g^2\right)}{8\eta_g \nu_g^2}\left[\frac{1}{2}\int_0^z dz' a_\rho^{(1)}{}_z\left(\frac{(C+1)z-(C-1)z'}{2}\right) a_\rho^{(1)}(z')\right. \\
&\left.-\frac{1}{C+1} a_\rho^{(1)'}(z) \int_0^z dz' a_\rho^{(1)}(z')\right] \\
&- \frac{C^3 k_g \nu_g^2 + k_g^3}{8\eta_g^2 \nu_g}\left[\frac{1}{2C}\int_0^z dz' a_\rho^{(1)}{}_z\left(\frac{(C+1)z+(C-1)z'}{2C}\right) a_\rho^{(1)}(z')\right. \\
&\left.+\frac{1}{C+1} a_\rho^{(1)'}(z) \int_0^z dz' a_\rho^{(1)}(z')\right] \\
&+ \frac{k_g\left(k_g^2+C\nu_g^2\right)}{8\eta_g \nu_g^2}\left[\frac{1}{2C}\int_0^z dz' a_\rho^{(1)}{}_z\left(\frac{(C+1)z+(C-1)z'}{2C}\right) a_\rho^{(1)}(z')\right. \\
&\left.-\frac{1}{C+1} a_\rho^{(1)'}(z) \int_0^z dz' a_\rho^{(1)}(z')\right] \\
&- \frac{\beta_0^2}{\alpha_0^2}\frac{k_g\left(k_g^2-\nu_g^2\right)}{4\nu_g^3}\left[\frac{1}{2}\int_0^z dz' a_\gamma^{(1)}{}_z\left(\frac{(C+1)z-(C-1)z'}{2}\right) a_\mu^{(1)}(z')\right. \\
&\left.+\frac{1}{C+1} a_\mu^{(1)'}(z) \int_0^z dz' a_\gamma^{(1)}(z')\right]
\end{aligned}
$$

$$
\begin{aligned}
&- \frac{1}{4\eta_g\nu_g^2}\left(k_g\frac{\omega^2}{\alpha_0^2} - 2\frac{\beta_0^2}{\alpha_0^2}k_g^3\right)\left[\frac{1}{2}\int_0^z dz' a_\gamma^{(1)}{}_z\left(\frac{(C+1)z-(C-1)\,z'}{2}\right)a_\mu^{(1)}\left(z'\right)\right.\\
&\left.-\frac{1}{C+1}a_\mu^{(1)'}(z)\int_0^z dz' a_\gamma^{(1)}(z')\right]\\
&+\frac{k_g\left(k_g^2+\nu_g^2\right)}{8\nu_g^3}\left[\frac{1}{2}\int_0^z dz' a_\gamma^{(1)}{}_z\left(\frac{(C+1)z-(C-1)\,z'}{2}\right)a_\rho^{(1)}\left(z'\right)\right.\\
&\left.+\frac{1}{C+1}a_\rho^{(1)'}(z)\int_0^z dz' a_\gamma^{(1)}(z')\right]\\
&-\frac{k_g\left(k_g^2+\nu_g^2\right)}{8\eta_g\nu_g^2}\left[\frac{1}{2}\int_0^z dz' a_\gamma^{(1)}{}_z\left(\frac{(C+1)z-(C-1)\,z'}{2}\right)a_\rho^{(1)}\left(z'\right)\right.\\
&\left.-\frac{1}{C+1}a_\rho^{(1)'}(z)\int_0^z dz' a_\gamma^{(1)}(z')\right]\\
&-\frac{1}{4\eta_g\nu_g^2}\left(\frac{\beta_0^2}{\alpha_0^2}Ck_g^3+\nu_g^2k_g-2Ck_g^5\frac{\beta_0^2}{\omega^2}-2k_g^3\nu_g^2\frac{\beta_0^2}{\omega^2}\right)\\
&\times\left[\frac{1}{2}\int_0^z dz' a_\rho^{(1)}{}_z\left(\frac{(C+1)z-(C-1)\,z'}{2}\right)a_\mu^{(1)}\left(z'\right)+\frac{1}{C+1}a_\mu^{(1)'}(z)\int_0^z dz' a_\rho^{(1)}(z')\right]\\
&-\frac{1}{4\eta_g\nu_g^2}\left(2\frac{\beta_0^2}{\alpha_0^2}Ck_g^3-2Ck_g^5\frac{\beta_0^2}{\omega^2}-2k_g^3\nu_g^2\frac{\beta_0^2}{\omega^2}\right)\\
&\times\left[\frac{1}{2}\int_0^z dz' a_\mu^{(1)}{}_z\left(\frac{(C+1)z-(C-1)\,z'}{2}\right)a_\rho^{(1)}\left(z'\right)+\frac{1}{C+1}a_\rho^{(1)'}(z)\int_0^z dz' a_\mu^{(1)}(z')\right]\\
&+\frac{1}{4\eta_g\nu_g^2}\left(\frac{\beta_0^2}{\alpha_0^2}C\nu_g^2k_g+k_g^3-2k_g^5\frac{\beta_0^2}{\omega^2}-2Ck_g^3\nu_g^2\frac{\beta_0^2}{\omega^2}\right)\\
&\times\left[\frac{1}{2}\int_0^z dz' a_\rho^{(1)}{}_z\left(\frac{(C+1)z-(C-1)\,z'}{2}\right)a_\mu^{(1)}\left(z'\right)-\frac{1}{C+1}a_\mu^{(1)'}(z)\int_0^z dz' a_\rho^{(1)}(z')\right]\\
&+\frac{1}{4\eta_g\nu_g^2}\left(2\frac{\beta_0^2}{\alpha_0^2}k_g^3-2k_g^5\frac{\beta_0^2}{\omega^2}-2Ck_g^3\nu_g^2\frac{\beta_0^2}{\omega^2}\right)\\
&\times\left[\frac{1}{2}\int_0^z dz' a_\mu^{(1)}{}_z\left(\frac{(C+1)z-(C-1)\,z'}{2}\right)a_\rho^{(1)}\left(z'\right)-\frac{1}{C+1}a_\rho^{(1)'}(z)\int_0^z dz' a_\mu^{(1)}(z')\right]\\
&-\frac{1}{4\eta_g^2\nu_g}\left(k_g^3-2k_g^5\frac{\beta_0^2}{\omega^2}+\frac{\beta_0^2}{\alpha_0^2}C^3\nu_g^2k_g-2C^3\nu_g^2k_g^3\frac{\beta_0^2}{\omega^2}\right)\\
&\times\left[\frac{1}{2C}\int_0^z dz' a_\rho^{(1)}{}_z\left(\frac{(C+1)z+(C-1)\,z'}{2C}\right)a_\mu^{(1)}\left(z'\right)+\frac{1}{C+1}a_\mu^{(1)'}(z)\int_0^z dz' a_\rho^{(1)}(z')\right]\\
&-\frac{1}{4\eta_g^2\nu_g}\left(-2C^3\nu_g^2k_g^3\frac{\beta_0^2}{\omega^2}-\frac{1}{2}k_g\frac{\omega^2}{\beta_0^2}+2C^2\nu_g^2k_g^3\frac{\beta_0^2}{\omega^2}\right)\\
&\times\left[\frac{1}{2C}\int_0^z dz' a_\mu^{(1)}{}_z\left(\frac{(C+1)z+(C-1)\,z'}{2C}\right)a_\rho^{(1)}\left(z'\right)+\frac{1}{C+1}a_\rho^{(1)'}(z)\int_0^z dz' a_\mu^{(1)}(z')\right]\\
&+\frac{1}{4\eta_g\nu_g^2}\left(C\nu_g^2k_g-2C\nu_g^2k_g^3\frac{\beta_0^2}{\omega^2}+\frac{\beta_0^2}{\alpha_0^2}k_g^3-2k_g^5\frac{\beta_0^2}{\omega^2}\right)
\end{aligned}
$$

$$
\begin{aligned}
&\times\left[\frac{1}{2C}\int_0^z dz' a_\rho^{(1)}{}_z\left(\frac{(C+1)z+(C-1)\,z'}{2C}\right)a_\mu^{(1)}\left(z'\right)-\frac{1}{C+1}a_\mu^{(1)'}(z)\int_0^z dz' a_\rho^{(1)}(z')\right]\\
&+\frac{1}{4\eta_g\nu_g^2}\left(2C^2\nu_g^2k_g^3\frac{\beta_0^2}{\omega^2}-2C\nu_g^2k_g^3\frac{\beta_0^2}{\omega^2}-\frac{1}{2}k_g\frac{\omega^2}{\beta_0^2}\right)\\
&\times\left[\frac{1}{2C}\int_0^z dz' a_\mu^{(1)}{}_z\left(\frac{(C+1)z+(C-1)\,z'}{2C}\right)a_\rho^{(1)}\left(z'\right)-\frac{1}{C+1}a_\rho^{(1)'}(z)\int_0^z dz' a_\mu^{(1)}(z')\right],
\end{aligned}
$$

the solution for Eq. (50), i.e.,

$$
\hat{G}_0^S\hat{V}_2^{SP}\hat{G}_0^P=-\hat{G}_0^S\hat{V}_1^{SP}\hat{G}_0^P\hat{V}_1^{PP}\hat{G}_0^P-\hat{G}_0^S\hat{V}_1^{SS}\hat{G}_0^S\hat{V}_1^{SP}\hat{G}_0^P,
$$

is

$$
\begin{aligned}
&\frac{1}{4}\left(\frac{k_g}{\nu_g}+\frac{k_g}{\eta_g}\right)a_\rho^{(2)}(z)+\frac{\beta_0^2}{2\omega^2}k_g\left(\nu_g+\eta_g\right)\left(1-\frac{k_g^2}{\nu_g\eta_g}\right)a_\mu^{(2)}(z)\\
=&\Bigg\{-\frac{1}{2\eta_g\nu_g^2}\left[2(C-1)\nu_g^2k_g^5\frac{\beta_0^4}{\omega^4}+\left(1-\frac{\beta_0^2}{\alpha_0^2}C\right)\nu_g^2k_g^3\frac{\beta_0^2}{\omega^2}\right]-\frac{\beta_0^2}{\alpha_0^2}\frac{k_g^3}{\nu_g}\frac{\beta_0^2}{\omega^2}+\frac{k_g}{2\eta_g}\left(2k_g^2\frac{\beta_0^2}{\omega^2}-1\right)\\
&+\left(\frac{1}{2C}+\frac{1}{C+1}\right)\frac{1}{4\eta_g^2\nu_g}\left(6k_g^3-12k_g^5\frac{\beta_0^2}{\omega^2}-k_g\frac{\omega^2}{\beta_0^2}+8k_g^7\frac{\beta_0^4}{\omega^4}+8C^3\nu_g^2k_g^5\frac{\beta_0^4}{\omega^4}\right.\\
&\left.-4\frac{\beta_0^2}{\alpha_0^2}C^3\nu_g^2k_g^3\frac{\beta_0^2}{\omega^2}\right)\\
&-\left(\frac{1}{2C}-\frac{1}{C+1}\right)\frac{1}{4\eta_g\nu_g^2}\left(4\frac{\beta_0^2}{\alpha_0^2}k_g^3-8k_g^5\frac{\beta_0^2}{\omega^2}-k_g\frac{\omega^2}{\alpha_0^2}+2k_g^3-4C\nu_g^2k_g^3\frac{\beta_0^2}{\omega^2}+8C\nu_g^2k_g^5\frac{\beta_0^4}{\omega^4}\right.\\
&\left.-4\frac{\beta_0^2}{\alpha_0^2}k_g^5\frac{\beta_0^2}{\omega^2}+8k_g^7\frac{\beta_0^4}{\omega^4}\right)\Bigg\}a_\mu^{(1)}(z)a_\mu^{(1)}(z)\\
&+\left[\left(\frac{1}{2}+\frac{1}{C+1}\right)\frac{k_g}{8\eta_g\nu_g^2}\left(Ck_g^2+\nu_g^2\right)-\left(\frac{1}{2}-\frac{1}{C+1}\right)\frac{k_g}{8\eta_g\nu_g^2}\left(k_g^2+C\nu_g^2\right)\right.\\
&\left.+\left(\frac{1}{2C}+\frac{1}{C+1}\right)\frac{k_g}{8\eta_g^2\nu_g}\left(C^3\nu_g^2+k_g^2\right)-\left(\frac{1}{2C}-\frac{1}{C+1}\right)\frac{k_g}{8\eta_g\nu_g^2}\left(k_g^2+C\nu_g^2\right)\right]a_\rho^{(1)}(z)a_\rho^{(1)}(z)\\
&+\left[\left(\frac{1}{2}+\frac{1}{C+1}\right)\frac{\beta_0^2}{\alpha_0^2}\frac{1}{4\nu_g^3}k_g\left(k_g^2-\nu_g^2\right)+\left(\frac{1}{2}-\frac{1}{C+1}\right)\frac{1}{4\eta_g\nu_g^2}\left(k_g\frac{\omega^2}{\alpha_0^2}-2\frac{\beta_0^2}{\alpha_0^2}k_g^3\right)\right.\\
&\left.+\frac{\beta_0^2}{\alpha_0^2}\frac{k_g}{2\nu_g}\right]a_\mu^{(1)}(z)a_\gamma^{(1)}(z)\\
&-\left[\left(\frac{1}{2}+\frac{1}{C+1}\right)\frac{k_g\left(k_g^2+\nu_g^2\right)}{8\nu_g^3}-\left(\frac{1}{2}-\frac{1}{C+1}\right)\frac{k_g\left(k_g^2+\nu_g^2\right)}{8\eta_g\nu_g^2}\right]a_\rho^{(1)}(z)a_\gamma^{(1)}(z)\\
&-\left[\left(\frac{1}{2}+\frac{1}{C+1}\right)\frac{1}{4\eta_g\nu_g^2}\left(2\nu_g^2k_g^3\frac{\beta_0^2}{\omega^2}-\nu_g^2k_g+2Ck_g^5\frac{\beta_0^2}{\omega^2}-\frac{\beta_0^2}{\alpha_0^2}Ck_g^3\right)\right.\\
&\left.-\left(\frac{1}{2}-\frac{1}{C+1}\right)\frac{1}{4\eta_g\nu_g^2}\left(2C\nu_g^2k_g^3\frac{\beta_0^2}{\omega^2}-\frac{\beta_0^2}{\alpha_0^2}C\nu_g^2k_g+2k_g^5\frac{\beta_0^2}{\omega^2}-k_g^3\right)\right.
\end{aligned}
$$

$$
\begin{aligned}
&-\left(\frac{1}{2C}+\frac{1}{C+1}\right)\frac{1}{4\eta_g^2\nu_g}\left(3k_g^3+\frac{\beta_0^2}{\alpha_0^2}C^3\nu_g^2k_g-4C^3\nu_g^2k_g^3\frac{\beta_0^2}{\omega^2}-4k_g^5\frac{\beta_0^2}{\omega^2}-\frac{1}{2}k_g\frac{\omega^2}{\beta_0^2}\right)\\
&+\left(\frac{1}{2C}-\frac{1}{C+1}\right)\frac{1}{4\eta_g\nu_g^2}\left(C\nu_g^2k_g+2k_g^3+\frac{\beta_0^2}{\alpha_0^2}k_g^3-4k_g^5\frac{\beta_0^2}{\omega^2}-4C\nu_g^2k_g^3\frac{\beta_0^2}{\omega^2}-\frac{1}{2}k_g\frac{\omega^2}{\beta_0^2}\right)\\
&-(C-1)\frac{k_g^3}{2\eta_g}\frac{\beta_0^2}{\omega^2}\Bigg]a_\rho^{(1)}(z)a_\mu^{(1)}(z)\\
&-\frac{1}{2\eta_g\nu_g^2}\left[2(C-1)\nu_g^2k_g^5\frac{\beta_0^4}{\omega^4}+\left(1-\frac{\beta_0^2}{\alpha_0^2}C\right)\nu_g^2k_g^3\frac{\beta_0^2}{\omega^2}\right]\\
&\times\int_0^z dz' a_\mu^{(1)}{}_z\left(\frac{(C+1)z-(C-1)\,z'}{2}\right)a_\mu^{(1)}\left(z'\right)\\
&+\frac{1}{4\eta_g^2\nu_g}\left(6k_g^3-12k_g^5\frac{\beta_0^2}{\omega^2}-k_g\frac{\omega^2}{\beta_0^2}+8k_g^7\frac{\beta_0^4}{\omega^4}+8C^3\nu_g^2k_g^5\frac{\beta_0^4}{\omega^4}-4\frac{\beta_0^2}{\alpha_0^2}C^3\nu_g^2k_g^3\frac{\beta_0^2}{\omega^2}\right)\\
&\times\left[\frac{1}{2C}\int_0^z dz' a_\mu^{(1)}{}_z\left(\frac{(C+1)z+(C-1)\,z'}{2C}\right)a_\mu^{(1)}\left(z'\right)+\frac{1}{C+1}a_\mu^{(1)'}(z)\int_0^z dz' a_\mu^{(1)}(z')\right]\\
&-\frac{1}{4\eta_g\nu_g^2}\left(4\frac{\beta_0^2}{\alpha_0^2}k_g^3-8k_g^5\frac{\beta_0^2}{\omega^2}-k_g\frac{\omega^2}{\alpha_0^2}+2k_g^3-4C\nu_g^2k_g^3\frac{\beta_0^2}{\omega^2}+8C\nu_g^2k_g^5\frac{\beta_0^4}{\omega^4}-4\frac{\beta_0^2}{\alpha_0^2}k_g^5\frac{\beta_0^2}{\omega^2}+8k_g^7\frac{\beta_0^4}{\omega^4}\right)\\
&\times\left[\frac{1}{2C}\int_0^z dz' a_\mu^{(1)}{}_z\left(\frac{(C+1)z+(C-1)\,z'}{2C}\right)a_\mu^{(1)}\left(z'\right)-\frac{1}{C+1}a_\mu^{(1)'}(z)\int_0^z dz' a_\mu^{(1)}(z')\right]\\
&+\frac{k_g\left(Ck_g^2+\nu_g^2\right)}{8\eta_g\nu_g^2}\left[\frac{1}{2}\int_0^z dz' a_\rho^{(1)}{}_z\left(\frac{(C+1)z-(C-1)\,z'}{2}\right)a_\rho^{(1)}\left(z'\right)\right.\\
&\left.+\frac{1}{C+1}a_\rho^{(1)'}(z)\int_0^z dz' a_\rho^{(1)}(z')\right]\\
&-\frac{k_g\left(k_g^2+C\nu_g^2\right)}{8\eta_g\nu_g^2}\left[\frac{1}{2}\int_0^z dz' a_\rho^{(1)}{}_z\left(\frac{(C+1)z-(C-1)\,z'}{2}\right)a_\rho^{(1)}\left(z'\right)\right.\\
&\left.-\frac{1}{C+1}a_\rho^{(1)'}(z)\int_0^z dz' a_\rho^{(1)}(z')\right]\\
&+\frac{C^3k_g\nu_g^2+k_g^3}{8\eta_g^2\nu_g}\left[\frac{1}{2C}\int_0^z dz' a_\rho^{(1)}{}_z\left(\frac{(C+1)z+(C-1)\,z'}{2C}\right)a_\rho^{(1)}\left(z'\right)\right.\\
&\left.+\frac{1}{C+1}a_\rho^{(1)'}(z)\int_0^z dz' a_\rho^{(1)}(z')\right]\\
&-\frac{k_g\left(k_g^2+C\nu_g^2\right)}{8\eta_g\nu_g^2}\left[\frac{1}{2C}\int_0^z dz' a_\rho^{(1)}{}_z\left(\frac{(C+1)z+(C-1)\,z'}{2C}\right)a_\rho^{(1)}\left(z'\right)\right.\\
&\left.-\frac{1}{C+1}a_\rho^{(1)'}(z)\int_0^z dz' a_\rho^{(1)}(z')\right]\\
&+\frac{\beta_0^2}{\alpha_0^2}\frac{k_g\left(k_g^2-\nu_g^2\right)}{4\nu_g^3}\left[\frac{1}{2}\int_0^z dz' a_\gamma^{(1)}{}_z\left(\frac{(C+1)z-(C-1)\,z'}{2}\right)a_\mu^{(1)}\left(z'\right)\right.
\end{aligned}
$$

$$
\begin{aligned}
&+\frac{1}{C+1}a_{\mu}^{(1)'}(z)\int_0^z dz' a_{\gamma}^{(1)}(z')\Bigg]\\
&+\frac{1}{4\eta_g\nu_g^2}\left(k_g\frac{\omega^2}{\alpha_0^2}-2\frac{\beta_0^2}{\alpha_0^2}k_g^3\right)\left[\frac{1}{2}\int_0^z dz' a_{\gamma}^{(1)}{}_z\left(\frac{(C+1)z-(C-1)\,z'}{2}\right)a_{\mu}^{(1)}\left(z'\right)\right.\\
&\left.-\frac{1}{C+1}a_{\mu}^{(1)'}(z)\int_0^z dz' a_{\gamma}^{(1)}(z')\right]\\
&-\frac{k_g\left(k_g^2+\nu_g^2\right)}{8\nu_g^3}\left[\frac{1}{2}\int_0^z dz' a_{\gamma}^{(1)}{}_z\left(\frac{(C+1)z-(C-1)\,z'}{2}\right)a_{\rho}^{(1)}\left(z'\right)\right.\\
&\left.+\frac{1}{C+1}a_{\rho}^{(1)'}(z)\int_0^z dz' a_{\gamma}^{(1)}(z')\right]\\
&+\frac{k_g\left(k_g^2+\nu_g^2\right)}{8\eta_g\nu_g^2}\left[\frac{1}{2}\int_0^z dz' a_{\gamma}^{(1)}{}_z\left(\frac{(C+1)z-(C-1)\,z'}{2}\right)a_{\rho}^{(1)}\left(z'\right)\right.\\
&\left.-\frac{1}{C+1}a_{\rho}^{(1)'}(z)\int_0^z dz' a_{\gamma}^{(1)}(z')\right]\\
&-\frac{1}{4\eta_g\nu_g^2}\left(2\nu_g^2k_g^3\frac{\beta_0^2}{\omega^2}-\nu_g^2k_g+2Ck_g^5\frac{\beta_0^2}{\omega^2}-\frac{\beta_0^2}{\alpha_0^2}Ck_g^3\right)\\
&\times\left[\frac{1}{2}\int_0^z dz' a_{\rho}^{(1)}{}_z\left(\frac{(C+1)z-(C-1)\,z'}{2}\right)a_{\mu}^{(1)}\left(z'\right)+\frac{1}{C+1}a_{\mu}^{(1)'}(z)\int_0^z dz' a_{\rho}^{(1)}(z')\right]\\
&+\frac{1}{4\eta_g\nu_g^2}\left(2C\nu_g^2k_g^3\frac{\beta_0^2}{\omega^2}-\frac{\beta_0^2}{\alpha_0^2}C\nu_g^2k_g+2k_g^5\frac{\beta_0^2}{\omega^2}-k_g^3\right)\\
&\times\left[\frac{1}{2}\int_0^z dz' a_{\rho}^{(1)}{}_z\left(\frac{(C+1)z-(C-1)\,z'}{2}\right)a_{\mu}^{(1)}\left(z'\right)-\frac{1}{C+1}a_{\mu}^{(1)'}(z)\int_0^z dz' a_{\rho}^{(1)}(z')\right]\\
&+(C-1)\frac{k_g^3}{2\eta_g}\frac{\beta_0^2}{\omega^2}\int_0^z dz' a_{\mu}^{(1)}{}_z\left(\frac{(C+1)z-(C-1)\,z'}{2}\right)a_{\rho}^{(1)}\left(z'\right)\\
&-\frac{1}{4\eta_g^2\nu_g}\left(-2k_g^3+2C^3\nu_g^2k_g^3\frac{\beta_0^2}{\omega^2}+2k_g^5\frac{\beta_0^2}{\omega^2}+\frac{1}{2}k_g\frac{\omega^2}{\beta_0^2}\right)\\
&\times\left[\frac{1}{2C}\int_0^z dz' a_{\mu}^{(1)}{}_z\left(\frac{(C+1)z+(C-1)\,z'}{2C}\right)a_{\rho}^{(1)}\left(z'\right)+\frac{1}{C+1}a_{\rho}^{(1)'}(z)\int_0^z dz' a_{\mu}^{(1)}(z')\right]\\
&-\frac{1}{4\eta_g^2\nu_g}\left(-k_g^3-\frac{\beta_0^2}{\alpha_0^2}C^3\nu_g^2k_g+2C^3\nu_g^2k_g^3\frac{\beta_0^2}{\omega^2}+2k_g^5\frac{\beta_0^2}{\omega^2}\right)\\
&\times\left[\frac{1}{2C}\int_0^z dz' a_{\rho}^{(1)}{}_z\left(\frac{(C+1)z+(C-1)\,z'}{2C}\right)a_{\mu}^{(1)}\left(z'\right)+\frac{1}{C+1}a_{\mu}^{(1)'}(z)\int_0^z dz' a_{\rho}^{(1)}(z')\right]\\
&-\frac{1}{4\eta_g\nu_g^2}\left(2k_g^3-2k_g^5\frac{\beta_0^2}{\omega^2}-2C\nu_g^2k_g^3\frac{\beta_0^2}{\omega^2}-\frac{1}{2}k_g\frac{\omega^2}{\beta_0^2}\right)\\
&\times\left[\frac{1}{2C}\int_0^z dz' a_{\mu}^{(1)}{}_z\left(\frac{(C+1)z+(C-1)\,z'}{2C}\right)a_{\rho}^{(1)}\left(z'\right)-\frac{1}{C+1}a_{\rho}^{(1)'}(z)\int_0^z dz' a_{\mu}^{(1)}(z')\right]\\
&-\frac{1}{4\eta_g\nu_g^2}\left(C\nu_g^2k_g+\frac{\beta_0^2}{\alpha_0^2}k_g^3-2k_g^5\frac{\beta_0^2}{\omega^2}-2C\nu_g^2k_g^3\frac{\beta_0^2}{\omega^2}\right)
\end{aligned}
$$

$$\times \left[\frac{1}{2C} \int_0^z dz' a_\rho^{(1)}{}_z \left(\frac{(C+1)z + (C-1)\,z'}{2C} \right) a_\mu^{(1)}\left(z'\right) - \frac{1}{C+1} a_\mu^{(1)'}(z) \int_0^z dz' a_\rho^{(1)}(z') \right],$$

and the solution for Eq. (**??**), i.e.,

$$\hat{G}_0^S \hat{V}_2^{SS} \hat{G}_0^S = -\hat{G}_0^S \hat{V}_1^{SP} \hat{G}_0^P \hat{V}_1^{PS} \hat{G}_0^S - \hat{G}_0^S \hat{V}_1^{SS} \hat{G}_0^S \hat{V}_1^{SS} \hat{G}_0^S,$$

is

$$\begin{aligned}
&-\frac{1}{4}\left(1-\frac{k_g^2}{\eta_g^2}\right) a_\rho^{(2)}(z) - \left[\frac{k_g^2+\eta_g^2}{4\eta_g^2} - \frac{2k_g^2}{k_g^2+\eta_g^2}\right] a_\mu^{(2)}(z) \\
=&-\left\{ \frac{1}{8\eta_g^4}\left(8k_g^2\eta_g^2 - \frac{\omega^4}{\beta_0^4}\right) - \frac{1}{4\eta_g^2}\left(\frac{\omega^2}{\beta_0^2} - 4\frac{\beta_0^2}{\omega^2}\eta_g^2 k_g^2\right) - \frac{\beta_0^2}{\alpha_0^2}k_g^2\frac{\beta_0^2}{\omega^2} \right. \\
&\left. + \frac{1}{\eta_g^2(C+1)}\left[k_g^2\left(\frac{\beta_0^4}{\alpha_0^4}C^2 - 1\right) - 4k_g^4\frac{\beta_0^2}{\omega^2}\left(\frac{\beta_0^2}{\alpha_0^2}C^2 - 1\right) + 4k_g^6\frac{\beta_0^4}{\omega^4}(C^2-1)\right] \right\} a_\mu^{(1)}(z) a_\mu^{(1)}(z) \\
&-\left[\frac{1}{8\eta_g^4}\left(\eta_g^4 - k_g^4\right) + \frac{1}{4\eta_g^2}k_g^2(C-1)\right] a_\rho^{(1)}(z) a_\rho^{(1)}(z) \\
&+\left\{ \frac{k_g^2}{\eta_g^2} - \frac{1}{\eta_g^2(C+1)}\left[k_g^2\left(\frac{\beta_0^2}{\alpha_0^2}C^2 - 1\right) - 2\frac{\beta_0^2}{\omega^2}k_g^4\left(C^2-1\right)\right] \right\} a_\mu^{(1)}(z) a_\rho^{(1)}(z) \\
&-\frac{1}{8\eta_g^4}\left(8k_g^2\eta_g^2 - \frac{\omega^4}{\beta_0^4}\right) a_\mu^{(1)'}(z) \int_0^z dz' a_\mu^{(1)}(z') \\
&-\frac{1}{8\eta_g^4}\left(\eta_g^4 - k_g^4\right) a_\rho^{(1)'}(z) \int_0^z dz' a_\rho^{(1)}(z') \\
&+\frac{k_g^2}{2\eta_g^2}\left[a_\mu^{(1)'}(z) \int_0^z dz' a_\rho^{(1)}(z') + a_\rho^{(1)'}(z) \int_0^z dz' a_\mu^{(1)}(z')\right] \\
&-\frac{1}{8\eta_g^2}\left(\eta_g^2 - 3k_g^2\right)\left[a_\mu^{(1)'}(z) \int_0^z dz' a_\rho^{(1)}(z') - a_\rho^{(1)'}(z) \int_0^z dz' a_\mu^{(1)}(z')\right] \\
&-\frac{1}{\eta_g^2(C+1)}\left[k_g^2\left(\frac{\beta_0^4}{\alpha_0^4}C^2 - 1\right) - 4k_g^4\frac{\beta_0^2}{\omega^2}\left(\frac{\beta_0^2}{\alpha_0^2}C^2 - 1\right) + 4k_g^6\frac{\beta_0^4}{\omega^4}(C^2-1)\right] \\
&\times \int_0^z dz' a_\mu^{(1)}{}_z \left(\frac{2Cz - (C-1)\,z'}{(C+1)} \right) a_\mu^{(1)}\left(z'\right) \\
&-\frac{1}{4\eta_g^2}k_g^2(C-1) \int_0^z dz' a_\rho^{(1)}{}_z \left(\frac{2Cz - (C-1)\,z'}{(C+1)} \right) a_\rho^{(1)}\left(z'\right) \\
&-\frac{1}{2\eta_g^2(C+1)}\left[k_g^2\left(\frac{\beta_0^2}{\alpha_0^2}C^2 - 1\right) - 2\frac{\beta_0^2}{\omega^2}k_g^4\left(C^2-1\right)\right] \\
&\times \left[\int_0^z dz' a_\mu^{(1)}{}_z \left(\frac{2Cz - (C-1)\,z'}{(C+1)} \right) a_\rho^{(1)}\left(z'\right) + \int_0^z dz' a_\rho^{(1)}{}_z \left(\frac{2Cz - (C-1)\,z'}{(C+1)} \right) a_\mu^{(1)}\left(z'\right)\right] \\
&+\frac{Ck_g^2}{2(C+1)\eta_g^2}\left(\frac{\beta_0^2}{\alpha_0^2} - 1\right) \\
&\times \left[\int_0^z dz' a_\mu^{(1)}{}_z \left(\frac{2Cz - (C-1)\,z'}{(C+1)} \right) a_\rho^{(1)}\left(z'\right) - \int_0^z dz' a_\rho^{(1)}{}_z \left(\frac{2Cz - (C-1)\,z'}{(C+1)} \right) a_\mu^{(1)}\left(z'\right)\right],
\end{aligned}$$

where $\eta_g = C\nu_g, k_g^2 + \nu_g^2 = \omega^2/\alpha_0^2$ and $k_g^2 + \eta_g^2 = \omega^2/\beta_0^2$.

After we solve all (four) of the second order equations, future research is to perform numerical tests with all four components of data available.

Conclusion

In this paper, a framework and algorithm have been developed for more accurate target identification. The elastic non-linear inversion requires all four components of data. In this paper we analyzed an algorithm which inputs only $\hat{D}^{PP}$. Although $\hat{D}^{PP}$ can itself provide useful non-linear direct inversion results, when we use $\hat{D}^{PP}$ to synthesize the other components, the implication of this research is that further value would derive from actually measuring $\hat{D}^{PP}$, $\hat{D}^{PS}$, $\hat{D}^{SP}$ and $\hat{D}^{SS}$, as the method requires. Pitfalls of indirect methods that use assumed aligned objectives, while sounding eminently persuasive and reasonable, can have a serious flaw in violating the fundamental physics behind non-linear inversion, and can never sense its problem, in any clear and definitive manner. There are very serious conceptual and practical consequences to that disconnect. For the case that all four components of data available, we also provided a consistent method to solve for all of the second terms. Further tests with the actual four components of data (in a 2-D world) are underway, to compare with $\hat{D}^{PP}$ and synthesized data components.

Acknowledgements

The M-OSRP sponsors are thanked for supporting this research. We are grateful to Robert Keys and Douglas Foster for useful comments and suggestions. We have been partially funded by and are grateful for NSF-CMG award DMS-0327778 and DOE Basic Sciences award DE-FG02-05ER15697.

Appendix A

In this Appendix, we give the different coefficients before every linear quantity $(a_\gamma^{(1)}, a_\rho^{(1)}, a_\mu^{(1)})$ — different incidence angle θ. For P to P case, we have

$$k_g^{PP} = \frac{\omega}{\alpha_0}\sin\theta^{PP},$$
$$\nu_g^{PP} = \frac{\omega}{\alpha_0}\cos\theta^{PP},$$

For S to P case,

$$k_g^{PS} = \frac{\omega}{\beta_0}\sin\theta^{PS},$$
$$\nu_g^{PS} = \frac{\omega}{\alpha_0}\sqrt{1 - \frac{\alpha_0^2}{\beta_0^2}\sin^2\theta^{PS}}$$

$$\eta_g^{PS} = \frac{\omega}{\beta_0}\cos\theta^{PS},$$

For P to S case,

$$k_g^{SP} = \frac{\omega}{\alpha_0}\sin\theta^{SP},$$
$$\nu_g^{SP} = \frac{\omega}{\alpha_0}\cos\theta^{SP}$$
$$\eta_g^{SP} = \frac{\omega}{\beta_0}\sqrt{1-\frac{\beta_0^2}{\alpha_0^2}\sin^2\theta^{SP}},$$

For S to S case,

$$k_g^{SS} = \frac{\omega}{\beta_0}\sin\theta^{SS},$$
$$\eta_g^{SS} = \frac{\omega}{\beta_0}\cos\theta^{SS},$$

Let the arguments of $a_\rho^{(1)}$ and $a_\mu^{(1)}$ in Eqs. (41), (42), (43) and (44) equal, we need

$$-2\nu_g^{PP} = -\nu_g^{PS} - \eta_g^{PS} = -\nu_g^{SP} - \eta_g^{SP} = -2\eta_g^{SS},$$

which leads to

$$2\frac{\omega}{\alpha_0}\cos\theta^{PP} = \frac{\omega}{\alpha_0}\sqrt{1-\frac{\alpha_0^2}{\beta_0^2}\sin^2\theta^{PS}} + \frac{\omega}{\beta_0}\cos\theta^{PS}$$
$$= \frac{\omega}{\alpha_0}\cos\theta^{SP} + \frac{\omega}{\beta_0}\sqrt{1-\frac{\beta_0^2}{\alpha_0^2}\sin^2\theta^{SP}} = 2\frac{\omega}{\beta_0}\cos\theta^{SS},$$

From the expression above, given θ^{PP}, we can find the corresponding θ^{PS}, θ^{SP} and θ^{SS}.

$$\theta^{PS} = \cos^{-1}\left[\frac{4b^2\cos^2\theta^{PP} + 1 - b^2}{4b\cos\theta^{PP}}\right],$$
$$\theta^{SP} = \cos^{-1}\left[\frac{4b^2\cos^2\theta^{PP} - 1 + b^2}{4b^2\cos\theta^{PP}}\right],$$
$$\theta^{SS} = \cos^{-1}\left(b\cos\theta^{PP}\right),$$

where $b = \frac{\beta_0}{\alpha_0}$.

References

Aki, K. and P. G. Richards. *Quantitative Seismology.* 2nd edition. University Science Books, 2002.

Araújo, F. V. *Linear and non-linear methods derived from scattering theory: backscattered tomography and internal multiple attenuation.* PhD thesis, Universidade Federal da Bahia, 1994.

Carvalho, P. M. *Free-surface multiple reflection elimination method based on nonlinear inversion of seismic data*. PhD thesis, Universidade Federal da Bahia, 1992.

Carvalho, P. M., A. B. Weglein, and R. H. Stolt. "Nonlinear inverse scattering for multiple suppression: Application to real data. part I." *62nd Ann. Internat. Mtg: Soc. of Expl. Geophys., Expanded Abstracts*. . Soc. Expl. Geophys., 1992. 1093–1095.

Clayton, R. W. and R. H. Stolt. "A Born-WKBJ inversion method for acoustic reflection data." *Geophysics* 46 (1981): 1559–1567.

Foster, D. J., R. G. Keys, and D. P. Schmitt. *Detecting subsurface hydrocarbons with elastic wavefields*. Springer-In Inverse Problems in Wave Progagation, Volume 90 of The IMA Volumes in Mathematics and its Applications, 1997.

Innanen, K. A. and A. B. Weglein. "Linear inversion for absorptive/dispersive medium parameters." *74th Annual Internat. Mtg., Soc. Expl. Geophys., Expanded Abstracts*. . Soc. Expl. Geophys., 2004. 1834–1837.

Innanen, K. A. and A. B. Weglein. "Towards non-linear construction of a Q-compensation operator directly from measured seismic reflection data." *75th Annual Internat. Mtg., Soc. Expl. Geophys., Expanded Abstracts*. . Soc. Expl. Geophys., 2005. 1693–1696.

Liu, F., A. B. Weglein K. A. Innanen, and B. G. Nita. "Extension of the non-linear depth imaging capability of the inverse scattering series to multidimensional media: strategies and numerical results." *9th Ann. Cong. SBGf, Expanded Abstracts*. . SBGf, 2005.

Liu, F., B. G. Nita, A. B. Weglein, and K. A. Innanen. "Inverse Scattering Series in the presence of lateral variations." *M-OSRP Annual Report* 3 (2004).

Liu, F. and A. B. Weglein. "Initial analysis of the inverse scattering series for a variable background." *M-OSRP Annual Report* 2 (2003): 210–225.

Matson, K. H. *An inverse-scattering series method for attenuating elastic multiples from multicomponent land and ocean bottom seismic data*. PhD thesis, University of British Columbia, 1997.

Ramírez, Adriana C. and Arthur B. Weglein. "An inverse scattering internal multiple elimination method: Beyond attenuation, a new algorithm and initial tests." *75th Annual Internat. Mtg., Soc. Expl. Geophys., Expanded Abstracts*. . Soc. Expl. Geophys., 2005. 2115–2118.

Shaw, S. A. and A. B. Weglein. "Imaging seismic reflection data at the correct depth without specifying an accurate velocity model: Initial examples of an inverse scattering subseries." *Frontiers of remote sensing information processing*. Ed. C. H. Chen. World Scientific Publishing Company, 2003. chapter 21, 469–484.

Shaw, S. A. and A. B. Weglein. "A leading order imaging series for prestack data acquired over a laterally invariant acoustic medium. Part II: Analysis for data missing low frequencies." *M-OSRP Annual Report* 3 (2004).

Shaw, S. A., A. B. Weglein, D. J. Foster, K. H. Matson, and R. G. Keys. "Convergence properties of a leading order depth imaging series." *73rd Annual Internat. Mtg., Soc. Expl. Geophys., Expanded Abstracts*. . Soc. Expl. Geophys., 2003. 937–940.

Shaw, S. A., A. B. Weglein, D. J. Foster, K. H. Matson, and R. G. Keys. "Isolation of a leading order depth imaging series and analysis of its convergence properties." *M-OSRP Annual Report* 2 (2003): 157–195.

Shaw, S. A., A. B. Weglein, D. J. Foster, K. H. Matson, and R. G. Keys. "Isolation of a leading order depth imaging series and analysis of its convergence properties." *Journal of Seismic Exploration* 2 (November 2004): 157–195.

Weglein, A. B., F. V. Araújo, P. M. Carvalho, R. H. Stolt, K. H. Matson, R. T. Coates, D. Corrigan, D. J. Foster, S. A. Shaw, and H. Zhang. "Inverse scattering series and seismic exploration." *Inverse Problems* 19 (2003): R27–R83.

Weglein, A. B., D. J. Foster, K. H. Matson, S. A. Shaw, P. M. Carvalho, and D. Corrigan. "Predicting the correct spatial location of reflectors without knowing or determining the precise medium and wave velocity: initial concept, algorithm and analytic and numerical example." *Journal of Seismic Exploration* 10 (2002): 367–382.

Weglein, A. B., F. A. Gasparotto, P. M. Carvalho, and R. H. Stolt. "An inverse-scattering series method for attenuating multiples in seismic reflection data." *Geophysics* 62 (1997): 1975–1989.

Weglein, A. B. and R. H. Stolt. 1992 "Approaches on linear and non-linear migration-inversion.". Personal Communication.

Weglein, A. B., P. B. Violette, and T. H. Keho. "Using multiparameter Born theory to obtain certain exact multiparameter inversion goals." *Geophysics* 51 (1986): 1069–1074.

Zhang, H. and A. B. Weglein. "The inverse scattering series for tasks associated with primaries: Depth imaging and direct non-linear inversion of 1D variable velocity and density acoustic media." *75th Annual Internat. Mtg., Soc. Expl. Geophys., Expanded Abstracts*. . Soc. Expl. Geophys., 2005. 1705–1708.

Towards a comprehensive inverse scattering framework for Q-compensation

K. A. Innanen and J. E. Lira

Abstract

A reasonable definition of Q-compensation is the estimation of an output (surface-recorded) primary data set that is identical to a given input, except that all absorptive propagation effects are absent. Inverse scattering provides a framework upon which to develop a variety of direct data-processing schemes fitting this definition. The framework is comprehensive in the sense that possible schemes deriving from it range from being highly non-linear and requiring no prior knowledge of the Q values or structure of the medium (and which as a result attempts to avoid the problems associated with standard Q processing when the incorrect Q value is used), to being linear but requiring a precise prior knowledge of the medium Q. Both are interpretable as being mappings to and from model space, with the map *to* model space steeped in absorptive-dispersive wave mathematics, and the map *back* being essentially acoustic. The algorithms are straightforwardly derived and synthetically exemplified for layered absorptive-dispersvie media.

1 Introduction

Consider a reflection seismic data set consisting of primaries that have been altered because of Q. A reasonable definition of Q-compensation is *the estimation of a further data set that is identical to the input, except that all absorptive propagation effects are absent.* Inverse scattering is a framework within which numerous algorithms that fit this definition, and that are based on a fully multidimensional and multi-parameter wave theory, can be developed. In this paper we present two examples.

The two examples are the two ends of a range of possible Q-compensation schemes derivable from within inverse scattering. (We say we are moving towards a "comprehensive framework" for Q-compensation because in principle it should be possible to derive an algorithm that sits anywhere in this range.) On one end are algorithms that are linear, and proceed with an accurate prior knowledge of the medium, including its Q structure. On the other are algorithms that are highly nonlinear, and proceed with no prior knowledge of the medium. The ultimate research aim would be to provide complete freedom to choose where one sits on this range when designing or using an algorithm.

We will take great pains to cast Q-compensation as a separate, independent step within the seismic processing chain. For instance, after non-linear absorptive-dispersive inversion equations are generated (which construct the depth profiles of P-wave velocity and Q), taking us, as it were, to the end of the processing chain, we proceed to suppress much of their behavior, and then map back to data space—apparently retreating to an earlier point on the chain. The reason is practical. As we shall see, correction for Q is treated in inverse scattering in a way highly coupled to both imaging, or reflector location, and parameter estimation. In fact, the raw equations attempt to accomplish

all of these tasks simultaneously. But, since in seismic processing the word *adequate* is subjective, a simple medium might be adequate to explain attenuation in the data events, and at the same time grossly inadequate to explain their phase and arrival times. It follows that we could easily find ourselves in a situation where the coupled algorithm, which images and compensates for Q all at once, does the latter task adequately and the former inadequately. To avoid situations like this, we define as our goal a Q-compensation algorithm that sits alone.

This current paper represents the progression, in an ongoing research project to determine the impact of absorption on linear and non-linear inverse scattering (Innanen and Weglein, 2003, 2005), to candidate algorithms suitable for a 2-parameter absorptive-dispersive medium exhibiting arbitrary variability in depth. The linear prototype algorithm is based on inversion equations with absorptive reference media (Innanen et al., 2008). The nonlinear algorithm has been discussed in its earlier incarnations in MOSRP05. Because it operates on primaries, and corrects for problems whose specific nature is determined by the duration of a wave in perturbed parts of the medium, the non-linear algorithm shares much with concurrent and ongoing direct non-linear imaging (Weglein et al., 2001; Shaw et al., 2004; Shaw, 2005; Liu et al., 2006; Liu, 2006) and inversion (Zhang and Weglein, 2005; Zhang, 2006) research.

The paper is organized as follows. In the remainder of this introductory section, we will review existing Q compensation methods, and comment on how well they fit into the parochial definition we have laid out in the first paragraph of the paper. We then introduce the various basic scattering quantities appropriate for absorptive-dispersive reference and actual media. In the following two sections we will present the linear and non-linear Q-compensation algorithms respectively, making regular use of the Appendices. In each case we provide simple synthetic examples of the algorithms.

Q-compensation and the seismic inverse problem

Many existing inverse Q filtering techniques (e.g., Clarke, 1968; Bickel and Natarajan, 1985; Hargreaves, 1992; Bickel, 1993; Duren and Trantham, 1997; Margrave, 1998; Wang, 2002, 2003; Zhang and Ulrych, 2007; Wang, 2006; Baan, 2008) fit well with the above definition. Generally, their output is indeed data-like, the result of a non-stationary deconvolution of the input data, and therefore identifiable as some form of reflectivity series in time. However, as one moves towards methods that are based on multidimensional and multiparameter wave theory, which we wish to do, it becomes less straightforward to arrange for the output to be data-like. At the opposite end of the continuum are absorptive-dispersive waveform inversion methods (e.g., Dahl and Ursin, 1992; Causse et al., 1999; Hicks and Pratt, 2001; Dasios et al., 2004), in which spatial distributions of medium parameters (including attenuation parameters) are estimated. These methods are wave-theoretic, and since, in applying them, attenuated data are used to determine sharp medium variations, some de facto form of Q-compensation is certainly taking place; but the output is far from data-like. We seek something that retains the data-to-data mapping sensibility of the deconvolution-type methods, while basing itself in full multidimensional - multiparameter wave theory. Migration or downward continuation schemes that incorporate attenuation (Mittet et al., 1995; Ribodetti and Virieux, 1998; Song and Innanen, 2002; Wang, 2003; Mittet, 2007) accomplish this to a limited degree: the image output (e.g., imaged wavefield-at-depth) has a slight data-like aspect, and a

wave-theoretic version of Q-compensation takes place in constructing it. But in designing direct Q compensation algorithms from the inverse scattering formalism, we identify most closely with the method of Hargreaves and Calvert (1991), which is based on multidimensional wave theory and returns a Q-compensated, non-imaged, pre-stack data set, and so falls closest to our parochial definition.

Absorptive-dispersive scattering quantities

Here we set out the scattering quantities to be used in both of the Q-compensation approaches discussed in this paper. Two fundamentally different sets of perturbations are required for the cases of absorptive and non-absorptive reference media.

Case I: Green's functions and perturbations for non-absorptive reference media

For the case of a non-absorptive reference medium, the Green's functions for a source at $\mathbf{x_s}$ and a receiver at $\mathbf{x}$ at angular frequency ω will satisfy

$$\left[\nabla^2 + \frac{\omega^2}{c_0^2}\right] G_0(\mathbf{x}|\mathbf{x_s};\omega) = \delta(\mathbf{x}-\mathbf{x_s}), \tag{1}$$

that is, be solutions for a homogeneous, constant density acoustic medium characterized by wavespeed c_0. The solution to equation (1) in 1D for a source at z_s and a receiver at z_g is

$$G_0(z_g|z_s;\omega) = \frac{e^{i\frac{\omega}{c_0}|z_g - z_s|}}{i2k}, \tag{2}$$

whereas in 2D with similar nomenclature we have instead

$$\begin{aligned} G_0(x_g, z_g|x, z;\omega) &= \frac{1}{2\pi}\int_{-\infty}^{\infty} dk'_x e^{ik'_x(x_g - x)} \frac{e^{iq'|z_g - z|}}{i2q'} \\ G_0(x, z|x_s, z_s;\omega) &= \frac{1}{2\pi}\int_{-\infty}^{\infty} dk'_x e^{ik'_x(x - x_s)} \frac{e^{iq'|z - z_s|}}{i2q'}, \end{aligned}$$

where $q'^2 = \omega^2/c_0^2 - k'^2_x$. Finally, Fourier transforming over x_g and x_s within $G_0(x_g, z_g|x, z;\omega)$ and $G_0(x, z|x_s, z_s;\omega)$ respectively produces the useful form:

$$\begin{aligned} G_0(k_g, z_g|x, z;\omega) &= e^{-ik_g x}\frac{e^{iq_g|z_g - z|}}{i2q_g}, \\ G_0(x, z|k_s, z_s;\omega) &= e^{ik_s x}\frac{e^{iq_s|z - z_s|}}{i2q_s}, \end{aligned} \tag{3}$$

where $q_g^2 = \omega^2/c_0^2 - k_g^2$ and $q_s^2 = \omega^2/c_0^2 - k_s^2$. We adopt the Fourier transform conventions of Clayton and Stolt (1981). We define wave propagation in the actual medium as satisfying a straightforward two parameter A-D wave model, in which the Green's function satisfies

$$\left[\nabla^2 + K^2\right] G(\mathbf{x}|\mathbf{x_s};K) = \delta(\mathbf{x}-\mathbf{x_s}), \tag{4}$$

where

$$K \equiv \frac{\omega}{c(\mathbf{x})}\left[1+\frac{F(\omega)}{Q(\mathbf{x})}\right], \tag{5}$$

and, importantly, where we have specifically extracted the function

$$F(\omega) = \frac{i}{2} - \frac{1}{\pi}\ln\left(\frac{\omega}{\omega_r}\right). \tag{6}$$

The reference frequency ω_r is a component of the A-D model, which in our numerical studies we choose to be the highest frequency in a given experiment. The nearly-constant Q model embodied in equations (5) and (6) is consistent with those described by Aki and Richards (2002), and with that of Kjartansson (1979) over a reasonable seismic bandwidth. The function $F(\omega)$ has two terms, one imaginary and one real and frequency-dependent; the former instills absorptive effects (i.e., attenuation proper) in the expression for a propagating wavefield, while the latter instills dispersive effects. Notice that the form of the A-D model has permitted us to separate out the space dependence of $Q(\mathbf{x})$ from the frequency-dependence produced by the dispersion, which we have placed in the function $F(\omega)$. The former will be treated as an unknown in the inverse scattering problem, and the latter as known. Solving for an attenuation parameter with unprescribed variation in both space and frequency does not appear to be tractable at present. Continuing in operator form (e.g., Weglein et al. (2003)), the reference wave equation and the actual wave equation, both based on equation (4) may be expressed as

$$\mathbf{L_0 G_0} = \mathbf{I}, \qquad \mathbf{LG} = \mathbf{I}, \tag{7}$$

respectively, where $\mathbf{I}$ is the operator form of the delta function source in equation (4). We then define perturbation and scattered field quantities as

$$\mathbf{V} = \mathbf{L_0} - \mathbf{L}, \qquad \psi = \mathbf{G} - \mathbf{G_0}, \tag{8}$$

respectively, after which the Scattering equation and forward scattering series arises,

$$\begin{aligned}\psi &= \mathbf{G_0 V G}, \\ &= \mathbf{G_0 V G_0} + \mathbf{G_0 V G_0 V G_0} + \mathbf{G_0 V G_0 V G_0 V G_0} + ... \quad .\end{aligned}$$

The perturbation operator $\mathbf{V}$ is the difference between two wave operators of the type in equation (4), a reference and an actual, namely:

$$\begin{aligned}\mathbf{V} &= \mathbf{L_0} - \mathbf{L} \\ &= \left[\nabla^2 + k^2\right] - \left[\nabla^2 + K^2\right] \\ &= \frac{\omega^2}{c_0^2} - \frac{\omega^2}{c^2(\mathbf{x})}\left[1+\frac{F(\omega)}{Q(\mathbf{x})}\right]^2 \\ &\approx \frac{\omega^2}{c_0^2} - \frac{\omega^2}{c^2(\mathbf{x})}\left[1+\frac{2F(\omega)}{Q(\mathbf{x})}\right],\end{aligned}$$

neglecting $1/Q^2$, a step that is already consistent with the approximations made in the development of the nearly-constant Q model (Kjartansson, 1979). We proceed by defining two dimensionless perturbation quantities:

$$\alpha(\mathbf{x}) = 1 - \frac{c_0^2(\mathbf{x})}{c^2(\mathbf{x})},$$
$$\beta(\mathbf{x}) = \frac{1}{Q(\mathbf{x})},$$

such that

$$\begin{aligned}\mathbf{V} &\approx \frac{\omega^2}{c_0^2} - \frac{\omega^2}{c_0^2}\left[1-\alpha(\mathbf{x})\right]\left[1+2F(\omega)\beta(\mathbf{x})\right] \\ &\approx \frac{\omega^2}{c_0^2}\left[\alpha(\mathbf{x}) - 2F(\omega)\beta(\mathbf{x})\right].\end{aligned}$$

Equation (9) further neglects the term containing the product $\alpha\beta$. The rationale for this is mathematical convenience; under many circumstances it is a good approximation, but we must expect it to act as a source of error given very large wavespeed contrasts. Within the inverse scattering series, the component of this perturbation that is linear in the data will then be written

$$\mathbf{V}_1 \equiv \frac{\omega^2}{c_0^2}\left[\alpha_1(\mathbf{x}) - 2F(\omega)\beta_1(\mathbf{x})\right]. \tag{9}$$

We emphasize that the perturbations appropriate for the absorptive reference medium case do not reduce to this form as the reference absorption parameter vanishes.

Case II: Green's functions and perturbations for absorptive reference media

The Green's functions for homogeneous absorptive reference media look very similar to the non-absorptive case; they do behave quite differently, however. We again make particular use of

$$\begin{aligned}G_0(x_g, z_g, x', z', \omega) &= \frac{1}{2\pi}\int dk_g e^{ik_g(x_g - x')}\frac{e^{iq_g|z_g - z'|}}{i2q_g}, \\ G_0(x', z', k_s, z_s, \omega) &= e^{ik_s x_s}\frac{e^{iq_s|z - z_s|}}{i2q_s},\end{aligned} \tag{10}$$

however, now the depth wavenumbers are altered: $q_g^2 = K^2 - k_g^2$, etc., and $K = \frac{\omega}{c_0}\left[1 + \frac{i}{2Q_0} - \frac{1}{\pi Q_0}\log\left(\frac{\omega}{\omega_r}\right)\right]$ as per Aki and Richards (2002). The scattering potential V is, as before, the difference between reference and actual absorptive differential operators. Defining $F(\omega) = i/2 - 1/\pi\log\left(\frac{\omega}{\omega_r}\right)$, we have

$$\mathbf{V} = \frac{\omega^2}{c_0^2}\left[1 + \frac{F(\omega)}{Q_0}\right]^2 - \frac{\omega^2}{c^2(\mathbf{x})}\left[1 + \frac{F(\omega)}{Q(\mathbf{x})}\right]^2. \tag{11}$$

We next express the two medium variables, c and Q, in a perturbational form that is fundamentally different from the non-absorptive case. We define

$$\begin{aligned} \alpha(z) &\equiv 1 - \frac{c_0^2}{c^2(\mathbf{x})} \\ \beta(z) &\equiv 1 - \frac{Q_0}{Q(\mathbf{x})}. \end{aligned} \tag{12}$$

Noting (1) that even if the reference medium is highly attenuative, e.g., $Q_0 = 10$, the terms in $1/Q_0^2$ will be an order of magnitude smaller than those in $1/Q_0$, and (2) that terms in the product $\alpha\beta$ are generally small also, neglecting smaller terms, we have, upon substitution,

$$\mathbf{V} \approx \frac{\omega^2}{c_0^2}\left[1 + 2\frac{F(\omega)}{Q_0}\right]\alpha(\mathbf{x}) + 2\frac{\omega^2}{c_0^2}\frac{F(\omega)}{Q_0}\beta(\mathbf{x}). \tag{13}$$

Again anticipating application of the inverse scattering series (Weglein et al., 2003), the component of $\mathbf{V}$ that is linear in the data, $\mathbf{V}_1$, is straightforwardly expressed in terms of the components of α and β that are themselves also linear in the data, α_1 and β_1, as

$$\mathbf{V}_1 \equiv \frac{\omega^2}{c_0^2}\left[1 + 2\frac{F(\omega)}{Q_0}\right]\alpha_1(\mathbf{x}) + 2\frac{\omega^2}{c_0^2}\frac{F(\omega)}{Q_0}\beta_1(\mathbf{x}). \tag{14}$$

We emphasize that the perturbation for the non-absorptive reference medium is *not* produced by letting $Q_0 \to \infty$ in equation (13).

2 Direct linear Q-compensation

Here we derive and exemplify a prototype direct linear Q compensation procedure. In terms of the range of potential inverse scattering Q-compensation algorithms, it sits at the end of the range at which we assume exact prior knowledge of Q. It is similar in requirements and capability to the method of Hargreaves and Calvert (1991), with the difference that the extension to a laterally- and vertically-varying Q model (an ongoing part of the research) will follow naturally from this derivation.

Approach

The linear Q compensation algorithm is derived in analogy to "migration-demigration" style processing algorithms, in which, through a well-defined set of differences between the migration and de-migration components, some specific goal of data processing occurs (e.g., Trad, 2003). In our case, we will (1) form a linear inverse scattering problem involving a homogeneous 2-parameter absorptive-dispersive reference medium, and (2) after solving it, map back to data space using a non-absorptive reference medium.

Linear Q-compensation

We begin with a set of linear inverse scattering data equations and a prescription for their solution (Innanen et al., 2008), which will require the forms for the absorptive reference Green's functions and an appropriate scattering potential derived in Case II in the introduction. We assume for present convenience (1) that the linear component of the scattering potential is a function of depth z only, and (2) we have line sources occupying the entire plane z_s, and a single line receiver at (x_g, z_g). Upon substitution of equations (10) and (14) into the first equation of the inverse scattering series, viz.

$$D'(x_g, z_g, k_s, z_s, \omega) = S(\omega) \int \int dx' dz' G_0(x_g, z_g, x', z', \omega) V_1(z') G_0(x', z', k_s, z_s, \omega), \tag{15}$$

where S is the (known) source wavelet, we have

$$D(k_s, \omega) = \alpha_1(-2q_s) + W(\omega)\beta_1(-2q_s), \tag{16}$$

where $W(\omega) = \frac{2F(\omega)}{Q_0}\left(1 + \frac{2F(\omega)}{Q_0}\right)^{-1}$, $F(\omega) = i/2 - 1/\pi \log(\omega/\omega_r)$, ω_r is a reference frequency, and D is related to D' by

$$D(k_s, \omega) = -4S^{-1}(\omega)\left(1 + \frac{2F(\omega)}{Q_0}\right)^{-1} \frac{q_s^2 c_0^2}{\omega^2} e^{-ik_s x_g} e^{iq_s(z_g + z_s)} D'(x_g, z_g, k_s, z_s, \omega). \tag{17}$$

D' should be thought of as the measured data, pre-processed as above to produce D. Equations (16) are the heart of the inversion, and, *c.f.* Innanen and Weglein (2007), the variability of W with temporal frequency for any given spectral component of the model parameters α_1 and β_1 determines the conditioning of the problem. In the linear steps in this paper we regularly use concepts and changes-of-variable as described by Clayton and Stolt (1981). Defining the depth wavenumber over which our perturbations are to be solved to be $k_z = -2q_s$, the equations become

$$D(k_s, \omega) = \alpha_1(k_z) + W(\omega)\beta_1(k_z). \tag{18}$$

At this stage we have several options. Ideally, we would subdivide the data into components $D(k_z, \theta)$ and solve the linear problem with sets of angles. However, the (k_z, θ) parametrization turns out to be inconvenient here, as there is no straightforward way of solving for $\omega(k_z, \theta)$. A more convenient choice, since the data equations are independent directly in terms of ω already, is to change variables from $D(k_s, \omega)$ to $D(k_z, \omega)$, and solve at each k_z using a set of $N > 2$ frequencies. To proceed in this way, we need to know what k_s value is associated with a particular pair k_z, ω. From the plane wave geometry we have

$$k_s^2 + q_s^2 = \frac{\omega^2}{c_0^2}\left[1 + \frac{F(\omega)}{Q_0}\right]^2, \tag{19}$$

hence

$$k_s(k_z, \omega) = \sqrt{\frac{\omega^2}{c_0^2}\left[1 + \frac{F(\omega)}{Q_0}\right]^2 - \frac{k_z^2}{4}}. \tag{20}$$

We then have the following prescription for performing the linear inversion:

1. From experimental geometry, sampling intervals, etc., determine a suitable (complex) wavenumber vector k_z.

2. Find in the data $D'(k_z,\omega) = \int\int dt dx_s e^{-i\omega t} e^{-i\sqrt{\frac{\omega^2}{c_0^2}\left[1+\frac{F(\omega)}{Q_0}\right]^2 - \frac{k_z^2}{4}}x_s} D'(x_s,t)$.

3. Process from $D' \rightarrow D$ using reference medium quantities and equation (17).

4. Now $D(k_z,\omega) = \alpha_1(k_z) + W(\omega)\beta_1(k_z)$ holds; solve for α_1 and β_1 for each k_z using pairs (or larger sets) of frequencies ω_1 and ω_2.

5. Calculate $\alpha_1(z|\omega_1,\omega_2) = \frac{1}{2\pi}\int dk_z e^{ik_z z}\alpha_1(k_z|\omega_1,\omega_2)$ and $\beta_1(z|\omega_1,\omega_2)$ $= \frac{1}{2\pi}\int dk_z e^{ik_z z}\beta_1(k_z|\omega_1,\omega_2)$. This is expected to be an unstable process, and the requirement of some dampening of large k_z values should be anticipated, especially in the presence of noise.

Presently we will use this linear inverse prescription to develop a linear Q compensation algorithm. First, however, let us briefly examine its direct use. Consider the purely acoustic model in the left panel of Figure 1. If we perform a linear acoustic inversion on the primaries reflecting from this model (see the non-bold profile in the bottom panel of Figure 3), we have an input ready for, e.g., the direct non-linear inversion algorithm of Shaw et al. (2004). However, if we embed this same velocity model in a homogeneous background absorptive medium with reference $Q_0 = 50$ (right panel of Figure 1), and perform the same (acoustic) inversion (top panel of Figure 3), the results are predictably distorted, and are inappropriate for use as input to Shaw's algorithm. However, assuming we have in hand the correct Q value for the background medium, which we do in this part of the paper, the above prescription[1] generates the linear wavespeed perturbation α_1 displayed in the middle and bottom panels of Figure 3. In the bottom panel the result is compared to the purely acoustic problem. This forms an input again appropriate for (e.g.) direct non-linear imaging.

In creating these results, we have employed a straightforward stabilization of the inverse transform by which we produce, e.g., $\alpha_1(z|\omega_1,\omega_2)$ from the data. Its effect will be noted in the forthcoming numerical examples, so let us first describe how it works. Consider one of the problematic integrals:

$$\alpha_1(z|\omega_1,\omega_2) = \frac{1}{2\pi}\int dk_z e^{ik_z z}\alpha_1(k_z|\omega_1,\omega_2). \tag{21}$$

The wavenumber k_z has a negative imaginary component, hence the integral requires that $\alpha_1(k_z|\omega_1,\omega_2)$ diminish with k_z at least as rapidly as this exponential grows. The part of α_1 that agrees with wave theory does so, if we have our reference medium properties correct, but any noise (for instance) almost certainly does not. Hence, even the bandlimited versions of it we consider are unstable. We define a taper function that has two components: (1) a gate function that truncates $e^{ik_z z}$ at a specified k_z value, that is (2) smooth by convolution with a Gaussian with a specified variance. The latter "shoulder" suppresses ringing of the stabilized solution. The integral is evidently also more unstable for large values of z. Hence, we make the cutoff k_z value a linearly decreasing function of

[1]Since we restrict ourselves in this numerical example to perturbations in wavespeed only, i.e., $\beta = 0$, the inversion is well-posed for normal incidence data.

depth, with the slope of this determined empirically for a given reference Q value. We will include specifics of the stabilization with each example to follow.

The Q compensation arises straightforwardly from the above inversion procedure – we simply map the corrected α_1, β_1 results linearly back to time using acoustic Green's functions. We begin with an example with the same geometry as that of Figure 1, but with a smaller contrast $c_1 = 1510$m/s, $c_2 = 1520$m/s, and a homogeneous reference medium of $c_0 = 1500$m/s and $Q_0 = 100$. The process is stabilized with the gate illustrated in Figure 4. The results are illustrated in Figure 5. In the top panel, we illustrate (in black) the input primary data plotted against the equivalent data (in red) that would have been measured if $Q_0 \to \infty$. The data is processed using the AD linear inverse equations, and re-mapped to data space using non-absorptive Green's functions otherwise identical to those used in the inverse step. The output is illustrated in the middle panel (in black), again plotted against the un-attenuated data set. The results differ from the benchmark "perfect" result, particularly in the lower corrected primary. However, this is full attributable to the tapering/stabilization, as we can see in the bottom panel when we compare the output with an equivalently tapered version of the un-attenuated data. In Figures 6–7 we repeat the procedure for a lower Q value.

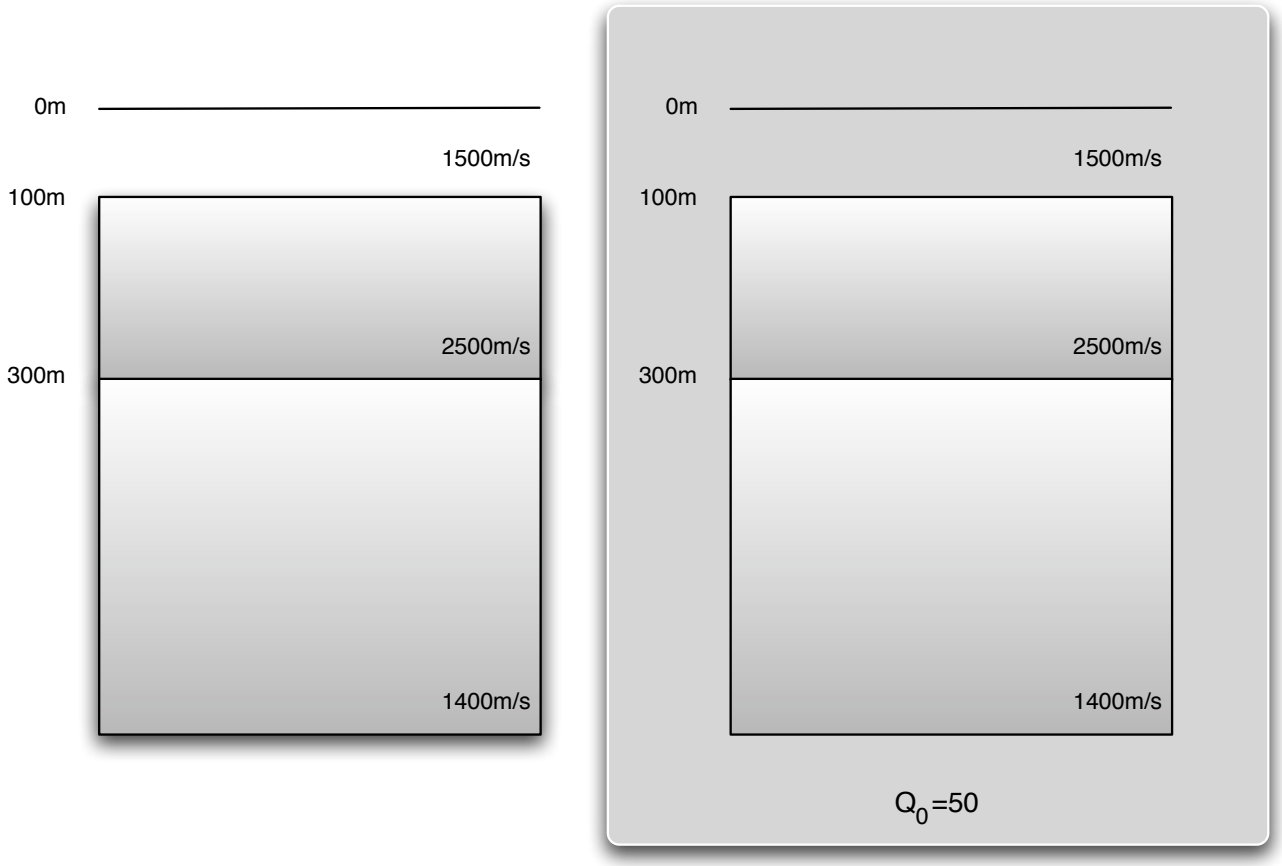

Figure 1: *Synthetic model used to illustrate the direct use of linear A-D equations with an absorptive reference medium. Left panel: a two-interface acoustic constant density profile. Right panel: the same model embedded in a homogeneous absorptive background characterized by* $Q_0 = 50$.

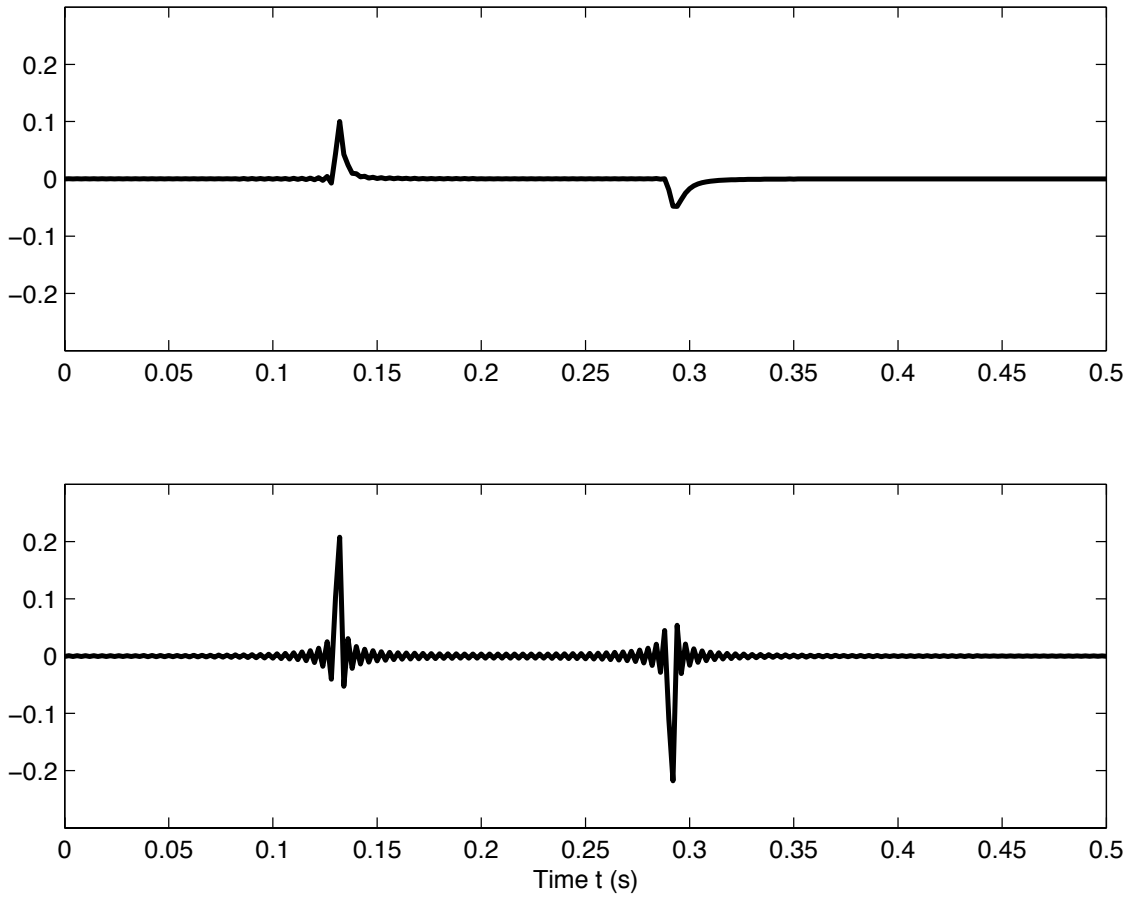

Figure 2: *Synthetically generated primary data. Top panel: primaries associated with the right-panel model in Figure 1. Bottom panel: primaries associated with the left-panel model in Figure 1.*

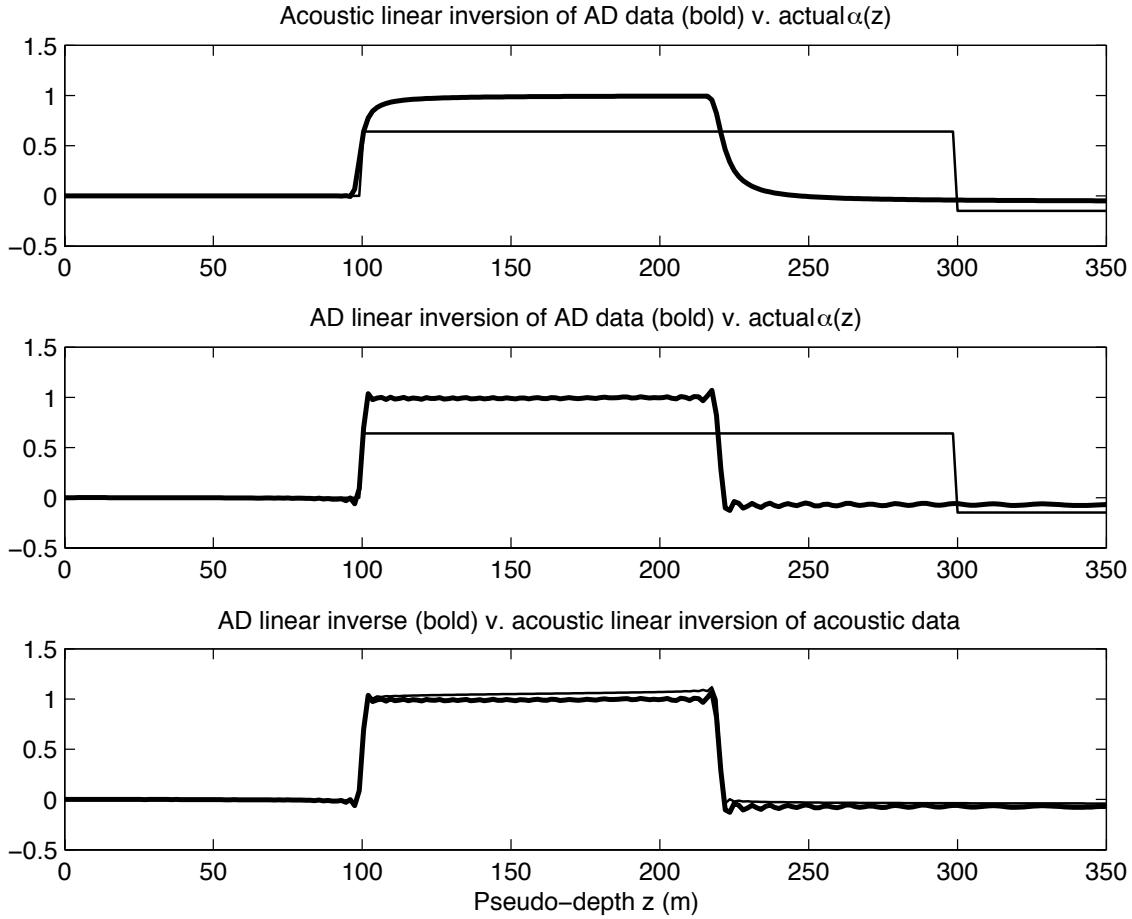

Figure 3: *A comparison of linear inversion results. Top panel: an example of what happens if we treat data from the top panel of Figure 2 with an acoustic linear inversion procedure (bold solid), plotted vs. the actual velocity perturbation. Not surprisingly, in addition to the amplitude and location problems to be corrected by non-linear direct inverse algorithms, the resolution of the reflectors is badly compromised. Middle panel: the linearized inversion of the data from the top panel of Figure 2, using the AD equations of this section (bold solid), again compared against the actual velocity perturbation. This time the results are suitable for input to, e.g., the imaging algorithm of Shaw et al. (2004). This is confirmed in the bottom panel, where we see that this output (again, bold solid) is very close to the linearized inversion of the acoustic data in the bottom panel of Figure 2 (plain solid).*

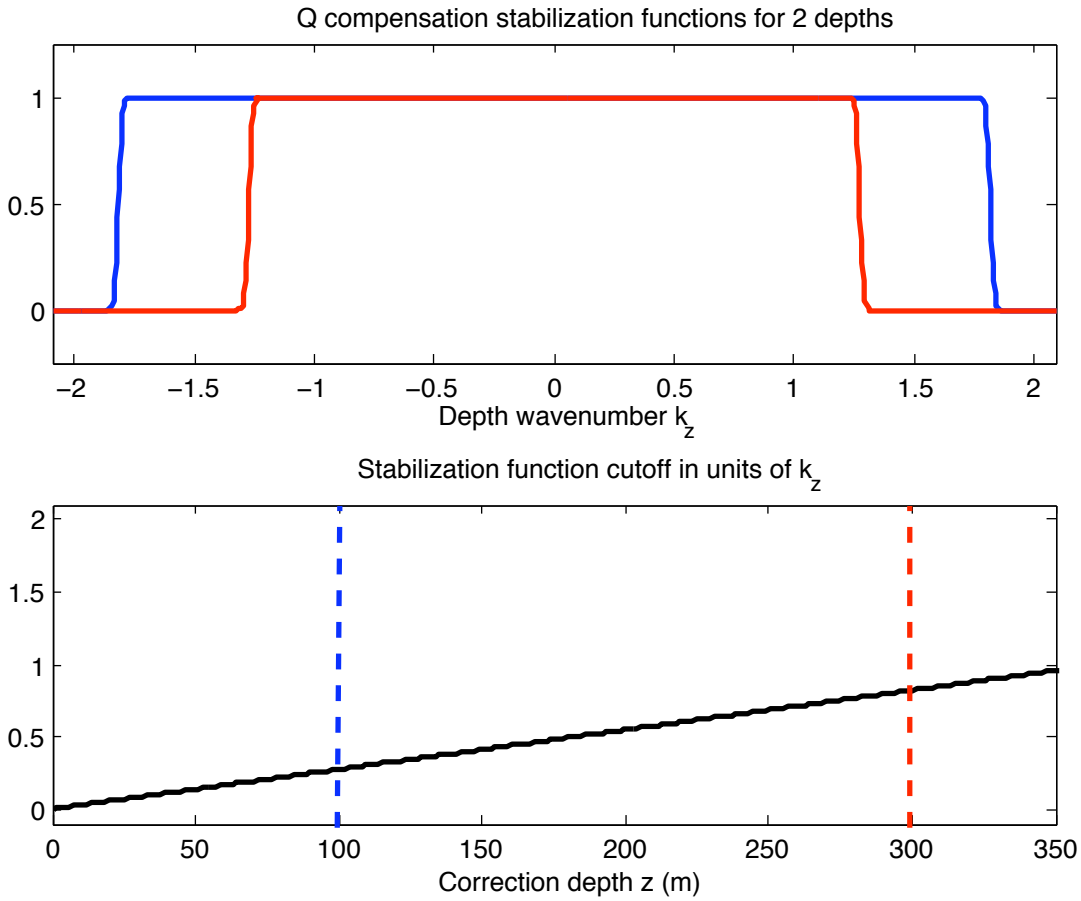

Figure 4: *Stabilization of Q compensation. Top panel: smoothed gate functions are defined to truncate the influence of large k_z values, stabilizing the procedure at the expense of resolution. Bottom panel: the width of the taper is made a linear function of depth, with the slope chosen empirically. In both panels, in blue is the taper at the depth of the shallow primary, and in red is the taper at the depth of the deeper primary.*

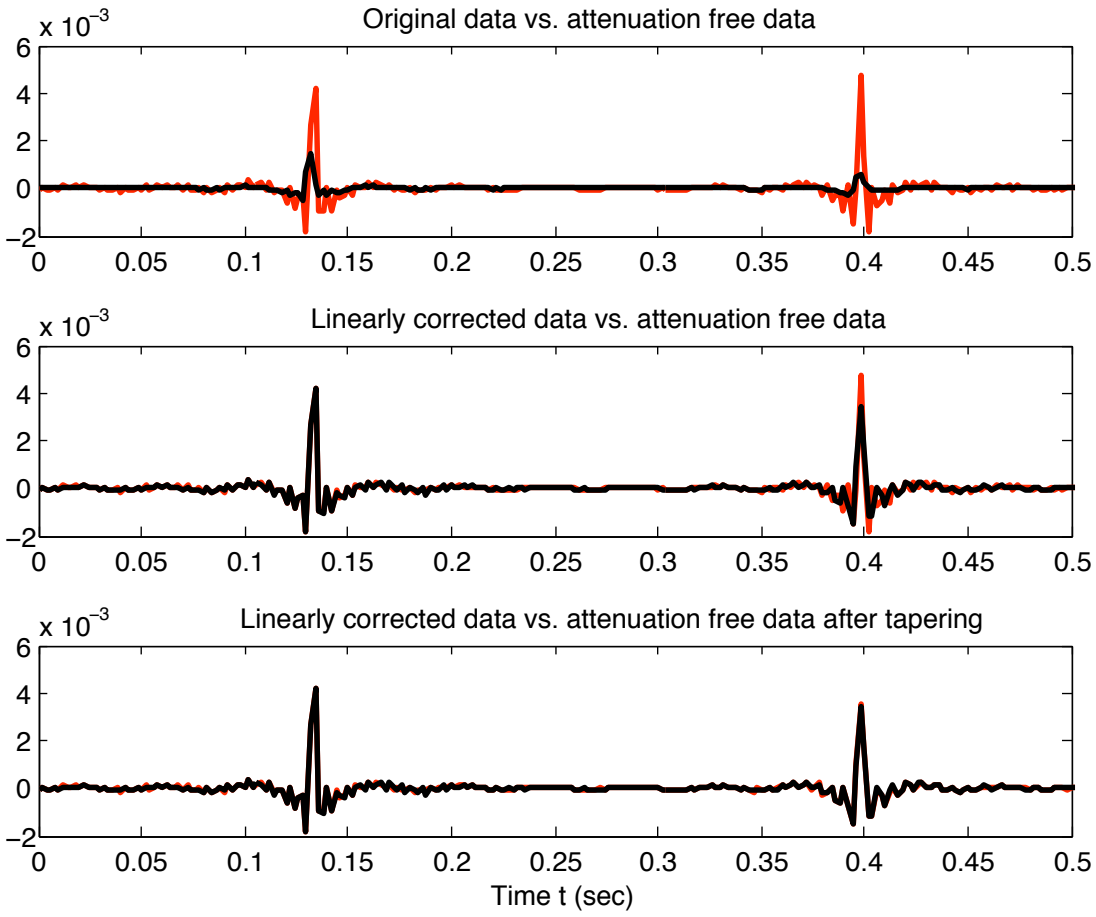

Figure 5: *Results of the direct linear Q compensation procedure for background $Q = 100$. Top panel: input data (black) compared to an equivalent data set constructed in the absence of Q (red). Middle panel: corrected data (black) compared to un-attenuated data (red); differences due to the stabilizing taper. Bottom panel: corrected data compared to tapered un-attenuated data (red).*

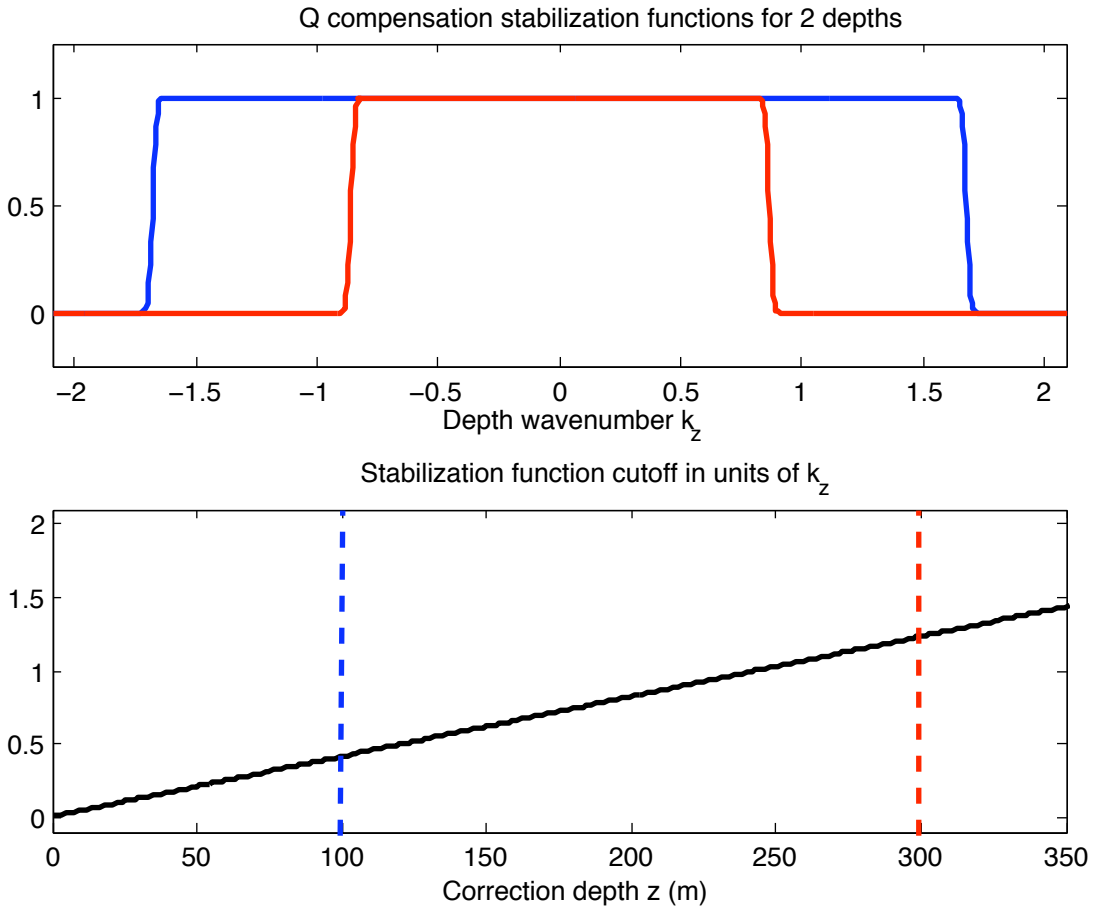

Figure 6: *Stabilization of Q compensation. Top panel: smoothed gate functions are defined to truncate the influence of large k_z values, stabilizing the procedure at the expense of resolution. Bottom panel: the width of the taper is made a linear function of depth, with the slope chosen empirically. In both panels, in blue is the taper at the depth of the shallow primary, and in red is the taper at the depth of the deeper primary.*

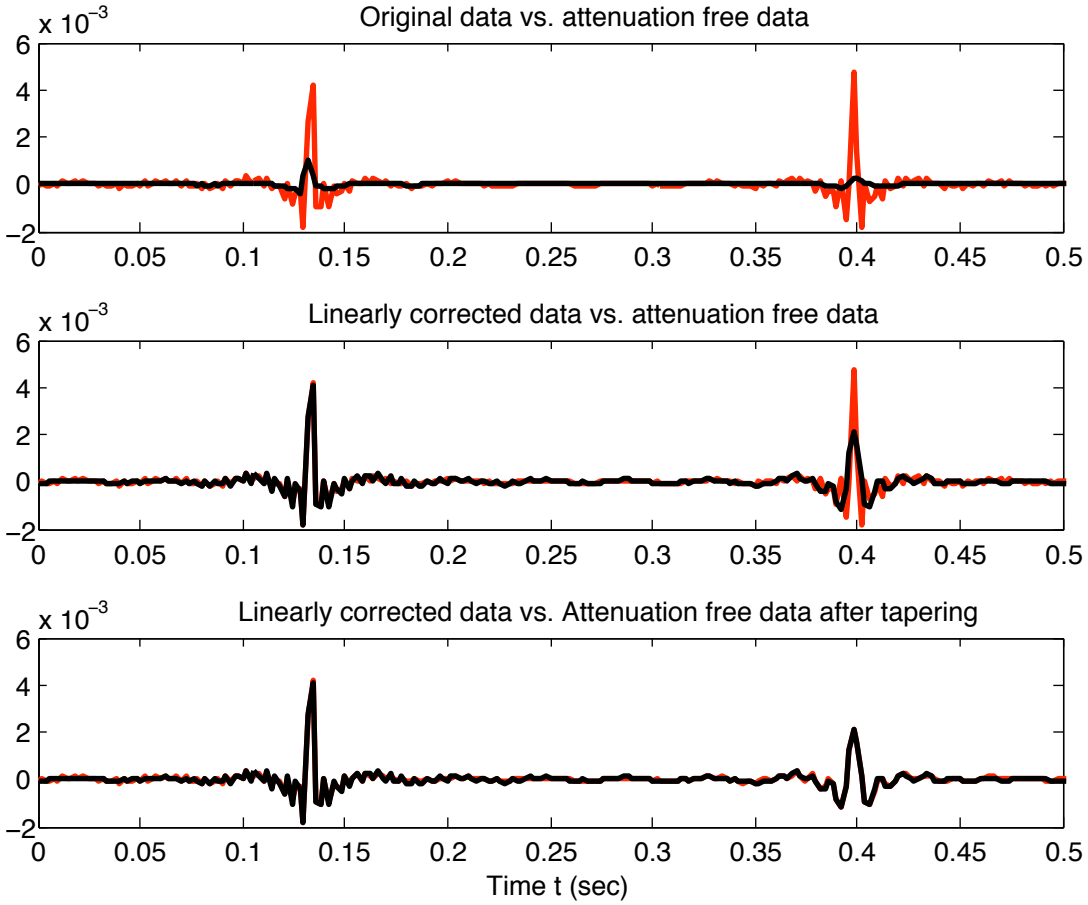

Figure 7: *Results of the direct linear Q compensation procedure for background $Q = 50$. Top panel: input data (black) compared to an equivalent data set constructed in the absence of Q (red). Middle panel: corrected data (black) compared to un-attenuated data (red); differences due to the stabilizing taper. Bottom panel: corrected data compared to tapered un-attenuated data (red).*

3 Direct non-linear Q-compensation

We next consider the opposite end of the range of Q-compensation algorithms derivable from inverse scattering. We attempt to derive algorithms that take full advantage of the inverse scattering series ability to perform inverse tasks using only reference medium properties and data (Weglein et al., 2003). If the reference and actual media differ signficantly, it follows that all resulting procedures occur in the absence of accurate prior medium information. The price of this desirable set of properties is stringent data requirements and algorithms that are highly non-linear. In the coming section, we will see how these general ideas play out in application to the absorption compensation problem.

Approach

The inverse scattering series in its pristine form takes as its input measurements of a scattered field, and creates as its output the perturbation that gave rise to the field. This runs counter to the goals of Q-compensation as stated in the introduction, because:

1. The scattered field in general contains all reflected events, including primaries and multiples, whereas we (having effective techniques for multiple suppression at hand) wish to perform inverse operations on primaries only;
2. Of all the processing steps enacted upon primaries within the full inverse problem, we wish one only, the correction for absorptive propagation, to actually be carried out;
3. We wish to estimate not the perturbation, a model-like quantity, but, rather, a data-like quantity, a set of reflected primaries that have been Q-compensated.

After posing the scattering problem to accommodate absorptive media, most of the strategy in the algorithm development we present is geared towards managing these three differences between our wishes and those of inverse scattering. Our route is as follows.

We begin by creating a forward model for absorptive-dispersive primaries based on the Born series. The result is a non-linear scattering-based series calculation of *primaries only* in a layered absorptive-dispersive medium, which is accurate for large, extended perturbations. This is useful, because it turns out that such partial series may be inverted, order-by-order, in exactly the same fashion as the full inverse scattering series, generating non-linear direct inversion procedures for primaries only. We continue, then, by carrying out this inversion upon the absorptive-dispersive primary series above. The resulting non-linear inverse scattering equations, which construct approximations of the actual wavespeed and Q perturbations in the medium, are of a form that addresses item (1.) above.

We next note that, because of the direct, analytical nature of the above inverse equations, it is clear where, and how, in the data-driven operations the correction for Q takes place. It is also clear how to suppress all of the other non-linear data operations. Doing so amounts to an extraction and

separate execution of the Q-compensation part of the full inversion of primary data; this addresses item (2.) above.

Finally, we point out that, given a homogeneous reference medium, the relationship between the linear components of the parameter perturbations and the data is very simple: essentially a Fourier transform. In the above procedure, all non-linear aspects of the processing, apart from those that are Q-related, have been suppressed. It follows that in all respects apart from absorption, the output maintains a simple, linear relationship with the data. We map this output trivially back to data-space. The final result, which has addressed item (3.) above, is deemed to be the Q-compensated data set.

Direct non-linear Q compensation

What follows is a skeletal derivation of our candidate scheme for direct, non-linear Q compensation; details are included in the Appendices. Using the definitions and quantities in Case I of the introduction, we construct the absorptive-dispersive scattering problem, restricting the medium such that α and β vary in depth only. Following the approach described above, we next form a partial Born series:

$$\psi_P = \psi_1 + \psi_2 + \psi_3..., \tag{22}$$

whose terms are adjudged, via arguments based on relative scattering geometry (Innanen, 2005), to construct reflected primaries that have been distorted by Q. At first order, for instance, we have

$$\begin{aligned}\psi_1(k_s,\omega) &= \int dx' \int dz' G_0(x_g, z_g, x', z', \omega) k^2 \gamma(z') G_0(x', z', k_s, z_s, \omega) \\ &= -\frac{1}{4\cos^2\theta} \int dz' e^{i2q_s z'} \gamma(z'),\end{aligned}$$

where

$$\gamma(z) = \alpha(z) - 2F(\omega)\beta(z),$$

and $\theta = \sin^{-1}\frac{k_s c_0}{\omega}$, and we have set $x_g = z_g = z_s = 0$. For another instance, at second order, we have

$$\psi_2(k_s,\omega) = -\frac{(-i2q_s)}{8\cos^4\theta} \int dz' e^{i2q_s z'} \gamma(z') \left(\int^{z'} dz'' \gamma(z'') \right).$$

Continuing the partial summation at all orders we produce a series for attenuated primaries, ψ_P, which we associate with the measured data $D \equiv \psi_P$:

$$\begin{aligned}D(k_s,\omega) =& \frac{-1}{4\cos^2\theta} \int dz' e^{i2q_s z'} \gamma(z') \\ & \times \sum_{n=0}^{\infty} \frac{1}{n!} \left(\frac{-iq_s}{\cos^2\theta} \int^{z'} dz'' \gamma(z'') \right)^n.\end{aligned} \tag{23}$$

Computing and summing a large number of these terms generates an analytic expression for the primary data. The full details of the derivation are presented in Appendix A. We next form an inverse series for the perturbations α and β, in which the n'th term is defined to be n'th order in the *primary* data modeled above. The full derivation and discussion of this is presented in Appendix B. Here we will describe some salient aspects of it. We let this series be

$$\begin{aligned}&[\alpha(z) - 2F(\omega)\beta(z)]\\ &\quad = [\alpha_1(z) - 2F(\omega)\beta_1(z)] + [\alpha_2(z) - 2F(\omega)\beta_2(z)] + \ldots \ .\end{aligned}$$

This is substituted into equation (35), and like orders are equated (Innanen, 2005), similarly to Carvalho's derivation of the full inverse scattering series (Carvalho, 1992). At first order, we have

$$D(k_s, \omega) = \frac{-1}{4\cos^2\theta}\int dz' e^{i2q_s z'}[\alpha_1(z') - 2F(\omega)\beta_1(z')]. \tag{24}$$

Innanen and Weglein (2007) describe in detail how this equation may be used to determine α_1 and β_1 as functions of pseudo-depth, as well as sets of incidence angles ϑ, and any desired weighting W. Importantly for what follows, the quantities α_1 and β_1 are interpretable as being either "model-like", if the actual perturbations are small and transient, and some scheme (e.g., Clayton and Stolt, 1981) of averaging is invoked to deal with the over-determinedness of the problem, or alternatively "data-like", if the perturbation is large and extended, and maximal variability of α_1 and β_1 with experimental variables is retained. Since we have chosen a homogeneous reference and are concerned with instances of large, extended perturbations, we are in the latter regime. It is accurate, therefore, to think of the α_1, β_1 quantities as being essentially linearly transformed and weighted versions of the input primary data.

At second order, we have

$$\begin{aligned}&\frac{1}{4\cos^2\theta}\int dz' e^{i2q_s z'}[\alpha_2(z'|\vartheta, W) - 2F(\omega)\beta_2(z'|\vartheta, W)]\\ &\quad = -\frac{[-i2q_s]}{8\cos^4\theta}\int dz' e^{i2q_s z'}[\alpha_1(z'|\vartheta, W) - 2F(\omega)\beta_1(z'|\vartheta, W)]\\ &\qquad \times \left(\int_0^{z'} dz''[\alpha_1(z''|\vartheta, W) - 2F(\omega)\beta_1(z''|\vartheta, W)]\right).\end{aligned}$$

In $\alpha_1(z'|\vartheta, W)$ and $\beta_1(z'|\vartheta, W)$ we have now explicitly included their dependence on incidence angles and weights; we point out that consequently, the second order terms α_2 and β_2 must also be functions of these quantities.

As we continue to higher orders, a pattern in the mathematics is discernible, that allows the n'th order equation to be straightforwardly predicted. Summing over all orders (by assuming the continuation of this pattern ad infinitum), and defining

$$\begin{aligned}\alpha_P(z|\vartheta, W) &\equiv \sum_{n=0}^{\infty}\alpha_{n+1}(z|\vartheta, W),\\ \beta_P(z|\vartheta, W) &\equiv \sum_{n=0}^{\infty}\beta_{n+1}(z|\vartheta, W),\end{aligned}$$

there results a closed form set of non-linear equations

$$\begin{aligned}&\alpha_P(k_z,\theta|\vartheta,W) - 2F(k_z,\theta)\beta_P(k_z,\theta|\vartheta,W)\\ &= \int dz' e^{-ik_z\left[z' + \frac{1}{2\cos^2\theta}\int_0^{z'} dz''[\alpha_1(z''|\vartheta,W) - 2F(k_z,\theta)\beta_1(z''|\vartheta,W)]\right]}\\ &\quad \times [\alpha_1(z'|\vartheta,W) - 2F(k_z,\theta)\beta_1(z'|\vartheta,W)],\end{aligned} \tag{25}$$

where again $k_z \equiv -2q_s$. This represents a complete inversion of the primary data (to within the accuracy of the primary approximation series in equation 35 in Appendix A), for a layered, 2-parameter, absorptive-dispersive medium. The quantities α_P and β_P are the non-linearly determined profiles associated with $c(z)$ and $Q(z)$. Each can be independently determined via equation (25), as is demonstrated in detail in Appendix C. This may be of independent interest.

However, our current goal is to accomplish a single inverse task, that of compensating for Q. To do this, we examine equation (25) more closely. We notice that the outputs, α_P and β_P, would be related linearly to the inputs, α_1 and β_1, except that α_1 and β_1 also appear in the argument of the exponential function in the integrand. We then make the following empirical statements. The role of α_1 in the argument of the exponential is to non-linearly process the input to accomplish tasks associated with wavespeed deviations between the reference and actual media (i.e., imaging). And, the role of β_1 in the argument is to accomplish Q related tasks, i.e., compensation. We peremptorily set α_1 in the argument to zero, and argue that as a consequence: (1) the (now altered) outputs α_P and β_P undergo non-linear correction for the attenuation and dispersion associated with Q, but (2) they undergo linear treatment in all other respects.

Calling the partially treated outputs α_Q and β_Q, we have instead

$$\begin{aligned}&\alpha_Q(k_z,\theta|\vartheta,W) - 2F(k_z,\theta)\beta_Q(k_z,\theta|\vartheta,W)\\ &= \int dz' e^{-ik_z\left[z' - \frac{F(k_z,\theta)}{\cos^2\theta}\int_0^{z'} dz''\beta_1(z''|\vartheta,W)\right]}\\ &\quad \times [\alpha_1(z'|\vartheta,W) - 2F(k_z,\theta)\beta_1(z'|\vartheta,W)].\end{aligned} \tag{26}$$

By assumption, within these equations only Q-compensation takes place as the data is processed. Finally, we will argue for an approach to make the output of this processing a data-like quantity. Equation (26) follows the basic template

$$A = \int e^B C. \tag{27}$$

By comparing this template (and equation 26) to the components of equation (24), it is evident that both A and C already have a strongly data-like aspect, with C representing the input and A representing the output, "processed," data. Even B shares this appearance, albeit with the α_1 component suppressed. It is, therefore, accurate to view the output data-like quantity A as being the consequence of weighted forms of the data (B) operating non-linearly upon themselves (C).

After constructing the input C and the operator B by linearly transforming and weighting the data, we apply equation (26), and, finally, use the relationship in equation (24) to map back to

the (k_s, ω) domain, through, in essence, a change of variables. Our suggestion is that this mapped quantity is a Q-compensated data set, in the sense of our introductory definition.

To exemplify this procedure, we construct a simple synthetic primary data set corresponding to the two-interface absorptive-dispersive model in Figure 8. The resulting primary data (Figure 9, upper panel) is used as input to the linear inverse scattering equations, which involves a transformation and weighting thereof. This synthetic is then used to construct both the operator e^B and the operand C as in equation (27). The Q-compensated data set (Figure 9, lower panel) is formed by transforming the result, A in equation (27), to the (k_s, ω) domain, and then performing straightforward inverse Fourier transforms. The Q-compensated results are compared in detail with the input in Figure 10 for three offsets, 0m, 110m, and 225m. We see high-quality results, albeit with slight under-correction at large angle.

In equation (26) there are two sets of angles: an input set (ϑ) that has been used in the linear step, in particular to construct the correction operator, and an output angle θ, which is varied to recover the full pre-stack data set. Empirically we have found that using sets of input angles ϑ which "cluster" around the output angle θ produces the best results. In the examples we present here, a $\vartheta = \{\theta, \theta + \Delta\theta\}$ was used for each θ of corrected data.

Noisy examples have not been included at this proof-of-concept stage; we have found our approach to share the basic response to noise of all standard Q compensation schemes. We point out that (as is often done) with a quick alteration to the function F as it appears in the argument in equation (25) we can transform this algorithm immediately into a "dispersion compensation" algorithm, which is well-conditioned and largely unaffected by noise.

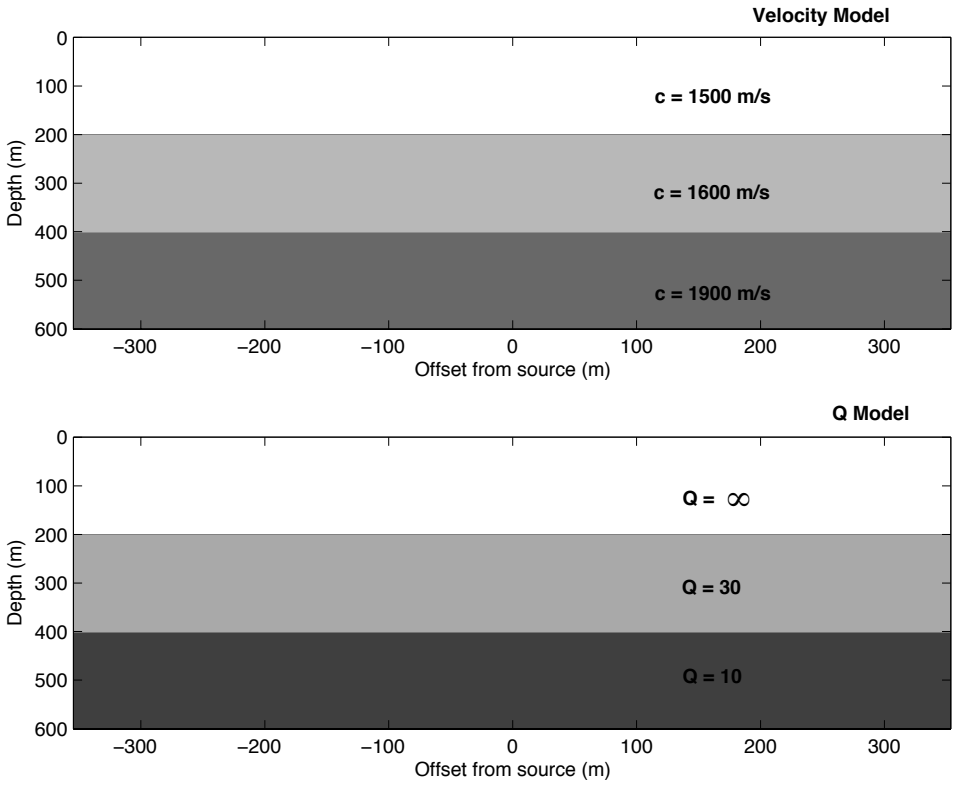

Figure 8: *Two interface absorptive-dispersive model.*

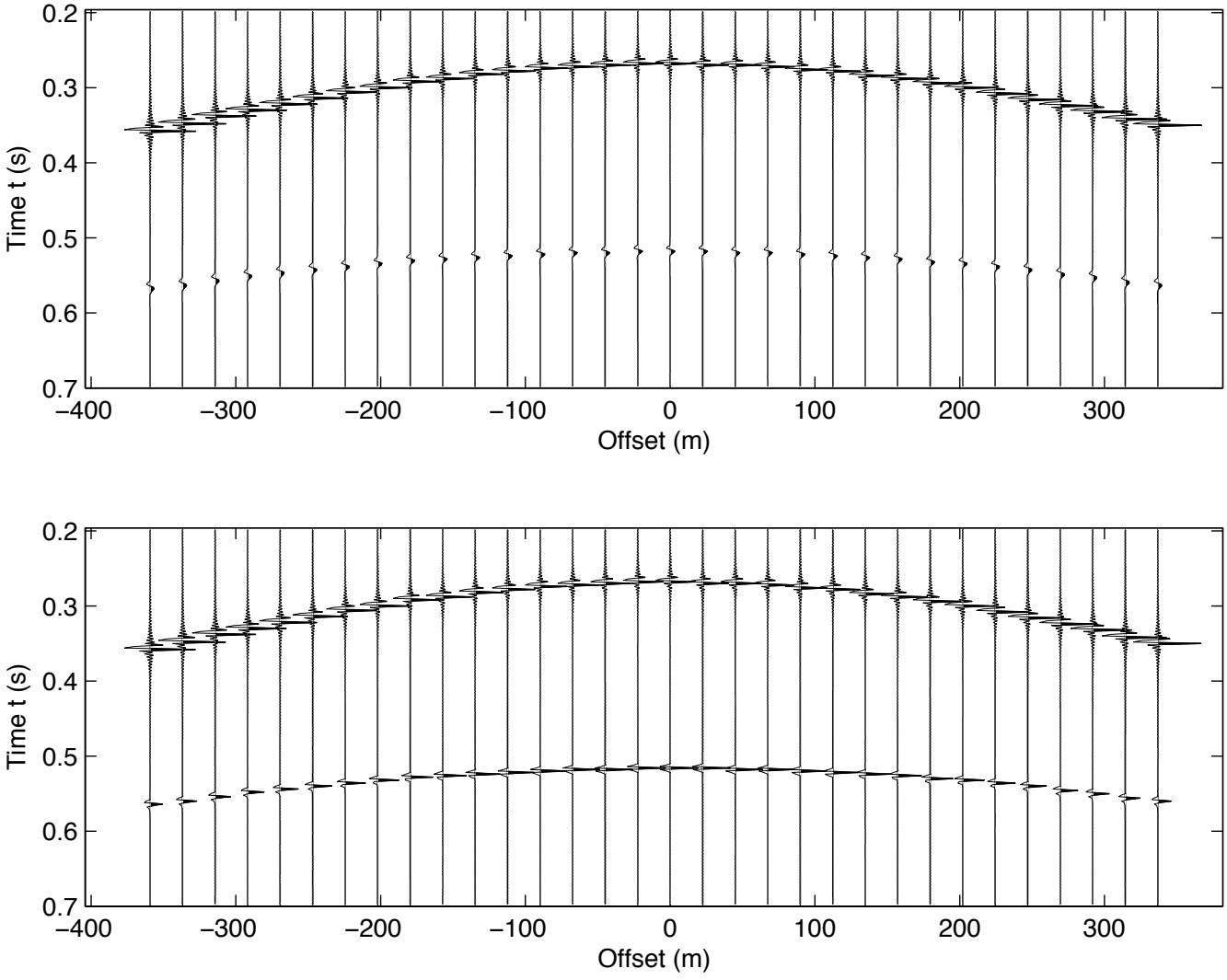

Figure 9: *Top panel: synthetic pre-stack input primary data from the model in Figure 8 (decimated for purposes of display); bottom panel: Q-compensated output data (likewise decimated).*

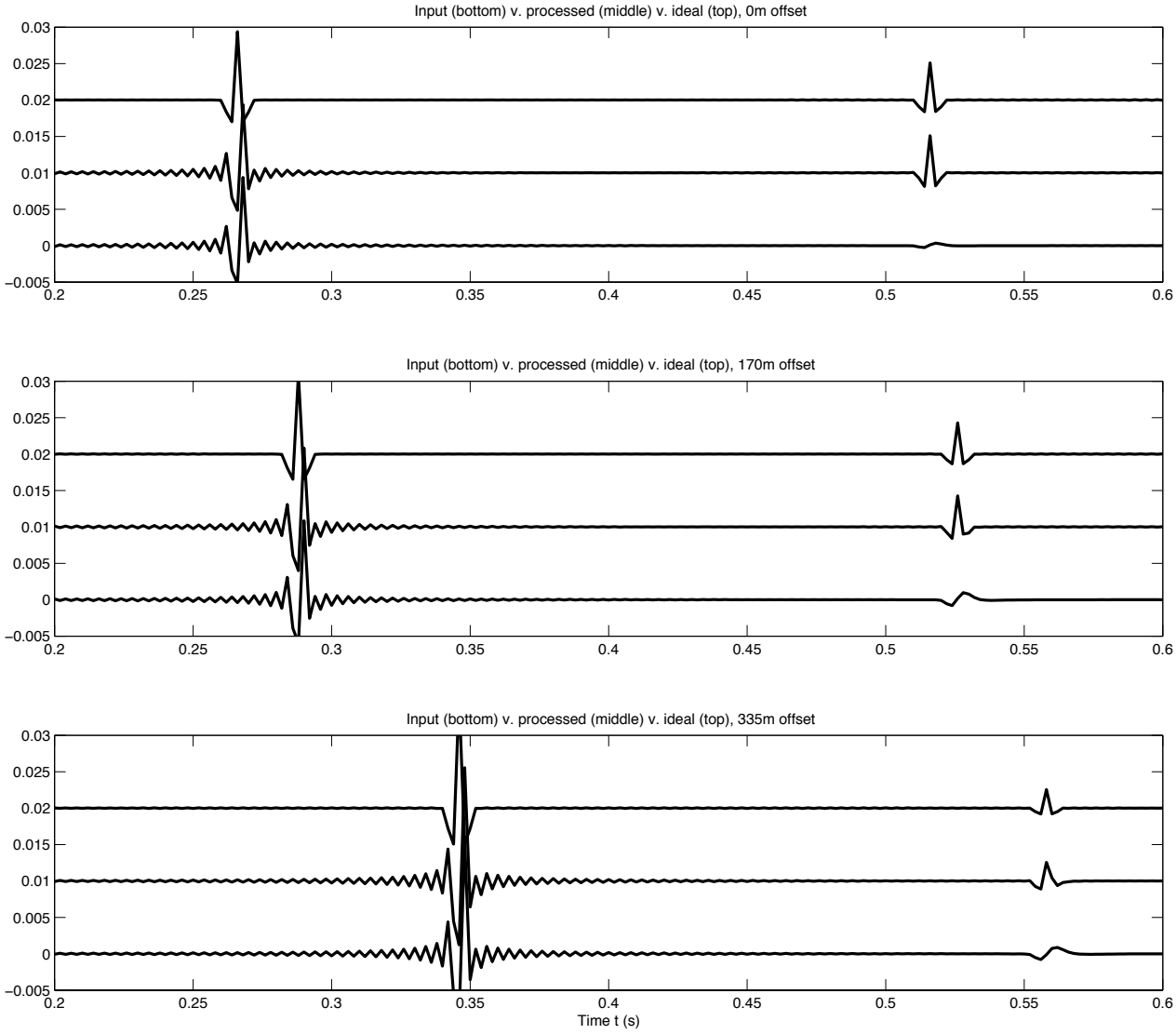

Figure 10: *Detail of Q compensation for three offsets of pre-stack data. Bottom trace in each panel is input, the middle trace is the output, and the top trace, for benchmarking, is an idealized trace constructed without Q, and normalized to the maximum value of the output traces.*

Discussion and conclusions

We choose as the definition of Q compensation, *the estimation of an output data set that is identical to the input, except that all absorptive propagation effects are absent*. We present two candidate schemes, based on linear and non-linear inverse scattering, whose output, we argue, fits this definition. In the non-linear algorithm, for which an accurate prior estimate of the Q structure of the medium is not required, a correction operator is automatically constructed from the data themselves, with minimal influence of or requirement for prior information. Synthetic examples illustrate the scheme in action, and are a compelling proof-of-concept result. We have made two rational, but intuitive, assumptions in deriving the scheme:

1. That, by suppressing certain components of the full non-linear inversion equations derived from inverse scattering, we completely isolate the Q compensation action inherent to the inversion.
2. That, with trivial linear transformation and changes of variable, the output of these inverse steps can be treated as an equivalent data set, different only from the input in the lack of absorption in the primary events.

We feel that the soundness of these steps is best argued for with success in testing, some of which we have provided with our proof-of-concept example.

Direct, non-linear methods bring a greatly reduced requirement for prior information as compared to their linear counterparts. But they demand broadband, densely sampled, wide-aperture, de-ghosted, deconvolved (of the *source* wavelet), and demultipled data in return. Data quality, bandwidth and coverage are the first requirements in considering methods such as this one.

The data set used in the above examples is broad-band, and includes low (sub-Hz) frequencies (although not close to zero frequency–the nearly constant Q model we are using in fact diverges at and near that limit). The requirement for this kind of data is typical of non-linear, wave theoretic inverse methods. The best outcome will result from actual acquisition of maximally low frequency data, of course; however, various assumptions, for instance that of a piecewise-constant overburden, can additionally be made, removing the sensitivity to cut-off of low frequencies.

Two other issues are at the forefront when it comes to contemplating field data application. The first has to do with the way in which the data are interrogated for information in constructing the operator (B in equation 27), which is described in detail by Innanen and Weglein (2007). Briefly, it is the frequency- and angle-dependence of the transmission-altered reflection coefficients of the primaries (loosely, a brand of AVO behaviour specific to absorptive-dispersive media) that drives the construction of the operator. That this behavior exists is a straightforward prediction of wave theory. However, it may appear as very subtle variations in field data. Detecting it is critical to the use of the method.

The second is a consequence of the algorithm's interest in amplitude variations in the data. As it stands, the algorithm considers data to be due to a 2-parameter, absorptive-dispersive, acoustic medium. When that is true, as in our synthetic examples, the results are of high quality. When

that is not true, as in a seismic field data application, the results will presumably suffer. One clear next step is to alter the construction of the corrective operator to be in accordance with a suitable anelastic (as opposed to an-acoustic) medium model.

Our aim is to build a theoretical framework from within which the user may select a suitable Q compensation algorithm, that optimally balances the degree of non-linearity (and the computational expense and sensitivity to data quality that this implies) with the degree of available prior knowledge of the Q structure (or velocity structure etc.) at hand.

Acknowledgements

The sponsors and personnel of M-OSRP are thanked. K. Innanen was supported by U.S. D.O.E. Grant No. DOE-De-FG02-05ER15697. J. Lira was supported by Petrobras.

References

Aki, K. and P. G. Richards. *Quantitative Seismology.* 2nd edition. University Science Books, 2002.

Baan, M. van der. "Time-varying wavelet estimation and deconvolution by kurtosis maximization." *Geophysics* 73 (2008): V11–V18.

Bickel, S. H. "Similarity and the inverse Q filter: The Pareto-Levy stretch." *Geophysics* 58 (1993): 1629.

Bickel, S. H. and R. R. Natarajan. "Plane-wave Q deconvolution." *Geophysics* 50 (1985): 1426–1439.

Carvalho, P. M. *Free-surface multiple reflection elimination method based on nonlinear inversion of seismic data.* PhD thesis, Universidade Federal da Bahia, 1992.

Causse, E., R. Mittet, and B. Ursin. "Preconditioning of full-waveform inversion in viscoacoustic media." *Geophysics* 64 (1999): 130–145.

Clarke, G. K. C. "Time-varying deconvolution filters." *Geophyics* 33 (1968): 936.

Clayton, R. W. and R. H. Stolt. "A Born-WKBJ inversion method for acoustic reflection data." *Geophysics* 46 (1981): 1559–1567.

Dahl, T. and B. Ursin. "Non-linear AVO inversion for a stack of anelastic layers." *Geophysical Prospecting* 40 (1992): 243.

Dasios, A., C. McCann, and T. Astin. "Least-squares inversion of in-situ sonic Q measurements: stability and resolution." *Geophysics* 69 (2004): 378–385.

Duren, R. E. and E. C. Trantham. "Sensitivity of the dispersion correction to Q error." *Geophysics* 62 (1997): 288–290.

Hargreaves, N. D. "Similarity and the inverse Q filter: some simple algorithms for inverse Q filtering." *Geophysics* 57 (1992): 944–947.

Hargreaves, N. D. and A. J. Calvert. "Inverse Q-filtering by Fourier transform." *Geophysics* 56 (1991): 519–527.

Hicks, G. and R. G. Pratt. "Reflection waveform inversion using local descent methods: estimating attenuation and velocity over a gas-sand deposit." *Geophysics* 66 (2001): 598–612.

Innanen, K. A. "Two non-linear forward and inverse approximations for wave fields in the presence of sustained medium perturbations." *Proceedings of the 75th Annual Meeting of the Society of Exploration Geophysicists, Houston, TX.* . Soc. Expl. Geophys., 2005.

Innanen, K. A., J. E. Lira, and A. B. Weglein. "An extension of linear inverse scattering methods for absorptive media to the case of an absorptive reference." *Proceedings of the EAGE, Rome, Italy.* . Eur. Ass. Geosci. Eng., 2008.

Innanen, K. A. and A. B. Weglein. "Construction of absorptive/dispersive wave fields with the forward scattering series." *Journal of Seismic Exploration* 12 (2003): 259–282.

Innanen, K. A. and A. B. Weglein. "Towards non-linear construction of a Q-compensation operator directly from reflection seismic data." *Proceedings of the 75th Annual Meeting of the Society of Exploration Geophysicists, Houston, TX.* . Soc. Expl. Geophys., 2005.

Innanen, K. A. and A. B. Weglein. "On the construction of an absorptive-dispersive medium model via direct linear inversion of reflected seismic primaries." *Inverse Problems* (2007): 2289–2310.

Kjartansson, E. "Constant-Q wave propagation and attenuation." *Journal of Geophysical Research* 84 (1979): 4737–4748.

Liu, F., A. B. Weglein, K. A. Innanen, and B. G. Nita. "Multi-dimensional seismic imaging using the inverse scattering series." *Proceedings of the 76th Annual Meeting of the Society of Exploration Geophysicists, New Orleans, LA.* . Soc. Expl. Geophys., 2006.

Liu, Fang. *Multi-dimensional depth imaging without an adequate velocity model*. PhD thesis, University of Houston, 2006.

Margrave, G. F. "Theory of nonstationary linear filtering in the Fourier domain with application to time-variant filtering." *Geophysics* 63 (1998): 244–259.

Mittet, R. "A simple design procedure for depth extrapolation operators that compensate for absorption and dispersion." *Geophysics* 72 (2007): S105–S112.

Mittet, R., R. Sollie, and K. Hostad. "Prestack depth migration with compensation for absorption and dispersion." *Geophysics* 60 (1995): 1485–1494.

Ribodetti, A. and J. Virieux. "Asymptotic theory for imaging the attenuation factor Q." *Geophysics* 63 (1998): 1767–1778.

Shaw, S. A. *An inverse scattering series algorithm for depth imaging of reflection data from a layered acoustic medium with an unknown velocity model*. PhD thesis, University of Houston, 2005.

Shaw, S. A., A. B. Weglein, D. J. Foster, K. H. Matson, and R. G. Keys. "Isolation of a leading order depth imaging series and analysis of its convergence properties." *Journal of Seismic Exploration* 2 (November 2004): 157–195.

Song, S. and K. A. Innanen. "Multiresolution modelling and wavefield reconstruction in attenuating media." *Geophysics* 67 (2002): 1192–1201.

Trad, Daniel. "Interpolation and multiple attenuation with migration operators." *Geophysics* 68 (November-December 2003): 2043–2054.

Wang, Y. "A stable and efficient approach of inverse Q filtering." *Geophysics* 67 (2002): 657–663.

Wang, Y. "Quantifying the effectiveness of stabilized inverse Q filtering." *Geophysics* 68 (2003): 337–345.

Wang, Y. "Inverse Q-filter for seismic resolution enhancement." *Geophysics* 71 (2006): V51–V60.

Weglein, A. B., F. V. Araújo, P. M. Carvalho, R. H. Stolt, K. H. Matson, R. T. Coates, D. Corrigan, D. J. Foster, S. A. Shaw, and H. Zhang. "Inverse Scattering Series and Seismic Exploration." *Inverse Problems* (2003): R27–R83.

Weglein, A. B., D. J. Foster, K. H. Matson, S. A. Shaw, P. M. Carvalho, and D. Corrigan. "An inverse-scattering sub-series for predicting the spatial location of reflectors without the precise reference medium and wave velocity." *71st Annual Internat. Mtg., Soc. Expl. Geophys., Expanded Abstracts*. . Soc. Expl. Geophys., 2001. 2108–2111.

Weglein, A. B., F. A. Gasparotto, P. M. Carvalho, and R. H. Stolt. "An Inverse-Scattering Series Method for Attenuating Multiples in Seismic Reflection Data." *Geophysics* 62 (November-December 1997): 1975–1989.

Zhang, C. and T. J. Ulrych. "Seismic absorption compensation: a least squares inverse scheme." *Geophysics* 72 (2007): R109–R114.

Zhang, H. *Direct non-linear acoustic and elastic inversion: towards fundamentally new comprehensive and realistic target identification*. PhD thesis, University of Houston, 2006.

Zhang, H. and A.B. Weglein. "The inverse scattering series for tasks associated with primaries: depth imaging and direct non-linear inversion of 1D variable velocity and density acoustic media." *SEG Technical Program Expanded Abstracts*. 2005, 1705–1708.

Appendix A
A scattering model of primaries in layered absorptive-dispersive media

In this appendix we take the scattering quantities defined in the introduction appropriate for non-absorptive reference media, and use them to construct the first three terms in the absorptive-dispersive Born series. The relative scattering geometry of these terms is next used to extract a subset of terms, which are adjudged to construct the absorptive-dispersive primaries. This pattern is used to deduce the full series expression.

We proceed assuming a non-absorptive reference medium. For plane waves at oblique incidence (i.e., a non-zero source plane wave angle θ) above a layered AD medium, with reflected waves detected at a lateral line receiver location x_g, the first order term of the Born series is

$$\begin{aligned}\psi_1(x_g, z_g, k_s, z_s, \omega) &= \int dx' \int dz' G_0(x_g, z_g, x', z', \omega) k^2 \gamma(z') G_0(x', z', k_s, z_s, \omega) \\ &= -\frac{1}{4}\frac{k^2}{q_s^2} e^{-iq_s(z_g+z_s)} e^{ik_s x_g} \int dz' e^{i2q_s z'} \gamma(z'),\end{aligned} \tag{28}$$

where

$$\gamma(z) = \alpha(z) - 2F(\omega)\beta(z). \tag{29}$$

This term constructs only primaries, and as such is defined as the first order term in the primary construction series also. For convenience we set $x_g = z_g = z_s = 0$, and rename the linear term ψ_{1P}, which has the form

$$\psi_{1P}(k_s, \omega) = -\frac{1}{4\cos^2\theta} \int dz' e^{i2q_s z'} \gamma(z'). \tag{30}$$

The second order term of the Born series is also needed in its entirety in the primary approximation. We have

$$\begin{aligned}\psi_2(x_g, z_g, k_s, z_s, \omega) = &\int dx' \int dz' G_0(x_g, z_g, x', z', \omega) k^2 \gamma(z') \\ &\times \int dx'' \int dz'' G_0(x', z', x'', z'', \omega) k^2 \gamma(z'') G_0(x'', z'', k_s, z_s, \omega),\end{aligned} \tag{31}$$

thus, again with $x_g = z_g = z_s = 0$,

$$\begin{aligned}\psi_{2P}(k_s, \omega) &= -\frac{1}{16\cos^4\theta}(-i2q_s) \int dz' e^{iq_s z'} \gamma(z') \int dz'' e^{iq_s|z'-z''|} \gamma(z'') e^{iq_s z''} \\ &= -\frac{1}{8\cos^4\theta}(-i2q_s) \int dz' e^{i2q_s z'} \gamma(z') \left(\int^{z'} dz'' \gamma(z'') \right).\end{aligned} \tag{32}$$

At third order, we begin with the full Born series term

$$\psi_3(k_s, \omega) = -\frac{1}{64\cos^6\theta}(-i2q_s)^2 \int dz' e^{iq_s z'} \gamma(z') \int dz'' e^{iq_s|z'-z''|} \gamma(z'') \int dz''' e^{iq_s|z''-z'''|} \gamma(z''') e^{iq_s z'''}, \tag{33}$$

but reject the component for which the "middle" scattering location z'' is shallower than both z' and z''', which has been adjudged to begin the construction of multiples (Weglein et al., 1997). This means rejecting 1 of the 4 components of equation (33) that arise when the absolute value bars are evaluated case-wise. Retaining the other three components, we have

$$\begin{aligned}\psi_{3P}(k_s,\omega) &= -\frac{1}{64\cos^6\theta}(-i2q_s)^2\int dz' e^{i2q_s z'}\gamma(z')\int^{z'} dz''\gamma(z'')\int^{z''} dz'''\gamma(z''') \\ &= -\frac{1}{32\cos^6\theta}(-i2q_s)^2\int dz' e^{i2q_s z'}\gamma(z')\left(\int^{z'} dz''\gamma(z'')\right)^2,\end{aligned} \tag{34}$$

where again for convenience $x_g = z_g = z_s = 0$ (for cases involving non-zero source receiver depths, or several x_g values, the simple exponential factors outside the integrals may be easily re-instated). The pattern visible from orders 1–3 persists at higher order. Summing all of terms that fit the same pattern creates an approximation of primaries appropriate for large, extended absorptive-dispersive perturbations. The approximation error that arises in this expression at very large perturbation sizes is due to terms at third order and beyond whose scattering geometry fits the criteria for retention, but which are not reproduced by this formula. Calling the approximation ψ_P, we have

$$\begin{aligned}\psi_P(k_s,\omega) &= \sum_{n=0}^{\infty}\psi_{nP}(k_s,\omega) \\ &= -\frac{1}{4\cos^2\theta}\int dz' e^{i2q_s z'}\gamma(z')\sum_{n=0}^{\infty}\frac{1}{n!}\left(-\frac{iq_s}{\cos^2\theta}\int^{z'} dz''\gamma(z'')\right)^n.\end{aligned} \tag{35}$$

This may be summed to closed form, as was done in direct non-linear imaging by Shaw et al. (2004):

$$\psi_P(k_s,\omega) = -\frac{1}{4\cos^2\theta}\int dz' e^{i2q_s\left[z'-(1/2)\cos^{-2}\theta\int^{z'} dz''\gamma(z'')\right]}\gamma(z'). \tag{36}$$

In this paper, the summed form is of less significance, since our aim will be to perform an order by order inversion. As the key result of this appendix, then, we have the series in equation (35), explicitly in terms of the wavespeed and Q perturbations α and β, respectively, given by

$$\psi_P(k_s,\omega) = \int dz' \frac{e^{i2q_s z'}}{4\cos^2\theta}[2F(\omega)\beta(z') - \alpha(z')]\sum_{n=0}^{\infty}\frac{1}{n!}\left(\frac{iq_s}{\cos^2\theta}\int^{z'} dz''[2F(\omega)\beta(z'') - \alpha(z'')]\right)^n. \tag{37}$$

Appendix B
Direct non-linear absorptive-dispersive inversion equations for layered media

In this appendix we perform a direct, order-by-order inversion of the absorptive-dispersive primary approximation derived in Appendix A. We assume that the data (1) contain only primaries, (2) have been deconvolved of the source wavelet, and (3) have been deghosted. These assumptions are typical for direct non-linear primary algorithms based on the inverse scattering series (Weglein et al., 2003). If this is the case, and if the perturbations α and β are of such a size and extent that equation (37) is accurate, we may write

$$\begin{aligned} & D(k_s,\omega) \\ & = -\frac{1}{4\cos^2\theta(k_s,\omega)}\int dz' e^{i2q_s(k_s,\omega)z'}[\alpha(z')-2F(\omega)\beta(z')] \\ & \quad -\frac{[-i2q_s(k_s,\omega)]}{8\cos^4\theta(k_s,\omega)}\int dz' e^{i2q_s(k_s,\omega)z'}[\alpha(z')-2F(\omega)\beta(z')]\left(\int_0^{z'} dz''[\alpha(z'')-2F(\omega)\beta(z'')]\right) \\ & \quad -\frac{[-i2q_s(k_s,\omega)]^2}{32\cos^6\theta(k_s,\omega)}\int dz' e^{i2q_s(k_s,\omega)z'}[\alpha(z')-2F(\omega)\beta(z')]\left(\int_0^{z'} dz''[\alpha(z'')-2F(\omega)\beta(z'')]\right)^2 \\ & \quad +..., \end{aligned} \tag{38}$$

where θ and q_s are particular arrangements of experimental variables k_s and ω:

$$\begin{aligned} \theta &= \sin^{-1}\frac{k_s c_0}{\omega}, \\ q_s &= \frac{\omega}{c_0}\sqrt{1-\frac{k_s^2 c_0^2}{\omega^2}}. \end{aligned} \tag{39}$$

The aim in the remainder of this appendix will be to directly invert equation (38).

An inverse series for absorptive-dispersive primaries

We form an inverse series for the perturbations α and β, in which the n'th term is defined to be n'th order in the *primary* data modeled in equation (37). Let this series be

$$\begin{aligned} & [\alpha(z)-2F(\omega)\beta(z)] \\ & = [\alpha_1(z)-2F(\omega)\beta_1(z)]+[\alpha_2(z)-2F(\omega)\beta_2(z)]+[\alpha_3(z)-2F(\omega)\beta_3(z)]+... \ . \end{aligned} \tag{40}$$

This is substituted into equation (38), and like orders are equated (Innanen, 2005), in a manner similar to Carvalho's derivation of the full inverse scattering series (Carvalho, 1992). At first order we have

$$D(k_s,\omega) = -\frac{1}{4\cos^2\theta(k_s,\omega)}\int dz' e^{i2q_s(k_s,\omega)z'}[\alpha_1(z')-2F(\omega)\beta_1(z')]. \tag{41}$$

At second order, we have

$$\frac{1}{4\cos^2\theta(k_s,\omega)}\int dz' e^{i2q_s(k_s,\omega)z'}[\alpha_2(z')-2F(\omega)\beta_2(z')]$$
$$=-\frac{[-i2q_s(k_s,\omega)]}{8\cos^4\theta(k_s,\omega)}\int dz' e^{i2q_s(k_s,\omega)z'}[\alpha_1(z')-2F(\omega)\beta_1(z')]\left(\int_0^{z'} dz''[\alpha_1(z'')-2F(\omega)\beta_1(z'')]\right). \tag{42}$$

At third order, we have

$$\frac{1}{4\cos^2\theta(k_s,\omega)}\int dz' e^{i2q_s(k_s,\omega)z'}[\alpha_3(z')-2F(\omega)\beta_3(z')]$$
$$=-\frac{[-i2q_s(k_s,\omega)]}{8\cos^4\theta(k_s,\omega)}\int dz' e^{i2q_s(k_s,\omega)z'}[\alpha_1(z')-2F(\omega)\beta_1(z')]\left(\int_0^{z'} dz''[\alpha_2(z'')-2F(\omega)\beta_2(z'')]\right)$$
$$-\frac{[-i2q_s(k_s,\omega)]}{8\cos^4\theta(k_s,\omega)}\int dz' e^{i2q_s(k_s,\omega)z'}[\alpha_2(z')-2F(\omega)\beta_2(z')]\left(\int_0^{z'} dz''[\alpha_1(z'')-2F(\omega)\beta_1(z'')]\right)$$
$$-\frac{[-i2q_s(k_s,\omega)]^2}{32\cos^6\theta(k_s,\omega)}\int dz' e^{i2q_s(k_s,\omega)z'}[\alpha_1(z')-2F(\omega)\beta_1(z')]\left(\int_0^{z'} dz''[\alpha_1(z'')-2F(\omega)\beta_1(z'')]\right)^2. \tag{43}$$

This continues. Just as in the full inverse scattering series, the sequential direct solution for each term, followed by their summation, produces the desired solution. Experience with the cascaded series that have been required to deal with the direct imaging of primaries (e.g., Weglein et al., 2003; Shaw et al., 2004), indicates that several tens of such terms will be required. Hence our approach will be to carry out the inversion explicitly on the first three orders only, thereafter attempting to deduce a pattern that holds over all orders.

First order

The construction of the first order components of the absorptive-dispersive perturbations α_1 and β_1 from the data (i.e., the solution of equation (41)), and the resulting issues of conditioning, detectability, and relationships with the actual medium perturbations, have been described in detail by Innanen and Weglein (2007), and will not be extensively reviewed here. Briefly put, two profiles, $\alpha_1(z|\vartheta,W)$ and $\beta_1(z|\vartheta,W)$, over layered absorptive-dispersive media, may be constructed given a single shot-record or receiver record of reflected primary data and the acoustic reference wavespeed c_0, which is assumed to agree with the actual medium at and above the sources and receivers. Since two or more plane wave incidence angles are required to construct the profiles, but many varied sets of these angles may be sufficient to do so, we define the quantity $\vartheta=\{\theta_1,\theta_2,...\}$ to represent the particular set of angles used. In addition, since the freedom also exists to weight the data at each angle, we define W to represent the particular weighting scheme (if any) chosen. The profiles are then functions of these quantities also.

Summarizing, we establish a mapping between

$$\begin{aligned} D(k_s,\omega) &\rightarrow \alpha_1(z|\vartheta,W), \\ D(k_s,\omega) &\rightarrow \beta_1(z|\vartheta,W). \end{aligned} \tag{44}$$

The mapping is simple, generally a linear combination of Fourier components of the data.

Second order

The second order term in equation (42) is already very close to the form we will find suitable for the eventual direct non-linear inverse equations. However, we make two comments. First, since all of the above relationships are expected to hold for all k_s and ω, by comparing integrands in equation (42), we see that instances of $\alpha_2 - F\beta_2$ occurring under Fourier integrals may be replaced by

$$\alpha_2(z) - 2F(\omega)\beta_2(z) = -\frac{[-i2q_s(k_s,\omega)]}{2\cos^2\theta(k_s,\omega)}[\alpha_1(z) - 2F(\omega)\beta_1(z)]\left(\int_0^z dz'[\alpha_1(z') - 2F(\omega)\beta_1(z')]\right). \tag{45}$$

This will be useful for manipulations at third order. Second, we change variables to θ and $k_z = -2q_s$:

$$\begin{aligned} \int dz' e^{-ik_z z'}&[\alpha_2(z'|\vartheta,W) - 2F(k_z,\theta)\beta_2(z'|\vartheta,W)] \\ &= \frac{-ik_z}{2\cos^2\theta}\int dz' e^{-ik_z z'}[\alpha_1(z'|\vartheta,W) - 2F(k_z,\theta)\beta_1(z'|\vartheta,W)] \\ &\quad\times\left(\int_0^{z'} dz''[\alpha_1(z''|\vartheta,W) - 2F(k_z,\theta)\beta_1(z''|\vartheta,W)]\right), \end{aligned} \tag{46}$$

where we have employed the specific forms for α_1 and β_1 derived above, including the set of angles ϑ and weights W. Since the first order input to the second order term has these dependences, so also must the second order perturbations $\alpha_2 = \alpha_2(z|\vartheta,W)$, $\beta_2 = \beta_2(z|\vartheta,W)$.

Third order

The third order problem requires a greater level of manipulation. The middle two terms in equation (43) may be re-written

$$\begin{aligned}
&-\frac{[-i2q_s(k_s,\omega)]}{8\cos^4\theta(k_s,\omega)}\int dz' e^{i2q_s(k_s,\omega)z'}[\alpha_1(z')-2F(\omega)\beta_1(z')]\left(\int_0^{z'} dz''[\alpha_2(z'')-2F(\omega)\beta_2(z'')]\right)\\
&-\frac{[-i2q_s(k_s,\omega)]}{8\cos^4\theta(k_s,\omega)}\int dz' e^{i2q_s(k_s,\omega)z'}[\alpha_2(z')-2F(\omega)\beta_2(z')]\left(\int_0^{z'} dz''[\alpha_1(z'')-2F(\omega)\beta_1(z'')]\right)\\
=&+\frac{[-i2q_s(k_s,\omega)]^2}{32\cos^4\theta(k_s,\omega)}\int dz' e^{i2q_s(k_s,\omega)z'}[\alpha_1(z')-2F(\omega)\beta_1(z')]\left(\int_0^{z'} dz''[\alpha_1(z'')-2F(\omega)\beta_1(z'')]\right)^2\\
&+\frac{[-i2q_s(k_s,\omega)]^2}{16\cos^4\theta(k_s,\omega)}\int dz' e^{i2q_s(k_s,\omega)z'}[\alpha_1(z')-2F(\omega)\beta_1(z')]\left(\int_0^{z'} dz''[\alpha_1(z'')-2F(\omega)\beta_1(z'')]\right)^2.
\end{aligned} \tag{47}$$

The second of these re-written forms is immediate; to derive the first, we have used the fact that for any integrable function f,

$$\begin{aligned}
&\int_{-\infty}^{z} f(z')\int_{-\infty}^{z'} f(z'')dz''dz'\\
&=\int_{-\infty}^{z}\frac{d}{dz'}\left(\int_{-\infty}^{z'} f(z'')dz''\right)\int_{-\infty}^{z'} f(z'')dz''\\
&=\frac{1}{2}\int_{-\infty}^{z}\frac{d}{dz'}\left(\int_{-\infty}^{z'} f(z'')dz''\right)^2 dz'\\
&=\frac{1}{2}\left(\int_{-\infty}^{z} f(z')dz'\right)^2.
\end{aligned} \tag{48}$$

The two terms in equation (47) are, then, of the same form, and sum to produce

$$+\frac{3[-i2q_s(k_s,\omega)]^2}{32\cos^6\theta(k_s,\omega)}\int dz' e^{i2q_s(k_s,\omega)z'}[\alpha_1(z')-2F(\omega)\beta_1(z')]\left(\int_0^{z'} dz''[\alpha_1(z'')-2F(\omega)\beta_1(z'')]\right)^2.$$

This expression is, in turn, of the same form as that of the last term in equation (43), and so the third order inverse equation may be re-expressed in full as

$$\begin{aligned}
&\frac{1}{4\cos^2\theta(k_s,\omega)}\int dz' e^{i2q_s(k_s,\omega)z'}[\alpha_3(z')-2F(\omega)\beta_3(z')]\\
=&\frac{[-i2q_s(k_s,\omega)]^2}{16\cos^6\theta(k_s,\omega)}\int dz' e^{i2q_s(k_s,\omega)z'}[\alpha_1(z')-2F(\omega)\beta_1(z')]\left(\int_0^{z'} dz''[\alpha_1(z'')-2F(\omega)\beta_1(z'')]\right)^2.
\end{aligned} \tag{49}$$

Simplifying, and changing variables to k_z and θ, we have

$$\begin{aligned}\int dz' e^{-ik_z z'}&[\alpha_3(z'|\vartheta,W) - 2F(k_z,\theta)\beta_3(z'|\vartheta,W)] \\ &= \frac{[-ik_z]^2}{4\cos^4\theta}\int dz' e^{-ik_z z'}[\alpha_1(z'|\vartheta,W) - 2F(k_z,\theta)\beta_1(z'|\vartheta,W)] \\ &\quad\times\left(\int_0^{z'} dz''[\alpha_1(z''|\vartheta,W) - 2F(k_z,\theta)\beta_1(z''|\vartheta,W)]\right)^2.\end{aligned} \tag{50}$$

Again, since at first and second orders the outputs are functions of the set of angles and weights used in the first order procedure, so must the third order terms, i.e., $\alpha_3 = \alpha_3(z'|\vartheta,W)$ and $\beta_3 = \beta_3(z'|\vartheta,W)$.

Direct non-linear absorptive-dispersive inversion equations

Examining equations (46) and (50), we see two things of interest. First, the results are an exact, full inversion of the primary approximation from the previous appendix. Second, within these inversion terms, a pattern is noticeable, whose form persists at higher order. In fact, α_{n+1} and β_{n+1} are related to α_1 and β_1 via

$$\begin{aligned}\int dz' e^{-ik_z z'}&[\alpha_{n+1}(z'|\vartheta,W) - 2F(k_z,\theta)\beta_{n+1}(z'|\vartheta,W)] \\ &= \frac{1}{n!}\left(\frac{-ik_z}{2\cos^2\theta}\right)^n\int dz' e^{-ik_z z'}[\alpha_1(z'|\vartheta,W) - 2F(k_z,\theta)\beta_1(z'|\vartheta,W)] \\ &\quad\times\left(\int_0^{z'} dz''[\alpha_1(z''|\vartheta,W) - 2F(k_z,\theta)\beta_1(z''|\vartheta,W)]\right)^n.\end{aligned} \tag{51}$$

Let us define

$$\begin{aligned}\alpha_P(z|\vartheta,W) &\equiv \sum_{n=0}^{\infty}\alpha_{n+1}(z'|\vartheta,W), \\ \beta_P(z|\vartheta,W) &\equiv \sum_{n=0}^{\infty}\beta_{n+1}(z'|\vartheta,W),\end{aligned} \tag{52}$$

bearing in mind that these sums produce quantities that are functions not only of depth z, but also of the set of angles ϑ and the weights W that were originally used to construct the linear components α_1 and β_1. If we create an instance of equation (51) for every value of $n \geq 0$ and add them together, the left-hand side becomes

$$\begin{aligned}&\sum_{n=0}^{\infty}\int dz' e^{-ik_z z'}[\alpha_{n+1}(z'|\vartheta,W) - 2F(k_z,\theta)\beta_{n+1}(z'|\vartheta,W)] \\ &= \int dz' e^{-ik_z z'}[\alpha_P(z'|\vartheta,W) - 2F(k_z,\theta)\beta_P(z'|\vartheta,W)],\end{aligned} \tag{53}$$

and the right-hand side becomes

$$\begin{aligned}
&\sum_{n=0}^{\infty} \frac{1}{n!} \left(\frac{-ik_z}{2\cos^2\theta} \right)^n \int dz' e^{-ik_z z'} [\alpha_1(z'|\vartheta, W) - 2F(k_z,\theta)\beta_1(z'|\vartheta, W)] \\
&\quad \times \left(\int_0^{z'} dz'' [\alpha_1(z''|\vartheta, W) - 2F(k_z,\theta)\beta_1(z''|\vartheta, W)] \right)^n \\
&= \int dz' e^{-ik_z z'} [\alpha_1(z'|\vartheta, W) - 2F(k_z,\theta)\beta_1(z'|\vartheta, W)] \\
&\quad \times \sum_{n=0}^{\infty} \frac{1}{n!} \left(\frac{-ik_z}{2\cos^2\theta} \int_0^{z'} dz'' [\alpha_1(z''|\vartheta, W) - 2F(k_z,\theta)\beta_1(z''|\vartheta, W)] \right)^n \\
&= \int dz' e^{-ik_z \left[z' + \frac{1}{2\cos^2\theta} \int_0^{z'} dz'' [\alpha_1(z''|\vartheta,W) - 2F(k_z,\theta)\beta_1(z''|\vartheta,W)] \right]} [\alpha_1(z'|\vartheta, W) - 2F(k_z,\theta)\beta_1(z'|\vartheta, W)],
\end{aligned} \tag{54}$$

where in the last step we have performed the collapsing step of Shaw et al. (2004). Equating these two expressions:

$$\begin{aligned}
&\int dz' e^{-ik_z z'} [\alpha_P(z'|\vartheta, W) - 2F(k_z,\theta)\beta_P(z'|\vartheta, W)] \\
&= \int dz' e^{-ik_z \left[z' + \frac{1}{2\cos^2\theta} \int_0^{z'} dz'' [\alpha_1(z''|\vartheta,W) - 2F(k_z,\theta)\beta_1(z''|\vartheta,W)] \right]} [\alpha_1(z'|\vartheta, W) - 2F(k_z,\theta)\beta_1(z'|\vartheta, W)],
\end{aligned} \tag{55}$$

we form the basic underlying equations of direct non-linear inversion for absorptive-dispersive primaries.

Appendix C
Absorptive-dispersive model construction via non-linear direct inversion

The aim in inverse scattering series applications may vary from the construction of spatial distributions of perturbation quantities (model-like quantities) to the construction of equivalent data sets (data-like quantities). The direct non-linear primary inversion quantities derived in Appendix B lend themselves to either goal. In this appendix we will derive the general form of the first of these constructions for layered, 2-parameter absorptive-dispersive media. They will be of independent interest to those wishing to directly determine the 2-parameter medium.

We begin with a straightforward manipulation of equation (55). Recognizing the left-hand side as a Fourier transform, we have

$$\alpha_P(k_z) - 2F(k_z,\theta)\beta_P(k_z) = \Delta(k_z,\theta|\vartheta,W), \tag{56}$$

where we define

$$\begin{aligned}\Delta(k_z,\theta|\vartheta,W) \equiv \int dz' e^{-ik_z\left[z' + \frac{1}{2\cos^2\theta}\int_0^{z'} dz''[\alpha_1(z''|\vartheta,W) - 2F(k_z,\theta)\beta_1(z''|\vartheta,W)]\right]} \\ \times\,[\alpha_1(z'|\vartheta,W) - 2F(k_z,\theta)\beta_1(z'|\vartheta,W)].\end{aligned} \tag{57}$$

We wish to separately calculate α_P and β_P at each relevant depth wavenumber k_z; given at least two angles per depth wavenumber k_z, this is an over-determined problem. Since over-determinedness is typically dealt with through a weighted averaging process (e.g., least squares), we will now be in the business of defining a set of angles and weights to work with. Some notational care will be required here, because, as we see in the linear quantities $\alpha_1(z|\vartheta,W)$ and $\beta_1(z|\vartheta,W)$ in equation (57), an earlier set of angles and weights, $\vartheta = \{\theta_1,\theta_2,...\}$ and W, is already in play here.

We proceed by defining a new set of angles $\widetilde{\vartheta} = \{\widetilde{\theta}_1,\widetilde{\theta}_2,...\} \neq \vartheta$ and weights $\widetilde{W} \neq W$. The mathematics of inversion do not require that $\widetilde{\vartheta}$ and $\widetilde{W}$ be related in any way to ϑ and W. During the construction of the direct Q compensation algorithms in this paper we will argue towards a relationship, but at present we will consider them distinct and un-related. Consequently, the final non-linear output must be considered in general to be a function of both.

Given the $N > 2$ angles that are contained in $\widetilde{\vartheta}$, equation (56) becomes

$$\mathbf{F}(k_z,\widetilde{\vartheta})\begin{bmatrix}\alpha_P(k_z)\\ \beta_P(k_z)\end{bmatrix} = \mathbf{\Delta}(k_z,\widetilde{\vartheta}|\vartheta,W), \tag{58}$$

where

$$\mathbf{F}(k_z,\widetilde{\vartheta}) = \begin{bmatrix}1 & -2F(k_z,\widetilde{\theta}_1)\\ 1 & -2F(k_z,\widetilde{\theta}_2)\\ \vdots & \vdots\\ 1 & -2F(k_z,\widetilde{\theta}_N)\end{bmatrix}, \tag{59}$$

and

$$\mathbf{\Delta}(k_z, \widetilde{\vartheta}|\vartheta, W) = \begin{bmatrix} \Delta(k_z, \widetilde{\theta}_1|\vartheta) \\ \Delta(k_z, \widetilde{\theta}_2|\vartheta) \\ \vdots \\ \Delta(k_z, \widetilde{\theta}_N|\vartheta) \end{bmatrix}. \tag{60}$$

Through whatever choices are made in inverting $\mathbf{F}(k_z, \widetilde{\vartheta})$ the new non-linear weights $\widetilde{W}$ are brought in. That is, $\mathbf{F}^{-1} = \mathbf{F}^{-1}(k_z, \widetilde{\vartheta}, \widetilde{W})$. Now, this means that the outputs α_P and β_P are dependent on k_z, but also on (1) the weights and angles used to create the linear output, ϑ and W, and on (2) the weights and angles used above to create the non-linear output, $\widetilde{\vartheta}$ and $\widetilde{W}$. That is,

$$\begin{bmatrix} \alpha_P(k_z|\widetilde{\vartheta}, \widetilde{W}, \vartheta, W) \\ \beta_P(k_z|\widetilde{\vartheta}, \widetilde{W}, \vartheta, W) \end{bmatrix} = \mathbf{F}^{-1}(k_z, \widetilde{\vartheta}, \widetilde{W})\mathbf{\Delta}(k_z, \widetilde{\vartheta}|\vartheta, W). \tag{61}$$

Finally, profiles may be generated through inverse Fourier transforms:

$$\begin{aligned} \alpha_P(z|\widetilde{\vartheta}, \widetilde{W}, \vartheta, W) &= \frac{1}{2\pi}\int dk_z e^{ik_z z}\alpha_P(k_z|\widetilde{\vartheta}, \widetilde{W}, \vartheta, W), \\ \beta_P(z|\widetilde{\vartheta}, \widetilde{W}, \vartheta, W) &= \frac{1}{2\pi}\int dk_z e^{ik_z z}\beta_P(k_z|\widetilde{\vartheta}, \widetilde{W}, \vartheta, W). \end{aligned} \tag{62}$$

The freedom to *twice* choose both the subsets of the data we use, and their weights, during the calculation of the profiles in equation (62), suggests a large range of types of inverse result is possible.